Aqueous Photochemistry of α-Keto Acids:

Building Complexity at Molecular and Supramolecular Scales

by

Rebecca Jean Rapf

A.B., Dartmouth College, 2012

A thesis submitted to the

Faculty of the Graduate School of the

University of Colorado in partial fulfillment

of the requirements for the degree of

Doctor of Philosophy

Department of Chemistry and Biochemistry

2017

This thesis entitled:
Aqueous Photochemistry of α-Keto Acids:
Building Complexity at Molecular and Supramolecular Scales
written by Rebecca Jean Rapf
has been approved for the Department of Chemistry and Biochemistry

_____
Prof. Veronica Vaida

_____
Prof. Joel Eaves

Date: _____

The final copy of this thesis has been examined and approved by the signatories, and we find that both the content and form meet acceptable standards of scholarly work in the above mentioned discipline.

Rapf, Rebecca Jean (Ph.D., Physical Chemistry)

Aqueous Photochemistry of α-Keto Acids: Building Complexity at Molecular and Supramolecular Scales

Thesis directed by Prof. Veronica Vaida

Sunlight-driven reactions of organic molecules contribute to the environmental processing of organic compounds, including the generation of molecular complexity via aqueous chemistry. This thesis focuses on the aqueous photochemistry of α-keto acids, and the implications of this reactivity for environmental chemistry of both the early and modern Earth. Beginning with pyruvic acid, the simplest α-keto acid, I have investigated the photochemical mechanisms governing their reactivity in aqueous solutions. Even in very dilute solutions with low concentrations of pyruvic acid, covalently-bonded dimers and trimers are formed from the recombination of photochemically-generated radical species. These mechanisms are readily generalizable to α-keto acids as a class of molecules, as shown for a series of alkyl α-keto acids. α-Keto acids are also shown to be capable of acting as photo-initiators, driving reactions of non-photoactive species.

The photochemistry of α-keto acids is known to be particularly sensitive to reaction conditions. One example of this sensitivity is the observed pH dependence and its effects on relative product yields, which is due in part to changes in the extent of hydration and deprotonation. These observed changes are consistent within the expanded mechanistic framework for the reactivity of α-keto acids.

Even simple starting solutions of a single alkyl α-keto acid species become a complex mixture of oligomeric species upon photolysis. This is due to the formation of reactive

intermediate species, which can further react in solution. The oligomers formed from this photochemistry are amphiphiles, many of which have two or three alkyl chains. The photoproducts generated from these alkyl α-keto acids are surface-active and spontaneously self-assemble into monodisperse, spherical aggregates over the course of photolysis, which has important environmental implications both for today and the early Earth. In the modern environment, this chemistry may contribute to the abiotic processes by which surface-active species are formed at the sea surface microlayer. The formation of such multi-tailed lipids and aggregates on the early Earth may help answer questions about how the first protocells evolved.

Acknowledgements

This thesis is the product of the collaboration and support I received along the way. The following is in no way intended to be an exhaustive list.

I would like to acknowledge the personal financial support I have received from a number of fellowships and awards: the NASA Earth and Spaces Science Fellowship, the CIRES Graduate Student Award, the Marion L. Sharrah Departmental Fellowship, and an RA position with the CU Center for the Study of Origins.

Of the many people who guided me through graduate school, Veronica Vaida stands heads and shoulders above the rest. You gave me every opportunity and urged me to make the most of all of them. I will always appreciate your creative and open-minded approach to science, as well as your commitment and care for your students. I have also been lucky to work with many collaborators who have broadened my horizons significantly: Barry Carpenter, Sheref Mansy, Laura Martini, Kevin Wilson, James Davies, Rob Walker, and Christine Gobrogge to name a few. Closer to home, I would like to thank Joel Eaves for allowing this simple experimentalist to pretend to be a theorist and for always trusting that my capabilities are up to the task, even when I'm skeptical. I am also grateful to the wonderful staff of the many core facilities, who go above and beyond the call of duty on a daily basis. In particular, I thank Jeremy Balsbaugh, Annette Erbse, and Rich Shoemaker who contributed a huge amount of time and thought to the work described in this thesis.

I am also grateful to my many other mentors and teachers who have been steadfast in their support and encouragement. My high school teachers, especially Mr. Clift, Mr. Fessler, Mrs. Hackman, Mrs. Knutson, and Mr. Urbatchka, taught me the importance of clear thinking and good writing, as well as the dangers of perfectionism. I am proof of the world-class education that can be provided by public schools, even in small, rural Wyoming

towns. I am also grateful to the Summer Science Program, which was my first glimpse of the research world and is always a reminder of just how much can be accomplished in a short period of time. I am also indebted to Molly Carpenter for her endless patience, sound advice, as well as leading by example in a way that I can only hope to emulate.

I am grateful to the Vaida group lab members past and present. To Elizabeth Griffith for deciding to do "just one more" experiment – I've spent a good five years because of it. And, especially to my cohort, the Three Muskeeters: To Jay Kroll for always reminding me of the role of wonder and curiosity in science. To Russell Perkins for the many, many brainstorming sessions over the years and your technical know-how – the only reason anything ever got done in lab. And to Allison Reed Harris for being my tireless and peerless editor and for reminding me that sometimes it's ok to say no. I could not imagine grad school without you.

I also have enjoyed the many hours spent at lunch playing bridge with Steven Strong and Alyssa Landin, as well as the fruitful scientific collaborations that have come, in part, from these games. I thank Allie Hunter for the countless conversations about science, society, and silliness, and Elise Wilkes for the many hours we spent in Kresge and for always being my virtual study-buddy.

I am also grateful to my family. To Aunt Bev and Mary Jane for their fierce interest in anything I have done. To Gramgunn for reminding me that it's never too late to try something new. I can only hope that my publishing record will live up to yours. And finally, to Mom and Dad for teaching me the value of kindness, the power of hard work, and the importance of knowing when to crump. Thank for you for allowing me to tag along on your many adventures.

Contents

Tables

Figures

Schemes

1. Introduction

Sunlight is the largest source of energy on Earth and has been since the time when the planet first cooled sufficiently to have a crust, more than 4 billion years ago.[1-3] Energy from the Sun drives, directly or indirectly, the vast majority of chemical and physical processes on Earth. The importance of the Sun in controlling climate and radiative forcing is recognized in the study of both the early and the modern Earth.[4-8] Modern atmospheric chemistry also recognizes the importance of photochemical processing of material, primarily through secondary reactions with hydroxyl radical.[9, 10] However, contributions from direct photochemistry of organic molecules to the reactivity of environmental systems have been limited. This is also the case in the study of prebiotic chemical evolution where the Sun has been largely viewed as a purely destructive force.[1, 11-13] Chapter 2 of this work highlights the capacity of sunlight to build molecular complexity and the likely importance of its role in the formation of more complex molecules needed for the evolution of life.[14]

This thesis focuses on the photochemistry of α-keto acids in the aqueous phase. These molecules are an interesting model system that demonstrates the surprisingly rich chemistry and interwoven networks of reactions that can occur even when starting with a simple single species in solution. Pyruvic acid, the simplest α-keto acid, is a small, three-carbon molecule, but its reactivity is extremely diverse and dependent on reaction conditions.[15-18] In Chapter 4, I discuss the detailed photochemical mechanisms that govern this reactivity in aqueous solution and suggest a new identification and mechanistic pathway for the formation of observed oligomeric species.[19] The mechanisms governing the photochemistry of pyruvic acid are robustly transferrable across α-keto acids as class, as discussed in Chapter 5.[20]

α-Keto acids, when dissolved in aqueous solution, hydrate to form the corresponding

geminal diol. As discussed in Chapter 6, the extent of hydration shifts as the solution pH is changed, as does the extent of deprotonation of both species, and these changes affect the branching ratio of the reactive pathways.[21] This behavior also highlights the broad theme that dissolving a pure compound in aqueous solution leads to a surprisingly complicated system, even before photolysis. Once illuminated with light, the solution complexity is only increased. The observed species generated from the photolysis of α-keto acids are in many cases not primary photoproducts but rather are generated from the subsequent reactions of reactive intermediate species. In some cases, these intermediates are themselves photoactive. In this way, even if initially only a single α-keto acid is present in a solution, photolysis rapidly generates multiple photoactive species that generate organic radicals that can combine with each other in a myriad of ways, building the system's chemical complexity. Crucially, this entangled mixture is governed by overarching mechanisms that are well understood and can be used to readily identify the majority of photoproducts in solution.

As shown in Chapters 7 and 8, α-keto acids also can be used as photo-initiators that drive reactions of species that are not themselves photoactive.[22] This suggests that α-keto acids in the natural environment may have an outsized effect in a mixture, even when present as only a minor component. This also speaks to the need to better quantify the contributions that direct photochemistry of organic species may play in the overall reactivity of species in the atmosphere, especially with comparison to the hydroxyl radical.

The aqueous photochemistry of α-keto acids is broadly characterized by the formation of oligomers.[15, 19, 20, 23-25] For the case of alkyl α-keto acids, photolysis results in the formation of a number of multi-tailed species in solution. The synthesis of double- and triple-tailed species from single-tailed precursors is intriguing as a source of higher molecular weight products that can contribute to the sea surface microlayer, as well as to the organic fraction

of atmospheric aerosols. Additionally, this provides a simple prebiotically plausible route for the formation of double-tailed lipids in the absence of biology, which has been a previously intractable problem.[26]

As discussed in Chapter 9, the photoproducts of alkyl α-keto acids are more surface-active[25] and spontaneously form monodisperse, spherical aggregates during the course of photolysis without external perturbation.[20, 25] Chapter 10 shows that these aggregates form abruptly when a critical aggregation concentration of multi-tailed photoproducts is reached, and electron microscopy suggests that despite initial evidence[25] these aggregates are unlikely to be vesicles.

To understand the mechanism of self-assembly of these photochemically generated aggregates, it is necessary to understand the fundamental intermolecular interactions that govern the self-assembly and diffusion of aggregates more broadly. Chapter 11 explores the nature of the diffusion of hydrophobic aggregates in the aqueous solution, specifically investigating whether the diffusion constant scales inversely with radius for particle sizes near the dewetting transition. Simple pictures of the intermolecular forces that govern the interactions of surfactant species may not be sufficient to explain the empirically observed behavior, as shown in Chapter 12 through investigation of fatty acids films at different salinity conditions.

A repeating motif present throughout all the studies in this thesis is the necessity of detailed, fundamental investigations that explore the mechanisms of seemingly simple systems to elucidate their underlying complexities. The mechanisms that underpin the behavior of model systems are often robust and self-consistent once known. Therefore, results from fundamental studies can then be applied more broadly to a wider range of systems, including those of mixtures that better resemble those present in the natural environment.

1.1 Bibliography:

1. Miller, S. L.; Urey, H. C. Organic compound synthesis on the primitive early Earth. *Science* **1959,** *130*, 245-251.

2. Deamer, D.; Weber, A. L. Bioenergetics and life's origins. *Cold Spring Harbor Persp. Biol.* **2010,** *2*, 1-16.

3. Crabtree, G. W.; Lewis, N. S. Solar energy conversion. *Physics Today* **2007,** *60*, 37-42.

4. Shaw, G. H. Earth's atmosphere–Hadean to early Proterozoic. *Chem. Erde Geochem.* **2008,** *68*, 235-264.

5. Sagan, C.; Chyba, C. The early faint sun paradox: Organic shielding of ultraviolet-labile greenhouse gases. *Science* **1997,** *276*, 1217-1221.

6. Hansen, J.; Sato, M.; Ruedy, R. Radiative forcing and climate response. *J. Geophys. Res. Atmos.* **1997,** *102*, 6831-6864.

7. Rosing, M. T.; Bird, D. K.; Sleep, N. H.; Bjerrum, C. J. No climate paradox under the faint early sun. *Nature* **2010,** *464*, 744-747.

8. Beer, J.; Mende, W.; Stellmacher, R. The role of the sun in climate forcing. *Quaternary Science Reviews* **2000,** *19*, 403-415.

9. Gligorovski, S.; Strekowski, R.; Barbati, S.; Vione, D. Environmental implications of hydroxyl radicals (•OH). *Chem. Rev.* **2015,** *115*, 13051-13092.

10. Finlayson-Pitts, B. J.; Pitts, J. N., *Chemistry of the upper and lower atmosphere.* Academic Press: San Diego, 1999.

11. Cleaves, H. J.; Miller, S. L. Oceanic protection of prebiotic organic compounds from UV radiation. *Proc. Natl. Acad. Sci.* **1998,** *95*, 7260-7263.

12. Cockell, C. S. The ultraviolet history of the terrestrial planets: Implications for biological evolution. *Planet. Space Sci.* **2000,** *48*, 203-214.

13. Margulis, L.; Walker, J. C. G.; Rambler, M. Reassessment of roles of oxygen and ultraviolet light in Precambrian evolution. *Nature* **1976,** *264*, 620-624.

14. Rapf, R. J.; Vaida, V. Sunlight as an energetic driver in the synthesis of molecules necessary for life. *Phys. Chem. Chem. Phys.* **2016,** *18*, 20067-20084.

15. Reed Harris, A. E.; Ervens, B.; Shoemaker, R. K.; Kroll, J. A.; Rapf, R. J.; Griffith, E. C.; Monod, A.; Vaida, V. Photochemical kinetics of pyruvic acid in aqueous solution. *J. Phys. Chem. A* **2014,** *118*, 8505-8516.

16. Griffith, E. C.; Carpenter, B. K.; Shoemaker, R. K.; Vaida, V. Photochemistry of aqueous pyruvic acid. *Proc. Natl. Acad. Sci.* **2013,** *110*, 11714-11719.

17. Reed Harris, A. E.; Doussin, J.-F.; Carpenter, B. K.; Vaida, V. Gas-phase photolysis of pyruvic acid: The effect of pressure on reaction rates and products. *J. Phys. Chem. A* **2016,** *120*, 10123-10133.

18. Reed Harris, A. E.; Pajunoja, A.; Cazaunau, M.; Gratien, A.; Pangui, E.; Monod, A.; Griffith, E. C.; Virtanen, A.; Doussin, J. F.; Vaida, V. Multiphase photochemistry of pyruvic acid under atmospheric conditions. *J. Phys. Chem. A* **2017,** *121*, 3327–3339.

19. Rapf, R. J.; Perkins, R. J.; Carpenter, B. K.; Vaida, V. Mechanistic description of photochemical oligomer formation from aqueous pyruvic acid. *J. Phys. Chem. A* **2017,** *121*, 4272–4282.

20. Rapf, R. J.; Perkins, R. J.; Yang, H.; Miyake, G. M.; Carpenter, B. K.; Vaida, V. Photochemical synthesis of oligomeric amphiphiles from alkyl oxoacids in aqueous environments. *J. Am. Chem. Soc.* **2017,** *139*, 6946–6959.

21. Rapf, R. J.; Dooley, M. R.; Kappes, K.; Perkins, R. J.; Vaida, V. pH dependence of the aqueous photochemistry of α -keto acids *J. Phys. Chem. A* **2017**, DOI: 10.1021/acs.jpca.7b08192.

22. Renard, P.; Reed Harris, A. E.; Rapf, R. J.; Rainer, S.; Demelas, C.; Coulomb, B.; Quivet, E.; Vaida, V.; Monod, A. Aqueous phase oligomerization of methyl vinyl ketone by atmospheric radical reactions. *J. Phys. Chem. C* **2014,** *118*, 29421-29430.

23. Leermakers, P. A.; Vesley, G. F. Photochemistry of alpha-keto acids and alpha-keto esters. 1. Photolysis of pyruvic acid and benzoylformic acid. *J. Am. Chem. Soc.* **1963,** *85*, 3776-3779.

24. Guzman, M. I.; Colussi, A. J.; Hoffmann, M. R. Photoinduced oligomerization of aqueous pyruvic acid. *J. Phys. Chem. A* **2006,** *110*, 3619-3626.

25. Griffith, E. C.; Rapf, R. J.; Shoemaker, R. K.; Carpenter, B. K.; Vaida, V. Photoinitiated synthesis of self-assembled vesicles. *J. Am. Chem. Soc.* **2014,** *136*, 3784-3787.

26. Monnard, P. A.; Deamer, D. W. Membrane self-assembly processes: Steps toward the first cellular life. *Anat. Rec.* **2002,** *268*, 196-207.

2. Sunlight as an Energetic Driver in the Synthesis of Molecules Necessary for Life*

2.1 Introduction:

Life is an inherently high-energy, out-of-equilibrium enterprise, and both the evolution and continuation of life require the input of energy to the system. Living organisms obtain energy autotrophically, chemotrophically, or heterotrophically, and then, through metabolism, create and replicate the complex biomolecules needed for their survival. Likewise, under prebiotic conditions without enzymatic assistance, the synthesis of such biomolecules from simpler organic molecules also requires energy from an external source.

Light from the Sun is the single largest energy source on both the ancient and modern Earth.[2-4] Even considering the lower luminosity of the early Sun, the amount of solar energy available on Earth was orders of magnitude greater than that provided by electrical discharges, shockwaves from impacts, radioactivity, volcanoes, and geothermal sources combined.[3, 4] Additionally, in the absence of atmospheric oxygen and ozone, which shield the surface of the Earth from ultraviolet photons today, there would have been more of this chemically useful high-energy light available on the surface of the prebiotic Earth. It stands to reason, then, that photochemical reactions may have played an important role in the development of larger, more complex molecules during the chemical evolution of biomolecules that eventually led to life.

In this chapter, we highlight the uniqueness of photochemistry in the abiotic synthesis of such molecules. Incoming solar radiation reaches Earth with high energy and low entropy, but is degraded into heat, motion, and ultimately thermal energy, which is re-

* This work was reproduced from Rapf, R.J and Vaida, V. Sunlight as an Energetic Driver in the Synthesis of Molecules Necessary for Life. *Physical Chemistry and Chemical Physics*, *18*, 20067-20084, 2016 with permission from the PCCP Owner Societies.[1]

radiated to space. This energy dispersal generates entropy, which can then drive large-scale processes such as weather systems, ocean currents, and life.

The low entropy energy provided by a star is, therefore, different from thermal sources of energy (geothermal, volcanic, hydrothermal vents, etc.) considered in origin of life scenarios. Excitation initiated by thermal sources causes energy to be distributed randomly throughout molecules. It therefore requires very high temperatures for any significant fraction of molecules to have sufficient energy to react. Photochemistry, on the other hand, relies on the absorption of a photon, which excites a specific molecule, localizing a great deal of energy while still allowing the temperature of the system to remain low. These characteristics lead to a great contrast between thermal chemistry and photochemistry; under conditions required for reaction, thermal chemistry always moves toward thermodynamic equilibrium, but photochemistry can move away from it. Photochemistry, therefore, allows for the direct generation of high-energy compounds and/or non-equilibrium systems without the need to invoke environmental changes, such as wet-dry cycles,[5, 6] as are required for thermal chemistry.

Furthermore, photochemistry is inherently molecule-specific because electronic and vibrational states are quantized and depend uniquely on the structure of the molecule. The functional groups of a molecule determine the shape of its potential energy surfaces, including the energy spacing between states, and govern the accessible reaction pathways. These potential energy surfaces are often affected by the molecule's environment (e.g. solvent conditions). Different environments can often alter reaction mechanisms and, at times, change the final products. Thus, photochemistry is not only molecule-specific but is also quite environment-specific.

Here, we briefly review the likely solar radiation and environmental conditions available on the early Earth before giving an overview of the processes that govern

photophysical and photochemical pathways. We then explore examples of prebiotically-plausible sunlight-driven chemical reactions that abiotically generate biologically-relevant compounds, including the generation of high energy species, lipids, and biopolymer precursors. We also will examine photostability as a possible evolutionary selection pressure.

2.2 Prebiotic Conditions and Constraints:

We are concerned with the period of chemical evolution prior to the origin of life. Assignment of definitive dates to the occurrence of specific milestones or incidents is always controversial when considering events that took place billions of years ago. The era of prebiotic chemistry leading to abiogenesis must have occurred after the Earth cooled enough to have liquid water on its surface and before the establishment of life.

While there is a paucity of geological evidence during the first billion years of Earth's existence, there is evidence for liquid water on the surface as early as 4.3 Gya.[7-9] The Earth also experienced a much higher rate of meteoritic impacts during this early period, particularly during the Late Heavy Bombardment (LHB).[10-14] It was initially proposed that this bombardment would have been intense enough to heat the oceans considerably, possibly even vaporizing them,[11] effectively sterilizing the Earth.[10] More recently, however, it has been suggested that rather than a cataclysmic LHB, there was instead a longer, relatively sustained period of moderate bombardment, heavier than the impact rate now, but not enough to sterilize the ocean.[12, 13] This implies that prebiotic chemistry may have been taking place throughout this period.

Constraining the upper limits of the time during which prebiotic chemistry took place is reliant on being able to date the emergence of life. Direct evidence of life, in the form of microfossils[15] and sedimentary remnants of microbial mats[16] has been found as far back as 3.2 Gya, suggesting life was well-established at that point. Prior to 3.2 Gya, there is

evidence in the form of stromatolites,[17-19] sedimentary structures,[20] and biogenic isotope fractionation[21-25] that suggests life may have been established by 3.5 Gya or even as early as 3.8 Gya.

For our purposes, we will discuss the likely conditions on the early Earth during the mid to late Hadean period and the early Archean period, or approximately 4.2 to 3.8 Gya, a reasonable time frame for abiogenesis that brackets the dates that others have invoked for prebiotic chemistry.[26-29]

2.2.1 Radiative Output of the Early Sun:

The Sun is a G-type star on the main Hertzsprung-Russell sequence, meaning it is of a medium size, has a moderate surface temperature, fuses hydrogen into helium, and has an expected lifetime of around 10 billion years.[30] Currently about 4.56 billion years old, the Sun was only 30 million years old when the Earth was formed 4.54 billion years ago.[29, 30] The Sun has evolved considerably over this time, and the solar spectrum of the early Sun differed from that of today.

As stars age, their luminosity increases, so the Sun of 4.5 billion years ago and of 3.8 billion years ago (Gya) was only 70% and 75% as luminous as it is today, respectively.[31] The spectral distribution of the early Sun also differed from that of the modern solar spectrum. The spectra of stars are often modeled as black body radiation, where both the luminosity and the peak in spectral output have a direct relationship to the surface temperature of the star. The decreased luminosity of the early Sun is due to the relatively cooler surface temperature of the star early in its evolution. Additionally, cooler black bodies have spectral outputs that peak at lower energies, i.e. the Earth radiates primarily in the infrared (IR). The modern Sun's spectral maximum is at about 500 nm (green light) but, using black body radiation as a guide, one would expect the early Sun to have had an output that peaked at longer wavelengths, and, consequently, a decreased output of higher

energy UV radiation than today. Interestingly, this appears not to be the case for young stars, which deviate from the expected black body radiation spectra and have considerably more UV radiation relative to what is predicted by black body radiation curves.[31, 32] It has been claimed that the young Sun may have had up to 10,000 times more UV radiation than it does today.[32] However, more recent studies have suggested that the increase may have been much more modest with the ratio of UV flux of the early Sun to that of the current Sun maximizing at about 10 times the current flux.[31] This increase in flux also occurs preferentially in the extreme UV at wavelengths less than 200 nm,[28, 31] while the flux in the middle and near UV (λ = 200 – 400 nm) may actually have been slightly lower for the early Sun.[31] As seen in Figure 2.1, the flux of the extraterrestrial solar spectrum of the early Sun (3.8 Gya) and the current Sun do differ significantly from each other. However, the changes in the Sun's spectrum itself are dwarfed by the changes in observed spectrum on the surface of the Earth caused by absorptions in the atmosphere.[33] We, therefore, will discuss the plausible environmental conditions on the early Earth during the period of prebiotic chemical evolution, including atmospheric composition, in order to evaluate the spectrum available for causing photochemical reactions.

2.2.2 Environmental Conditions on the Early Earth:

The composition of the atmosphere can have major impacts not only on the light that reaches the surface of the Earth, but also on the species available for reaction. Photochemistry can (and does) take place throughout the atmosphere as well as on the surface (both terrestrial and oceanic) of the Earth. However, when considering the productive photochemistry that may have contributed to chemical evolution, we will consider mainly the lower atmosphere because of the higher concentration of organic molecules near the Earth's surface. The atmospheric composition at high altitude was likely important in terms of filtering the sunlight that reached the surface and initiating radical

photochemistry, but it is the troposphere, the surface, and shallow oceans that we will focus on as major regions of photochemical interest for the origins of life.

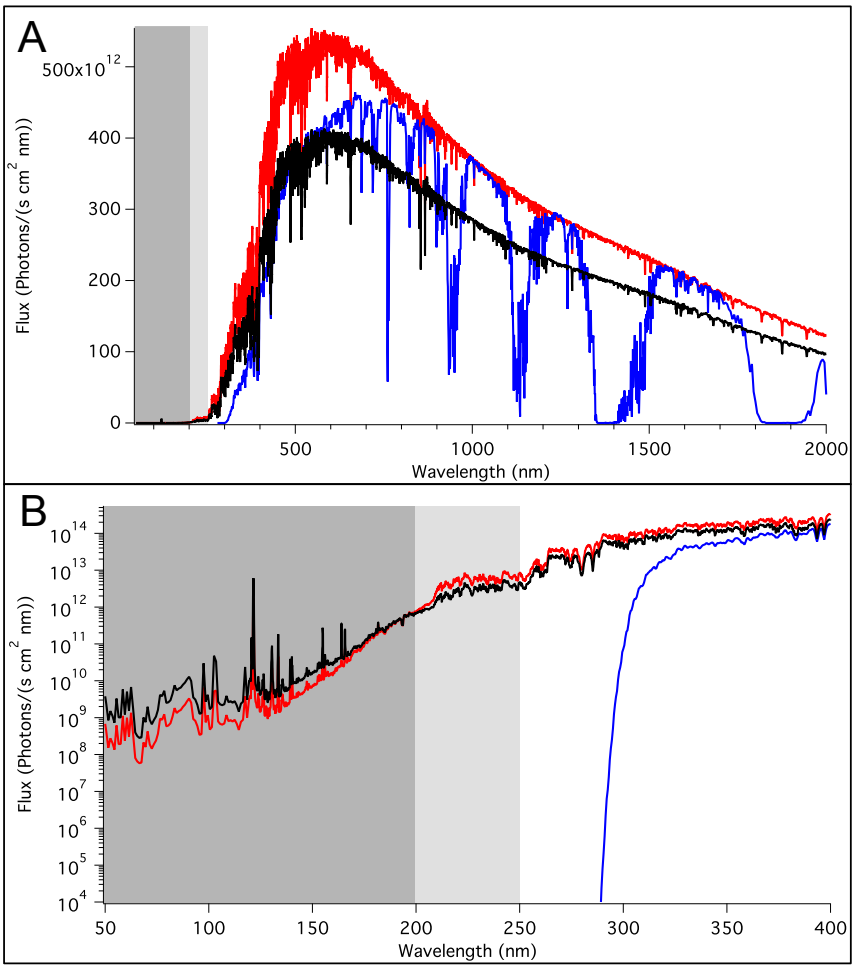

Figure 2.1. A) Photon flux of the current extraterrestrial solar spectrum (red) compared to the calculated extraterrestrial spectrum of the Sun 3.8 Gya (black) as given in Claire et al. 2012[31] and to the spectrum of solar radiation that reaches the surface of the modern Earth (blue) as given in the NREL reference AM 1.5 atmosphere.[33] B) Inset of the UV region of interest for most photochemistry with photon flux on a logarithmic scale. The grey boxes in both A and B show likely regions of attenuation by the prebiotic atmosphere. The dark grey region (< 200 nm) would have been almost completely attenuated, while the radiation in the lighter grey region (200-250 nm) would have been modestly attenuated. These regions of attenuation are in agreement with Ranjan and Sasselov 2016.[28]

The early atmosphere contained very little oxygen or other species that are generated by reactions with molecular oxygen, such as ozone. The exact composition of the atmosphere during the Hadean has been controversial, though most agree that it was not oxidizing.[30, 34-37] Yet, while many concur that it was likely reducing during the Hadean,[30, 34,

[35] some argue that the global atmosphere was neutral at the advent of life,[36, 37] perhaps with locally reducing environments (e.g. near volcanoes).[37] The dominant species in the atmosphere were most likely N_2 and CO_2.[34, 38] Some have considered that there might have been up to 100 bar of CO_2 during this period,[39] but it is more commonly assumed that the overall atmospheric pressure was close to the 1 bar of today. Additionally, constraints from paleosols[40, 41] and banded iron formations[42] suggest that upper limit to the mixing ratio of CO_2 during the Archean was somewhere between 3 to 50 times the present atmospheric level. Using these constraints, the early Earth's atmosphere has been modeled with mixing ratios of N_2 and CO_2 of roughly 0.9 and 0.1, respectively,[28, 43] with other minor trace gases included.

Methane has the potential to be another key component of the early atmosphere. Some have proposed a relatively high concentration of CH_4, which would create organic hazes that may have formed as an early UV shield.[44] However, this requires a ratio of CH_4/CO_2 ratio of 0.1,[45] which is a very high ratio considering there would be no biotic sources of methane. Instead it is more likely that only trace amounts of methane existed and has been modeled with concentrations between 0 and 1 ppm.[28, 43, 46] Other trace gases with significance for prebiotic photochemistry include HCN, NH_3, H_2S, and volatile organics, such as aldehydes and ketones. The expected prebiotic mixing ratios of these species are not well-constrained. The amount of HCN, for example, is dependent on assumptions about the concentration of CH_4.[47] Regardless, while these are important feedstock species for further chemistry, the expected steady state mixing ratios of these trace gases would be very small.

Following periods of significant volcanic activity, SO_2 outgassing from magma and lava would have also been an important constituent of the atmospheric mixture.[48-50] Although, given its reactivity,[51, 52] the steady-state mixing ratio was likely relatively small. Water vapor is also outgassed by magma,[36] and, while the majority of it was rapidly condensed to

liquid, H_2O was likely a significant component of the atmosphere, just as it is today. The specific mixing ratio of water in the atmosphere, however, is, and would have been, heavily temperature and therefore altitude dependent.[44-46]

The surface temperature of the early Earth is another controversial point in determining the likely environmental conditions present. At the lower luminosities of billions of years ago, less radiation would have reached the surface of the Earth, resulting in a surface temperature below the freezing point of water.[53] Considering this, it is plausible that the Earth was completely icebound,[53] in a similar manner to the later "Snowball Earth" periods that have been suggested.[54] However, given the geological evidence of liquid water on the Earth at this time,[55, 56] this is at least an incomplete picture of the early Earth. This is the so-called faint young sun paradox,[53] based on the conflicting data between decreased solar luminosity and evidence of liquid water. This paradox can be reconciled by invoking an atmospheric composition with sufficient greenhouse gases to trap enough heat on the Earth to compensate for the lower influx of light.[38, 57-59] Climate models have shown that the circulation of the Earth's atmosphere[60-62] would have been sufficient to keep an open ocean in the mid-latitudes[43, 60-62] even with modest amounts of greenhouse gases that are consistent with the constraints on CO_2 concentrations,[40-42] especially when combined with other warming mechanisms such as changes in albedo and cloud condensation nuclei.[43] Some have even suggested that the climate of the early Archean may have been quite warm with ocean temperatures of 60 – 80 °C,[63, 64] although more recent analyses have found the upper limit on temperature to be 40 °C.[65, 66] While the oceanic temperature is likely to have played a role in the various rates of critical chemical reactions, such as hydrolysis, water temperature is not a key environmental factor that we must consider here. Photochemistry, unlike thermal chemistry, is relatively insensitive to the temperature of the surroundings. Therefore, for our purposes, it is sufficient to assume that

the temperatures at the surface of the Earth were such that there would have been surface liquid water during the period of chemical evolution.

Assuming that there was liquid water present, the oceans of the early Earth likely covered almost the entire surface due to the lack of continent formation in the Hadean.[67, 68] The composition of this global ocean is difficult to predict, but it likely contained both inorganic and organic species. Prebiotic organic material in the ocean was likely comprised primarily of small, monomeric molecules in relatively dilute concentrations (the so-called "prebiotic soup") although local pockets of increased molecular complexity and concentration would have existed. The majority of the inorganic species were probably ionic species from salts, with total concentrations thought to be higher than that of today,[34, 37, 39, 69-72] perhaps roughly 1.5 to 2 times higher.[73, 74] The composition of the ions present in the early ocean is a matter of debate, however. Na^+ is generally agreed to have been an important species in the early oceans. Many assume that NaCl was the major salt as it is now,[39, 75] but some have suggested that, rather than chloride, bicarbonate may have been the predominant counterion.[72] Adding to the uncertainty, the pH of the early oceans is not well constrained, with estimates ranging from a pH of 4 to 9.[34, 37, 39, 70-72, 76] While very little can be said about the likely conditions of the early ocean with much certainty, the presence of a global ocean would have provided a large, bulk aqueous medium in which prebiotic chemistry could occur.

In addition to the bulk aqueous environment of the oceans, air-water interfaces provide unique reactive environments where different chemistry may occur than in bulk phases.[77, 78] Such interfaces would have been present on the surfaces of oceans, lakes, clouds, and fogs. Atmospheric aerosols, small liquid or solid particles suspended in the atmosphere, would also have provided a significant source of surfaces. Aerosols can be formed from many sources, including dust, soot, sea spray, and condensation of gaseous species. Collectively,

these globally distributed atmospheric particles have an enormous surface area.[79]

It is likely that most aerosols in the prebiotic atmosphere would have had some water content that would be found primarily on the outside of these particles. Even fairly hydrophobic particles will take up some water,[80-83] with the extent of uptake relying heavily on the relative humidity of the atmosphere. Relative humidity is very dependent on the temperature of the atmosphere and therefore difficult to predict for the prebiotic Earth. It is plausible, however, that most of the aerosols generated in the lower atmospheric region that we are considering in this chapter would have had at least some surface coverage of water, generating air-water interfaces. In addition, aerosols with water surfaces can be formed directly by wind action on a liquid ocean. Such aqueous aerosols would be widely available, not only on Earth, but also on any rotating planet with an atmosphere and liquid water on the planet's surface.[84]

On modern Earth, the total surface area of aerosols is larger than that of all other water sources combined.[85] Even when considering the surface area of only marine aerosols, this is on the order of 10^{15} m^2; comparatively, the surface area of the oceans is roughly 10^{14} m^2.[85, 86] This makes atmospheric aerosols a particularly important environment for interfacial chemistry. Aqueous surfaces provide a means for concentrating and orienting simple organic molecules, while also ameliorating some of the thermodynamic and kinetic constraints for reactions that are unfavorable in bulk water.[77, 87, 88] Today's aerosols are known to have significant organic content, some of which will partition preferentially to the surface of the particle.[84, 89-93] Even many small, soluble organic molecules, such as amino acids, partition preferentially to the surface.[94]

Atmospheric aerosols also provide an important connection between an ocean and the atmosphere, allowing for exchange of material between the liquid and the vapor phase, as shown in Figure 2.2.[84, 89, 95-97] With lifetimes on the order of weeks, aerosols provide a means

for global transport of material, connecting localized molecular sources such as meteoric impacts with broader oceanic and atmospheric ones. For example, even modern aerosols have been shown to have significant meteoritic content,[93] despite the lower bombardment rates on today's Earth. Additionally, during their lifetime, aerosols sample a wide-range of temperature, humidity, and photon flux conditions in the atmosphere, meaning that organic molecules on their surface are far from thermodynamic equilibrium.[84, 98] Such fluctuations have been discussed as a necessity in driving a wide variety of chemical reactions under plausible prebiotic conditions.[99] Aerosols are far more acidic than the bulk ocean; atmospheric CO_2 partitions to the liquid phase, forming carbonic acid. Likewise, sulfuric acid formed from atmospheric SO_2 rapidly partitions to aerosols. Consequently, prebiotic aerosols would likely have been acidic, even if the prebiotic ocean was basic. Aerosols also likely had a higher concentration of salt due to the selective evaporation of water in the atmosphere.

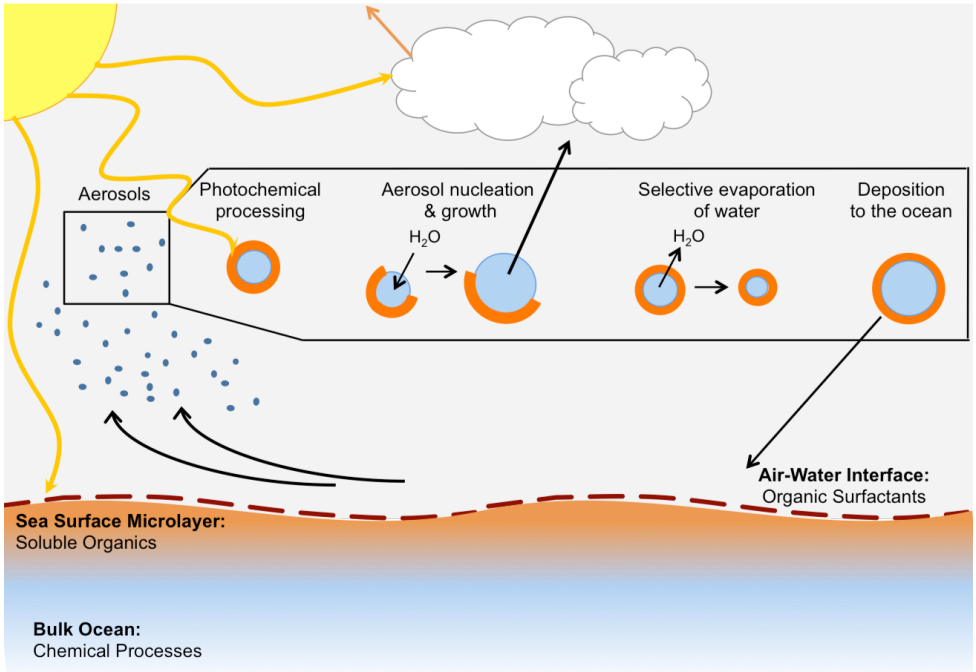

Figure 2.2. Schematic of the life cycle of aqueous atmospheric aerosols (orange areas represent surface-active organics, and light blue represents the aqueous core of the particle), highlighting the ocean-atmosphere interactions.

In addition to air-water interfaces, mineral surfaces are also a potentially favorable reaction environment. Rock and clay surfaces help with "selection, concentration, and organization"[100] of the disordered prebiotic soup and are known to promote key organic reactions.[100-103] Widespread terrestrial continents and even plate tectonics are thought not to have formed until after the Hadean (< 4.03 Gya),[67] but mineral surfaces would have played an important role on the ocean floor, near hydrothermal vents, and on volcanic islands. The mineral inventory of the early Earth would have been smaller than today, but was still diverse. Hazen has reviewed the minerals that were likely present during the Hadean.[104, 105] These are expected to have included chondritic minerals found on meteorites, igneous rocks, and minerals formed from aqueous and hydrothermal alteration.[104] Both mineral surfaces and aqueous transition metal ions derived from them would have been important prebiotic catalysts, including in photochemical reactions.

2.2.3 Expected Terrestrial Solar Spectrum:

The prebiotic Earth's surface would have been reached by far more high-energy light than present day (see Figure 2.1),[28, 106, 107] because of the absence of the UV screening from a stratospheric ozone layer. The modern ozone layer begins filtering light at around 360 nm and ensures that essentially no light below 290 nm reaches the surface of the Earth. While likely not as efficient as ozone, other species in the prebiotic atmosphere would have screened some of the UV light, particularly the very high-energy light in the far-UV (FUV, λ < 200 nm), which is known to break even strong covalent bonds and destroy molecules.[108] This is particularly interesting because the FUV is the region where the young Sun has preferential increase in photon flux compared to the spectrum today. The total flux of photons produced by the Sun in this region remains very low, but because these photons are so high in energy they remain an important source of energy to consider. However, FUV radiation is readily absorbed by many atmospheric species, including CO_2[109, 110] and H_2O.[111,

[112] Thus much of the FUV radiation would have been filtered by prebiotically-plausible atmospheric species.[28, 108, 113]

The near-UV radiation (NUV, 200 nm < λ < 400 nm) that is screened by ozone today was likely transmitted to the Earth's surface with minimal loss due to absorption. Some have suggested that the UV may have been mitigated to some extent by physical screening, such as scattering from organic hazes or fractal aerosols,[44, 114-116]but these species are unlikely to have been as effective as ozone and, in the case of the hazes, require a fairly high concentration of CH_4 in the atmosphere which may not be plausible prebiotically.[45] Using assumptions similar to the likely atmosphere of the early Earth presented here and ignoring the contribution of possible organic hazes, the Sasselov group has recently modeled the likely attenuation of the early solar spectrum by the gaseous species in the prebiotic atmosphere.[28, 113] They report that, while almost all of the FUV light below 200 nm is filtered, the UV light between 200 and 350 nm is only modestly screened, with the majority of attenuation occurring between 200 and 250 nm,[28, 113] as shown in Figure 2.1.

Beyond the screening provided by gases in the atmosphere, UV light can be filtered by condensed phases as well. Liquid water is the most obvious source of attenuation and determines the depth of water column in the ocean that may have been productive environments for photochemistry. The attenuation of UV light as a function of column depth depends heavily on the wavelength of the light. While FUV light with λ < 200 nm doesn't penetrate past 1 m of water, NUV light penetrates to a depth of at least 10 m.[28, 117] This suggests that the photochemically-active zone of the ocean, while shallow, is certainly not limited to its surface. Aqueous photochemistry in the bulk oceans may be advantageous because it could harness useful NUV while protected from the higher energy, more destructive FUV light.

Examining the likely environmental conditions on the early Earth and their effect on

the solar radiation from the young Sun, we agree with the predictions by Sasselov's group[28, 113] that FUV light of wavelengths less than 200 nm would have been screened by species at high altitudes in the atmosphere, potentially generating reactive radicals and intermediates. Broadband solar radiation from the UV to the infrared would still have been available, with significant fluxes in the photochemically useful NUV region. As stated above, the early Sun's lower luminosity but relatively larger output of UV radiation coupled with the lack of UV screening by the Earth's atmosphere ensured that the early Earth's surface was bathed in significantly more high-energy light relative to today. This in conjunction with the variety of auspicious environments (aqueous, interfacial, and gaseous) present on the early Earth would have allowed for a wide-variety of photochemical processes to occur.

2.3 Photophysics and Photochemistry:

We begin our discussion of photochemistry broadly, giving a general overview of the defining principles of photophysics and photochemistry. We also consider what molecules may be relevant to prebiotic photochemistry by examining the photo-properties of key classes of functional groups. We will see in the specific examples of prebiotically-relevant, sunlight-driven reactions given in Section 2.4 that several molecules undergo similar photochemical processes, but result in a variety of different products with differing functions. For example, both pyruvic acid and 2-oxooctanoic acid follow the same photochemical mechanism in aqueous solution, but the species produced from this chemistry are different, generating either high energy, potential metabolic species or more complex, double-tailed lipids, respectively. We have referred back to Section 2.3.1 within our later discussion of specific photochemical reactions where applicable to give grounding to these processes.

2.3.1 Principles of Photophysics and Photochemistry:

Photochemistry can occur when the absorption of radiation by a molecule has sufficient energy to induce chemical transformations. Here, we give a brief overview of some of the key concepts and terminology of molecular photochemistry and photophysics that will be used in the following sections. For a more detailed explanation of the principles governing photochemistry see the textbook "Modern Molecular Photochemistry of Organic Molecules" by Turro et al.[118]

Using the conceptual framework of quantum mechanics, the photophysical and photochemical properties of molecules can be described by electronic and nuclear motion on potential energy surfaces. A potential energy surface is a multidimensional representation of the potential energy of a polyatomic molecule as a function of nuclear configuration for a specific electronic state. It can be convenient to represent these complicated multidimensional surfaces as 2-dimensional potential energy curves, as shown in Figure 2.3. When a molecule absorbs a photon it is promoted from its ground state configuration to some higher energy excited state (e.g. S_0 and S_1 in Figure 2.3, respectively). The excitation energy can be dissipated radiatively or nonradiatively and, in some instances, can lead to reaction.

In polyatomic molecules with significant density of states, absorption to higher electronic surfaces (Path A in Figure 2.3) results in rapid radiationless decay to the lowest excited singlet manifold by internal conversion (Path B). Emission of radiation from the lowest excited singlet state via fluorescence (Path E) and, following intersystem crossing to the lowest triplet state (Path C), phosphorescence (Path D) can be observed. Both compete with other non-radiative processes, including reaction (Paths G, H, and I).

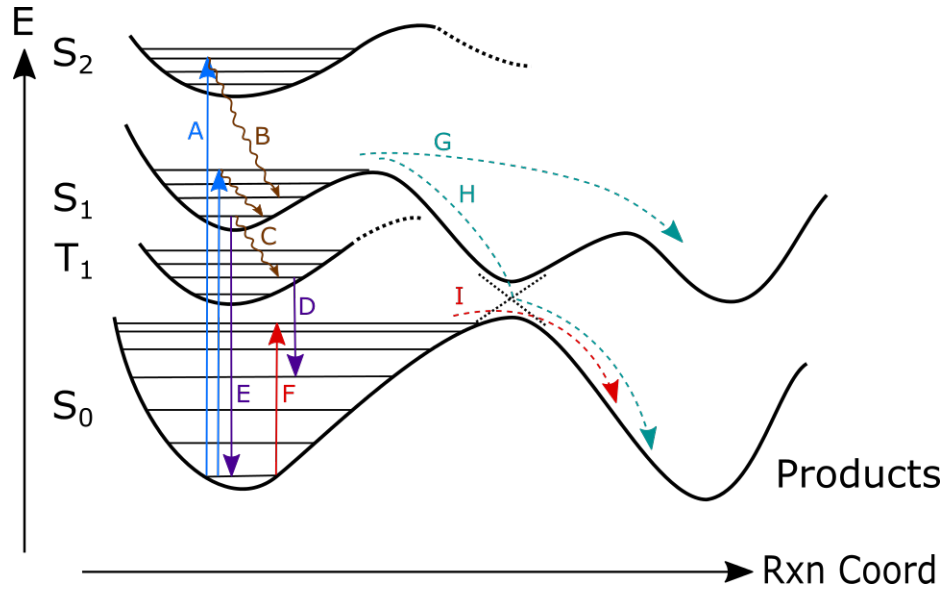

Figure 2.3. Schematic of the potential photophysical and photochemical pathways following excitation of a molecule. The singlet ground state (S_0) absorbs a photon and is excited to higher energy singlet states (S_1 and S_2) (A). The energy can dissipate via non-radiative pathways, such as internal conversion (B) to a lower singlet state or intersystem crossing (C) to the triplet state (T_1). The system can also return to the ground state by emitting a photon via phosphorescence (D) or fluorescence (E). Alternatively, the S_0 state can be excited to a specific high vibrational level (F) at or near the ground electronic state barrier for reaction. Chemistry follows absorption of a photon directly on the excited state (G), by crossing to another state through a conical intersection (H), or on the vibrationally-excited ground electronic state (I).

These photophysical and photochemical processes are competitive, and the probability of energy dissipation by a given path will vary by molecular system. If photochemistry and non-radiative decay are slow, significant fluorescence may be observed as a molecule returns to its electronic ground state. Photochemical reactions will be efficient when the rates of reaction are fast compared to alternative photophysical processes.

Every molecule has a unique set of quantized energy levels that determine its photophysical and photochemical properties. However, classes of molecules with similar chromophores (functional groups) will absorb radiation in similar regions of the electromagnetic spectrum and tend to have similar chemistry. For example, aldehydes and ketones are excited to reactive states by absorption of light in the NUV at 300 to 400 nm through a $n \rightarrow \pi^*$ partially forbidden transition. Molecules containing conjugated C-C or C-O

double bonds absorb light at lower and lower energies as the degree of conjugation between the double bonds increases. For example, ethylene absorbs at 200 nm, but the absorption spectrum shifts from the ultraviolet to the visible for butadiene, hexatriene, and octatetraene.[119-121] Such unsaturated compounds have short atmospheric lifetimes today due to oxidation by O_3 and OH, but could have been prevalent in the reducing or neutral atmosphere of early Earth.

In principle, photochemical reactions take place on the initial excited potential energy surface. However, electronic potential energy surfaces may interact at certain molecular geometries and energies, allowing coupling between electronic states and rapid energy transfer from one to another. Such an interaction affects the photochemical yield and product distributions. Following absorption of a photon and generation of a molecular excited electronic state, the system can evolve to a favorable nuclear geometry, where the wavefunctions of the two states are nearly degenerate in energy. This point, where the two potential energy surfaces intersect, is referred to as a conical intersection. The rate of crossing between two states can become very fast in the presence of such a conical intersection (Path H in Figure 2.3), due to the significant the non-adiabatic coupling between states. In favorable circumstances, motion through a conical intersection can occur with rates comparable to vibrational relaxation. Such crossing of two electronic surfaces rarely occurs in diatomic molecules but is often observed in polyatomic organic molecules, including in many of the examples discussed in Section 2.4 (e.g. pyruvic acid and nucleobases).

Systems with conical intersections or curve crossings can be difficult to study, though recent experimental and theoretical methods have been developed to treat some complex systems dynamically.[122, 123] The presence of non-reactive conical intersections that result in rapid non-radiative decay to the electronic ground state may make excited-state lifetimes

too short for slower photochemical processes to occur. The observed photostability of a molecule upon UV excitation is often due to such conical intersections. Photostability has been suggested as an important property of early organic and biological molecules needed for the evolution of life,[124-126] and is discussed more in Section 2.5 below.

Photochemistry can also be initiated by absorption of a lower energy visible or IR photon that promotes the molecule to a highly vibrationally-excited energy level on the molecule's electronic ground state, close to the reaction barrier. Formally, only fundamental vibrational transitions between adjacent vibrational levels are allowed, but, due to anharmonicity, overtone transitions to high vibrational levels do occur with sufficient intensity to drive reaction in polyatomic molecules containing O-H, C-H or N-H groups.[127-131] However, the intensity of each overtone transition decreases with each successive vibrational level. Following absorption by the chromophore, intramolecular energy redistribution (IVR) transfers the energy to other modes, including the reaction coordinate.[131] This process can be of some significance if the molecule possesses a weak bond (for example O-O in H_2O_2 or N-O in HNO_3), leading to reaction upon absorption of low-energy red light. Competition between IVR and reaction has been a topic of interest in this field.[132-135] We note that vibrational overtone chemistry happens on the ground electronic state potential without heating the molecule and is significantly different from the thermochemical processes driven at high temperature.

2.3.2 Environmental Effects on Photochemistry:

The environment surrounding a molecule will alter its photophysical and photochemical properties. In the gas phase, for instance, photolysis rates and mechanisms will be altered by collisional deactivation rates. In condensed phase, the presence of solvent differentially stabilizes the ground and excited states, producing spectral shifts in the chromophores of interest. Quantum yields for reactions of organic molecules in condensed phases depend on

the environment,[136-138] which can induce changes in the absorption cross sections, alter vibrational relaxation rates, and promote recombination within a solvent cage. In biology, the protein environment tunes the absorption spectra of light sensitive systems.[139-141] Similar effects can be induced by ice matrices, hydrogen bonding in condensed phases, and at mineral and organic surfaces. Spectroscopy can be used to observe shifts in absorption spectra, changes in absorption cross-sections, usually from enhancement of the intensity of forbidden transitions, and changes in line widths,[142-144] giving information about the effect of the solvent or matrix.

While the environmental effects on photochemical reactions have been studied widely for matrices, crystals, and organic solvents, with some exceptions, there is comparatively little information available concerning aqueous environments.[138] Recently, the photochemistry of organic and inorganic compounds in aqueous solutions that are important in today's environment has been reviewed,[138, 145-147] providing a useful guide for the contemporary atmosphere. The effects of aqueous conditions on photochemistry can be particularly impactful if the molecule undergoes structural changes in water. Water-soluble organic compounds in the gas-phase of the atmosphere will partition to aerosols and fog and cloud drops.[148, 149] Molecules with carbonyl functional groups are among the most photoreactive compounds in the contemporary atmosphere. However, most aldehydes and, to some extent, ketones hydrate to photochemically-inactive geminal-diol forms in aqueous environments,[150-154] removing the chromophore functionality. Theoretical approaches have found that, in the contemporary atmosphere, aqueous quantum yields for photolysis of carbonyls seldom compete with the rate of oxidation by hydroxyl (OH) radicals (further discussion below in Section 2.3.4) dissolved in these aqueous media.[155] However, the extent of hydration and, therefore, the change in photochemical quantum yields in aqueous solutions are molecule dependent and cannot be derived from structurally similar

compounds.[155] Photochemistry of carbonyl-containing compounds is expected to have been a more significant process on early Earth than it is today given that far less OH radical would have been available in prebiotic environments, underscoring the importance of examining the environment for molecules of interest.

In addition to environmental effects from bulk phases, changes due to interfaces must also be considered.[78, 146] We have mentioned how both mineral dust surfaces[100, 105, 156] and air-water interfaces[77, 87, 88, 95] can align and concentrate molecules. It has been suggested that photochemical reactions possible in condensed phases and at surfaces might be enhanced in aerosols, fogs and clouds in the atmosphere.[84, 92, 157] Gas phase photochemistry may also be promoted if a surface is encountered.[158] The advantages and special role of atmospheric aerosols in the origin of life have been examined;[84, 89, 95-98, 159-161] here, we point out that only a sparse literature exists on the photochemistry of interfacial films[162, 163] on aqueous or mineral dust substrates.[164-166] For example, stearic acid upon irradiation at 230-250 nm, reacts via C-C bond scission, breaking apart into smaller components.[163] This chemistry has implications for fatty acids with shorter alkyl chains that are expected to have been prebiotically available. The surface activity of organic molecules in aqueous solution has been implicated as a factor in the photochemical synthesis of larger, more complicated molecules.[167]

2.3.3 Indirect Excitation via Photosensitization:

Absorption of solar radiation can lead to energy transfer from the excited molecule (donor) to another molecule (acceptor), which does not absorb available radiation efficiently. The acceptor molecule is excited by energy transfer (i.e. is photosensitized) and can react in interesting ways. The donor molecule (i.e. the photosensitizer) itself does not participate in the reaction of interest.

In modern environmental chemistry, the most commonly used photosensitizers are large

organic molecules, such as chlorophyll or humic acid. These photosensitizers have been used to generate unsaturated and branched-chain oxygenated volatile products as well as carboxylic acids from non-photoactive species.[168-171] Photosensitizers like humic acid are not considered prebiotically-relevant species; however, there are prebiotic analogs to such productive photosensitization. Both organic molecules, such as porphyrins[117, 172, 173] and polycyclic aromatic hydrocarbons (PAHs),[174, 175] and inorganic systems, including minerals[176-178] and transition metal ions,[179, 180] have been proposed as prebiotically-plausible photosensitizers.

PAHs, for example, absorb light in the near-UV to blue region and have been shown to harness solar energy.[181, 182] This solar energy may then be transferred into the system, either by generating an electron gradient or by donating an electron directly to an acceptor molecule. PAHs and their derivatives have been shown to be good charge transfer mediators,[183, 184] and are likely to assist in photoredox reactions. PAHs included in lipid bilayers have been able to generate gradients across a membrane, by transferring an electron to an acceptor molecule encapsulated within the enclosure.[174, 185, 186] Porphyrins have also shown this ability to drive gradients across membranes[187, 188] and have long been proposed as potential precursors to photosynthetic pigments.[172]

Photocatalysis also readily occurs in the natural environment on mineral dust surfaces.[164-166, 189, 190] Metal oxides and sulfides, which may absorb radiation to generate electron-hole pairs and subsequently electron transfer resulting in redox chemistry, are also of prebiotic interest. Transition metal complexes, such as ferrocyanide, have been used to generate pH gradients that drive this photoredox chemistry.[191] Photocatalysis performed on semiconductor particles or surfaces can also lead to a wide variety of chemistries, and has been studied in depth for applications outside of prebiotic chemistry, but the same principles apply.[192]

Consideration of photosensitization also highlights the importance of heterogeneous photochemistry that occurs at interfaces. In the case of sensitization by minerals, the molecules being sensitized must be in contact with the mineral surface, resulting in an inherent coupling of interfacial effects with the sensitizing effects. For molecular photosensitizers, interfacial effects can still play an important role, due to the ability of interfaces to concentrate and align the sensitizers with the reactants.

2.3.4 Unimolecular and Bimolecular Photochemical Reactions:

The energy of a UV photon is comparable to the energy of a covalent bond; therefore, UV light is useful in photochemistry as it has the ability to break such bonds. The initial step in most photochemical reactions leads to the unimolecular decomposition of the precursor molecule, forming extremely reactive species, such as radicals (neutral species with one unpaired valence electron) and carbenes (neutral organic species with two unshared valence electrons on a carbon). These reactive species can then initiate bimolecular chemistry, including the synthesis of larger molecules.

Indeed, the production of hydroxyl radical, OH, is considered to be perhaps the most important photochemical process in modern atmospheric chemistry[193] because of the subsequent reactions in which it participates. OH is at the center of the reaction networks that govern nitrogen, sulfur, halogens, and organics cycling in the atmosphere. In the modern atmosphere, OH is produced primarily by the photodissociation of O_3 at high altitude into O_2 and an excited atomic $O(^1D)$, which goes on to react with a water molecule making two hydroxyl radicals.[85] OH radicals can also be produced directly by photolysis of a peroxide species[85] or of water.[111] While the direct photolysis of water is a minor source today, this would have been the primary source of any OH present in the prebiotic atmosphere due to the lack of O_2 and O_3.

The concentration of OH would likely have been very small because the photolysis of

H_2O requires UV light with wavelength < 180 nm[112] but also because of the reactivity of OH. The lifetime of a given OH radical in the modern atmosphere is less than a second,[194] and the steady state mixing ratio today is < 1 ppt.[195, 196] The reactivity of OH is such that it is likely quenched rapidly upon its interaction with another species. At the high altitudes where direct photolysis of water might occur, this depletion would most likely occur by collisions with CO_2, or even, potentially, from reaction with the products of the photolysis of CO_2 (e.g. CO).[197, 198] However, some OH may have been transported from the high altitudes, where it is formed, to lower altitudes that would have had relatively higher concentrations of organic species. Even today, the concentration of OH in the lower troposphere comes primarily from the transport of OH generated in the upper troposphere.[193] Whatever OH there was would have acted primarily to abstract hydrogen from any trace organic species, such as methane, generating organic radicals. Through such hydrogen abstraction, OH has been shown to act as a radical initiator in the generation of complex polymer chains.[199-201]

However, because of the lack of its major production pathway under prebiotic conditions, OH is likely not the most important photochemically-generated radical species to consider. Rather, in prebiotic chemistry, the more important reactive species would have been organic radicals generated from the photolysis of prebiotically-available organic molecules in gas phase, condensed phase, or at interfaces. It is plausible that these organic radicals may have served a similar role in the prebiotic atmosphere that OH serves today. Pyruvic acid is capable of polymerizing non-photoactive species by abstracting hydrogen in the same manner as OH, and there is evidence that this polymerization is favored in the absence of oxygen.[200]

High-energy UV light has historically been discussed in prebiotic chemistry primarily as a destructive force and a hazard in chemical evolution, simply breaking apart useful molecules.[106, 107, 126, 202, 203] There have been many studies exploring the damage caused by

high-energy radiation. Mononucleotides, for example, are known to fragment upon photochemical excitation, cleaving either at the phosphodiester bond or the glycosidic bond.[204] One of the benefits considered by those who propose that life originated at deep hydrothermal vents in the ocean is that the environment would be protected from UV light.[100, 205] We illustrate here that even if photolysis leads to the generation of smaller species, these species are often highly reactive. Therefore, photochemical reactions are capable of generating complex molecules via subsequent radical chemistry, especially in environments where excess energy is effectively dissipated.

2.4 Sunlight-Initiated Reactions under Prebiotic Constraints:

In the following, we highlight a few examples of the role that photochemistry can play in the abiotic synthesis of the molecules and molecular precursors necessary for life. We show that high-energy solar radiation can be harnessed and used to generate larger, more complex molecules. For the sake of clarity and applicability, we choose to focus on cases of prebiotic photochemical steps in syntheses that lead to the production of cellular components, i.e. sugars, metabolites, lipids, amino acids, and nucleic acids.

2.4.1 Photochemistry of High Energy Species:

The generation of organic molecules that store chemical energy in their bonds, which may be used later for necessary chemical reactions, is the hallmark of metabolism. Today sugars are the primary fuels for metabolism, acting as reservoirs of both the energy and carbon needed for later biological reactions.

Prebiotically, the formose reaction was a possible source of sugar formation.[206] The formose reaction generates a large mixture of sugar species through a series of aldolic reactions of formaldehyde and glyceraldehyde.[206, 207] Aldehydes can be readily synthesized photochemically by UV light.[208-210] Prebiotically-relevant syntheses of formaldehyde and glyceraldehyde have been demonstrated using gas-phase photochemistry of CO_2 and H_2O.[211]

Transition metal ion complexes have been used as photosensitizers in the photooxidation of alcohols, yielding formaldehyde and glyceraldehyde,[212] although the prebiotic-plausibility of the conditions used has been questioned.[213] Glycoaldehyde and glyceraldehyde have been generated from hydrogen cyanide, HCN, in the presence of a tricyanocuprate complex, $[Cu(CN)_3]^{2-}$,[180] which transfers energy to the system either by photooxidation[180] or photoionization.[214]

Aldehydes are themselves photoactive species, and photochemical mechanisms for the formose reaction have been suggested,[215, 216] in addition to the normal thermal approach. These photochemical reactions are unlikely to occur in high yield in aqueous environments because of the dominance of the hydration of aldehydes and ketones to geminal diols, which are not good chromophores in the NUV where radiation is available. However, photosensitization from minerals or organic pigments may allow for the photochemical formation of simple sugars from the aqueous mixture of aldehydes and geminal diols.[212, 217]

It has also been suggested[218] that in the first forms of a pre-enzymatic primitive metabolism, "driver reactions" were coupled directly to an energy source. Shapiro[218] proposed pyruvic acid (and its deprotonated form, pyruvate) as a potential candidate. Pyruvic acid exemplifies the chemistry these types of driver molecules are capable of, while also being at the core of metabolism in almost all known aerobic and anaerobic organisms. It has even been proposed that coupling to a zinc sulfide photosensitizer allows pyruvic acid to drive the reductive citric acid cycle via photoelectrochemistry.[178] Pyruvic acid is itself photoactive and even on the contemporary Earth, direct photolysis is its primary atmospheric sink.[219-223] Therefore, we will review its photochemistry in some detail as outlined in Figure 2.4 to further illustrate the idea that sunlight can be used to provide energy stored in chemical bonds and drive reactions necessary for life.

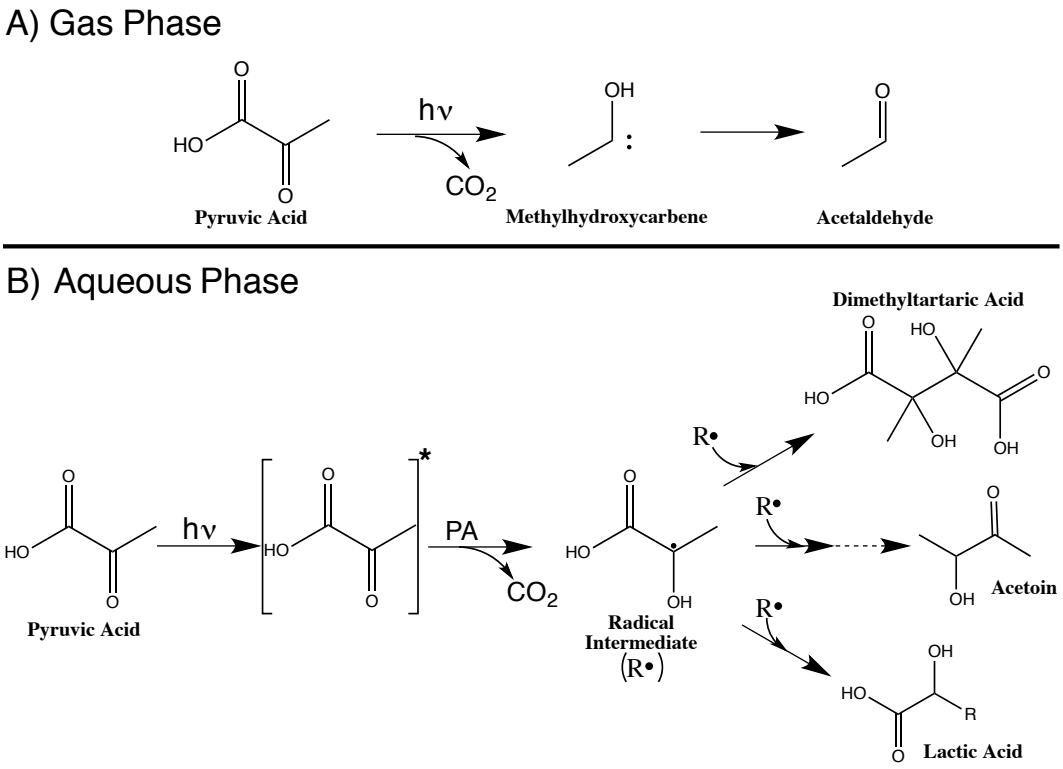

Figure 2.4. Simplified reaction scheme of the photochemistry of pyruvic acid A) in the gas phase[224, 225] and B) in the aqueous phase.[219, 220]

Pyruvic acid is a prebiotically-plausible, three-carbon α-keto acid that absorbs light in the NUV. It can be synthesized abiotically directly from CO_2 and H_2O at high temperatures and pressures,[178, 226, 227] conditions such as those found at hydrothermal vents, as well as synthesized exogenously and delivered to Earth on meteorites.[228, 229] In the gas phase,[224, 225, 230, 231] pyruvic acid is excited electronically by absorption of a near UV photon (λ_{max} ~350 nm, spectrum shown in Figure 2.5) to the first singlet (n-π*) state. The products, methylhydroxycarbene and CO_2, are formed primarily on the ground electronic state after passage through a conical intersection between the S_1 and S_0 states, similar to pathway H in Figure 2.3.[232, 233] Methylhydroxycarbene, a very reactive species, can rearrange to form acetaldehyde.[224, 225] Acetaldehyde, itself, absorbs NUV radiation and can generate further radical species photochemically.

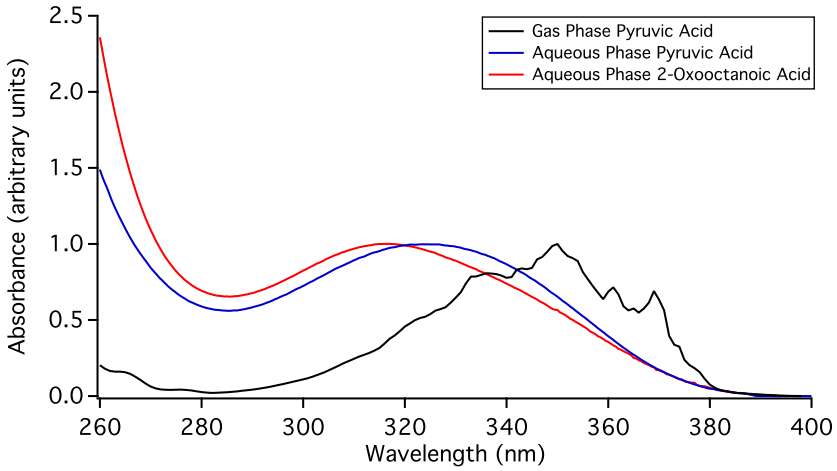

Figure 2.5. Normalized absorbance spectra of the transition to the singlet n-π state of pyruvic acid in the gas phase (black, data from Horowitz et al. 2001[234]) and aqueous phase (blue) and 2-oxooctanoic acid in the aqueous phase (red).*

Photochemistry of pyruvic acid in the gas phase can also be driven by lower-energy, visible, red photons via excitation of vibrational overtone transitions, as in pathway I in Figure 2.3.[235] While the same products are expected, the methylhydroxycarbene would be formed with little to no internal energy, unlike in the case of UV excitation of pyruvic acid. This carbene would not have enough internal energy to rearrange to acetaldehyde and, therefore, would remain ready for further bimolecular reactions,[235] leading to more complex species. The chemical fate of the "cold" methylhydroxycarbene, however, has not been investigated to date.

The electronic states of pyruvic acid are significantly influenced by environmental conditions. In the aqueous phase, an alternate photochemical pathway becomes accessible, leading to a new mechanism and different products.[219-223] The aqueous pyruvic acid photochemistry begins by absorption of a near UV photon (λ_{max} ~320 nm, spectrum shown in Figure 2.5) and excitation to the S_1 state; however, due to solvent effects, it is possible and efficient to proceed by intersystem crossing and internal conversion to the n-π* triplet (T_1) state. This excited species undergoes concerted decarboxylation while also abstracting the acidic hydrogen from a neighboring pyruvic acid molecule, forming reactive radical

intermediates that initiate further chemistry.[200, 220, 236] This chemistry generates a variety of interesting species, including small oligomers (e.g. dimethyltartaric acid) and molecules with metabolic importance today, such as lactic acid and acetoin.[219-223] Lactic acid plays a wide variety of roles in biology and metabolism; it has even been proposed to be preferentially preferred as an energy source to glucose in some cases.[237, 238] Lactic acid has also been used to help with prebiotic polymerization of amino acids, generating depsipeptides.[5] Acetoin can function as a pH regulator and is used in energy storage as a substitute for glucose in modern bacterial cells.[239, 240]

The aqueous phase photochemistry of pyruvic acid is also dependent on environmental conditions, such as pH and atmospheric composition, changing both the relative yield and favored reaction pathways. The aqueous photochemistry described above is favored at acidic pH; photochemical reaction under high pH conditions results in a nearly 20-fold decrease in yield.[221] Further, the dissolved gases in the aqueous solution shift the observed product ratios: when oxygen is removed from the solution, which better mimics the likely prebiotic conditions, the production of oligomers is greatly increased.[220] Pyruvic acid photochemistry in the gas and condensed phases illustrates that molecular complexity can be generated by harnessing energy from the Sun under prebiotically-relevant conditions.

2.4.2 Photochemistry of Lipids and Membrane Components:

The aqueous photochemistry of pyruvic acid can be extended to other α-keto acids (or oxoacids). For example, 2-oxooctanoic acid (2-OOA) is an 8-carbon α-keto acid with a 6-carbon alkyl tail. Oxoacids and other molecules of similar chemical functionality have been found in meteoritic samples,[228, 241] and the short, 8-carbon chain of 2-OOA is among the most prevalent length synthesized in the common Fischer-Tropsch type synthesis of lipids (molecules with 7-9 carbons are most common).[242, 243] Upon irradiation using a solar

simulator, 2-OOA follows the same photochemical mechanism as pyruvic acid in aqueous solution (spectrum shown in Figure 2.5), reacting to form dihexyltartaric acid (DHTA).[167] Because of its alkyl chain 2-OOA partitions preferentially to surfaces, which may promote photochemistry because the enhancement of the local concentration at the interface makes it more likely that the photochemically generated radicals would encounter each other to form DHTA. The formation of DHTA is interesting, not simply because it is an example of using photochemistry to make a carbon-carbon bond, but because the molecule formed is a double-tailed surfactant, as shown in Figure 2.6.

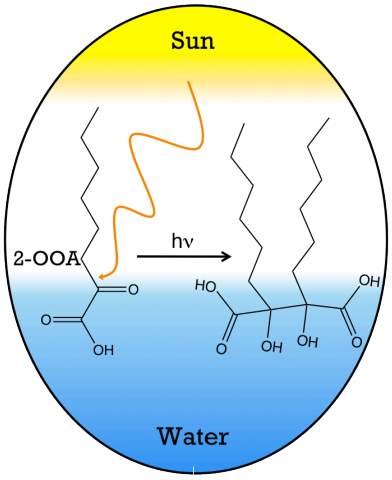

Figure 2.6. Photochemical synthesis of double-tailed dihexyltartaric acid (DHTA) from 2-oxooctanoic acid (2-OOA) in aqueous solution.

Surfactants, or amphiphiles with hydrophilic "head" and hydrophobic "tail" groups, are the key components of organic films, membranes, and enclosures, which are recognized to be of vital importance for cellular life.[244-246] The library of known molecules that self-assemble into vesicles is relatively small. The modern cell membrane is composed of phospholipids (surfactants with two hydrophobic tails and a polar phosphate head group), which assemble into a bilayer in aqueous environments. Models of primitive cellular constructs, on the other hand, tend to use simple vesicles composed of single-tailed, fatty acids.[247-249] Such fatty acids were prebiotically-available,[249-251] having been found in

meteorites[228, 241] as well as synthesized endogenously, including from the photooxidation of alkanes by photosensitization from PAHs.[175, 252] However, generating vesicles and protocells spontaneously from these simple lipids requires high concentrations, and the enclosures formed are stable only over a relatively narrow range of conditions,[253-255] although their robustness can be increased when other species are incorporated into the membrane.[185, 256-258] Vesicles formed from double-tailed surfactants, such as phospholipids, have increased stability, are insensitive to salts, and self-assemble spontaneously at lower concentrations, but they have not generally been considered prebiotically-relevant because there has been lack of satisfactory abiotic syntheses.[253]

The photochemical synthesis of DHTA from 2-OOA opens up another potential class of lipid molecules for these studies.[167] By generating a relatively short, double-tailed lipid, we are able to explore some of the chemical space between the complex phospholipids and the simple fatty acids, using a prebiotically-plausible synthesis that only requires sunlight and water. As the photochemistry proceeds, and with no further perturbation of the reaction system, the products spontaneously self-assemble into stable, uniform aggregates that are tentatively classified as vesicles.[167] This indicates that aqueous organic photochemistry can be used to form more complex membrane components from simple precursors.

2.4.3 Photochemistry of Biopolymer Precursors:

Long-stranded biopolymers are at the center of life, performing the critical functions of information storage and enzyme catalysis. Both proteins and nucleic acids strands are formed by a series of condensation reactions that connect monomers together by forming either amide bonds in the case of peptides or glycosidic and phosphodiester bonds in the case of oligonucleotides. Many of the prebiotically-relevant syntheses of the amino acids, nucleobases, nucleosides, and nucleotides that make up these biopolymers include

photochemical steps.

Abiotic syntheses of amino acids from simple gaseous species in the presence of water have been conducted for a wide variety of atmospheric compositions since the initial Urey-Miller experiments.[259-261] These experiments most commonly use electrical discharges as their energy source. However, UV irradiation of the gaseous mixtures (e.g. CH_4, C_2H_6, NH_3, H_2O H_2S) results in the photochemical production of amino acids, although with relatively low yields.[262-264] Formation of amino acids via aqueous phase photochemistry has also been observed.[179, 265-267] Examples of this include UV irradiation of organic precursors in the presence of nitrate salts,[266] but these environmental conditions are likely not prebiotically plausible. Amino acids have also been synthesized photochemically on interstellar ice analogues,[268-272] suggesting the importance of heterogeneous photochemistry; although, the UV radiation used in these ice studies is commonly Lyman-α[269] or a combination of Lyman-α and a narrow band of FUV light centered at 160 nm, which are less relevant to the surface of early Earth.[270-272]

The natural bases that compose RNA and DNA today, adenine, guanine, thymine, cytosine, and uracil, are composed of either purine or pyrimidine rings. Consideration of the abiotic synthesis of these nucleic acid components generally begins with hydrogen cyanide, HCN. HCN, is an important source of reactive carbon and nitrogen that is used in the synthesis of not only to nucleobases, but also to metabolic species (as discussed in Section 2.4.1 above).[273] HCN is found in the interstellar medium and on comets[274-278] and is assumed to have been widely available on the early Earth.[47, 278] A photochemical source of HCN at very short wavelengths has also been proposed.[279]

The prebiotically-available HCN can then be oligomerized to form a tetramer, *cis*-2,3-diaminomaleonitrile (*cis*-DAMN). *Cis*-DAMN is photolyzed to form the reactive intermediate, 5-aminoimidazole-4-carbonitrile (AICN). AICN subsequently forms purine

nucleobases.[280-283] The photochemical step to form AICN is widely acknowledged to be critical to this process,[280-283] but its mechanism is still not well-known.[283] It has also been shown that purine and pyrimidine bases can be formed from formamide either by photosensitization with TiO_2,[176, 177] or by direct excitation using NUV (200-254 nm) light at 130 °C.[284] The energetics of the photochemical radical pathways associated with this chemistry have been calculated and appear to be more favorable at lower, more relevant temperatures.[285] The formamide pathways to purines and pyrimidines may not be totally separate from HCN pathways, however. Direct excitation of formamide with UV light has been shown to generate formidic acid and further decomposition into HCN and water.[286]

It has also been shown that pyrimidine bases can be synthesized using an HCN-independent pathway. In this case, an acetylene atmosphere above a mixture of water, ice, and urea is irradiated (λ ~185-254 nm), generating cytosine and uracil.[287] Uracil and thymine can also be produced by the photodehydration of 5,6-dihydrouracil, a pyrimidine derivative that is synthesized from the conventional pyrimidine synthesis route of drying β-alanine and urea.[288]

Nucleobases are incorporated into nucleic acids as nucleotides, which have sugar and phosphate groups in addition to the base. Historically, formation of nucleotides has been attempted by sequential addition of the sugar and phosphate to a nucleobase. It is possible to make nucleosides (base and sugar) in this manner, but these syntheses tend to be complicated. Formation of pyrimidine nucleosides is more difficult than for purines, but they have been generated in multi-step schemes, which include a photochemical rearrangement step.[289] A more promising approach is the abiotic synthesis of pyrimidine ribonucleotides, which avoids connecting free nucleobases and sugars via condensation reactions, and, instead, generates nucleotides through amino-oxazoline and anhydronucleoside intermediates, which circumvents the condensation reactions required

to attach the sugar and base.[290] In this synthesis, UV light is used in the abiotic synthesis of a uracil ribonucleotide derivative, driving the conversion of the cytosine-based activated ribonucleotide to the uracil form via photohydration.[290]

2.5 Photostability as an Evolutionary Driving Force:

Modern life requires only a remarkably small library of molecules to function, relying on only 20-odd amino acids and 5 nucleobases. This sparseness would not be predicted based on the constraints of prebiotic chemistry alone. More than 80 amino acids and at least 7 nucleobases have been unambiguously identified in meteorites,[291] suggesting that there are readily available abiotic pathways to synthesize many molecules that are similar to those used in life today and that evolutionary selection has led to the modern biological library.

The photostability of prebiotic molecules against UV radiation may have provided an evolutionary pressure, helping to determine which molecules were ultimately selected for life.[124-126] This has been particularly well studied for the case of nucleobases and small nucleic acid polymers.[292-294] During prebiotic chemical evolution, it is very likely that there were many more purine and pyrimidine-based molecules that could have functioned as nucleobases than the 5 bases used today. While there would have been other, very important selective pressures related to structure and function, it is also possible to consider the effect of external pressures, including UV radiation. It is remarkable how the five canonical bases are quite photostable despite absorbing UV light ($\lambda \sim 250$-290 nm). The excess energy is rapidly dissipated to the surroundings,[126, 293-295] circumventing reaction. This property of the individual nucleobases has been shown to hold when they are connected into an oligonucleotide strand, indicating that questions of photostability may have broader impacts on the viability of replication as well.[293]

The canonical nucleobases have very low fluorescence quantum yields, indicating very competitive non-radiative processes and implying subpicosecond excited-state lifetimes.[294]

This ultrafast relaxation back to the ground state minimizes the opportunity the nucleobase has for reaction.[296] The deactivation is linked to efficient conical intersections between the first excited singlet state and the ground state,[294] but this is far from a complete description. The detailed photophysics governing this energy dissipation has been the subject of many investigations, which have been reviewed by Serrano-Andres, et al.[293] and Crespo-Hernandez et al.[296]

The conical intersection between the S_1 and S_0 state, for instance, is not sufficient to explain the differences in photostability between the canonical nucleobases, their structural isomers, and close derivatives.[293] Small changes to the structure of the molecule appear to have considerable effect on the accessibility of the conical intersection.[293, 294] The tautomers and close derivatives of the natural nucleobases, which may have been incorporated in prebiotic biopolymers,[297, 298] tend to have much longer excited-state lifetimes, which means they have more opportunity to undergo photochemical reaction.[293, 296] This may indicate that the non-canonical nucleobases would have photochemically reacted, and therefore mutated more often, preventing them from participating in replication, and ultimately leading to their non-selection for the genetic codes.[293] Non-canonical nucleobases that have photostability comparable to the canonical bases may be better candidates for a pre-RNA biopolymer.[299] The difference in relative photostability has been exploited to destroy the competing pyrimidine nucleotides generated during the synthesis of a uracil ribonucleotide derivative.[290] Interestingly, an exception to this increase in excited-state lifetime of the mutated nucleobases occurs for the methylated derivatives: they have comparable photostability to the natural bases.[293, 296, 300] These methylated nucleobases would have a similar response to a photostability selection pressure and would not be removed from the genetic code based on this criterion. This is particularly intriguing given that the most common modified nucleobases found in DNA today are methylated nucleobases.[293, 301, 302]

Photostability, then, may have been one of the forces that resulted in the selection of the biomolecules of life used in life today. Synthesis of larger organic molecules via photochemistry requires harnessing energy from the Sun, but it is also necessary for the molecules formed to be reasonably stable in order for that energy to be useful in furthering chemical evolution. In at least some cases, the initial photoactive precursor molecules, such as pyruvic acid or 2-OOA, generate products that do not have the same chromophores and, therefore, are less photoactive and are more stable with respect to photolysis.[77, 167, 220] Environmental conditions are also likely to be of importance in considering photostability.

2.6 Conclusions:

In this chapter, we have shown that photochemistry and photostability likely played an important role in the period of prebiotic chemical evolution prior to the origin of life. Abiotically synthesized simple organic molecules can harness energy from the Earth's single largest source, solar radiation, and convert it into high-energy chemical bonds. The Sun provides broadband radiation to the Earth, ranging from the far UV to the infrared. While FUV light would have been screened by atmospheric species, considerably more of the photochemically-useful near UV reached the early Earth's surface. In spite of its advantages compared with thermal and discharge energy sources, solar radiation has not been as extensively considered in origin of life scenarios. Because photochemistry relies on absorption of a photon by a molecule, it is very dependent on the energy, wavelength, and photon flux of radiation. Laboratory studies often use monochromatic or narrow-band light sources, providing only a few wavelengths of light that may not overlap optimally with the absorbance of the molecule of interest, which may change chemical outcomes and yields. Using broadband radiation to simulate the spectral output of the Sun in laboratory studies, such as Xe arc lamps, would likely provide more prebiotically-relevant photochemical results.

As an inherently non-equilibrium process, photochemistry differs from conventional thermal chemistry because it allows for the direct generation of high-energy species under low temperature conditions. One consequence of the ability to synthesize molecules under relatively gentle conditions is that the environment in which synthesis occurs could be more conducive for the subsequent self-assembly necessary for life (e.g. vesicle formation or protein folding) than high temperature or high pressure settings. Different photochemical pathways are favored under different environmental conditions, which allows for a wide array of reactions and products, especially considering the variety of auspicious gaseous, aqueous, and interfacial environments present on the early Earth. Atmospheric aerosols may have been important in connecting these disparate environments and providing transport of material between them.

In any environment, direct photolysis of molecules can create reactive species, an important subset of which is organic radicals. These radicals can then initiate chemistry that generates larger, high-energy molecules. Photochemistry, especially in the aqueous phase, provides a viable means of increasing molecular complexity under prebiotically-relevant conditions. With the radiation conditions available from the solar spectrum on early Earth, it is likely that photochemistry played a role in the evolution of prebiotic molecules necessary for the evolution of life.

2.7 Bibliography:

1. Rapf, R. J.; Vaida, V. Sunlight as an energetic driver in the synthesis of molecules necessary for life. *Phys. Chem. Chem. Phys.* **2016,** *18*, 20067-20084.

2. Crabtree, G. W.; Lewis, N. S. Solar energy conversion. *Physics Today* **2007,** *60*, 37-42.

3. Deamer, D.; Weber, A. L. Bioenergetics and life's origins. *Cold Spring Harbor Persp. Biol.* **2010,** *2*, 1-16.

4. Miller, S. L.; Urey, H. C. Organic compound synthesis on the primitive early Earth. *Science* **1959,** *130*, 245-251.

5. Forsythe, J. G.; Yu, S.-S.; Mamajanov, I.; Grover, M. A.; Krishnamurthy, R.; Fernandez, F. M.; Hud, N. V. Ester-mediated amide bond formation driven by wet-dry cycles: A possible path to polypeptides on the prebiotic Earth. *Angew. Chem. Int. Ed.* **2015,** *54*, 9871-9875.

6. Mamajanov, I.; MacDonald, P. J.; Ying, J.; Duncanson, D. M.; Dowdy, G. R.; Walker, C. A.; Engelhart, A. E.; Fernández, F. M.; Grover, M. A.; Hud, N. V. Ester formation and hydrolysis during wet–dry cycles: Generation of far-from-equilibrium polymers in a model prebiotic reaction. *Macromolecules* **2014,** *47*, 1334-1343.

7. Mojzsis, S. J.; Harrison, T. M.; Pidgeon, R. T. Oxygen-isotope evidence from ancient zircons for liquid water at the Earth's surface 4,300 myr ago. *Nature* **2001,** *409*, 178-181.

8. Peck, W. H.; Valley, J. W.; Wilde, S. A.; Graham, C. M. Oxygen isotope ratios and rare earth elements in 3.3 to 4.4 Ga zircons: Ion microprobe evidence for high delta O-18 continental crust and oceans in the early Archean. *Geochim. Cosmochim. Acta* **2001,** *65*, 4215-4229.

9. Wilde, S. A.; Valley, J. W.; Peck, W. H.; Graham, C. M. Evidence from detrital zircons for the existence of continental crust and oceans on the Earth 4.4 Gyr ago. *Nature* **2001,** *409*, 175-178.

10. Maher, K. A.; Stevenson, D. J. Impact frustration of the origin of life. *Nature* **1988,** *331*, 612-614.

11. Sleep, N. H.; Zahnle, K. J.; Kasting, J. F.; Morowitz, H. J. Annihilation of ecosystems by large asteroid impacts on the early Earth. *Nature* **1989,** *342*, 139-142.

12. Abramov, O.; Kring, D. A.; Mojzsis, S. J. The impact environment of the Hadean Earth. *Chem. Erde Geochem.* **2013,** *73*, 227-248.

13. Abramov, O.; Mojzsis, S. J. Microbial habitability of the Hadean Earth during the late heavy bombardment. *Nature* **2009,** *459*, 419-422.

14. Chapman, C. R.; Cohen, B. A.; Grinspoon, D. H. What are the real constraints on the existence and magnitude of the late heavy bombardment? *Icarus* **2007,** *189*, 233-245.

15. Javaux, E. J.; Marshall, C. P.; Bekker, A. Organic-walled microfossils in 3.2-billion-year-old shallow-marine siliciclastic deposits. *Nature* **2010,** *463*, 934-938.

16. Noffke, N.; Eriksson, K. A.; Hazen, R. M.; Simpson, E. L. A new window into early Archean life: Microbial mats in Earth's oldest siliciclastic tidal deposits (3.2 Ga moodies group, south africa). *Geology* **2006,** *34*, 253-256.

17. Hofmann, H. J.; Grey, K.; Hickman, A. H.; Thorpe, R. I. Origin of 3.45 Ga coniform stromatolites in Warrawoona group, Western Australia. *Geol. Soc. Am. Bull.* **1999,** *111*, 1256-1262.

18. Buick, R.; Dunlop, J. S. R.; Groves, D. I. Stromatolite recognition in ancient rocks - an appraisal of irregularly laminated structures in an early archean chert-barite unit from north-pole, western-australia. *Alcheringa* **1981,** *5*, 161-181.

19. Buick, R.; Groves, D. I.; Dunlop, J. S. R. Abiological origin of described stromatolites older than 3.2 ga - comment *Geology* **1995,** *23*, 191.

20. Noffke, N.; Christian, D.; Wacey, D.; Hazen, R. M. Microbially induced sedimentary structures recording an ancient ecosystem in the ca. 3.48 billion-year-old Dresser formation, Pilbara, Western Australia. *Astrobio.* **2013,** *13*, 1103-1124.

21. Ohtomo, Y.; Kakegawa, T.; Ishida, A.; Nagase, T.; Rosing, M. T. Evidence for biogenic graphite in early Archaean Isua metasedimentary rocks. *Nat. Geosci.* **2014,** *7*, 25-28.

22. Schidlowski, M. A 3,800-million-year isotopic record of life from carbon in sedimentary rocks. *Nature* **1988,** *333*, 313-318.

23. Mojzsis, S. J.; Arrhenius, G.; McKeegan, K. D.; Harrison, T. M.; Nutman, A. P.; Friend, C. R. L. Evidence for life on Earth before 3,800 million years ago. *Nature* **1996,** *384*, 55-59.

24. Rosing, M. T. C-13-depleted carbon microparticles in > 3700-Ma sea-floor sedimentary rocks from west Greenland. *Science* **1999,** *283*, 674-676.

25. Rosing, M. T.; Frei, R. U-rich Archaean sea-floor sediments from Greenland: Indications of >3700 Ma oxygenic photosynthesis. *Earth. Planet. Sci. Lett.* **2004,** *217*, 237-244.

26. Joyce, G. F. The antiquity of RNA-based evolution. *Nature* **2002,** *418*, 214-221.

27. Sutherland, J. D.; Whitfield, J. N. Prebiotic chemistry: A bioorganic perspective. *Tetrahedron* **1997,** *53*, 11493-11527.

28. Ranjan, S.; Sasselov, D. D. Influence of the UV environment on the synthesis of prebiotic molecules. *Astrobio.* **2016,** *16*, 68-88.

29. Daniel, I.; Oger, P.; Winter, R. Origins of life and biochemistry under high-pressure conditions. *Chem. Soc. Rev.* **2006,** *35*, 858-875.

30. Ryden, B.; Peterson, B. M., *Foundations of astrophysics*. Addison-Wesley: San Francisco, 2010.

31. Claire, M. W.; Sheets, J.; Cohen, M.; Ribas, I.; Meadows, V. S.; Catling, D. C. The evolution of solar flux from 0.1 nm to 160 μm: Quantitative estimates for planetary studies. *Astrophys. J.* **2012,** *757*, 95.

32. Canuto, V. M.; Levine, J. S.; Augustsson, T. R.; Imhoff, C. L. UV radiation from the young sun and oxygen and ozone levels in the prebiological paleoatmosphere. *Nature* **1982,** *296*, 816-820.

33. Gueymard, C. A. Parameterized transmittance model for direct beam and circumsolar spectral irradiance. *Solar Energy* **2001,** *71*, 325-346.

34. Morse, J. W.; Mackenzie, F. T. Hadean ocean carbonate geochemistry. *Aquat. Geochem.* **1998,** *4*, 301-319.

35. Zaia, D. A. M.; Zaia, C. T. B. V.; Santana, H. D. Which amino acids should be used in prebiotic chemistry studies? *Origins Life Evol. Biosphere* **2008,** *38*, 469-88.

36. Trail, D.; Watson, E. B.; Tailby, N. D. The oxidation state of Hadean magmas and implications for early Earth's atmosphere. *Nature* **2011,** *480*, 79-82.

37. Bada, J. L. New insights into prebiotic chemistry from Stanley Miller's spark discharge experiments. *Chem. Soc. Rev.* **2013,** *42*, 2186.

38. Kasting, J. F., Atmospheric composition of Hadean-Early Archean Earth: The importance of CO. In *Earth's early atmosphere and surface environment*, Shaw, G. H., Ed. 2014; Vol. 504, pp 19-28.

39. Sleep, N. H. The Hadean-Archaean environment. *Cold Spring Harbor Persp. Biol.* **2010,** *2*, a002527.

40. Driese, S. G.; Jirsa, M. A.; Ren, M.; Brantley, S. L.; Sheldon, N. D.; Parker, D.; Schmitz, M. Neoarchean paleoweathering of tonalite and metabasalt: Implications for reconstructions of 2.69 Ga early terrestrial ecosystems and paleoatmospheric chemistry. *Precambrian Res.* **2011,** *189*, 1-17.

41. Sheldon, N. D. Precambrian paleosols and atmospheric CO_2 levels. *Precambrian Res.* **2006,** *147*, 148-155.

42. Rosing, M. T.; Bird, D. K.; Sleep, N. H.; Bjerrum, C. J. No climate paradox under the faint early sun. *Nature* **2010,** *464*, 744-747.

43. Wolf, E.; Toon, O. Controls on the Archean climate system investigated with a global climate model. *Astrobio.* **2014,** *14*, 241-253.

44. Wolf, E. T.; Toon, O. B. Fractal organic hazes provided an ultraviolet shield for early Earth. *Science* **2010,** *328*, 1266-1268.

45. DeWitt, H. L.; Trainer, M. G.; Pavlov, A. A.; Hasenkopf, C. A.; Aiken, A. C.; Jimenez, J. L.; McKay, C. P.; Toon, O. B.; Tolbert, M. A. Reduction in haze formation rate on prebiotic Earth in the presence of hydrogen. *Astrobio.* **2009,** *9*, 447-453.

46. Kaltenegger, L.; Traub, W. A.; Jucks, K. W. Spectral evolution of an Earth-like planet. *Astrophys. J.* **2007,** *658*, 598.

47. Tian, F.; Kasting, J. F.; Zahnle, K. Revisiting HCN formation in Earth's early atmosphere. *Earth. Planet. Sci. Lett.* **2011,** *308*, 417-423.

48. Gerlach, T. M.; Nordlie, B. E. C-O-H-S gaseous system: 1. Composition limits and trends in basaltic cases. *Am. J. Sci.* **1975,** *275*, 353-376.

49. Gerlach, T. M.; Nordlie, B. E. C-O-H-S gaseous system: 2. Temperature, atomic composition, and molecular equilibria in volcanic gases. *Am. J. Sci.* **1975,** *275*, 377-394.

50. Gerlach, T. M.; Nordlie, B. E. C-O-H-S gaseous system: 3. Magmatic gases compatible with oxides and sulfides in basaltic magmas. *Am. J. Sci.* **1975,** *275*, 395-410.

51. Whitehill, A. R.; Jiang, B.; Guo, H.; Ono, S. SO_2 photolysis as a source for sulfur mass-independent isotope signatures in stratospehric aerosols. *Atmo. Chem. Phys.* **2015,** *15*, 1843-1864.

52. Whitehill, A. R.; Ono, S. Excitation band dependence of sulfur isotope mass-independent fractionation during photochemistry of sulfur dioxide using broadband light sources. *Geochim. Cosmochim. Acta* **2012,** *94*, 238-253.

53. Sagan, C.; Chyba, C. The early faint sun paradox: Organic shielding of ultraviolet-labile greenhouse gases. *Science* **1997,** *276*, 1217-1221.

54. Hoffman, P. F.; Kaufman, A. J.; Halverson, G. P.; Schrag, D. P. A Neoproterozoic snowball Earth. *Science* **1998,** *281*, 1342-1346.

55. Condon, D. J.; Prave, A. R.; Benn, D. I. Neoproterozoic glacial-rainout intevals: Observations and implications. *Geology* **2002,** *30*, 35-38.

56. Cavosie, A. J.; Valley, J. W.; Wilde, S. A.; E.I.M.F. Magmatic δ 18O in 4400–3900 Ma detrital zircons: A record of the alteration and recycling of crust in the early Archean. *Earth. Planet. Sci. Lett.* **2005,** *235*, 663-681.

57. Pierrehumbert, R. T. High levels of atmospheric carbon dioxide necessary for the termination of global glaciation. *Nature* **2004,** *429*, 646-649.

58. Kasting, J. F. Earth's early atmosphere. *Science* **1993,** *259*, 920-926.

59. Kasting, J. F.; Ono, S. Palaeoclimates: The first two billion years. *Philos. Trans. R. Soc. London, Ser. B* **2006,** *361*, 917-929.

60. Wolf, E.; Toon, O. Hospitable Archean climates simulated by a general circulation model. *Astrobio.* **2013,** *13*, 656-673.

61. Kunze, M.; Godolt, M.; Langematz, U.; Grenfell, J.; Hamann-Reinus, A.; Rauer, H. Investigating the early Earth faint young sun problem with a general circulation model. *Planet. Space Sci.* **2014,** *98*, 77-92.

62. Charnay, B.; Forget, F.; Wordsworth, R.; Leconte, J.; Millour, E.; Codron, F.; Spiga, A. Exploring the faint young sun problem and the possible climates of the Archean Earth with a 3D GCM. *J. Geophys. Res. Atmos.* **2013,** *118*, 10414-10431.

63. Knauth, L. P.; Lowe, D. R. High Archean climatic temperature inferred from oxygen isotope geochemistry of cherts in the 3.5 Ga Swaziland supergroup, South Africa. *Geol. Soc. Am. Bull.* **2003,** *115*, 566-580.

64. Robert, F.; Chaussidon, M. A palaeotemperature curve for the Precambrian oceans based on silicon isotopes in cherts. *Nature* **2006,** *443*, 969-972.

65. Hren, M.; Tice, M.; Chamberlain, C. Oxygen and hydrogen isotope evidence for a temperate climate 3.42 billion years ago. *Nature* **2009,** *462*, 205-208.

66. Blake, R. E.; Chang, S. J.; Lepland, A. Phosphate oxygen isotopic evidence for a temperate and biologically active Archaean ocean. *Nature* **2010,** *464*, 1029-1032.

67. Hazen, R. M.; Downs, R. T.; Kah, L.; Sverjensky, D., Carbon mineral evolution. In *Carbon in Earth*, Hazen, R. M.; Jones, A. P.; Baross, J. A., Eds. 2013; Vol. 75, pp 79-107.

68. Williams, R. J. P.; da Silva, J., *The natural selection of the chemical elements: The environment and life's chemistry*. Clarendon Press; Oxford University Press: 1996.

69. Plankensteiner, K.; Reiner, H.; Rode, B. M. Amino acids on the rampant primordial Earth: Electric discharges and the hot salty ocean. *Molec. Divers.* **2006,** *10*, 3-7.

70. Grotzinger, J.; Kasting, J. New constraints on Precambrian ocean composition. *J. Geol.* **1993,** *101*, 235-243.

71. Shibuya, T.; Komiya, T.; Nakamura, K.; Takai, K.; Maruyama, S. Highly alkaline, high-temperature hydrothermal fluids in the early Archean ocean. *Precambrian Res.* **2010,** *182*, 230-238.

72. Kempe, S.; Degens, E. T. An early soda ocean? *Chem. Geol.* **1985,** *53*, 95-108.

73. Knauth, L. P. Salinity history of the Earth's early ocean [letter]. *Nature* **1998,** *395*, 554-555.

74. Knauth, L. P. Temperature and salinity history of the precambrian ocean: Implications for the course of microbial evolution. *Palaeogeogr. Palaeoclimatol. Palaeoecol.* **2005,** *219*, 53-69.

75. Holland, H. D., *The chemical evolution of the atmosphere and oceans*. Princeton University Press: 1984; p 598.

76. Sugisaki, R.; Horiuchi, Y.; Sugitani, K.; Adachi, M. Acid character of Archean ocean waters revealed by 3.3-Ga-old ferruginous chert compositions, Western Australia. *Proc. Jpn. Acad., Ser. B* **1995,** *71*, 170-174.

77. Griffith, E. C.; Vaida, V. In situ observation of peptide bond formation at the water-air interface. *Proc. Natl. Acad. Sci.* **2012,** *109*, 15697-15701.

78. Donaldson, D. J.; Vaida, V. The influence of organic films at the air-aqueous boundary on atmospheric processes. *Chem. Rev.* **2006,** *106*, 1445-1461.

79. Tuck, A. F., *Atmospheric turbulence: A molecular dynamics perspective*. Oxford University Press: Oxford, U.K., 2008.

80. Rudich, Y. Laboratory perspectives on the chemical transformations of organic matter in atmospheric particles. *Chem. Rev.* **2003,** *103*, 5097-5124.

81. Demou, E.; Visram, H.; Donaldson, D.; Makar, P. A. Uptake of water by organic films: The dependence on the film oxidation state. *Atmos. Environ.* **2003,** *37*, 3529-3537.

82. Asad, A.; Mmereki, B.; Donaldson, D. Enhanced uptake of water by oxidatively processed oleic acid. *Atmo. Chem. Phys.* **2004,** *4*, 2083-2089.

83. Broekhuizen, K. E.; Thornberry, T.; Kumar, P. P.; Abbatt, J. P. Formation of cloud condensation nuclei by oxidative processing: Unsaturated fatty acids. *J. Geophys. Res. Atmos.* **2004,** *109*, D24206.

84. Dobson, C. M.; Ellison, G. B.; Tuck, A. F.; Vaida, V. Atmospheric aerosols as prebiotic chemical reactors. *Proc. Natl. Acad. Sci.* **2000,** *97*, 11864-11868.

85. Finlayson-Pitts, B. J.; Pitts, J. N., *Chemistry of the upper and lower atmosphere*. Academic Press: San Diego, 1999.

86. Seinfeld, J. H.; Pandis, S. N., *Atmospheric chemistry and physics: From air pollution to climate change*. John Wiley & Sons, Inc.: New York, 1998.

87. Nilson, F. P. R. Possible impact of a primordial oil slick on atmospheric and chemical evolution. *Origins Life Evol. Biosphere* **2002,** *32*, 247-253.

88. Pohorille, A.; Wilson, M. A. Molecular-dynamics studies of simple membrane water interfaces: Structure and functions in the beginnings of cellular life. *Origins Life Evol. Biosphere* **1995,** *25*, 21-46.

89. Donaldson, D. J.; Tervahattu, H.; Tuck, A. F.; Vaida, V. Organic aerosols and the origin of life: An hypothesis. *Origins Life Evol. Biosphere* **2004,** *34*, 57-67.

90. Gilman, J. B.; Tervahattu, H.; Vaida, V. Interfacial properties of mixed films of long-chain organics at the air-water interface. *Atmos. Environ.* **2006,** *40*, 6606-6614.

91. Tervahattu, H.; Hartonen, K.; Kerminen, V. M.; Kupiainen, K.; Aarnio, P.; Koskentalo, T.; Tuck, A. F.; Vaida, V. New evidence of an organic layer on marine aerosols. *J. Geophys. Res.* **2002,** *107*, 4053-4060.

92. Ellison, G. B.; Tuck, A. F.; Vaida, V. Atmospheric processing of organic aerosols. *J. Geophys. Res. Atmos.* **1999,** *104*, 11633-11641.

93. Murphy, D.; Thomson, D.; Mahoney, M. In situ measurements of organics, meteoritic material, mercury, and other elements in aerosols at 5 to 19 kilometers. *Science* **1998,** *282*, 1664-1669.

94. Demou, E.; Donaldson, D. J. Adsorption of atmospheric gases at the air-water interface. 4: The influence of salts. *J. Phys. Chem. A* **2002,** *106*, 982-987.

95. Griffith, E. C.; Tuck, A. F.; Vaida, V. Ocean-atmosphere interactions in the emergence of complexity in simple chemical systems. *Acc. Chem. Res.* **2012,** *45*, 2106-2113.

96. Lerman, L., The primordial bubble: Water, symmetry-breaking, and the origin of life. In *Water and life: The unique properties of water*, Lynden-Bell, R. M.; Morris, S. C.; Barrow, J. D.; Finney, J. L.; Harper Jr., C. L., Eds. CRC Press: Boca Raton, FL, 2010; pp 259 - 290.

97. Tverdislov, V. A.; Yakovenko, L. V. Physical aspects of the emergence of living cell precursors: The ion and chiral asymmetries as two fundamental asymmetry types. *Moscow Univ. Phys. Bull.* **2008,** *63*, 151-163.

98. Tuck, A. The role of atmospheric aerosols in the origin of life. *Surv. Geophys.* **2002,** *23*, 379-409.

99. Powner, M. W.; Sutherland, J. D. Prebiotic chemistry: A new modus operandi. *Philos. Trans. R. Soc. London, Ser. B* **2011,** *366*, 2870-2877.

100. Hazen, R. M.; Sverjensky, D. A. Mineral surfaces, geochemical complexities, and the origins of life. *Cold Spring Harbor Persp. Biol.* **2010,** *2*, a002162.

101. Cairns-Smith, A. G.; Hartman, H., *Clay minerals and the origin of life*. Press Syndicate of the University of Cambridge: Cambridge, 1986.

102. Ferris, J. P. Montmorillonite-catalysed formation of RNA oligomers: The possible role of catalysis in the origins of life. *Philos. Trans. R. Soc. London, Ser. B* **2006,** *361*, 1777-1786.

103. Huber, C.; Wachtershauser, G. Peptides by activation of amino acids with CO on (Ni,Fe)S surfaces: Implications for the origin of life. *Science* **1998,** *281*, 670-672.

104. Hazen, R. M. Paleomineralogy of the Hadean eon: A preliminary species list. *Am. J. Sci.* **2013,** *313*, 807-843.

105. Hazen, R. M.; Papineau, D.; Leeker, W. B.; Downs, R. T.; Ferry, J. M.; McCoy, T. J.; Sverjensky, D. A.; Yang, H. Mineral evolution. *Am. Mineral.* **2008,** *93*, 1693-1720.

106. Cockell, C. S. Biological effects of high ultraviolet radiation on early Earth: A theoretical evaluation. *J. Theor. Bio.* **1998,** *193*, 717-729.

107. Cleaves, H. J.; Miller, S. L. Oceanic protection of prebiotic organic compounds from UV radiation. *Proc. Natl. Acad. Sci.* **1998,** *95*, 7260-7263.

108. Venot, O.; Fray, N.; Bénilan, Y.; Gazeau, M.-C.; Hébrard, E.; Larcher, G.; Schwell, M.; Dobrijevic, M.; Selsis, F. High-temperature measurements of VUV-absorption cross sections of CO_2 and their application to exoplanets. *Astron. Astrophys.* **2013,** *551*, A131.

109. Huestis, D. L.; Berkowitz, J. Critical evaluation of the photoabsorption cross section of CO_2 from 0.125 to 201.6 nm at room temperature. *Adv. Geosci.* **2010,** *25*, 229-242.

110. Thompson, B.; Harteck, P.; Reeves, R. Ultraviolet absorption coefficients of CO_2, CO, O_2, H_2O, N_2O, NH_3, NO, SO_2, and CH_4 between 1850 and 4000 A. *J. Geophys. Res.* **1963,** *68*, 6431-6436.

111. Engel, V.; Staemmler, V.; Vander Wal, R.; Crim, F.; Sension, R.; Hudson, B.; Andresen, P.; Hennig, S.; Weide, K.; Schinke, R. Photodissociation of water in the first absorption band: A prototype for dissociation on a repulsive potential energy surface. *J. Phys. Chem.* **1992,** *96*, 3201-3213.

112. Gürtler, P.; Saile, V.; Koch, E. Rydberg series in the absorption spectra of H_2O and D_2O in the vacuum ultraviolet. *Chem. Phys. Lett.* **1977,** *51*, 386-391.

113. Rugheimer, S.; Segura, A.; Kaltenegger, L.; Sasselov, D. UV surface environment of earth-like planets orbiting FGKM stars through geological evolution. *Astrophys. J.* **2015,** *806*, 137.

114. Trainer, M. G. Atmospheric prebiotic chemistry and organic hazes. *Curr. Org. Chem.* **2013,** *17*, 1710-1723.

115. Trainer, M. G.; Pavlov, A. A.; DeWitt, H. L.; Jimenez, J. L.; McKay, C. P.; Toon, O. B.; Tolbert, M. A. Organic haze on Titan and the early Earth. *Proc. Natl. Acad. Sci.* **2006,** *103*, 18035-18042.

116. Trainer, M. G.; Pavlov, A. A.; Curtis, D. B.; Mckay, C. P.; Worsnop, D. R.; Delia, A. E.; Toohey, D. W.; Toon, O. B.; Tolbert, M. A. Haze aerosols in the atmosphere of early Earth: Manna from heaven. *Astrobio.* **2004,** *4*, 409-419.

117. Mauzerall, D., Oceanic photochemistry and evolution of elements and cofactors in the early stages of the evolution of life. In *Evolution of primary producers in the sea*, Falkowski, P. G.; Knoll, A. H., Eds. Elsevier: Amsterdam, 2007; pp 7-19.

118. Turro, N. J.; Ramamurthy, V.; Scaiano, J. C., *Modern molecular photochemistry of organic molecules*. University Science Books: Sausalito, California, 2010.

119. Leopold, D. G.; Pendley, R. D.; Roebber, J. L.; Hemley, R. J.; Vaida, V. Direct absorption-spectroscopy of jet-cooled polyenes 2. The 1 $^1B_u^+ \leftarrow 1\ ^1A_g^-$ transitions of butadienes and hexatrienes. *J. Chem. Phys.* **1984,** *81*, 4218-4229.

120. Leopold, D. G.; Vaida, V.; Granville, M. F. Direct absorption-spectroscopy of jet-cooled polyenes 1. The 1 $^1B_u^+ \leftarrow 1\ ^1A_g^-$ transition of trans, trans-1,3,5,7-octatetraene. *J. Chem. Phys.* **1984,** *81*, 4210-4217.

121. Vaida, V.; McClelland, G. M. Electronic absorption-spectroscopy of cooled supersonic expansions - dynamics of the $^1B_{1u}$ state of trans-butadiene. *Chem. Phys. Lett.* **1980,** *71*, 436-439.

122. Mitric, R.; Petersen, J.; Bonacic-Koutecky, V. Laser-field-induced surface-hopping method for the simulation and control of ultrafast photodynamics. *Phys. Rev. A* **2009,** *79*, 053416.

123. Domcke, W.; Yarkony, D.; Köppel, H., *Conical intersections: Electronic structure, dynamics & spectroscopy*. World Scientific: 2004; Vol. 15.

124. Michaelian, K.; Iop, A non-linear irreversible thermodynamic perspective on organic pigment proliferation and biological evolution. In *4th national meeting in chaos, complex system and time series*, 2013; Vol. 475.

125. Michaelian, K.; Simeonov, A. Fundamental molecules of life are pigments which arose and co-evolved as a response to the thermodynamic imperative of dissipating the prevailing solar spectrum. *Biogeosciences* **2015,** *12*, 4913-4937.

126. Sagan, C. Ultraviolet selection pressure on the earliest organisms. *J. Theor. Bio.* **1973,** *39*, 195-200.

127. Henry, B. R. Use of local modes in the description of highly vibrationally excited molecules. *Acc. Chem. Res.* **1977,** *10*, 207-213.

128. Crim, F. F. Selective excitation studies of unimolecular reaction dynamics. *Annu. Rev. Phys. Chem.* **1984,** *35*, 657-691.

129. Donaldson, D. J.; Tuck, A. F.; Vaida, V. Atmospheric photochemistry via vibrational overtone absorption. *Chem. Rev.* **2003,** *103*, 4717-4729.

130. Donaldson, D. J.; George, C.; Vaida, V. Red sky at night: Long-wavelengths photochemistry in the atmosphere. *Environ. Sci. Technol.* **2010,** *44*, 5321-5326.

131. Henry, B. R.; Kjaergaard, H. G. Local modes. *Can. J. Chem.* **2002,** *80*, 1635-1642.

132. Uzer, T.; Hynes, J. T.; Reinhardt, W. P. Classical dynamics of intramolecular energy-flow and overtone-induced dissociation in HO_2H and HO_2D. *J. Chem. Phys.* **1986,** *85*, 5791-5804.

133. Lu, D. H.; Hase, W. L. Classical trajectory calculation of the benzene overtone spectra. *J. Phys. Chem.* **1988,** *92*, 3217-3225.

134. Heller, E. J.; Davis, M. J. Molecular overtone bandwidths from classical trajectories. *J. Phys. Chem.* **1980,** *84*, 1999-2001.

135. Sibert, E. L.; Hynes, J. T.; Reinhardt, W. P. Classical dynamics of highly excited CH and CD overtones in benzene and perdeuterobenzene. *J. Chem. Phys.* **1984,** *81*, 1135-1144.

136. Kahan, T. F.; Kwamena, N. O. A.; Donaldson, D. J. Different photolysis kinetics at the surface of frozen freshwater vs. frozen salt solutions. *Atmo. Chem. Phys.* **2010,** *10*, 10917-10922.

137. Epstein, S. A.; Nizkorodov, S. A. A comparison of the chemical sinks of atmospheric organics in the gas and aqueous phase. *Atmo. Chem. Phys.* **2012,** *12*, 8205-8222.

138. Vaida, V. Perspective: Water cluster mediated atmospheric chemistry. *J. Chem. Phys.* **2011,** *135*, Art. Nr. 020901.

139. Gromov, E. V.; Burghardt, I.; Koeppel, H.; Cederbaum, L. S. Electronic structure of the PYP chromophore in its native protein environment. *J. Am. Chem. Soc.* **2007,** *129*, 6798-6806.

140. Brondsted Nielsen, M. Model systems for understanding absorption tuning by opsin proteins. *Chem. Soc. Rev.* **2009,** *38*, 913-924.

141. Gromov, E. V.; Burghardt, I.; Koeppel, H.; Cederbaum, L. S. Native hydrogen bonding network of the photoactive yellow protein (PYP) chromophore: Impact on the electronic structure and photoinduced isomerization. *J. Photochem. Photobiol., A* **2012,** *234*, 123-134.

142. Vaida, V.; Donaldson, D. J.; Sapers, S. P.; Naaman, R.; Child, M. S. Spectroscopic probe of intramolecular predissociation dynamics in clusters. *J. Phys. Chem.* **1989,** *93*, 513-520.

143. Robinson, G. W. Intensity enhancement of forbidden electronic transitions by weak intermolecular interactions. *J. Chem. Phys.* **1967,** *46*, 572-585.

144. Long, C. A.; Ewing, G. E. Spectroscopic investigation of van der Waals molecules. 1. Infrared and visible spectra of O_2 *J. Chem. Phys.* **1973,** *58*, 4824-4834.

145. Herrmann, H.; Schaefer, T.; Tilgner, A.; Styler, S. A.; Weller, C.; Teich, M.; Otto, T. Tropospheric aqueous-phase chemistry: Kinetics, mechanisms, and its coupling to a changing gas phase. *Chem. Rev.* **2015,** *115*, 4259–4334.

146. Vaida, V. Spectroscopy of photoreactive systems: Implications for atmospheric chemistry. *J. Phys. Chem. A* **2009,** *113*, 5-18.

147. Vaida, V.; Feierabend, K. J.; Rontu, N.; Takahashi, K. Sunlight-initiated photochemistry: Excited vibrational states of atmospheric chromophores. *Int. J. Photoenergy* **2008**, Art. No. 138091.

148. Faccini, M. C.; Mircea, M.; Fuzzi, S.; Charlson, R. J. Cloud albedo enhancement by surface-active organic solutes in growing droplets. *Nature* **1999,** *401*, 257-259.

149. Ervens, B.; Turpin, B. J.; Weber, R. J. Secondary aerosol formation in cloud droplets and aqueous particles (aqSOA): A review of laboratory, field and model studies. *Atmo. Chem. Phys.* **2011,** *11*, 11069-11102.

150. Axson, J. L.; Takahashi, K.; De Haan, D. O.; Vaida, V. Gas-phase water-mediated equilibrium between methylglyoxal and its geminal diol. *Proc. Natl. Acad. Sci.* **2010,** *107*, 6687-6692.

151. Bell, R. P.; Rand, M. H.; Wynnejones, K. M. A. Kinetics of hydration of acetaldehyde. *Trans. Faraday Soc.* **1956,** *52*, 1093-1102.

152. Buschmann, H. J.; Dutkiewicz, E.; Knoche, W. The reversible hydration of carbonyl compounds in aqueous solution.2. The kinetics of the keto gem-diol transition. *Ber. Bunsen-Ges. Phys. Chem* **1982,** *86*, 129-134.

153. Wolfe, S.; Kim, C.-K.; Yang, K.; Weinberg, N.; Shi, Z. Hydration of the carbonyl group: A theoretical study of the cooperative mechanism. *J. Am. Chem. Soc.* **1995,** *117*, 4240-4260.

154. Plath, K. L.; Axson, J. L.; Nelson, G. C.; Takahashi, K.; Skodje, R. T.; Vaida, V. Gas-phase vibrational spectra of glyoxylic acid and its gem diol monohydrate. Implications for atmospheric chemistry. *React. Kinet. Catal. Lett.* **2009,** *96*, 209-224.

155. Epstein, S. A.; Tapavicza, E.; Furche, F.; Nizkorodov, S. A. Direct photolysis of carbonyl compounds dissolved in cloud and fog droplets. *Atmo. Chem. Phys.* **2013,** *13*, 9461-9477.

156. Hazen, R. M. Mineral surfaces and the prebiotic selection and organization of biomolecules. *Am. Mineral.* **2006,** *91*, 1715-1729.

157. George, C.; Ammann, M.; D'Anna, B.; Donaldson, D. J.; Nizkorodov, S. A. Heterogeneous photochemistry in the atmosphere. *Chem. Rev.* **2015,** *115*, 4218-4258.

158. Martins-Costa, M. T. C.; Anglada, J. M.; Francisco, J. S.; Ruiz-Lopez, M. F. Reactivity of volatile organic compounds at the surface of a water droplet. *J. Am. Chem. Soc.* **2012,** *134*, 11821-11827.

159. Goldacre, R. J., Surface films, their collapse on compression, the shape and size of cells and the origin of life. In *Surface phenomena in chemistry and biology*, Danielli, J. F.; Parkhurst, K. G. A.; Riddiford, A. C., Eds. Pergamon Press: New York, 1958; pp 12 - 27.

160. Shah, D. O., The origin of membranes and related surface phenomena. In *Exobio.*, Ponnamperuma, C., Ed. North-Holland Publishing Co.: Amsterdam, 1972; pp 235 - 265.

161. Lerman, L.; Teng, J., In the beginning. In *Origins: Genesis, evolution and diversity of life*, Seckbach, J., Ed. Kluwer Academic Publishers: Dordrecht, The Netherlands, 2004; pp 35 - 55.

162. Rideal, E. K.; Mitchell, J. S. Photochemical reactions in monolayers: I. Photochemical properties of the ketoimino linkage. *Proc. R. Soc. London, Ser. A* **1937,** *159*, 0206-0228.

163. Pilpel, N.; Hunter, B. F. J. Oxidation and decomposition of monomolecular films of stearic acid under ultraviolet irradiation. *J. Colloid Interface Sci.* **1970,** *33*, 615-622.

164. Gankanda, A.; Grassian, V. H. Nitrate photochemistry on laboratory proxies of mineral dust aerosol: Wavelength dependence and action spectra. *J. Phys. Chem. C* **2014,** *118*, 29117-29125.

165. Chen, H.; Nanayakkara, C. E.; Grassian, V. H. Titanium dioxide photocatalysis in atmospheric chemistry. *Chem. Rev.* **2012,** *112*, 5919-5948.

166. Cwiertny, D. M.; Young, M. A.; Grassian, V. H. Chemistry and photochemistry of mineral dust aerosol. *Annu. Rev. Phys. Chem.* **2008,** *59*, 27-51.

167. Griffith, E. C.; Rapf, R. J.; Shoemaker, R. K.; Carpenter, B. K.; Vaida, V. Photoinitiated synthesis of self-assembled vesicles. *J. Am. Chem. Soc.* **2014,** *136*, 3784-3787.

168. Reeser, D.; Jammoul, A.; Clifford, D.; Brigante, M.; D'Anna, B.; George, C.; Donaldson, D. J. Photoenhanced reaction of ozone with chlorophyll at the seawater surface. *J. Phys. Chem. C* **2009,** *113*, 2071-2077.

169. Ciuraru, R.; Fine, L.; van Pinxteren, M.; D'Anna, B.; Herrmann, H.; George, C. Photosensitized production of functionalized and unsaturated organic compounds at the air-sea interface. *Sci. Rep.* **2015,** *5*, 12741

170. Fu, H.; Ciuraru, R.; Dupart, Y.; Passananti, M.; Tinel, L.; Rossignol, S.; Perrier, S.; Donaldson, D. J.; Chen, J.; George, C. Photosensitized production of atmospherically reactive organic compounds at the air/aqueous interface. *J. Am. Chem. Soc.* **2015,** *137*, 8348-8351.

171. Reeser, D. I.; George, C.; Donaldson, D. J. Photooxidation of halides by chlorophyll at the air-salt water interface. *J. Phys. Chem. A* **2009,** *113*, 8591-8595.

172. Deamer, D. W. The first living systems: A bioenergetic perspective. *Microbio. Mol. Bio. Rev.* **1997,** *61*, 239 - 261.

173. Mercer-Smith, J. A.; Mauzerall, D. C. Photochemistry of porphyrins: A model for the origin of photosynthesis. *Photochem. Photobiol.* **1984,** *39*, 397-405.

174. Deamer, D. W. Polycyclic aromatic hydrocarbons: Primitive pigment systems in the prebiotic environment. *Adv. Space Res.* **1992,** *12*, 183-189.

175. Ehrenfreund, P.; Rasmussen, S.; Cleaves, J.; Chen, L. H. Experimentally tracing the key steps in the origin of life: The aromatic world. *Astrobio.* **2006,** *6*, 490-520.

176. Saladino, R.; Ciambecchini, U.; Crestini, C.; Costanzo, G.; Negri, R.; Di Mauro, E. One-pot TiO_2-catalyzed synthesis of nucleic bases and acyclonucleosides from formamide: Implications for the origin of life. *ChemBioChem* **2003,** *4*, 514-521.

177. Senanayake, S. D.; Idriss, H. Photocatalysis and the origin of life: Synthesis of nucleoside bases from formamide on TiO_2(001) single surfaces. *Proc. Natl. Acad. Sci.* **2006,** *103*, 1194-1198.

178. Guzman, M. I.; Martin, S. T. Prebiotic metabolism: Production by mineral photoelectrochemistry of alpha-ketocarboxylic acids in the reductive tricarboxylic acid cycle. *Astrobio.* **2009,** *9*, 833-842.

179. Bahadur, K.; Ranganayaki, S.; Santamaria, L. Photosynthesis of amino-acids from paraformaldehyde involving the fixation of nitrogen in the presence of colloidal molybdenum oxide as catalyst. *Nature* **1958,** *182*, 1668.

180. Ritson, D.; Sutherland, J. D. Prebiotic synthesis of simple sugars by photoredox systems chemistry. *Nature Chem.* **2012,** *4*, 895-899.

181. Pagni, R. M.; Sigman, M. E., The photochemistry of PAHs and PCBs in water and on solids. In *Environmental photochemistry*, Springer: 1999; pp 139-179.

182. Baek, S.; Field, R.; Goldstone, M.; Kirk, P.; Lester, J.; Perry, R. A review of atmospheric polycyclic aromatic hydrocarbons: Sources, fate and behavior. *Water, Air, Soil Pollut.* **1991,** *60*, 279-300.

183. Chen, L. H.; Geiger, C.; Perlstein, J.; Whitten, D. G. Self-assembly of styryl naphthalene amphiphiles in aqueous dispersions and interfacial films: Aggregate structure, assembly properties, photochemistry, and photophysics. *J. Phys. Chem. B* **1999,** *103*, 9161-9167.

184. Chen, L. H.; Lucia, L.; Whitten, D. G. Cooperative electron transfer fragmentation reactions. Amplification of a photoreaction through a tandem chain fragmentation of acceptor and donor pinacols. *J. Am. Chem. Soc.* **1998,** *120*, 439-440.

185. Cape, J. L.; Monnard, P.-A.; Boncella, J. M. Prebiotically relevant mixed fatty acid vesicles support anionic solute encapsulation and photochemically catalyzed trans-membrane charge transport. *Chem. Sci.* **2011,** *2*, 661-671.

186. Escabi-Perez, J. R.; Romero, A.; Lukac, S.; Fendler, J. H. Aspects of artificial photosynthesis: Photoionization and electron transfer in dihexadecyl phosphate vesicles. *J. Am. Chem. Soc.* **1979,** *101*, 2231-2233.

187. Seta, P.; Bienvenue, E.; Moore, A. L.; Mathis, P.; Bensasson, R. V.; Liddell, P.; Pessiki, P. J.; Joy, A.; Moore, T. A.; Gust, D. Photodriven transmembrane charge separation and electron transfer by a carotenoporphyrin–quinone triad. *Nature* **1985,** *316*, 653-655.

188. Sun, K.; Mauzerall, D. Charge transfer across a single lipid-water interface causes ion pumping across the bilayer. *Biophys. J.* **1996,** *71*, 309-316.

189. Herrmann, J. M. Heterogeneous photocatalysis: Fundamentals and applications to the removal of various types of aqueous pollutants. *Catal. Today* **1999,** *53*, 115-129.

190. Hoffmann, M. R.; Martin, S. T.; Choi, W. Y.; Bahnemann, D. W. Environmental applications of semiconductor photocatalysis. *Chem. Rev.* **1995,** *95*, 69-96.

191. Deamer, D.; Harang, E. Light-dependent pH gradients are generated in liposomes containing ferrocyanide. *BioSystems* **1990,** *24*, 1-4.

192. Nakata, K.; Fujishima, A. TiO_2 photocatalysis: Design and applications. *J. Photochem. Photobio. C* **2012,** *13*, 169-189.

193. Gligorovski, S.; Strekowski, R.; Barbati, S.; Vione, D. Environmental implications of hydroxyl radicals (•OH). *Chem. Rev.* **2015,** *115*, 13051-13092.

194. Monks, P. S. Gas-phase radical chemistry in the troposphere. *Chem. Soc. Rev.* **2005,** *34*, 376-395.

195. Crutzen, P. J.; Zimmermann, P. H. The changing photochemistry of the troposphere. *Tellus B* **1991,** *43*, 136-151.

196. Lelieveld, J.; Gromov, S.; Pozzer, A.; Taraborrelli, D. Global tropospheric hydroxyl distribution, budget and reactivity. *Atmos. Chem. Phys. Discuss.* **2016,** *2016*, 1-25.

197. Reeves Jr, R. R.; Harteck, P.; Thompson, B. A.; Waldron, R. W. Photochemical equilibrium studies of carbon dioxide and their significance for the venus atmosphere. *J. Phys. Chem.* **1966,** *70*, 1637-1640.

198. Garcia, R. R.; López - Puertas, M.; Funke, B.; Marsh, D. R.; Kinnison, D. E.; Smith, A. K.; González - Galindo, F. On the distribution of CO_2 and CO in the mesosphere and lower thermosphere. *J. Geophys. Res. Atmos.* **2014,** *119*, 5700-5718.

199. Liu, Y.; Siekmann, F.; Renard, P.; Zein, A. E.; Salque, G.; Haddad, I. E.; Temime-Roussel, B.; Voisin, D.; Thissen, R.; Monod, A. Oligomer and SOA formation through aqueous phase photooxidation of methacrolein and methyl vinyl ketone. *Atmos. Environ.* **2012,** *49*, 123-129.

200. Renard, P.; Reed Harris, A. E.; Rapf, R. J.; Rainer, S.; Demelas, C.; Coulomb, B.; Quivet, E.; Vaida, V.; Monod, A. Aqueous phase oligomerization of methyl vinyl ketone by atmospheric radical reactions. *J. Phys. Chem. C* **2014,** *118*, 29421-29430.

201. Renard, P.; Siekmann, F.; Gandolfo, A.; Socorro, J.; Salque, G.; Ravier, S.; Quivet, E.; Clement, J. L.; Traikia, M.; Delort, A. M., et al. Radical mechanisms of methyl vinyl ketone oligomerization through aqueous phase OH-oxidation: On the paradoxical role of dissolved molecular oxygen. *Atmo. Chem. Phys.* **2013,** *13*, 6473-6491.

202. Margulis, L.; Walker, J. C. G.; Rambler, M. Reassessment of roles of oxygen and ultraviolet light in Precambrian evolution. *Nature* **1976,** *264*, 620-624.

203. Cockell, C. S. The ultraviolet history of the terrestrial planets: Implications for biological evolution. *Planet. Space Sci.* **2000,** *48*, 203-214.

204. Marcum, J. C.; Kaufman, S. H.; Weber, J. M. UV-photodissociation of non-cyclic and cyclic mononucleotides. *Int. J. Mass Spectrom.* **2011,** *303*, 129-136.

205. Russell, M. J.; Nitschke, W.; Branscomb, E. The inevitable journey to being. *Philos. Trans. R. Soc. London, Ser. B* **2013,** *368*, 20120254.

206. Butlerov, A. Bildung einer zuckerartigen substanz durch synthese (formation of a sugar-like substance by synthesis). *Justus Liebigs Ann Chem* **1861,** *120*, 295-298.

207. Breslow, R. On the mechanism of the formose reaction. *Tetrahedron Lett.* **1959,** *1*, 22-26.

208. Ferris, J. P.; Chen, C. T. Chemical evolution XXVI: Photochemistry of methane, nitrogen and water mixtures as a model for the atmosphere of primitive Earth. *J. Am. Chem. Soc.* **1975,** *97*, 2962-2967.

209. Bar-Nun, A.; Chang, S. Photochemical-reactions of water and carbon-monoxide in earths primitive atmosphere. *J. Geophys. Res. Oceans* **1983,** *88*, 6662-6672.

210. Bar-Nun, A.; Hartman, H. Synthesis of organic-compounds from carbon-monoxide and water by UV photolysis. *Origins Life Evol. Biosphere* **1978,** *9*, 93-101.

211. Pinto, J. P.; Gladstone, G. R.; Yung, Y. L. Photochemical production of formaldehyde in earths primitive atmosphere. *Science* **1980,** *210*, 183-184.

212. Eisch, J. J.; Munson, P. R.; Gitua, J. N. The potential of photochemical transitionmetal reactions in prebiotic organic synthesis. I. Observed conversion of methanol into ethylene glycol as possible prototype for sugar alcohol formation. *Origins Life Evol. Biosphere* **2004,** *34*, 441-454.

213. Dondi, D.; Merli, D.; Pretali, L., Prebiotic photochemistry. In *Photochemistry: Volume 38*, The Royal Society of Chemistry: 2010; Vol. 38, pp 330-343.

214. Banerjee, A.; Ganguly, G.; Tripathi, R.; Nair, N. N.; Paul, A. Unearthing the mechanism of prebiotic nitrile bond reduction in hydrogen cyanide through a curious association of two molecular radical anions. *Chem. Eur. J.* **2014,** *20*, 6348-6357.

215. Pestunova, O.; Simonov, A.; Snytnikov, V.; Stoyanovsky, V.; Parmon, V. Putative mechanism of the sugar formation on prebiotic Earth initiated by UV-radiation. *Adv. Space Res.* **2005,** *36*, 214-219.

216. Baly, E. C. C.; Heilbron, I. M.; Barker, W. F. Cx.—photocatalysis. Part I. The synthesis of formaldehyde and carbohydrates from carbon dioxide and water. *J. Chem. Soc. Trans.* **1921,** *119*, 1025-1035.

217. Schwartz, A. W.; De Graaf, R. The prebiotic synthesis of carbohydrates: A reassessment. *J. Mol. Evo.* **1993,** *36*, 101-106.

218. Shapiro, R. Small molecule interactions were central to the origin of life. *Q. Rev. Bio.* **2006,** *81*, 105-125.

219. Griffith, E. C.; Carpenter, B. K.; Shoemaker, R. K.; Vaida, V. Photochemistry of aqueous pyruvic acid. *Proc. Natl. Acad. Sci.* **2013,** *110*, 11714-11719.

220. Reed Harris, A. E.; Ervens, B.; Shoemaker, R. K.; Kroll, J. A.; Rapf, R. J.; Griffith, E. C.; Monod, A.; Vaida, V. Photochemical kinetics of pyruvic acid in aqueous solution. *J. Phys. Chem. A* **2014,** *118*, 8505-8516.

221. Leermakers, P. A.; Vesley, G. F. Photochemistry of alpha-keto acids and alpha-keto esters. 1. Photolysis of pyruvic acid and benzoylformic acid. *J. Am. Chem. Soc.* **1963,** *85*, 3776-3779.

222. Leermakers, P. A.; Vesley, G. F. Photolysis of pyruvic acid in solution. *J. Org. Chem.* **1963,** *28*, 1160-1161.

223. Guzman, M. I.; Colussi, A. J.; Hoffmann, M. R. Photoinduced oligomerization of aqueous pyruvic acid. *J. Phys. Chem. A* **2006,** *110*, 3619-3626.

224. Vesley, G. F.; Leermakers, P. A. Photochemistry of alpha-keto acids and alpha-keto esters. 3. Photolysis of pyruvic acid in vapor phase. *J. Phys. Chem.* **1964,** *68*, 2364-2366.

225. Yamamoto, S.; Back, R. A. The photolysis and thermal decomposition of pyruvic acid in the gas phase. *Can. J. Chem.* **1985,** *63*, 549-554.

226. Hazen, R. M.; Deamer, D. W. Hydrothermal reactions of pyruvic acid: Synthesis, selection, and self-assembly of amphiphilic molecules. *Origins Life Evol. Biosphere* **2007,** *37*, 143-152.

227. Cody, G. D.; Boctor, N. Z.; Filley, T. R.; Hazen, R. M.; Scott, J. H.; Sharma, A.; Yoder, H. S. Primordial carbonylated iron-sulfur compounds and the synthesis of pyruvate. *Science* **2000,** *289*, 1337 -1340.

228. Cooper, G.; Reed, C.; Nguyen, D.; Carter, M.; Wang, Y. Detection and formation scenario of citric acid, pyruvic acid, and other possible metabolism precursors in carbonaceous meteorites. *Proc. Natl. Acad. Sci.* **2011,** *108*, 14015-14020.

229. Pizzarello, S.; Lahav, M. On the emergence of biochemical homochirality: An elusive beginning. *Origins Life Evol. Biosphere* **2010,** *40*, 1-2.

230. Mellouki, A.; Mu, Y. J. On the atmospheric degradation of pyruvic acid in the gas phase. *J. Photochem. Photobiol., A* **2003,** *157*, 295-300.

231. Berges, M. G.; Warneck, P. Product quantum yields for the 350 nm photodecomposition of pyruvic acid in air. *Ber. Bunsen-Ges. Phys. Chem* **1992,** *96*, 413-416.

232. Chang, X.-P.; Fang, Q.; Cui, G. Mechanistic photodecarboxylation of pyruvic acid: Excited-state proton transfer and three-state intersection. *J. Chem. Phys.* **2014,** *141*, 154311.

233. da Silva, G. Decomposition of pyruvic acid on the ground-state potential energy surface. *J. Phys. Chem. A* **2015,** *120* 276–283.

234. Horowitz, A.; Meller, R.; Moortgat, G. K. The UV–vis absorption cross sections of the α-dicarbonyl compounds: Pyruvic acid, biacetyl and glyoxal. *J. Photochem. Photobiol., A* **2001,** *146*, 19-27.

235. Takahashi, K.; Plath, K. L.; Skodje, R. T.; Vaida, V. Dynamics of vibrational overtone excited pyruvic acid in the gas phase: Line broadening through hydrogen-atom chattering. *J. Phys. Chem. A* **2008,** *112*, 7321-7331.

236. Griffith, E. C.; Shoemaker, R. K.; Vaida, V. Sunlight-initiated chemistry of aqueous pyruvic acid: Building complexity in the origin of life. *Origins Life Evol. Biosphere* **2013,** *43*, 341-352.

237. Zilberter, Y.; Zilberter, T.; Bregestovski, P. Neuronal activity in vitro and the in vivo reality: The role of energy homeostasis. *Trends Pharmacol. Sci.* **2010,** *31*, 394-401.

238. Wyss, M. T.; Jolivet, R.; Buck, A.; Magistretti, P. J.; Weber, B. In vivo evidence for lactate as a neuronal energy source. *J. Neurosci.* **2011,** *31*, 7477-7485.

239. Hugenholtz, J. Citrate metabolism in lactic acid bacteria. *FEMS Microbiol. Rev.* **1993,** *12*, 165-178.

240. Xiao, Z. J.; Xu, P. Acetoin metabolism in bacteria. *Crit. Rev. Microbio.* **2007,** *33*, 127-140.

241. Pizzarello, S. Prebiotic chemical evolution: A meteoritic perspective. *Rend. Lincei.* **2011,** *22*, 153-163.

242. McCollom, T. M.; Ritter, G.; Simoneit, B. R. T. Lipid synthesis under hydrothermal conditions by Fischer-Tropsch-type reactions. *Origins Life Evol. Biosphere* **1999,** *29*, 153-166.

243. Rushdi, A. I.; Simoneit, B. R. T. Lipid formation by aqueous Fischer-Tropsch-type synthesis over a temperature range of 100 to 400 °C. *Origins Life Evol. Biosphere* **2001,** *31*, 103-118.

244. Hargreaves, W. R.; Mulvihill, S. J.; Deamer, D. W. Synthesis of phospholipids and membranes in prebiotic conditions. *Nature* **1977,** *266*, 78-80.

245. Rao, M.; Eichberg, J.; Oro, J. Synthesis of phosphatidylcholine under possible primitive Earth conditions *J. Mol. Evo.* **1982,** *18*, 196-202.

246. Stano, P.; D'Aguanno, E.; Bolz, J.; Fahr, A.; Luisi, P. L. A remarkable self-organization process as the origin of primitive functional cells. *Angew. Chem. Int. Ed.* **2013,** *52*, 13397-13400.

247. Mansy, S. S. Membrane transport in primitive cells. *Cold Spring Harbor Persp. Biol.* **2010,** *2*, 14.

248. Budin, I.; Szostak, J. W. Physical effects underlying the transition from primitive to modern cell membranes. *Proc. Natl. Acad. Sci.* **2011,** *108*, 5249-5254.

249. Hanczyc, M. M.; Fujikawa, S. M.; Szostak, J. W. Experimental models of primitive cellular compartments: Encapsulation, growth, and division. *Science* **2003,** *302*, 618-622.

250. Pohorille, A.; Deamer, D. Self-assembly and function of primitive cell membranes. *Res. Microbiol.* **2009,** *160*, 449-456.

251. Luisi, P. L.; Walde, P.; Oberholzer, T. Lipid vesicles as possible intermediates in the origin of life. *Curr. Opin. Colloid Interface Sci.* **1999,** *4*, 33-39.

252. Deamer, D., Sources and syntheses of prebiotic amphiphiles. In *Self-production of supramolecular structures*, Springer: 1994; pp 217-229.

253. Monnard, P. A.; Deamer, D. W. Membrane self-assembly processes: Steps toward the first cellular life. *Anat. Rec.* **2002,** *268*, 196-207.

254. Morigaki, K.; Walde, P. Fatty acid vesicles. *Curr. Opin. Colloid Interface Sci.* **2007,** *12*, 75-80.

255. Monnard, P. A.; Apel, C. L.; Kanavarioti, A.; Deamer, D. W. Influence of ionic inorganic solutes on self-assembly and polymerization processes related to early forms of life: Implications for a prebiotic aqueous medium. *Astrobio.* **2002,** *2*, 139-152.

256. Black, R. A.; Blosser, M. C.; Stottrup, B. L.; Tavakley, R.; Deamer, D. W.; Keller, S. L. Nucleobases bind to and stabilize aggregates of a prebiotic amphiphile, providing a viable mechanism for the emergence of protocells. *Proc. Natl. Acad. Sci.* **2013,** *110*, 13272-13276.

257. Apel, C. L.; Deamer, D. W.; Mautner, M. N. Self-assembled vesicles of monocarboxylic acids and alcohols: Conditions for stability and for the encapsulation of biopolymers. *Biochim. Biophys. Acta-Biomembranes* **2002,** *1559*, 1-9.

258. Maurer, S. E.; Deamer, D. W.; Boncella, J. M.; Monnard, P. A. Chemical evolution of amphiphiles: Glycerol monoacyl derivatives stabilize plausible prebiotic membranes. *Astrobio.* **2009,** *9*, 979-987.

259. Miller, S. L. A production of amino acids under possible primitive Earth conditions. *Science* **1953,** *117*, 528-529.

260. Cleaves, H. J.; Chalmers, J. H.; Lazcano, A.; Miller, S. L.; Bada, J. L. A reassessment of prebiotic organic synthesis in neutral planetary atmospheres. *Origins Life Evol. Biosphere* **2008,** *38*, 105-115.

261. McCollom, T. M. Miller-Urey and beyond: What have we learned about prebiotic organic synthesis reactions in the past 60 years? *Ann. Rev. Earth Planet. Sci.* **2013,** *41*, 207-229.

262. Groth, W. E.; Vonweyssenhoff, H. Photochemical formation of organic compounds from mixtures of simple gases. *Planet. Space Sci.* **1960,** *2*, 79-85.

263. Khare, B. N.; Sagan, C. Synthesis of cystine in simulated primitive conditions. *Nature* **1971,** *232*, 577-579.

264. Sagan, C.; Khare, B. N. Long-wavelength ultraviolet photoproduction of amino acids on primitive earth. *Science* **1971,** *173*, 417-420.

265. Sarker, P. K.; Takahashi, J. I.; Obayashi, Y.; Kaneko, T.; Kobayashi, K. Photo-alteration of hydantoins against UV light and its relevance to prebiotic chemistry. *Adv. Space Res.* **2013,** *51*, 2235-2240.

266. Bahadur, K. Photosynthesis of amino-acids from paraformaldehyde and potassium nitrate. *Nature* **1954,** *173*, 1141.

267. Santamaria, L.; Fleischmann, L. Photochemical synthesis of amino acids from paraformaldehyde catalysed by inorganic agents. *Experientia* **1966,** *22*, 430-431.

268. Cottin, H.; Gazeau, M. C.; Raulin, F. Cometary organic chemistry: A review from observations, numerical and experimental simulations. *Planet. Space Sci.* **1999,** *47*, 1141-1162.

269. Munoz Caro, G. M.; Meierhenrich, U. J.; Schutte, W. A.; Barbier, B.; Arcones Segovia, A.; Rosenbauer, H.; Thiemann, W. H. P.; Brack, A.; Greenberg, J. M. Amino acids from ultraviolet irradiation of interstellar ice analogues. *Nature* **2002,** *416*, 403-6.

270. Bernstein, M. P.; Dworkin, J. P.; Sandford, S. A.; Cooper, G. W.; Allamandola, L. J. Racemic amino acids from the ultraviolet photolysis of interstellar ice analogues. *Nature* **2002,** *416*, 401-403.

271. Elsila, J. E.; Dworkin, J. P.; Bernstein, M. P.; Martin, M. P.; Sandford, S. A. Mechanisms of amino acid formation in interstellar ice analogs. *Astrophys. J.* **2007,** *660*, 911-918.

272. Nuevo, M.; Auger, G.; Blanot, D.; d'Hendecourt, L. A detailed study of the amino acids produced from the vacuum UV irradiation of interstellar ice analogs. *Origins Life Evol. Biosphere* **2008,** *38*, 37-56.

273. Sutherland, J. D. The origin of life-out of the blue. *Angew. Chem. Int. Ed.* **2016,** *55*, 104-121.

274. Cernicharo, J.; Agundez, M.; Kahane, C.; Guelin, M.; Goicoechea, J. R.; Marcelino, N.; De Beck, E.; Decin, L. Probing the dust formation region in IRC +10216 with the high vibrational states of hydrogen cyanide. *Astron. Astrophys.* **2011,** *529*, L3.

275. Matthews, C. N.; Minard, R. D. Hydrogen cyanide polymers, comets and the origin of life. *Faraday Discuss.* **2006,** *133*, 393-401.

276. Schilke, P.; Menten, K. M. Detection of a second, strong submillimeter HCN laser line toward carbon stars. *Astrophys. J.* **2003,** *583*, 446-450.

277. Snyder, L. E.; Buhl, D. Observations of radio emission from interstellar hydrogen cyanide. *Astrophys. J.* **1971,** *163*, L47.

278. Ehrenfreund, P.; Charnley, S. B. Organic molecules in the interstellar medium, comets, and meteorites: A voyage from dark clouds to the early Earth. *Ann. Rev. Astron. Astrophys.* **2000,** *38*, 427-483.

279. Zahnle, K. J. Photochemistry of methane and the formation of hydrocyanic acid (HCN) in the earths early atmosphere. *J. Geophys. Res. Atmos.* **1986,** *91*, 2819-2834.

280. Sanchez, R. A.; Ferris, J. P.; Orgel, L. E. Studies in prebiotic synthesis. 2. Synthesis of purine precursors and amino acids from aqueous hydrogen cyanide. *J. Mol. Biol.* **1967,** *30*, 223-253.

281. Sanchez, R. A.; Ferris, J. P.; Orgel, L. E. Studies in prebiotic synthesis. 4. Conversion of 4-aminoimidazole-5-carbonitrile derivatives to purines. *J. Mol. Biol.* **1968,** *38*, 121-128.

282. Al-Azmi, A.; Elassar, A. Z. A.; Booth, B. L. The chemistry of diaminomaleonitrile and its utility in heterocyclic synthesis. *Tetrahedron* **2003,** *59*, 2749-2763.

283. Boulanger, E.; Anoop, A.; Nachtigallova, D.; Thiel, W.; Barbatti, M. Photochemical steps in the prebiotic synthesis of purine precursors from HCN. *Angew. Chem. Int. Ed.* **2013,** *52*, 8000-8003.

284. Barks, H. L.; Buckley, R.; Grieves, G. A.; Di Mauro, E.; Hud, N. V.; Orlando, T. M. Guanine, adenine, and hypoxanthine production in UV-irradiated formamide solutions: Relaxation of the requirements for prebiotic purine nucleobase formation. *ChemBioChem* **2010,** *11*, 1240-1243.

285. Nguyen, H. T.; Jeilani, Y. A.; Hung, H. M.; Nguyen, M. T. Radical pathways for the prebiotic formation of pyrimidine bases from formamide. *J. Phys. Chem. A* **2015,** *119*, 8871-8883.

286. Duvernay, F.; Trivella, A.; Borget, F.; Coussan, S.; Aycard, J. P.; Chiavassa, T. Matrix isolation fourier transform infrared study of photodecomposition of formimidic acid. *J. Phys. Chem. A* **2005,** *109*, 11155-11162.

287. Menor-Salvan, C.; Marin-Yaseli, M. R. A new route for the prebiotic synthesis of nucleobases and hydantoins in water/ice solutions involving the photochemistry of acetylene. *Chem. Eur. J.* **2013,** *19*, 6488-6497.

288. Schwartz, A. W.; Chittenden, G. J. F. Synthesis of uracil and thymine under simulated prebiotic conditions. *Biosystems* **1977,** *9*, 87-92.

289. Sanchez, R. A.; Orgel, L. E. Studies in prebiotic synthesis. 5. Synthesis and photo anomerization of pyrimidine nucleosides. *J. Mol. Biol.* **1970,** *47*, 531-543.

290. Powner, M. W.; Gerland, B.; Sutherland, J. D. Synthesis of activated pyrimidine ribonucleotides in prebiotically plausible conditions. *Nature* **2009,** *459*, 239-242.

291. Burton, A. S.; Stern, J. C.; Elsila, J. E.; Glavin, D. P.; Dworkin, J. P. Understanding prebiotic chemistry through the analysis of extraterrestrial amino acids and nucleobases in meteorites. *Chem. Soc. Rev.* **2012,** *41*, 5459-5472.

292. Rios, A. C.; Tor, Y. On the origin of the canonical nucleobases: An assessment of selection pressures across chemical and early biological evolution. *Isr. J. Chem.* **2013,** *53*, 469-483.

293. Serrano-Andres, L.; Merchan, M. Are the five natural DNA/RNA base monomers a good choice from natural selection? A photochemical perspective. *J. Photochem. Photobio. C* **2009,** *10*, 21-32.

294. Gustavsson, T.; Improta, R.; Markovitsi, D. DNA/RNA: Building blocks of life under UV irradiation. *J. Phys. Chem. Lett.* **2010,** *1*, 2025-2030.

295. Mulkidjanian, A. Y.; Cherepanov, D. A.; Galperin, M. Y. Survival of the fittest before the beginning of life: Selection of the first oligonucleotide-like polymers by UV light. *BMC Evol. Bio.* **2003,** *3*, 12.

296. Crespo-Hernandez, C. E.; Cohen, B.; Hare, P. M.; Kohler, B. Ultrafast excited-state dynamics in nucleic acids. *Chem. Rev.* **2004,** *104*, 1977-2019.

297. Switzer, C.; Moroney, S. E.; Benner, S. A. Enzymatic incorporation of a new base pair into DNA and RNA. *J. Am. Chem. Soc.* **1989,** *111*, 8322-8323.

298. Piccirilli, J. A.; Benner, S. A.; Krauch, T.; Moroney, S. E.; Benner, S. A. Enzymatic incorporation of a new base pair into DNA and RNA extends the genetic alphabet. *Nature* **1990,** *343*, 33-37.

299. Brister, M. M.; Pollum, M.; Crespo-Hernandez, C. E. Photochemical etiology of promising ancestors of the RNA nucleobases. *Phys. Chem. Chem. Phys.* **2016**.

300. Samoylova, E.; Lippert, H.; Ullrich, S.; Hertel, I. V.; Radloff, W.; Schultz, T. Dynamics of photoinduced processes in adenine and thymine base pairs. *J. Am. Chem. Soc.* **2005,** *127*, 1782-1786.

301. Bird, A. DNA methylation patterns and epigenetic memory. *Genes Dev.* **2002,** *16*, 6-21.

302. Li, H. Y.; Savage, T.; Obermoeller, R. D.; Kazianis, S.; Walter, R. B. Parental 5-methylcytosine methylation patterns are stable upon interspecies hybridization of xiphophorus (Teleostei : Poeciliidae) fish. *Comp. Biochem. Phys. B* **2002,** *133*, 581-595.

3. Experimental and Theoretical Methods:

3.1 Introduction:

The research described in the following chapters is largely centered on the aqueous phase photochemistry of α-keto acids, including product identification, mechanism development, and characterization of photo-initiated aggregation. Additional experimental and theoretical studies related to understanding more broadly the behavior of amphiphilic and hydrophobic species in aqueous solution were also conducted. These studies necessitated the use of a wide-range of both *in situ* and offline analytical techniques, including mass spectrometry, NMR and UV-vis spectroscopy, microscopy, and dynamic light scattering. Additionally, surface-sensitive measurements were conducted using a Langmuir trough. Theoretical molecular dynamics simulations were also conducted, complementing the experimental investigations. This chapter is designed to give a broad overview of the methods and techniques used throughout the thesis, as well as relevant data analysis procedures. Study-specific experimental details are given in the methods section of the corresponding chapters.

3.2 Materials:

The majority of molecules used in these studies were purchased commercially in the highest purity available. In many cases, however, this purity was not sufficient, and it was necessary to remove additional impurities before further use. Typically this was achieved by distilling compounds at reduced pressure (<1 Torr), using an apparatus similar to that shown in Figure 3.1. The compound of interest was heated gently until distillation was observed, using either a water bath or, in the case of longer-tailed species, a heating mantle. The distillate was collected in a flask that was cooled by liquid nitrogen once distillation was observed to have begun. Following distillation, the distillate was stored at

either 4 °C (pyruvic acid) or room temperature (fatty acid and alcohols) until used for further experiments. Distilled pyruvic acid forms oligomers spontaneously even in the dark.[1] These species grow in on the order of weeks, and, therefore, care was taken to only use pyruvic acid that had been distilled within one month of use.

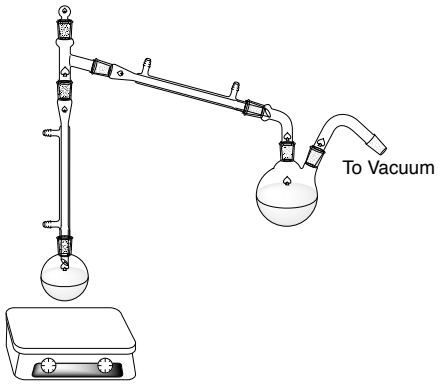

Figure 3.1. Schematic of the distillation apparatus used to purify compounds under study.

Pyruvic acid and 2-oxooctanoic acid (OOA) are commercially available, but the other alkyl α-keto acids under study (2-oxohexanoic acid (OHA), 2-oxodecanoic acid (ODA), and 2-oxododecanoic acid (ODDA)), require custom synthesis. All three species were synthesized and purified by Dr. Haishen Yang in the lab of Dr. Garret Miyake at CU Boulder. Details of the synthesis for each molecule are given in Appendix E, but a brief overview of the procedure is provided here.[2]

A solution of Grignard reagent, prepared from the appropriate 1-bromoalkane and the suspension of magnesium in THF, was added dropwise under N_2 atmosphere to a cold (–78 °C) solution of diethyloxalate in THF. After the addition was complete, the reaction mixture was stirred at –78 °C for at least an additional hour. The reaction was quenched with 2 N HCl, and the aqueous layer was extracted with either ether or hexanes. The combined organic layers were washed with saturated NaCl, dried over $MgSO_4$, and evaporated. The crude product was purified either by distillation under reduced pressure to give a colorless oil (OHA) or by recrystallization in hexanes to give a white solid (ODA and ODDA).

In some cases, additional properties of α-keto acids were characterized, including the determination of effective pK_a values for pyruvic acid and OOA. These values were determined by titration with NaOH. Acid dissociation constant values were determined following the general fitting routine given in Harris's *Quantitative Chemical Analysis* textbook,[3] modified to account for changing ionic strength as in Papanastasiou and Ziogas 1995.[4] A detailed description of the iterative fitting procedure is included Appendix F.

3.3 Photochemical Experiments:

The photochemical experiments conducted throughout this thesis are designed to provide insight into the environmental chemical processes of the both the modern and early Earth. Therefore, it is essential to use a light source whose spectral output closely resembles that of the Sun. For this reason, a continuous, high pressure 450 W xenon arc lamp (Newport) was used for all photochemical experiments conducted in the Vaida laboratory. Xe arc lamps are common solar simulators as their spectral output closely matches that of the Sun because both have similar black body temperatures (Figure 3.2). The early Sun was ~25% less luminous than the modern Sun, but it had a relatively larger output of UV radiation.[5] For our purposes, the flux provided by a Xe arc lamp can be used to model the spectral output of the Sun both today and ~4 Gya ago.

The actinic flux that reaches the surface of the modern Earth has been filtered by the stratospheric ozone layer, which enforces a high-energy cut-off of UV light of ~290 nm. The output of a xenon arc lamp can be similarly filtered using a Pyrex® lens. However, far more high energy UV light would have reached the surface of the early Earth during the period of chemical evolution when very little oxygen was present in the atmosphere.[6] All photochemical experiments were run using the unfiltered Xe arc lamp as a light source unless otherwise specified.

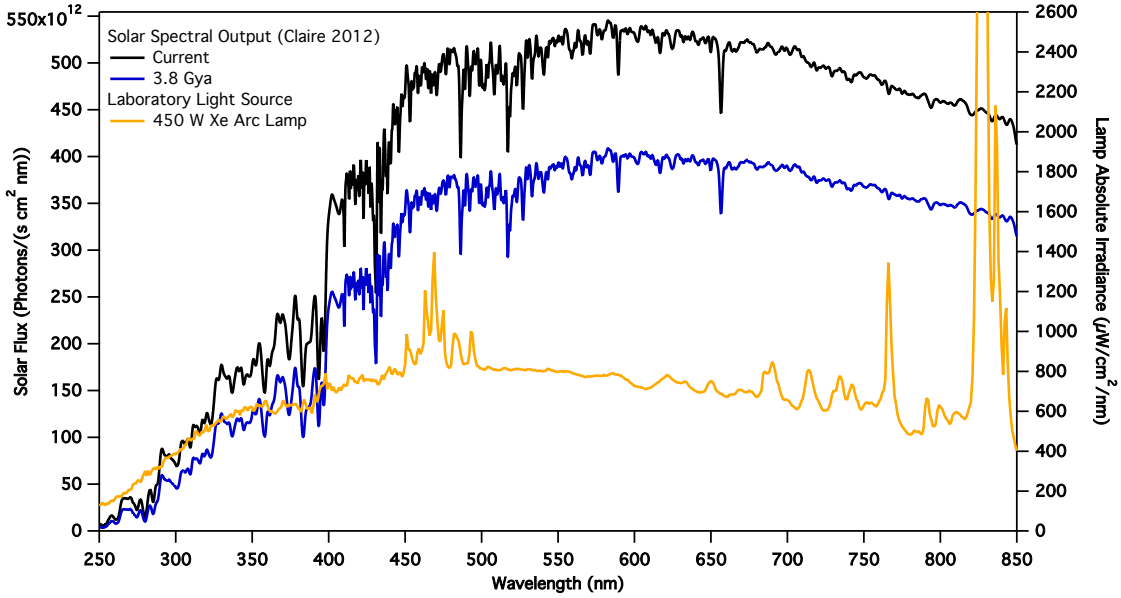

Figure 3.2. Modeled spectral output from the modern (black) and early Sun (3.8 Gya, blue) from Claire et al. 2012[5] compared to the flux of the Xe arc lamp used in the photochemical experiments.

Solutions were photolyzed in a glass reactor equipped with a quartz window to allow the transmission of UV light (Figure 3.3). The reactor was placed in a temperature-controlled water bath that was held at either 4 or 20 °C. The reactor contains two ports, one of which was used to purge solutions with either nitrogen or oxygen, and the other of which was used to remove aliquots as needed during the course of photolysis. When purging with gas, a slight positive pressure was maintained in the reactor to prevent contamination from air, and excess pressure was vented to the atmosphere.

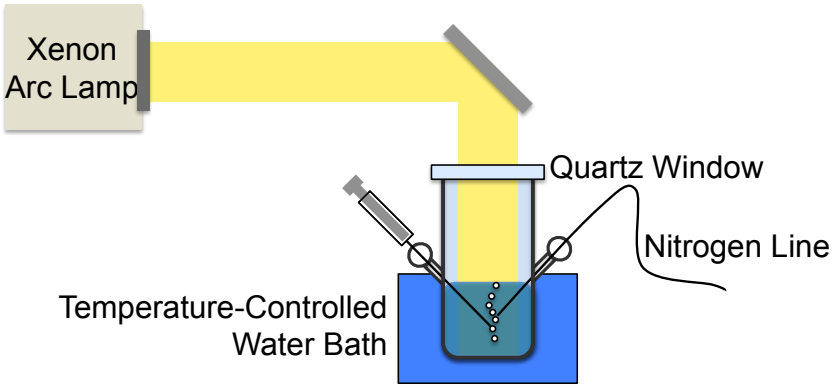

Figure 3.3. Schematic of the reactor used for aqueous photochemical experiments. This figure was adapted from a similar diagram by Allison Reed Harris.[7]

The majority of photochemical experiments were conducted with this Xe arc lamp and analysis of the photochemical products was conducted offline for post-photolysis samples and compared to their pre-photolysis controls. In some cases aliquots were taken at intermediate time-points to monitor the progression of the reaction. These offline analytical techniques are discussed below. However, online *in situ* analysis of the dynamic light scattering of solutions of alkyl α-keto acids was also conducted, obtaining time-resolved information about the formation of aggregates. Because of the experimental requirements, a different light source, the Energetiq EQ-99 Laser-Driven Light Source (LDLS), was used to induce photochemistry. The LDLS uses a continuous wave laser to heat a xenon plasma. The spectral output is similar to that of a Xe arc lamp but is more stable. The EQ-99 power output is significantly lower than that of the 450 W Xe arc lamp, but is still capable of driving observable photochemistry albeit on a slower timescale.

The LDLS was equipped with a U330 Filter (Edmund Optics). This filter allows transmission of UV light from ~230 nm to ~400 nm but removes visible light from ~400 nm to ~660 nm, as well as any higher energy UV light. Figure 3.4 shows both the filtered and unfiltered spectral output of the LDLS that was used experimentally to illuminate the cuvette.

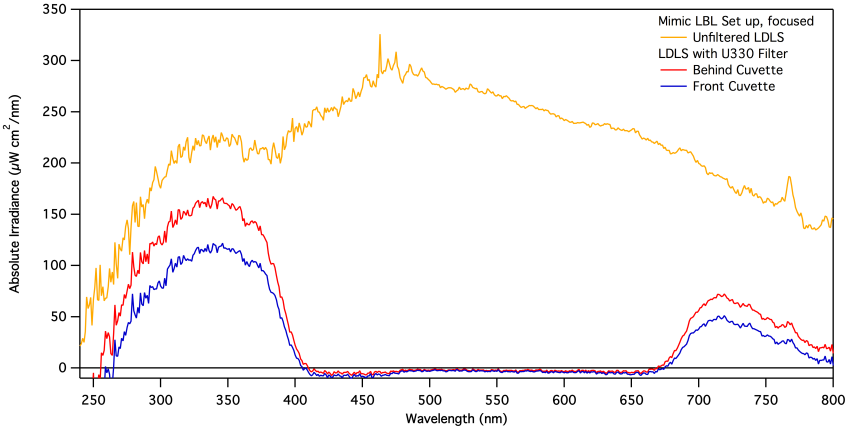

Figure 3.4. Spectral output of the Energetiq EQ-99 laser driven light source unfiltered (gold) and with the U330 filter, measured in front of (blue) and behind (red) the cuvette position.

3.4 Mass Spectrometry:

The workhorse analytical technique used throughout this thesis is high-resolution mass spectrometry (MS) because of its unique ability to readily identify individual components of complex mixtures of species.[8] Mass spectrometry takes advantage of the behavior of charged species in the presences of either an electric or magnetic field to separate species by their mass to charge ratio (m/z). A multitude of ionization techniques can be used to generate these ions, and are generally characterized as either hard or soft ionization processes. Hard ionization processes impart more energy to the system and generally result in more fragmentation of species. Soft ionization techniques, on the other hand, are less harsh, impart less energy, and result in less fragmentation. Electrospray ionization (ESI) is one such soft ionization technique that is particularly useful for the analysis of organic molecules. Liquid is drawn into a capillary and a voltage is applied across this liquid, aerosolizing it. The aerosol then rapidly evaporates, releasing charged species into the gas phase that can then be separated by a mass analyzer and subsequently detected. ESI can be used to generate either positively or negatively charged ions. Negative mode ESI was used throughout the experiments described here because the acidic nature of the species under study makes them more amenable to deprotonation than protonation.

Because of the nature of the ESI process, certain species are ionized more readily than others in solution. Namely, more surface-active species are often preferentially ionized to comparable molecules that are less hydrophobic. Additionally, the functionalization or other properties of a molecule can control its ionization efficiency. In mixtures, molecules that have a lower concentration but a better ionization efficiency may be observed more intensely than species that are less easily ionized. In some cases, molecules may not be ionized at all, such as fatty alcohols, which do not deprotonate. For these reasons, the MS analyses conducted here were not designed to be absolutely quantitative, and intensities of

analytes are used for relative comparisons only. It is also important to note that the absence of detection of a species cannot be used to say that it is not present in solution.

All high-resolution ESI$^-$ MS experiments were performed on a Waters Synapt G2 HDMS mass spectrometer in the Central Analytical Mass Spectrometry Facility at CU Boulder under the guidance of Dr. Jeremy Balsbaugh. Instrument parameters remained constant, and were as follows: analyzer, resolution mode; capillary voltage, 1.5 kV; source temperature, 80 °C; sampling cone, 30 V; extraction cone, 5 V; source gas flow, 0.00 mL/min; desolvation temperature, 150 °C; cone gas flow, 0.0 L/h; desolvation gas flow, 500.0 L/h. These instrument parameters were deliberately chosen to to minimize the potential for in-source fragmentation and reactions due to ionization.[9]

High-resolution MS is capable of measuring the m/z of analytes very precisely, allowing for the determination of exact elemental compositions of a species based on the differing mass defect of atoms of different elements. Accurate mass measurements greatly reduce the number of possible molecular formulas for a given analyte, but, in some cases, more than one combination of elements is plausible. For this reason, the chemical formula of a given analyte was assigned based both on the agreement of m/z of the main ion of a species with the theoretical m/z (mass difference typically < 10 ppm), as well as the first isotope. Additionally, the experimental ratio of the first isotope to the main ion was compared to the expected natural abundance.

A conservative intensity threshold of 10^4 counts was applied for analyte identification to avoid incorrect ion assignments to noise peaks; the noise threshold is about 1000 counts. For comparative purposes, categories of signal intensity are defined as follows: “strong” ions display intensities greater than 10^6 counts, “medium” ions display intensities greater than 10^5 counts, and “weak” ions display intensities greater that 10^4 counts for the monoisotopic ion in all cases. It is important to note that these intensity categories do not necessarily

correlate directly to absolute analyte concentrations and are used for relative comparisons only.

3.5 Spectroscopy:

A number of spectroscopic techniques were used to complement the mass spectrometry analysis. Spectroscopy uses the interaction of electromagnetic radiation with matter to probe the fundamental characteristics of that matter. For molecules, radiation of varying wavelengths can be used to determine the electronic, vibrational, and rotational energy levels of a given species. The quantized energy levels within a molecule ensure that only radiation of a specific wavelength will be able to promote the transition from one energy level to another. Because the spacing of energy levels is characteristic of molecular structure, a spectrum of these absorptions (or, conversely, emissions) can be used to deduce the nature of the species being analyzed.

3.5.1 UV-Visible Spectroscopy

Light in the ultraviolet and visible region typically will promote electronic transitions in a molecule. The amount of energy required to promote a molecule from its ground excited state to an excited state is largely governed by the molecule's functionalization.[10] As for instance, the degree of unsaturation of the molecule is increased by the addition of more double bonds, observed electronic transitions will shift to the red. This shift is compounded if the conjugation of a molecule also increases. Similarly, increasing the oxidation of the functional group present for a given molecule (e.g. alcohol < carboxylic acid < α-keto acid) will lower the energy required to promote it to an excited state.

The selection rules that govern the transition from ground to excited electronic states are less strict for real molecules because of anharmonicity. However, generally transitions from a state of one multiplicity to another that require a spin flip are forbidden, e.g. if the ground state is a singlet, direct excitation to a triplet excited state is spin forbidden.[11] This

means then that, while the reactive state of the α-keto acids in aqueous solutions is the first excited triple state, (T_1, $^3(n, \pi^*)$), the initial excitation that promotes photochemistry and that can be monitored by UV-vis spectroscopy is, instead, to the first excited singlet state (S_1, $^1(n, \pi^*)$). The S_1 state is higher in energy than the T_1 state, and the molecule transitions to the T_1 state by internal conversion and intersystem crossing.

UV-vis spectroscopy was used primarily to characterize the absorption of organic species in solution, and, in some cases to determine the composition of a mixture of species in solution. It was used to track the photochemical decay α-keto acids in solution, as well as the corresponding growth of photochemical products. Additionally, UV-vis spectroscopy is sensitive to light scattering due to the presence of aggregates in solution and was employed to monitor solutions for aggregates. All UV-vis experiments were conducted using a Varian (Agilent) Cary 5000 spectrometer with a 0.1 s average time, 0.5 nm data interval, and a 0.5 nm spectral bandwidth, unless otherwise specified.

3.5.2 Nuclear Magnetic Resonance Spectroscopy:

Nuclear magnetic resonance spectroscopy (NMR) uses low energy radio waves to induce the orientation of atomic nuclei that are held within a magnetic field, which breaks the degeneracy of the nuclear spin states. Only atoms with an overall non-zero spin are visible to this technique because their magnetic moment is also non-zero. However, odd isotopes (e.g. ^{1}H and ^{13}C) will interact with and absorb this radiation, and the specific frequencies at which this occurs can be used as a detailed probe of the chemical environment of that atom. Because of this NMR is the main modern analytical tool used to determine molecular structure.

^{1}H NMR was used throughout these experiments and was most often conducted in aqueous solution. This requires water suppression techniques be employed to prevent signal from the water swamping that of the molecules of interest. All one-dimensional NMR

spectra were obtained by either Russell Perkins or Dr. Rich Shoemaker, using a Varian INOVA-500 NMR spectrometer operating at 23 °C and 499.60 MHz for ^{1}H detection. To perform experiments in aqueous solution, an optimized WET solvent suppression pulse sequence was used to eliminate >99% of the H_2O signal.[12]

Additional two-dimensional NMR experiments were performed and analyzed by Dr. Rich Shoemaker. In particular, diffusion-ordered spectroscopy (DOSY) NMR was used to characterize the species present in aqueous solutions of alkyl α-keto acids both before and after photolysis, including aggregates. High resolution 2D-DOSY NMR was performed as for the one-dimensional aqueous solutions, but with the addition of the convection and non-uniform-gradient compensated stimulated PFG echo pulse sequence that is available in the VNMRJ 3.2A instrument (Agilent Technologies, Inc.). The data analysis was performed using the VNMRJ software, including non-uniform gradient compensation, and multi-component fitting of the DOSY decay curves.[13, 14]

3.6 Microscopy:

In addition to analytical techniques used to determine the molecular products formed photochemically, several tools were used to characterize the formation of aggregates in post-photolysis solutions. These included direct imaging of the aggregates via microscopy.

3.6.1 Confocal Optical Microscopy

Both phase contrast and fluorescence confocal optical microscopies were employed. Confocal microscopy uses a lens to focus the light used to illuminate a sample into a focal plane.[15] The light is then passed through an aperture to eliminate contributions from any light outside this focal plane before detection. This increases the resolution of the microscope compared to wide-field techniques, including vertical resolution that is achieved by moving the height of the focal plane within the sample.

Phase contrast microscopy uses monochromatic polarized light and monitors changes in

refractive index between the solvent and structures of interest. The resultant shifts in the phase of the light are shown as differences in the brightness of the image. It can be used to determine the shape of aggregates in solution.

Fluorescence microscopy can also be used to visualize aggregates in solution but requires the addition of a dye. This stain acts as a fluorophore that is excited by a laser of the correct wavelength. Due to the Stokes shift, the light that is emitted from the fluorophore is longer in wavelength. Monitoring the emission of a fluorophore rather than its absorption allows for more sensitivity because there is comparatively little background signal. Many dyes can be used in fluorescence microscopy. We chose to use the lipophilic Rhodamine 6G that preferentially partitions to and binds with membranes in solution.[16] It is possible also to instead encapsulate a hydrophilic dye, such as HPTS, within vesicles. The small aggregates generated during photolysis of alkyl α-keto acids are on the order of 200 nm in diameter, which is close to the diffraction limit for optical microscopy. Additionally these small particles diffuse quite rapidly, which limits the utility of these measurements. All optical microscopy images were taken using the Nikon A1R confocal microscope in the BioFrontiers Advanced Light Microscopy Core with assistance from Dr. Kevin Dean and Dr. Joe Dragavon.

3.6.2 Transmission Electron Microscopy:

The resolution of electron microscopy is not restricted by the diffraction limit of light like optical microscopy, and, therefore, it can be used to investigate smaller particles in solution. Transmission electron microscopy (TEM) is conducted by "illuminating" a sample with a beam of electrons rather than photons. Differences in the absorption of electrons with the sample are used to generate an image. TEM requires that samples be affixed on a grid prior to imaging, and this can be done either through flash freezing or by blotting on a grid, usually followed by the addition of a stain. Both cryogenic (cryo-TEM) and negative

stain TEM methods were used. All electron microscope images were obtained at the University of Colorado, Boulder EM Services Core Facility in the MCDB Department, with the technical assistance of facility staff.

Negative stain TEM images were obtained as follows. 6-8µl of sample was applied to a glow-discharged, carbon coated TEM grid and left to incubate for ~2 min. The sample was then blotted with filter paper to a thin layer, so all sample attached to the grid remained hydrated, followed by a wash in a droplet of water, and then blotted again to a thin layer of liquid. 5µl of stain was then applied to sample for ~15 sec, then blotted off; this step was then repeated. The stain used was a commercially available product called "UranylLess," which is pH neutral and non-radioactive. Negative stained grids were then viewed and imaged on an FEI Tecnai T12 Spirit Biotwin (LaB6) 120kV TEM.

For cryo-TEM, 4 µl of sample (at room temperature) was applied to a lacey carbon coated TEM grid in the humidified chamber of an FEI Vitrobot Mark IV plunge freezer, blotted away for ~4 to 5 seconds (leaving a thin film of hydrated sample on the grid), and then plunged into a liquid nitrogen (LN_2) chilled vessel of liquid ethane. The thin sample layer coupled with fast heat transfer rate of liquid ethane allows the sample solution to become vitrified, or frozen without the formation of crystalline ice. Grids were then stored in LN_2 until transferred to a cryoTEM sample rod (Gatan model 626), maintaining a temperature below -170º C while in the vacuum of the TEM. Samples were imaged on an FEI Tecnai F20 FEG-TEM operating at 200kV, and imaged with a Gatan US4000 CCD. Total electron dose was limited to ~30 electrons/square-Å per image. Cryo-TEM is a less sensitive technique than negative-stain TEM, and, therefore, analyzed samples were concentrated by the removing of water via rotary evaporation to a final concentration roughly six times that of the original sample to ensure enough aggregates were visible within the TEM grid.

3.7 Dynamic Light Scattering:

In addition to direct imaging, indirect methods were also used to characterize the size of the photochemically generated aggregates. Chief among these was dynamic light scattering (DLS). Solutions that contain particles scatter light. When a beam of monochromatic light is used to illuminate such a solution, the scattering caused by particles causes fluctuations in the intensity of the scattered light due to constructive and destructive interference. The intensity of this scattered light can be monitored at a known scattering angle, typically 90°, and used to extract the diffusion constant of the particles in solution.[17] This is possible because particles in solution undergo Brownian motion, and the rate of diffusion is dependent on the size of the particles.

The intensity fluctuations observed in the scattered light are, over long time scales, random, but over short timescales these fluctuations are correlated to each other.[18] That is, the scattering light intensity at any given time is due to a particular arrangement of particles in solution. The particles move randomly, but within a given time step they can only travel a finite distance from their starting position. Therefore, the scattering at one time-point is related to the scattering at the next time-point because the arrangement of species in solution at time-point 2 has evolved from the arrangement at time-point 1. The arrangement at time-point 3 is also correlated with that from time-point 1, but this dependence is weaker. By some time-point N, the arrangement of particles in solution no longer has any correlation with the arrangement at time-point 1. Therefore, it is possible to fit intensity of scattered light to an auto-correlation function, and the timescale of the decay of the function is related to the diffusion constant of particles in solution. As particles diffuse faster in solution, the auto-correlation function will decay faster.

For solutions of monodisperse aggregates, the correlation function can be fit to a single exponential of the form,

$$C = e^{-2\Gamma\tau},$$

where τ is the delay time and Γ is the decay constant. Γ can be directly related to the diffusion constant, D, of any aggregates in solution,

$$\Gamma = Dq^2 = D\left(\frac{4\pi n}{\lambda}\sin\frac{\Theta}{2}\right)^2,$$

where n is the refractive index of the solution, λ is the wavelength of the laser, and θ is the scattering angle. The diffusion constant can then be related to the radius of the particle, R, using the Stokes-Einstein equation,

$$D = \frac{k_B T}{6\pi\eta R},$$

where η is the solvent viscosity and T is the temperature of the solution. In this manner, experimental auto-correlation functions at each time-point were fit with a single-adjustable parameter, particle radius, R, and error in radius is reported as the standard deviation of the fit.

DLS measurements were obtained at CU Boulder in the Biochemistry Shared Instrument Core with aid from Dr. Annette Erbse using a Titan DynaPro instrument (Wyatt Technology). Because of the sensitivity of this instrument, post-photolysis solutions were diluted 10-fold before analysis. All measurements were obtained at 20 °C.

3.7.1 Time-Resolved, *In Situ* Dynamic Light Scattering

In situ DLS measurements of the scattering of solutions of α-keto acids during photolysis were conducted in the laboratory of Dr. Kevin Wilson at Lawrence Berkeley National Lab. This allowed for time-resolved measurements of the formation of aggregates over the course of photolysis. The photochemistry in these experiments was conducted using the Energetiq LDLS described above as the photolysis source and was coupled to the DLS apparatus, as shown in Figure 3.5.

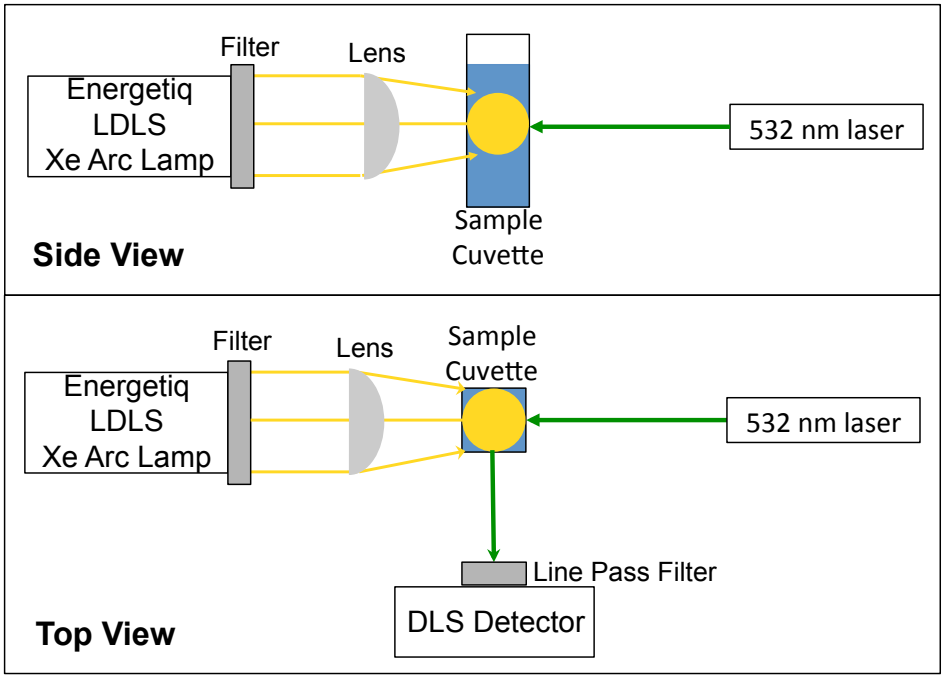

Figure 3.5. Schematic of experimental set-up used in the in situ *time-resolved dynamic light scattering measurements conducted at LBL, including both a side-view showing the illumination of the cuvette, as well as a top-down view of the scattering detector.*

The cuvette was illuminated in roughly the vertical center using slightly focused light from the LDLS with a spot size roughly the diameter of the cuvette (~1 cm). Scattering was monitored within the illuminated portion of the cuvette, unless otherwise specified. Light scattering from either a 532 nm 4.5 mW diode laser (Thorlabs) or a 632 nm 4 mW HeNe laser (Melles Griot) was monitored at 90° from illumination by a PMT detector. The PMT was equipped with a line pass filter of appropriate wavelength to ensure only scattering from the laser light was detected, and the LDLS was equipped with a UV330 filter remove its output of both 532 nm and 632 nm light. The detector was connected to an ALV-6010 / 200 Multiple Tau Digital Correlator, and this software was used to extract scattering information, including counts and auto-correlation functions. The scattering data were fit using a Python script adapted from Dr. James Davies.

3.8 Langmuir Trough

The phase behavior of amphiphilic, surface-active molecules was monitored using

surface-sensitive techniques, namely a Langmuir trough. Langmuir troughs are deceptively simple instruments that provide a means of studying monolayer films of organic material on a liquid subphase, usually by measurement of changes in the surface tension.[19] Organic molecules, particularly amphiphiles with a hydrophilic head group and a hydrophobic alkyl tail, are known to partition to the air-water interface and reduce the surface tension of water. Studies of this phenomenon date back centuries,[20] when, for instance, Benjamin Franklin noted the "stilling of waves" in a rough ocean when oil was poured over the side of a ship, and continued to experiment on this system under the more controlled experimental conditions afforded by ponds and lakes.[21] Agnes Pockel in the mid-nineteenth century observed the changes caused by the addition of soap to water while doing dishes and developed the first trough used to study surface tension of organics on water.[22] Irving Langmuir modified the Pockels trough to a version similar to that used today. [23] Katherine Blodgett also developed techniques that allowed for the transfer of films to a solid support.[24] Troughs equipped with a dipper are referred to as Langmuir-Blodgett troughs, while those without are simply Langmuir troughs.

Langmuir troughs are typically simple PTFE (Teflon) dishes that have controllable barriers that can be opened or closed, changing the surface area of the trough. A number of tools can be used to measure changes in surface tension, but we use a Wilhelmy microbalance. Detailed descriptions of how such balances work have been given elsewhere,[25, 26] but a brief outline follows. Surface tension, γ, is a measure of force per unit length or energy per unit area. It can useful to consider changes in surface tension as changes in the amount of energy that must be supplied to increase surface area. Therefore, when a hydrophilic probe with a low contact angle with water is placed in an aqueous solution, there is a net energy cost to create new surface area around the probe that results in a restoring force that pulls the probe into the solution. The resultant change in height of

the probe, or, equivalently the force required to keep the probe at a constant height, can be used to extract a measurement of surface tension. In practice, it is more convenient to measure surface pressure (π), or the deviation of surface tension from that of pure water, $\pi = \gamma_{H2O} - \gamma$.

Langmuir troughs can be used to measure the surface-partitioning effects of both soluble and insoluble surfactants. Soluble surfactants are usually dissolved in the aqueous subphase, and changes in surface pressure are monitored as the species partition to the surface. The surface thermodynamics of this behavior are often quantified using the Gibbs adsorption isotherm formalism, which can be used to determine the surface excess concentration of the species.[27, 28]

On the other hand, insoluble surfactants like those under study here are generally deposited on the surface of the aqueous subphase, using a spreading solvent, such as chloroform, that is allowed to evaporate, leaving a monolayer film. The phase behavior of this film can be obtained through compression isotherms, where the barriers of the trough are closed, inducing phase transitions as the film is compressed.[19, 29] A typical compression isotherm of stearic acid is shown in Figure 3.6.

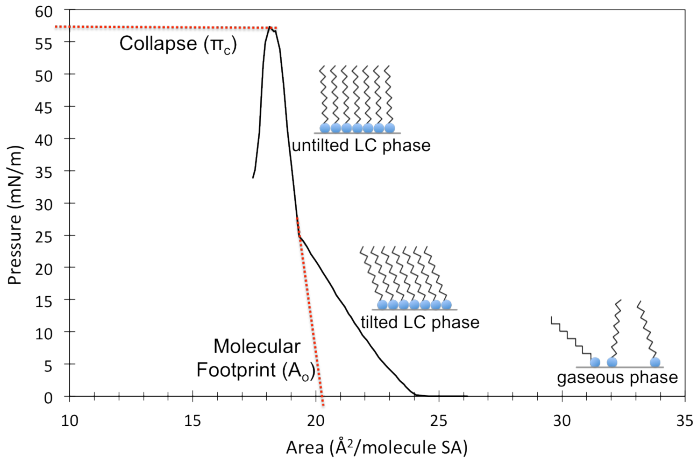

Figure 3.6. Representative compression isotherm of stearic acid deposited on water, showing the two-dimensional phases of the film, as well as the molecular footprint and collapse pressure. This figure is reproduced from the thesis of Elizabeth Griffith.[25]

Long-tailed fatty acids, such as stearic acid, transition from a two-dimensional gas phase to a tilted-condensed phase before transitioning to the more ordered untilted-condensed phase. Surface pressure continues to increase with further compression until the film is no longer stable and collapses into three-dimensional structures.[30] The footprint of a molecule, or the average mean molecular area that it takes up within the film, can also be determined by extrapolation from the slope of the surface pressure change.

3.9 Molecular Dynamics Simulations:

In addition to the experimental techniques outlined above, theoretical molecular dynamics (MD) simulations were also conducted. Classical MD is a computational method that can be used to investigate physical behavior of species on a molecular level. These simulations are realized by initialization of a system of particles or atoms defined by empirical potentials. Trajectories for these species are then calculated by solving Newton's equations of motion numerically over a series of time-steps within a given statistical mechanical ensemble. All MD simulations were conducted using LAMMPS[31] and were run on the Janus and Summit supercomputers at CU. Details of the specific simulations are given in Chapter 11.

3.10 Bibliography:

1. Perkins, R. J.; Shoemaker, R. K.; Carpenter, B. K.; Vaida, V. Chemical equilibria and kinetics in aqueous solutions of zymonic acid. *J. Phys. Chem. A* **2016,** *120*, 10096-10107.

2. Rapf, R. J.; Perkins, R. J.; Yang, H.; Miyake, G. M.; Carpenter, B. K.; Vaida, V. Photochemical synthesis of oligomeric amphiphiles from alkyl oxoacids in aqueous environments. *J. Am. Chem. Soc.* **2017,** *139*, 6946–6959.

3. Harris, D. C., *Quantitative chemical analysis*. 7th ed.; W.H. Freeman and Company: New York, 2007.

4. Papanastasiou, G.; Ziogas, I. Simultaneous determination of equivalence volumes and acid dissociation constants from potentiometric titration data. *Talanta* **1995,** *42*, 827-836.

5. Claire, M. W.; Sheets, J.; Cohen, M.; Ribas, I.; Meadows, V. S.; Catling, D. C. The evolution of solar flux from 0.1 nm to 160 μm: Quantitative estimates for planetary studies. *Astrophys. J.* **2012,** *757*, 95.

6. Ranjan, S.; Sasselov, D. D. Influence of the UV environment on the synthesis of prebiotic molecules. *Astrobio.* **2016,** *16*, 68-88.

7. Reed Harris, A. E. A kinetic and mechanistic study of the photochemistry of pyruvic acid: Implications for the atmosphere. University of Colorado Boulder, 2017.

8. Cech, N. B.; Enke, C. G. Practical implications of some recent studies in electrospray ionization fundamentals. *Mass Spectrom. Rev.* **2001,** *20*, 362-387.

9. Rapf, R. J.; Perkins, R. J.; Carpenter, B. K.; Vaida, V. Mechanistic description of photochemical oligomer formation from aqueous pyruvic acid. *J. Phys. Chem. A* **2017,** *121*, 4272–4282.

10. Skoog, D. A.; Holler, F. J.; Mieman, T. A., *Principles of instrumental analysis*. 5th ed.; Brooks/Cole: United States, 1998.

11. Demtröder, W., *Molecular physics: Theoretical principles and experimental methods*. Blackwell Science: Oxford, 2005.

12. Ogg, R. J.; Kingsley, R.; Taylor, J. S. WET, a T 1-and B 1-insensitive water-suppression method for in vivo localized ^{1}H NMR spectroscopy. *J. Magn. Reson., Ser B* **1994,** *104*, 1-10.

13. Nilsson, M.; Connell, M. A.; Davis, A. L.; Morris, G. A. Biexponential fitting of diffusion-ordered NMR data: Practicalities and limitations. *Anal. Chem.* **2006,** *78*, 3040-3045.

14. Nilsson, M.; Morris, G. A. Improved DECRA processing of DOSY data: Correcting for non-uniform field gradients. *Magn. Reson. Chem.* **2007,** *45*, 656-660.

15. Price, R. L.; Jerome, W. G. J., *Basic confocal microscopy*. Springer Science & Business Media: 2011.

16. Griffith, E. C.; Rapf, R. J.; Shoemaker, R. K.; Carpenter, B. K.; Vaida, V. Photoinitiated synthesis of self-assembled vesicles. *J. Am. Chem. Soc.* **2014,** *136*, 3784-3787.

17. Clark, N. A.; Lunacek, J. H.; Benedek, G. B. A study of Brownian motion using light scattering. *Am. J. Phys.* **1970,** *38*, 575-585.

18. Gillespie, D. T. Fluctuation and dissipation in Brownian motion. *Am. J. Phys.* **1993,** *61*, 1077-1083.

19. Kaganer, V. M.; Mohwald, H.; Dutta, P. Structure and phase transitions in Langmuir monolayers. *Rev. Mod. Phys.* **1999,** *71*, 779-819.

20. Greene, J. E. Tracing the 4000 year history of organic thin films: From monolayers on liquids to multilayers on solids. *Appl. Phys. Rev.* **2015,** *2*, 011101.

21. Wang, D.-N.; Stieglitz, H.; Marden, J.; Tamm, Lukas K. Benjamin Franklin, Philadelphia's favorite son, was a membrane biophysicist. *Biophys. J.* **2013,** *104*, 287-291.

22. Pockels, A. On the relative contamination of the water-surface by equal quantities of different substances. *Nature* **1892,** *46*, 418-419.

23. Langmuir, I. The constitution and fundamental properties of solids and liquids. II. Liquids. *J. Am. Chem. Soc.* **1917,** *39*, 1848-1906.

24. Blodgett, K. B. Films built by depositing successive monomolecular layers on a solid surface. *J. Am. Chem. Soc.* **1935,** *57*, 1007-1022.

25. Griffith, E. C. Chemical and physical changes unique in and on water: Implications for life and its origins. University of Colorado, Boulder, 2014.

26. Perkins, R. J. Beyond hydrophobicity: Aqueous interfaces, interactions, and reactions. University of Colorado Boulder, 2017.

27. Gibbs, J. W.; Bumstead, H. A., *Thermodynamics*. Longmans, Green and Company: 1906.

28. Guggenheim, E.; Adam, N. The thermodynamics of adsorption at the surface of solutions. *Proc. R. Soc. London, Ser. A* **1933,** *139*, 218-236.

29. Knobler, C. M.; Desai, R. C. Phase transitions in monolayers. *Annu. Rev. Phys. Chem.* **1992,** *43*, 207-236.

30. Smith, R. D.; Berg, J. C. The collapse of surfactant monolayers at the air—water interface. *J. Colloid Interface Sci.* **1980,** *74*, 273-286.

31. Plimpton, S. Fast parallel algorithms for short-range molecular dynamics. *J. Comp. Phys.* **1995,** *117*, 1-19, lammps.sandia.gov.

4. Mechanistic Description of Photochemical Oligomer Formation from Aqueous Pyruvic Acid*

4.1 Introduction:

Atmospheric aerosols are known to contribute to pollution-related smog and haze, affecting visibility and human health;[2, 3] in addition, they have considerable influence over the global radiative budget.[4-11] The impact of atmospheric aerosols on radiative forcing is currently the largest source of uncertainty in climate models, with significant contributions to the accumulated error occurring from the effort to quantify secondary organic aerosol (SOA).[12] SOA, particles generated in the atmosphere through the oxidation of volatile organic compounds (VOCs), are the major contributor to aerosol mass in remote areas.[9, 13, 14] Recent work suggests that oligomers formed from aqueous phase photochemistry of small organics may contribute significantly to the formation and development of SOA.[9, 10, 15-23] Therefore, the generation of such molecular complexity via multiphase chemistry is critical in the understanding of the formation of SOA.

The chemistry governing the formation of SOA from small organics is inherently complex, involving interwoven networks of reactions between many species. As we show, even a single, simple three-carbon molecule can yield surprisingly rich chemistry. Here we examine the aqueous phase photochemistry of a model species, pyruvic acid, under acidic, anaerobic conditions, suggesting a new identification and mechanistic pathway for observed oligomeric species. By developing mechanistically the potential reactive pathways for aqueous pyruvic acid, we may add to the understanding of its possible photochemical fates in the natural environment.

---

* This work was reproduced in part with permission from Rapf, R.J.; Perkins, R.J.; Carpenter, B.K.; Vaida, V. Mechanistic description of photochemical oligomer formation from aqueous pyruvic acid. *Journal Physical Chemistry A*, *121*, 4272–4282, 2017. Copyright 2017 American Chemical Society.[1]

Pyruvic acid, a key oxidation product of isoprene in the environment,[24-26] is found in both the gas and aqueous phases in the atmosphere.[24, 27-35] The simplest of the α-keto acids, pyruvic acid has also been used as a proxy for atmospheric α-dicarbonyls.[25, 26, 29, 36] Pyruvic acid absorbs light in the near-UV from the solar photon flux reaching the surface of the Earth and is oxidized relatively slowly by H_2O_2 and the hydroxyl radical (OH).[37-41] Consequently, the main atmospheric sink for pyruvic acid is direct photolysis; in the aqueous phase, this photochemistry has been linked to oligomer formation and the production of SOA.[22, 38, 42-46]

While a seemingly simple, three-carbon molecule, pyruvic acid's reactivity is extremely diverse and dependent on reaction conditions. Its chemistry spans a wide variety of processes and environmental conditions, including gas and aqueous photochemistry,[38, 43-61] multiphase photochemistry,[62] oxidation by H_2O_2 and hydroxyl radicals,[26, 37, 39-41] thermal decomposition,[63-65] and multiphoton pyrolysis.[66] Pyruvic acid is also known to spontaneously oligomerize in aqueous solution or as a pure liquid, even in the dark, forming a variety dimer species that include zymonic acid and parapyruvic acid.[67]

The photochemical pathways available to pyruvic acid are strongly phase dependent. In the gas phase, absorption of a UV photon (λ_{max} ~350 nm) promotes ground state pyruvic acid to the first excited singlet state (S_1, $^1(n, \pi^*)$), whereupon it decomposes, forming CO_2 and acetaldehyde, with additional minor products.[37, 49, 55, 56, 58-60, 68, 69] However, the species produced by this gas phase photochemistry can be affected by changing the buffer gas, total pressure, and composition.[59] Different photochemical pathways become accessible in the aqueous phase than in gas phase[42, 44-46, 57, 61] because interactions with water affect pyruvic acid's electronic structure, changing its photophysical and photochemical mechanisms. The λ_{max} of the S_1, $^1(n, \pi^*)$, state shifts to the blue (λ_{max} ~320 nm) such that, following excitation, intersystem crossing and internal conversion to the T_1, $^3(n, \pi^*)$ state occurs, subsequently

generating organic radicals. These radicals then react further, often recombining to generate oligomeric species.

Recent work on the aqueous photochemistry of pyruvic acid has exposed its extreme sensitivity to the environment: the rate of decomposition and resulting products are dependent on both the concentration of pyruvic acid and on the atmospheric composition.[38, 62] This sensitivity to reaction conditions likely explains some of the discrepancies in the literature about some minor photoproducts;[38, 42-46, 70, 71] however, there is broad agreement that the major aqueous photochemical pathways generate more complex oligomeric species,[38, 43, 44] including covalently bonded dimers and trimers[72] of pyruvic acid. In this chapter, we structurally characterize oligomeric species and propose a new mechanistic pathway by which these oligomers are photochemically formed through reactions with reactive intermediate species.

4.2 Experimental Section:

Pyruvic acid (98%, Sigma-Aldrich) was distilled twice under reduced pressure (< 1 Torr) while heating gently (< 55 °C) and diluted with 18.2 MΩ water (3 ppb TOC) to make solutions of 10, 1, and 0.5 mM concentration. For each 100 mL volume solution, 10 mL of the solution was saved as a pre-photolysis control, and the remaining 90 mL of solution were illuminated for 5 hours in a temperature-stabilized water bath at 4 °C with a 450 W Xe arc lamp (Newport). The lower concentration solutions (1 mM and 0.5 mM) were also irradiated with the water bath held at 20 °C. There was no difference in observed products based on water bath temperature. Unless otherwise specified, all solutions were purged with N_2 to displace dissolved O_2, beginning one hour prior to the start of photolysis and continuing for the duration of the experiment. Oxygen-depleted conditions are known to favor formation of the oligomeric species under study here,[38] allowing for easier analysis and identification of products at relatively low reaction concentrations. The irradiated

solutions were allowed to come to room temperature before any further analysis was conducted.

The solutions were used without adjustment from their natural pH, meaning all photochemical experiments were conducted under acidic conditions. There is a slight variance in the pH of the solutions as a function of the concentration of pyruvic acid, increasing with decreasing concentration. The pH of the 10 mM pyruvic acid solutions was ~2.4 and rises to approximately 3.5 for the 0.5 mM pre-photolysis solutions.

The Xe arc lamp used was not filtered, meaning that its output extends into the UV to about 220 nm as shown in Figure D.1. Because of the extended light in the UV, under our experimental conditions, it is likely some excitation to the S_2, $^1(\pi, \pi^*)$, state in addition to the S_1 state also occurs. However, as is common with excitation to higher excited states,[73 74] it is likely that the system in the S_2 rapidly undergoes internal conversion to the lower S_1 state before following the same photochemical pathway of intersystem crossing and internal conversion to the reactive T_1 state. The photochemical products observed here using with the unfiltered Xe arc lamp are in good agreement with the previous results generated with a filtered Xe arc lamp with wavelengths $\lambda < 300$ nm removed from the spectrum.[38] In the latter case, the radiation provided can excite the S_1 but not the S_2 state, suggesting the same reactive photochemical pathway is preserved. The rate of photochemistry is, however, increased when the light is not filtered, as would be expected when more photons are present. These observations are consistent with those in the literature, which have shown, for example, that the photochemistry of nonanoic acid in aqueous solution using a filtered Xe arc lamp is observed to slow but not result in significantly different products than when not filtered.[75]

4.2.1 Electronic Structure Calculations: Calculations with the composite CBS-QB3

model[76] and using the Gaussian 09 suite of programs[77] were conducted on the relative barriers to H-atom abstraction from the methyl and carboxyl groups of pyruvic acid S_0 by pyruvic acid T_1, $^3(n,\pi^*)$. The calculations suggested that the activation enthalpy for the former is only 1.47 kcal/mol greater than that for the latter.

4.2.2 UV-Vis Spectroscopy: Pre- and post-photolysis solutions of the oxoacids were scanned using a Varian (Agilent) Cary 5000 spectrometer with a 0.1 s average time, 0.5 nm data interval, and a 0.5 nm spectral bandwidth.

4.2.3 NMR Analysis: NMR experiments were obtained at 23 °C using a Varian INOVA-500 NMR spectrometer operating at 499.60 MHz for ^1H detection. To perform experiments in aqueous solution, an optimized WET solvent suppression pulse sequence was used to eliminate >99% of the H_2O signal.[78]

4.2.4 Mass Spectrometry Analysis: High resolution mass spectrometry was performed on a Waters Synapt G2 HDMS mass spectrometer using electrospray ionization operated in negative mode. Instrument parameters and details of the analysis procedure are given in Chapter 3.4.

The instrument parameters were chosen to minimize the potential for in-source fragmentation and reactions due to ionization. Under the ionization conditions used here, we observe both $[M\text{-}H]^-$ and singly charged adduct ions for the analytes of interest. The adducts identified are formed from two or more deprotonated organic species coordinated to a metal ion, yielding a non-covalent adduct ion with a net charge of -1. In the pyruvic acid solutions, especially before photolysis, we observe adduct ions consisting of multiple deprotonated pyruvic acid molecules coordinated with a positive counterion, usually Na^+ or Ca^{2+} at quite high intensities, as shown in Table D.1 and Figure D.2. To minimize the presence of adduct ions, all photochemical experiments were conducted in 18.2 MΩ water

without the addition of salt and any such metal ions are assumed to be only present in trace quantities.

4.3 Results and Discussion:

The aqueous chemistry of pyruvic acid is generally defined by the formation of oligomeric species, under both light and dark conditions. The aqueous phase photochemistry of pyruvic acid has been studied previously in the literature[42, 44-46, 57, 61, 62] and is known to generate a surprisingly complex mixture of observed photoproducts, many of which have been assigned following the literature mechanism.[38, 44] Here, studying the aqueous phase photochemistry of pyruvic acid with high-resolution negative mode electrospray ionization mass spectrometry (ESI^- MS), we are able to suggest a new structural identification for oligomeric photoproducts. The new mechanistic pathway we suggest for these products is informed by a recent investigation of the dark oligomerization processes of pyruvic acid,[67] as well as recent results examining the multiphase photochemistry of pyruvic acid in an environmental simulation chamber.[62]

4.3.1 Pre-Photolysis Solutions and Dark Processes

The generation of covalently-bonded dimers of pyruvic acid in the dark has been known since the 19th century;[79-81] nevertheless, these dark processes have been largely ignored by the modern literature. Recently, however, it has been demonstrated that pyruvic acid, either pure or in aqueous solution, will spontaneously dimerize, likely through an aldol addition reaction.[67] The dimerization products include parapyruvic acid and zymonic acid, the lactone enol form of parapyruvic acid (see Scheme 4.2 for structures). In aqueous solution, there is an equilibrium between pyruvic acid, parapyruvic acid, zymonic acid, and their tautomers and hydrates, which depends on the concentration and pH of the solution.[67]

When studying the photochemical products generated by pyruvic acid, it is necessary to consider whether the oligomerization processes that take place in the dark may be

contributing to the identified products. However, such dark oligomerization processes do not occur on a timescale that competes with the observed photochemistry. As observed in the MS data, the rate of formation of these dimerization products in pure, distilled pyruvic acid stored 4 °C occurs over the course of weeks. As shown by NMR analysis in Figure D.3, there is very little contamination present in the 10 mM aqueous solutions before photolysis, with conservative estimates placing an upper limit on zymonic acid of < 0.1%. As mentioned above, the equilibrium between pyruvic acid and the various forms of parapyruvic and zymonic acid shifts as a function of concentration. In the dilute aqueous solutions under which photochemistry was conducted here, the equilibrium favors the reformation of monomeric pyruvic acid from dimerization products that may have been formed in the pure pyruvic acid. The kinetics of this shift are slow, but they provide reassurance that further dark dimerization products are not formed quickly enough to influence either the light-initiated chemistry or analysis in these experiments.

Although the overall concentration of the pyruvic acid dimers formed by dark reactions is low in our pre-photolysis samples, the presence of zymonic acid species is detectable by our ESI$^-$ MS analysis. There are six species derived from zymonic acid, including parapyruvic acid, that exist in aqueous solution.[67] Because these are closely related tautomers and enols, the chemical formulas of these species overlap. For example, using ESI$^-$ MS we detect an ion with an average experimental m/z for [M-H]$^-$ of 175.0239, which suggests the molecular formula $C_6H_8O_6$. This likely represents both parapyruvic acid and the closed ring form of the zymonic acid diol. Of the equilibrium species of zymonic acid in aqueous solution, these structures are the favored species.[67] In our analysis of the MS data (see Table 4.1 and Table D.1), we applied a conservative intensity threshold of 10^4 counts for analyte identifications to avoid incorrect ion assignments to noise peaks (see Chapter 3.4 for more detail). The ions that correspond to parapyruvic acid and the closed zymonic

diol are consistently observed above the threshold for the 10 mM pyruvic acid solutions before photolysis. Ions corresponding to the other zymonic acid species were observed occasionally at the threshold of intensity but were not consistently observed above the intensity cutoff we implemented. At the lower pyruvic acid solution concentrations (e.g. 1 mM and 0.5 mM), ions from zymonic acid are not generally observed in the mass spectra above the threshold. It is not surprising that the presence of zymonic acid is not observable at low concentrations of pyruvic acid; an already very low concentration of the contaminant is spread over multiple equilibrium structures, making it less likely that it would rise above our conservative threshold for detection.

Table 4.1. Select Compiled Pyruvic Acid Photochemistry ESI^- MS Data[a]

Assigned Formula $[M-H]^-$	Assigned Structure	Average Experimental m/z[b]	Theoretical m/z	Mass Diff. (ppm)	Pre-Photolysis	Post-Photolysis
Pre-Photolysis Species						
$C_3H_3O_3$	Pyruvic Acid	87.0091 ± 0.0005	87.0082	10.8	Strong	Strong
$C_3H_5O_4$	2,2-Dihydroxy-propanoic Acid	105.0190 ± 0.0007	105.0188	2.3	Weak	Below Threshold
$C_6H_7O_6$	Parapyruvic Acid[c]	175.0243 ± 0.0004	175.0243	0.21	Weak	Below Threshold
Key Photochemical Products						
$C_4H_7O_2$	Acetoin	87.0454 ± 0.0007	87.0446	8.7	Below Threshold	Medium
$C_3H_5O_3$	Lactic Acid	89.0239 ± 0.0003	89.0239	0.45	Below Threshold	Weak
$C_5H_7O_4$	Acetolactic Acid	131.0354 ± 0.001	131.0345	6.6	Below Threshold	Medium
$C_7H_{11}O_5$	DMOHA[d]	175.0617 ± 0.0006	175.0607	5.5	Below Threshold	Strong
$C_6H_9O_6$	Dimethyltartaric Acid	177.0409 ± 0.0005	177.0400	5.0	Below Threshold	Strong
$C_8H_{11}O_7$	CDMOHA[e]	219.0512 ± 0.0009	219.0505	3.2	Below Threshold	Medium

[a]Chemical formulas are assigned as the ionized $[M-H]^-$ species, structures are assigned as the neutral species. [b]The experimental m/z is the observed average across experiments, and the uncertainty given is the 95% confidence interval. [c]The peak assigned to parapyruvic acid likely also has contributions from the closed ring form of zymonic acid diol as well.[d]DMOHA = 2,4-dihydroxy-2-methyl-5-oxohexanoic acid [e]CDMOHA = 4-carboxy-2,4-dihydroxy-2-methyl-5-oxohexanoic acid

Parapyruvic acid and other zymonic acid derivatives are not generally observed in the post-photolysis solutions with intensities that rise above our threshold for detection. The lack of signal from parapyruvic acid in the ESI^- MS of post-photolysis solutions suggests that most of it has been consumed during the photochemical experiments. This is not surprising because parapyruvic acid is itself an α-keto acid and therefore photoactive. Similarly, if any parapyruvic acid was generated photochemically during the course of photolysis, it may not be detected in the post-photolysis samples. This raises the possibility that these species might also be synthesized photochemically and act as reactive oligomeric intermediate species whose further chemistry contributes to the observed photoproducts in the light-initiated chemistry of pyruvic acid, as is discussed in detail below. The recent observation of zymonic acid as a photoproduct generated from the photolysis of multiphase pyruvic acid under atmospherically-relevant conditions in environmental simulation chamber studies[62] lends credence to the photochemical formation and subsequent photochemistry of parapyruvic acid that may take place in aqueous solution.

4.3.2 Photochemical Oligomerization Processes

As mentioned above, photochemistry in aqueous solution begins upon absorption of a photon by the α-keto acid in the near UV. The absorption maximum of this transition occurs for pyruvic acid at a wavelength of ~320 nm (Figure D.1). In aqueous solution, the ketone group of pyruvic acid can be hydrated to form a geminal diol, 2,2,dihydroxypropanoic acid, (2,2-DHPA).[82-85] Unlike the ketone form, the geminal diol conformer does not absorb light within the solar spectrum. Many α-dicarbonyl species undergo almost complete hydration to the diol form in aqueous solution, where catalysis by water, acid, or base lowers the relatively high reaction barriers.[86-88] Pyruvic acid retains significant amounts of the ketonic functionality. The extent of hydration is both pH- and temperature-dependent,[83, 89] but, at 298 K, aqueous pyruvic acid generally exists as ~40% in the keto and ~60% in the diol

form.[38, 43, 84, 85] However, this ratio is concentration dependent as well. For the 10 mM solutions of pyruvic acid investigated here, the ratio is closer to 50% keto and 50% diol (Figure D.3). This ratio shifts during the photochemical experiments to slightly favor the keto form, which is likely due to the coupled effects of the depletion of pyruvic acid and subsequent slight decrease in acidity of the solution. All photochemical experiments were conducted without adjusting the solutions from their natural pH. The pH of the solution is increased slightly as the concentration of pyruvic acid is lowered. For the 0.5 mM pre-photolysis solutions, the pH is approximately 3.5, compared to ~2.4 for 10 mM solutions. At this lower concentration and higher pH, the amount of pyruvic acid in the keto conformer increases to about 75% (Figure D.4).

While all photochemical experiments were conducted under acidic conditions, the pH of the solutions are near the effective pK_a for pyruvic acid solutions of 2.49,[90] implying the protonation state of pyruvic acid is important to consider. This literature value is an effective pK_a because the keto and diol conformers have different, individual pK_a values, of 2.18 and 3.6, respectively.[83] Under our reaction conditions, then, more than 50% of the keto form of pyruvic acid is in its anionic form, pyruvate, for all concentrations, which reduces the number of photoactive protonated species in solution.

Regardless of the exact ratio of keto and diol conformer and their respective protonation states, the presence of significant amounts of protonated keto conformer in aqueous solution means that photochemistry is still a major reactive pathway under such conditions. However, interactions with the solvent shift the accessible electronic states for aqueous pyruvic acid, which favors photochemical mechanisms in the aqueous phase that follow different pathways than in the gas phase, as shown in Scheme 4.1.

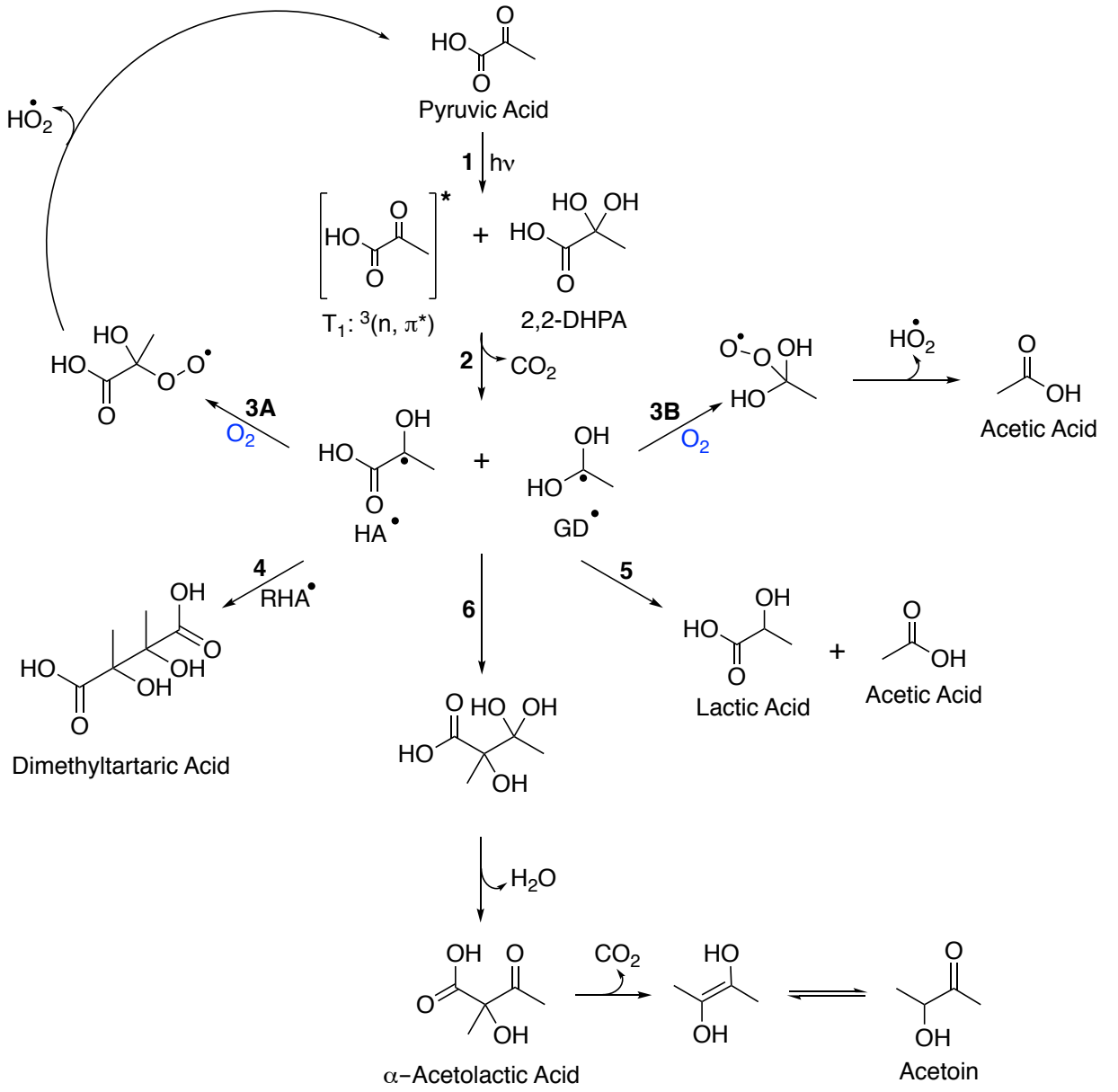

Scheme 4.1. Aqueous photochemical pathways for pyruvic acid.[38, 44]

In the aqueous phase, chemistry occurs from the T_1, $^3(n, \pi^*)$, state (Reaction 1 in Scheme 4.1). As has been shown previously in the literature, the excited T_1 state can abstract a hydrogen from the carboxyl group of another pyruvic acid molecule and decarboxylates to form two radical species (Reaction 2 in Scheme 4.1), one with hydroxyl acid functionality, $CH_3\dot{C}(OH)CO_2H$, denoted as HA• and one with geminal diol functionality, $CH_3\dot{C}(OH)_2$, denoted as GD•.[38, 44] The hydrogen abstraction from another pyruvic acid molecule can

either occur from the keto form of the molecule or from its geminal diol form, 2,2-DHPA, though abstraction from the diol is favored energetically.[44] Because 10 mM pyruvic acid under our reaction conditions is approximately 50% in the diol form, it is likely that abstraction from the diol is the major pathway. It has also been suggested that proton-coupled electron transfer can also occur,[43, 61] which would generate the same reactive radicals from the T_1 excited state of pyruvic acid.

The HA• and GD• radicals that are formed following hydrogen abstraction from the carboxyl group of either pyruvic acid or 2,2-DHPA, then go on to react further following a number of pathways, which are summarized in Scheme 4.1[38, 44] with MS results given in Table 4.1. The branching ratio of the pathways, and therefore the yields of the generated species, is influenced by the environmental conditions under which the aqueous photochemistry is conducted. Under our reaction conditions, at 10 mM concentration under a nitrogen atmosphere, approximately 90% of the pyruvic acid is consumed during five hours of photolysis (Figure D.3).

As is consistent with the previous literature, the main products observed from the aqueous phase photochemistry of pyruvic acid are oligomeric species, such as dimethyltartaric acid (DMTA), following Reaction 4 of Scheme 4.1. DMTA is formed by the recombination of two HA• radicals.[43, 44] For this recombination to happen, the HA• radicals must be able to escape from the initial solvent cage surrounding the generated HA• and GD• radicals in order to encounter a second HA• radical. Because these radicals must both undergo cage escape and encounter one another in dilute solution to form dimethyltartaric acid, HA• radicals must be relatively long-lived species. This observation is consistent with the stabilization of HA• by the captodative effect, enabled by the presence of both electron-donating and electron-withdrawing groups.[91]

DMTA is not the only observed oligomeric product species. Previous ^{1}H NMR studies

have observed a number of oligomeric photoproducts that remain unidentified.[38, 44] Additionally, MS analyses consistently observe an oligomeric photoproduct ion that that is detected with similar intensity to DMTA and likely represents the chemical formula $C_7H_{12}O_5$.[38, 43] The formation of this product cannot be explained following the mechanisms described in Scheme 4.1. It has been suggested previously that this species may be one of two possible structures, 2-(hydroxyethanyloxy)-2-carboxy-3oxobutane or 2-(3-oxobutan-2-yloxy)-2-hydroxypropanoic acid.[43, 71] Here, we propose that this product may be produced by further photochemistry of reactive oligomeric intermediates generated during photolysis with pyruvic acid.

The previously known mechanism for pyruvic acid aqueous photochemistry generates HA• and GD• following hydrogen abstraction from the carboxyl group of pyruvic acid or 2,2-DHPA.[44] Using electronic structure calculations, we examined the possibility of hydrogen abstraction from the methyl group rather than the carboxyl group of a neutral pyruvic acid molecule, which, at the CBS-QB3 level, show that methyl hydrogen abstraction has a transition state that is 1.47 kcal/mol higher in enthalpy than that for abstraction from the carboxyl hydrogen. This is a small difference in energy that is close to the likely error in the method, suggesting that hydrogen abstraction from the methyl group is likely competitive with hydrogen abstraction from the carboxyl group of pyruvic acid. Abstraction from the methyl group may be further favored because, for all pyruvic acid concentrations under our reaction conditions, more than 50% of the keto form of pyruvic acid (pK_a = 2.18)[83] is in its anionic form, pyruvate. Photochemistry under high pH conditions (pH = 6.1), where most of the pyruvic acid is deprotonated, has been observed to be considerably slower than under more acidic conditions,[45] suggesting that hydrogen abstraction from the carboxyl group is indeed favored. However, for deprotonated pyruvate molecules only the methyl group is available for abstraction. While perhaps not the major location of abstraction, it is

likely some abstraction from the methyl group of pyruvic acid occurs during the photochemical experiments (Reaction 1 of Scheme 4.2), yielding two radicals, HA• and one with oxoacid functionality, $\dot{C}H_2C(O)CO_2H$, denoted as OA•. It is worth noting that it is unlikely that proton-coupled electron transfer could generate the OA• radical.

The recombination of HA• and OA• (Reaction 2 of Scheme 4.2) generates parapyruvic acid, suggesting that it is a dimer of pyruvic acid that can be generated photochemically, in addition to dark oligomerization processes.[67] Each radical pair generated by hydrogen abstraction at the methyl group (Reaction 1 of Scheme 4.2) will have an overall net triplet characteristic, meaning that intra-cage geminate recombination to form parapyruvic acid will not occur. Instead, either intersystem crossing back to the singlet state or cage escape must take place before the radicals can react further, either of which is possible. The relative probability of these two possibilities, however, is difficult to predict.

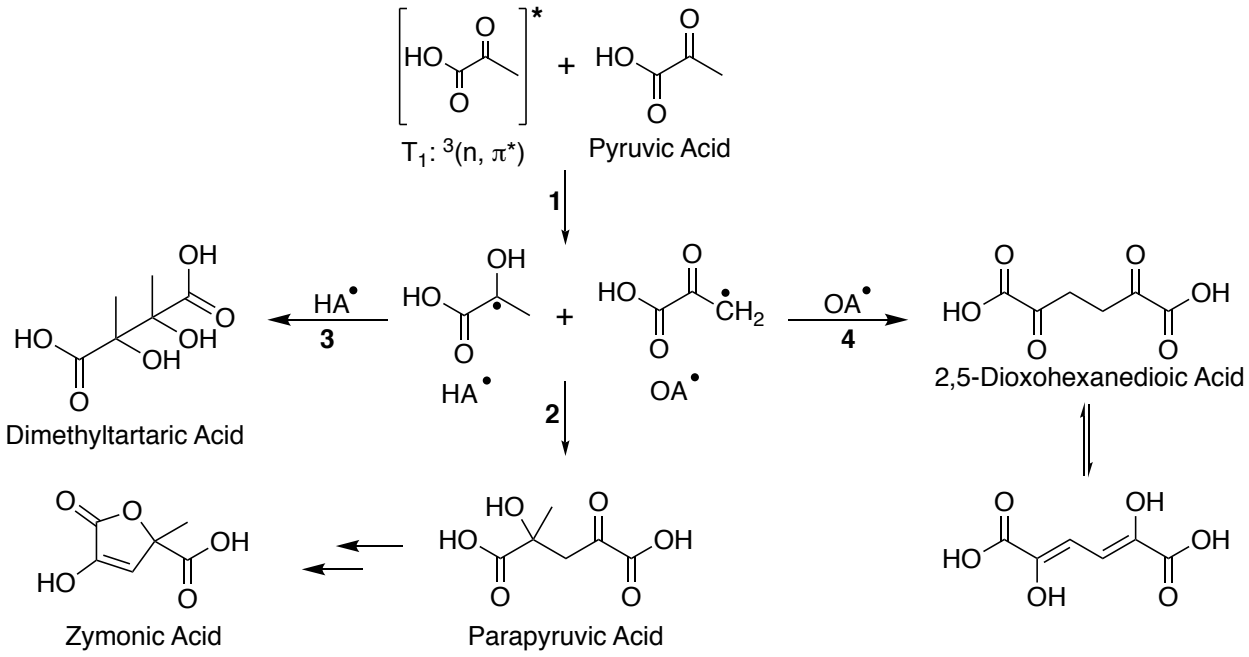

Scheme 4.2. Photochemical generation of parapyruvic acid via hydrogen abstraction from the methyl group of pyruvic acid.

If intersystem crossing back to the singlet state was the dominant pathway, one would expect only to see the recombination product between HA• and OA•, generating

parapyruvic acid. In the case of the radicals undergoing cage escape, the recombination product of each radical with itself would also be observed, in addition to the cross product between radicals. As is discussed above, the recombination of two HA• radicals generates DMTA, which is shown in Reaction 4 of Scheme 4.1 and in Reaction 3 of Scheme 4.2. The recombination of two OA• radicals would generate the dioxoacid compound shown by Reaction 4 of Scheme 4.2. This dioxoacid, 2,5 dioxohexanedioic acid (DOHDA, $C_6H_6O_6$), would likely exist in equilibrium with its enol form, though we do not observe such a peak in the MS data. However, the absence of detection does not mean that this species is not formed. OA•, unlike HA•, is not stabilized by the captodative effect, so its lifetime would be expected to be somewhat shorter. It is also less likely to encounter another OA• radical after undergoing cage escape because, while the energetics are not prohibitive, hydrogen abstraction from the methyl group of pyruvic acid is less likely than from the carboxyl group and thus OA• concentrations are expected to be small. Additionally, the keto form of DOHDA will be in equilibrium with the enol form of the acid in aqueous solution. Both the keto and enol forms of DOHDA are likely to be themselves photoactive: the keto form has two α-keto acid groups and the enol form has a conjugated double bond system. This means that any DOHDA that might be generated during illumination may go on to react, further depleting its concentration in the post-photolysis solution and limiting our ability to detect it. It is possible that such reactions can account for some of the minor photoproducts that we currently have not identified.

Because we do not observe DOHDA in the MS data, we are unable to conclusively state whether intersystem crossing back to the singlet state or cage escape is the favored mechanistic pathway. We tentatively favor cage escape as the more likely path by which HA• and OA• may react with each other to form parapyruvic acid. Our reasons are twofold. First, because it provides another mechanistic pathway by which DMTA, a product

observed in high concentrations, can be formed, and, secondly, because cage escape has been demonstrated to occur for both HA• and GD•, as shown in Scheme 4.1.

Regardless of the path by which recombination of HA• and OA• occurs, it seems likely that parapyruvic acid is formed photochemically during the course of the illumination of pyruvic acid. This reactivity will reduce its concentration in solution and is likely the main reason it is not detected in the post-photolysis MS data with an intensity above the threshold we implement here. Parapyruvic acid, itself an α-keto acid, has the same reactive functionality as pyruvic acid, and is, therefore, capable of undergoing the same photochemistry as pyruvic acid, as shown in Scheme 4.3. Therefore, any trace parapyruvic acid in the initial pre-photolysis solution, as well as any generated photochemically, can also be excited by near-UV photons. An excited parapyruvic acid molecule may then abstract a hydrogen from either a pyruvic acid or 2,2-DHPA molecule, which would be followed by decarboxylation as in the pathway originally shown in Reaction 2 of Scheme 4.1.

This generates both the familiar GD• and a parapyruvic radical, $CO_2HC(CH_3)OH\dot{C}(OH)CO_2H$ denoted as PPA•, shown in Reaction 1 of Scheme 4.3. These two radical species can then combine, following Reaction 2 and 3 of Scheme 4.3, generating 4-carboxy-2,4-dihydroxy 2-methyl-5-oxohexanoic acid (CDMOHA) and, following decarboxylation (Reaction 4 of Scheme 4.3), 2,4-dihydroxy-2-methyl-5-oxohexanoic acid (DMOHA). CDMOHA has a chemical formula of $C_8H_{12}O_7$ and we observe, correspondingly, a species in the MS data with an average experimental m/z for $[M\text{-}H]^-$ of 219.0517. DMOHA's chemical formula is $C_7H_{12}O_5$. We posit that the oligomeric photoproduct that is detected in the MS data with a high intensity, both here and in the literature,[38, 43] can be assigned to DMOHA and explained by the photochemical mechanism given in Scheme 4.3.

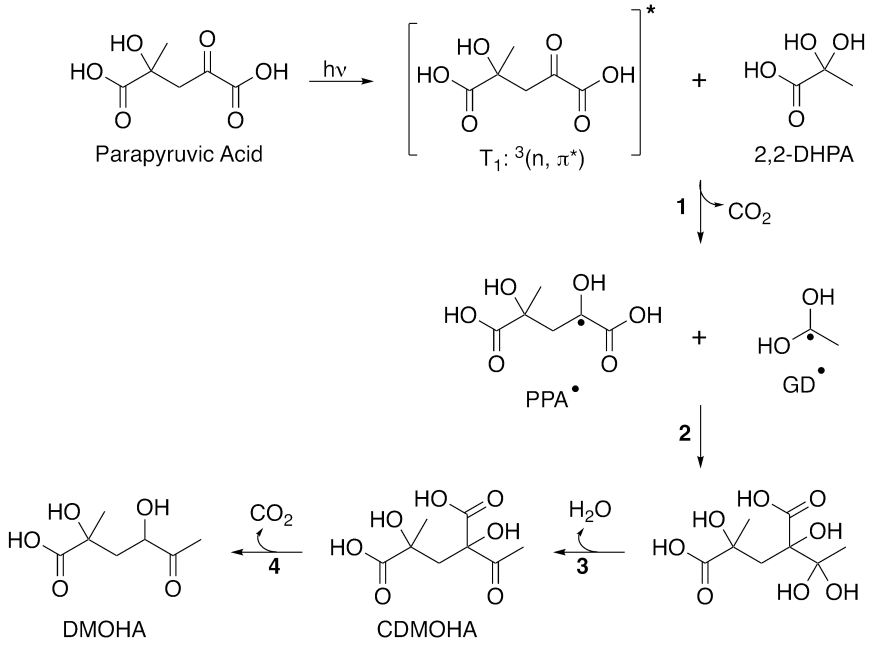

Scheme 4.3. Photochemistry of parapyruvic acid to generate trimer species.

These structures, CDMOHA and DMOHA, are consistent with the MS results presented here and the known chemistry of pyruvic acid and zymonic acid.[38, 44, 67] The mechanistic pathway presented in Scheme 4.3 is further supported because it directly parallels one of the accepted mechanistic pathways for aqueous pyruvic acid photochemistry in the literature.[44, 46] As shown by Reaction 6 of Scheme 4.1, the recombination of the HA• and GD• radicals followed by the subsequent dehydration to form α-acetolactic acid, which then decarboxylates to form acetoin.[44] Consistent with this mechanism, we observe a species with an accurate mass corresponding to the chemical formula $C_5H_8O_4$, which is mostly likely acetolactic acid. Acetolactic acid, as a β-keto acid, will thermally decarboxylate into acetoin under ambient temperature conditions in aqueous solution. The rate of this decomposition is both pH and temperature dependent, increasing as temperature is raised and pH is lowered.[92] The time required for complete decarboxylation of aqueous acetolactic acid at 20 °C ranges from a few hours at a pH of 1.0[43] to two weeks at a pH of 4.65.[93] For our reaction conditions that are not buffered or pH adjusted (dependent on pyruvic acid

concentration, pH ~2.4 for 10 mM pre-photolysis solutions), it is reasonable to expect that acetolactic acid generated photochemically would be partially decarboxylated, allowing us to observe both acetolactic acid and acetoin during post-photolysis analysis.

Acetoin has been widely reported in the literature as a known product of the aqueous photochemistry of pyruvic acid.[38, 42, 44-46] It is readily apparent that the pathway presented in Scheme 4.3 is wholly analogous to the pathway presented by Reaction 6 of Scheme 4.1, where the intermediate species, CDMOHA, corresponds to acetolactic acid and DMOHA corresponds to acetoin. Griffith et al. (2013) unambiguously identified acetoin as a minor product by COSY NMR.[44] Here we identify acetoin as a photoproduct using ESI^- MS as well (Table 4.1).

The observation of acetoin as a product of the aqueous photochemistry of pyruvic acid has been a point of contention in the literature.[43, 44, 70, 71] This discrepancy likely stems in part from the fact that acetoin is not a primary photoproduct, but, is instead formed from the thermal decarboxylation from a larger oligomer generated by radical-radical recombination. Indeed, several of the observed photoproducts of the light-initiated chemistry of pyruvic acid are not directly formed from the simple recombination of pyruvic acid-derived radicals. Rather, species that are generated by these initial recombination processes, such as 2-methyl-2,3,3-trihydroxybutanoic acid, go on to further react, forming species such as acetolactic acid and acetoin, as shown in Reaction 6 of Scheme 4.1. Such species can decompose into smaller product species, as is observed in the dehydration reactions that form acetolactic acid and CDMOHA and the decarboxylation reactions that form acetoin and DMOHA. But oligomeric intermediates can also react to generate larger oligomeric species, as is observed when parapyruvic acid, a dimer of pyruvic acid, is photochemically excited and reacts with another pyruvic acid molecule, ultimately generating DMOHA, a trimer of pyruvic acid. The generation and subsequent reactions of

intermediate species, especially oligomeric intermediates, is not always appreciated. Because of this reactivity, both an increase in molecular complexity by the generation of oligomeric species and the generation of a complex mixture of molecules within the solution are observed. These interconnected reactions mean that even the three-carbon pyruvic acid generates a diverse library of products upon photolysis in aqueous solution. The combination of the reaction pathways outlined in Schemes 4.1–4.3, can explain the majority of the photochemical products observed in the MS data. This includes both acetic acid and lactic acid as shown in Reaction 5 of Scheme 4.1. Acetic acid has been observed by NMR previously[44] and is readily seen in the NMR of the experiments conducted here (Figures D.3 and D.4). Lactic acid was conclusively identified as a photoproduct by COSY and DOSY NMR.[44] Here, for the first time here we have observed the formation of lactic acid in the MS data as well (Table 4.1). However, there remain a number of minor photoproducts; we observe several of which that have not been previously reported in the literature and have not yet been identified. For completeness, we report the detailed MS data in Table D.1.

That the observed chemistry is so rich, even at very low pyruvic acid concentrations (from 0.5 mM to 10 mM) is, perhaps, surprising. We are able to detect more minor photoproducts in the 10 mM post-photolysis solutions in the MS, which is likely due to the lower concentration of products formed in solutions with lower initial pyruvic acid concentrations, as we used the same ionization parameters for all MS analyses. The main oligomeric products, including DMTA and DMOHA, are observed in the 0.5 mM post-photolysis solutions. The formation of these products requires that two radicals escape their initial solvent cage, encounter each other, and recombine before they are quenched. Even the initial generation of these radicals requires that a photoexcited species encounter another molecule in solution before quenching. Under more dilute conditions, the chance of such encounters occurring decreases. A kinetics analysis of the aqueous pyruvic acid

photochemistry under anaerobic conditions found that the rates of depletion of pyruvic acid were roughly equivalent between 100 mM and 20 mM solutions,[38] suggesting both these concentrations are above this dilute limit. While a formal investigation of the kinetics of photolysis as a function of concentration was outside the scope of this study, the observed consumption of pyruvic acid in the NMR after five hours of photolysis is lower for the low concentration solutions, as would be expected for radical-driven chemistry. For the solutions of 0.5 mM, the depletion of pyruvic acid was observed by NMR to be closer to 50% (Figure D.4), compared to the roughly 90% depletion observed for the 10 mM solutions. This observed decrease in reactivity is likely due to a combination of factors, all stemming from the low concentrations of pyruvic acid used. As mentioned above, in the 0.5 mM solutions, pyruvic acid exists primarily as the keto conformer and the higher pH of the solution (~3.5) means that more exists as pyruvate, both of which likely slow reaction compared to the 10 mM solutions. In the low concentration limit, it would also be expected that the probability of two species encountering each other before quenching decreases to essentially zero and only unimolecular homolysis products would be observed. It has previously been suggested that the transition from bimolecular to unimolecular processes would occur for solutions around 10 mM pyruvic acid.[43, 61] Here, however, we demonstrate that under our reaction conditions bimolecular processes still readily occur even in very dilute solutions.

It is important to consider the implications of the reaction conditions used here, as the aqueous photochemistry of pyruvic acid is extremely sensitive to its environmental surroundings. This sensitivity helps explain differences between reported products in the literature.[38, 42-46, 70, 71] As shown in Scheme 4.1, a number of pathways exist for the further reactions of HA• and GD• to give the observed photoproducts. The branching ratio of these pathways is influenced by the environmental conditions under which the aqueous photochemistry is conducted. For example, it has been shown that the composition of the

atmosphere under which the photochemistry is conducted can strongly influence this branching ratio.[38] Reactions 3A and 3B of Scheme 4.1 involve the reaction of the radical species with oxygen. Reaction 3A is a pathway by which pyruvic acid is regenerated, therefore slowing the kinetics of pyruvic photolysis.[38] Reaction 3B forms acetic acid. In the high oxygen concentration limit, obtained by bubbling pure O_2 through the photolysis reactor, the branching ratio is such that only acetic acid is observed as a photoproduct using NMR (Figure D.5). Here, we are reliant on our combined, complementary NMR and ESI$^-$ MS analyses: while acetic acid is formed and readily observed by NMR, it is not seen in the MS. Acetic acid is difficult to observe by the ESI$^-$ MS used here, likely because, as a small molecule, it is toward the low mass range of our instrument, and the signal and mass accuracy of the instrument decrease as ion m/z is decreased. Even at 100 mM concentration, acetic acid is observed only weakly in the ESI$^-$ MS, as shown in Figure D.6. It is not surprising that we do not observe it as a photoproduct in the MS when the concentration is much lower.

The effect to the branching ratio of the photochemical pathways under a pure O_2 atmosphere is extreme, but it serves as an example highlighting the differences in observable products created by different reaction conditions. In environments that are not saturated with O_2, the familiar oligomeric species discussed above are readily formed. In oxygen-limited conditions, these oligomers are the major observable products. Because we were interested primarily in these oligomeric species, we chose to conduct our photochemical experiments under a nitrogen atmosphere in order to maximize our ability to observe such species at low concentrations. Under conditions free of dissolved O_2 Reaction 3 of Scheme 4.1 is effectively removed, and lifetimes of excited state pyruvic acid are effectively increased by removing the quenching effects of O_2. The oxygen-limited conditions may account for the persistence of bimolecular photochemical processes even at very dilute

concentrations in the experiments reported here.

While the branching ratio observed for reactions under oxygen-depleted conditions is not directly comparable to those that might occur in the natural environment, the products observed and the mechanistic insight behind their formation provide us with a better understanding of the complexity of reactions that occur in the natural environment. Biasing the branching ratio toward oligomeric species for laboratory studies simply aids in the ability to analyze the resultant products at low concentrations, it does not change the nature of the species generated. Oxygen-limited conditions may additionally be relevant for certain systems found in the natural environment as well. Photolysis of pyruvic acid in the bulk aqueous phase open to air has been shown to deplete oxygen from the reaction vessel.[38, 94] Atmospheric aerosols in the modern atmosphere are unlikely to be depleted in oxygen, but even under conditions where dissolved O_2 is not depleted reactions to form oligomers are still active.[38, 62, 94]

The observation that the formation of more complex, oligomeric species is favored under anoxic conditions does raise intriguing possibilities for the relevance of this chemistry in the ancient, prebiotic environment. Unlike the modern atmosphere, the prebiotic atmosphere contained very little O_2 and ozone, allowing more UV light to reach the troposphere and Earth's surface.[95, 96] Aqueous photochemistry of pyruvic acid has been shown to be competitive with hydroxyl radical reaction in the modern environment.[38] The absence of oxygen in the prebiotic atmosphere suggests that the photochemistry of carbonyl-containing compounds would be expected be an even more significant process on the ancient Earth than it is today, given that far less OH radical would have been available in prebiotic environments. The generation of oligomers under prebiotically-relevant conditions demonstrates that pyruvic acid can harness sunlight and convert it into usable chemical energy stored in complex, reactive molecules. In addition to being an important

atmospheric species, pyruvic acid is also at the center of metabolism,[97-101] and it has been suggested that its photochemistry may have driven protometabolic cycles.[96, 100-102]

4.4 Conclusions:

In this work, the aqueous phase photochemistry of pyruvic acid was investigated at low concentrations under an anaerobic, N_2 atmosphere. Even in very dilute solutions with low concentrations of pyruvic acid, covalently-bonded dimers and trimers are formed from the recombination of photochemically-generated radical species. We have shown that it is energetically possible for an excited pyruvic acid molecule to abstract a hydrogen from the methyl hydrogen group of another pyruvic acid molecule in addition to hydrogen abstraction from the carboxyl group. This generates a new radical, OA•, which can recombine with HA• to form parapyruvic acid, a dimer of pyruvic acid known to be generated via dark oligomerization processes.[67]

Several of the observed species in the post-photolysis solutions are not primary photoproducts of pyruvic acid but are, rather, generated from the further reactions of oligomeric intermediates. Such intermediate species can decompose by dehydration or decarboxylation, but they can also undergo further photochemical reactions to generate larger molecules. We have proposed that parapyruvic acid, itself an α-keto acid, when photoexcited follows the same photochemical pathways as pyruvic acid, cross-reacting with pyruvic acid to form 2,4-dihydroxy-2-methyl-5-oxohexanoic acid, a trimer of pyruvic acid.

Pyruvic acid's photochemistry is known to be incredibly sensitive to environmental conditions, with completely different reaction pathways available in the aqueous phase than in the gas phase. Within the aqueous phase, the composition of dissolved gases in solution has a strong influence on the branching ratio of these pathways. This network of reactions yields a diverse library of photoproducts even when considering only a simple model system of a single species. This highlights that the formation of SOA from the

aqueous chemistry of small organics under atmospheric conditions is reliant on a Gordian Knot of interwoven networks of reactions between many species. However, while a complex mixture of products is generated from the aqueous photochemistry of pyruvic acid, the mechanisms governing their formation are robust and self-consistent, suggesting that by understanding in detail the photochemistry of model species, mechanistic motifs may be found across classes of molecules that help untangle the reactive behavior of more complex mixtures of species.

4.5 Bibliography:

1. Rapf, R. J.; Perkins, R. J.; Carpenter, B. K.; Vaida, V. Mechanistic description of photochemical oligomer formation from aqueous pyruvic acid. *J. Phys. Chem. A* **2017,** *121*, 4272–4282.

2. Perraud, V.; Bruns, E. A.; Ezell, M. J.; Johnson, S. N.; Yu, Y.; Alexander, M. L.; Zelenyuk, A.; Imre, D.; Chang, W. L.; Dabdub, D., et al. Nonequilibrium atmospheric secondary organic aerosol formation and growth. *Proc. Natl. Acad. Sci.* **2012,** *109*, 2836-2841.

3. Harrison, R. M.; Yin, J. Particulate matter in the atmosphere: Which particle properties are important for its effects on health? *Sci. Total Environ.* **2000,** *249*, 85-101.

4. Finlayson-Pitts, B. J.; Pitts, J. N., *Chemistry of the upper and lower atmosphere*. Academic Press: San Diego, 1999.

5. Hinds, W. C., *Aerosol technology : Properties, behavior, and measurement of airborne particles*. 2nd ed.; Wiley: New York, 1999.

6. Ervens, B. Modeling the processing of aerosol and trace gases in clouds and fogs. *Chem. Rev.* **2015,** *115*, 4157-4198.

7. Lohmann, U.; Feichter, J. Global indirect aerosol effects: A review. *Atmo. Chem. Phys.* **2005,** *5*, 715-737.

8. Hansen, J.; Sato, M.; Ruedy, R. Radiative forcing and climate response. *J. Geophys. Res. Atmos.* **1997,** *102*, 6831-6864.

9. Hallquist, M.; Wenger, J. C.; Baltensperger, U.; Rudich, Y.; Simpson, D.; Claeys, M.; Dommen, J.; Donahue, N. M.; George, C.; Goldstein, A. H., et al. The formation, properties and impact of secondary organic aerosol: Current and emerging issues. *Atmos. Chem. Phys.* **2009,** *9*, 5155-5236.

10. Ervens, B.; Turpin, B. J.; Weber, R. J. Secondary aerosol formation in cloud droplets and aqueous particles (aqSOA): A review of laboratory, field and model studies. *Atmo. Chem. Phys.* **2011,** *11*, 11069-11102.

11. Seinfeld, J. H.; Pandis, S. N., *Atmospheric chemistry and physics: From air pollution to climate change*. John Wiley & Sons, Inc.: New York, 1998.

12. Boucher, O.; Randall, D.; Artaxo, P.; Bretherton, C.; Feingold, G.; Forster, P.; Kerminen, V. M.; Kondo, Y.; Liao, H.; Lohmann, U., et al., Clouds and aerosols. In *Climate change 2013: The physical science basis. Contribution of working group I to the fifth assessment report of the intergovernmental panel on climate change*, Stocker, T. F.; Qin, D.; Plattner, G. K.; Tignor, M.; Allen, S. K.; Boschung, J.; Nauels, A.; Xia, Y.; Bex, V.; Midgley, P. M., Eds. Cambridge Univ. Press, : Cambridge, U.K. and New York, NY, USA, 2013; pp 465-570.

13. Heald, C. L.; Jacob, D. J.; Park, R. J.; Russell, L. M.; Huebert, B. J.; Seinfeld, J. H.; Liao, H.; Weber, R. J. A large organic aerosol source in the free troposphere missing from current models. *Geophys. Res. Lett.* **2005,** *32*, L18809.

14. Jimenez, J. L.; Canagaratna, M. R.; Donahue, N. M.; Prevot, A. S. H.; Zhang, Q.; Kroll, J. H.; DeCarlo, P. F.; Allan, J. D.; Coe, H.; Ng, N. L., et al. Evolution of organic aerosols in the atmosphere. *Science* **2009,** *326*, 1525-1529.

15. Carlton, A. G.; Wiedinmyer, C.; Kroll, J. H. A review of secondary organic aerosol (SOA) formation from isoprene. *Atmo. Chem. Phys.* **2009,** *9*, 4987-5005.

16. Monod, A.; Carlier, P. Impact of clouds on the tropospheric ozone budget: Direct effect of multiphase photochemistry of soluble organic compounds. *Atmos. Environ.* **1999,** *33*, 4431-4446.

17. Kroll, J. H.; Ng, N. L.; Murphy, S. M.; Flagan, R. C.; Seinfeld, J. H. Secondary organic aerosol formation from isoprene photooxidation. *Environ. Sci. Technol.* **2006,** *40*, 1869-1877.

18. Claeys, M.; Graham, B.; Vas, G.; Wang, W.; Vermeylen, R.; Pashynska, V.; Cafmeyer, J.; Guyon, P.; Andreae, M. O.; Artaxo, P. Formation of secondary organic aerosols through photooxidation of isoprene. *Science* **2004,** *303*, 1173-1176.

19. Kroll, J. H.; Ng, N. L.; Murphy, S. M.; Flagan, R. C.; Seinfeld, J. H. Secondary organic aerosol formation from isoprene photooxidation under high - nox conditions. *Geophys. Res. Lett.* **2005,** *32*, L18808.

20. Brégonzio-Rozier, L.; Giorio, C.; Siekmann, F.; Pangui, E.; Morales, S.; Temime-Roussel, B.; Gratien, A.; Michoud, V.; Cazaunau, M.; DeWitt, H. Secondary organic aerosol formation from isoprene photooxidation during cloud condensation–evaporation cycles. *Atmo. Chem. Phys.* **2016,** *16*, 1747-1760.

21. George, C.; Ammann, M.; D'Anna, B.; Donaldson, D. J.; Nizkorodov, S. A. Heterogeneous photochemistry in the atmosphere. *Chem. Rev.* **2015,** *115*, 4218-4258.

22. Boris, A. J.; Desyaterik, Y.; Collett, J. L. How do components of real cloud water affect aqueous pyruvate oxidation? *Atmo. Res.* **2014,** *143*, 95-106.

23. Vaida, V. Spectroscopy of photoreactive systems: Implications for atmospheric chemistry. *J. Phys. Chem. A* **2009,** *113*, 5-18.

24. Altieri, K. E.; Carlton, A. G.; Lim, H.-J.; Turpin, B. J.; Seitzinger, S. P. Evidence for oligomer formation in clouds: Reactions of isoprene oxidation products. *Environ. Sci. Technol.* **2006,** *40*, 4956-4960.

25. Ervens, B.; Carlton, A. G.; Turpin, B. J.; Altieri, K. E.; Kreidenweis, S. M.; Feingold, G. Secondary organic aerosol yields from cloud-processing of isoprene oxidation products. *Geophys. Res. Lett.* **2008,** *35*, L02816.

26. Carlton, A. G.; Turpin, B. J.; Lim, H.-J.; Altieri, K. E.; Seitzinger, S. Link between isoprene and secondary organic aerosol (SOA): Pyruvic acid oxidation yields low volatility organic acids in clouds. *Geophys. Res. Lett.* **2006,** *33*, L06822.

27. Kawamura, K.; Kasukabe, H.; Barrie, L. A. Source and reaction pathways of dicarboxylic acids, ketoacids and dicarbonyls in arctic aerosols: One year of observations. *Atmos. Environ.* **1996,** *30*, 1709-1722.

28. Sempere, R.; Kawamura, K. Comparative distributions of dicarboxylic acids and related polar compounds in snow, rain, and aerosols from urban atmosphere. *Atmos. Environ.* **1994,** *28*, 449-459.

29. Nguyen, T. B.; Bateman, A. P.; Bones, D. L.; Nizkorodov, S. A.; Laskin, J.; Laskin, A. High-resolution mass spectrometry analysis of secondary organic aerosol generated by ozonolysis of isoprene. *Atmos. Environ.* **2010,** *44*, 1032-1042.

30. Veres, P. R.; Roberts, J. M.; Cochran, A. K.; Gilman, J. B.; Kuster, W. C.; Holloway, J. S.; Graus, M.; Flynn, J.; Lefer, B.; Warneke, C., et al. Evidence of rapid production of organic acids in an urban air mass. *Geophys. Res. Lett.* **2011,** *38*, L17807.

31. Warneck, P. Multi-phase chemistry of C-2 and C-3 organic compounds in the marine atmosphere. *J. Atmos. Chem.* **2005,** *51*, 119-159.

32. Andreae, M. O.; Talbot, R. W.; Li, S. M. Atmospheric measurements of pyruvic and formic acid. *J. Geophys. Res. Atmos.* **1987,** *92*, 6635-6641.

33. Ho, K.; Lee, S.; Cao, J.; Kawamura, K.; Watanabe, T.; Cheng, Y.; Chow, J. C. Dicarboxylic acids, ketocarboxylic acids and dicarbonyls in the urban roadside area of Hong Kong. *Atmos. Environ.* **2006,** *40*, 3030-3040.

34. Talbot, R.; Andreae, M.; Berresheim, H.; Jacob, D. J.; Beecher, K. Sources and sinks of formic, acetic, and pyruvic acids over central Amazonia: 2. Wet season. *J. Geophys. Res. Atmos.* **1990,** *95*, 16799-16811.

35. Veres, P.; Roberts, J. M.; Burling, I. R.; Warneke, C.; de Gouw, J.; Yokelson, R. J. Measurements of gas‐phase inorganic and organic acids from biomass fires by

negative - ion proton - transfer chemical - ionization mass spectrometry. *J. Geophys. Res. Atmos.* **2010,** *115*, D23302.

36. Kawamura, K.; Kasukabe, H.; Barrie, L. A. Secondary formation of water-soluble organic acids and alpha-dicarbonyls and their contributions to total carbon and water-soluble organic carbon: Photochemical aging of organic aerosols in the arctic spring. *J. Geophys. Res. Atmos.* **2010,** *115*, D21306.

37. Mellouki, A.; Mu, Y. J. On the atmospheric degradation of pyruvic acid in the gas phase. *J. Photochem. Photobiol., A* **2003,** *157*, 295-300.

38. Reed Harris, A. E.; Ervens, B.; Shoemaker, R. K.; Kroll, J. A.; Rapf, R. J.; Griffith, E. C.; Monod, A.; Vaida, V. Photochemical kinetics of pyruvic acid in aqueous solution. *J. Phys. Chem. A* **2014,** *118*, 8505-8516.

39. Lopalco, A.; Dalwadi, G.; Niu, S.; Schowen, R. L.; Douglas, J.; Stella, V. J. Mechanism of decarboxylation of pyruvic acid in the presence of hydrogen peroxide. *J. Pharm. Sci.* **2016,** *105*, 705-713.

40. Stefan, M. I.; Bolton, J. R. Reinvestigation of the acetone degradation mechanism in dilute aqueous solution by the UV/H_2O_2 process. *Environ. Sci. Technol.* **1999,** *33*, 870-873.

41. Schöne, L.; Herrmann, H. Kinetic measurements of the reactivity of hydrogen peroxide and ozone towards small atmospherically relevant aldehydes, ketones and organic acids in aqueous solutions. *Atmo. Chem. Phys.* **2014,** *14*, 4503.

42. Leermakers, P. A.; Vesley, G. F. Photochemistry of alpha-keto acids and alpha-keto esters. 1. Photolysis of pyruvic acid and benzoylformic acid. *J. Am. Chem. Soc.* **1963,** *85*, 3776-3779.

43. Guzman, M. I.; Colussi, A. J.; Hoffmann, M. R. Photoinduced oligomerization of aqueous pyruvic acid. *J. Phys. Chem. A* **2006,** *110*, 3619-3626.

44. Griffith, E. C.; Carpenter, B. K.; Shoemaker, R. K.; Vaida, V. Photochemistry of aqueous pyruvic acid. *Proc. Natl. Acad. Sci.* **2013,** *110*, 11714-11719.

45. Leermakers, P. A.; Vesley, G. F. Photolysis of pyruvic acid in solution. *J. Org. Chem.* **1963,** *28*, 1160-1161.

46. Closs, G. L.; Miller, R. J. Photo-reduction and photodecarboxylation of pyruvic acid - applications of CIDNP to mechanistic photochemistry. *J. Am. Chem. Soc.* **1978,** *100*, 3483-3494.

47. Hall, G. E.; Muckerman, J. T.; Preses, J. M.; Weston, R. E.; Flynn, G. W. Time-resolved FTIR studies of the photodissociation of pyruvic-acid at 193 nm. *Chem. Phys. Lett.* **1992,** *193*, 77-83.

48. Rincon, A. G.; Guzman, M. I.; Hoffmann, M. R.; Colussi, A. J. Optical absorptivity versus molecular composition of model organic aerosol matter. *J. Phys. Chem. A* **2009,** *113*, 10512-10520.

49. Vesley, G. F.; Leermakers, P. A. Photochemistry of alpha-keto acids and alpha-keto esters .3. Photolysis of pyruvic acid in vapor phase. *J. Phys. Chem.* **1964,** *68*, 2364-2366.

50. Dhanya, S.; Maity, D. K.; Upadhyaya, H. P.; Kumar, A.; Naik, P. D.; Saini, R. D. Dynamics of OH formation in photodissociation of pyruvic acid at 193 nm. *J. Chem. Phys.* **2003,** *118*, 10093-10100.

51. Oneill, J. A.; Kreutz, T. G.; Flynn, G. W. IR diode-laser study of vibrational-energy distribution in CO_2 produced by UV excimer laser photofragmentation of pyruvic-acid. *J. Chem. Phys.* **1987,** *87*, 4598-4605.

52. Wood, C. F.; Oneill, J. A.; Flynn, G. W. Infrared diode-laser probes of photofragmentation products - bending excitation in CO_2 produced by excimer laser photolysis of pyruvic-acid. *Chem. Phys. Lett.* **1984,** *109*, 317-323.

53. Berges, M. G.; Warneck, P. Product quantum yields for the 350 nm photodecomposition of pyruvic acid in air. *Ber. Bunsen-Ges. Phys. Chem* **1992,** *96*, 413-416.

54. Grosjean, D. Atmospheric reactions of pyruvic-acid. *Atmos. Environ.* **1983,** *17*, 2379-2382.

55. Yamamoto, S.; Back, R. A. The photolysis and thermal decomposition of pyruvic acid in the gas phase. *Can. J. Chem.* **1985,** *63*, 549-554.

56. Plath, K. L.; Takahashi, K.; Skodje, R. T.; Vaida, V. Fundamental and overtone vibrational spectra of gas-phase pyruvic acid. *J. Phys. Chem. A* **2009,** *113*, 7294-7303.

57. Larsen, M. C.; Vaida, V. Near infrared photochemistry of pyruvic acid in aqueous solution. *J. Phys. Chem. A* **2012,** *116*, 5840-5846.

58. Takahashi, K.; Plath, K. L.; Skodje, R. T.; Vaida, V. Dynamics of vibrational overtone excited pyruvic acid in the gas phase: Line broadening through hydrogen-atom chattering. *J. Phys. Chem. A* **2008,** *112*, 7321-7331.

59. Reed Harris, A. E.; Doussin, J.-F.; Carpenter, B. K.; Vaida, V. Gas-phase photolysis of pyruvic acid: The effect of pressure on reaction rates and products. *J. Phys. Chem. A* **2016,** *120*, 10123-10133.

60. Chang, X.-P.; Fang, Q.; Cui, G. Mechanistic photodecarboxylation of pyruvic acid: Excited-state proton transfer and three-state intersection. *J. Chem. Phys.* **2014,** *141*, 154311.

61. Davidson, R. S.; Goodwin, D.; De Violet, P. F. The mechanism of the photo-induced decarboxylation of pyruvic acid in solution. *Chem. Phys. Lett.* **1981,** *78*, 471-474.

62. Reed Harris, A. E.; Pajunoja, A.; Cazaunau, M.; Gratien, A.; Pangui, E.; Monod, A.; Griffith, E. C.; Virtanen, A.; Doussin, J. F.; Vaida, V. Multiphase photochemistry of pyruvic acid under atmospheric conditions. *J. Phys. Chem. A* **2017,** *121*, 3327–3339.

63. Saito, K.; Sasaki, G.; Okada, K.; Tanaka, S. Unimolecular decomposition of pyruvic acid - an experimental and theoretical study. *J. Phys. Chem.* **1994,** *98*, 3756-3761.

64. Taylor, R. The mechanism of thermal eliminations XXIII: [1] the thermal-decomposition of pyruvic-acid. *Int. J. Chem. Kinet.* **1987,** *19*, 709-713.

65. da Silva, G. Decomposition of pyruvic acid on the ground-state potential energy surface. *J. Phys. Chem. A* **2015,** *120* 276–283.

66. Colberg, M. R.; Watkins, R. J.; Krogh, O. D. Vibrationally excited carbon-dioxide produced by infrared multiphoton pyrolysis. *J. Phys. Chem.* **1984,** *88*, 2817-2821.

67. Perkins, R. J.; Shoemaker, R. K.; Carpenter, B. K.; Vaida, V. Chemical equilibria and kinetics in aqueous solutions of zymonic acid. *J. Phys. Chem. A* **2016,** *120*, 10096-10107.

68. Horowitz, A.; Meller, R.; Moortgat, G. K. The UV–vis absorption cross sections of the α -dicarbonyl compounds: Pyruvic acid, biacetyl and glyoxal. *J. Photochem. Photobiol., A* **2001,** *146*, 19-27.

69. Schreiner, P. R.; Reisenauer, H. P.; Ley, D.; Gerbig, D.; Wu, C.-H.; Allen, W. D. Methylhydroxycarbene: Tunneling control of a chemical reaction. *Science* **2011,** *332*, 1300-1303.

70. Griffith, E. C.; Carpenter, B. K.; Shoemaker, R. K.; Vaida, V. Reply to eugene et al.: Photochemistry of aqueous pyruvic acid. *Proc. Natl. Acad. Sci.* **2013,** *110*, E4276-E4276.

71. Eugene, A. J.; Xia, S.-S.; Guzman, M. I. Negative production of acetoin in the photochemistry of aqueous pyruvic acid. *Proc. Natl. Acad. Sci.* **2013,** *110*, E4274-E4275.

72. If not specified the terms “dimer” and “trimer” are used here to refer to covalently-bonded oligomeric species, rather than non-covalently associated species.

73. Leermakers, P. A.; Vesley, G. F. Organic photochemistry and the excited state. *J. Chem. Educ* **1964,** *41*, 535.

74. Turro, N. J.; Ramamurthy, V.; Scaiano, J. C., *Modern molecular photochemistry of organic molecules*. University Science Books: Sausalito, California, 2010.

75. Rossignol, S.; Tinel, L.; Bianco, A.; Passananti, M.; Brigante, M.; Donaldson, D. J.; George, C. Atmospheric photochemistry at a fatty acid–coated air-water interface. *Science* **2016,** *353*, 699-702.

76. Montgomery, J. A.; Frisch, M. J.; Ochterski, J. W.; Petersson, G. A. A complete basis set model chemistry. Vi. Use of density functional geometries and frequencies. *J. Chem. Phys.* **1999,** *110*, 2822-2827.

77. Frisch, M. J.; Trucks, G. W.; Schlegel, H. B.; Scuseria, G. E.; Robb, M. A.; Cheeseman, J. R.; Scalmani, G.; Barone, V.; Petersson, G. A.; Nakatsuji, H., et al. *Gaussian 09, revision d.01*, Gaussian, Inc.: Wallingford, CT, 2016.

78. Ogg, R. J.; Kingsley, R.; Taylor, J. S. WET, a T 1-and B 1-insensitive water-suppression method for in vivo localized ^{1}H NMR spectroscopy. *Journal of Magnetic Resonance, Series B* **1994,** *104*, 1-10.

79. Wolff, L. Ueber ein neues condensationsproduct der brenztraubensäure. *Justus Liebigs Ann. Chem.* **1901,** *317* 1–22.

80. Prey, V.; Waldmann, E.; Berbalk, H. Zur kenntnis der brenztraubensäure. *Monatshefte für Chemie und verwandte Teile anderer Wissenschaften* **1955,** *86*, 408-413.

81. Wolff, L. II. Ueber die parabrenztraubensäure. *Justus Liebigs Ann Chem* **1899,** *305*, 154-165.

82. Schnitzler, E. G.; Seifert, N. A.; Ghosh, S.; Thomas, J.; Xu, Y.; Jäger, W. Hydration of the simplest α-keto acid: A rotational spectroscopic and ab initio study of the pyruvic acid–water complex. *Phys. Chem. Chem. Phys.* **2017,** *19* 4440-4446.

83. Pocker, Y.; Meany, J. E.; Nist, B. J.; Zadorojny, C. Reversible hydration of pyruvic acid. I. Equilibrium studies. *J. Phys. Chem.* **1969,** *73*, 2879-2882.

84. Buschmann, H. J.; Dutkiewicz, E.; Knoche, W. The reversible hydration of carbonyl compounds in aqueous solution. 2. The kinetics of the keto gem-diol transition. *Ber. Bunsen-Ges. Phys. Chem* **1982,** *86*, 129-134.

85. Buschmann, H. J.; Füldner, H. H.; Knoche, W. The reversible hydration of carbonyl compounds in aqueous solution. Part I, the keto/gem - diol equilibrium. *Ber. Bunsen-Ges. Phys. Chem* **1980,** *84*, 41-44.

86. Vaida, V. Perspective: Water cluster mediated atmospheric chemistry. *J. Chem. Phys.* **2011,** *135*, Art. Nr. 020901.

87. Kumar, M.; Francisco, J. S. The role of catalysis in alkanediol decomposition: Implications for general detection of alkanediols and their formation in the atmosphere. *J. Phys. Chem. A* **2015,** *119*, 9821-9833.

88. Kramer, Z. C.; Takahashi, H.; Vaida, V.; Skodje, R. T. Will water act as a photocatalyst for cluster phase chemical reactions? Vibrational overtone-induced dehydration reaction of methanediol. *J. Chem. Phys.* **2012,** *136*, 164302.

89. Maroń, M. K.; Takahashi, K.; Shoemaker, R. K.; Vaida, V. Hydration of pyruvic acid to its geminal-diol, 2, 2-dihydroxypropanoic acid, in a water-restricted environment. *Chem. Phys. Lett.* **2011,** *513*, 184-190.

90. Pedersen, K. J. The dissociation constants of pyruvic and oxaloacetic acid. *Acta Chem. Scand.* **1952,** *6*, 243-256.

91. Viehe, H. G.; Janousek, Z.; Merenyi, R.; Stella, L. The captodative effect. *Acc. Chem. Res.* **1985,** *18*, 148-154.

92. Ronkainen, P.; Brummer, S.; Suomalainen, H. Diacetyl and formic acid as decomposition products of 2-acetolactic acid. *Acta Chem. Scand.* **1970,** *24*, 3404-3406.

93. De Man, J. The formation of diacetyl and acetoin from α - acetolactic acid. *Recl. Trav. Chim. Pays-Bas* **1959,** *78*, 480-486.

94. Renard, P.; Reed Harris, A. E.; Rapf, R. J.; Rainer, S.; Demelas, C.; Coulomb, B.; Quivet, E.; Vaida, V.; Monod, A. Aqueous phase oligomerization of methyl vinyl ketone by atmospheric radical reactions. *J. Phys. Chem. C* **2014,** *118*, 29421-29430.

95. Ranjan, S.; Sasselov, D. D. Influence of the UV environment on the synthesis of prebiotic molecules. *Astrobio.* **2016,** *16*, 68-88.

96. Rapf, R. J.; Vaida, V. Sunlight as an energetic driver in the synthesis of molecules necessary for life. *Phys. Chem. Chem. Phys.* **2016,** *18*, 20067-20084.

97. Cooper, G.; Reed, C.; Nguyen, D.; Carter, M.; Wang, Y. Detection and formation scenario of citric acid, pyruvic acid, and other possible metabolism precursors in carbonaceous meteorites. *Proc. Natl. Acad. Sci.* **2011,** *108*, 14015-14020.

98. Voet, D.; Voet, J. G., *Biochemistry*. 4 ed.; John Wiley and Sons, Inc: Hoboken, NJ, 2011.

99. Cody, G. D.; Boctor, N. Z.; Filley, T. R.; Hazen, R. M.; Scott, J. H.; Sharma, A.; Yoder, H. S. Primordial carbonylated iron-sulfur compounds and the synthesis of pyruvate. *Science* **2000,** *289*, 1337 -1340.

100. Griffith, E. C.; Shoemaker, R. K.; Vaida, V. Sunlight-initiated chemistry of aqueous pyruvic acid: Building complexity in the origin of life. *Origins Life Evol. Biosphere* **2013,** *43*, 341-352.

101. Guzman, M. I.; Martin, S. T. Prebiotic metabolism: Production by mineral photoelectrochemistry of alpha-ketocarboxylic acids in the reductive tricarboxylic acid cycle. *Astrobio.* **2009,** *9*, 833-842.

102. Shapiro, R. Small molecule interactions were central to the origin of life. *Q. Rev. Bio.* **2006,** *81*, 105-125.

5. Photochemical Synthesis of Oligomeric Amphiphiles from Alkyl Oxoacids in Aqueous Environments*

5.1 Introduction:

The reactivity and synthesis of lipid-like molecules are of interest for environmental chemistry of both the modern and ancient Earth.[2-10] In the environment, lipid-like molecules selectively partition to air-water interfaces. Sunlight can drive photo-initiated chemistry of organic species at air-water interfaces, such as the sea-surface microlayer (SML).[11-17] The SML contains high concentrations of amphiphilic organic molecules and, as the boundary layer between the ocean and atmosphere, connects processes at the sea surface with the atmosphere, including the generation of sea spray aerosol. Recent work suggests that oligomers formed from aqueous phase photochemistry of small organic molecules may contribute significantly to the formation and development of secondary organic aerosol (SOA).[18-26] The surface-active molecules found in the SML are often biological in origin,[15, 27, 28] but abiotic photochemical sources may be additional, important contributors.[12, 13, 24, 29-31] Such sunlight-driven reactions are critical in the understanding of the formation of marine-derived primary organic aerosol and SOA,[32-38] influencing visibility, human health, cloud formation, and radiative forcing.[18, 20, 39-46]

The present study investigates the photochemistry of a series of amphiphilic α-keto acids, also known as 2-oxoacids that will be referred to as oxoacids here, with varying alkyl tail lengths. Such oxoacids have been identified at the ocean surface and are significant contributors to the environment today[15, 47, 48] and likely would have been found on the early Earth.[49-52] In this chapter, we describe the general photochemical mechanism for α-keto

*This work was reproduced in part with permission from Rapf, R.J.; Perkins, R.J., Yang, H.; Miyake, G.M.; Carpenter, B.K.; Vaida, V. Photochemical Synthesis of Oligomeric Amphiphiles from Alkyl Oxoacids in Aqueous Environments. *Journal of the American Chemical Society*, *139*, 6946–6959, 2017. Copyright 2017 American Chemical Society.[1]

acids in aqueous solution under acidic conditions, investigating the effect of the alkyl tail length. By demonstrating this mechanistic understanding of the photochemistry of α-keto acids, we show its generalizability across a class of molecules, widening the library of species whose photolysis may contribute to the reactivity found in natural environments.

Previously, the photochemistry of the simplest of α-keto acid, pyruvic acid, has been studied in detail in both the gas[53-60] and aqueous phases,[29, 61-69] due to its atmospheric relevance.[48, 70-78] Like all α-keto acids, pyruvic acid absorbs light in the near-UV within the spectral range of wavelengths of sunlight that are available near the surface of the Earth, and direct photolysis is its main atmospheric sink.[29, 57, 58] In the aqueous phase, pyruvic acid readily forms oligomers,[29, 63, 64, 67, 79] including in atmospherically-relevant, multiphase studies using an environmental simulation chamber.[68] These covalently-bonded dimers and trimers[80] are generated in relatively high yields from the recombination of photochemically-generated organic radicals and are the major observed photoproducts, especially under oxygen-limited reaction conditions.[29, 63, 64, 67]

In this study, we examine the photo-reactivity in aqueous solution at unadjusted pH of four oxoacids (shown in Scheme 5.1) with differing saturated, linear alkyl chains, ranging from the four-carbon butyl tail of 2-oxohexanoic acid to the 10-carbon decyl tail of 2-oxododecanoic acid, and compare these results to the known photochemistry of pyruvic acid, possessing a single-carbon methyl tail. We demonstrate that the pyruvic acid photochemical mechanism is transferrable to molecules with the same reactive functional groups, including those compounds with longer alkyl chains that are relevant to the generation of the large, surface-active oligomer species that contribute to the SML. These longer-tailed species also follow additional reactive pathways that are not available to the short-tailed pyruvic acid, increasing the complexity of the mixture of photoproducts generated.

Organic photochemistry, as investigated here, also has significant implications for the

study of prebiotic chemical evolution and the generation of biomolecules in the absence of enzymatic assistance,[5] including the abiotic synthesis of lipid molecules.[5, 52] The synthesis of lipid molecules is interesting, not only because of the formation of a carbon-carbon bond in the absence of biology, but also because of the importance of such molecules in the formation of membranous enclosures. Such enclosures form the basis for protocells and are recognized as vital to developing and sustaining life.[10, 81-87]

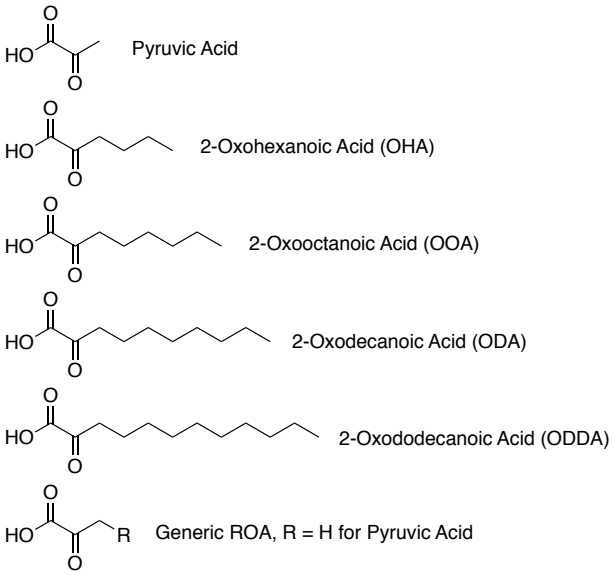

Scheme 5.1. Structures of pyruvic acid and the four oxoacids studied in this investigation: 2-oxohexanoic acid (OHA), 2-oxooctanoic acid (OOA), 2-oxodecanoic acid (ODA), 2-oxododecanoic acid (ODDA).

5.2 Experimental Section:

2-Oxooctanoic acid (OOA, ≥99.0%, Sigma-Aldrich) was diluted with 18.2 MΩ water (3 ppb TOC) to obtain solutions of 6, 3, and 1 mM and sonicated until fully dissolved. Solutions were filtered before use with a 0.1 μM syringe filter (MillexVV). The remaining alkyl oxoacids, 2-oxohexanoic acid (OHA), 2-oxodecanoic acid (ODA), and 2-oxododecanoic acid (ODDA), were synthesized as described in Chapter 3.2 and diluted in the same manner as OOA to obtain 1 mM solutions. 6 mM OHA and 3 mM ODA solutions were also used. Solutions consisting of mixtures of 1:1 OOA:ODA were obtained in the same manner with

either 3 mM or 1.5 mM concentrations of each oxoacid, giving a total amphiphile concentration of either 6 or 3 mM, respectively. It has recently been suggested that solutions of OOA at similar concentrations to those used here can result in the formation of vesicles.[88] We do not observe this under our experimental procedure. Dynamic light scattering of the pre-photolysis solutions (OHA, OOA, ODA, and OOA/ODA) confirmed that aggregates were not detectable in our solutions prior to irradiation.

The solutions were used without adjustment from their natural pH, meaning all photolyses were conducted under acidic conditions. There is a slight variance in the pH of the solutions as a function of the concentration of ROA. For example, the 6 mM OOA solutions are pH ~2.5, increasing slightly to ~2.8 and ~3.3 for the solutions at 3 mM and 1 mM, respectively. The pH of the solutions at a given concentration of ROA does not change significantly as the identity of the ROA is changed. The pH of 3 mM ODA is also ~2.8, and the observed pH for each ROA at 1 mM varies only slightly, between ~3.3 and ~3.7. These pH ranges are in keeping with the previously observed pH for solutions of pyruvic acid at similar concentrations (10 mM ~2.4 and 0.5 mM ~3.5).[67] This is suggestive that the pK_a of each ROA does not change significantly as alkyl tail length is varied. The effective pK_a of OOA has recently been determined to be 2.78,[88] which is similar to the well-known effective pK_a of pyruvic acid of 2.49.[89] The term effective is used to describe these pK_a values because the titration method of determining pK_a necessarily includes contributions from both the keto and geminal-diol conformers in solution (discussed below), which each also have individual values of pK_a.[90]

For each photolysis, 100 mL solutions were prepared, saving 10 mL as a pre-photolysis control, and photolyzing the remaining 90 mL of solution for 5 hours, using a 450 W ozone-free Xe arc lamp (Newport). Solution temperature was controlled by a temperature-stabilized water bath. For the 1 mM solutions of each oxoacid the water bath was held at 20

°C because of solubility concerns for ODDA. The higher concentrations of OHA, ODA, and OOA were also conducted at 4 °C. No difference was observed in products with changes in the water bath temperature. Unless otherwise stated, each solution was purged with N_2, in order to displace dissolved O_2. Solutions were purged for the duration of photolysis, beginning for one hour prior to the start of illumination. After photolysis, the solutions were brought to room temperature before any further analyses were conducted.

The absorption maximum of the excitation from the ground state to the S_1, $^1(n, \pi^*)$, state for each of the oxoacids examined here occurs at λ_{max} ~315 nm. This is a slight blue shift from that of pyruvic acid (λ_{max} ~320 nm),[29, 67] but there is not an a significant change in the absorption maximum as a function of changing alkyl tail length as for the four oxoacids investigated here (spectra shown in Figure E.1).

The spectral output of the unfiltered Xe arc lamp used in these studies extends into the UV to about 220 nm as shown in Figure E.1. Therefore, it is likely that, under our experimental conditions, some excitation to the S_2, $^1(\pi, \pi^*)$, state also occurs in addition to excitation to the S_1 state. This is unlikely to alter any reaction pathways, as it is known that, upon excitation to higher excited states, such as the S_2 state, systems often rapidly undergo internal conversion to the first excited (S_1) state.[91, 92] This process is expected to occur here, allowing the normal photochemical pathway of intersystem crossing and internal conversion from the S_1 state to the reactive T_1 state to follow. It has been previously observed that the photochemical products generated from the photolysis of pyruvic acid using an unfiltered Xe arc lamp[67] are in good agreement to those obtained when the Xe lamp is filtered to remove wavelengths $\lambda < 300$ nm;[29] however, the rate of photolysis is slowed when the Xe lamp is filtered, as would be expected when fewer photons are present. The S_2 state cannot be excited with $\lambda > 300$ nm, suggesting the same reactive photochemical pathways are followed when the lamp remains unfiltered, without additional

reactive pathways stemming from excitation to the S_2 state. This is consistent with other observations in the literature, which have shown, for example, that the photochemistry of nonanoic acid in aqueous solution is faster but does not result in the formation of different products when an unfiltered Xe arc lamp is used.[13]

5.2.1 Synthesis of Alkyl Oxoacids: The same general procedure was used to synthesize each of 2-oxohexanoic acid, 2-oxodecanoic acid, and 2-oxododecanoic acid. The general synthetic procedure is outlined in Chapter 3.2. Detailed information and characterization of each synthesized oxoacid are given in Appendix E, along with ^{1}H and ^{13}C NMR spectra (Figures E.2-E.4).

5.2.2 Product Analysis: Detailed information and instrument parameters for the analytical techniques used to characterize the photolysis solutions (dynamic light scattering, UV-vis and NMR spectroscopy, and high resolution negative mode electrospray ionization mass spectrometry) are given in Chapter 3. In the ESI^- MS, both $[M-H]^-$ and singly-charged adduct ions are observed for the analytes of interest under the ionization conditions used here. The observed non-covalent adduct ions are formed from the coordination of two or more deprotonated organic species with a metal ion and a net charge of -1. We observe, primarily in the pre-photolysis controls, adduct ions consisting of multiple deprotonated oxoacid molecules coordinated with a positive counterion, usually Na^+ or Ca^{2+}. All photolyses were conducted in 18.2 MΩ water without the addition of salt to minimize the presence of such adduct ions, and any metal ions are assumed to be present only in trace quantities in solution. The ESI^- MS analysis procedure used is described in Chapter 3.4.

5.3 Results And Discussion:

Here we report on the generation of surface-active oligomers from the aqueous photochemistry of a series of four α-keto acids with differing alkyl tail lengths (2-

oxohexanoic acid (OHA), 2-oxooctanoic acid (OOA), 2-oxodecanoic acid (ODA), and 2-oxododecanoic acid (ODDA) shown in Scheme 5.1). The photochemical mechanisms governing this chemistry follow those that have been previously reported in the literature,[52, 93-95] primarily from detailed studies of the aqueous photolysis of pyruvic acid.[29, 62, 64, 65, 67, 96, 97] Here, we perform a detailed high-resolution negative mode electrospray ionization mass spectrometry (ESI^-MS) analysis, supported by NMR studies, to show that this chemistry is robust and broadly transferable to a whole class of molecules with the same reactive functionality and generates multi-tailed lipids.

The aqueous photolysis of each oxoacid we study here follows the same general mechanism, regardless of the alkyl tail length, detailed descriptions of which can be found in previous work on pyruvic acid.[29, 64, 67] For clarity, here we will describe briefly the mechanistic pathways of this chemistry for the general case of an oxoacid with an arbitrary alkyl tail, R, abbreviated as ROA. The photochemistry holds for each of the specific alkyl tails examined (R = $(CH_2)_2CH_3$, $(CH_2)_4CH_3$, $(CH_2)_6CH_3$, and $(CH_2)_8CH_3$). Similarities and differences between the known photochemical behavior of pyruvic acid (R = H) will be discussed when relevant.

The solubility of the molecules investigated decreases as a function of chain length, so to facilitate comparison across alkyl tail lengths, photolyses for each oxoacid were conducted at concentrations of ~1 mM and at 20 °C. These experimental conditions approached the solubility limit of ODDA. Photolyses of 6 mM and 3 mM OOA and 3 mM 2-oxodecanoic acid ODA were also conducted at 4 °C. There were no observable differences in the products generated during photolysis when the water bath temperature was changed from 4 °C to 20 °C for OOA and ODA.

Despite the low concentrations required, photochemical products were still readily observed for each oxoacid. Averaged MS results for OOA are given in Table 5.1 with

representative mass spectra for both the pre- and post-photolysis solutions of OOA given in Figure 5.1. A summary of the MS results for the other alkyl oxoacids, OHA, ODA, and ODDA, are given in Table 5.2. Detailed MS results for each oxoacid are also given in the supporting information (Figures E.5-E.7 and Tables E.1-E.4).

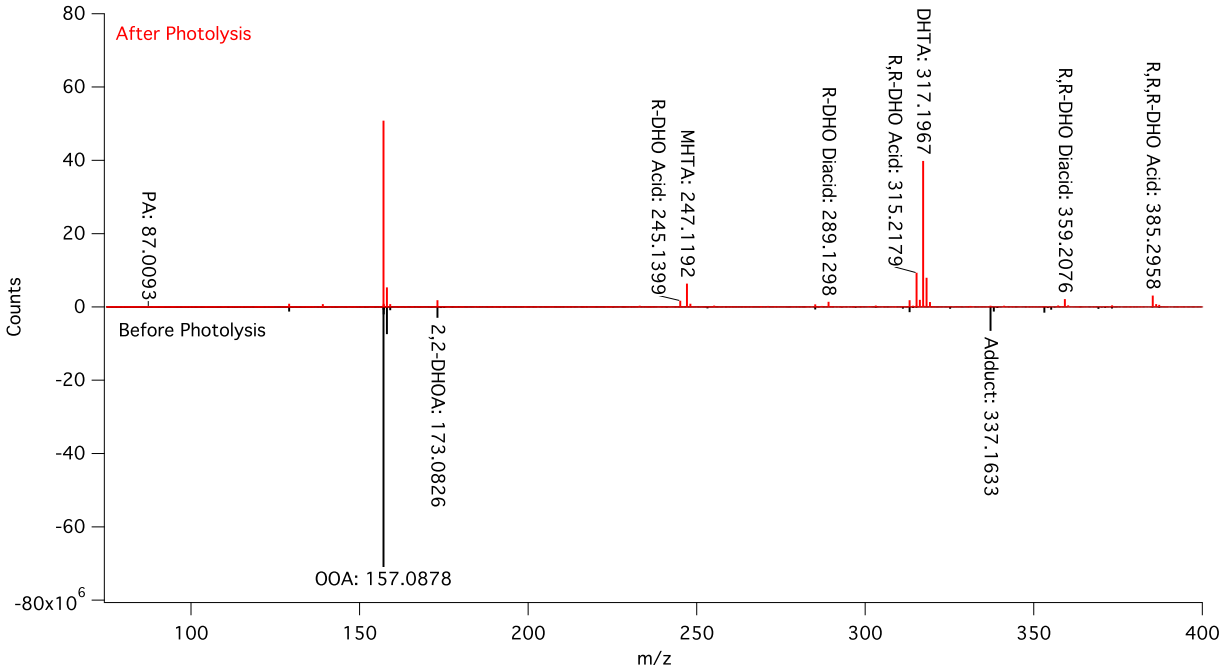

Figure 5.1. Representative MS of 3 mM OOA pre (black, counts multiplied by -1 for ease of presentation) and post (red) 5 hours of photolysis in N_2; high molecular weight products are not observed.

In aqueous solution, the ketone group of ROA can be hydrated to the geminal diol form of the acid, R,gemdiol-alkanoic acid (RGDA).[29, 64, 67] These 2,2-dihydroxyalkanoic acids, unlike the ketone form, do not absorb light within the solar spectrum. Unlike many α-dicarbonyl species, which are almost completely hydrated in aqueous solution, oxoacids retain a significant amount of ketonic functionality.[90, 98, 99] It has been shown for pyruvic acid that the extent of hydration is concentration-, pH-, and temperature-dependent,[67, 90, 99-101] with percentages of diol conformer ranging from ~65% at 100 mM to ~50% at 10 mM concentrations.[29, 63, 67] The longer-tailed oxoacid species under study here retain significantly more ketonic functionality in aqueous solution than pyruvic acid. 6 mM OOA

at ambient temperature exists as roughly 80% keto and 20% diol in solution as characterized by NMR (Figure E.8). Both conformers are also observed in the MS data (Figure 5.1 and Table 5.1). The ratio of keto to diol conformers does not appear to change as a function of tail length for any of the longer-tailed species we investigate here. For example, ODA, which has two more carbons than OOA in its alkyl chain, also exists as approximately 80% keto conformer in solution under our reaction conditions (Figure E.9).

Table 5.1. Select Compiled 2-Oxooctanoic Acid Photolysis Mass Spectra Data[a]

Assigned Formula $[M-H]^-$	Assigned Structure	Average Experimental m/z[b]	Theoretical m/z	Mass Diff. (ppm)	Pre-Photolysis	Post-Photolysis
$C_3H_3O_3$	Pyruvic Acid	87.0092 ± 0.0006	87.0082	10.9	Below Threshold	Weak
$C_8H_{13}O_3$	2-Oxooctanoic Acid	157.0880 ± 0.0005	157.0865	9.6	Strong	Strong
$C_8H_{13}O_4$	2,2-DHOA[c] (OOA Diol)	173.0826 ± 0.0004	173.0814	7.0	Medium	Medium
$C_6H_9O_6$	Dimethyl-tartaric Acid	177.0411 ± 0.0005	177.0400	6.6	Below Threshold	Weak
$C_{12}H_{21}O_5$	R-DHO Acid	245.1400 ± 0.0005	245.1389	4.4	Below Threshold	Medium
$C_{11}H_{19}O_6$	Methylhexyl-tartaric Acid	247.1193 ± 0.0005	247.1182	4.6	Below Threshold	Strong
$C_{13}H_{21}O_7$	R-DHO Diacid	289.1301 ± 0.001	289.1288	4.7	Below Threshold	Medium
$C_{17}H_{31}O_5$	R,R-DHO Acid	315.2181 ± 0.0006	315.2172	3.0	Below Threshold	Strong
$C_{16}H_{29}O_6$	Dihexyltartaric Acid	317.1973 ± 0.0005	317.1965	2.8	Below Threshold	Strong
$C_{18}H_{31}O_7$	R,R-DHO Diacid	359.2071 ± 0.0007	359.2070	0.29	Below Threshold	Medium
$C_{22}H_{41}O_5$	R,R,R-DHO Acid	385.2958 ± 0.0003	385.2954	0.83	Below Threshold	Medium
$C_{23}H_{41}O_7$	R,R,R-DHO Diacid	429.2855 ± 0.0008	429.2860	-1.2	Below Threshold	Weak

[a]Chemical formulas are assigned as the ionized $[M-H]^-$ species; structures are assigned as the neutral species. [b]The experimental m/z is the observed average across experiments, and the uncertainty given is the 95% confidence interval. [c]2,2-DHOA = 2,2-dihydroxyoctanoic acid, the gem-diol form of OOA.

Additionally, even under our acidic reaction conditions, because the effective pK_a of

alkyl oxoacids is about ~2.6,[88, 89] a significant percentage of ROA that are deprotonated in solution, with preferential deprotonation of the photoactive, keto conformer.[90] This reduces the number of photoactive protonated species available for excitation, and at higher pH the rate of photolysis for pyruvic acid has been observed to slow.[65] However, under our acidic reaction conditions, the photochemistry still readily proceeds.

Table 5.2. Summary of Key MS Data for OHA, ODA, ODDA[a]

	[M-H]⁻	Avg. Exp. *m/z*[b] (ppm)	[M-H]⁻	Avg. Exp. *m/z*[b] (ppm)	[M-H]⁻	Avg. Exp. *m/z*[b] (ppm)	**Pre-hn**[c]	**Post-hn**[c]
Identity	2-Oxohexanoic Acid, R = $(CH_2)_2CH_3$		2-Oxodecanoic Acid, R = $(CH_2)_6CH_3$		2-Oxododecanoic Acid, R = $(CH_2)_8CH_3$			
ROA	$C_6H_9O_3$	129.0550 (-1.5)	$C_{10}H_{17}O_3$	185.1186 (4.5)	$C_{12}H_{21}O_3$	213.1502 (5.2)	**S**	**S**
R-DHO Acid	$C_{10}H_{17}O_5$	217.1077 (0.3)	$C_{14}H_{25}O_5$	273.1708 (1.9)	$C_{16}H_{29}O_5$	301.2025 (3.2)	**B.T.**	**M**
R,M-TA[d]	$C_9H_{15}O_6$	219.0868 (-0.5)	$C_{13}H_{23}O_6$	275.1500 (1.8)	$C_{15}H_{27}O_6$	303.1820 (4.0)	**B.T.**	**M**
R,R-DHO Acid	$C_{13}H_{23}O_5$	259.1546 (-1.5)	$C_{21}H_{39}O_5$	371.2805 (1.9)	$C_{25}H_{47}O_5$	427.3450 (6.1)	**B.T.**	**M**
R,R-TA[e]	$C_{12}H_{21}O_6$	261.1339 (0.0)	$C_{20}H_{37}O_6$	373.2595 (1.2)	$C_{24}H_{45}O_6$	429.3215 (-0.3)	**B.T.**	**S**
R,R,R-DHO Acid	$C_{16}H_{29}O_5$	301.2015 (0.6)	$C_{28}H_{53}O_5$	469.3890 (-0.7)	B.T.		**B.T.**	**M**

[a]Chemical formulas are assigned as the ionized [M-H]⁻ species; structures are assigned as the neutral species. [b]The experimental *m/z* is the average observed mass across experiments. Values in parentheses are the averaged mass differences from the theoretical *m/z* given in ppm. [c]Relative intensities of the observed MS species are given as S = Strong, M = Medium, B.T. = Below Threshold. [d]R,M-TA = R,Methyl-tartaric Acid, [e]R,R-TA = R,R-Tartaric Acid

In aqueous solution, photolysis begins when the oxoacid, ROA, is excited by a UV photon from the ground state to the S_1, $^1(n, \pi^*)$, state (λ_{max} ~315 nm), which is followed by intersystem crossing and internal conversion to the T_1, $^3(n, \pi^*)$, state (Reaction 1 of Scheme 5.2). ROA in the excited T_1 state then form radical species by abstracting a hydrogen from another oxoacid, which can occur via two different pathways (Scheme 5.2),[67] depending on the site of hydrogen abstraction. In the first (Reaction 2 of Scheme 5.2), hydrogen

abstraction occurs at the carboxyl group of either ROA or its geminal diol form (RGDA) and is followed by decarboxylation to form two radical species, one with hydroxy-acid functionality (denoted RHA•) and one with geminal diol functionality (denoted RGD•). For pyruvic acid, abstraction from the diol form is favored energetically, but it has been shown that abstraction from the keto conformer can also occur.[64] Even with the lower amounts of diol observed for ROA compared to pyruvic acid, it is clear from the products observed by ESI^- MS that hydrogen abstraction at the carboxyl group readily occurs for all the oxoacids under consideration here and is likely the dominant site of abstraction.

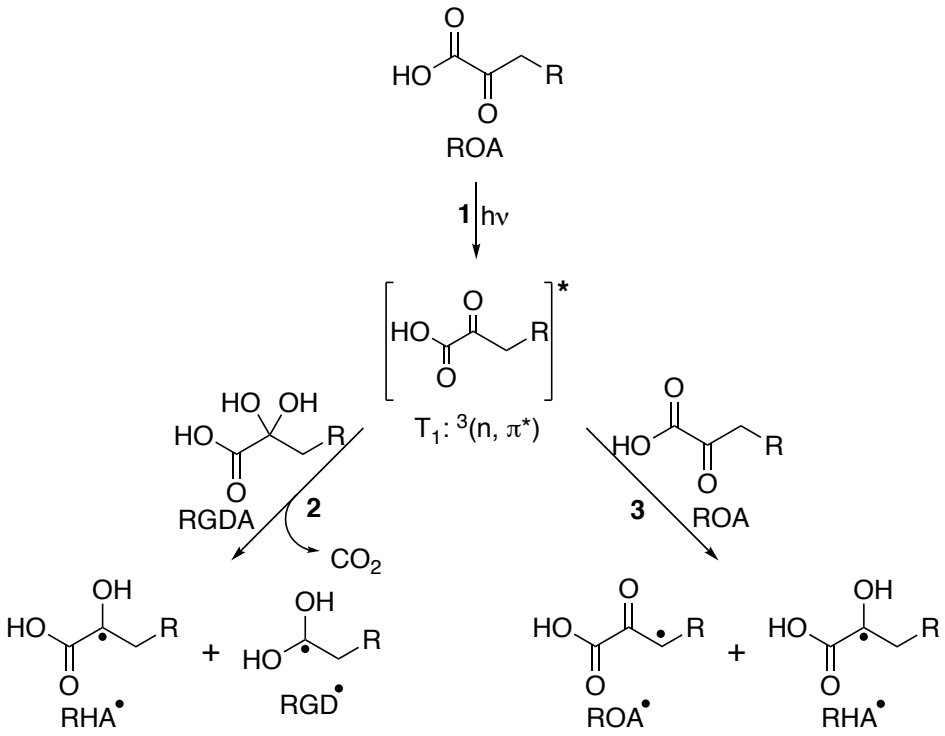

Scheme 5.2. Formation pathways of radical species during the aqueous photolysis of oxoacids.[102]

In the second possible pathway (Reaction 3 of Scheme 5.2), the excited ROA in the T_1 state abstracts a hydrogen from the alkyl tail of another, ground state ROA. Calculations have shown that hydrogen abstraction from the methyl group of pyruvic acid is likely to be competitive with hydrogen abstraction from the carboxyl group.[67] This competitiveness of

this pathway is also likely increased in dilute solutions where pH is slightly higher because the methyl group becomes the only site available for abstraction when the keto form of pyruvic acid is deprotonated.[67] It is reasonable, then, to assume that abstraction from the alkyl tail for ROA is likewise energetically-competitive, occurring to some extent during photolysis, yielding both a radical that retains oxoacid functionality (ROA•) and RHA•. We have drawn, throughout our discussion, the hydrogen abstraction to form ROA• as occurring at the β-CH_2 group. While abstraction from this site may be favored, it can, in principle, occur anywhere along the alkyl chain.[103] Products that are generated from subsequent reactions of ROA• are observed in the MS of post-photolysis solutions, but ESI^- MS alone cannot differentiate where along the alkyl chain hydrogen abstraction has occurred. It is likely that the observation of a given chemical formula in the MS data corresponds to a mixture of constitutional isomers.

The three radical species (RHA•, RGD•, and ROA•) generated by these two hydrogen abstraction processes can recombine following a variety of pathways, explaining the majority of the observed photoproducts for each of the oxoacids under study here (Tables 5.1 and 5.2, with detailed MS results for each ROA in Table E.1-E.4). The products observed from further reactions of the radical pair, RHA• and RGD•, generated by hydrogen abstraction from the carboxyl group, are outlined in Scheme 5.3. Tartaric acid derivatives with two alkyl chains (R,R-tartaric acid), are formed from the recombination of two RHA• radicals, as shown by Reaction 4 of Scheme 5.3. R,R-tartaric acid (*e.g.* dihexyltartaric acid for OOA) appears to be one of the major photochemical products formed during photolysis for each of the oxoacids under study here. It is observed as the photoproduct with the highest intensity in the MS data in each of the post-photolysis solutions analyzed, regardless of whether the photolysis was conducted in air or under N_2. However, this is only a relative comparison as our ESI^- MS analysis was not designed to be

absolutely quantitative. The "R"s used in the names of product species throughout our discussion simply denote the presence of an alkyl chain; the "R"s do not represent an attempt at assigning the stereochemistry of these molecules, even though these tartaric acid derivatives do contain chiral centers (the implications of which are discussed further below).

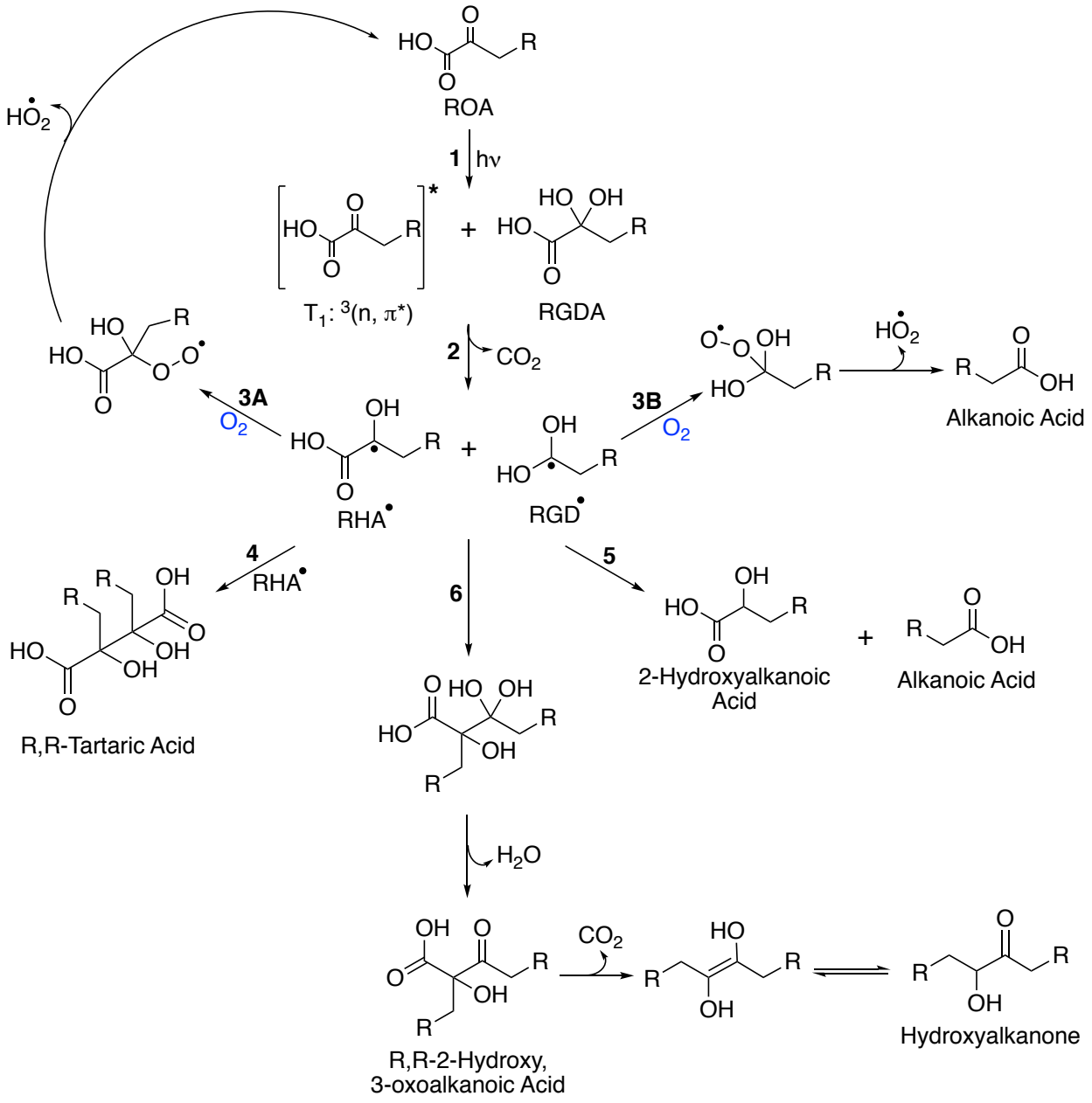

Scheme 5.3. General photochemical pathways of alkyl oxoacids following carboxyl hydrogen abstraction.

Further reactions stemming from the recombination of RHA• and ROA• generated by hydrogen abstraction from the alkyl tail of ROA account for several of the other main photoproducts observed by MS. As shown in Reaction 2 of Scheme 5.4, the recombination of RHA• and ROA• forms a derivative of parapyruvic acid with two alkyl chains, R,R-parapyruvic acid (R,R-PPA), which is observed in the MS for each of the ROA under study here (Table E.1-E.4). The reactions in Scheme 5.4 have been drawn showing hydrogen abstraction occurring at the β-CH_2 group, but it is possible for the hydrogen abstraction that generates ROA• to occur anywhere along the alkyl tail.

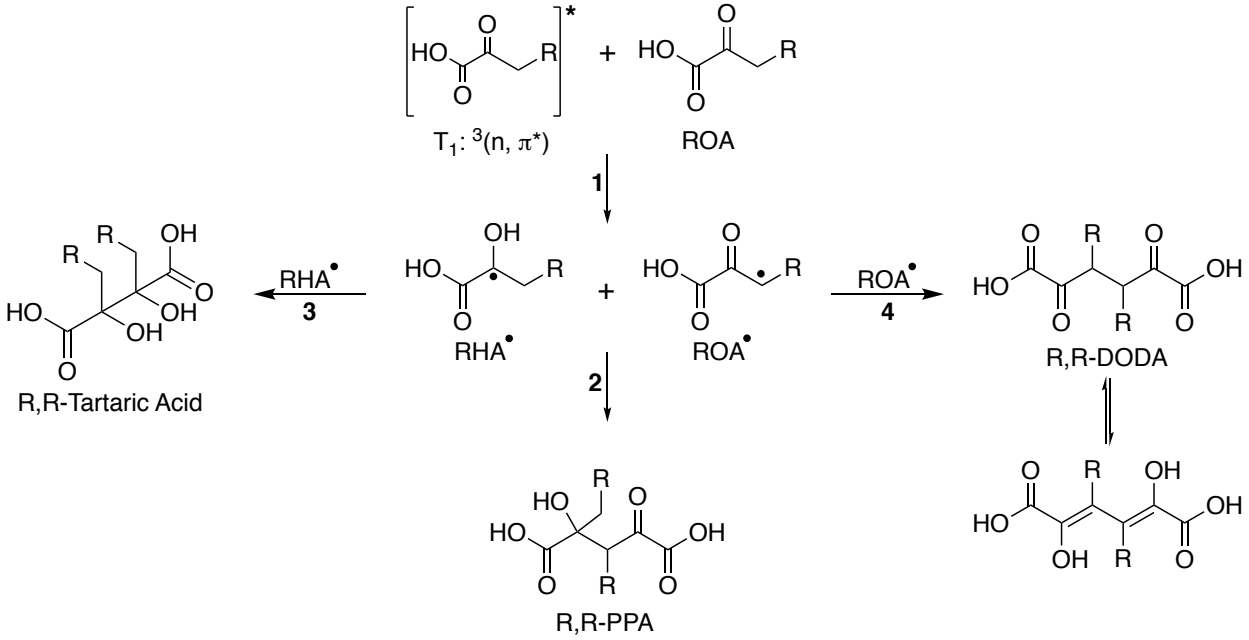

Scheme 5.4. Potential recombination pathways for alkyl oxoacids following alkyl hydrogen abstraction to form ROA•, here shown at the β-CH_2 site.[102]

In addition to the R,R-PPA and R,R-tartaric acid species, we have tentatively detected dioxoacid species, R,R-dioxodiacid (R,R-DODA), as photoproducts for most of ROA under study. Generated from the recombination of two ROA• radicals, as shown in Reaction 4 of Scheme 5.4, R,R-DODA likely exists in equilibrium with the enol in aqueous solution. In the post-photolysis solutions for OHA, ODA, and ODDA, we observe ions corresponding to the chemical formulas of R,R-DODA in the MS (Table E.2-E.4). Although, because the

intensities of the observed ions are at the cut-off threshold for detection for all three oxoacids, these assignments are tentative. However, these tentative detections help answer questions about the photochemical mechanism underlying the production of R,R-PPA.[67] The recombination of ROA• and RHA• that generates R,R-PPA cannot occur immediately after the two radicals are generated by hydrogen abstraction along the alkyl tail (Reaction 1 of Scheme 5.4) because the radical pair generated has an overall net triplet character, preventing intra-cage geminate recombination. Instead, before the radicals can react further, they must either undergo intersystem crossing back to the singlet state or undergo cage escape, either of which is possible. If intersystem crossing back to the singlet state is favored, then only R,R-PPA species should be detected; however, if the radicals undergo cage escape then products from each of the potential recombination processes for the RHA• and ROA• radicals should also be observed. As shown in Reaction 3 of Scheme 5.4, the recombination of RHA• radicals formed from this channel can also contribute to the formation of R,R-tartaric acid, while the recombination of ROA• radicals leads to R,R-DODA as mentioned above. In the previous study of pyruvic acid that initially proposed this mechanism, the dioxoacid, 2,5-dioxohexanedioic acid, was not observed in the MS,[67] possibly because of its own ability to react photochemically. This means that there was no way of differentiating between cage escape and intersystem crossing back to the singlet state, which would only generate parapyruvic acid as a product.[67] Here, the presence of R,R-DODA species, suggests that cage escape is the favored route by which the generated radical pair can recombine, rather than intersystem crossing back to the singlet state.

Regardless of the path by which they are formed, the R,R-PPA species created by the recombination of RHA• and ROA• are themselves photoactive. They are also α-keto acids and can, therefore, undergo the same photochemistry as other alkyl oxoacids, as shown in Scheme 5.5. Photoexcited R,R-PPA can then encounter another ROA, or the corresponding

RGDA in solution, which then decarboxylates, following the pathway outlined in Reaction 2 of Scheme 5.3, generating both a RGD• radical and a R,R-PPA radical (R,R-PPA•), as shown in Reaction 1 of Scheme 5.5. These two radicals can then combine, following Reaction 2 and 3 of Scheme 5.5, generating a dihydroxyoxodialkanoic acid with three alkyl chains (R,R,R-DHO Diacid) and, following decarboxylation, a dihydroxyoxoalkanoic acid (R,R,R-DHO Acid). The R,R,R-DHO acid is observed in the MS for each of the ROA except for ODDA (Table 5.1 and Table 5.2). The intermediate, R,R,R-DHO diacid is, however, observed for ODDA (Table E.4), as it is for ODA and OOA. For OHA, the R,R,R-DHO diacid is observed readily at 6 mM, but it is below the threshold for detection in the 1 mM solutions.

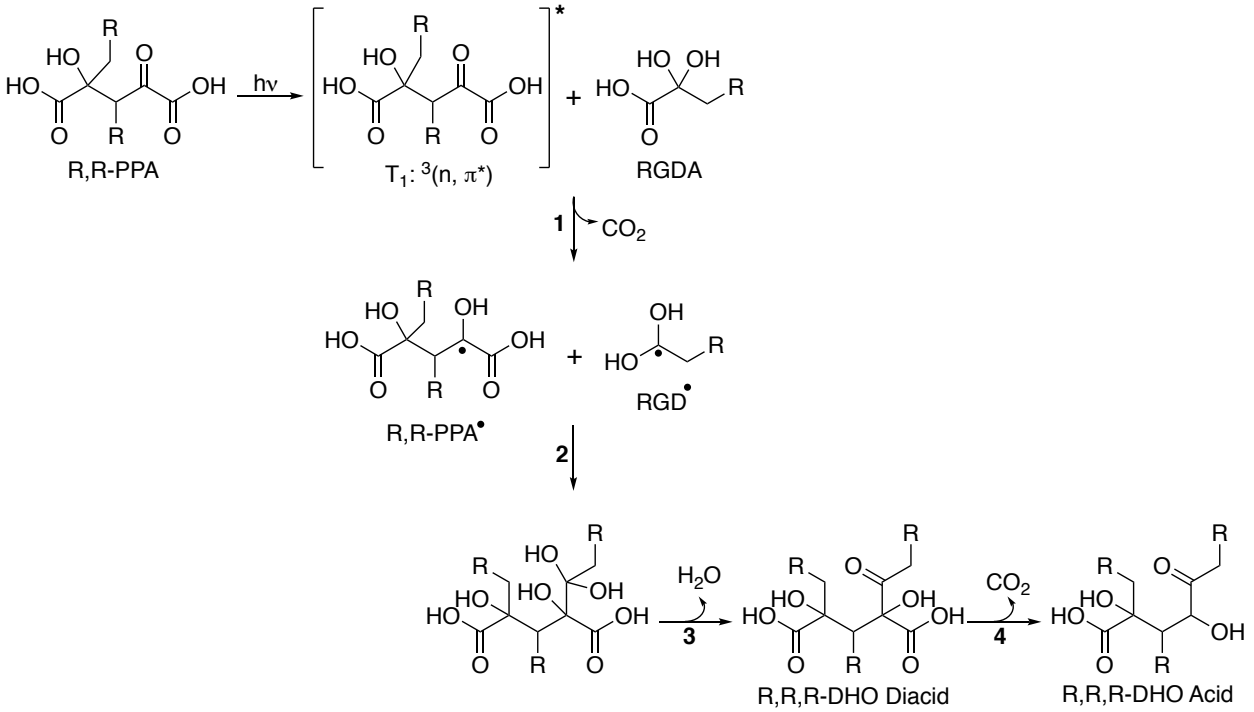

Scheme 5.5. *Photochemistry of R,R-PPA (here shown as formed from a β-CH_2 ROA•) to generate trimer species of ROA.*[102]

In addition to the photochemical pathways discussed above where organic radicals are generated from bimolecular interactions, there is also a unimolecular photochemical reaction pathway.[52] For the four ROA species investigated here, photoexcitation can lead to

an intramolecular Norrish Type II reaction as shown in Scheme 5.6. This is in contrast to pyruvic acid, which does not have an alkyl chain with the γ-carbon that is necessary for this chemistry to proceed. There has been some debate in the literature as to whether the Norrish Type II reaction happens from the singlet or the triplet state,[93, 94] with Davidson et al. 1981 presenting evidence for its occurrence on the singlet state.[94] Regardless of the manifold on which it occurs, the Norrish Type II reaction generates a biradical on the oxoacid (Reaction 1 Scheme 5.6) that then leads to homolytic bond cleavage (Reaction 2 Scheme 5.6).

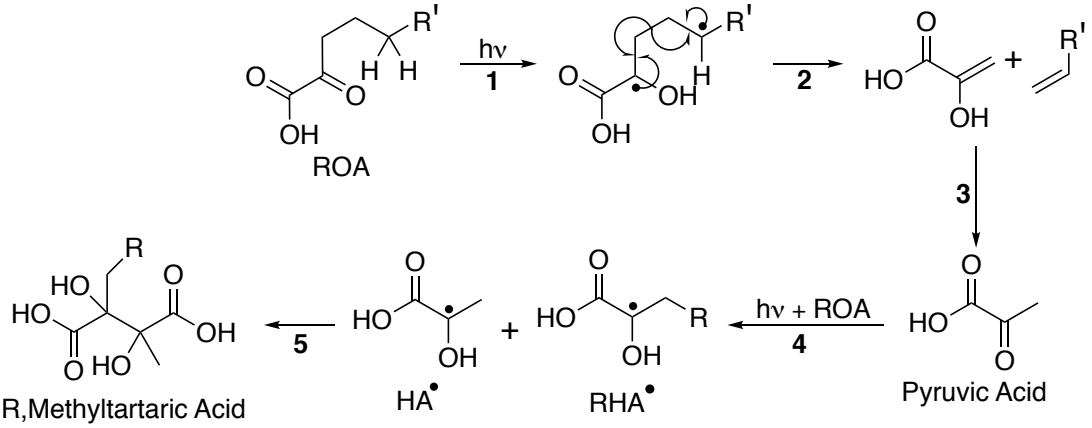

Scheme 5.6. General Norrish Type II reaction scheme for ROA.

This additional pathway adds considerably to the complexity of the photoproducts observed for longer-tailed alkyl oxoacids compared to pyruvic acid. The 2-hydroxy-3-propenoic acid generated by bond cleavage of the ROA in Reaction 2 of Scheme 5.6, can rearrange to form pyruvic acid, as shown in Reaction 3 of Scheme 5.6. This photochemically synthesized pyruvic acid can, of course, undergo all of its normal aqueous photochemistry,[29, 64, 67] including generating dimethyltartaric acid and 2,4-dihydroxy-2-methyl-5-oxohexanoic acid (DMOHA). Both of these species are observed in post-photolysis solutions for each ROA. The intensities of these species in the MS are near the threshold for detection, as would be expected given the probability of two minor species encountering each other in

solution.

It is far more likely that the photochemically generated pyruvic acid would encounter an ROA molecule, leading to a crossreaction between the two species. The most direct reaction involves the encounter of two radicals with hydroxy-acid functionality, HA• from pyruvic acid and RHA• from ROA. The recombination of these two species forms a tartaric acid derivative with one methyl and one alkyl chain, R,methyl-tartaric acid (Reaction 5 of Scheme 5.6). The R,methyltartaric acid species generated by this process was also observed clearly by MS as one of the main photoproducts for each of the four oxoacids.

As the radical species under study here are promiscuous and because of the formation of pyruvic acid from ROA via the Norrish Type II reaction, the photolysis of ROA leads to complex mixtures of products. Intermediate species, such as R,R-PPA and pyruvic acid, that can go on themselves to do further photochemistry, widely expand the photoproducts that can be formed. The formation of pyruvic acid in solution with ROA means that not only can R,R-PPA be formed from two ROA• radicals recombining, but R-PPA from the recombination of one ROA• and the pyruvic OA• and even parapyruvic acid itself from the recombination of two OA• can be formed. R-PPA species are observed for each of the oxoacids, although not for 1 mM OHA. The presence of parapyruvic acid is not observed by MS, but its concentration would be expected to be low due to the relatively low statistical probability of its formation.

R,R-PPA, R-PPA, and parapyruvic acid are oligomeric intermediate species that can go on to interact with either another ROA or pyruvic acid molecule in solution, following the reactions outlined in Scheme 5.5. This leads to the possible formation of several DHO diacid and DHO acid species, a few of which are shown in Scheme 5.7 for OOA. Even assuming the only site of hydrogen abstraction on the alkyl tail of ROA is the β-CH_2 group, there are a number of constitutional isomers possible for the R-DHO acid and R,R-DHO acids. Scheme

5.7 shows two such R,R-DHO acids, one generated by the reaction of R,R-PPA with a pyruvic acid molecule and one generated by the reaction of one of the potential isomers of R-PPA with OOA. Clearly there are other possible reactions that generate species with the same chemical formula and reactive functionality but different tail positions. Considering the potential for hydrogen abstraction from multiple sites along the alkyl tail considerably expands the pool of potential constitutional isomers generated by this chemistry as well. R,R-DHO acid and R-DHO acids are observed in the MS of the post-photolysis solutions for each of the ROA studied here, as are the corresponding diacid intermediates, with each observable peak likely corresponding to a mixture of constitutional isomers.

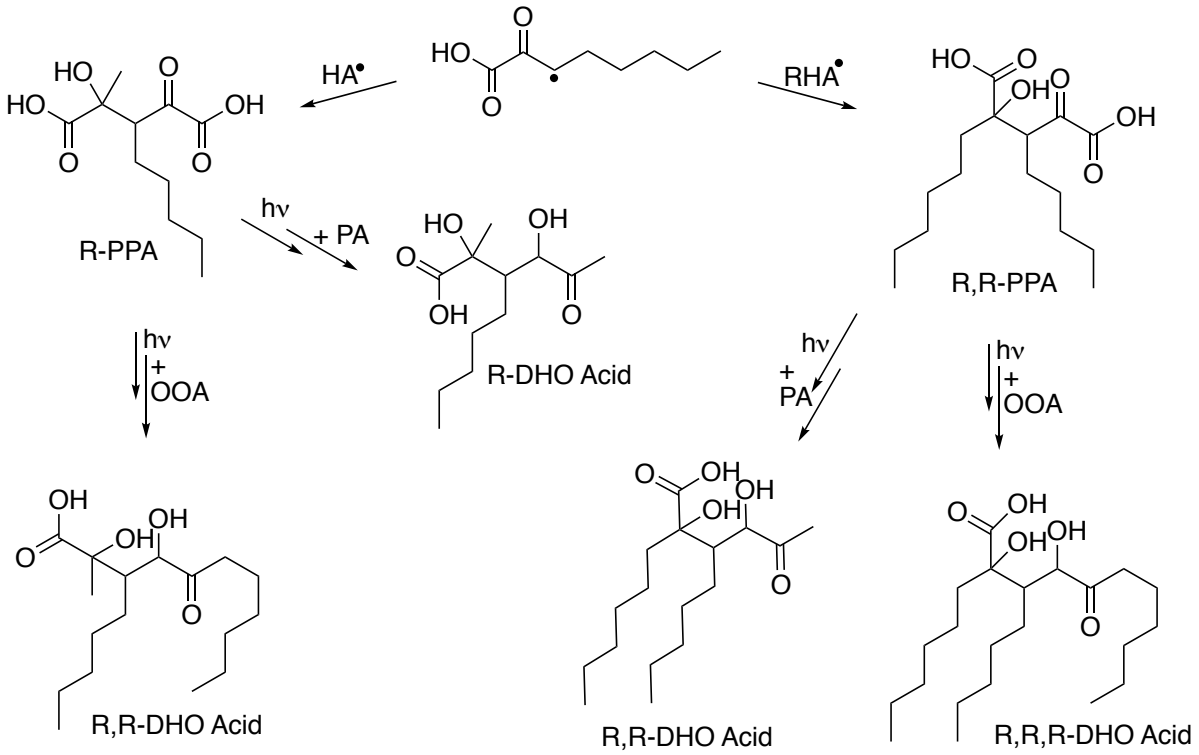

Scheme 5.7. *Select possible reaction pathways for ROA• derived from hydrogen abstraction from the β-CH_2 of OOA to form R,R,R-DHO acid species, where R = $(CH_2)_4CH_3$.*[102]

Pathways that generate reactive intermediate species, such as the formation of R,R-PPA and pyruvic acid, ensure that even an initial solution of a single ROA develops into a complex, interconnected network of reactions that generate a rich mixture of oligomeric

photoproducts upon photolysis. The generated radicals by the photolysis of oxoacids are capable of interacting not just with another identical oxoacid molecule but also with other radical species present in solution. Here, we show that the ability for cross-reactions carries through to the reaction between two different ROAs in solution, photolyzing a mixed solution of OOA and ODA. A representative post-photolysis mass spectrum is shown in Figure 5.2, with key results in Table 5.3 (a representative pre-photolysis spectrum is given in Figure E.10).

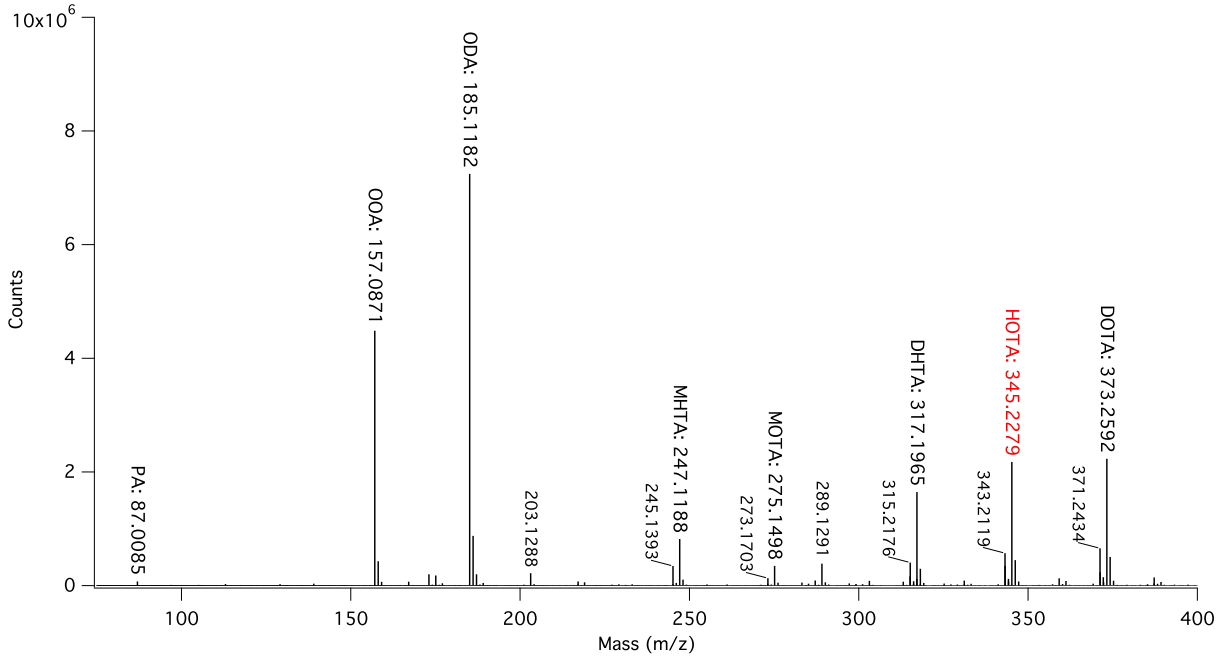

Figure 5.2. Representative MS of 3 mM OOA and 3 mM ODA after 5 hours of photolysis under N_2.

As shown in Scheme 5.6, when both OOA and ODA are in solution, the R,R-tartaric acid species generated are not only the corresponding dihexyltartaric acid (DHTA) and dioctyltartartic acid (DOTA), but also the tartaric acid species with differing tail lengths, hexyloctyltartaric acid (HOTA). As shown in Figure 5.2, when equal amounts of OOA and ODA are present in solution, the amount to HOTA generated is comparable to both DOTA and DHTA, suggesting that there is no great preference for like radicals to recombine with each other. This observation is likely because in order to form the R,R-tartaric acid, RHA•

must undergo cage escape and so there is no particular preference for either the partner in the solvent cage or the radicals they encounter following cage escape.

In addition to the mixed R,R'-tartaric acid, HOTA, the mixed DHO acid and DHO diacid products are also observed, as shown in Table 5.3. The R,R'-PPA species is formed from the recombination of either a ROA• and a R'HA• or a R'OA• and a RHA•. Any ROA• radical may, in principle, have the radical anywhere along the alkyl tail, as well, which further expands the number of possible isomers. Each of R,R-PPA, R',R'-PPA, R-PPA, R'-PPA, parapyruvic acid, and this new species R,R'-PPA can go on to react with either OOA, ODA, or pyruvic acid in solution. Of the many possible recombination products, the mixed trimer species, R,R',R'-DHO acid, R,R,R'-DHO acid, and the R,R'-DHO acid are newly observed photoproducts, along with the corresponding DHO diacid intermediate species.

Table 5.3. New photoproducts from the mixed photolysis of OOA and ODA[a]

Assigned Formula $[M-H]^-$	Assigned Structure	Average Experimental m/z[b]	Mass Diff. (ppm)	Pre-Photolysis	Post-Photolysis
$C_{18}H_{31}O_6$	R,R'-PPA	343.2113	-2.5	Medium	Medium
$C_{19}H_{35}O_5$	R,R'-DHO Acid	343.2490	1.5	Below Threshold	Medium
$C_{18}H_{33}O_6$	HexylOctyl-Tartaric Acid	345.2280	0.75	Below Threshold	Strong
$C_{20}H_{35}O_7$	R,-R' DHO Diacid	387.2380	-0.80	Below Threshold	Medium
$C_{24}H_{45}O_5$	R,R,R'-DHO Acid	413.2370	0.65	Below Threshold	Medium
$C_{26}H_{49}O_5$	R,R',R'-DHO Acid	441.3575	-1.2	Below Threshold	Medium
$C_{25}H_{45}O_7$	R,R,R'-DHO Diacid	457.3175	2.0	Below Threshold	Weak
$C_{27}H_{49}O_7$	R,R',R'-DHO Diacid	485.3480	0.27	Below Threshold	Weak

[a]Chemical formulas are assigned as the ionized $[M-H]^-$ species; structures are assigned as the neutral species. Here, R = $(CH_2)_4CH_3$ from OOA and R' = $(CH_2)_6CH_3$ from ODA. [b]The experimental m/z is the average observed mass across experiments.

Clearly, the introduction of even one other starting species greatly adds to the already complex mixture of photoproducts that may be generated from alkyl oxoacids. However, it is worth noting that, while there are many possible oligomeric photoproducts that may be

generated, each with several potential constitutional isomers, the photochemistry under study here can be explained using variants on well-understood mechanistic motifs,[29, 52, 64, 67] identifying a clear majority of the observed photochemical products, even for the mixed ROA solutions. Indeed, even the generation of R,R-DHO acid from the further reactions of R,R-PPA is, essentially, an equivalent reaction pathway to that which forms hydroxyalkanone (acetoin for pyruvic acid[64]) from the decarboxylation of the β-keto acid, R,R-2-hydroxy, 3-oxoalkanoic acid, which is generated from the recombination of RHA• and RGD•, as shown in Reaction 6 of Scheme 5.3.[67] The R,R-2-hydroxy, 3-oxoalkanoic acids are observed by MS for each ROA (Tables E.1-E.4) and for OOA the hydroxyalkanone is also observed as a minor photoproduct. However, this species is not observed above our detection threshold for any of the other ROA.

Simple fatty acid species (alkanoic acid) are also generated as a minor product from the photolysis of ROA, following Reaction 5 of Scheme 5.3. The alkanoic acid (e.g. heptanoic acid for OOA) is detected both before and after photolysis. It is likely that fatty acids are a common contaminant of the initial ROA starting material, just as acetic acid is a known contaminant of pyruvic acid. Interestingly, the corresponding 2-hydroxyalkanoic acid is not observed by MS for the ROA examined here. It has been previously shown that simple carboxylic acids do not have a strong intensity in the ESI^- MS under the experimental conditions used here,[67] and, given the presence of many other more surface-active photoproducts, the intensity of the MS signal is not quantitatively reflective of their concentration in solution. However, this may also indicate that the branching ratio of products observed for the longer-tailed, alkyl ROA differs somewhat from pyruvic acid. While both acetic acid and lactic acid generated from pyruvic acid following Reaction 5 of Scheme 5.3 are minor photoproducts under oxygen-limited conditions, they are readily observed by NMR[29, 64, 67] and lactic acid has been observed by MS as well.[67]

Small changes in product branching ratios between pyruvic acid and the longer-tailed ROA, such as OOA, would not be surprising. It also appears as though OOA has a slower rate of reaction than pyruvic acid. Quantifying the amount of OOA consumed during photolysis is more difficult than for pyruvic because of the additional signal in the NMR due to the hydrogens on the alkyl chains, but we estimate that for the 3 mM OOA solutions approximately 30% of the OOA is consumed after five hours of photolysis. This is a smaller yield than for pyruvic acid (~90% consumed) under similar reaction conditions.[67] It is possible that we are underestimating the consumption of OOA, as signal from some H atoms may be lost through the production of volatile species that partition to the gas phase, the formation of water, or, due to the large aggregates we observe, which will have low NMR response. The aggregates formed by OOA photolysis are discussed further below.

There are several likely contributing factors for this apparent decrease in reactivity for the longer-tailed oxoacid. Hydrogen abstraction is favored energetically from the diol form of the oxoacid rather than the keto form, therefore, the chemistry might be less favorable because the ratio of diol to keto shifts for the longer-tailed species. For solubility reasons, we used lower concentrations of OOA than PA (~3-6 mM OOA vs. 10 mM PA). Because the chemistry used to generate the oligomeric products relies on radical species encountering each other, the kinetics of reaction likely decrease for lower concentrations of oxoacid.

While the product yields and the exact branching ratios may differ slightly between pyruvic acid and the ROA studied here, the chemistry retains its sensitivity to environmental conditions even when longer alkyl chains are added to the oxoacids. The ESI^- MS experiments used here were not designed to be quantitative, but these results can be used to infer qualitative differences in product yields when comparing very similar samples, especially if the effect is large. As shown in Figure 5.3, the difference between the post-photolysis samples that were irradiated in air versus in nitrogen is stark. While the

oligomeric dihexyltartaric acid is the major observed product under both conditions, considerably more of the oligomeric products are formed in a nitrogen environment. Interestingly, while this effect is also seen in the NMR, the overall decrease in OOA concentration is only modestly increased under a nitrogen atmosphere (Figure E.11), shifting from approximately 20% consumption in air to 30% in nitrogen following five hours of photolysis. As mentioned above, this relatively small shift could be due to the loss of signal when the generated products are tied up into larger aggregates. Additionally, because the products generated by photolysis are oligomers of OOA, even a relatively modest change in overall consumption can have a large effect on the formation and yield of photoproducts. For example, there is a noticeable decrease in the relative amounts of the oligomeric photoproducts that are formed from the further reactions of species generated by photolysis, such as methylhexyltartaric acid and the DHO acid species. This result suggests that those processes that require two photochemical steps are less favored in the presence of oxygen, which can act as a radical quencher.

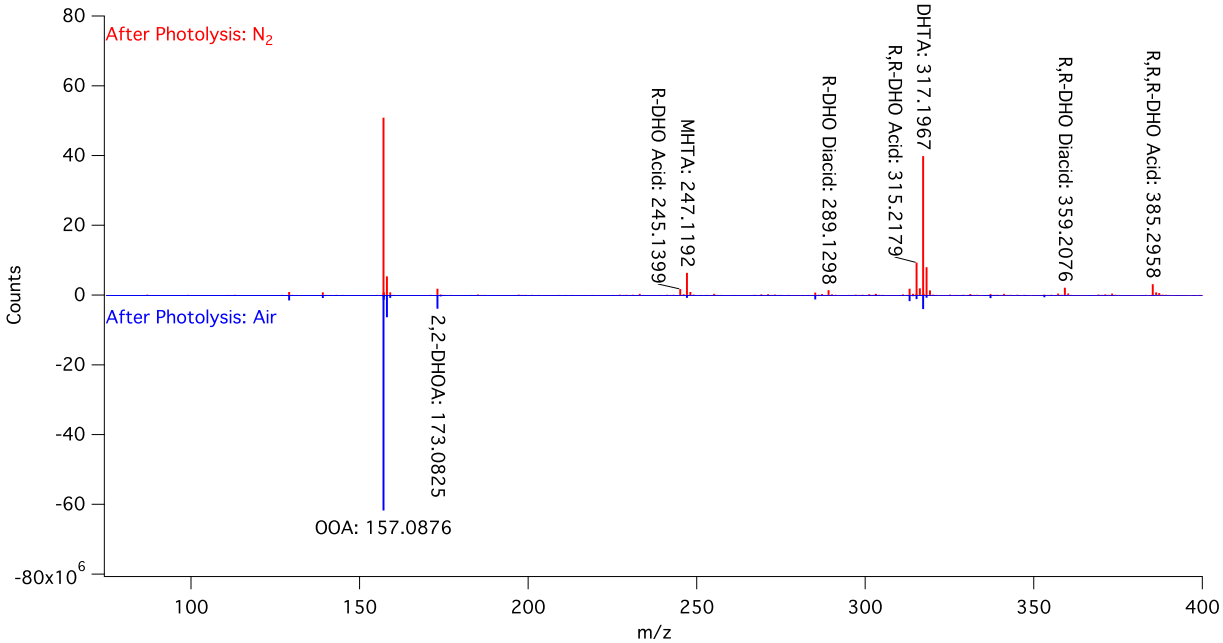

Figure 5.3. Representative MS of 3 mM OOA after five hours of photolysis under N_2 (red) and open to air (blue, counts multiplied by -1 for ease of presentation).

We have observed here, for the first time, that environmental conditions such as the concentration of oxygen in the photolysis reactor, affects the longer-tailed oxoacids in the same manner as was demonstrated for pyruvic acid.[29] The increased yield of such oligomers in the absence of oxygen is to be expected, given both that oxygen is known to quench triplet state chemistry, and that oxoacids may be regenerated through reactions with oxygen (Reaction 3A in Scheme 5.3). However, it is worth noting that, while the formation of oligomeric products is reduced when oxygen is present in solution, oligomers are still formed and are the major observable product. This is consistent with previous studies on pyruvic acid that show that oligomers are formed in the presence of oxygen,[29, 69] including under conditions that closely replicate the modern atmosphere.[68] Nevertheless, the ability to shift the reaction branching ratios by shifting environmental conditions has significant implications, especially for longer, lipid-like oxoacids.

Anoxic conditions favor the formation of more complex oligomeric species, many of which have two or three alkyl chains. This dependence is intriguing because the prebiotic atmosphere, unlike that of today, contained very little O_2 and ozone, allowing more UV light to reach the Earth's surface.[5, 104] The absence of oxygen in the prebiotic atmosphere would render the common, modern photo-oxidation reactions with hydroxyl radical negligible, and makes it likely that direct photochemistry of carbonyl-containing compounds would be a more significant process on the ancient Earth than it is today. This points to the potential of such chemistry to generate more complex, double- and triple-tailed amphiphiles under prebiotically-relevant conditions. This chemistry is among one of the only processes by which multi-tailed lipids from single-tailed precursors can be formed simply and in relatively high yields under prebiotically-plausible conditions and using prebiotically-plausible precursors.[5, 52]

The generation of a large library of photoproducts, including that of mixed oligomeric

species from two different ROA, shows the specificity of the photochemistry governing the formation of the radicals from oxoacids, while also demonstrating their ability to react promiscuously with other species in solution. The reactivity of mixtures and the ways in which such mixtures produce molecular complexity is inherently more applicable to environmental chemistry whether on the modern or ancient Earth than single molecule systems.

The photochemical pathways followed by oxoacids are robust and readily generalizable to the series of molecules under study here. While, for example, the Norrish Type II reaction pathway is accessible for the longer-tailed oxoacids, it is remarkable how consistent the generated photoproducts are across alkyl tail lengths. Although, within the photochemical framework there are many constitutional isomers possible for the R,R-DHO acids generated by Scheme 5.5 for the longer-tailed species, which we cannot distinguish within the scope of this study, it is remarkable how well a relatively simple mechanistic framework can describe the observed photochemistry. For each ROA under study, almost all significant ions that are observed in the MS corresponding to oligomeric species can be identified in this way, with only a few minor ions escaping classification. One might expect that as the molecules under study are increased in size, the complexity of the observed products would also increase. This is, however, not the case. If anything the observed MS are "cleaner" than those of pyruvic acid under similar reaction conditions.[67] This could be because of the surface partitioning of the longer-tailed species during mass spectrometry analysis, which is biased towards observation of the more surface-active species, a bias that increases with the longer alkyl tail of the starting oxoacid. Or, it could be because of the steric effects of the oligomerization process cutting off further reaction channels that produce minor products.

5.3.1 Properties of Generated Photoproducts

The major products, the tartaric acid derivatives and DHO acids, are interesting because they are molecules with chiral centers that have been produced from achiral starting materials. The tartaric acid derivatives produced, R,-R-tartaric acid and the R-methyl-tartaric acid, have two chiral centers. For the double-tailed, R,-R-tartaric acid molecules, one of the three stereoisomers produced is a meso isomer; however, in the case of the R,-methyl-tartaric acid molecules and the mixed HOTA molecule, there is no meso-isomer. In the case of the DHO acids, for oxoacids larger than pyruvic acid, there are always at least two chiral centers on each molecule, with the potential for three. The molecules generated are almost certainly a racemic mixture of all the possible isomers. However, as has been noted in the literature, enantioselective environments may be able to generate an optically active product mixture.[105-108]

The abiotic production of chiral molecules under environmentally-relevant conditions points to the importance of understanding the sources of chiral molecules in the modern environment. The SML and the surfaces of aerosols have been shown to contain chiral molecules, including lipids,[109] but these are almost always assumed to be biotic in origin.[15, 27, 28] However, as demonstrated here, it is possible to make chiral molecules in high yields from very simple, achiral precursors, suggesting that the potential for abiotic environmental sources of chirality should not be discounted.

During photolysis, oligomeric photoproducts with two and three alkyl chains are generated from single-chained ROA species. These multi-tailed amphiphilic products will likely have more surface activity than starting material, as has been shown for OOA.[52] The increase in surface activity during photolysis also translates to a reduction in the critical aggregation concentration. Each of the oxoacids is observed to undergo self-assembly, forming aggregates that scatter light and turn the solutions visibly cloudy. For OHA, OOA,

and the mixed solutions of OOA and ODA the aggregates were characterized using DLS, and found to be monodisperse and uniform, with sizes ranging from ~150 nm to ~250 nm in diameter, depending on the ROA (Table 5.4). This aggregation behavior has been previously reported for OOA, with microscopy indicating a spherical morphology.[52] However, even the very short-chained OHA is observed to assemble into such aggregates, with an average size of ~250 nm in diameter, larger than the ~160 nm observed for OOA. Prior to photolysis, the precursor oxoacids do not form aggregates, as confirmed by DLS, and are below their critical aggregation concentration (except for, perhaps, ODDA), but as the photolysis generates multi-tailed oligomeric species aggregation is observed, even at 1 mM initial starting concentrations, for all oxoacids. The generated oligomers, therefore, have much lower critical aggregation concentrations than the starting material, as would be expected for multi-tailed species.[110]

Table 5.4. Average sizes of aggregates observed by dynamic light scattering

ROA	**Avg. Observed Diameter (nm)**[a]
OHA	250 ± 20
OOA	160 ± 20
Mixed OOA/ODA	150 ± 10

[a]Uncertainty is expressed as a 95% confidence interval.

The diameters of the aggregates observed here for OHA, OOA, and the mixed OOA:ODA are too large to be simple micelles, and the monodispersity in their size indicates ordered aggregation. It has previously been speculated that the aggregates observed for OOA may be vesicles,[52] and the observed decrease in size as a function of increasing tail length is also suggestive that these aggregates are vesicles. The ratio of head group size to alkyl tail length is quite large for the oligomeric species generated from the photolysis of OHA, corresponding to a larger packing parameter[111] than for the longer tail-length oligomers. The packing parameter for the multi-tailed lipids generated from the photolysis of each of

the alkyl oxoacids studied here is likely near one, a regime that generally is associated with bilayer formation.[111] If bilayers are formed, species with a higher packing parameter generally assemble into lower curvature, larger structures, which is consistent with the trend in size of aggregate observed here.

5.4 Conclusions:

We have shown that the photochemical reaction mechanisms for α-keto acids in aqueous solution are readily generalizable to a series of molecules with differing alkyl chain lengths. Differences in reactivity due to chain length might be expected, but for all of the oxoacids under study here the chemical reactivity between molecules is surprisingly consistent, although a new intramolecular Norrish Type II pathway is accessible for alkyl oxoacids with a γ-CH_2 group that is not available to the shorter pyruvic acid.

Even a simple starting solution of a single alkyl oxoacid species becomes a complex mixture of oligomeric species upon photolysis. This is due in large part to the formation of reactive intermediate species with the same α-keto functionality, including pyruvic acid and parapyruvic acid derivatives. These species also undergo photochemistry and the organic radicals generated from each of the oxoacids can react indiscriminately with each other in aqueous solution. For processes that form radicals on the alkyl chain of an oxoacid, it is likely that hydrogen abstraction occurs at multiple sites along the alkyl chain, allowing for the formation of several constitutional isomers with the same chemical formula that cannot be distinguished from each other via the MS analysis conducted here. However, despite this, the products are not intractable as the majority of the observed species can be readily identified using simple mechanistic schemes.

The oligomers formed from this photochemistry are amphiphiles, many of which have two or three alkyl chains. The generation of chiral, multi-tailed species with increased surface activity and their subsequent self-assembly into monodisperse, spherical aggregates

has important environmental implications both for today and the early Earth.[5] In the modern environment, this chemistry may contribute to the abiotic processes by which surface-active species are formed at the sea surface microlayer.[30] Prebiotically, the photochemical reactions of alkyl oxoacids are one of the only demonstrated processes by which multi-tailed lipids can be formed simply and in relatively high yields from prebiotically-relevant starting materials. The properties of these multi-tailed lipids, as well as their propensity to self-assemble into ordered aggregates shown here, demonstrate their potential importance in the generation of primitive enclosures.

5.5 Bibliography:

1. Rapf, R. J.; Perkins, R. J.; Yang, H.; Miyake, G. M.; Carpenter, B. K.; Vaida, V. Photochemical synthesis of oligomeric amphiphiles from alkyl oxoacids in aqueous environments. *J. Am. Chem. Soc.* **2017,** *139*, 6946–6959.

2. Miyazaki, Y.; Sawano, M.; Kawamura, K. Low-molecular-weight hydroxyacids in marine atmospheric aerosol: Evidence of a marine microbial origin. *Biogeosciences* **2014,** *11*, 4407-4414.

3. Rinaldi, M.; Decesari, S.; Finessi, E.; Giulianelli, L.; Carbone, C.; Fuzzi, S.; Dowd, C. D.; Ceburnis, D.; Facchini, M. C. Primary and secondary organic marine aerosol and oceanic biological activity: Recent results and new perspectives for future studies. *Adv. Meteorol.* **2010,** *2010*, Article ID 310682.

4. Thornton, D. C. O.; Brooks, S. D.; Chen, J. Protein and carbohydrate exopolymer particles in the sea surface microlayer (SML). *Front. Mar. Sci.* **2016,** *3*.

5. Rapf, R. J.; Vaida, V. Sunlight as an energetic driver in the synthesis of molecules necessary for life. *Phys. Chem. Chem. Phys.* **2016,** *18*, 20067-20084.

6. Donaldson, D. J.; Vaida, V. The influence of organic films at the air-aqueous boundary on atmospheric processes. *Chem. Rev.* **2006,** *106*, 1445-1461.

7. Griffith, E. C.; Tuck, A. F.; Vaida, V. Ocean-atmosphere interactions in the emergence of complexity in simple chemical systems. *Acc. Chem. Res.* **2012,** *45*, 2106-2113.

8. Deamer, D.; Weber, A. L. Bioenergetics and life's origins. *Cold Spring Harbor Persp. Biol.* **2010,** *2*, 1-16.

9. Stano, P.; D'Aguanno, E.; Bolz, J.; Fahr, A.; Luisi, P. L. A remarkable self-organization process as the origin of primitive functional cells. *Angew. Chem. Int. Ed.* **2013,** *52*, 13397-13400.

10. Monnard, P.-A.; Walde, P. Current ideas about prebiological compartmentalization. *Life* **2015,** *5*, 1239-1263.

11. Cunliffe, M.; Engel, A.; Frka, S.; Gasparovic, B.; Guitart, C.; Murrell, J. C.; Salter, M.; Stolle, C.; Upstill-Goddard, R.; Wurl, O. Sea surface microlayers: A unified physiochemical and biological perspective of the air-ocean interface. *Prog. Oceanogr.* **2013,** *109*, 104-116.

12. Ciuraru, R.; Fine, L.; Pinxteren, M. v.; D'Anna, B.; Herrmann, H.; George, C. Unravelling new processes at interfaces: Photochemical isoprene production at the sea surface. *Environ. Sci. Technol.* **2015**, 13199–13205.

13. Rossignol, S.; Tinel, L.; Bianco, A.; Passananti, M.; Brigante, M.; Donaldson, D. J.; George, C. Atmospheric photochemistry at a fatty acid–coated air-water interface. *Science* **2016,** *353*, 699-702.

14. Chiu, R.; Tinel, L.; Gonzalez, L.; Ciuraru, R.; Bernard, F.; George, C.; Volkamer, R. UV photochemistry of carboxylic acids at the air-sea boundary: A relevant source of glyoxal and other oxygenated VOC in the marine atmosphere. *Geophys. Res. Lett.* **2017,** *44*, 1079-1087.

15. Cochran, R. E.; Laskina, O.; Jayarathne, T.; Laskin, A.; Laskin, J.; Lin, P.; Sultana, C.; Lee, C.; Moore, K. A.; Cappa, C. D. Analysis of organic anionic surfactants in fine and coarse fractions of freshly emitted sea spray aerosol. *Environ. Sci. Technol.* **2016,** *50*, 2477-2486.

16. Tervahattu, H.; Hartonen, K.; Kerminen, V. M.; Kupiainen, K.; Aarnio, P.; Koskentalo, T.; Tuck, A. F.; Vaida, V. New evidence of an organic layer on marine aerosols. *J. Geophys. Res.* **2002,** *107*, 4053-4060.

17. Tervahattu, H.; Juhanoja, J.; Vaida, V.; Tuck, A. F.; Niemi, J. V.; Kupiainen, K.; Kulmala, M.; Vehkamaki, H. Fatty acids on continental sulfate aerosol particles. *J. Geophys. Res.* **2005,** *110*, Article number D06207.

18. Ervens, B.; Turpin, B. J.; Weber, R. J. Secondary aerosol formation in cloud droplets and aqueous particles (aqSOA): A review of laboratory, field and model studies. *Atmo. Chem. Phys.* **2011,** *11*, 11069-11102.

19. Carlton, A. G.; Wiedinmyer, C.; Kroll, J. H. A review of secondary organic aerosol (SOA) formation from isoprene. *Atmo. Chem. Phys.* **2009,** *9*, 4987-5005.

20. Hallquist, M.; Wenger, J. C.; Baltensperger, U.; Rudich, Y.; Simpson, D.; Claeys, M.; Dommen, J.; Donahue, N. M.; George, C.; Goldstein, A. H., et al. The formation, properties and impact of secondary organic aerosol: Current and emerging issues. *Atmos. Chem. Phys.* **2009,** *9*, 5155-5236.

21. Herrmann, H. Kinetics of aqueous phase reactions relevant for atmospheric chemistry. *Chem. Rev.* **2003,** *103*, 4691-4716.

22. Herrmann, H.; Schaefer, T.; Tilgner, A.; Styler, S. A.; Weller, C.; Teich, M.; Otto, T. Tropospheric aqueous-phase chemistry: Kinetics, mechanisms, and its coupling to a changing gas phase. *Chem. Rev.* **2015,** *115*, 4259–4334.

23. Brégonzio-Rozier, L.; Giorio, C.; Siekmann, F.; Pangui, E.; Morales, S.; Temime-Roussel, B.; Gratien, A.; Michoud, V.; Cazaunau, M.; DeWitt, H. Secondary organic aerosol formation from isoprene photooxidation during cloud condensation–evaporation cycles. *Atmo. Chem. Phys.* **2016,** *16*, 1747-1760.

24. Renard, P.; Reed Harris, A. E.; Rapf, R. J.; Rainer, S.; Demelas, C.; Coulomb, B.; Quivet, E.; Vaida, V.; Monod, A. Aqueous phase oligomerization of methyl vinyl ketone by atmospheric radical reactions. *J. Phys. Chem. C* **2014,** *118*, 29421-29430.

25. Renard, P.; Siekmann, F.; Gandolfo, A.; Socorro, J.; Salque, G.; Ravier, S.; Quivet, E.; Clement, J. L.; Traikia, M.; Delort, A. M., et al. Radical mechanisms of methyl vinyl ketone oligomerization through aqueous phase OH-oxidation: On the paradoxical role of dissolved molecular oxygen. *Atmo. Chem. Phys.* **2013,** *13*, 6473-6491.

26. Vaida, V. Spectroscopy of photoreactive systems: Implications for atmospheric chemistry. *J. Phys. Chem. A* **2009,** *113*, 5-18.

27. Alves, C. A. Chemistry between the sea surface microlayer and marine aerosols. *Quim. Nova* **2014,** *37*, 1382-1400.

28. Wang, X.; Sultana, C. M.; Trueblood, J.; Hill, T. C. J.; Malfatti, F.; Lee, C.; Laskina, O.; Moore, K. A.; Beall, C. M.; McCluskey, C. S., et al. Microbial control of sea spray aerosol composition: A tale of two blooms. *ACS Cent. Sci.* **2015,** *1*, 124-131.

29. Reed Harris, A. E.; Ervens, B.; Shoemaker, R. K.; Kroll, J. A.; Rapf, R. J.; Griffith, E. C.; Monod, A.; Vaida, V. Photochemical kinetics of pyruvic acid in aqueous solution. *J. Phys. Chem. A* **2014,** *118*, 8505-8516.

30. Vaida, V. Atmospheric radical chemistry revisited. *Science* **2016,** *353*, 650-650.

31. Vaida, V. Ocean sea spray, clouds, and climate. *ACS Cent. Sci.* **2015,** *1*, 112-114.

32. Hoque, M. M. M.; Kawamura, K.; Uematsu, M. Spatio-temporal distributions of dicarboxylic acids, ω-oxocarboxylic acids, pyruvic acid, α-dicarbonyls and fatty acids in the marine aerosols from the north and south Pacific. *Atmo. Res.* **2017,** *185*, 158-168.

33. Mochida, M.; Kitamori, Y.; Kawamura, K.; Nojiri, Y.; Suzuki, K. Fatty acids in the marine atmosphere: Factors governing their concentrations and evaluation of organic films on sea-salt particles. *J. Geophys. Res. Atmos.* **2002,** *107*, 4325.

34. Kawamura, K.; Umemoto, N.; Mochida, M.; Bertram, T.; Howell, S.; Huebert, B. J. Water-soluble dicarboxylic acids in the tropospheric aerosols collected over east Asia and western north Pacific by ACE-Asia C-130 aircraft. *J. Geophys. Res. Atmos.* **2003,** *108*, 8639.

35. Long, M.; Keene, W.; Kieber, D.; Frossard, A.; Russell, L.; Maben, J.; Kinsey, J.; Quinn, P.; Bates, T. Light - enhanced primary marine aerosol production from biologically productive seawater. *Geophys. Res. Lett.* **2014,** *41*, 2661-2670.

36. Galloway, M. M.; Powelson, M. H.; Sedehi, N.; Wood, S. E.; Millage, K. D.; Kononenko, J. A.; Rynaski, A. D.; De Haan, D. O. Secondary organic aerosol formation during evaporation of droplets containing atmospheric aldehydes, amines, and ammonium sulfate. *Environ. Sci. Technol.* **2014,** *48*, 14417-14425.

37. George, C.; Ammann, M.; D'Anna, B.; Donaldson, D. J.; Nizkorodov, S. A. Heterogeneous photochemistry in the atmosphere. *Chem. Rev.* **2015,** *115*, 4218-4258.

38. Rudich, Y. Laboratory perspectives on the chemical transformations of organic matter in atmospheric particles. *Chem. Rev.* **2003,** *103*, 5097-5124.

39. Perraud, V.; Bruns, E. A.; Ezell, M. J.; Johnson, S. N.; Yu, Y.; Alexander, M. L.; Zelenyuk, A.; Imre, D.; Chang, W. L.; Dabdub, D., et al. Nonequilibrium atmospheric secondary organic aerosol formation and growth. *Proc. Natl. Acad. Sci.* **2012,** *109*, 2836-2841.

40. Harrison, R. M.; Yin, J. Particulate matter in the atmosphere: Which particle properties are important for its effects on health? *Sci. Total Environ.* **2000,** *249*, 85-101.

41. Finlayson-Pitts, B. J.; Pitts, J. N., *Chemistry of the upper and lower atmosphere*. Academic Press: San Diego, 1999.

42. Hinds, W. C., *Aerosol technology : Properties, behavior, and measurement of airborne particles*. 2nd ed.; Wiley: New York, 1999.

43. Ervens, B. Modeling the processing of aerosol and trace gases in clouds and fogs. *Chem. Rev.* **2015,** *115*, 4157-4198.

44. Lohmann, U.; Feichter, J. Global indirect aerosol effects: A review. *Atmo. Chem. Phys.* **2005,** *5*, 715-737.

45. Hansen, J.; Sato, M.; Ruedy, R. Radiative forcing and climate response. *J. Geophys. Res. Atmos.* **1997,** *102*, 6831-6864.

46. Seinfeld, J. H.; Pandis, S. N., *Atmospheric chemistry and physics: From air pollution to climate change*. John Wiley & Sons, Inc.: New York, 1998.

47. Chebbi, A.; Carlier, P. Carboxylic acids in the troposphere, occurrence, sources, and sinks: A review. *Atmos. Environ.* **1996,** *30*, 4233-4249.

48. Ho, K.; Lee, S.; Cao, J.; Kawamura, K.; Watanabe, T.; Cheng, Y.; Chow, J. C. Dicarboxylic acids, ketocarboxylic acids and dicarbonyls in the urban roadside area of Hong Kong. *Atmos. Environ.* **2006,** *40*, 3030-3040.

49. Cooper, G.; Reed, C.; Nguyen, D.; Carter, M.; Wang, Y. Detection and formation scenario of citric acid, pyruvic acid, and other possible metabolism precursors in carbonaceous meteorites. *Proc. Natl. Acad. Sci.* **2011,** *108*, 14015-14020.

50. Pizzarello, S. Prebiotic chemical evolution: A meteoritic perspective. *Rend. Lincei.* **2011,** *22*, 153-163.

51. McCollom, T. M.; Ritter, G.; Simoneit, B. R. T. Lipid synthesis under hydrothermal conditions by Fischer-Tropsch-type reactions. *Origins Life Evol. Biosphere* **1999,** *29*, 153-166.

52. Griffith, E. C.; Rapf, R. J.; Shoemaker, R. K.; Carpenter, B. K.; Vaida, V. Photoinitiated synthesis of self-assembled vesicles. *J. Am. Chem. Soc.* **2014,** *136*, 3784-3787.

53. Plath, K. L.; Takahashi, K.; Skodje, R. T.; Vaida, V. Fundamental and overtone vibrational spectra of gas-phase pyruvic acid. *J. Phys. Chem. A* **2009,** *113*, 7294-7303.

54. Vesley, G. F.; Leermakers, P. A. Photochemistry of alpha-keto acids and alpha-keto esters .3. Photolysis of pyruvic acid in vapor phase. *J. Phys. Chem.* **1964,** *68*, 2364-2366.

55. Takahashi, K.; Plath, K. L.; Skodje, R. T.; Vaida, V. Dynamics of vibrational overtone excited pyruvic acid in the gas phase: Line broadening through hydrogen-atom chattering. *J. Phys. Chem. A* **2008,** *112*, 7321-7331.

56. Yamamoto, S.; Back, R. A. The photolysis and thermal decomposition of pyruvic acid in the gas phase. *Can. J. Chem.* **1985,** *63*, 549-554.

57. Mellouki, A.; Mu, Y. J. On the atmospheric degradation of pyruvic acid in the gas phase. *J. Photochem. Photobiol., A* **2003,** *157*, 295-300.

58. Horowitz, A.; Meller, R.; Moortgat, G. K. The UV–vis absorption cross sections of the α -dicarbonyl compounds: Pyruvic acid, biacetyl and glyoxal. *J. Photochem. Photobiol., A* **2001,** *146*, 19-27.

59. Schreiner, P. R.; Reisenauer, H. P.; Ley, D.; Gerbig, D.; Wu, C.-H.; Allen, W. D. Methylhydroxycarbene: Tunneling control of a chemical reaction. *Science* **2011,** *332*, 1300-1303.

60. Reed Harris, A. E.; Doussin, J.-F.; Carpenter, B. K.; Vaida, V. Gas-phase photolysis of pyruvic acid: The effect of pressure on reaction rates and products. *J. Phys. Chem. A* **2016,** *120*, 10123-10133.

61. Rincon, A. G.; Guzman, M. I.; Hoffmann, M. R.; Colussi, A. J. Optical absorptivity versus molecular composition of model organic aerosol matter. *J. Phys. Chem. A* **2009,** *113*, 10512-10520.

62. Closs, G. L.; Miller, R. J. Photo-reduction and photodecarboxylation of pyruvic acid - applications of CIDNP to mechanistic photochemistry. *J. Am. Chem. Soc.* **1978,** *100*, 3483-3494.

63. Guzman, M. I.; Colussi, A. J.; Hoffmann, M. R. Photoinduced oligomerization of aqueous pyruvic acid. *J. Phys. Chem. A* **2006,** *110*, 3619-3626.

64. Griffith, E. C.; Carpenter, B. K.; Shoemaker, R. K.; Vaida, V. Photochemistry of aqueous pyruvic acid. *Proc. Natl. Acad. Sci.* **2013,** *110*, 11714-11719.

65. Leermakers, P. A.; Vesley, G. F. Photolysis of pyruvic acid in solution. *J. Org. Chem.* **1963,** *28*, 1160-1161.

66. Larsen, M. C.; Vaida, V. Near infrared photochemistry of pyruvic acid in aqueous solution. *J. Phys. Chem. A* **2012,** *116*, 5840-5846.

67. Rapf, R. J.; Perkins, R. J.; Carpenter, B. K.; Vaida, V. Mechanistic description of photochemical oligomer formation from aqueous pyruvic acid. *J. Phys. Chem. A* **2017,** *121*, 4272–4282.

68. Reed Harris, A. E.; Pajunoja, A.; Cazaunau, M.; Gratien, A.; Pangui, E.; Monod, A.; Griffith, E. C.; Virtanen, A.; Doussin, J. F.; Vaida, V. Multiphase photochemistry of pyruvic acid under atmospheric conditions. *J. Phys. Chem. A* **2017,** *121*, 3327–3339.

69. Eugene, A. J.; Guzman, M. I. Reactivity of ketyl and acetyl radicals from direct solar actinic photolysis of aqueous pyruvic acid. *J. Phys. Chem. A* **2017,** *121*, 2924–2935.

70. Kawamura, K.; Kasukabe, H.; Barrie, L. A. Source and reaction pathways of dicarboxylic acids, ketoacids and dicarbonyls in Arctic aerosols: One year of observations. *Atmos. Environ.* **1996,** *30*, 1709-1722.

71. Sempere, R.; Kawamura, K. Comparative distributions of dicarboxylic acids and related polar compounds in snow, rain, and aerosols from urban atmosphere. *Atmos. Environ.* **1994,** *28*, 449-459.

72. Nguyen, T. B.; Bateman, A. P.; Bones, D. L.; Nizkorodov, S. A.; Laskin, J.; Laskin, A. High-resolution mass spectrometry analysis of secondary organic aerosol generated by ozonolysis of isoprene. *Atmos. Environ.* **2010,** *44*, 1032-1042.

73. Veres, P. R.; Roberts, J. M.; Cochran, A. K.; Gilman, J. B.; Kuster, W. C.; Holloway, J. S.; Graus, M.; Flynn, J.; Lefer, B.; Warneke, C., et al. Evidence of rapid production of organic acids in an urban air mass. *Geophys. Res. Lett.* **2011,** *38*, L17807.

74. Warneck, P. Multi-phase chemistry of C-2 and C-3 organic compounds in the marine atmosphere. *J. Atmos. Chem.* **2005,** *51*, 119-159.

75. Altieri, K. E.; Carlton, A. G.; Lim, H.-J.; Turpin, B. J.; Seitzinger, S. P. Evidence for oligomer formation in clouds: Reactions of isoprene oxidation products. *Environ. Sci. Technol.* **2006,** *40*, 4956-4960.

76. Andreae, M. O.; Talbot, R. W.; Li, S. M. Atmospheric measurements of pyruvic and formic acid. *J. Geophys. Res. Atmos.* **1987,** *92*, 6635-6641.

77. Talbot, R.; Andreae, M.; Berresheim, H.; Jacob, D. J.; Beecher, K. Sources and sinks of formic, acetic, and pyruvic acids over central Amazonia: 2. Wet season. *J. Geophys. Res. Atmos.* **1990,** *95*, 16799-16811.

78. Veres, P.; Roberts, J. M.; Burling, I. R.; Warneke, C.; de Gouw, J.; Yokelson, R. J. Measurements of gas‐phase inorganic and organic acids from biomass fires by negative‐ion proton‐transfer chemical‐ionization mass spectrometry. *J. Geophys. Res. Atmos.* **2010,** *115*, D23302.

79. Perkins, R. J.; Shoemaker, R. K.; Carpenter, B. K.; Vaida, V. Chemical equilibria and kinetics in aqueous solutions of zymonic acid. *J. Phys. Chem. A* **2016,** *120*, 10096-10107.

80. The terms “dimer” and “trimer” are used to refer to covalently-bonded oligomeric species, unless otherwise specified.

81. Hargreaves, W. R.; Mulvihill, S. J.; Deamer, D. W. Synthesis of phospholipids and membranes in prebiotic conditions. *Nature* **1977,** *266*, 78-80.

82. Rao, M.; Eichberg, J.; Oro, J. Synthesis of phosphatidylcholine under possible primitive Earth conditions *J. Mol. Evo.* **1982,** *18*, 196-202.

83. Stano, P.; D'Aguanno, E.; Bolz, J.; Fahr, A.; Luisi, P. L. A remarkable self-organization process as the origin of primitive functional cells. *Angew. Chem. Int. Ed.* **2013,** *52*, 13397-13400.

84. Chen, I. A.; Walde, P. From self-assembled vesicles to protocells. *Cold Spring Harbor Persp. Biol.* **2010,** *2*.

85. Pohorille, A.; Deamer, D. Self-assembly and function of primitive cell membranes. *Res. Microbiol.* **2009,** *160*, 449-456.

86. Hanczyc, M.; Fujikawa, S.; Szostak, J. Experimental models of primitive cellular compartments: Encapsulation, growth, and division. *Science (New York, N.Y.)* **2003,** *302*, 618-22.

87. Mansy, S. S.; Szostak, J. W. Reconstructing the emergence of cellular life through the synthesis of model protocells. *Cold Spring Harb. Symp. Quant. Bio.* **2009,** *74*, 47 -54.

88. Xu, H.; Du, N.; Song, Y.; Song, S.; Hou, W. Vesicles of 2-ketooctanoic acid in water. *Soft Matter* **2017,** *13*, 2246-2252

89. Pedersen, K. J. The dissociation constants of pyruvic and oxaloacetic acid. *Acta Chem. Scand.* **1952,** *6*, 243-256.

90. Pocker, Y.; Meany, J. E.; Nist, B. J.; Zadorojny, C. Reversible hydration of pyruvic acid. I. Equilibrium studies. *J. Phys. Chem.* **1969,** *73*, 2879-2882.

91. Leermakers, P. A.; Vesley, G. F. Organic photochemistry and the excited state. *J. Chem. Educ* **1964,** *41*, 535.

92. Turro, N. J.; Ramamurthy, V.; Scaiano, J. C., *Modern molecular photochemistry of organic molecules*. University Science Books: Sausalito, California, 2010.

93. Evans, T. R.; Leermakers, P. A. Photochemistry of alpha-keto acids and alpha.-keto esters VI. V. The Norrish Type II process in alpha-keto acids. Photolysis of alpha-ketodecanoic acid in benzene. *J. Am. Chem. Soc.* **1968,** *90*, 1840-1842.

94. Davidson, R. S.; Goodwin, D.; de Violet, P. F. The mechanism of the Norrish Type II reaction of α-keto-acids and esters. *Tetrahedron Lett.* **1981,** *22*, 2485-2486.

95. Davidson, R. S.; Goodwin, D. The role of electron transfer processes in the photoinduced decarboxylation reaction of α-oxo-carboxylic acids. *J. Chem. Soc., Perkin Trans. 2* **1982**, 1559-1564.

96. Davidson, R. S.; Goodwin, D.; De Violet, P. F. The mechanism of the photo-induced decarboxylation of pyruvic acid in solution. *Chem. Phys. Lett.* **1981,** *78*, 471-474.

97. Leermakers, P. A.; Vesley, G. F. Photochemistry of alpha-keto acids and alpha-keto esters. 1. Photolysis of pyruvic acid and benzoylformic acid. *J. Am. Chem. Soc.* **1963,** *85*, 3776-3779.

98. Axson, J. L.; Takahashi, K.; De Haan, D. O.; Vaida, V. Gas-phase water-mediated equilibrium between methylglyoxal and its geminal diol. *Proc. Natl. Acad. Sci.* **2010,** *107*, 6687-6692.

99. Buschmann, H. J.; Dutkiewicz, E.; Knoche, W. The reversible hydration of carbonyl compounds in aqueous solution. 2. The kinetics of the keto gem-diol transition. *Ber. Bunsen-Ges. Phys. Chem* **1982,** *86*, 129-134.

100. Maroń, M. K.; Takahashi, K.; Shoemaker, R. K.; Vaida, V. Hydration of pyruvic acid to its geminal-diol, 2, 2-dihydroxypropanoic acid, in a water-restricted environment. *Chem. Phys. Lett.* **2011,** *513*, 184-190.

101. Buschmann, H. J.; Füldner, H. H.; Knoche, W. The reversible hydration of carbonyl compounds in aqueous solution. Part I, the keto/gem - diol equilibrium. *Ber. Bunsen-Ges. Phys. Chem* **1980,** *84*, 41-44.

102. Here, ROA• is shown with the radical on the β-CH_2 group for ease of presentation. Hydrogen abstraction can, in principle, occur anywhere along the alkyl chain.

103. Brocks, J. J.; Beckhaus, H.-D.; Beckwith, A. L.; Rüchardt, C. Estimation of bond dissociation energies and radical stabilization energies by esr spectroscopy. *J. Org. Chem.* **1998,** *63*, 1935-1943.

104. Ranjan, S.; Sasselov, D. D. Influence of the UV environment on the synthesis of prebiotic molecules. *Astrobio.* **2016,** *16*, 68-88.

105. Albrecht, M.; Borba, A.; Barbu-Debus, K. L.; Dittrich, B.; Fausto, R.; Grimme, S.; Mahjoub, A.; Nedić, M.; Schmitt, U.; Schrader, L., et al. Chirality influence on the aggregation of methyl mandelate. *New J. Chem.* **2010,** *34*, 1266-1285.

106. Dong, H.; Ignés-Mullol, J.; Claret, J.; Pérez, L.; Pinazo, A.; Sagués, F. Interfacial chiral selection by bulk species. *Chem. Eur. J.* **2014,** *20*, 7396-7401.

107. Toxvaerd, S. Origin of homochirality in biosystems. *Int. J. Molec. Sci.* **2009,** *10*, 1290-1299.

108. Pizzarello, S.; Weber, A. L. Stereoselective syntheses of pentose sugars under realistic prebiotic conditions. *Origins Life Evol. Biosphere* **2009,** *40*, 3-10.

109. Martinez, I. S.; Peterson, M. D.; Ebben, C. J.; Hayes, P. L.; Artaxo, P.; Martin, S. T.; Geiger, F. M. On molecular chirality within naturally occurring secondary organic aerosol particles from the central amazon basin. *Phys. Chem. Chem. Phys.* **2011,** *13*, 12114-12122.

110. Tanford, C., *The hydrophobic effect: Formation of micelles and biological membranes 2d ed.* J. Wiley.: 1980.

111. Gradzielski, M. a. Vesicles and vesicle gels-structure and dynamics of formation. *J. Phys.: Condens. Matter* **2003,** *15*, R655.

6. pH Dependence of the Aqueous Photochemistry of α-Keto Acids

6.1 Introduction:

The aqueous photochemistry of organic species has been increasingly recognized as an important contributor to environmental chemistry on both the modern and early Earth.[1-3] The generation of more complex oligomeric species from the photolysis of simple organic molecules is of particular interest because recent work has shown that these species may contribute significantly to the formation and processing of organic aerosols.[4-9] The study described here expands the understanding of these photolysis reactions in the natural environment by investigating the pH dependence of α-keto acid photolysis product distributions and reaction rates.

The organic content of primary organic aerosols (POA) generated from sea spray can be enriched by contributions from the sea-surface microlayer (SML).[10] This organic-rich layer provides a connection between the ocean and the atmosphere, linking two disparate environments and allowing for the transport of material between them. The organic material in the SML is primarily provided by biological sources,[11-15] but abiotic photochemically-processed sources may also be important contributors.[8, 9, 13, 15-17] In addition to POA, secondary organic aerosols (SOA) can be formed from further reactions of organic material, either in the gas or particle phase, including aqueous phase photochemical processes.[2, 7, 18-23]

One class of molecules whose aqueous photochemistry in the context of SOA formation has attracted considerable interest is the α-keto acids. Pyruvic acid, the simplest α-keto acid, is an oxidation product of isoprene[24-26] and is found in abundance in both the gas and aqueous phase in the atmosphere.[24, 27-33] Keto acids with longer alkyl chains, such as 2-oxooctanoic acid (OOA), have been found at the ocean surface and contribute to the surface-

active organic material found in the SML.[15, 29, 34] Regardless of alkyl chain length, α-keto acids absorb light in the near-UV at wavelengths of relevance for actinic flux and readily undergo photochemistry that, in the aqueous phase, is characterized by the formation of oligomers.[5, 35-41] The mechanisms governing this photochemistry have been studied in detail.[5, 38-44] However, the photochemistry, to date, has largely only been explored under acidic conditions. To the best of our knowledge, the photochemistry of pyruvic acid under higher pH conditions has only been briefly mentioned once in the literature, when Leermakers and Vesley in 1963 reported that the photochemistry of pyruvic acid at pH of 6.1 was observed to slow significantly and produced less CO_2 compared to solutions of pyruvic acid at lower pH.[43] In the present study, we undertake a detailed examination of the organic photoproducts formed under high pH conditions, which allows for mechanistic insight into the behavior of α-keto acids in different environments.

It is surprising that the role of the acidity of the solution has been largely ignored, given the environmental importance of α-keto acids and the range of pH conditions in the natural environment. The ocean, for example, is basic with a pH of ~8, and the SML is thought also to likely be basic.[45, 46] Atmospheric aerosols, on the other hand, are usually acidic with pH values that range from ~0 to ~5.[47-52] Aerosols derived from sea spray may initially be basic, but partitioning of gaseous atmospheric species, such as SO_2, NO_2, and CO_2, into the aqueous phase will rapidly acidify due to the formation of the corresponding acids (H_2SO_4, HNO_3, and H_2CO_3). This acidification process means that organic molecules, even on a single aerosol, may experience a wide range of conditions. We use investigations of the extent of protonation and hydration as a function of pH, together with a detailed mechanistic understanding, to successfully predict the experimentally observed photoproducts.

6.2 Experimental Section:

Pyruvic acid (98%, Sigma Aldrich) was distilled by heating gently (<55 °C) under reduced pressure (<1 Torr) to remove impurities. The purified pyruvic acid was used within one month of distillation to minimize the presence of oligomeric species generated by dark processes.[53] Pyruvic acid was diluted with 18.2 MΩ (3 ppb TOC) water to make solutions of 10 mM concentration (unadjusted pH = 2.37 ± 0.04). 2-oxooctanoic acid (OOA, ≥99.0%, Sigma Aldrich) was used without further purification and diluted to a final concentration of either 6 or 3 mM (3 mM unadjusted pH = 2.80 ± 0.05). Solutions of OOA were sonicated until fully dissolved. Solution pH was determined using a Corning pH meter and adjusted by addition of either sodium hydroxide (1 M stock solutions, 98.0%, Fisher Scientific) or hydrochloric acid (~37%, Mallinckrodt), as appropriate.

For photolysis, 250 mL solutions of α-keto acids were prepared. Of this, 20 mL was saved as a pre-photolysis control, and the remaining solution was placed in a temperature-controlled water bath at 20 °C and illuminated using an unfiltered 450 W Xe arc lamp (Newport) for 5 hours with 10 mL aliquots taken hourly. Additionally, 100 mL solutions were prepared (10 mL saved as a pre-photolysis control) and photolyzed for 5 hours at 4 °C without hourly aliquots. No difference was observed in products with changes in the water bath temperature or solution volume. All solutions were purged continuously with N_2, beginning one hour prior to the start of photolysis. Purging the reactor with N_2 allows for the displacement of dissolved O_2 in solution. As shown previously,[5] oxygen-depleted conditions favor the formation of oligomers, which allows for the identification of products under very dilute reaction conditions. It is important to note that, while the presence of oxygen slows the rate of photochemical formation,[5] these same oligomeric products are generated from the photochemistry of pyruvic acid under atmospherically-relevant conditions.[35]

6.2.1 Determination of Acid Dissociation Constants:

Effective acid dissociation constants for both pyruvic acid and OOA were determined by titration with NaOH. A detailed discussion of why the titration method for determining acid dissociation constants can only give "effective" values for α-keto acids is given in the Section 6.3.1. Each titration was conducted with 25 mL of either 10 mM pyruvic acid or 3 mM OOA and the addition of 15 mM or 10 mM NaOH, respectively. The NaOH concentration was standardized using potassium hydrogen phthalate.

Acid dissociation constant values were determined following the general fitting routine given in Harris's *Quantitative Chemical Analysis* textbook,[54] modified to account for changing ionic strength as in Papanastasiou and Ziogas 1995.[55] A detailed description of the iterative fitting procedure is included in Appendix F.1. pK_a values were determined for each individual titration and then averaged.

6.2.2 Spectroscopic and Spectrometric Analysis:

Solutions were characterized using a variety of analytical techniques, including UV-Vis and NMR spectroscopy and high-resolution negative mode electrospray ionization mass spectrometry (ESI^- MS). Instrument parameters are given Chapter 3. All UV-vis spectra were baseline corrected. To allow for direct comparison between multiple experimental runs, the absorbance of all spectra were scaled to a nominal concentration of 10 mM for pyruvic acid and 3 mM for OOA, unless otherwise specified.

Analysis of the mass spectrometry data followed the procedure outlined in Chapter 3.4. Because of the variance in total intensity in the mass spectra as a function of pH, relative intensities were used to compare photoproduct distributions at different pH values. The analysis conducted here was not designed to be absolutely quantitative. Analyte intensities may not correlate directly to absolute analyte concentrations and are used for relative comparisons only.

6.3 Results and Discussion:

The effects of changing pH on the photochemical reactivity of two α-keto acids, pyruvic acid and 2-oxooctanoic acid (OOA), were examined and are reported below. While seemingly simple molecules, α-keto acids have deceptively complex behavior in aqueous solution, and this, in turn, impacts the observed photochemistry. Therefore, in order to determine how changes in pH might affect the photochemical reactivity of α-keto acids, it is necessary first to understand how the precursor behaves in aqueous solutions of varying acidity.

6.3.1 Characterization of α-Keto Acids in Aqueous Solution

Pyruvic acid, when dissolved in aqueous solution, exists as a mixture of the keto form and its hydrate, the geminal diol 2,2-dihydroxypropanoic acid (2,2-DHPA), as shown in Scheme 6.1. The extent of hydration of the solution is known to be both temperature and pH dependent,[56] but it is usually reported that solutions of pyruvic acid at 298 K, which have not been pH adjusted, exist as approximately 65% diol and 35% keto in solution.[36, 38, 57-59] This ratio does not appear to rapidly change near ambient temperatures, as analysis of NMR spectra of solutions of 100 mM pyruvic acid (pH = 2.06) taken at 23 °C are 60% diol and 40% keto (Figure 6.1).[5] This is, however, an oversimplification. Because the molecules of interest are acidic, the pH and, therefore, the equilibrium between forms shifts when the concentration of the solution is changed. This is particularly important for dilute solutions. As has been previously reported,[39] solutions of 10 mM pyruvic acid (pH ~2.4) exist as approximately 50% diol and 50% keto. The pH of very dilute 0.5 mM solutions rises to ~3.5 and consequently the percentage of keto form rises to ~75%.[39]

The longer-tailed OOA is also hydrated in aqueous solution to give a geminal diol, 2,2-dihydroxyoctanoic acid (2,2-DHOA). Solutions of 6 mM OOA at unadjusted pH (~2.5) exist as approximately 80% keto and 20% diol.[41] This is a higher percentage of keto form in solution than would be expected for comparable solutions of pyruvic acid, suggesting that

longer-tailed oxoacids favor a relatively lower extent of hydration.

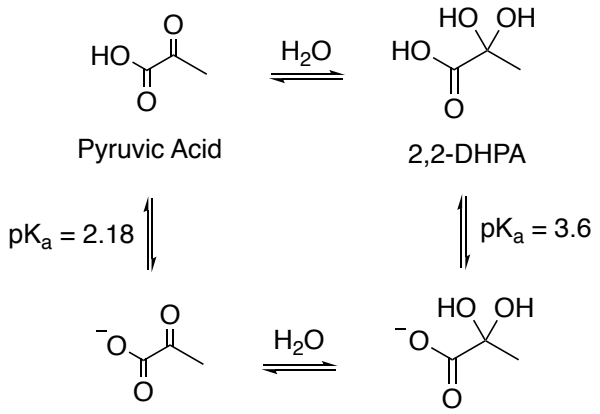

Scheme 6.1. Equilibria of species found in aqueous solutions of pyruvic acid.[57, 60]

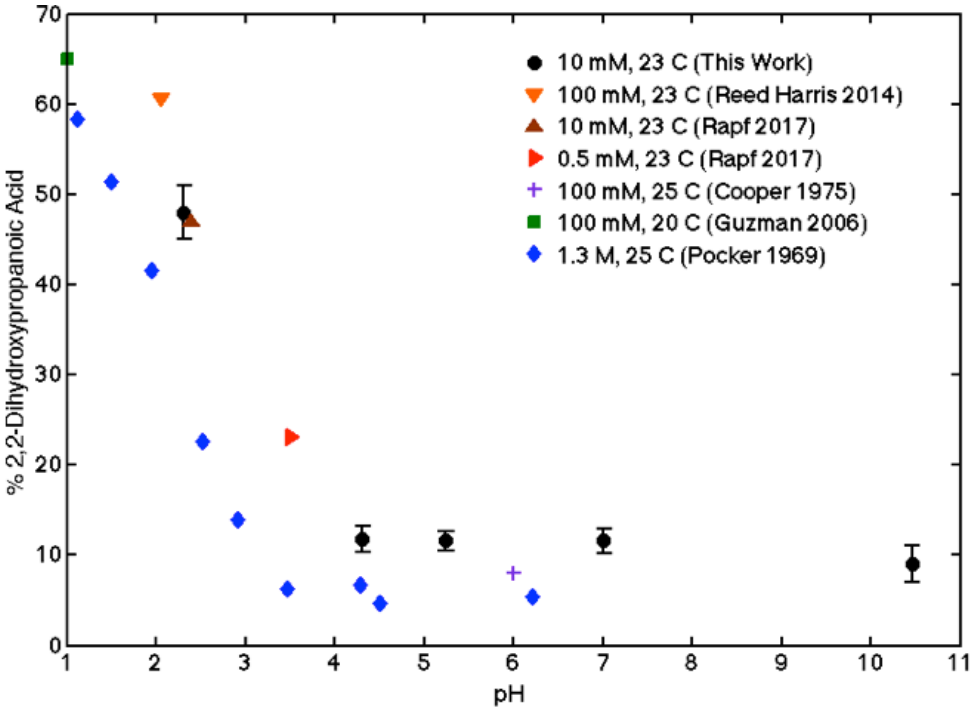

Figure 6.1. Percent composition of 2,2-dihydroxypropanoic acid, the geminal diol hydrate of pyruvic acid, as a function of solution pH as determined by NMR. Compositions obtained in this work for 10 mM pyruvic acid at 23 °C (black circles, error given as the standard deviation of the mean) are compared to previous literature values for solutions of 0.5 mM (brown triangle), 10 mM (red triangle),[39] *and 100 mM at 23 °C (orange triangle),*[5] *as well as 100 mM solutions at 20 °C (green square),*[36] *25 °C (purple cross),*[61] *and 1.3 M solutions at 25 °C (blue diamond).*[56]

To study in more detail the pH dependence of the extent of hydration, we examined the ratio between the keto and diol forms using ^{1}H NMR for 10 mM pyruvic acid solutions under varying pH conditions, as shown in Figure 6.1. Representative NMR spectra for

unadjusted pH (2.31) and high pH (10.46) are shown in Figure F.1. The amount of diol in solution dramatically decreases as the pH of the solution is increased, before rapidly stabilizing at ~11% diol in solution. This behavior matches qualitatively to values obtained previously in the literature,[5, 36, 39, 56, 61] where sigmoidal curves resembling the titration curve of a weak acid have been obtained, and the inflection point of these curves have be used to estimate the pK_a (~2.2) of the keto form of pyruvic acid.[56] This suggests, as would be expected, a strong interdependence between the extent of hydration and the extent of deprotonation of pyruvic acid in solution.

As shown in Scheme 6.1, pure pyruvic acid exists as four species in solution: both the keto and diol forms and their respective conjugate bases. As the pH of the solution is changed and the ratio of diol and keto species shifts, so too does the ratio of protonated and deprotonated species. Here, the term "protonated" is used to describe a neutral species that has not been deprotonated. A simple titration of a solution of pyruvic acid (Figure F.2) with NaOH can be used to extract an effective pK_a value for the solution. Fitting the titration data and accounting for ionic strength, the effective acid dissociation constant of pyruvic acid was determined to be 2.51 ± 0.05, in good agreement with the literature value of 2.49.[57, 62] A detailed description of the fitting procedure is given in the supporting information. This value is an effective dissociation constant because both the keto and diol forms are being deprotonated in solution and each has an individual acid dissociation constant of 2.18[57] and 3.6,[60] respectively.

Unlike pyruvic acid, the acid dissociation constants of OOA are not well known in the literature. The effective pK_a value for OOA has recently been reported for the first time, giving a value of 2.78.[63] This value was estimated from titration with NaOH, but the data were not rigorously fit.[63] Here, we have obtained an experimental value of 2.49 ± 0.04 for the effective pK_a of OOA using the same fitting technique as above for pyruvic acid (Figure

F.3). The close agreement we obtain between the effective pK_a values for pyruvic acid and OOA is not surprising given their identical functional groups and suggests that the presence of an alkyl tail is not a significant contributor to the protonation behavior.[58] While the individual pK_a values for the keto and diol forms of OOA have not been determined, it is reasonable to assume that they are very similar to those of pyruvic acid, and this assumption has been made throughout the discussion that follows.

The effective pK_a of the α-keto acids can be used to obtain a rough estimate of the number of deprotonated species in solution. For example, a solution of 10 mM pyruvic acid at pH 2.4 would be expected to be ~40% deprotonated using the effective pK_a value. However, this is an oversimplification because more keto pyruvic acid will be deprotonated than the corresponding diol for a given pH. Instead, the expected percentages of deprotonated keto and diol can be solved for explicitly using their individual pK_a values and the experimentally determined keto/diol ratios, as described in the supporting information. Doing so for our example 10 mM pyruvic acid solution, approximately 64% of keto and 6% of diol species will be deprotonated. Interestingly, a weighted average using the experimentally determined keto and diol concentrations predicts that ~36% of the total species in solution will be deprotonated, recovering the result obtained using the effective pK_a value.

Similar calculations can be repeated for any solution whose pH has been adjusted by addition of NaOH; the expected composition of species in solution for various pH conditions is given in Figure F.4. In the high pH limit, both the keto and diol forms are completely deprotonated (>99%), as would be expected. However, because both the keto and diol are relatively strong acids, it is important to remember that the “high pH limit” is, in fact, reached while the overall pH of the solution is still acidic. That is, for any solution of pyruvic acid whose pH is ≥5.6, more than 99% of both the keto and diol forms will be

deprotonated. Even for solutions at pH 3.5, which would normally be considered quite acidic, ~45% of the diol and ~96% of the keto form is deprotonated.

Aqueous natural environments cover a wide variety of acidities, as discussed in the introduction. The ocean is slightly basic (~8), and fresh waters are near neutral pH. The acidity of aqueous aerosols is more difficult to measure,[64] but they are generally acidic, spanning pH values from ~0 to ~5 with considerable variability between particles.[47] While some aerosols are clearly in the low pH limit, when considering the full scope of natural aqueous environments, it is clear that if α-keto acids are found in the aqueous phase, they will likely be in their keto form and the deprotonated species will play an important role in its reactivity.

The large extent of deprotonation of the keto form of pyruvic acid, even at relatively low pH, is important to consider, because the keto form of pyruvic acid is the photoactive species. Traditionally, only the protonated form of the keto has been considered when discussing the photochemistry of pyruvic acid,[5, 36-39, 42] largely because at higher concentrations (e.g. 100 mM and pH 2.06[5]) the natural pH is lower, and the majority of the keto form is protonated. In some cases, the pH of solutions has been lowered to ensure the protonation of species in solution.[36, 37] However, it seems clear that the deprotonated keto species must play a key role in the fate of pyruvic acid and other α-keto acids in the atmosphere.

Pyruvic acid is known to generate primarily oligomeric species from its aqueous photochemistry under acidic conditions.[5, 36-39] However, pyruvic acid can also undergo oligomerization reactions in the dark, forming species such as zymonic acid.[53] The formation of zymonic acid and other larger oligomers via dark oligomerization processes is thought to be base catalyzed and has been shown to be far more prevalent at high pH.[65] To minimize the contributions of these dark oligomerization processes, all experiments were

conducted using dilute solutions of pyruvic acid, where the equilibrium shifts to favor monomeric pyruvic acid over oligomeric species in solution. 10 mM solutions of pyruvic acid of varying acidities were monitored using ^{1}H NMR and show no significant growth of oligomeric species as the solutions were aged in the dark (Figure F.5). Indeed, solutions at pH 10.5 appear to enrich slightly in pyruvic acid over the course of 24 hours with a corresponding slight decrease in zymonic acid species. Under these dilute solution conditions, dark oligomerization processes do not appear to occur on a timescale that would compete with photochemical oligomerization or complicate the interpretation of post-photolysis analysis. Pre-photolysis samples of all experiments were kept and analyzed at the same time as the post-photolysis samples as a further control to ensure only photochemically-generated products were considered.

6.3.2 UV Absorption Spectra of α-Keto Acids as a Function of pH

Photolysis of α-keto acids in the aqueous phase begins when the keto form absorbs a near-UV photon and is excited to the first excited singlet ^{1}(n, π*) state (S_1). The system can then undergo rapid intersystem crossing and internal conversion to the reactive ^{3}(n, π*) T_1 state.[38] The diol form does not absorb light within the solar spectrum and, therefore, is not considered to be a photoactive species. The absorption cross-section of the S_1 state for a given solution of pyruvic acid can be monitored by UV-vis spectroscopy, and previous studies have reported the λ_{max} for this broad transition at ~320 nm.[5, 36-39, 44] Similarly, the λ_{max} for OOA occurs ~315 nm.[41]

Here, we examined changes in this UV absorption for solutions of 10 mM pyruvic acid of varying pH (Figure 6.2), showing a dramatic increase in the intensity of absorption as the pH of solution is raised. Additionally, a very slight shift of the transition wavelength maximum to the blue is also observed, with a change in λ_{max} from 320 nm to 316 nm. This blue shift can be observed more clearly when the absorbance of all spectra is normalized at

λ_{max}, as shown in Figure F.6. In the other limit, lowering the pH to 1.54 causes the absorbance to decrease and shift slightly to the red. As pH is raised from 3.38 to 10.46 the intensity and shape of the spectra continue to change slightly, but this is a small effect compared to the difference between the unadjusted pH solution and that at pH 3.38. While not surprising, given the rapid changes in the protonation and hydration states of pyruvic acid in the range from pH 1.5 to 3.4, this again demonstrates that the so-called high pH limit is rapidly reached, even for acidic solutions. Likewise, 3 mM solutions of OOA show a very similar increase in absorbance and slight blue shift (from 315 nm to 312 nm) as pH is increased, as shown in Figure F.7.

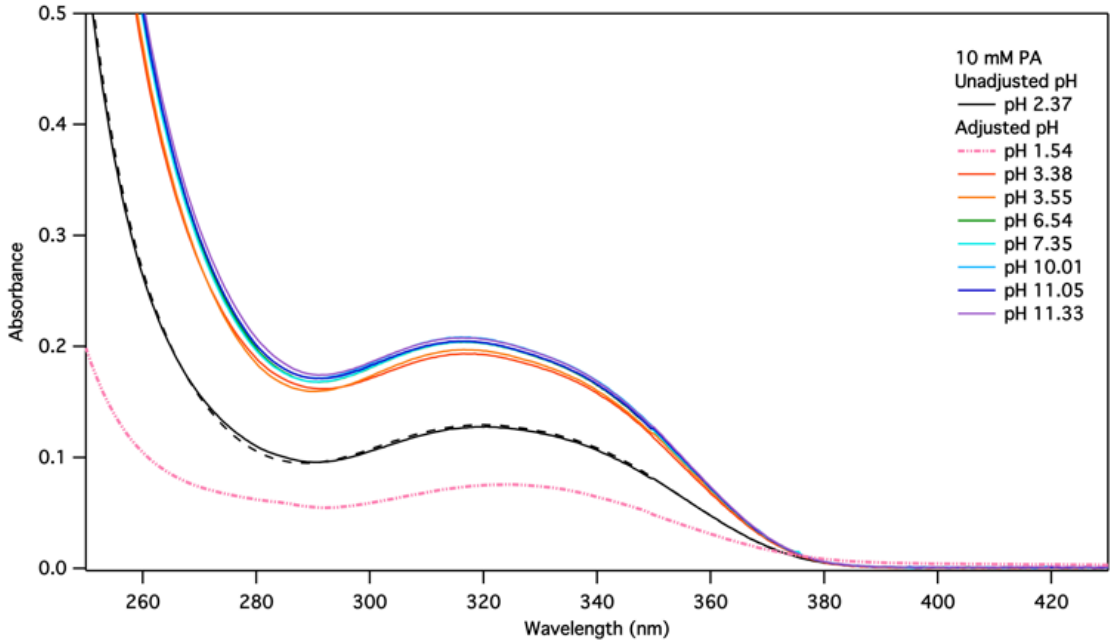

Figure 6.2. Representative UV-vis absorption spectra of 10 mM pyruvic acid solutions over a range of pH conditions from 1.54 to 11.33.

The changes in absorbance can be understood by considering that both the protonated and deprotonated forms of the keto α-keto acid contribute to the observed peak. As the pH of the solution is raised, the overall percentage of keto form increases to approximately 90%, which, in turn, leads to the increase in absorbance intensity. Regardless of protonation, the keto form contains a chromophore and absorbs light within the actinic flux,

unlike the diol form. It is likely, however, that the slight difference in the shape of the absorbance is due to the increased contribution of the deprotonated form, which has a slightly higher energy transition to the S_1 state than the protonated form.

The electronic structure of deprotonated α-keto acids would be expected to be slightly different from that of the protonated form. Predicting the nature of this difference is, however, difficult. Deprotonated species tend to be more delocalized, which would imply a slight red shift from the ground state. However, in the aqueous phase, interactions between the more polar deprotonated species and water likely stabilize the ground state, increasing the energy of the transition to the S_1 state, resulting in a shift to the blue. The relative size of these two opposite effects is difficult to predict, but it appears, in this case, that they essentially offset, resulting in only a very subtle shift in the shape of the absorption spectrum as a function of pH. This suggests that the electronic states for the protonated and deprotonated keto species are quite similar. This is reasonable given that the only difference between the two species is the presence of a proton, and the number of electrons has not been changed.

6.3.3. Photolysis of α-Keto Acids at varying pH

Studies of the aqueous photochemistry of pyruvic acid have previously only explicitly considered photolysis of its protonated keto form.[5, 36-39] However, as demonstrated above, in dilute solution, even at the natural, acidic pH (~2.4), more than half of the keto species are deprotonated. This percentage rapidly increases as the pH of the solution is raised. As mentioned above, the only previous report in the literature about the photolysis of pyruvic acid under high pH conditions (~6.1, >99% deprotonated) mentions that the photolysis is observed to proceed more slowly, as determined by UV spectrophotometric analysis, at less than a third of the rate observed for their 0.285 M samples at unadjusted pH.[43] A reduction in the amount of CO_2 produced during the course of photolysis was also observed, but no

other reaction products were identified, nor was any attempt made to rationalize the slowed time evolution of the reaction.

Such a decrease in the rate of reaction observed in the high pH limit is not, however, due to a reduction in the number of photoactive species in solution. Rather, as shown in Figure 6.2, the absorbance of the solution increases as the pH of the solution is raised, as the keto form becomes more favored. From comparison of the UV data it appears that very similar S_1 states can be accessed for both the protonated and deprotonated keto forms. However, because the photolysis discussed by Leermakers and Vesley was monitored only by the decay of pyruvic acid and the formation of CO_2, it is not possible to extract further information about the subsequent reactive pathways the photoexcited pyruvic acid follows. Therefore, in this study, we examine the generated aqueous photoproducts, particularly those oligomeric species whose formation we understand with mechanistic detail,[5, 38, 39, 41] to determine whether similar photochemical pathways are accessible across acidities for α-keto acids.

Dilute solutions of 10 mM pyruvic acid were photolyzed for 5 hours with a xenon arc lamp, unlike Leermakers and Vesley who used much more concentrated solutions (285 mM) and a mercury arc lamp.[43] Despite these experimental differences, when photolysis is monitored by UV-vis spectroscopy, the decay of pyruvic acid is indeed slowed under higher pH conditions, as shown in Figure 6.3. ^{1}H NMR analysis (shown in Figure F.8) confirms this as the relative consumption of pyruvic acid over the course of 5 hours of photolysis is reduced at high pH to ~30% compared to ~90% at unadjusted pH. A full analysis of kinetics is beyond the scope of this paper, but it is readily apparent that the relative rate of consumption of pyruvic acid is reduced in the high pH limit. As previously discussed, the high pH limit for reaction is reached around a solution pH of 5.6. Therefore, it is not surprising that photolyses conducted for solutions above this point behave very similarly

and have essentially identical UV spectra across the course of reaction.

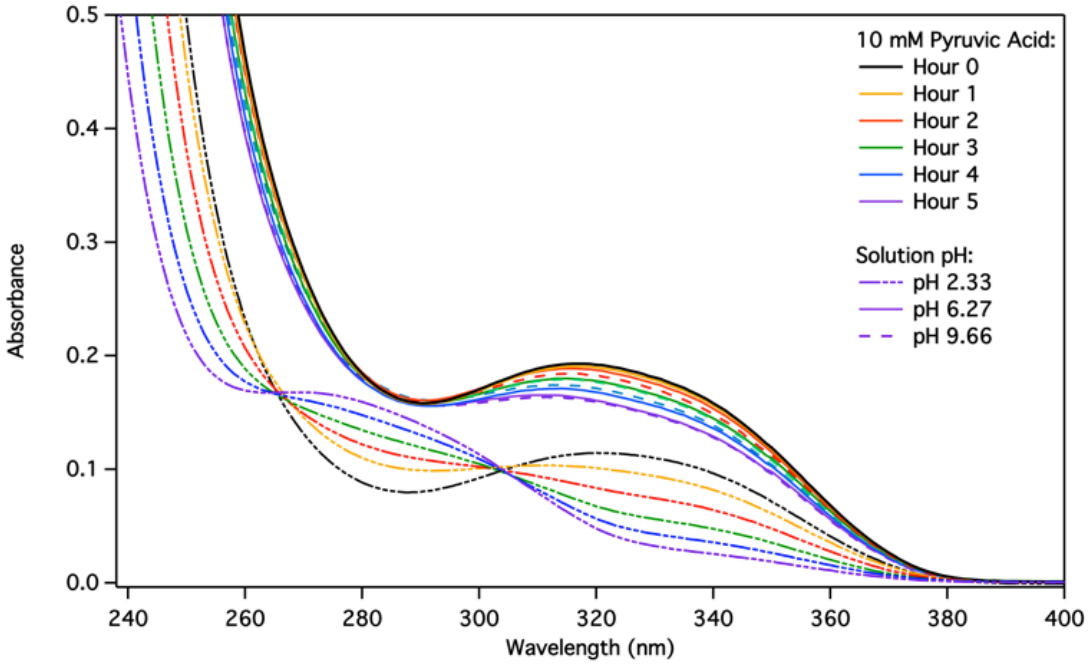

Figure 6.3. Representative UV-vis absorption spectra for the photolysis of 10 mM pyruvic acid over 5 hours for solutions at unadjusted pH (2.33, dash-dot), pH 6.27 (solid), and pH 9.66 (dashed).

The shape of the UV spectra over the course of photolysis in the high pH limit, however, differs distinctively from that of unadjusted pH solutions. UV spectra of pyruvic acid during photolysis generally feature prominently a double isosbestic point,[5] a feature which is retained here for our dilute solutions at unadjusted pH. This strong feature (~265-305 nm) is a convolution of contributions from photoproducts, including both acetoin and oligomeric photoproducts.[38] It is observable even at relatively low extents of reaction and should be observable for the high pH solutions despite the decreased overall consumption of pyruvic acid. However, the high pH solutions appear to have no such feature, and the shape of their UV spectra is characterized solely by the decay of pyruvic acid without a corresponding increasing peak. This suggests that a different product distribution is generated under high pH conditions. Similar analysis of UV spectra for OOA is difficult because of scattering, caused by the formation of aggregates in solution as photolysis progresses,[40, 41] which

obscures any potentially interesting features of the spectra.

^{1}H NMR spectra of post-photolysis solutions of pyruvic acid (Figure F.8) also show this apparent shift in relative mixture of photoproducts, although, importantly it appears largely that this is a shift in the relative composition. However, the complexity of the mixture of species in solution, as well as changes in chemical shift at different acidities, makes detailed analysis of these data difficult. Therefore, we turn to high resolution negative mode electrospray ionization mass spectrometry (ESI$^-$ MS) for more detailed product analysis for both pyruvic acid and OOA.

The ESI$^-$ MS techniques used here are not designed to be quantitative, and, in complex mixtures, like those under study here, the differing ionization efficiencies of species in solution can greatly influence the observed analytes. Therefore, signal intensity may not correlate directly with absolute analyte concentration and care must be taken to ensure that MS results are not over-interpreted. However, relative comparisons and qualitative trends between similar samples may be derived using these techniques.

ESI$^-$ MS data was analyzed for both pre- and post-photolysis solutions of both pyruvic acid and OOA in the high pH limit, following the analysis procedure of Rapf et al. 2017[39] and detailed results are given in Tables F.1 and F.2. For solutions of pure pyruvic acid and OOA before photolysis look very similar across all pH ranges as shown in Figures F.9 and F.10, respectively. In addition to signal due to the $[M\text{-}H]^-$ ion for each α-keto acid (m/z = 87.0085 ± 0.0003 for pyruvic acid and m/z = 157.0867 ± 0.0003 for OOA), adduct species consisting of two or more deprotonated α-keto acid molecules coordinated with a positively charged ion, usually Na^+ or Ca^{2+}, are observed. In the unadjusted pH solutions, these are trace ions only as 18.2 MΩ water is used without further addition of salt. However, when NaOH is added to adjust the solution pH, more sodium ions are present in solution, and, accordingly, the relative intensity of adduct signal is increased.

As shown in Figure 6.4, significantly more signal due to pyruvic acid, in both its free and adduct ions, remains following photolysis in the high pH limit than under unadjusted pH conditions, consistent with both the NMR and UV spectra discussed above, and again suggesting that the reaction is slowed at high pH. Interestingly, it appears that the same species are generated photochemically regardless of pH regime.

However, while the same species appear to be generally present in solution, there are noticeable differences in the relative ratios of products formed between high and low pH solutions, indicating that the branching ratios governing the further reactions of pyruvic acid are changed as pH is raised. This shift in the ratio of photoproducts likely accounts for some of the observed differences in the shape of the UV spectra of post-photolysis pyruvic acid at high pH.

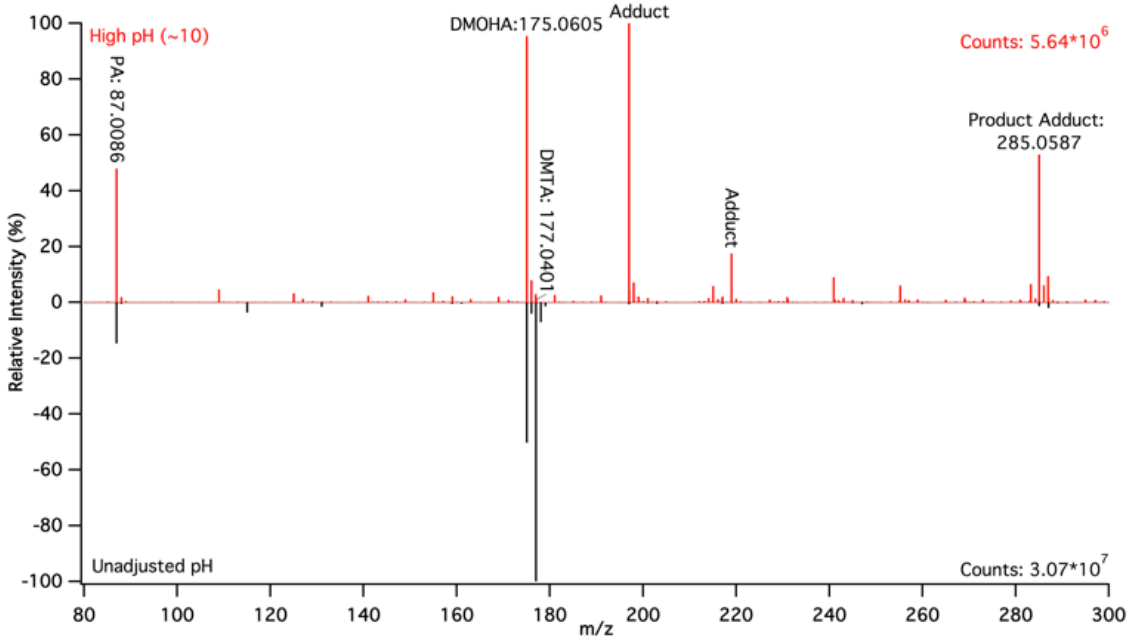

Figure 6.4. Representative ESI⁻ MS of 10 mM pyruvic acid after 5 hours of photolysis at unadjusted pH (black, multiplied by -1 for ease of presentation) and pH ~10 (initial pH = 9.66, red). Note: DMTA peak in high pH is about half the intensity it appears due to the presence of a closely overlapping peak.

The mechanisms by which organic radicals generated from hydrogen abstraction by triplet state pyruvic acid and subsequently recombine have been previously discussed in

detail.[5, 38, 39, 42] A simplified version of these pathways is shown in Scheme 6.2.

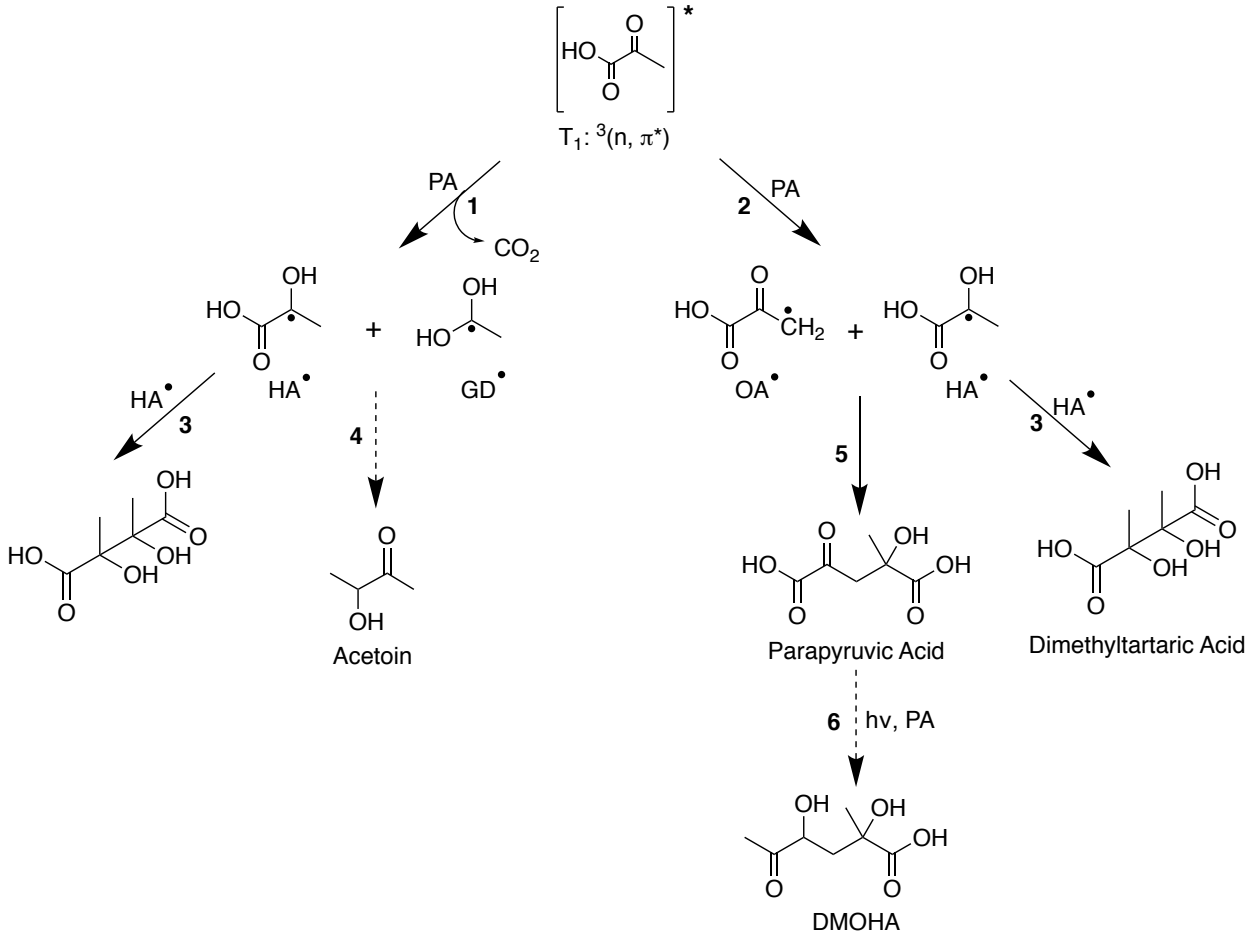

Scheme 6.2. Simplified reaction network for the aqueous phase photochemistry of pyruvic acid. Dashed arrows indicate multiple reactive steps occur between shown species.[38, 39]

Briefly, hydrogen abstraction can occur either from the carboxyl group (Reaction 1 of Scheme 6.2) or from the methyl group (Reaction 2 of Scheme 6.2) of pyruvic acid. Hydrogen abstraction from the carboxyl group can occur from either the diol or keto form of pyruvic acid, although abstraction from the diol form is slightly favored energetically.[38] While hydrogen abstraction for the carboxyl group is likely the dominant reactive pathway in acidic solution, it has also recently been shown that hydrogen abstraction from the methyl group is energetically competitive.[39] The radicals generated from these two abstraction pathways, include one with hydroxyl acid functionality, $CH_3\dot{C}(OH)CO_2H$ (HA•), one with geminal diol functionality, $CH_3\dot{C}(OH)_2$ (GD•), and one with oxoacid functionality,

$\dot{C}H_2C(O)CO_2H$ (OA•).[39] These radicals then go on to do further chemistry, yielding the observable photoproducts. For example, recombination of two HA• radicals (Reaction 3 of Scheme 6.2) gives dimethyltartaric acid (DMTA), a dimer[66] of pyruvic acid.[38] Recombination of HA• with OA• generates parapyruvic acid, itself an α-keto acid that is photoactive (Reaction 5 of Scheme 6.2). Following a second photochemical step involving the cross-reaction between parapyruvic acid and pyruvic acid and subsequent dehydration and decarboxylation, 2,4-dihydroxy-2-methyl-5-oxohexanoic acid (DMOHA) is generated as the observable photoproduct (Reaction 6 of Scheme 6.2). DMTA and DMOHA are generally considered the most important oligomeric products of this photochemistry and are observed with the highest intensity by ESI^- MS, although a number of other product species have also been identified.[5, 38, 39] More interestingly, because these two products are generated from the recombination of radicals formed from hydrogen abstraction at different sites, their relative ratio can be used as a probe of the relative amount of hydrogen abstraction occurring from the carboxyl versus methyl group of pyruvic acid.

Comparison of solutions at different pH under the same experimental conditions and concentration regime reveals changes in the relative branching ratio as the pH of the solution is changed. Mechanistically, we can predict that high pH conditions should favor the formation of DMOHA over DMTA. This is expected because hydrogen abstraction from the carboxyl group of pyruvic acid cannot occur if the carboxyl group is deprotonated. Instead, the only remaining site for abstraction is the methyl group. This, therefore, will increase the relative amount of products stemming from the methyl abstraction pathway (Reaction 2 of Scheme 6.2), leading the production of relatively more DMOHA than DMTA under high pH conditions. A secondary contributing factor to the shift in hydrogen abstraction to favor the methyl site is the change in keto/diol ratio. Hydrogen abstraction from the protonated diol appears to be favored over the protonated ketone energetically,[38]

which means that residual or transiently protonated species are also less likely to react at high pH, due to the reduced diol content at high pH.

As seen in Figure 6.4, this mechanistic prediction is borne out and considerably more DMOHA is observed in the high pH limit compared to DMTA. While the overall yield of products is reduced under high pH conditions, as discussed above, the relative amount of DMOHA has clearly increased. Additionally, the intensity of the ion at m/z = 285.0592 ± 0.0005 is increased significantly under high pH conditions. This appears to be a product adduct, corresponding to a sodium ion coordinated to two singly deprotonated species, which here are likely DMOHA and pyruvic acid. Again, it is not surprising that the relative intensity of adducts increases when more than a trace amount of sodium is present in solution due to the addition of NaOH to adjust the solution pH.

The ESI$^-$ MS measurements conducted here were not designed to be absolutely quantitative, and ionization efficiency of species are known to change under different solutions conditions.[67] Therefore, to ensure that the observed difference in relative product ratios was not an artifact of the high pH solution conditions, samples of post-photolysis solutions that were conducted in the high pH limit were adjusted back to low pH and analyzed and vice versa (Figures F.11 and F.12). These controls showed relatively minor differences in ionization efficiency for the oligomeric species of interest, e.g. DMOHA and DMTA for pyruvic acid. This means that the observed change in the relative intensity of the two products as a function of pH is reflective of a change in the branching ratio of the reactive pathways.

A similar shift in product distribution is observed for OOA as well (Figure 6.5). α-Keto acids with longer alkyl chains undergo largely the same photochemistry as the shorter pyruvic acid,[40, 41] where hydrogen abstraction from the methyl group of pyruvic acid becomes hydrogen abstraction from the alkyl tail of OOA. However, there is an additional

intramolecular Norrish Type II reactive pathway that is accessible to alkyl α-keto acids that contain a γ-carbon that results in the formation of pyruvic acid.[40, 41, 68, 69] This pyruvic acid can, of course, react photochemically, and the products generated from the cross-reaction between radicals generated from both pyruvic acid and OOA photochemistry are observed.[41]

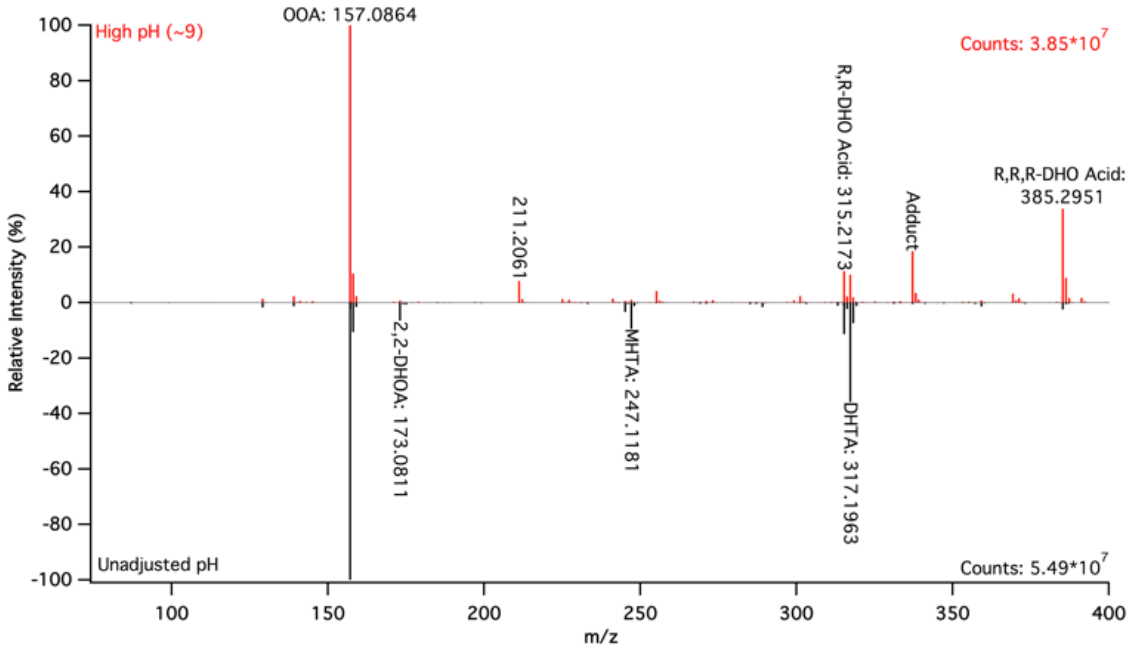

Figure 6.5. Representative ESI⁻ MS of 3 mM 2-oxooctanoic acid after 5 hours of photolysis at unadjusted pH (black, multiplied by -1 for ease of presentation) and pH ~9 (initial pH = 8.91, red).

For example, methylhexyltartaric acid (MHTA, Figure 6.6) is generated from the recombination of an HA• radical of pyruvic acid with an RHA• radical from OOA. Because of the multiple photoactive species present in solution during photolysis (OOA, pyruvic acid, and various parapyruvic acid derivatives), it is possible to generate oligomeric products with one, two, or three alkyl tails, examples of which are shown in Figure 6.6. The species in Figure 6.6 are those generated when hydrogen abstraction occurred at the β-CH_2 group of the alkyl tail of OOA. This is expected to be the favored site of abstraction,[41, 70] but it is likely that hydrogen abstraction can occur along the alkyl tail and the observed oligomeric products are likely a mixture of constitutional isomers.

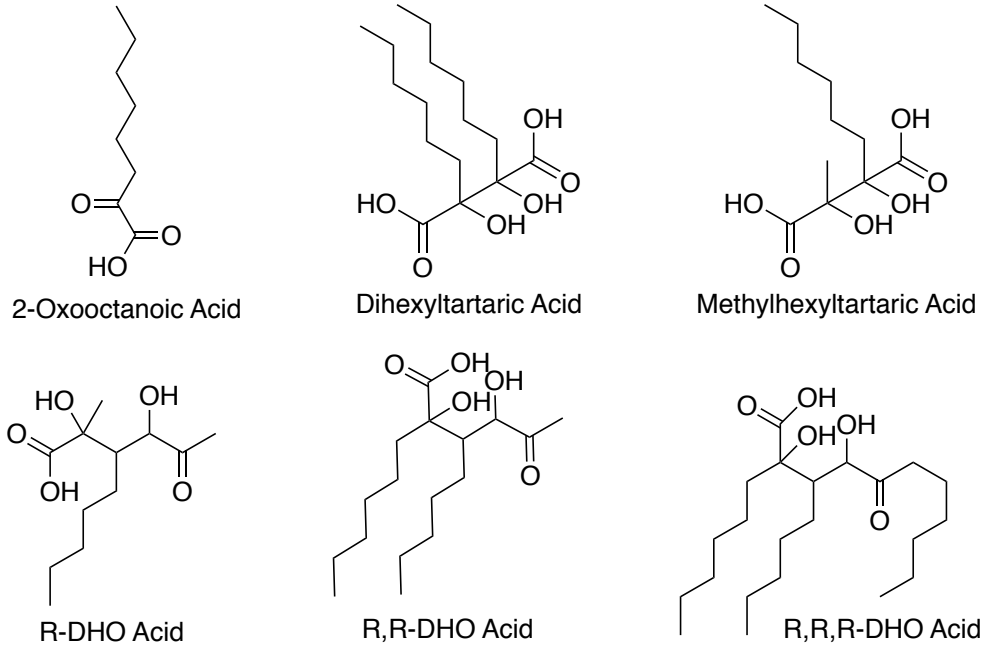

Figure 6.6. Structure of 2-oxooctanoic acid and selected photochemical products.[41] Note: the dihydroxyoxoalkanoic acid species shown are representative structures derived from hydrogen abstraction at the β-CH_2 site. Other structural isomers are likely also formed.

Under unadjusted pH conditions, the formation of the tartaric acid derivatives is clearly favored, as dihexyltartaric acid (DHTA) and the mixed MHTA are observed with the highest intensity by ESI^- MS (Figure 6.5). When photolysis is conducted in the high pH limit, the relative intensity of the dihydroxyoxoalkanoic acid species increases dramatically, particularly for the triple-tailed species (R,R,R-DHO acid), as would be mechanistically predicted. While relative intensity of the double-tailed R,R-DHO acid also increases, it appears to be a less dramatic increase, and signal from the single-tailed R-DHO acid does not appear to be particularly enhanced. Indeed, the species that are generated from the cross reactions of pyruvic acid with OOA are relatively suppressed, with a notable decrease in the relative intensity of MHTA. This suggests that the Norrish Type II reaction that forms pyruvic acid may preferentially suppressed under high pH conditions. Additionally, there appear to be a few other very minor products generated under high pH conditions (*e.g.* m/z = 211.2065 ± 0.0003) that are not formed in significant amounts under low pH

conditions. These species are as yet unidentified but suggest that there may be details as yet missing from our understanding of the reactive pathways of α-keto acids.

While the high pH limit is reached while solutions are still quite acidic, it is interesting to consider how the pH of solution changes over the course of photolysis (Figure F.13). It is known that for solutions of pyruvic acid, the pH increases slightly over the course of photolysis.[5] Under the dilute conditions at unadjusted pH used here, we observe a similar slight increase in pH of ~0.5 over the course of photolysis. Solutions with an initial pH of ~10, also show a relatively slight change in pH during photolysis, typically decreasing slightly by ~0.8. However, solutions at intermediate pH initially (~4-6) show a much larger change in pH over the course of photolysis, increasing to a pH of ~8.5. This change occurs because the dilute solutions near these pH values are near the equivalence point of pyruvic acid, and, therefore, are not well buffered (Figure F.2). This considerable increase in pH does not affect the observed photochemistry because the solution was already in the high pH limit, but it is possible that the further reactivity of the generated species might be affected. Dilute pyruvic acid is unlikely to be important drivers of the overall acidity of atmospheric particles, but it is important to consider how this behavior may affect more complex laboratory studies, for instance.

Broadly speaking, however, the vast majority of the observed products of α-keto acids can be explained using our mechanistic framework, and with the experimental pH dependence of the relative branching ratios of the reactive pathways matching the predicted behavior. That the mechanistic framework for the aqueous photochemistry of α-keto acids that was developed under low pH conditions is in good agreement with the products observed under high pH conditions suggests that the reactive pathways are similar regardless of the acidity of solution. This leads us to conclude that the electronic states of the deprotonated keto form are similar to those of the protonated keto form, and a

reactive triplet state is still readily accessible. While the observed slowing of the photochemistry in the high pH limit might be explained by a lowered efficiency in intersystem crossing to the reactive triple state of the deprotonated form, we suggest that changes in composition of the solution as pH is increased are responsible for the majority of the experimental decrease in reactivity. In the high pH limit, ~90% of an α-keto acid exists as its deprotonated keto form, which substantially changes the efficiency and availability of sites for hydrogen abstraction, accounting for both the slowed photolysis and the shift in the ratio of observed products.

6.4 Conclusions:

We have, for the first time, investigated in detail the pH dependence of the aqueous phase photochemistry of α-keto acids. When an α-keto acid is dissolved in water, it exists in equilibrium with its geminal diol hydrate in solution. The extent of hydration is lowered as pH is raised, reaching a composition of about 10% diol and 90% keto for pyruvic acid in the high pH limit. In the high pH limit, both the keto and diol forms are completely deprotonated (>99%). These are relatively strong acids, therefore, the "high pH limit" is reached under even quite acidic conditions. The photoactive keto form of pyruvic acid, for instance, is more than 95% deprotonated for a solution pH of 3.5. We have shown that the previously developed detailed mechanistic framework holds at high pH, and deprotonated α-keto acids can access the same reactive pathways as their protonated counterparts, although the photochemistry is observed to slow under high pH conditions. The relative branching ratio also shifts to favor products generated by radicals stemming from alkyl hydrogen abstraction, as is predicted mechanistically.

This work is particularly relevant for understanding the fate of organics in the ocean and atmospheric aerosols, where reaction rates and product distributions will change as the pH conditions of these systems are altered through transport and chemical processing.

While the photochemistry of α-keto acids and the sensitivity to reaction conditions have been the subject of considerable scrutiny, the effects of the acidity of the reaction environment have been ignored. In aqueous environments, molecules that would be a single compound in the gas phase will often exist as a mixture of species in solution, whose composition may change drastically as the solution conditions are changed. We have shown that, for this system, we can translate the known mechanistic framework to understand the observed changes in the aqueous phase composition, rate of reactivity, and the relative product yields.

6.5 Bibliography:

1. Rapf, R. J.; Vaida, V. Sunlight as an energetic driver in the synthesis of molecules necessary for life. *Phys. Chem. Chem. Phys.* **2016,** *18*, 20067-20084.

2. George, C.; Ammann, M.; D'Anna, B.; Donaldson, D. J.; Nizkorodov, S. A. Heterogeneous photochemistry in the atmosphere. *Chem. Rev.* **2015,** *115*, 4218-4258.

3. George, C.; D'Anna, B.; Herrmann, H.; Weller, C.; Vaida, V.; Donaldson, D.; Bartels-Rausch, T.; Ammann, M., Emerging areas in atmospheric photochemistry. In *Atmospheric and aerosol chemistry*, Springer: 2014; pp 1-53.

4. Renard, P.; Reed Harris, A. E.; Rapf, R. J.; Rainer, S.; Demelas, C.; Coulomb, B.; Quivet, E.; Vaida, V.; Monod, A. Aqueous phase oligomerization of methyl vinyl ketone by atmospheric radical reactions. *J. Phys. Chem. C* **2014,** *118*, 29421-29430.

5. Reed Harris, A. E.; Ervens, B.; Shoemaker, R. K.; Kroll, J. A.; Rapf, R. J.; Griffith, E. C.; Monod, A.; Vaida, V. Photochemical kinetics of pyruvic acid in aqueous solution. *J. Phys. Chem. A* **2014,** *118*, 8505-8516.

6. Vaida, V. Atmospheric radical chemistry revisited. *Science* **2016,** *353*, 650-650.

7. Bernard, F.; Ciuraru, R.; Boréave, A.; George, C. Photosensitized formation of secondary organic aerosols above the air/water interface. *Environ. Sci. Technol.* **2016,** *50*, 8678-8686.

8. Ciuraru, R.; Fine, L.; Pinxteren, M. V.; D'Anna, B.; Herrmann, H.; George, C. Unravelling new processes at interfaces: Photochemical isoprene production at the sea surface. *Environ. Sci. Technol.* **2015**, 13199–13205.

9. Rossignol, S.; Tinel, L.; Bianco, A.; Passananti, M.; Brigante, M.; Donaldson, D. J.; George, C. Atmospheric photochemistry at a fatty acid–coated air-water interface. *Science* **2016,** *353*, 699-702.

10. Quinn, P. K.; Collins, D. B.; Grassian, V. H.; Prather, K. A.; Bates, T. S. Chemistry and related properties of freshly emitted sea spray aerosol. *Chem. Rev.* **2015,** *115*, 4383-4399.

11. Alves, C. A. Chemistry between the sea surface microlayer and marine aerosols. *Quim. Nova* **2014,** *37*, 1382-1400.

12. Wang, X.; Sultana, C. M.; Trueblood, J.; Hill, T. C. J.; Malfatti, F.; Lee, C.; Laskina, O.; Moore, K. A.; Beall, C. M.; McCluskey, C. S., et al. Microbial control of sea spray aerosol composition: A tale of two blooms. *ACS Cent. Sci.* **2015,** *1*, 124-131.

13. Cunliffe, M.; Engel, A.; Frka, S.; Gasparovic, B.; Guitart, C.; Murrell, J. C.; Salter, M.; Stolle, C.; Upstill-Goddard, R.; Wurl, O. Sea surface microlayers: A unified physiochemical and biological perspective of the air-ocean interface. *Prog. Oceanogr.* **2013,** *109*, 104-116.

14. Engel, A.; Bange, H. W.; Cunliffe, M.; Burrows, S. M.; Friedrichs, G.; Galgani, L.; Herrmann, H.; Hertkorn, N.; Johnson, M.; Liss, P. S., et al. The ocean's vital skin: Toward an integrated understanding of the sea surface microlayer. *Front. Mar. Sci.* **2017,** *4*.

15. Cochran, R. E.; Laskina, O.; Jayarathne, T.; Laskin, A.; Laskin, J.; Lin, P.; Sultana, C.; Lee, C.; Moore, K. A.; Cappa, C. D. Analysis of organic anionic surfactants in fine and coarse fractions of freshly emitted sea spray aerosol. *Environ. Sci. Technol.* **2016,** *50*, 2477-2486.

16. Chiu, R.; Tinel, L.; Gonzalez, L.; Ciuraru, R.; Bernard, F.; George, C.; Volkamer, R. UV photochemistry of carboxylic acids at the air-sea boundary: A relevant source of glyoxal and other oxygenated VOC in the marine atmosphere. *Geophys. Res. Lett.* **2017,** *44*, 1079-1087.

17. Tervahattu, H.; Hartonen, K.; Kerminen, V. M.; Kupiainen, K.; Aarnio, P.; Koskentalo, T.; Tuck, A. F.; Vaida, V. New evidence of an organic layer on marine aerosols. *J. Geophys. Res.* **2002,** *107*, 4053-4060.

18. Long, M.; Keene, W.; Kieber, D.; Frossard, A.; Russell, L.; Maben, J.; Kinsey, J.; Quinn, P.; Bates, T. Light - enhanced primary marine aerosol production from biologically productive seawater. *Geophys. Res. Lett.* **2014,** *41*, 2661-2670.

19. Galloway, M. M.; Powelson, M. H.; Sedehi, N.; Wood, S. E.; Millage, K. D.; Kononenko, J. A.; Rynaski, A. D.; De Haan, D. O. Secondary organic aerosol formation during evaporation of droplets containing atmospheric aldehydes, amines, and ammonium sulfate. *Environ. Sci. Technol.* **2014,** *48*, 14417-14425.

20. Rudich, Y. Laboratory perspectives on the chemical transformations of organic matter in atmospheric particles. *Chem. Rev.* **2003,** *103*, 5097-5124.

21. Ervens, B.; Turpin, B. J.; Weber, R. J. Secondary aerosol formation in cloud droplets and aqueous particles (aqSOA): A review of laboratory, field and model studies. *Atmo. Chem. Phys.* **2011,** *11*, 11069-11102.

22. Carlton, A. G.; Wiedinmyer, C.; Kroll, J. H. A review of secondary organic aerosol (SOA) formation from isoprene. *Atmo. Chem. Phys.* **2009,** *9*, 4987-5005.

23. Hallquist, M.; Wenger, J. C.; Baltensperger, U.; Rudich, Y.; Simpson, D.; Claeys, M.; Dommen, J.; Donahue, N. M.; George, C.; Goldstein, A. H., et al. The formation, properties and impact of secondary organic aerosol: Current and emerging issues. *Atmos. Chem. Phys.* **2009,** *9*, 5155-5236.

24. Altieri, K. E.; Carlton, A. G.; Lim, H.-J.; Turpin, B. J.; Seitzinger, S. P. Evidence for oligomer formation in clouds: Reactions of isoprene oxidation products. *Environ. Sci. Technol.* **2006,** *40*, 4956-4960.

25. Ervens, B.; Carlton, A. G.; Turpin, B. J.; Altieri, K. E.; Kreidenweis, S. M.; Feingold, G. Secondary organic aerosol yields from cloud-processing of isoprene oxidation products. *Geophys. Res. Lett.* **2008,** *35*, L02816.

26. Carlton, A. G.; Turpin, B. J.; Lim, H.-J.; Altieri, K. E.; Seitzinger, S. Link between isoprene and secondary organic aerosol (SOA): Pyruvic acid oxidation yields low volatility organic acids in clouds. *Geophys. Res. Lett.* **2006,** *33*, L06822.

27. Warneck, P. Multi-phase chemistry of C-2 and C-3 organic compounds in the marine atmosphere. *J. Atmos. Chem.* **2005,** *51*, 119-159.

28. Andreae, M. O.; Talbot, R. W.; Li, S. M. Atmospheric measurements of pyruvic and formic acid. *J. Geophys. Res. Atmos.* **1987,** *92*, 6635-6641.

29. Ho, K.; Lee, S.; Cao, J.; Kawamura, K.; Watanabe, T.; Cheng, Y.; Chow, J. C. Dicarboxylic acids, ketocarboxylic acids and dicarbonyls in the urban roadside area of Hong Kong. *Atmos. Environ.* **2006,** *40*, 3030-3040.

30. Talbot, R.; Andreae, M.; Berresheim, H.; Jacob, D. J.; Beecher, K. Sources and sinks of formic, acetic, and pyruvic acids over central Amazonia: 2. Wet season. *J. Geophys. Res. Atmos.* **1990,** *95*, 16799-16811.

31. Veres, P.; Roberts, J. M.; Burling, I. R.; Warneke, C.; de Gouw, J.; Yokelson, R. J. Measurements of gas-phase inorganic and organic acids from biomass fires by negative-ion proton-transfer chemical - ionization mass spectrometry. *J. Geophys. Res. Atmos.* **2010,** *115*, D23302.

32. Hoque, M. M. M.; Kawamura, K.; Uematsu, M. Spatio-temporal distributions of dicarboxylic acids, ω-oxocarboxylic acids, pyruvic acid, α-dicarbonyls and fatty acids in the marine aerosols from the north and south Pacific. *Atmo. Res.* **2017,** *185*, 158-168.

33. Hoque, M. M. M.; Kawamura, K. Longitudinal distributions of dicarboxylic acids, ω-oxoacids, pyruvic acid, α-dicarbonyls, and fatty acids in the marine aerosols from the

central Pacific including equatorial upwelling. *Global Biogeochem. Cycles* **2016,** *30*, 534-548.

34. Chebbi, A.; Carlier, P. Carboxylic acids in the troposphere, occurrence, sources, and sinks: A review. *Atmos. Environ.* **1996,** *30*, 4233-4249.

35. Reed Harris, A. E.; Pajunoja, A.; Cazaunau, M.; Gratien, A.; Pangui, E.; Monod, A.; Griffith, E. C.; Virtanen, A.; Doussin, J. F.; Vaida, V. Multiphase photochemistry of pyruvic acid under atmospheric conditions. *J. Phys. Chem. A* **2017,** *121*, 3327–3339.

36. Guzman, M. I.; Colussi, A. J.; Hoffmann, M. R. Photoinduced oligomerization of aqueous pyruvic acid. *J. Phys. Chem. A* **2006,** *110*, 3619-3626.

37. Eugene, A. J.; Guzman, M. I. Reactivity of ketyl and acetyl radicals from direct solar actinic photolysis of aqueous pyruvic acid. *J. Phys. Chem. A* **2017,** *121*, 2924–2935.

38. Griffith, E. C.; Carpenter, B. K.; Shoemaker, R. K.; Vaida, V. Photochemistry of aqueous pyruvic acid. *Proc. Natl. Acad. Sci.* **2013,** *110*, 11714-11719.

39. Rapf, R. J.; Perkins, R. J.; Carpenter, B. K.; Vaida, V. Mechanistic description of photochemical oligomer formation from aqueous pyruvic acid. *J. Phys. Chem. A* **2017,** *121*, 4272–4282.

40. Griffith, E. C.; Rapf, R. J.; Shoemaker, R. K.; Carpenter, B. K.; Vaida, V. Photoinitiated synthesis of self-assembled vesicles. *J. Am. Chem. Soc.* **2014,** *136*, 3784-3787.

41. Rapf, R. J.; Perkins, R. J.; Yang, H.; Miyake, G. M.; Carpenter, B. K.; Vaida, V. Photochemical synthesis of oligomeric amphiphiles from alkyl oxoacids in aqueous environments. *J. Am. Chem. Soc.* **2017,** *139*, 6946–6959.

42. Closs, G. L.; Miller, R. J. Photo-reduction and photodecarboxylation of pyruvic acid - applications of CIDNP to mechanistic photochemistry. *J. Am. Chem. Soc.* **1978,** *100*, 3483-3494.

43. Leermakers, P. A.; Vesley, G. F. Photolysis of pyruvic acid in solution. *J. Org. Chem.* **1963,** *28*, 1160-1161.

44. Leermakers, P. A.; Vesley, G. F. Photochemistry of alpha-keto acids and alpha-keto esters. 1. Photolysis of pyruvic acid and benzoylformic acid. *J. Am. Chem. Soc.* **1963,** *85*, 3776-3779.

45. Zhang, Z.; Cai, W.; Liu, L.; Liu, C.; Chen, F. Direct determination of thickness of sea surface microlayer using a pH microelectrode at original location. *Science in China Series B: Chemistry* **2003,** *46*, 339-351.

46. Zhang, Z. B.; Liu, L.; Liu, C.; Cai, W. Studies on the sea surface microlayer. II. The layer of sudden change of physical and chemical properties. *J. Colloid Interface Sci.* **2003,** *264*, 148-159.

47. Craig, R. L.; Nandy, L.; Axson, J. L.; Dutcher, C. S.; Ault, A. P. Spectroscopic determination of aerosol pH from acid–base equilibria in inorganic, organic, and mixed systems. *J. Phys. Chem. A* **2017,** *121*, 5690-5699.

48. Bougiatioti, A.; Nikolaou, P.; Stavroulas, I.; Kouvarakis, G.; Weber, R.; Nenes, A.; Kanakidou, M.; Mihalopoulos, N. Particle water and pH in the eastern Mediterranean: Source variability and implications for nutrient availability. *Atmos. Chem. Phys.* **2016,** *16*, 4579-4591.

49. Weber, R. J.; Guo, H.; Russell, A. G.; Nenes, A. High aerosol acidity despite declining atmospheric sulfate concentrations over the past 15 years. *Nat. Geosci.* **2016,** *9*, 282-285.

50. Young, A. H.; Keene, W. C.; Pszenny, A. A. P.; Sander, R.; Thornton, J. A.; Riedel, T. P.; Maben, J. R. Phase partitioning of soluble trace gases with size-resolved aerosols in near-surface continental air over northern Colorado, USA, during winter. *J. Geophys. Res. Atmos.* **2013,** *118*, 9414-9427.

51. Murphy, J. G.; Gregoire, P.; Tevlin, A.; Wentworth, G.; Ellis, R.; Markovic, M.; VandenBoer, T. Observational constraints on particle acidity using measurements and modelling of particles and gases. *Faraday Discuss.* **2017**.

52. Guo, H.; Xu, L.; Bougiatioti, A.; Cerully, K. M.; Capps, S. L.; Hite Jr, J.; Carlton, A.; Lee, S.; Bergin, M.; Ng, N. Fine-particle water and pH in the southeastern United States. *Atmos. Chem. Phys* **2015,** *15*, 5211-5228.

53. Perkins, R. J.; Shoemaker, R. K.; Carpenter, B. K.; Vaida, V. Chemical equilibria and kinetics in aqueous solutions of zymonic acid. *J. Phys. Chem. A* **2016,** *120*, 10096-10107.

54. Harris, D. C., *Quantitative chemical analysis*. 7th ed.; W.H. Freeman and Company: New York, 2007.

55. Papanastasiou, G.; Ziogas, I. Simultaneous determination of equivalence volumes and acid dissociation constants from potentiometric titration data. *Talanta* **1995,** *42*, 827-836.

56. Pocker, Y.; Meany, J. E.; Nist, B. J.; Zadorojny, C. Reversible hydration of pyruvic acid. I. Equilibrium studies. *J. Phys. Chem.* **1969,** *73*, 2879-2882.

57. Strehlow, H. Die kinetik der hydratation von α-ketocarbonsäuren. *Zeitschrift für Elektrochemie* **1962,** *66*, 392-396.

58. Buschmann, H. J.; Dutkiewicz, E.; Knoche, W. The reversible hydration of carbonyl compounds in aqueous solution. 2. The kinetics of the keto gem-diol transition. *Ber. Bunsen-Ges. Phys. Chem* **1982,** *86*, 129-134.

59. Buschmann, H. J.; Füldner, H. H.; Knoche, W. The reversible hydration of carbonyl compounds in aqueous solution. Part I, the keto/gem - diol equilibrium. *Ber. Bunsen-Ges. Phys. Chem* **1980,** *84*, 41-44.

60. Becker, M. Über magnetische kernresonanzspektren wäßriger brenztraubensäurelösungen. *Ber. Bunsen-Ges. Phys. Chem* **1964,** *68*, 669-676.

61. Cooper, A. J.; Redfield, A. G. Proton magnetic resonance studies of alpha-keto acids. *J. Biol. Chem.* **1975,** *250*, 527-32.

62. Pedersen, K. J. The dissociation constants of pyruvic and oxaloacetic acid. *Acta Chem. Scand.* **1952,** *6*, 243-256.

63. Xu, H.; Du, N.; Song, Y.; Song, S.; Hou, W. Vesicles of 2-ketooctanoic acid in water. *Soft Matter* **2017,** *13*, 2246-2252

64. Hennigan, C.; Izumi, J.; Sullivan, A.; Weber, R.; Nenes, A. A critical evaluation of proxy methods used to estimate the acidity of atmospheric particles. *Atmo. Chem. Phys.* **2015,** *15*, 2775.

65. Perkins, R. J.; Vaida, V. Zymonic acid as a prebiotic sugar analogue. *Origins Life Evol. Biosphere* **2017**, Submitted.

66. The terms “dimer” and “trimer” are used to refer to covalently-bonded oligomeric species, unless otherwise specified.

67. Cech, N. B.; Enke, C. G. Practical implications of some recent studies in electrospray ionization fundamentals. *Mass Spectrom. Rev.* **2001,** *20*, 362-387.

68. Davidson, R. S.; Goodwin, D.; de Violet, P. F. The mechanism of the Norrish Type II reaction of α-keto-acids and esters. *Tetrahedron Lett.* **1981,** *22*, 2485-2486.

69. Evans, T. R.; Leermakers, P. A. Photochemistry of alpha-keto acids and alpha-keto esters VI. V. The Norrish Type II process in alpha-keto acids. Photolysis of alpha-ketodecanoic acid in benzene. *J. Am. Chem. Soc.* **1968,** *90*, 1840-1842.

70. Brocks, J. J.; Beckhaus, H.-D.; Beckwith, A. L.; Rüchardt, C. Estimation of bond dissociation energies and radical stabilization energies by ESR spectroscopy. *J. Org. Chem.* **1998,** *63*, 1935-1943.

7. Aqueous Phase Oligomerization of Methyl Vinyl Ketone by Atmospheric Radical Reactions*

7.1 Introduction:

Aerosols play an important role in many atmospheric processes, including cloud nucleation, radiation scattering, and smog evolution, which significantly impact human health and climate.[2-4] Furthermore, quantification of their overall effect on the Earth's radiative budget contributes the largest source of uncertainty in current climate models, motivating fundamental research regarding the chemical and physical properties of aerosols. In addition to inorganic particles, the impact of organic material on aerosol light scattering and cloud initiation has recently been recognized.[5] Globally, only 20% of the organic aerosol mass is emitted directly.[5, 6] Therefore, understanding the formation and growth mechanisms for secondary organic aerosol (SOA) is particularly important. SOA production from the gas phase oxidation of volatile organic compounds (VOC) has been extensively studied.[2, 5, 6] Recently, however, it has become clear that aqueous phase photochemistry, which generates high molecular weight compounds that remain condensed upon water evaporation, is another essential pathway to form SOA.[2, 3, 7-11] Solution phase processes can be very different from those in the gas phase, thus aqueous SOA may have unique and characteristic properties.[3, 12-14] Additionally, products from these aqueous reactions can partition to the surface of a particle and change its morphology and hygroscopicity, which will in turn affect its lifetime and atmospheric consequences.[15-19]

Isoprene is one important organic compound in the atmosphere, as it comprises about a

*This work was reproduced in part with permission from Renard, P., Reed Harris, A.E., Rapf, R.J., Ravier, S., Smaani, A., Demelas, C., Coulomb, B., Quivet, E., Vaida, V., & Monod, A. "Aqueous Phase Oligomerization of Methyl Vinyl Ketone by Atmospheric Radical Reactions." *J. Phys. Chem. C.*, *118*(50), 29421–29430, 2014. Copyright 2014 American Chemical Society.[1]

third of annual global non-methane VOC emissions.[20] Methyl vinyl ketone (MVK), an α, β-unsaturated water-soluble organic compound, is among the key oxidative products from isoprene.[21] While the oxidation of isoprene in the gas phase has been linked to formation of SOA,[22-24] this direct gas-phase SOA formation has not been observed to evolve through an MVK intermediate. [22, 24] However, laboratory studies have shown that the aqueous reactivity of some carbonyl compounds, including MVK, creates high molecular weight products that may contribute to SOA formation.[7, 8, 13, 25-36] MVK bears highly reactive functional groups (i.e. conjugated carbon-carbon and carbon-oxygen double bonds), which play a major role in the aqueous chemistry that yields these high molecular weight products through i) acid-catalyzed aldol reactions;[36] and/or ii) acid-catalyzed hydration followed by oligomerization;[36] and/or iii) radical chemistry.[7, 35] The aqueous phase reactivity of MVK towards •OH radicals has been studied by several authors.[7, 34, 35, 37] In particular, Renard et al.[7] showed that photooxidation of MVK by •OH in the aqueous phase proceeds *via* a radical mechanism to create large multifunctional species, or oligomers.[†] MVK oxidation by •OH yields initiator radicals, which react with MVK to form oligomers by addition to the vinyl double bond.[7]

In addition to photooxidation initiated by •OH, direct photochemistry of some aldehydes and ketones can be an important tropospheric sink.[35, 38] Pyruvic acid (PA), another oxidative product of isoprene, reacts photolytically without •OH in both the gas and aqueous phases.[12, 38-48] Unlike MVK, which has very low quantum yields for photolysis in the solar spectrum, photolysis dominates over the •OH chemistry for PA.[12] The direct aqueous photochemistry of PA proceeds through the excited $^3(n, \pi^*)$ state, which initiates radical chemistry through a hydrogen atom abstraction reaction. This yields reactive radicals that

[†] Polymers consisting of a small number (<30) of repeat units are called oligomers in this context.

combine to form various products, including dimethyltartaric acid and other oligomers.[7, 14, 40] Moreover, it has been shown that under certain atmospheric conditions, such as some cloud droplets (liquid water content (LWC) = 0.5 g m^{-3}, pH = 3) or wet aerosols (LWC = 17.6 μg m^{-3}, pH = 1), the aqueous photolysis of PA can be of equal or greater importance to the gas phase photolysis.[12] Since this reaction increases the molecular weight of compounds in solution, it is important to consider when analyzing aerosol processing.

While the •OH-oxidation of isolated aldehydes or ketones, such as MVK, has been investigated, mixed systems in which photochemically generated radicals other than HO_x trigger oligomerization in solution have been overlooked.[7, 14] These reactions, however, are expected to be highly atmospherically relevant, as oxidative products of isoprene are formed simultaneously and likely interact. Because aqueous PA is effective in activating radical chemistry through photolysis under atmospheric actinic flux, the present study investigates the ability of PA to initiate oligomerization of MVK. Here, we show that upon irradiation of a mixed solution of MVK and PA, similar oligomers to the products observed by Renard et al.[7] from the •OH oxidation of MVK, are formed under a range of initial concentrations. These products are significant in at least two ways: i) this is a new mechanism for creating oligomers in solution may be atmospherically relevant and ii) we show here that the products are surface active and may, therefore, change optical properties at air-water interfaces in the environment and potentially contribute to SOA formation.[15-19]

7.2 Experimental Section:

In this chapter, we used a photoreactor to generate radicals from the photolysis of either pyruvic acid or hydrogen peroxide that then initiate MVK oligomerization reactions. Aqueous aliquots sampled at different photoreaction times were analyzed using liquid chromatography coupled to ultra-violet absorbance spectroscopy (LC-UV) and liquid

chromatography coupled to mass spectrometry (LC-MS) in order to quantify the reactants, identify the oligomers produced, and establish a basic mechanism. The products from the reaction initiated by intermediates in the pyruvic acid photolysis were compared to that from the reaction initiated by •OH. Finally, the surface activity of all products was investigated using a Langmuir trough equipped with a Wilhelmy balance.

7.2.1 Photochemical Reaction and Conditions:

Described in Renard et al.,[7] a 450 cm^3 stirred Pyrex thermostated photoreactor was equipped with a 1000 W xenon arc lamp (LSB 551, Lot Oriel) and a glass filter, air mass 0 (LSZ 185, Lot Oriel). Photochemical reactions for the surface activity analysis were performed using a similar setup (described by Reed Harris et al.[12]) with a 450 W xenon arc lamp (Newport) and a pyrex lens used to filter radiation below 300 nm.

Reactive radicals to initiate oligomerization were prepared by irradiation of Ultra High Quality (UHQ) water (18.2 MΩ, Millipore) with H_2O_2 (50%, stabilized, Sigma Aldrich) or pyruvic acid (98%, Sigma Aldrich) for 10 minutes. MVK (99%, Sigma Aldrich) was then introduced to begin the reaction and photolysis of the mixture continued for a duration of 300 minutes. Renard et al.[7] showed that a change in temperature affects only the kinetics of the reaction of MVK with •OH, and not the reaction products. Therefore, in this work, all experiments were performed at 25 °C. Solutions were unbuffered and dissolved oxygen concentrations were not constrained. The temperature, pH, and dissolved oxygen concentrations were continuously monitored in the reaction solution using a Consort C3020 multi-parameter analyzer.

Tan et al.[31] have shown the important impact of initial concentrations on oligomer formation for α-dicarbonyls. The PA experiments were therefore carried out at three different initial MVK concentrations, 0.2, 2, and 20 mM, which are comparable to the total

concentrations of unsaturated water-soluble organic compound in wet aerosol.[7, 49, 50] The initial pyruvic acid concentrations (4, 10, and 100 mM, respectively) were also chosen to be consistent with observed amounts of pyruvic acid in the particulate phase in the atmosphere.[51] For the •OH-experiments, we used the same highest initial concentration of MVK (20 mM) as in Renard et al.[7] The estimation of the resulting •OH concentrations in these studies (10^{-15} - 10^{-14} M) were close to estimated values for cloud and fog droplets.[52, 53]

A solution of pyruvic acid with MVK under dark conditions was monitored by LC-UV for the same duration as the photochemical experiments. Neither was significantly consumed, indicating that no substantial reaction between them occurs without irradiation. Additionally, the direct photolysis of PA (100 mM), in the absence of MVK, as seen in Reed Harris, et al.[12], yielded much shorter oligomers than is observed for the photolysis of the mixed solution of pyruvic acid with MVK. These control experiments ensure that the observed oligomerization is initiated by MVK reaction with •OH or intermediates in the PA photolysis.

7.2.2 Reactants and Products Analysis:

LC-MS Analyses: Aliquots of the solution sampled from the photoreactor were analyzed for organic species using an ultra-high performance liquid chromatographic (UPLC) system coupled to a time of flight mass spectrometer equipped with an electrospray ionization (ESI) source and an ion mobility cell (Synapt-G2 HDMS, Waters). The resolution of the mass spectrometer (18,000 at m/z 400) allowed determination of the chemical formula of the oligomer series. Data were collected from m/z 50 to 1200 in both ionization modes. The chromatographic separations are carried out on an UPLC column (HSS T3 C18, 2.1 × 100 mm – 1.8 µm; Waters) at 40°C. The mobile phases consist in (A) 0.1 % formic acid in water (Biosolve, 99 %) and (B) acetonitrile (Biosolve, ULC/MS). The gradient elution is performed

at a flow rate of 600 μL min^{-1} using 5 to 95 % of B within 7 min and held at 95 % of B for 1.5 min.

LC-UV Analyses: An UPLC system (Accela 600 auto sampler, Accela 600 pump, Thermo Scientific) coupled to a diode array detector (Accela 600 PDA detector; Thermo Scientific) was used to monitor the concentrations of MVK and PA sampled from the photoreactor. The LC separation was performed using a Hypersil GOLD column (100 x 2.1 mm - 1.9 μm, Thermo Scientific) at 40 °C and at a flow rate of 300 μL min^{-1}. The mobile phase was water/acetonitrile (98:2) (v/v) and the injection volume was set to 2 μL. The spectra were recorded from 200 to 360 nm.

Both PA and MVK show an intense absorption band (K-band; π → π* transition) in aqueous solution that peaks at 205 and 211 nm, respectively and a weak absorption band (R-band; n → π* transition) that peaks at 319 and 308 nm, respectively. Pyruvic acid has a retention time of 0.5 min and MVK has a retention time of 1.8 minutes. The absorption intensity at 211 nm and 229 nm were found to be directly proportional to both the PA and the MVK concentrations in the range of the studied concentrations. MVK oxidation by pyruvic acid photolysis was followed by monitoring at 211 nm for the lowest concentrations ($[PA]_0$ = 4 mM and $[MVK]_0$ = 0.2 mM) and at 229 nm for higher concentrations ($[PA]_0$ = 10 and 100 mM and $[MVK]_0$ = 2 and 20 mM).

IC-MS Analyses: Quantification of organic acids in the solutions was performed with an ion chromatography system (Dionex ICS3000) driven by Chromeleon software (version 6.80); composed of a SP-5 gradient pump, an AS40 autosampler, a CD25 conductivity detector; and coupled to a Thermo Scientific Surveyor MSQ (Thermo Electron, USA) mass spectrometer operated in the ESI negative mode. A 4 mm ASRS 300 electrolytic suppressor operated in external water mode (7 mL min^{-1}) was placed before the conductivity cell. An

additional peristaltic pump was used to wash the entrance cone of the mass spectrometer with water at a flow rate of 0.4 mL min^{-1} during measurements. The chromatographic separations were carried out on an IonPac AS11-HC column 4 x 250 mm (Dionex) coupled to a guard column (Dionex AG11-HC, 4 x 50 mm). Samples were injected automatically using a 25 µL loop injection valve. The analysis was performed at 35 °C with a flow rate set at 0.8 mL min^{-1}. Eluent A (UHQ water) and eluent B (100 mM NaOH) were flushed with purified helium gas for 30 min and kept under a nitrogen atmosphere during the procedure. Separation was carried out using an eluent gradient, as follows (min, B %): 0, 1 %; 12, 5 %; 30, 19 %; 40, 40 %. The analytes were monitored using the selected ion-monitoring (SIM) mode, and signal areas (counts/min) of each peak were used for quantification.

7.2.3 Surface Activity Studies:

The surface activity of solutions both before and after photolysis was determined using a Langmuir trough equipped with a Wilhelmy balance (KSV-NIMA, Biolin Scientific). The custom-built PTFE Langmuir trough (52 x 7 x 0.5 cm) described previously has computer-controlled mechanical barriers, which allow for control of surface area (A).[54] In the experiments presented here, the barriers were opened to a maximum of 300 cm^2 and closed to a minimum area of 30 cm^2 with a constant barrier speed of 75 cm^2 min^{-1}. The trough was filled with ~200 mL of the solution of interest while the barriers were fully opened, and the system was equilibrated for one hour before compression to allow the surface-active species to partition to the surface.

The Wilhelmy balance measures surface pressure (π), or the difference in surface tension between the solution of interest (γ) and that of pure water (γ_0), $\pi = \gamma_0 - \gamma$. By measuring surface pressure as a function of surface area, surface pressure – area (π – A) isotherms are obtained, which allow for an understanding of surface thermodynamics of the

system.[55] Here, such isotherms are used as a measure of the extent of preferential surface partitioning of molecules based on their hydrophobicity. The more hydrophobic a molecule, the more it partitions to the surface, which disrupts the normal surface tension of water and increases surface pressure. A system with increased surface pressure is indicative of its greater surface activity.

7.3 Results and Discussion:

7.3.1 Photo-Reaction Products of MVK Oxidation by PA

In aqueous solution, pyruvic acid (PA) hydrates to its geminal diol, 2,2-dihydroxypropanoic acid (~60%).[14, 56] Photolysis of unhydrated PA begins with excitation to $^1(n, \pi^*)$, followed by intersystem crossing and internal conversion to $^3(n, \pi^*)$. PA in the triplet exited state (PA*) then abstracts a hydrogen atom from 2,2-dihydroxypropanoic acid, inducing decarboxylation and creation of two radicals, $CH_3C^{\bullet}(OH)C(O)OH$ (alpha lactyl radical, or $PA^{\bullet}$) and $CH_3C^{\bullet}(OH)_2$ (hydrated acetyl radical, or $AA^{\bullet}$). Recombinations of these radicals yield small oligomers, including dimethyltartaric acid (a major product), and minor products including acetoin, lactic acid, and acetic acid.[12, 14] In this study, we aim to form high molecular weight compounds from MVK radical chemistry initiated by intermediates in the pyruvic acid photolysis, namely $PA^{\bullet}$, $AA^{\bullet}$, or PA*.‡ The mechanism proposed here is similar to MVK photooxidation by $^{\bullet}OH$, with the new observation that organic radicals, such as those created by PA photolysis, can also start radical oligomerization chemistry.

The aqueous phase oligomerization of MVK initiated by photolysis of pyruvic acid leads to the formation of several series of oligomers similar to the observed products from the MVK $^{\bullet}OH$-oxidation reaction in Renard et al.[7] Figure 7.1 shows a comparison of combined

‡All three intermediates, $PA^{\bullet}$, $AA^{\bullet}$, and PA*, may initiate radical chemistry, but for simplicity in the text we refer to these initiator radicals using $PA^{\bullet}$ as our example.

LC-MS spectra (retention time range: 0-4 min), between MVK PA-photolysis ($[MVK]_0$ = 20 mM, $[PA]_0$ = 100 mM) and MVK $^{\bullet}$OH-oxidation ($[MVK]_0$ = 20 mM, $[H_2O_2]_0$ = 400 mM).

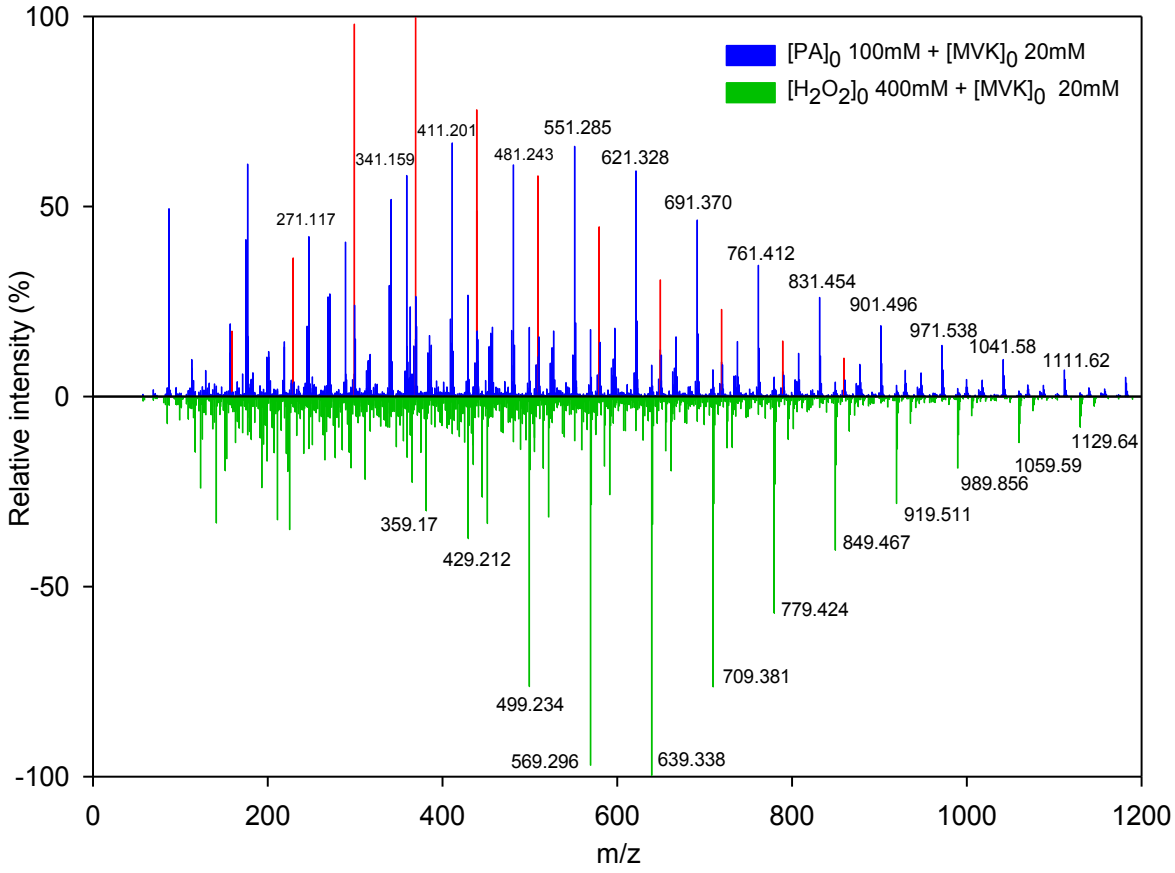

Figure 7.1. Combined mass spectra for MVK PA-photolysis (blue, $[MVK]_0$ = 20 mM, $[PA]_0$ = 100 mM) and MVK $^{\bullet}$OH-oxidation (green, $[MVK]_0$ = 20 mM, $[H_2O_2]_0$ = 400 mM) at reaction time of 50 min, obtained using LC-MS for the retention time range 0 to 4 min, in the negative mode. Series S160 ($PA\text{-}(MVK)_n$, see Table 7.1) is highlighted in red.

In both experiments, oligomer series are clearly visible, with regular spacing of 70.042 amu, which corresponds to the exact mass of MVK. Both systems extend up to *m/z* 1200, corresponding to 17 monomer units. Table 7.1 lists the oligomer series identified by LC-MS in both modes from MVK PA-photolysis (Figure 7.1). Identification is performed, as in Renard et al.[7] on the most intense series, which were further confirmed by MS/MS analyses.

Table 7.1. Oligomer series from MVK PA-photolysis identified by LC-MS. All products were detected as their protonated molecules ([M + H]+) or sodium adducts ([M + Na]+) in the positive mode, and their deprotonated molecules ([M − H]−) in the negative mode

Oligomer series		Detected ions	
Name[a]	Formulas	Formulas[b]	m/z[b]
S138	MVK-$(MVK)_n$	$[C_8H_{10}O_2, +H]^+$	139.0759
S140		$[C_8H_{12}O_2, +H]^+$	141.0916
S156	MVK-OH-$(MVK)_n$	$[C_8H_{12}O_3, +Na]^+$	179.0684
S158	PA-$(MVK)_n$	$[C_7H_{10}O_4, -H]^-$	157.0501
S160		$[C_7H_{12}O_4, -H]^-$	159.0657
S200	$C_5H_8O_4$-$(MVK)_n$	$[C_9H_{12}O_5, -H]^-$	199.0606
S202		$[C_9H_{14}O_5, -H]^-$	201.0763
S218	$C_4H_6O_6$-$(MVK)_n$	$[C_8H_{10}O_7, -H]^-$	217.0348
S220		$[C_8H_{12}O_7, -H]^-$	219.0505

[a]For each series, the name is given by "S" followed by a number corresponding to the nominal mass of the smallest oligomer of the series, i.e. $(MVK)_{n=1}$. [b]Formula and m/z of ions corresponding to the smallest oligomer of each series.

Some of the oligomer series (S138, S140 and S156) are similar to those described in Renard et al.[7] and can be explained by a common mechanism, i.e. H-abstraction from MVK. Other series, including S158, S160, S200, S202, S218 and S220, are specific to the PA-photolysis. In particular, S158 and S160 correspond to PA•-addition to MVK, as illustrated in Figure 7.2, and discussed further below.

In this work, we also detected by IC-MS (Figure G.1) low molecular weight reaction products in addition to larger oligomers. Acetic, oxalic, and succinic acids were produced during the reaction of MVK with both PA• and •OH as radical initiators. The presence of common acids regardless of radical initiator is a further indication of the similarity of the oligomerization mechanisms. Lactic acid, however, was observed during photolysis of PA with MVK but not during MVK •OH-oxidation. Lactic acid is also seen in the photolysis of

pyruvic acid alone, formed by H-abstraction from AA• by PA•.[12, 14, 57] The presence of lactic acid in the mixed solution of MVK and PA, therefore, is likely due to this PA• chemistry rather than some difference in oligomerization mechanism due to the specific initiator radical.

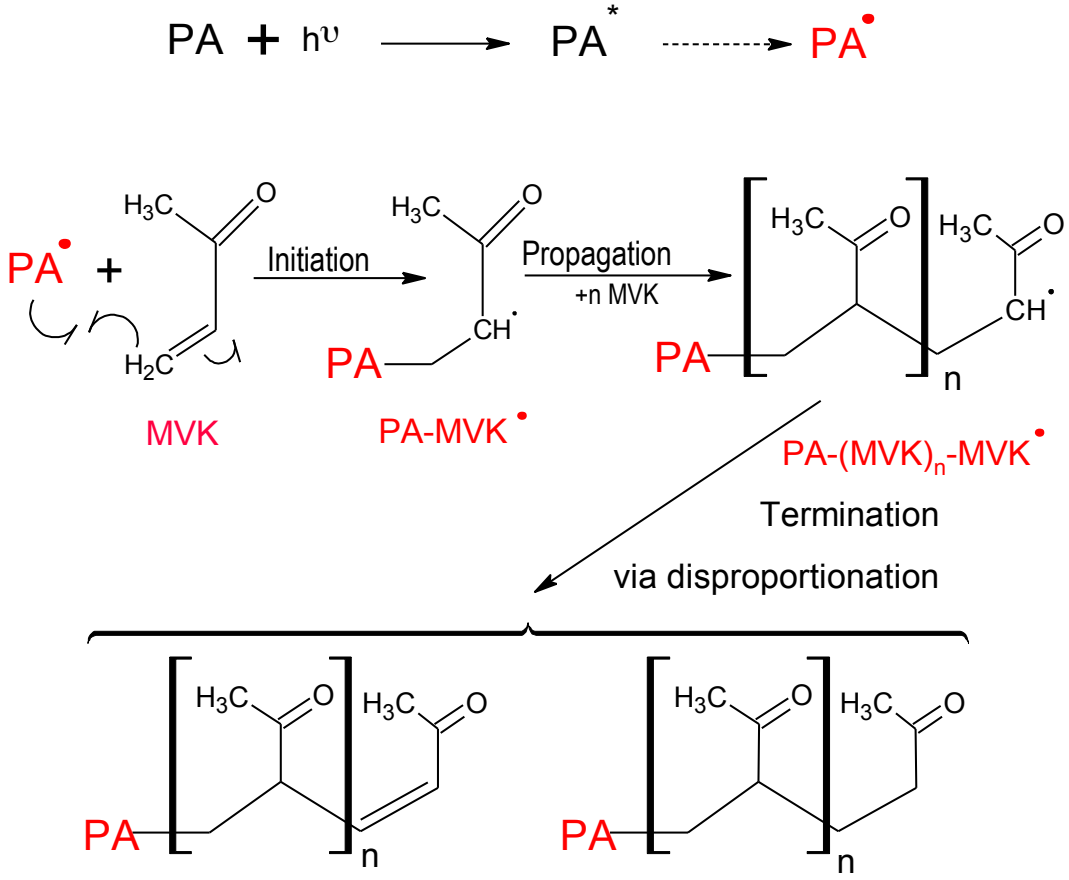

Figure 7.2. Proposed mechanism of radical oligomerization of PA-(MVK)$_n$ series in the aqueous phase, initiated by PA-photolysis. PA• is an initiator radical; MVK is the monomer, n is the degree of oligomerization, i.e. chain length. For clarity, only the external radical additions are shown.

Based on the mechanism for MVK radical oligomerization initiated by •OH-oxidation detailed in Renard et al.,[7] we propose a similar process for oligomerization of MVK initiated by PA• (Figure 7.2) to explain the formation of oligomer series S158 and S160 (Table 7.1). The reaction proceeds primarily as proposed by Renard et al.:[7] oligomerization begins when PA• opens the vinyl double bond of MVK and forms another radical (PA-MVK•) that

continues to add MVK monomer units until radical termination. Termination occurs by bimolecular reaction between two radicals, via either recombination or disproportionation. This yields two oligomer series, one saturated and one unsaturated terminal group.[58] For clarity, Figure 7.2 depicts only reactions in which PA$^{\bullet}$ adds to the β-carbon of MVK, as this is favored over addition to the α-carbon.[7, 59] However, either reaction is possible with PA*, AA$^{\bullet}$, or PA$^{\bullet}$, leading to a number of isomers that grows exponentially with oligomer chain length.

This chemical mechanism is justified by three experimental observations: i) the regular mass spacing of 70.042 amu observed in mass spectra (Figure 7.1) corresponds exactly to the mass of the monomeric MVK; ii) the faster consumption of MVK compared to that of pyruvic acid (19 mM of MVK is consumed within 95 min while 12 mM of PA is consumed within this time) (Figure 7.3); and iii) the strong dependence of oligomer chain length on initial MVK concentration (see next section).

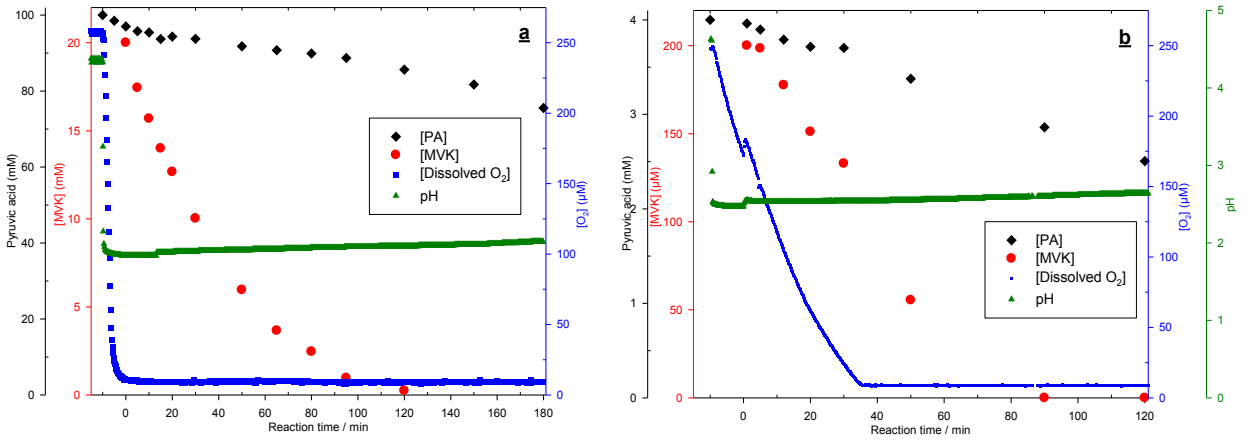

Figure 7.3. Time profile of the concentrations of PA, MVK, and dissolved O_2, as well as pH during MVK PA-photolysis a) for high initial precursor concentrations ($[MVK]_0$ = 20 mM, $[PA]_0$ = 100 mM); b) for very low initial precursor concentrations ($[MVK]_0$ = 0.2 mM, $[PA]_0$ = 4 mM). Data were recorded beginning at reaction time, t = -15 min, with introduction of PA at t = -10 min and MVK at t = 0 min.

7.3.2 Effect of Reaction Conditions on MVK Oligomerization:

In this study, we observe MVK oligomerization under a variety of initial reactant and dissolved oxygen concentrations. Specifically, the reaction was performed at three different initial MVK concentrations 20 mM ($[PA]_0$ = 100 mM), 2mM ($[PA]_0$ = 10 mM), and 0.2 mM ($[PA]_0$ = 4 mM) and the results compared.

First, we provide a brief comment on the effect of the radical initiator ($PA^{\bullet}$ vs $^{\bullet}OH$) on the kinetics of MVK oligomerization to illustrate the role of dissolved oxygen. The observed kinetics of MVK degradation by PA-photolysis are distinct from those performed through $^{\bullet}OH$-oxidation and dependent on initial PA concentrations (Figures 7.3 and G.2). This contrast may be due to different concentrations of dissolved O_2 between the systems, as O_2 is known to slow free radical photo-oligomerization.[60] The slowed kinetics is caused by O_2 quenching the excited state of the photoinitiator and/or by fast O_2-addition on primary initiating and propagating radicals. This yields peroxyl radicals ($RO_2^{\bullet}$), which are moderately reactive and can terminate propagation or may even initiate slow reactions of polymerization in specific cases.[61, 62] Under our $^{\bullet}OH$-oxidation of MVK experimental conditions, photolysis of H_2O_2 induces supersaturated oxygen conditions prior to MVK introduction (mechanism shown in Table G.1).[7] The result is a slow initial decay of MVK (Figure G.2) relative to the remainder of the reaction. Conversely, in the MVK with PA-photolysis experiments, conducted at high initial concentrations, the photolysis of 100mM PA consumes most of the dissolved oxygen present (decreasing from 258 to 12 μM) during the 10 minutes of photolysis prior to addition of MVK (Figure 7.3A). Therefore, oligomerization occurs quickly upon addition of MVK, inducing a faster initial decay of MVK than in the $^{\bullet}OH$-oxidation experiments (Figure G.2).

Due to the tendency of PA*, $PA^{\bullet}$, and $AA^{\bullet}$ to consume O_2 under high initial

concentrations of photoinitiators, the experiment presented above (Figure 7.1) was performed under depleted dissolved oxygen concentrations ($[O_2] \leq 12$ μM, Figure 7.3A). To test for oligomerization under more relevant atmospheric conditions, we explored the influence of the presence of dissolved O_2 on product formation using low initial precursor concentrations ($[MVK]_0 = 0.2$ mM and $[PA]_0 = 4$ mM, compared with $[MVK]_0 = 20$ mM and $[PA]_0 = 100$ mM in Figure 7.1) (Figure 7.3 and Figure G.3). Because of the lower pyruvic acid concentration, this investigation shows a much slower depletion in dissolved O_2 before MVK is added, causing substantial amounts of O_2 to be present in the solution during the MVK and PA reaction. Under these conditions, molecular weight compounds up to m/z 300, including some oligomers, are observed (as compared with m/z 1200 in Figure 7.1). Although oxygen reactivity towards $PA^{\bullet}$ is by far the dominating process under these conditions,[12] PA addition to MVK is still competitive. The oligomer series (S160) PA-$(MVK)_n$ is detected under these conditions (for n=1, and a very weak signal for n=2) at t=5 minutes of reaction (Figure G.3), when $[O_2] = 160$ μM (Figure 7.3B). This result shows that the initiation reaction by $PA^{\bullet}$ on MVK (Figure 7.2) remains active under more atmospherically relevant amounts of dissolved oxygen.

The smaller oligomers observed in the low concentration conditions above may be due both to the presence of oxygen acting as a radical quencher as well as the low concentrations used. Initial concentrations of photooxidation precursors are known to influence the kinetics of oligomerization and the size of resulting oligomers.[7, 61] We explored these issues by comparing reactions with initial MVK concentrations of 20 mM ($[PA]_0 = 100$ mM) and 2 mM ($[PA]_0 = 10$ mM). Both of these reactions were depleted in dissolved oxygen ($[O_2] \leq 12$ μM) when MVK was added, and thus the kinetic and product differences can be attributed solely to reactant concentrations. The lower the concentrations, the faster the

oligomers reached the maximum of LC-MS relative intensity. For example, while this peak in oligomer intensity was reached after 50 min for 20 mM MVK, it was reached in 15 minutes for 2 mM MVK. Figure 7.4 compares the mass spectra for these two reactions at their peak in oligomer intensity (50 min and 15 min, respectively).

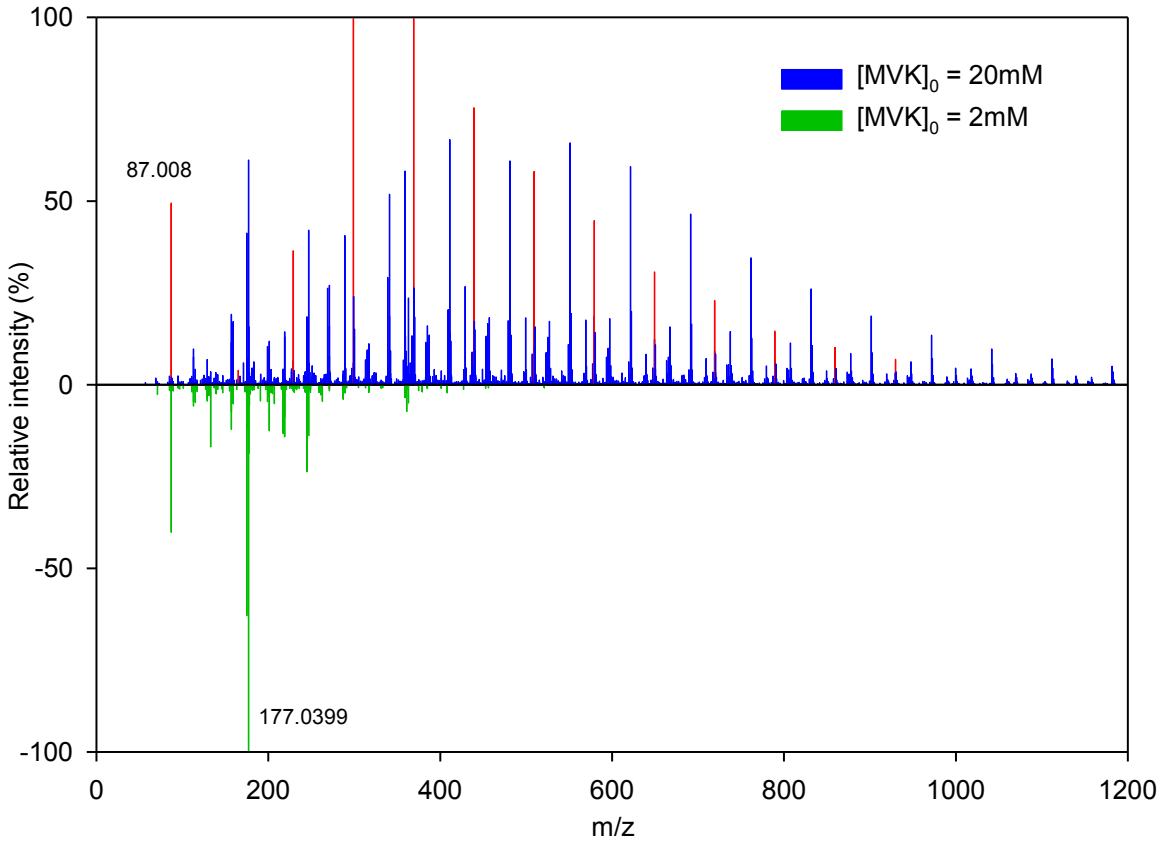

Figure 7.4. Combined mass spectra of the peak relative oligomer intensity of the MVK PA-photolysis at two different initial reactant concentrations, higher (blue, $[MVK]_0$ = 20 mM, $[PA]_0$ = 100 mM, t = 50 min) and lower (green, $[MVK]_0$ = 2 mM, $[PA]_0$ = 10 mM, t = 15 min), obtained using LC-MS for the retention time range 0 to 4 min, in the negative mode. The peak labeled at m/z 87.008 corresponds to pyruvic acid; the peak labeled at m/z 177.0399 corresponds to the recombination of $PA^{\bullet}$ + $PA^{\bullet}$, dimethyltartaric acid. In the top panel, PA and Series S160 ($PA\text{-}(MVK)_n$, see Table 7.1) is highlighted in red.

Upon inspection of these mass spectra, it is clear the initial concentrations of MVK and PA also strongly affected the extent of oligomerization (Figure 7.4). In both experiments, the same major series of oligomers were observed, but chain lengths increased with increasing initial MVK concentration. At the lower initial concentration of MVK (2 mM),

oligomers up to m/z 400 are formed, and the recombination of radicals becomes important as compared to addition to MVK. The most intense peak (m/z 177.04) in the 2mM MVK reaction (Figure 7.4) corresponds to the recombination of two $PA^{\bullet}$ to make dimethyltartaric acid. Conversely, the higher initial concentration of MVK (20 mM) allows for more propagation and thus longer chain lengths, resulting in the formation of high molecular weight reaction products up to m/z 1200 (Figure 7.4).

The combined results from the three different initial reactant concentrations demonstrates that the same oligomer series are produced in the MVK and PA photolysis regardless of the initial reactant or dissolved oxygen concentrations. However, the size of the oligomers formed increases with increasing initial reactant concentrations and decreasing concentrations of dissolved oxygen.

7.3.3 Surface Activity of Reaction Photoproducts:

π – A isotherms taken of a monolayer of a single surfactant yield quantitative thermodynamic information about the behavior and ordering of the surfactant at the surface of an aqueous solution.[63] Specifically, the molecular footprint of the surfactant is obtained. The difficulty of extracting quantitative values increases as the system complexity increases. Monitoring the preferential partitioning of soluble molecules to the surface from a bulk solution presents experimental and conceptual challenges in obtaining numerical results. In this study, π – A isotherms were taken of mixtures of molecules, including post-photolysis products, in a bulk solution, making quantitative speciation and analysis untenable. This complexity does not, however, preclude making very useful, qualitative comparisons between reagents, products, and different reaction systems.

The post-photolysis solutions containing the photooxidation products of MVK (at 20 mM) clearly show increased surface partitioning compared to the pre-photolysis controls,

regardless of precursors (see Figure 7.5).[§]

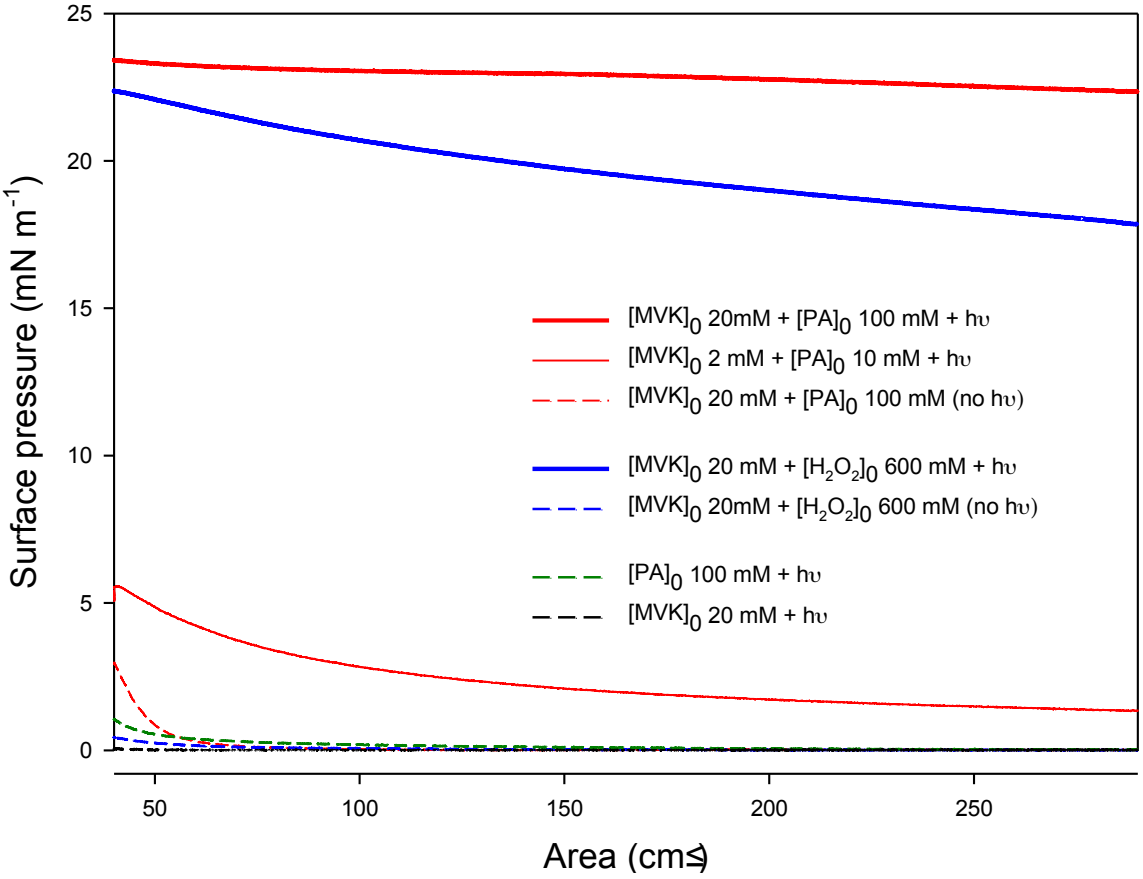

Figure 7.5. Surface pressure-area isotherms for aqueous phase oligomerization of methyl vinyl ketone by radical reactions and control experiments. Dashed lines correspond to control experiments, which show very little surface activity compared to the radical oligomerization reaction products shown in solid ($[MVK]_0$ = 20 mM) and thin ($[MVK]_0$ = 2 mM) lines. The initial H_2O_2 concentration was increased from 400 mM to compensate for the decrease in reaction kinetics due to the 450 W Xe arc lamp used in these studies.

For both control experiments (MVK + H_2O_2 and MVK + PA, no irradiation), the pre-photolysis solutions show little surface activity, with only minor increases in surface pressure at low surface areas. This is a further confirmation that very little oligomerization of MVK occurs without photochemical radical initiation. In contrast, the post-photolysis oxidation products of MVK show very significant partitioning to the surface, indicating that

[§]The initial concentration of H_2O_2 was increased to 600 mM for the surface activity studies in order to compensate for the decrease in reaction kinetics associated with the 450 W xenon lamp compared to the 1000 W lamp.

the oligomers formed during photolysis have considerable surface activity. Qualitatively, the post-photolysis products appear to have close to the same degree of surface activity using either •OH-oxidation or PA-photolysis. This is another indication that a similar degree of oligomerization of MVK occurs for initiation with either •OH or PA• radicals. Additionally, at the higher initial MVK and PA concentrations (20 mM and 100 mM, respectively), the post-photolysis solution shows a larger increase in surface pressure than for the less concentrated solution (Figure 7.5), which is consistent with the higher concentration of longer-chained oligomers formed under these conditions and observed by LC-MS analysis.

7.4 Atmospheric Implications:

It is increasingly recognized that aqueous phase photooxidation reactions initiated by •OH radicals can create high molecular weight oligomers in atmospheric particles. When water evaporates, these oligomers likely remain in the particulate phase, thus increasing SOA mass.[10, 11, 35] The results obtained in this study suggest that similar reactions can be triggered by organic radicals in solution, demonstrating a new mechanism by which SOA can be created. In this work, we show that MVK, an unsaturated, water-soluble organic compound, produces oligomers of similar mass via both •OH-oxidation and PA-photolysis.

The experimental conditions investigated in this study indicate that, under depleted concentrations of dissolved oxygen (≤ 12 μM), initial reactant concentrations greatly affect the oligomer chain length, with a chain length decrease by a factor of 3 when initial concentrations of MVK and PA are decreased by an order of magnitude. Using even lower initial precursor concentrations results in much slower depletion of dissolved oxygen concentrations, and show that the initiation reaction of pyruvic acid excited triplet state and/or PA• radical on MVK remains active under the presence of more atmospherically

relevant amounts of unsaturated water soluble organic compounds and dissolved oxygen ($[O_2]$ = 160 μM). The mechanisms for O_2 inhibition on photopolymerization have been extensively investigated focusing on industrial applications for the production of long chain polymers ($m/z \geq 10\,000$),[62] but extremely limited studies have investigated this complex chemistry under environmental conditions for the formation of oligomers with $m/z < 2000$.[7, 50, 64] More studies are thus needed to investigate the likely different precursors and oligomer chain lengths of atmospheric relevance.

Furthermore, it is interesting to compare the efficiency of the initiation steps between MVK •OH-oxidation and MVK PA-photolysis. A simple estimate (Table G.2) shows that under atmospheric conditions where aqueous concentrations of •OH radicals are limited and where pyruvic acid is highly concentrated such as in wet aerosols,[51, 59] the initiation steps between MVK •OH-oxidation and MVK PA-photolysis can be of the same order of magnitude. This estimation emphasizes the relevance of studying radical oligomerization initiated by radicals other than •OH, and especially those arising from the photolysis of atmospheric organic compounds.

The resulting products from both reactions are surface active, indicating that these oligomers partition preferentially to an air-water interface, such as the surface of an aerosol. This partitioning could facilitate oligomerization by increasing the concentration of radicals at the surface and may lead to SOA formation or a change in the atmospheric processing of the particle. This is a new mechanism for the formation of organic oligomers, as well as a demonstration of the surface partitioning of the resultant high molecular weight compounds. Surface organic coatings have long been proposed to exist on atmospheric aerosols providing hydrophobic enclosures that, upon aging, can be oxidized in the atmosphere to acquire hydrophilic sites.[17, 65, 66] As field measurements of atmospheric

particles provided molecular speciation, it was confirmed that surface active organics are important components in atmospheric particles with consequences to their optical and chemical properties and overall effect on climate.[18, 19, 67-74]

Organic surface films can also provide barriers to transport across the air-particle interface, inhibiting uptake of gas phase species.[75-80] These organic films can be an auspicious medium for solubilizing gas phase organic species which may perhaps explain the observed non-Henry's law concentration of organics in field samples.[81] Organic surfactant films provide a special reaction environment, which affects heterogeneous atmospheric chemistry, changing the hygroscopic properties of organically coated particles during their atmospheric lifetime.[18, 82-87] Organic films may affect the morphological, optical and chemical properties of atmospheric aerosols, having potentially important consequences to the direct and indirect effects on the Earth's climate.[88] The results presented here highlight a new, atmospherically plausible, way to create surface-active oligomers, which may play a role in the aerosol processing and surface chemistry of the atmosphere.

7.5 Bibliography:

1. Renard, P.; Reed Harris, A. E.; Rapf, R. J.; Rainer, S.; Demelas, C.; Coulomb, B.; Quivet, E.; Vaida, V.; Monod, A. Aqueous phase oligomerization of methyl vinyl ketone by atmospheric radical reactions. *J. Phys. Chem. C* **2014,** *118*, 29421-29430.

2. Hallquist, M.; Wenger, J. C.; Baltensperger, U.; Rudich, Y.; Simpson, D.; Claeys, M.; Dommen, J.; Donahue, N. M.; George, C.; Goldstein, A. H., et al. The formation, properties and impact of secondary organic aerosol: Current and emerging issues. *Atmopheric Chemistry and Physics* **2009,** *9*, 5155-5236.

3. George, C.; D'Anna, B.; Herrmann, H.; Weller, C.; Vaida, V.; Donaldson, D.; Bartels-Rausch, T.; Ammann, M., Emerging areas in atmospheric photochemistry. In *Atmospheric and aerosol chemistry*, Springer: 2014; pp 1-53.

4. Ervens, B.; Turpin, B. J.; Weber, R. J. Secondary aerosol formation in cloud droplets and aqueous particles (aqSOA): A review of laboratory, field and model studies. *Atmo. Chem. Phys.* **2011,** *11*, 11069-11102.

5. Kanakidou, M.; Seinfeld, J.; Pandis, S.; Barnes, I.; Dentener, F.; Facchini, M.; Dingenen, R. V.; Ervens, B.; Nenes, A.; Nielsen, C. Organic aerosol and global climate modelling: A review. *Atmo. Chem. Phys.* **2005,** *5*, 1053-1123.

6. Spracklen, D.; Jimenez, J.; Carslaw, K.; Worsnop, D.; Evans, M.; Mann, G.; Zhang, Q.; Canagaratna, M.; Allan, J.; Coe, H. Aerosol mass spectrometer constraint on the global secondary organic aerosol budget. *Atmo. Chem. Phys.* **2011,** *11*, 12109-12136.

7. Renard, P.; Siekmann, F.; Gandolfo, A.; Socorro, J.; Salque, G.; Ravier, S.; Quivet, E.; Clement, J. L.; Traikia, M.; Delort, A. M., et al. Radical mechanisms of methyl vinyl ketone oligomerization through aqueous phase OH-oxidation: On the paradoxical role of dissolved molecular oxygen. *Atmo. Chem. Phys.* **2013,** *13*, 6473-6491.

8. Carlton, A. G.; Wiedinmyer, C.; Kroll, J. H. A review of secondary organic aerosol (SOA) formation from isoprene. *Atmo. Chem. Phys.* **2009,** *9*, 4987-5005.

9. Volkamer, R.; Jimenez, J. L.; San Martini, F.; Dzepina, K.; Zhang, Q.; Salcedo, D.; Molina, L. T.; Worsnop, D. R.; Molina, M. J. Secondary organic aerosol formation from anthropogenic air pollution: Rapid and higher than expected. *Geophys. Res. Lett.* **2006,** *33*.

10. Loeffler, K. W.; Koehler, C. A.; Paul, N. M.; De Haan, D. O. Oligomer formation in evaporating aqueous glyoxal and methylglyoxal solutions. *Environ. Sci. Technol.* **2006,** *40*, 6318-6323.

11. Carlton, A. G.; Turpin, B. J.; Lim, H.-J.; Altieri, K. E.; Seitzinger, S. Link between isoprene and secondary organic aerosol (SOA): Pyruvic acid oxidation yields low volatility organic acids in clouds. *Geophys. Res. Lett.* **2006,** *33*, L06822.

12. Reed Harris, A. E.; Ervens, B.; Shoemaker, R. K.; Kroll, J. A.; Rapf, R. J.; Griffith, E. C.; Monod, A.; Vaida, V. Photochemical kinetics of pyruvic acid in aqueous solution. *J. Phys. Chem. A* **2014,** *118*, 8505-8516.

13. Renard, P.; Siekmann, F.; Salque, G.; Demelas, C.; Coulomb, B.; Vassalo, L.; Ravier, S.; Temime-Roussel, B.; Voisin, D.; Monod, A. Aqueous-phase oligomerization of methyl vinyl ketone through photooxidation: Part 1: Aging processes of oligomers. *Atmo. Chem. Phys.* **2015,** *15*, 21-35.

14. Griffith, E. C.; Carpenter, B. K.; Shoemaker, R. K.; Vaida, V. Photochemistry of aqueous pyruvic acid. *Proc. Natl. Acad. Sci.* **2013,** *110*, 11714-11719.

15. Finlayson-Pitts, B. J.; Pitts, J. N., *Chemistry of the upper and lower atmosphere*. Academic Press: San Diego, 1999.

16. Sorjamaa, R.; Svenningsson, B.; Raatikainen, T.; Henning, S.; Bilde, M.; Laaksonen, A. The role of surfactants in Köhler theory reconsidered. *Atmo. Chem. Phys.* **2004,** *4*, 2107-2117.

17. Charlson, R. J.; Seinfeld, J. H.; Nenes, A.; Kulmala, M.; Laaksonen, A.; Facchini, M. C. Reshaping the theory of cloud formation. *Science* **2001,** *292*, 2025-2026.

18. Ellison, G. B.; Tuck, A. F.; Vaida, V. Atmospheric processing of organic aerosols. *J. Geophys. Res. Atmos.* **1999,** *104*, 11633-11641.

19. Donaldson, D. J.; Vaida, V. The influence of organic films at the air-aqueous boundary on atmospheric processes. *Chem. Rev.* **2006,** *106*, 1445-1461.

20. Guenther, C. Estimates of global terrestrial isoprene emissions using MEGAN (model of emissions of gases and aerosols from nature). *Atmo. Chem. Phys.* **2006,** *6*.

21. Lee, W.; Baasandorj, M.; Stevens, P. S.; Hites, R. A. Monitoring OH-initiated oxidation kinetics of isoprene and its products using online mass spectrometry. *Environ. Sci. Technol.* **2005,** *39*, 1030-1036.

22. Kroll, J. H.; Ng, N. L.; Murphy, S. M.; Flagan, R. C.; Seinfeld, J. H. Secondary organic aerosol formation from isoprene photooxidation. *Environ. Sci. Technol.* **2006,** *40*, 1869-1877.

23. Dommen, J.; Metzger, A.; Duplissy, J.; Kalberer, M.; Alfarra, M.; Gascho, A.; Weingartner, E.; Prevot, A.; Verheggen, B.; Baltensperger, U. Laboratory observation of oligomers in the aerosol from isoprene/NO_x photooxidation. *Geophys. Res. Lett.* **2006,** *33*.

24. Surratt, J. D.; Murphy, S. M.; Kroll, J. H.; Ng, N. L.; Hildebrandt, L.; Sorooshian, A.; Szmigielski, R.; Vermeylen, R.; Maenhaut, W.; Claeys, M. Chemical composition of secondary organic aerosol formed from the photooxidation of isoprene. *J. Phys. Chem. A* **2006,** *110*, 9665-9690.

25. Ortiz-Montalvo, D. L.; Lim, Y. B.; Perri, M. J.; Seitzinger, S. P.; Turpin, B. J. Volatility and yield of glycolaldehyde SOA formed through aqueous photochemistry and droplet evaporation. *Aerosol Sci. Technol.* **2012,** *46*, 1002-1014.

26. Altieri, K. E.; Carlton, A. G.; Lim, H.-J.; Turpin, B. J.; Seitzinger, S. P. Evidence for oligomer formation in clouds: Reactions of isoprene oxidation products. *Environ. Sci. Technol.* **2006,** *40*, 4956-4960.

27. Haddad, I. E.; Liu, Y.; Nieto-Gligorovski, L.; Michaud, V.; Temime-Roussel, B.; Quivet, E.; Marchand, N.; Sellegri, K.; Monod, A. In-cloud processes of methacrolein under simulated conditions: Part 2: Formation of secondary organic aerosol. *Atmo. Chem. Phys.* **2009,** *9*, 5107-5117.

28. Altieri, K.; Seitzinger, S.; Carlton, A.; Turpin, B.; Klein, G.; Marshall, A. Oligomers formed through in-cloud methylglyoxal reactions: Chemical composition, properties, and mechanisms investigated by ultra-high resolution FT-ICR mass spectrometry. *Atmos. Environ.* **2008,** *42*, 1476-1490.

29. Perri, M. J.; Seitzinger, S.; Turpin, B. J. Secondary organic aerosol production from aqueous photooxidation of glycolaldehyde: Laboratory experiments. *Atmos. Environ.* **2009,** *43*, 1487-1497.

30. Tan, Y.; Carlton, A. G.; Seitzinger, S. P.; Turpin, B. J. SOA from methylglyoxal in clouds and wet aerosols: Measurement and prediction of key products. *Atmos. Environ.* **2010,** *44*, 5218-5226.

31. Tan, Y.; Perri, M. J.; Seitzinger, S. P.; Turpin, B. J. Effects of precursor concentration and acidic sulfate in aqueous glyoxal–OH radical oxidation and implications for secondary organic aerosol. *Environ. Sci. Technol.* **2009,** *43*, 8105-8112.

32. Lim, Y. B.; Tan, Y.; Turpin, B. J. Chemical insights, explicit chemistry, and yields of secondary organic aerosol from OH radical oxidation of methylglyoxal and glyoxal in the aqueous phase. *Atmo. Chem. Phys.* **2013,** *13*, 8651-8667.

33. Donaldson, D.; Valsaraj, K. T. Adsorption and reaction of trace gas-phase organic compounds on atmospheric water film surfaces: A critical review. *Environ. Sci. Technol.* **2010,** *44*, 865-873.

34. Zhang, X.; Chen, Z.; Zhao, Y. Laboratory simulation for the aqueous OH-oxidation of methyl vinyl ketone and methacrolein: Significance to the in-cloud SOA production. *Atmo. Chem. Phys.* **2010,** *10*, 9551-9561.

35. Liu, Y.; Siekmann, F.; Renard, P.; Zein, A. E.; Salque, G.; Haddad, I. E.; Temime-Roussel, B.; Voisin, D.; Thissen, R.; Monod, A. Oligomer and SOA formation through aqueous phase photooxidation of methacrolein and methyl vinyl ketone. *Atmos. Environ.* **2012,** *49*, 123-129.

36. Chan, K. M.; Huang, D. D.; Li, Y. J.; Chan, M. N.; Seinfeld, J. H.; Chan, C. K. Oligomeric products and formation mechanisms from acid-catalyzed reactions of methyl vinyl ketone on acidic sulfate particles. *J. Atmos. Chem.* **2013,** *70*, 1-18.

37. Schöne, L.; Schindelka, J.; Szeremeta, E.; Schaefer, T.; Hoffmann, D.; Rudzinski, K. J.; Szmigielski, R.; Herrmann, H. Atmospheric aqueous phase radical chemistry of the isoprene oxidation products methacrolein, methyl vinyl ketone, methacrylic acid and acrylic acid–kinetics and product studies. *Phys. Chem. Chem. Phys.* **2014,** *16*, 6257-6272.

38. Epstein, S. A.; Tapavicza, E.; Furche, F.; Nizkorodov, S. A. Direct photolysis of carbonyl compounds dissolved in cloud and fog droplets. *Atmo. Chem. Phys.* **2013,** *13*, 9461-9477.

39. Closs, G. L.; Miller, R. J. Photo-reduction and photodecarboxylation of pyruvic acid - applications of CIDNP to mechanistic photochemistry. *J. Am. Chem. Soc.* **1978,** *100*, 3483-3494.

40. Guzman, M. I.; Colussi, A. J.; Hoffmann, M. R. Photoinduced oligomerization of aqueous pyruvic acid. *J. Phys. Chem. A* **2006,** *110*, 3619-3626.

41. Larsen, M. C.; Vaida, V. Near infrared photochemistry of pyruvic acid in aqueous solution. *J. Phys. Chem. A* **2012,** *116*, 5840-5846.

42. Leermakers, P. A.; Vesley, G. F. Photochemistry of alpha-keto acids and alpha-keto esters. 1. Photolysis of pyruvic acid and benzoylformic acid. *J. Am. Chem. Soc.* **1963,** *85*, 3776-3779.

43. Leermakers, P. A.; Vesley, G. F. Photolysis of pyruvic acid in solution. *J. Org. Chem.* **1963,** *28*, 1160-1161.

44. Mellouki, A.; Mu, Y. J. On the atmospheric degradation of pyruvic acid in the gas phase. *J. Photochem. Photobiol., A* **2003,** *157*, 295-300.

45. Plath, K. L.; Takahashi, K.; Skodje, R. T.; Vaida, V. Fundamental and overtone vibrational spectra of gas-phase pyruvic acid. *J. Phys. Chem. A* **2009,** *113*, 7294-7303.

46. Takahashi, K.; Plath, K. L.; Skodje, R. T.; Vaida, V. Dynamics of vibrational overtone excited pyruvic acid in the gas phase: Line broadening through hydrogen-atom chattering. *J. Phys. Chem. A* **2008,** *112*, 7321-7331.

47. Vesley, G. F.; Leermakers, P. A. Photochemistry of alpha-keto acids and alpha-keto esters. 3. Photolysis of pyruvic acid in vapor phase. *J. Phys. Chem.* **1964,** *68*, 2364-2366.

48. Yamamoto, S.; Back, R. A. The photolysis and thermal decomposition of pyruvic acid in the gas phase. *Can. J. Chem.* **1985,** *63*, 549-554.

49. Ervens, B.; Wang, Y.; Eagar, J.; Leaitch, W.; Macdonald, A.; Valsaraj, K.; Herckes, P. Dissolved organic carbon (DOC) and select aldehydes in cloud and fog water: The role of the aqueous phase in impacting trace gas budgets. *Atmo. Chem. Phys.* **2013,** *13*, 5117-5135.

50. Kameel, F. R.; Hoffmann, M. R.; Colussi, A. J. OH radical-initiated chemistry of isoprene in aqueous media. Atmospheric implications. *J. Phys. Chem. A* **2013,** *117*, 5117-5123.

51. Bao, L.; Matsumoto, M.; Kubota, T.; Sekiguchi, K.; Wang, Q.; Sakamoto, K. Gas/particle partitioning of low-molecular-weight dicarboxylic acids at a suburban site in Saitama, Japan. *Atmos. Environ.* **2012,** *47*, 546-553.

52. Herrmann, H.; Hoffmann, D.; Schaefer, T.; Bräuer, P.; Tilgner, A. Tropospheric aqueous-phase free-radical chemistry: Radical sources, spectra, reaction kinetics and prediction tools. *ChemPhysChem* **2010,** *11*, 3796-3822.

53. Arakaki, T.; Anastasio, C.; Kuroki, Y.; Nakajima, H.; Okada, K.; Kotani, Y.; Handa, D.; Azechi, S.; Kimura, T.; Tsuhako, A. A general scavenging rate constant for reaction of hydroxyl radical with organic carbon in atmospheric waters. *Environ. Sci. Technol.* **2013,** *47*, 8196-8203.

54. Griffith, E. C.; Adams, E. M.; Allen, H. C.; Vaida, V. Hydrophobic collapse of a stearic acid film by adsorbed l-phenylalanine at the air-water interface. *J. Phys. Chem. B* **2012,** *116*, 7849-7857.

55. Adamson, A. W.; Gast, A. P., *Physical chemistry of surfaces*. 6 ed.; John Wiley & Sons, Inc.: New York, 1997.

56. Maroń, M. K.; Takahashi, K.; Shoemaker, R. K.; Vaida, V. Hydration of pyruvic acid to its geminal-diol, 2, 2-dihydroxypropanoic acid, in a water-restricted environment. *Chem. Phys. Lett.* **2011,** *513*, 184-190.

57. Griffith, E. C.; Shoemaker, R. K.; Vaida, V. Sunlight-initiated chemistry of aqueous pyruvic acid: Building complexity in the origin of life. *Origins Life Evol. Biosphere* **2013,** *43*, 341-352.

58. Gibian, M. J.; Corley, R. C. Organic radical-radical reactions. Disproportionation vs. Combination. *Chem. Rev.* **1973,** *73*, 441-464.

59. Ervens, B.; Sorooshian, A.; Lim, Y. B.; Turpin, B. J. Key parameters controlling OH - initiated formation of secondary organic aerosol in the aqueous phase (aqSOA). *J. Geophys. Res. Atmos.* **2014,** *119*, 3997-4016.

60. Decker, C.; Jenkins, A. D. Kinetic approach of oxygen inhibition in ultraviolet-and laser-induced polymerizations. *Macromolecules* **1985,** *18*, 1241-1244.

61. Odian, G., *Principles of polymerization*. John Wiley & Sons: Hoboken, New Jersey, 2004.

62. Ligon, S. C.; Husar, B.; Wutzel, H.; Holman, R.; Liska, R. Strategies to reduce oxygen inhibition in photoinduced polymerization. *Chem. Rev.* **2014,** *114*, 557-589.

63. Ervens, B.; Volkamer, R. Glyoxal processing by aerosol multiphase chemistry: Towards a kinetic modeling framework of secondary organic aerosol formation in aqueous particles. *Atmo. Chem. Phys.* **2010,** *10*, 8219-8244.

64. Kameel, F. R.; Riboni, F.; Hoffmann, M.; Enami, S.; Colussi, A. Fenton oxidation of gaseous isoprene on aqueous surfaces. *Journal of Physical Chemistry C* **2014,** *118*, 29151-29158.

65. Dobson, C. M.; Ellison, G. B.; Tuck, A. F.; Vaida, V. Atmospheric aerosols as prebiotic chemical reactors. *Proc. Natl. Acad. Sci.* **2000,** *97*, 11864-11868.

66. Gill, P.; Graedel, T.; Weschler, C. Organic films on atmospheric aerosol particles, fog droplets, cloud droplets, raindrops, and snowflakes. *Rev. Geophys.* **1983,** *21*, 903-920.

67. Rudich, Y.; Riziq, A.; Erlick, C.; Adler, G.; Trainic, M.; Lang, N. Optical properties of aerosols with organic components using cavity ring down spectrometry. *Geochim. Cosmochim* **2009**, A1130-A1130.

68. Kaku, K.; Hegg, D.; Covert, D.; Santarpia, J.; Jonsson, H.; Buzorius, G.; Collins, D. Organics in the northeastern Pacific and their impacts on aerosol hygroscopicity in the subsaturated and supersaturated regimes. *Atmo. Chem. Phys.* **2006,** *6*, 4101-4115.

69. Gilman, J. B.; Tervahattu, H.; Vaida, V. Interfacial properties of mixed films of long-chain organics at the air-water interface. *Atmos. Environ.* **2006,** *40*, 6606-6614.

70. Prather, K. A.; Bertram, T. H.; Grassian, V. H.; Deane, G. B.; Stokes, M. D.; DeMott, P. J.; Aluwihare, L. I.; Palenik, B. P.; Azam, F.; Seinfeld, J. H., et al. Bringing the ocean into the laboratory to probe the chemical complexity of sea spray aerosol. *Proc. Natl. Acad. Sci.* **2013,** *110*, 7550-7555.

71. McNeill, V. F.; Sareen, N.; Schwier, A. N., Surface-active organics in atmospheric aerosols. In *Atmospheric and aerosol chemistry*, McNeill, V. F.; Ariya, P. A., Eds. 2014; Vol. 339, pp 201-259.

72. Tervahattu, H.; Hartonen, K.; Kerminen, V. M.; Kupiainen, K.; Aarnio, P.; Koskentalo, T.; Tuck, A. F.; Vaida, V. New evidence of an organic layer on marine aerosols. *J. Geophys. Res.* **2002,** *107*, 4053-4060.

73. Tervahattu, H.; Juhanoja, J.; Vaida, V.; Tuck, A. F.; Niemi, J. V.; Kupiainen, K.; Kulmala, M.; Vehkamaki, H. Fatty acids on continental sulfate aerosol particles. *J. Geophys. Res.* **2005,** *110*, Article number D06207.

74. Prather, K. A.; Hatch, C. D.; Grassian, V. H. Analysis of atmospheric aerosols. *Annu. Rev. Anal. Chem.* **2008,** *1*, 485-514.

75. Barnes, G. The effects of monolayers on the evaporation of liquids. *Adv. Colloid Interface Sci.* **1986,** *25*, 89-200.

76. Gilman, J. B.; Vaida, V. Permeability of acetic acid through organic films at the air-aqueous interface. *J. Phys. Chem. A* **2006,** *110*, 7581-7587.

77. Mmereki, B. T.; Donaldson, D. Direct observation of the kinetics of an atmospherically important reaction at the air−aqueous interface. *J. Phys. Chem. A* **2003,** *107*, 11038-11042.

78. Asad, A.; Mmereki, B.; Donaldson, D. Enhanced uptake of water by oxidatively processed oleic acid. *Atmo. Chem. Phys.* **2004,** *4*, 2083-2089.

79. Davies, J. F.; Miles, R. E.; Haddrell, A. E.; Reid, J. P. Influence of organic films on the evaporation and condensation of water in aerosol. *Proc. Natl. Acad. Sci.* **2013,** *110*, 8807-8812.

80. Park, S. C.; Burden, D. K.; Nathanson, G. M. Surfactant control of gas transport and reaction at the surface of sulfuric acid. *Acc. Chem. Res.* **2009,** *42*, 379-387.

81. Lo, J.-H. A.; Lee, W.-M. G. Effect of surfactant film on solubility of hydrophobic organic compounds in fog droplets. *Chemosphere* **1996,** *33*, 1391-1408.

82. Bertram, A. K.; Ivanov, A. V.; Hunter, M.; Molina, L. T.; Molina, M. J. The reaction probability of OH on organic surfaces of tropospheric interest. *J. Phys. Chem. A* **2001,** *105*, 9415-9421.

83. Eliason, T. L.; Gilman, J. B.; Vaida, V. Oxidation of organic films relevant to atmospheric aerosols. *Atmos. Environ.* **2004,** *38*, 1367-1378.

84. Rudich, Y. Laboratory perspectives on the chemical transformations of organic matter in atmospheric particles. *Chem. Rev.* **2003,** *103*, 5097-5124.

85. Rudich, Y.; Donahue, N. M.; Mentel, T. F. Aging of organic aerosol: Bridging the gap between laboratory and field studies. *Annu. Rev. Phys. Chem.* **2007,** *58*, 321-352.

86. Chakraborty, P.; Zachariah, M. R. On the structure of organic-coated water droplets: From "net water attractors" to "oily" drops. *J. Geophys. Res.* **2011,** *116*, Art. Nr. D21205.

87. Blower, P. G.; Shamay, E.; Kringle, L.; Ota, S. T.; Richmond, G. L. Surface behavior of malonic acid adsorption at the air/water interface. *J. Phys. Chem. A* **2013,** *117*, 2529-2542.

88. Li, Y.; Ezell, M. J.; Finlayson-Pitts, B. J. The impact of organic coatings on light scattering by sodium chloride particles. *Atmos. Environ.* **2011,** *45*, 4123-4132.

8. Photo-Initiated Reactions of Lipids by α-Keto Acids in Aqueous Solution

8.1 Introduction:

The Sun is by far the largest source of energy to the planet, and it controls, directly or indirectly, the vast majority of physical, chemical, and biological processes that take place on the Earth.[1-3] Atmospheric chemistry is undeniably driven by photochemical processing, often from secondary reactions involving the further reactions of photochemically generated radical species.[4] Indeed, photochemistry and photo-oxidation in the literature have often been synonymous with hydroxyl radical reactions (OH).[5, 6] Recently, however, there has been increased interest in the direct photochemistry of organic species, in both the gas and particle phase in the atmosphere, as well as at the sea surface microlayer.[4, 7-13, 14] These photoactive organic species have also been shown to be capable of initiating further reactions with species that are not themselves photoactive.[8, 11, 12, 15-17] Such indirect photochemical processes include either energy transfer from the initially excited molecule to the excited state of another molecule (photosensitization), or, as is studied here, the reaction of one photochemically-excited species with another, non-photoactive species (photo-initiation).

Reaction with OH is often considered to be the controlling factor governing the fate of species in the atmosphere because of its ability to react indiscriminately with most species, even those that are not particularly reactive.[5] Organic radicals may act similarly but such processes have been subject to much less investigation in atmospheric chemistry. The contributions from organic radical reactions have rarely been compared to those of the ubiquitous OH radical reactions,[18] but it has been shown that pyruvic acid is capable of initiating polymerization of methyl vinyl ketone (MVK) that is comparable to that initiated

by reaction of OH in the aqueous phase.[19] Both MVK and pyruvic acid are oxidation products of isoprene.[20-23] MVK is a highly reactive species that, upon radical initiation, rapidly forms high molecular weight products.[15, 19, 21, 24-36] Pyruvic acid, an α-keto acid whose photochemistry has been studied extensively,[7, 14, 37-48] reacts in the aqueous phase to generate oligomeric species via radical recombination.[7, 43-48] In this study, we show that α-keto acids can act as radical initiators, not only for highly reactive species like MVK, but also for unreactive fatty acids and fatty alcohols, leading to the generation of lipid-like, covalently-bonded molecules from the cross-reaction.

The reactions of these surface-active species are of particular interest because of the ubiquity of fatty acids and fatty alcohols in the sea surface microlayer[49, 50] as well as their ability to partition and persist on atmospheric aerosol particles.[50-54] The chemistry of these simple lipids, especially the fatty acids, has been studied to examine their volatile products, but comparatively little attention has been paid to their condensed phase products. The formation of higher molecular weight products through photo-initiated processes, as shown here, has the potential to modify the surfactant layer and contribute to secondary organic aerosols formation. Beyond this, the cross-reactions between a photo-initiator species and non-photoactive species that are discussed in this work show the disproportionately large effect a species may have on the overall reactivity of a mixture, even when the photoactive species is only a minor component.

8.2 Experimental Section:

Pyruvic acid (98%), hexanoic acid (>99.5%), 1-hexanol (hexanol, 98%), nonanoic acid (96%), and 1-nonanol (nonanol, 98%) were obtained from Sigma-Aldrich and distilled by heating under reduced pressure (< 1 Torr) to remove impurities. Pyruvic acid was distilled at <55 °C and used within one month of distillation to ensure oligomers from dark processes were minimized.[55] Hexanol was heated to ~50 °C, hexanoic acid ~80 °C, and nonanoic acid

and nonanol were heated to ~180 °C during distillation. In each case noticeable yellow impurities were removed upon distillation, leaving a clear, colorless liquid. Representative NMR spectra before and after distillation are shown in Figures H.1-H.4. 2-oxooctanoic acid (OOA, ≥99.0%, Sigma Aldrich) was used without further purification.

Photolysis solutions were made in a ~1:2 ratio of α-keto acid initiator to fatty acid or alcohol, in the combinations reported in Table 8.1. Control solutions of 10 mM pyruvic acid, 0.5 mM OOA, 20 mM hexanoic acid, 20 mM hexanol, 1 mM nonanoic acid, and 0.8 mM nonanol were also photolyzed, as were solutions of 6 mM OOA and 100 mM nonanoic acid dissolved in methanol (Fisher Scientific, 99.9%). Solutions were made using 18.2 MΩ (3 ppb TOC) water and then sonicated until fully dissolved. All solutions were used at their natural pH of the solution without further adjustment.

Table 8.1 Experimental Solution Compositions

	α-keto Acid Conc. (mM)	Fatty Acid/Alcohol Conc. (mM)
Pyruvic Acid and Hexanoic Acid	10	20
	0.5	1
Pyruvic Acid and Hexanol	10	20
Pyruvic Acid and Nonanoic Acid	0.5	1
Pyruvic Acid and Nonanol	0.5	0.8
OOA and Nonanol	0.5	0.9

Photolyses were conducted as described in Rapf et al. 2017.[45] Briefly, for each experiment, 100 mL of solution was made and ~10 mL were saved as a pre-photolysis control. The remaining solution was photolyzed for 5 hours using an unfiltered 450 W Xe arc lamp (Newport). Higher concentration solutions were photolyzed in a temperature-stabilized water bath at 4 °C, while the lower concentration solutions were photolyzed at 20 °C due to solubility concerns for nonanoic acid and nonanol. No differences in products were observed with changing water bath temperature. All solutions were purged with N_2 beginning one hour before the start of photolysis and continuing throughout the experiment

to eliminate oxygen from the reactor. Oxygen-limited conditions favor the formation of oligomeric products from the aqueous photochemistry of α-keto acids,[46] which allows for easier identification and analysis of minor products, such as those under study here.

A variety of analytical techniques, including UV-Vis and NMR spectroscopy and high-resolution negative mode electrospray ionization mass spectrometry (ESI^- MS) were used to characterize solutions. The parameters used for each instrument are included in Chapter 3. Analysis of mass spectrometry data followed the procedure outlined Chapter 3.4. All ions assigned to a particular analyte were within at least 15 ppm of the theoretical mass for each experiment with typical mass differences of <10 ppm. The analyses conducted here were not designed to be absolutely quantitative, and analyte intensities may not correlate directly to absolute concentrations and are used only for relative comparison.

8.3 Results and Discussion:

The aqueous phase photochemistry of α-keto acids, including pyruvic acid and OOA, has been studied in detail[7, 43-48, 56] with mechanistic understanding of the available reactive pathways[44-46, 57] and their dependence on reaction conditions, such as solution pH[48] and the presence of oxygen.[46] The photochemistry of these species is characterized largely by the formation of radicals that recombine to form oligomeric species, including covalently-bonded dimers and trimers.[58] It has been previously shown that pyruvic acid can act as a radical initiator in the polymerization of methyl vinyl ketone (MVK).[19] Here, we examined the ability of these α-keto acids to initiate reactions with the fatty acids and fatty alcohols, hexanoic acid, nonanoic acid, 1-hexanol, and 1-nonanol, which themselves do not absorb actinic radiation.

In addition to the mixed solutions of α-keto acids and fatty acid or alcohol, control solutions consisting of the individual fatty acids and alcohols were also photolyzed. While fatty acids and fatty alcohols are not generally considered photoactive species within the

relevant actinic spectrum, it has recently been suggested that some fatty acids, including nonanoic acid, may undergo photochemistry themselves, perhaps due to an enhancement of the triplet state at the air-water interface.[9, 17, 59] Our experimental conditions were chosen to probe bulk phase photochemistry and used dilute concentrations of all species. Under our experimental conditions, the distilled fatty acids and fatty alcohols do not appear to undergo photochemistry, with essentially no changes observed in either NMR or ESI^- MS between the pre- and post-photolysis solutions (Figures H.5-H.12, Tables H.1-H.4). ESI^- MS experiments are of limited use for identifying the fatty alcohols, hexanol and nonanol, as they are not expected to deprotonate under the ionization conditions used here, but changes were not observed upon photolysis, which is further confirmed by the NMR spectra. The dilute solutions used here may prevent observation of minor photochemical pathways. These dilute concentrations are necessary because of solubility concerns for fatty acids and alcohols in water, but it is worth noting that 100 mM solutions of nonanoic acid dissolved in methanol show similarly negligible changes in the ESI^- MS data between pre- and post-photolysis (Figure H.13).

Each of the fatty acids and fatty alcohols has weak absorbance in their respective UV-vis absorption spectra at ~270 nm (Figures H.14 and H.15), whose intensity is slightly decreased following distillation (Figures H.16). For nonanoic acid, this peak has previously been assigned to its triplet state.[59] It is intriguing that the fatty alcohols also have a peak in this same wavelength region given that their electronic structures are quite different. Interestingly, upon photolysis of 20 mM hexanoic acid, while no new photoproducts are detected by NMR or ESI^- MS, the 270 nm peak in the UV-vis absorption spectra appears to be preferentially depleted compared to the acid peak at ~204 nm (Figure H.17). Such behavior could potentially be explained if the observed 270 nm peak was due, at least in part, to an impurity. The identity of this impurity is not known, but Appendix C contains

preliminary evidence for one potential contaminant. Regardless, these experimental controls make it clear that under our conditions, any observed photochemistry for the fatty acids and fatty alcohols stems from the α-keto acids acting as radical initiators.

As observed both by NMR and ESI$^-$ MS (Figure 8.1, Figures H.18-H.27), the mixed solutions of fatty acids/alcohols with an α-keto acid initiator are dominated by photoproducts generated by radical recombination reactions between α-keto acid species (Figures H.28, H.29).[45, 57] Detailed ESI$^-$ MS results are given in Appendix H (Tables H.1-H.5). It is not surprising that reactions between photoactive species dominate the observed results for these photolyses, but new photoproducts are observed for the mixed solutions that are not present in either the α-keto acid or fatty acid/alcohol control photolyses. Namely, as shown in Table 8.2, for each of the mixed solutions under consideration here, a new analyte is observed with an m/z corresponding to the molecular formula expected for the cross-product between the α-keto acid and the fatty acid/alcohol, evidence that organic radicals generated by photolysis of α-keto acids can react with fatty acids and alcohols. Figure 8.1 shows representative ESI$^-$ MS data for the post-photolysis solution of 0.5 mM pyruvic acid and 0.8 mM nonanol, showing both the expected products for the photolysis of pyruvic acid, as well as the cross-product between pyruvic acid and nonanol (theoretical m/z = 231.1597). Full spectra, including pre-photolysis and methanol controls, are given for all photolyses between α-keto acid and fatty acid/alcohol in Figures H.23-27.

While not included in these results, we expect the cross-product of OOA and nonanoic acid to also be formed. However, the expected molecular formula from this product matches that of one of the major photoproducts of OOA, making its detection difficult. Similarly, it appears there is a very minor product generated by the photolysis of pyruvic acid with the same chemical formula as the cross-product of pyruvic acid and hexanoic acid. In this case, however, the intensity observed is increased dramatically in the mixed photolysis case,

suggesting the new cross-product is, indeed, formed. It is unlikely that this change is simply due to differences in ionization efficiency, given the similar intensities observed for the other analytes across solution conditions. The cross-products for pyruvic acid with hexanol, nonanoic acid, and nonanol, as well as for OOA with nonanol, are observed following photolysis without any interference from photoproducts generated from the individual α-keto acids.

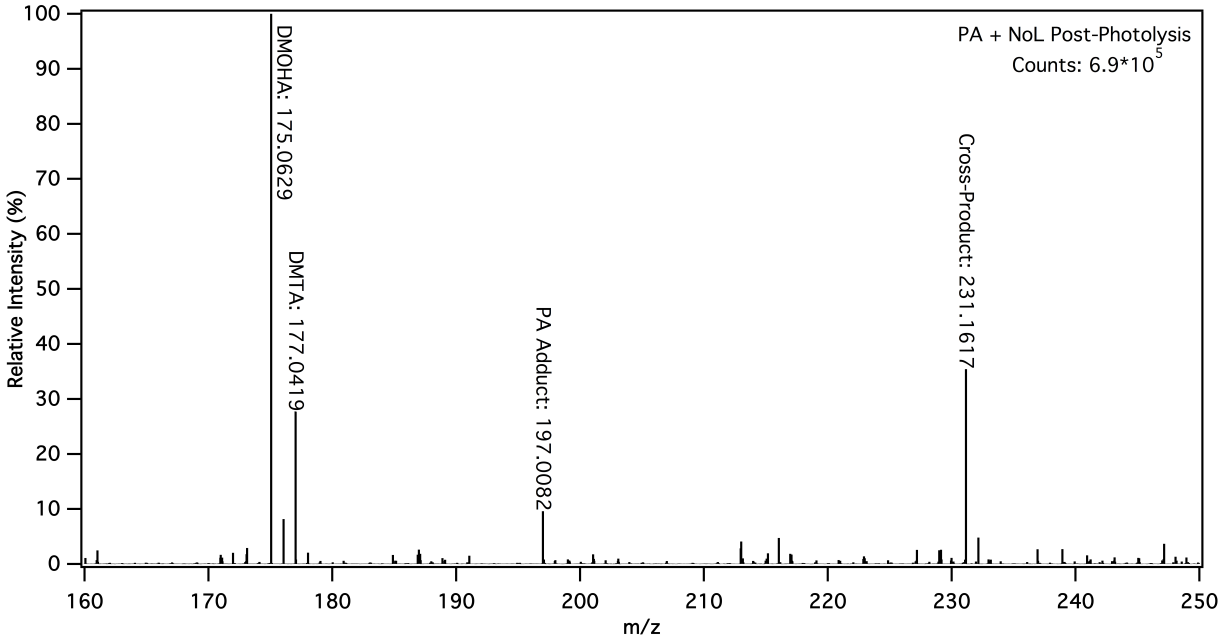

Figure 8.1. Representative ESI⁻ MS of a solution of 0.5 mM pyruvic acid and 0.8 mM nonanol after 5 hours of photolysis highlighting the formation of the mixed cross-product between the two species compared to major pyruvic acid photolysis products, dimethyl-tartaric acid (DMTA) and 2,4-dihydroxy-2-methyl-5-oxohexanoic acid (DMOHA).[44, 45]

Table 8.2. ESI⁻ MS data for the cross-product between α-keto acid initiator and fatty acid or fatty alcohol species

	Assigned Formula [M-H]-	Theor. m/z	Exp. m/z	Mass Diff. (ppm)	Pre-hν	Post-hν
Pyruvic Acid + Hexanoic Acid	$C_9H_{15}O_5^-$	203.0920	203.0926	3.2	B.T.	M*
Pyruvic Acid + Hexanol	$C_9H_{17}O_4^-$	189.1127	189.1143	8.5	B.T.	M
Pyruvic Acid + Nonanoic Acid	$C_{12}H_{21}O_5^-$	245.1389	245.1400	4.4	B.T.	M
Pyruvic Acid + Nonanol	$C_{12}H_{23}O_4^-$	231.1597	231.1607	4.6	B.T.	M
OOA + Nonanol	$C_{17}H_{33}O_4^-$	301.2379	301.2390	3.5	B.T.	M
OOA in Methanol	$C_9H_{17}O_4^-$	189.1127	189.1130	1.5	W	S

*There is also weak overlapping photoproduct generated with the same chemical formula in the control photolysis of pyruvic acid.

We propose that this cross-product is formed by hydrogen abstraction from the ground state fatty acid/alcohol by the triplet state α-keto acid, leading to radical formation. This radical can then recombine with an α-keto acid radical in solution, forming the cross-product. A proposed mechanism for this process is shown for hexanoic acid and pyruvic acid in Scheme 8.1. The favored site of hydrogen abstraction on carboxylic acids is a matter of some debate in the literature.[60-64] We have drawn hydrogen abstraction as occurring from the α-position of hexanoic acid, as is generally assumed to be favored for longer-tailed carboxylic acids.[60, 62]

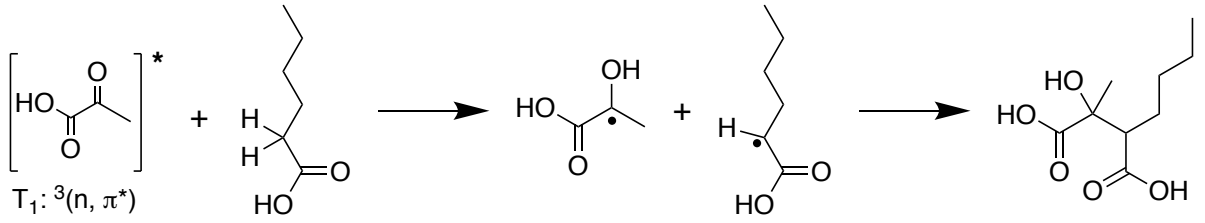

Scheme 8.1. Proposed hydrogen abstraction and recombination pathway to form the cross-product between hexanoic acid and pyruvic acid.

There is sufficient energy for the α-keto acid triplet state to induce hydrogen abstraction. Electronic structure calculations suggest that this is, in fact, possible. CBS-QB3 calculations for hydrogen abstraction from the α-position of propionic acid by triplet state pyruvic acid show that because of the relatively strong O-H bond that is formed after abstraction, this process is exothermic by ~17 kcal/mol. It is perhaps worth noting that the calculation of the OH bond strength in this context requires that the heat of formation of the radical be compared with that of a hydrogen atom and pyruvic acid in its T_1 state, not the ground state as would be usual for a bond energy calculation. The longer-tailed fatty acids ought to behave similarly to propionic acid, and it is likely that hydrogen abstraction can occur analogously for the fatty alcohols. While hydrogen abstraction may be favored at the α-position, because ESI$^-$ MS does not give structural information, it is certainly possible that the observed cross-products are due to a mix of constitutional isomers resulting from

hydrogen abstraction at other sites on the molecule.

In principle, the radicals generated from hydrogen abstraction from the fatty acid/alcohol could recombine with each other to form the corresponding dimer product; however, these products are not observed here by ESI^- MS. This is likely because of the dilute concentrations used, making it statistically likely that these radicals would first encounter a radical generated from an α-keto acid species. Also, any such oligomeric products may not be detected by ESI^- MS, especially those derived from the fatty alcohols, if they are not readily ionizable.

In addition to the dilute solutions of α-keto acids and fatty acids dissolved in water, 6 mM OOA was dissolved in methanol and photolyzed at 4 °C. The photoproducts observed with the highest intensity by ESI^- MS are the same species generated during the aqueous photolysis of OOA (Figure H.30, Table H.6). However, there is also an observable analyte that corresponds to the cross-product between OOA and methanol (exp. m/z = 189.1147). It is difficult to speculate on the relative ability of OOA to abstract a hydrogen from methanol compared to the other fatty alcohols under study here because the ratio of methanol is much larger than the 2:1 used in the other cases. However, the ability of OOA to cross-react with methanol is intriguing. Methanol is generally thought of as quite inert, so this observed cross-reaction is suggestive that the organic radicals generated by the photolysis of α-keto acids are highly capable of hydrogen abstraction for many species, not just those under consideration here.

In particular, the ability of a few photo-active molecules to induce further reactions of non-photoactive species is of importance when considering the chemistry of air-water interfaces, such as those found on the SML or atmospheric aerosols. Lipids, such as those under study here, partition preferentially to air-water interfaces and there is a considerable enrichment of organic material at surfaces.[65] Higher localized concentrations make it more

likely for an organic radical to encounter and react with another species before being quenched, which may further enhance the effect of a few photo-initiators. Beyond favorable reaction conditions, the SML provides a rich mixture of species for potential reaction,[50, 66, 67] expanding beyond simple single-molecule systems. In this way, we are able to bring our fundamental mechanistic understanding of a model chemical system to bear on larger, more complicated environmental questions. Here, we have focused on the condensed phase products generated, using sunlight to build molecular complexity. The higher molecular weight products formed from photo-initiated processes are likely to be more surface-active than the simple lipids used as starting materials. This chemistry will further modify aqueous surfaces and generates further organic material that could contribute to the formation of secondary organic aerosol.

8.4 Conclusions:

α-Keto acids as a class of molecule are able to act as radical initiators, promoting photo-initiated reactions of fatty acids and fatty alcohols. We have demonstrated this by showing in five different cases that the cross-product between α-keto acid initiator and non-photoactive species is formed during photolysis in aqueous solution. In addition, photolysis of 2-oxooctanoic acid dissolved in methanol is also observed to form the corresponding cross-product between the two. Electronic structure calculations show that hydrogen abstraction from a fatty acid by the triplet excited state α-keto acid is energetically possible. The cross-product, then, is likely formed by recombination of an α-keto acid radical with a fatty acid/alcohol radical. Fatty acid and alcohols are not considered particularly reactive species, which suggests that α-keto acids are likely to be able to act as radical initiators for a number of atmospherically-relevant species found in the sea surface microlayer and on atmospheric aerosol particles. It is necessary to better quantify the role that organic radical

reactions and photo-initiated processes may play in the overall reactivity of organic species in the atmosphere, especially with comparison to the hydroxyl radical.

8.5 Bibliography:

1. Miller, S. L.; Urey, H. C. Organic compound synthesis on the primitive early Earth. *Science* **1959,** *130*, 245-251.

2. Deamer, D.; Weber, A. L. Bioenergetics and life's origins. *Cold Spring Harbor Persp. Biol.* **2010,** *2*, 1-16.

3. Crabtree, G. W.; Lewis, N. S. Solar energy conversion. *Physics Today* **2007,** *60*, 37-42.

4. George, C.; Ammann, M.; D'Anna, B.; Donaldson, D. J.; Nizkorodov, S. A. Heterogeneous photochemistry in the atmosphere. *Chem. Rev.* **2015,** *115*, 4218-4258.

5. Gligorovski, S.; Strekowski, R.; Barbati, S.; Vione, D. Environmental implications of hydroxyl radicals (•OH). *Chem. Rev.* **2015,** *115*, 13051-13092.

6. Finlayson-Pitts, B. J.; Pitts, J. N., *Chemistry of the upper and lower atmosphere.* Academic Press: San Diego, 1999.

7. Reed Harris, A. E.; Pajunoja, A.; Cazaunau, M.; Gratien, A.; Pangui, E.; Monod, A.; Griffith, E. C.; Virtanen, A.; Doussin, J. F.; Vaida, V. Multiphase photochemistry of pyruvic acid under atmospheric conditions. *J. Phys. Chem. A* **2017,** *121*, 3327–3339.

8. Bernard, F.; Ciuraru, R.; Boréave, A.; George, C. Photosensitized formation of secondary organic aerosols above the air/water interface. *Environ. Sci. Technol.* **2016,** *50*, 8678-8686.

9. Chiu, R.; Tinel, L.; Gonzalez, L.; Ciuraru, R.; Bernard, F.; George, C.; Volkamer, R. UV photochemistry of carboxylic acids at the air-sea boundary: A relevant source of glyoxal and other oxygenated VOC in the marine atmosphere. *Geophys. Res. Lett.* **2017,** *44*, 1079-1087.

10. Ciuraru, R.; Fine, L.; Pinxteren, M. v.; D'Anna, B.; Herrmann, H.; George, C. Unravelling new processes at interfaces: Photochemical isoprene production at the sea surface. *Environ. Sci. Technol.* **2015**, 13199–13205.

11. Fu, H.; Ciuraru, R.; Dupart, Y.; Passananti, M.; Tinel, L.; Rossignol, S.; Perrier, S.; Donaldson, D. J.; Chen, J.; George, C. Photosensitized production of atmospherically reactive organic compounds at the air/aqueous interface. *J. Am. Chem. Soc.* **2015,** *137*, 8348-8351.

12. Ciuraru, R.; Fine, L.; van Pinxteren, M.; D'Anna, B.; Herrmann, H.; George, C. Photosensitized production of functionalized and unsaturated organic compounds at the air-sea interface. *Sci. Rep.* **2015,** *5*, 12741

13. George, C.; D'Anna, B.; Herrmann, H.; Weller, C.; Vaida, V.; Donaldson, D.; Bartels-Rausch, T.; Ammann, M., Emerging areas in atmospheric photochemistry. In *Atmospheric and aerosol chemistry*, Springer: 2014; pp 1-53.

14. Reed Harris, A. E.; Doussin, J.-F.; Carpenter, B. K.; Vaida, V. Gas-phase photolysis of pyruvic acid: The effect of pressure on reaction rates and products. *J. Phys. Chem. A* **2016,** *120*, 10123-10133.

15. Renard, P.; Siekmann, F.; Gandolfo, A.; Socorro, J.; Salque, G.; Ravier, S.; Quivet, E.; Clement, J. L.; Traikia, M.; Delort, A. M., et al. Radical mechanisms of methyl vinyl ketone oligomerization through aqueous phase OH-oxidation: On the paradoxical role of dissolved molecular oxygen. *Atmo. Chem. Phys.* **2013,** *13*, 6473-6491.

16. Tinel, L.; Rossignol, S.; Ciuraru, R.; Dumas, S.; George, C. Photosensitized reactions initiated by 6-carboxypterin: Singlet and triplet reactivity. *Phys. Chem. Chem. Phys.* **2016,** *18*, 17105-17115.

17. Tinel, L.; Rossignol, S.; Bianco, A.; Passananti, M.; Perrier, S.; Wang, X.; Brigante, M.; Donaldson, D. J.; George, C. Mechanistic insights on the photosensitized chemistry of a fatty acid at the air/water interface. *Environ. Sci. Technol.* **2016,** *50*, 11041-11048.

18. Epstein, S. A.; Nizkorodov, S. A. A comparison of the chemical sinks of atmospheric organics in the gas and aqueous phase. *Atmo. Chem. Phys.* **2012,** *12*, 8205-8222.

19. Renard, P.; Reed Harris, A. E.; Rapf, R. J.; Rainer, S.; Demelas, C.; Coulomb, B.; Quivet, E.; Vaida, V.; Monod, A. Aqueous phase oligomerization of methyl vinyl ketone by atmospheric radical reactions. *J. Phys. Chem. C* **2014,** *118*, 29421-29430.

20. Lee, W.; Baasandorj, M.; Stevens, P. S.; Hites, R. A. Monitoring OH-initiated oxidation kinetics of isoprene and its products using online mass spectrometry. *Environ. Sci. Technol.* **2005,** *39*, 1030-1036.

21. Altieri, K. E.; Carlton, A. G.; Lim, H.-J.; Turpin, B. J.; Seitzinger, S. P. Evidence for oligomer formation in clouds: Reactions of isoprene oxidation products. *Environ. Sci. Technol.* **2006,** *40*, 4956-4960.

22. Ervens, B.; Carlton, A. G.; Turpin, B. J.; Altieri, K. E.; Kreidenweis, S. M.; Feingold, G. Secondary organic aerosol yields from cloud-processing of isoprene oxidation products. *Geophys. Res. Lett.* **2008,** *35*, L02816.

23. Carlton, A. G.; Turpin, B. J.; Lim, H.-J.; Altieri, K. E.; Seitzinger, S. Link between isoprene and secondary organic aerosol (SOA): Pyruvic acid oxidation yields low volatility organic acids in clouds. *Geophys. Res. Lett.* **2006,** *33*, L06822.

24. Carlton, A. G.; Wiedinmyer, C.; Kroll, J. H. A review of secondary organic aerosol (SOA) formation from isoprene. *Atmo. Chem. Phys.* **2009,** *9*, 4987-5005.

25. Ortiz-Montalvo, D. L.; Lim, Y. B.; Perri, M. J.; Seitzinger, S. P.; Turpin, B. J. Volatility and yield of glycolaldehyde SOA formed through aqueous photochemistry and droplet evaporation. *Aerosol Sci. Technol.* **2012,** *46*, 1002-1014.

26. Renard, P.; Siekmann, F.; Salque, G.; Demelas, C.; Coulomb, B.; Vassalo, L.; Ravier, S.; Temime-Roussel, B.; Voisin, D.; Monod, A. Aqueous-phase oligomerization of methyl vinyl ketone through photooxidation. Part 1: Aging processes of oligomers. *Atmo. Chem. Phys.* **2015,** *15*, 21-35.

27. Haddad, I. E.; Liu, Y.; Nieto-Gligorovski, L.; Michaud, V.; Temime-Roussel, B.; Quivet, E.; Marchand, N.; Sellegri, K.; Monod, A. In-cloud processes of methacrolein under simulated conditions. Part 2: Formation of secondary organic aerosol. *Atmo. Chem. Phys.* **2009,** *9*, 5107-5117.

28. Altieri, K.; Seitzinger, S.; Carlton, A.; Turpin, B.; Klein, G.; Marshall, A. Oligomers formed through in-cloud methylglyoxal reactions: Chemical composition, properties, and mechanisms investigated by ultra-high resolution FT-ICR mass spectrometry. *Atmos. Environ.* **2008,** *42*, 1476-1490.

29. Perri, M. J.; Seitzinger, S.; Turpin, B. J. Secondary organic aerosol production from aqueous photooxidation of glycolaldehyde: Laboratory experiments. *Atmos. Environ.* **2009,** *43*, 1487-1497.

30. Tan, Y.; Carlton, A. G.; Seitzinger, S. P.; Turpin, B. J. SOA from methylglyoxal in clouds and wet aerosols: Measurement and prediction of key products. *Atmos. Environ.* **2010,** *44*, 5218-5226.

31. Tan, Y.; Perri, M. J.; Seitzinger, S. P.; Turpin, B. J. Effects of precursor concentration and acidic sulfate in aqueous glyoxal–OH radical oxidation and implications for secondary organic aerosol. *Environ. Sci. Technol.* **2009,** *43*, 8105-8112.

32. Lim, Y. B.; Tan, Y.; Turpin, B. J. Chemical insights, explicit chemistry, and yields of secondary organic aerosol from OH radical oxidation of methylglyoxal and glyoxal in the aqueous phase. *Atmo. Chem. Phys.* **2013,** *13*, 8651-8667.

33. Donaldson, D.; Valsaraj, K. T. Adsorption and reaction of trace gas-phase organic compounds on atmospheric water film surfaces: A critical review. *Environ. Sci. Technol.* **2010,** *44*, 865-873.

34. Zhang, X.; Chen, Z.; Zhao, Y. Laboratory simulation for the aqueous OH-oxidation of methyl vinyl ketone and methacrolein: Significance to the in-cloud SOA production. *Atmo. Chem. Phys.* **2010,** *10*, 9551-9561.

35. Liu, Y.; Siekmann, F.; Renard, P.; Zein, A. E.; Salque, G.; Haddad, I. E.; Temime-Roussel, B.; Voisin, D.; Thissen, R.; Monod, A. Oligomer and SOA formation through aqueous phase photooxidation of methacrolein and methyl vinyl ketone. *Atmos. Environ.* **2012,** *49*, 123-129.

36. Chan, K. M.; Huang, D. D.; Li, Y. J.; Chan, M. N.; Seinfeld, J. H.; Chan, C. K. Oligomeric products and formation mechanisms from acid-catalyzed reactions of methyl vinyl ketone on acidic sulfate particles. *J. Atmos. Chem.* **2013,** *70*, 1-18.

37. Chang, X.-P.; Fang, Q.; Cui, G. Mechanistic photodecarboxylation of pyruvic acid: Excited-state proton transfer and three-state intersection. *J. Chem. Phys.* **2014,** *141*, 154311.

38. Guzman, M. I.; Hoffmann, M. R.; Colussi, A. J. Photolysis of pyruvic acid in ice: Possible relevance to CO and CO_2 ice core record anomalies. *J. Geophys. Res.* **2007,** *112*, D10123.

39. Davidson, R. S.; Goodwin, D.; De Violet, P. F. The mechanism of the photo-induced decarboxylation of pyruvic acid in solution. *Chem. Phys. Lett.* **1981,** *78*, 471-474.

40. Yamamoto, S.; Back, R. A. The photolysis and thermal decomposition of pyruvic acid in the gas phase. *Can. J. Chem.* **1985,** *63*, 549-554.

41. Vesley, G. F.; Leermakers, P. A. Photochemistry of alpha-keto acids and alpha-keto esters. 3. Photolysis of pyruvic acid in vapor phase. *J. Phys. Chem.* **1964,** *68*, 2364-2366.

42. Leermakers, P. A.; Vesley, G. F. Photolysis of pyruvic acid in solution. *J. Org. Chem.* **1963,** *28*, 1160-1161.

43. Guzman, M. I.; Colussi, A. J.; Hoffmann, M. R. Photoinduced oligomerization of aqueous pyruvic acid. *J. Phys. Chem. A* **2006,** *110*, 3619-3626.

44. Griffith, E. C.; Carpenter, B. K.; Shoemaker, R. K.; Vaida, V. Photochemistry of aqueous pyruvic acid. *Proc. Natl. Acad. Sci.* **2013,** *110*, 11714-11719.

45. Rapf, R. J.; Perkins, R. J.; Carpenter, B. K.; Vaida, V. Mechanistic description of photochemical oligomer formation from aqueous pyruvic acid. *J. Phys. Chem. A* **2017,** *121*, 4272–4282.

46. Reed Harris, A. E.; Ervens, B.; Shoemaker, R. K.; Kroll, J. A.; Rapf, R. J.; Griffith, E. C.; Monod, A.; Vaida, V. Photochemical kinetics of pyruvic acid in aqueous solution. *J. Phys. Chem. A* **2014,** *118*, 8505-8516.

47. Eugene, A. J.; Guzman, M. I. Reactivity of ketyl and acetyl radicals from direct solar actinic photolysis of aqueous pyruvic acid. *J. Phys. Chem. A* **2017,** *121*, 2924–2935.

48. Rapf, R. J.; Dooley, M. R.; Kappes, K.; Perkins, R. J.; Vaida, V. pH dependence of the aqueous photochemistry of α -keto acids *J. Phys. Chem. A* **2017**, DOI: 10.1021/acs.jpca.7b08192.

49. Cochran, R. E.; Laskina, O.; Jayarathne, T.; Laskin, A.; Laskin, J.; Lin, P.; Sultana, C.; Lee, C.; Moore, K. A.; Cappa, C. D. Analysis of organic anionic surfactants in fine and coarse fractions of freshly emitted sea spray aerosol. *Environ. Sci. Technol.* **2016,** *50*, 2477-2486.

50. Cochran, R. E.; Laskina, O.; Trueblood, J. V.; Estillore, A. D.; Morris, H. S.; Jayarathne, T.; Sultana, C. M.; Lee, C.; Lin, P.; Laskin, J., et al. Molecular diversity of sea spray aerosol particles: Impact of ocean biology on particle composition and hygroscopicity. *Chem* **2017,** *2*, 655-667.

51. Tervahattu, H.; Hartonen, K.; Kerminen, V. M.; Kupiainen, K.; Aarnio, P.; Koskentalo, T.; Tuck, A. F.; Vaida, V. New evidence of an organic layer on marine aerosols. *J. Geophys. Res.* **2002,** *107*, 4053-4060.

52. Tervahattu, H.; Juhanoja, J.; Vaida, V.; Tuck, A. F.; Niemi, J. V.; Kupiainen, K.; Kulmala, M.; Vehkamaki, H. Fatty acids on continental sulfate aerosol particles. *J. Geophys. Res.* **2005,** *110*, Article number D06207.

53. Gilman, J. B.; Eliason, T. L.; Fast, A.; Vaida, V. Selectivity and stability of organic films at the air-aqueous interface. *J. Colloid Interface Sci.* **2004,** *280*, 234-243.

54. Gilman, J. B.; Tervahattu, H.; Vaida, V. Interfacial properties of mixed films of long-chain organics at the air-water interface. *Atmos. Environ.* **2006,** *40*, 6606-6614.

55. Perkins, R. J.; Shoemaker, R. K.; Carpenter, B. K.; Vaida, V. Chemical equilibria and kinetics in aqueous solutions of zymonic acid. *J. Phys. Chem. A* **2016,** *120*, 10096-10107.

56. Closs, G. L.; Miller, R. J. Photo-reduction and photodecarboxylation of pyruvic acid - applications of CIDNP to mechanistic photochemistry. *J. Am. Chem. Soc.* **1978,** *100*, 3483-3494.

57. Rapf, R. J.; Perkins, R. J.; Yang, H.; Miyake, G. M.; Carpenter, B. K.; Vaida, V. Photochemical synthesis of oligomeric amphiphiles from alkyl oxoacids in aqueous environments. *J. Am. Chem. Soc.* **2017,** *139*, 6946–6959.

58. If not specified the terms “dimer” and “trimer” are used here to refer to covalently-bonded oligomeric species, rather than non-covalently associated species.

59. Rossignol, S.; Tinel, L.; Bianco, A.; Passananti, M.; Brigante, M.; Donaldson, D. J.; George, C. Atmospheric photochemistry at a fatty acid–coated air-water interface. *Science* **2016,** *353*, 699-702.

60. Brocks, J. J.; Beckhaus, H.-D.; Beckwith, A. L.; Rüchardt, C. Estimation of bond dissociation energies and radical stabilization energies by ESR spectroscopy. *J. Org. Chem.* **1998,** *63*, 1935-1943.

61. Ogata, Y.; Tomizawa, K.; Takagi, K. Photo-oxidation of formic, acetic, and propionic acids with aqueous hydrogen peroxide. *Can. J. Chem.* **1981,** *59*, 14-18.

62. Sun, W.; Yang, L.; Yu, L.; Saeys, M. Ab initio reaction path analysis for the initial hydrogen abstraction from organic acids by hydroxyl radicals. *J. Phys. Chem. A* **2009,** *113*, 7852-7860.

63. Alvarez-Idaboy, J. R.; Mora-Diez, N.; Boyd, R. J.; Vivier-Bunge, A. On the importance of prereactive complexes in molecule-radical reactions: Hydrogen abstraction from aldehydes by OH. *J. Am. Chem. Soc.* **2001,** *123*, 2018-2024.

64. Butkovskaya, N. I.; Kukui, A.; Pouvesle, N.; Le Bras, G. Rate constant and mechanism of the reaction of OH radicals with acetic acid in the temperature range of 229-300 K. *J. Phys. Chem. A* **2004,** *108*, 7021-7026.

65. Donaldson, D. J.; Vaida, V. The influence of organic films at the air-aqueous boundary on atmospheric processes. *Chem. Rev.* **2006,** *106*, 1445-1461.

66. Quinn, P. K.; Collins, D. B.; Grassian, V. H.; Prather, K. A.; Bates, T. S. Chemistry and related properties of freshly emitted sea spray aerosol. *Chem. Rev.* **2015,** *115*, 4383-4399.

67. Cochran, R. E.; Ryder, O. S.; Grassian, V. H.; Prather, K. A. Sea spray aerosol: The chemical link between the oceans, atmosphere, and climate. *Acc. Chem. Res.* **2017,** *50*, 599-604.

9. Photoinitiated Synthesis of Self-Assembled Vesicles*

9.1 Introduction:

The unique properties of aqueous solutions of aggregated amphiphiles have been a subject of considerable interest in a wide-range of fields.[2-5] In addition, enclosures are universally considered necessary for life.[6] The search for the emergence of such primitive cellular constructs in the origin of life on Earth requires the existence and/or synthesis of a prebiotically plausible membrane component (a surfactant), followed by self-assembly into a stable enclosed structure.[7] Although much work has been performed studying the properties of vesicles composed of various surfactants,[8-11] the synthesis of such self-assembled structures and their components under plausible prebiotic conditions has received much less attention. Here we show the photochemical synthesis of a double-tailed surfactant from a single-tailed one followed by spontaneous self-assembly into stable vesicles. The single-tailed surfactant utilized, 2-oxooctanoic acid (OOA, an 8-carbon α-keto acid), is a plausible prebiotic molecule: oxoacids and other molecules of similar chemical functionality have been found in meteoritic samples,[12, 13] and the short, 8-carbon chain of OOA is among the most prevalent length synthesized in the common Fischer-Tropsch type synthesis of lipids (C7 – C9 are most common).[14, 15] With no further perturbation of the reaction system, as the photochemistry proceeds, the products spontaneously self-assemble into stable vesicles. These vesicles were found to be monodisperse (200 nm in diameter), to be temporally (over several months) and thermally (between at least 4 – 22 °C) stable, and to persist in the presence of $MgCl_2$ salt. This work provides a potential photochemical route for the synthesis of membrane components and a stable primitive enclosure under

* This work was reproduced in part with permission from Griffith, E.C.; Rapf, R.J.; Shoemaker, R.K.; Carpenter, B.K.; Vaida, V. Photoinitiated synthesis of self-assembled vesicles. *Journal of the American Chemical Society*, 136: 3784-3787, 2014. Copyright 2014 American Chemical Society.[1]

prebiotically relevant conditions, and contributes to understanding the evolution of primitive membrane structures.

9.2 Materials and Methods:

OOA (≥99%) was obtained from Sigma-Aldrich and was used without further purification. A 6 mM aqueous solution of OOA was prepared in DI water and sonicated until dissolved, followed by filtration through a 0.1 μm syringe filter to remove any dust or other particulates prior to photolysis. The final solution was then photolyzed, unstirred, using a 450-W Xe arc lamp (Newport) for 5 hours while kept at a constant temperature of 4 °C in a temperature-controlled water bath. The Xe arc lamp is used here as a solar simulator due to its significant overlap with the solar spectrum (wavelength output ~ 200 - 2500 nm, corresponding to a color temperature of ~5800K). The electronic spectrum of aqueous OOA was obtained using a USB2000 miniature fiber optic UV-visible spectrometer from Ocean Optics.

Following photolysis, the reaction products were detected using ESI-TOF mass spectrometry. The self-assembled vesicles were stained with 10 μM Rhodamine 6G (BioReagent, Sigma) and visualized by fluorescence microscopy (Nikon A1R confocal microscope). The size of vesicles in solution was determined by dynamic light scattering (DLS, DynaPro Titan, Wyatt Technology) after 10-fold dilution at 20 °C. Microscope images of the diluted sample were also obtained to ensure that no change occurred to the vesicles themselves with dilution. It is important to note that these vesicles are quite small and diffuse quickly. Thus, when imaging using the fluorescence microscope, they are diffusing in and out of focus while the image is being obtained. Sometimes this causes them to appear diverse in size with some appearing much larger than the reported diameter using DLS. However, this is a limitation of the fluorescence microscope technique, and the DLS data indicates that these vesicles are indeed monodisperse with a diameter of ~200 nm.

High resolution 2D-DOSY NMR was performed on a Varian INOVA 500-MHz NMR spectrometer operating at 499.60 MHz for ^{1}H observation using WET[16] suppression of the H_2O resonance, combined with the convection and non-uniform-gradient compensated stimulated PFG echo pulse sequence that is available in the VNMRJ 3.2A instrument (Agilent Technologies, Inc.). The data analysis was performed using the VNMRJ software, including non-uniform gradient compensation, and multi-component fitting of the DOSY decay curves.[17, 18]

For surface-activity analysis, the pre- and post-photolysis solutions were identically extracted with chloroform to separate out the hydrophobic components. The chloroform solutions then sat overnight to allow for evaporation of the solvent, and were subsequently re-solvated in a small amount of chloroform for deposition on the Langmuir trough. 100μl of the chloroform extract (either before or after photolysis) was deposited dropwise on an aqueous subphase on the Langmuir trough. After allowing 15 minutes for chloroform evaporation, π – A isotherms were recorded (barrier speed constant at 75 cm^2/min).

Surface pressure – area (π – A) isotherms were obtained using a custom built PTFE Langmuir trough (52 x 7 x 0.5 cm) with computer-controlled, PTFE mechanical barriers allowing for control of surface area (A), coupled with a Wilhelmy balance (KSV-NIMA, Biolin Scientific) to measure surface pressure (π). The π – A isotherm yields surface thermodynamic information and is used here as an indication of surfactant hydrophobicity through a measure of its surface activity.

9.3 Results and Discussion:

OOA first absorbs light through its carbonyl chromophore with an absorption maximum of ~320 nm (Figure 9.1). OOA has the same reactive functionality as pyruvic acid and follows the same general photochemical mechanism.[19-21] This generates organic radical species that can recombine to form oligomeric products, including, notably, dihexyltartaric

acid (DHTA). Figure 9.2 outlines the photochemical mechanism that results in the production DHTA (Figure 9.2A) as well as its detection by mass spectrometry (Figure 9.2B).

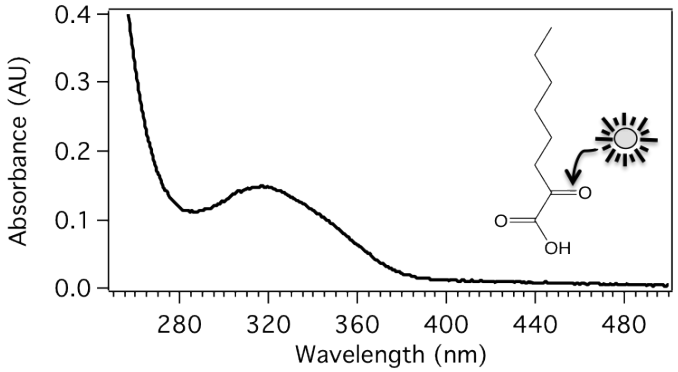

Figure 9.1. Electronic absorption spectrum of 6 mM OOA in water with inset illustrating absorption of light by the carbonyl chromophore.

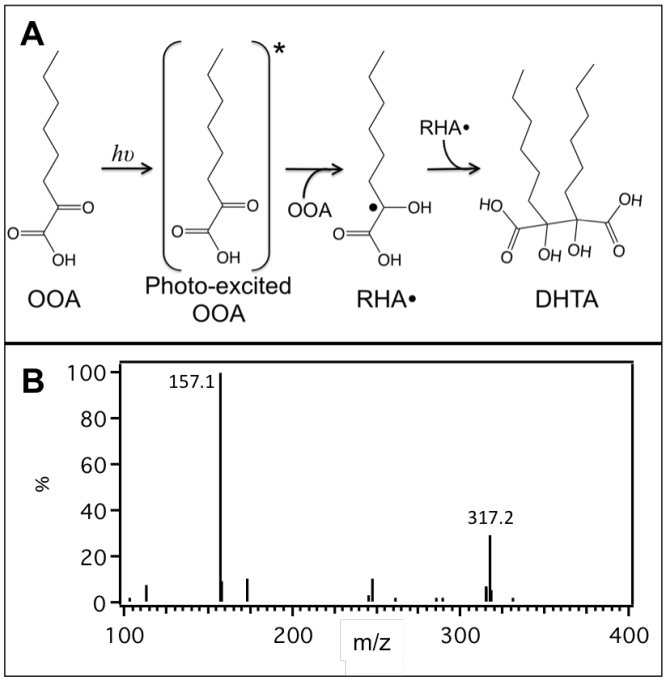

Figure 9.2. (A) Photochemical reaction mechanism of single-tailed OOA to produce the double-tailed DHTA, (B) Mass spectrum of photolysis products with peaks due to DHTA (317.2 m/z) and unreacted OOA (157.1 m/z) indicated.

The products of photolysis, when extracted into chloroform, were observed to be more surface active than the precursor solution of OOA using Langmuir trough methods (Figure 9.3), confirming the greater hydrophobicity of the photolysis products. In addition to the double-tailed dimer DHTA, another dimer product was detected at 247.1 m/z in the mass

spectrum. This product is formed through a Norrish Type II photochemical reaction mechanism, but remains as a single-tailed surfactant with similar hydrophobicity to OOA and is thus not discussed further in detail here.

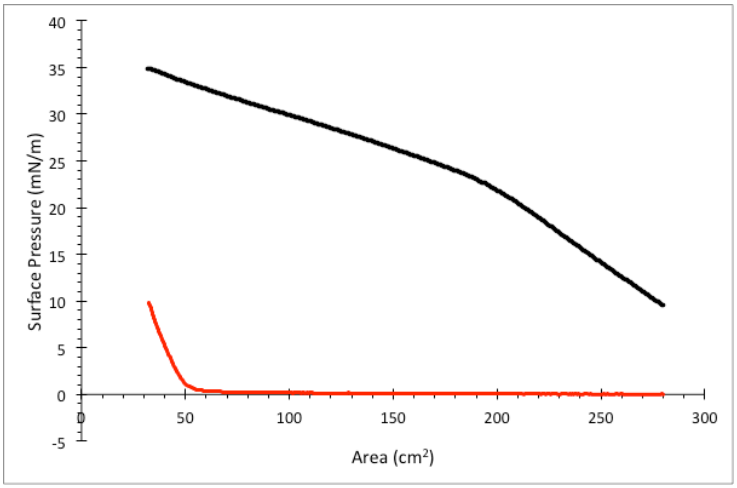

Figure 9.3. π – A isotherms of chloroform extract before photolysis (red) and after 8 hours of photolysis (black), illustrating greater surface activity of photolysis products.

Prior to exposure to light, the OOA solution is clear and devoid of detectable particles (image on left in Figure 9.4A), as determined using fluorescence microscopy and DLS. Although the critical bilayer concentration (CBC) of OOA is not known, similar surfactants have CBCs greater than 100 mM,[22] and thus vesicles are not expected, and indeed were not observed, at the low concentration of 6 mM used in this work. Over the course of photolysis, however, the solution becomes opalescent (image on right in Figure 9.4A) indicating the presence of particulates in solution. These particles were observed microscopically using both phase contrast microscopy (Figure 9.5) and fluorescence microscopy after staining with the membrane stain Rhodamine 6G (Figure 9.4B), appearing to be spherical. Further, they were determined to be monodisperse with a narrow size distribution centered around 200 nm in diameter using DLS (Figure 9.4C). These particles were stable in solution for several months, over the temperature range of 4 – 22°C, and in the presence of $MgCl_2$ salt (Figure 9.6). At 200 nm in diameter, they are too large to be micelles, and their long-term stability

in solution as well as their apparent spherical shape suggests that disordered aggregates of monomers are unlikely.

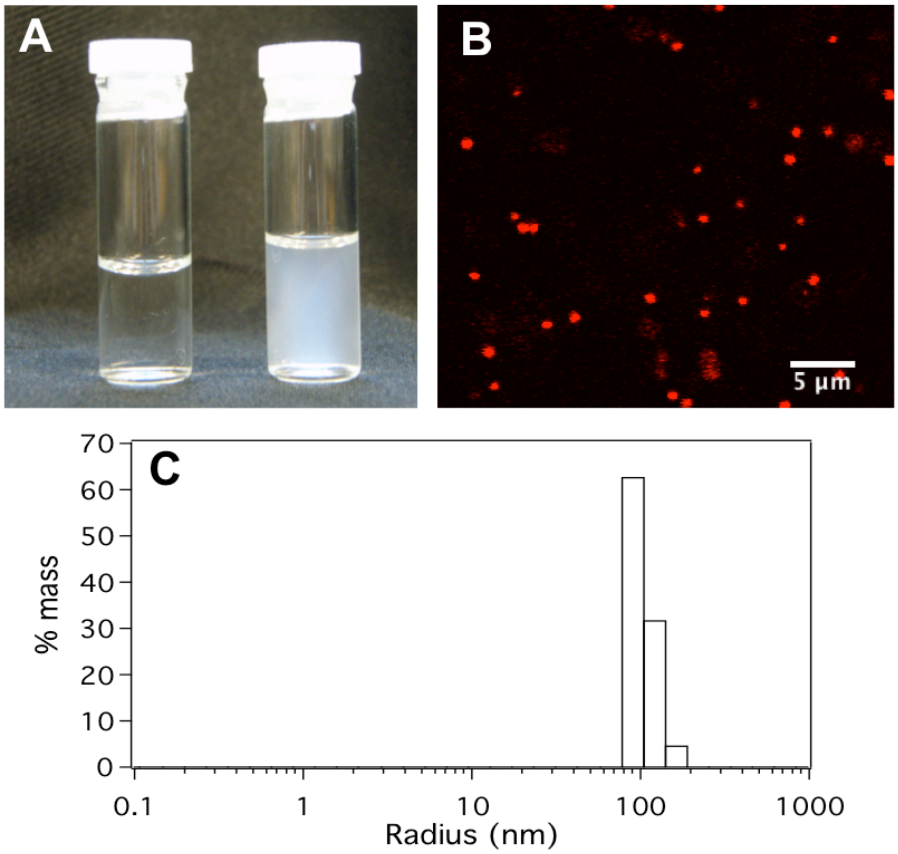

Figure 9.4. Characterization of self-assembled vesicles. (A) Photograph of clear OOA solution before photolysis (left) and opalescent solution after photolysis (right), (B) Fluorescence microscope image of vesicles stained with Rhodamine 6G, (C) Dynamic light scattering of vesicles formed illustrating mean radius of ~100 nm.

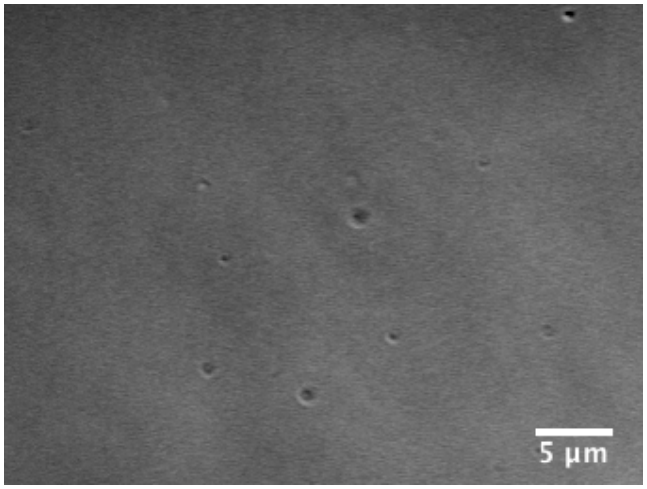

Figure 9.5. Phase contrast microscope image of unstained OOA solution after 5 hours of photolysis illustrating existence of particles in the absence of Rhodamine 6G stain.

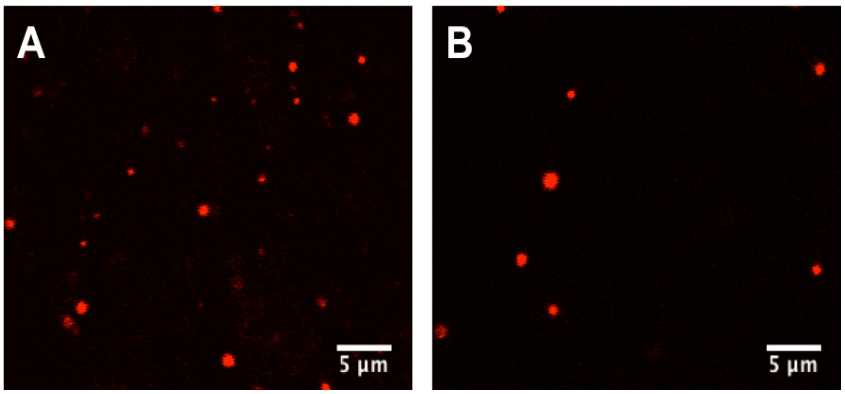

Figure 9.6. Indication of stability of self-assembled vesicles. Fluorescence microscope images of (A) stained vesicles after 5 weeks at 4 °C and (B) in the presence of 16 mM $MgCl_2$.

In addition, the Diffusion Ordered Spectroscopy (DOSY) NMR (Figure 9.7) spectrum detects these particulates as being much larger than any monomers in solution and to be very slowly diffusing (Figure 9.7A), yielding a diffusion coefficient of 4 x 10^{-8} cm^2/s, consistent with the value of 3 x 10^{-8} cm^2/s determined by DLS. This is in contrast to the measured diffusion coefficient of the aqueous free monomer (OOA), measured by DOSY NMR to be 7 x 10^{-6} cm^2/s. When looking at the decay of the NMR signal with gradient strength (Figure 9.7B), it is also apparent that the signals due to the hydrocarbon chain protons specifically near the ends of the tails exhibit a two-component decay profile: one short decay with sharp signals sitting atop broadened signals with a very long decay. This is indicative of two types of environments present in solution, one of monomers and one of similar molecules with confined motion. Additional information about the confined molecules can be obtained by noting the absence in signal from the protons closest to the polar head-groups at large gradient strength. This is common in lipid vesicles,[23] where the NMR signals from the protons on the rigid head groups are broadened due to dipolar relaxation, while the signals from the more flexible tails exhibit less dipolar broadening and are thusly easier to detect. Therefore, taken together with the size, monodispersity, and stability, this data indicates that the particulates detected in solution are ordered structures consistent with self-assembled vesicles.

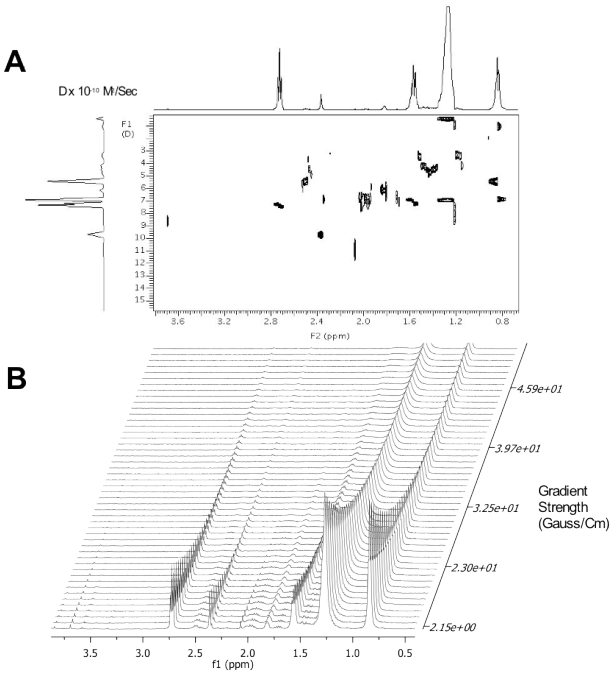

Figure 9.7. DOSY NMR illustrating the diffusion coefficients observed in the mixture of photolysis products, including the superposition of decay profiles for rapidly and slowly diffusion components, in the 0.5-1.5 ppm range of the NMR spectrum. (A) Full DOSY plot. (B) Decay of NMR signal with increase in gradient strength.

This chapter illustrates the advantageous environment provided by the water surface region. OOA, as a soluble surfactant, partitions significantly to the water surface (Figure 9.8), resulting in an inhomogeneous distribution of OOA molecules in solution. The surface excess concentration of OOA allows for a local concentration that is greater than the nominal bulk concentration of 6 mM. This increases the probability of contact between reactive species, thereby increasing the reaction yield. In addition, it allows for orientation of the hydrocarbon tail of OOA, resulting in a greater propensity to undergo the photochemical reaction mechanism illustrated in Figure 9.2A forming the DHTA, rather than the Norrish type II reaction resulting in a single-tailed dimer. The Norrish type II reaction necessitates more motion of the hydrocarbon tail, allowing it to fold over on itself, a situation requiring a more dilute solute environment (less likely in the surface region). Water surfaces, such as those found on oceans, lakes, and atmospheric aerosol particles,

have been implicated as unique prebiotic reaction environments previously.[24-31] Here, we add an additional example of the advantageous environment provided by the water surface for chemistry.

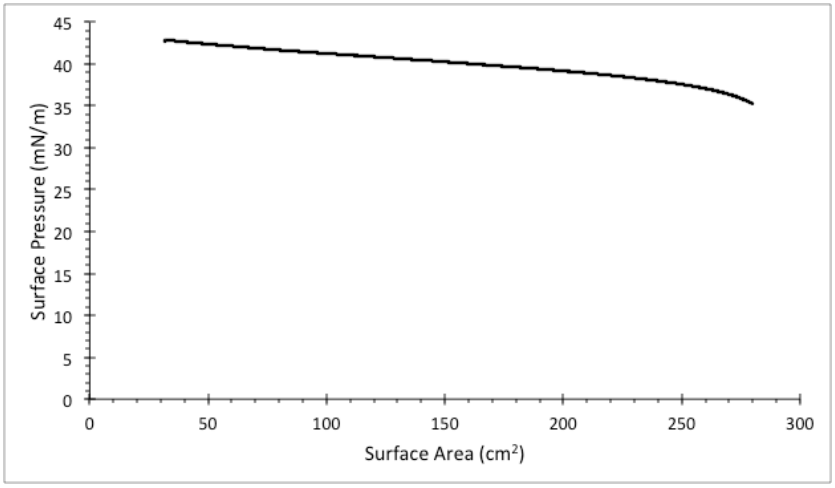

Figure 9.8: *π – A isotherm of aqueous OOA (6mM) illustrating significant surface partitioning in bulk aqueous solution, indicated by the increased surface pressure even at large molecular areas prior to surface compression.*

Thus far, simple vesicles (enclosures) composed of fatty acids have been used as a model system for primitive cellular constructs; they have the ability to mimic many functions of modern life and their monomers (fatty acids) are plausible components on early Earth.[6-9, 11, 14, 32, 33] However, such protocells are unlikely to have been the first enclosures due to the very specific environmental constraints put on their synthesis and stability (requisite pH, high concentration, intolerance of vesicles to salts).[34, 35] Modern cells are enclosed in a membrane composed of primarily double-tailed surfactants having none of the constraints put on fatty acid vesicles, however their prebiotic synthesis is often thought to be too difficult due to their chemical complexity.[22] Here we provide an alternative, sunlight-driven route to primitive enclosures in addition to what has been traditionally considered. Beginning with a dilute solution of a short single-chained soluble surfactant, well below its CBC, simulated sunlight prompts synthesis of a double-tailed surfactant followed by self-assembly without external perturbation. No complicated synthetic steps or preparations are

required nor are high concentrations of surfactant. In addition, the resultant vesicles are stable over time and persist in the presence of Mg^{2+} ions, a likely component of the early ocean.[36] In contrast, the more common models of fatty acid vesicles are unstable in the presence of divalent cations.[35]

Regardless as to whether or not the first enclosures were composed of single-tailed surfactants, a transition is needed at some point in molecular evolutionary history to membrane constituents with a double-tailed structure, as they are prevalent throughout modern biology. Once mixed membranes composed of both single and double-tailed surfactants are facilitated, even with minimal double-tailed surfactant, unique competition and subsequent evolution has been seen to emerge.[37] The present study illustrates a simple, prebiotically plausible transition from single-tailed to double-tailed surfactants using only the energy provided by the early sun. Therefore, the work presented here provides a possible route to the prebiotic synthesis of a simple enclosure as well as a potential contribution to primitive membrane evolution.

9.4 Bibliography:

1. Griffith, E. C.; Rapf, R. J.; Shoemaker, R. K.; Carpenter, B. K.; Vaida, V. Photoinitiated synthesis of self-assembled vesicles. *J. Am. Chem. Soc.* **2014,** *136*, 3784-3787.

2. Menger, F. M.; Shi, L.; Rizvi, S. A. A. Self-assembling systems: Mining a rich vein. *J. Colloid Interface Sci.* **2010,** *344*, 241-246.

3. Maibaum, L.; Dinner, A. R.; Chandler, D. Micelle formation and the hydrophobic effect. *J. Phys. Chem. B* **2004,** *108*, 6778-6781.

4. Whitelam, S.; Rogers, C.; Pasqua, A.; Paavola, C.; Trent, J.; Geissler, P. L. The impact of conformational fluctuations on self-assembly: Cooperative aggregation of archaeal chaperonin proteins. *Nano Lett.* **2009,** *9*, 292-297.

5. Lee, O.-S.; Cho, V.; Schatz, G. C. Modeling the self-assembly of peptide amphiphiles into fibers using coarse-grained molecular dynamics. *Nano Lett.* **2012,** *12*, 4907-4913.

6. Szostak, J. W.; Bartel, D. P.; Luisi, P. L. Synthesizing life. *Nature* **2001,** *409*, 387-390.

7. Pohorille, A.; Deamer, D. Self-assembly and function of primitive cell membranes. *Res. Microbiol.* **2009,** *160*, 449-456.

8. Hanczyc, M. M.; Fujikawa, S. M.; Szostak, J. W. Experimental models of primitive cellular compartments: Encapsulation, growth, and division. *Science* **2003,** *302*, 618-622.

9. Luisi, P. L.; Walde, P.; Oberholzer, T. Lipid vesicles as possible intermediates in the origin of life. *Curr. Opin. Colloid Interface Sci.* **1999,** *4*, 33-39.

10. Apel, C. L.; Deamer, D. W.; Mautner, M. N. Self-assembled vesicles of monocarboxylic acids and alcohols: Conditions for stability and for the encapsulation of biopolymers. *Biochim. Biophys. Acta-Biomembranes* **2002,** *1559*, 1-9.

11. Mansy, S. S. Membrane transport in primitive cells. *Cold Spring Harbor Persp. Biol.* **2010,** *2*, 14.

12. Cooper, G.; Reed, C.; Nguyen, D.; Carter, M.; Wang, Y. Detection and formation scenario of citric acid, pyruvic acid, and other possible metabolism precursors in carbonaceous meteorites. *Proc. Natl. Acad. Sci.* **2011,** *108*, 14015-14020.

13. Pizzarello, S. Prebiotic chemical evolution: A meteoritic perspective. *Rend. Lincei.* **2011,** *22*, 153-163.

14. McCollom, T. M.; Ritter, G.; Simoneit, B. R. Lipid synthesis under hydrothermal conditions by Fischer-Tropsch-type reactions. *Origins Life Evol. Biosphere* **1999,** *29*, 153-166.

15. Rushdi, A. I.; Simoneit, B. R. T. Lipid formation by aqueous Fischer-Tropsch-Type synthesis over a temperature range of 100 to 400 °C. *Origins Life Evol. Biosphere* **2001,** *31*, 103-118.

16. Ogg, R. J.; Kingsley, R.; Taylor, J. S. WET, a T 1-and B 1-insensitive water-suppression method for in vivo localized ^{1}H NMR spectroscopy. *Journal of Magnetic Resonance, Series B* **1994,** *104*, 1-10.

17. Nilsson, M.; Morris, G. A. Improved DECRA processing of DOSY data: Correcting for non-uniform field gradients. *Magn. Reson. Chem.* **2007,** *45*, 656-660.

18. Nilsson, M.; Connell, M. A.; Davis, A. L.; Morris, G. A. Biexponential fitting of diffusion-ordered NMR data: Practicalities and limitations. *Anal. Chem.* **2006,** *78*, 3040-3045.

19. Griffith, E. C.; Carpenter, B. K.; Shoemaker, R. K.; Vaida, V. Photochemistry of aqueous pyruvic acid. *Proc. Natl. Acad. Sci.* **2013,** *110*, 11714-11719.

20. Guzman, M. I.; Colussi, A. J.; Hoffmann, M. R. Photoinduced oligomerization of aqueous pyruvic acid. *J. Phys. Chem. A* **2006,** *110*, 3619-3626.

21. Leermakers, P. A.; Vesley, G. F. Photochemistry of alpha-keto acids and alpha-keto esters. 1. Photolysis of pyruvic acid and benzoylformic acid. *J. Am. Chem. Soc.* **1963,** *85*, 3776-3779.

22. Monnard, P. A.; Deamer, D. W. Membrane self-assembly processes: Steps toward the first cellular life. *Anat. Rec.* **2002,** *268*, 196-207.

23. Veatch, S. L.; Polozov, I. V.; Gawrisch, K.; Keller, S. L. Liquid domains in vesicles investigated by NMR and fluorescence microscopy. *Biophys. J.* **2004,** *86*, 2910-2922.

24. Griffith, E. C.; Tuck, A. F.; Vaida, V. Ocean-atmosphere interactions in the emergence of complexity in simple chemical systems. *Acc. Chem. Res.* **2012,** *45*, 2106-2113.

25. Griffith, E. C.; Vaida, V. In situ observation of peptide bond formation at the water-air interface. *Proc. Natl. Acad. Sci.* **2012,** *109*, 15697-15701.

26. Dobson, C. M.; Ellison, G. B.; Tuck, A. F.; Vaida, V. Atmospheric aerosols as prebiotic chemical reactors. *Proc. Natl. Acad. Sci.* **2000,** *97*, 11864-11868.

27. Tverdislov, V. A.; Yakovenko, L. V. Physical aspects of the emergence of living cell precursors: The ion and chiral asymmetries as two fundamental asymmetry types. *Moscow Univ. Phys. Bull.* **2008,** *63*, 151-163.

28. Lerman, L., The primordial bubble: Water, symmetry-breaking, and the origin of life. In *Water and life: The unique properties of water*, Lynden-Bell, R. M.; Morris, S. C.; Barrow, J. D.; Finney, J. L.; Harper Jr., C. L., Eds. CRC Press: Boca Raton, FL, 2010; pp 259 - 290.

29. Tuck, A. The role of atmospheric aerosols in the origin of life. *Surv. Geophys.* **2002,** *23*, 379-409.

30. Goldacre, R. J., Surface films, their collapse on compression, the shape and size of cells and the origin of life. In *Surface phenomena in chemistry and biology*, Danielli, J. F.; Parkhurst, K. G. A.; Riddiford, A. C., Eds. Pergamon Press: New York, 1958; pp 12 - 27.

31. Fallah-Araghi, A.; Meguellati, K.; Baret, J.-C.; El Harrak, A.; Mangeat, T.; Karplus, M.; Ladame, S.; Marques, C. M.; Griffiths, A. D. Enhanced chemical synthesis at soft interfaces: A universal reaction-adsorption mechanism in microcompartments. *Phys. Rev. Lett.* **2014,** *112*.

32. Chen, I. A.; Roberts, R. W.; Szostak, J. W. The emergence of competition between model protocells. *Science* **2004,** *305*, 1474-1476.

33. Stano, P.; D'Aguanno, E.; Bolz, J.; Fahr, A.; Luisi, P. L. A remarkable self-organization process as the origin of primitive functional cells. *Angew. Chem. Int. Ed.* **2013,** *52*, 13397-13400.

34. Morigaki, K.; Walde, P. Fatty acid vesicles. *Curr. Opin. Colloid Interface Sci.* **2007,** *12*, 75-80.

35. Monnard, P. A.; Apel, C. L.; Kanavarioti, A.; Deamer, D. W. Influence of ionic inorganic solutes on self-assembly and polymerization processes related to early forms of life: Implications for a prebiotic aqueous medium. *Astrobio.* **2002,** *2*, 139-152.

36. Anbar, A. D. Oceans elements and evolution. *Science* **2008,** *322* 1481-1483.

37. Budin, I.; Szostak, J. W. Physical effects underlying the transition from primitive to modern cell membranes. *Proc. Natl. Acad. Sci.* **2011,** *108*, 5249-5254.

10. *In Situ* Characterization of Photochemical Aggregate Formation from Alkyl α-Keto Acids

10.1 Introduction:

The photolysis of alkyl α-keto acids is characterized by the formation of aggregates. These aggregates self-assemble during the course of photolysis without any external perturbation to the system. As described in Chapters 5 and 9, the nature of these aggregates has been examined using optical microscopy and dynamic light scattering (DLS) of post-photolysis solutions. From these measurements, it is clear that the aggregates formed are spherical, relatively monodisperse in size, and have an average radius of approximately ~80-100 nm. These particles also appear to be extremely temporally stable in aqueous solution, persisting without obvious coagulation or phase separation in solution for years. Indeed, samples from July 2013 are largely unchanged more than four years after photolysis. Given these characteristics, it was initially concluded that these aggregates were likely to be vesicles (Chapter 9).[1] However, attempts to confirm this identification via other techniques, including dye encapsulation, differential scanning calorimetry, centrifugation, and resuspension, were largely inconclusive. Details of these attempted experiments are given in Appendix B. Here, using time-resolved dynamic light scattering and electron microscopy, we report in more detail on the nature and kinetics of the self-assembly process and the nature of the aggregates formed during photolysis.

The formation of aggregates and the mechanism of their self-assembly is a hugely important topic for a vast array of different fields, including biomedical drug delivery applications, biophysics, and materials science, as well as the study of origins of life and emergence of the first membranous enclosures.[2-5] Three-dimensional aggregates can take many forms, from micelles and vesicles to coacervates and colloidal suspensions.

Aggregates in aqueous solution are often composed of amphiphiles, or molecules with both a hydrophobic tail and a hydrophilic head group. When interactions between the amphiphile molecules are more favorable than interactions with the solvent, aggregation occurs. The details governing the self-assembly of species into aggregates varies depending on the molecular system in question. As discussed in Chapter 12, even the aggregation behavior of simple fatty acids is governed by complex interactions with solvent and salts that are still not fully understood.

Broadly speaking, however, two major regimes of self-assembly exist. In the first, aggregation occurs gradually, stepping up in size before the final aggregate size is reached. This can occur either by the incremental addition of molecules to each other, growing from small molecular to larger microscopic aggregates, as often occurs in the formation of small clusters[6, 7] or aerosol particles.[8] Another example of incremental growth is the much-discussed micelle to vesicle transition, where molecules first aggregate into smaller micelles before the transition to vesicles can occur.[9, 10] The second regime of self-assembly is more abrupt and a critical concentration of molecules in solution must be reached before aggregation occurs. Once this so-called critical aggregation concentration (CAC) is reached, the solution rapidly transitions from containing soluble species to particles. This second regime of assembly is commonly observed in the formation of micelles and vesicles from lipids,[2, 11-13] as well as in the formation of some colloids.[5] Although, it is important to note, as outlined in Appendix A, there are some indications that there may be some crossover between these two regimes of self-assembly, as preliminary evidence suggests that simple lipids may diffuse as dimers in solution when at concentrations below the bulk CAC. Nevertheless, when considering aggregation it is important to determine which of these two types of self-assembly is the dominant process to better understand the structures formed.

The aggregates formed from alkyl α-keto acids in our experiments are generated

photochemically. While it has been reported in the literature that the precursors, 2-oxooctanoic acid (OOA), is capable of forming vesicles in a similar manner to fatty acids,[14, 15] we have not previously seen evidence for their formation.[1, 16] Rather, we begin with a sample containing no aggregates that are detectable by either optical microscopy or DLS and then aggregates are formed during the course of photolysis. As photolysis proceeds, the single-tailed OOA reacts to form multi-tailed oligomeric products.[1, 16] These products are significantly more surface-active than the starting material[1] and, therefore, likely to self-assemble more readily than the precursors.[17] While the exact composition of the generated aggregates has not been determined, it seems highly likely that the multi-tailed photoproducts are the major components; although, it also seems reasonable that some OOA would also be incorporated.

It is difficult to determine *a priori* the more likely method of self-assembly for this system. Preliminary DOSY results suggest that the precursor α-keto acids may diffuse as dimers or small clusters in solution (Appendix A), which suggests that incremental growth may be likely. However, the ordered nature and apparent monodispersity of the formed aggregates points to a distinct change of phase. Luckily, this system is in many ways perfectly designed to test this question, as the concentration of multi-tailed species is slowly increased as photolysis proceeds, essentially resulting in a titration of these species into the solution. In this way, by monitoring the solution with DLS during photolysis, we are able to monitor the formation of aggregates *in situ* and in real time. This, combined with electron microscopy, allows us to gain key new insights into the formation and nature of the resultant aggregates.

10.2 Experimental Section:

All *in situ*, time-resolved dynamic light scattering (DLS) measurements were designed and conducted at Lawrence Berkeley National Lab in Dr. Kevin Wilson's lab. I conducted

all experiments at LBL in collaboration with Dr. James Davies. Additional control experiments and electron microscopy measurements were performed at CU Boulder.

10.2.1 Time-Resolved Dynamic Light Scattering:

2-oxooctanoic acid (OOA, ≥99.0%, Sigma-Aldrich) was diluted in 18.2 MΩ water to a final concentration of 5 mM and sonicated until fully dissolved. Solutions were filtered before use with a 0.1 μM syringe filter (MillexVV). These filtered solutions were then placed into a standard quartz cuvette (~4 mL) and capped.

This solution was then photolyzed using an Energetiq EQ-99 Laser-Driven Light Source (LDLS) equipped with a UV330 Filter (Edmund Optics). This filter allows UV light from ~230 nm to ~400 nm through but removes visible light from ~400 nm to ~660 nm, as well as any higher energy UV light. The cuvette was illuminated in roughly the vertical center using slightly focused light from the LDLS with a spot size roughly the diameter of the cuvette (~1 cm).

The formation of aggregates in the experimental solutions was monitored by observing the light scattering from either a 532 nm or 632 nm laser at 90° to the illumination via a PMT detector equipped with a line pass filter of appropriate wavelength to ensure only scattering from the laser light was detected. This detector was connected to an ALV-6010 / 200 Multiple Tau Digital Correlator, and its software was used to extract scattering information, including counts and auto-correlation functions. More details of this experimental apparatus, including a schematic, are given in Chapter 3.7.1.

The LDLS has a much lower photon flux than the 450 W Xe arc lamp used for photochemistry in Boulder. As a result, the rate of reaction was significantly slower. Full photochemical experiments were conducted on the order of ~20 hours and scattering measurements of 30 seconds duration were obtained in duplicate every 10 minutes.

Additional experiments were conducted for ~5 hours taking 5 measurements every 10 minutes to obtain higher resolution for the behavior of the system over early time scales.

Using a Python script adapted from Dr. James Davies, experimental auto-correlation functions were normalized and, using the built-in SciPy function curve_fit, were fit to a single exponential of the form,

$$C = e^{-2\Gamma\tau},$$

where τ is the delay time and Γ is the decay constant. Γ can be directly related to the diffusion constant, D, of any aggregates in solution,

$$\Gamma = Dq^2 = D\left(\frac{4\pi n}{\lambda}\sin\frac{\Theta}{2}\right)^2,$$

where n is the refractive index of the solution, λ is the wavelength of the laser, and θ is the scattering angle. The diffusion constant can then be related to the radius of the particle, R, using the Stokes-Einstein equation,

$$D = \frac{k_B T}{6\pi\eta R},$$

where η is the solvent viscosity and T is the temperature of the solution. In this manner, experimental auto-correlation functions at each time-point were fit with a single-adjustable parameter, particle radius, R, and error in radius is reported as the standard deviation of the fit.

10.2.2 Electron Microscopy:

Photochemical experiments at CU Boulder were conducted in the same manner as described in Rapf et al. 2017,[16] using 100 mL solutions of 6 mM OOA that were sparged with N_2 and photolyzed for 5 hours at 4 °C using an unfiltered 450 W Xe arc lamp (Newport). High-resolution electrospray ionization mass spectrometry (ESI^- MS), of post-photolysis solutions from illumination with the unfiltered 450 W XE lamp were compared with those from the filtered LDLS and no significant differences in photoproducts were observed.

Pre- and post-photolysis solutions were analyzed using both negative-staining and cryogenic transmission electron microscopy (TEM). Negative-staining TEM was conducted using samples at their natural concentration. For cyro-TEM, it was necessary to concentrate the solutions via rotary evaporation to approximately 6x the photolysis concentration in order to obtain enough aggregates per grid for analysis. Both pre- and post-photolysis solutions were concentrated to allow for comparison. The parameters used for both negative-staining and cryo-TEM measurements are given in Chapter 3.6.2.

10.3 Results and Discussion:

Previous analysis of the aggregates formed during the photolysis of OOA has relied primarily on the comparison of pre- and post-photolysis solutions, which cannot reveal the nature of the self-assembly. In the experimental set-up in Boulder, photolyses are conducted with a 450 W Xe arc lamp and samples are illuminated for 5 hours. Visually, solutions of OOA appear cloudy after 3 hours of photolysis, and UV-vis spectroscopy of aliquots taken during photolysis show scattering following one hour of photolysis. However, these coarse-grained attempts at understanding the kinetics of this assembly again cannot answer whether the aggregates are formed by incremental growth or by an abrupt change in phase. Instead we turn to time-resolved DLS measurements taken *in situ* during photolysis described below to answer this question.

Using a similar experimental set-up and a similar filter (FUV11M, Thorlabs), to that used in the DLS measurements at LBL, UV-vis spectroscopy suggests that ~5.5 hours of photolysis with the filtered LDLS corresponds to ~3 hours of photolysis using the unfiltered 450 W Xe arc lamp (Figure 10.1). Interestingly, the LDLS appears to slow the kinetics of the reaction sufficiently that a slight decrease in the absorption of OOA (λ_{max} ~ 315 nm) can be observed before being obscured by scattering. The observed behavior closely matches the known changes in pyruvic acid's absorption spectrum upon photolysis.[18, 19]

The starting solutions of 5 and 6 mM OOA prior to photolysis do not contain aggregates that are observable to the DLS. This is in contrast to the recent reports by Xu et al. that OOA in similar concentrations can form polydisperse vesicles (~30-200 nm with some at 500 nm diameter).[14, 15] The reported CVC for OOA is ~1.4 mM;[14] however, this is a very low CVC for a single-tailed lipid with a 6-carbon alkyl tail,[13] and there appears to be some confusion as the solubility limit of OOA is given as ~28 mM in the same report.[14] Clearly, the system cannot both be soluble at 28 mM while also forming vesicles at ~1 mM. We suggest that the likely solubility limit and critical aggregation concentration lay between these two values.

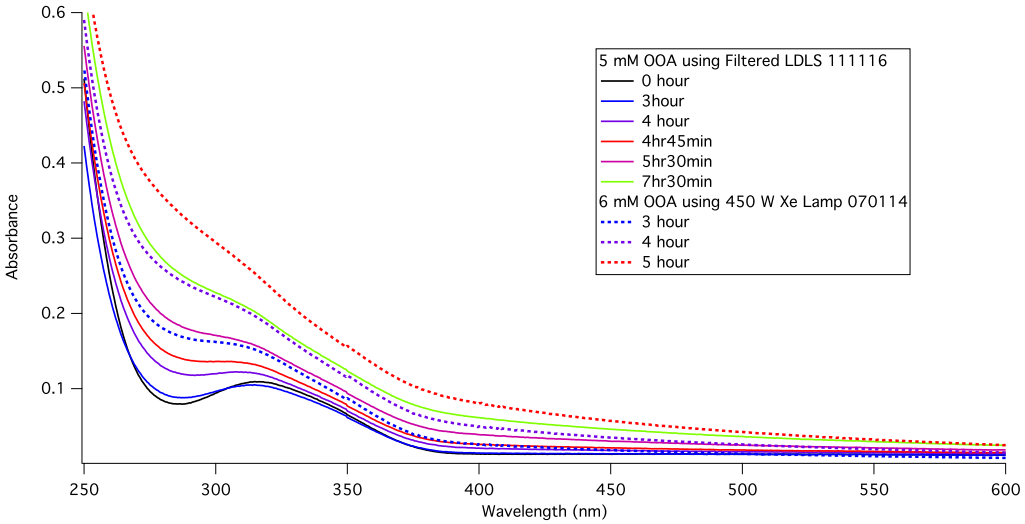

Figure 10.1. UV-vis absorbance spectra of OOA over the course of photolysis using a filtered LDLS (solid) or unfiltered 450 W Xe arc lamp (dashed).

Interestingly, however, Xu et al. suggest that the vesicles formed from OOA may be generated from dimers of OOA held together by intermolecular force.[14] Here, it is important to note that these dimers are not the same as the covalently-bonded multi-tailed oligomers generated by photochemistry, e.g. dihexyltartaric acid, but rather two OOA molecules held together by either Van der Waals or hydrogen bonding interactions. This supposition would be consistent with the preliminary evidence seen via DOSY NMR that the similar α-keto acids may be diffusing as dimers in solution, as discussed in Appendix A.

While it is certainly possible that small clusters, such as these dimers are present in solution, we observe no evidence for the formation of larger aggregates, such as vesicles under our experimental conditions. Optical microscopy, DLS, and UV-vis spectroscopy show no signs of aggregate formation prior to photolysis. A few small aggregates are apparent in negative-staining TEM, but these do not resemble the vesicles suggested by Xu et al.[14] and appear to be present in only trace amounts and may be an artifact of the drying process for TEM analysis. This suggests that it is reasonable to assume that under our experimental conditions the initial pre-photolysis solutions are free from significant aggregation, and any aggregates observed in the post-photolysis solutions are due to photochemical processes.

The background input count rate of the pre-photolysis solutions was ~10 kHz when using the 632 nm laser. The slightly more powerful, and, therefore, more sensitive 532 nm laser had a background count rate of ~30 kHz. This background count rate is largely noise and not attributable to "real" scattering. Figure 10.2 shows a representative normalized auto-correlation function for an early time-point in the photolysis, where the signal is clearly dominated by noise and no real correlation is observed. While our numerical fitting procedure extracts a radius from this data, it has no physical meaning.

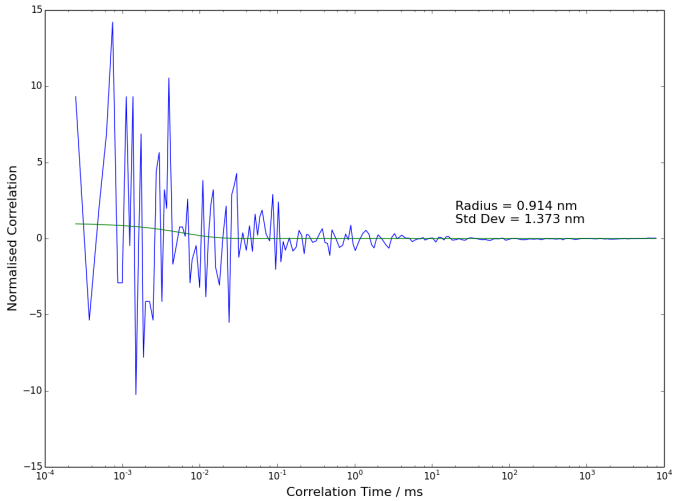

Figure 10.2. Representative normalized correlation data (blue) and attempted fit (green) for an early time-point during the photolysis of OOA before aggregates are formed.

As shown in Figure 10.3, the solutions remain at this background level count rate for the initial phase of photolysis, but, after ~2.5 hours of photolysis, the counts begin to increase, indicating more scattering in the solution. The counts then continue to increase smoothly until eventually beginning to level out to a steady level following ~20 hours of photolysis. The initial uptick in count rate is sudden and counts increase quite rapidly, as shown in Figure 10.4, with a noticeable increase even across 30-second measurements within a replicate set of measurements.

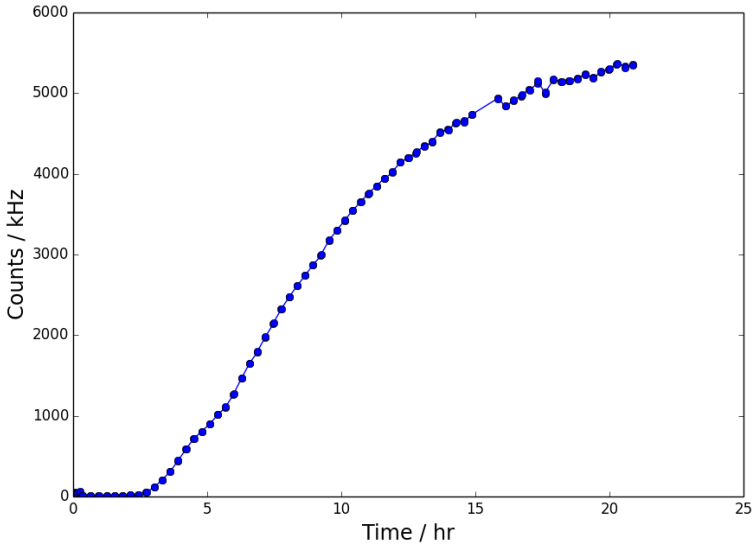

Figure 10.3. Scattering count rate over the course of photolysis of a 5 mM solution OOA as measured by illumination from a 532 nm laser.

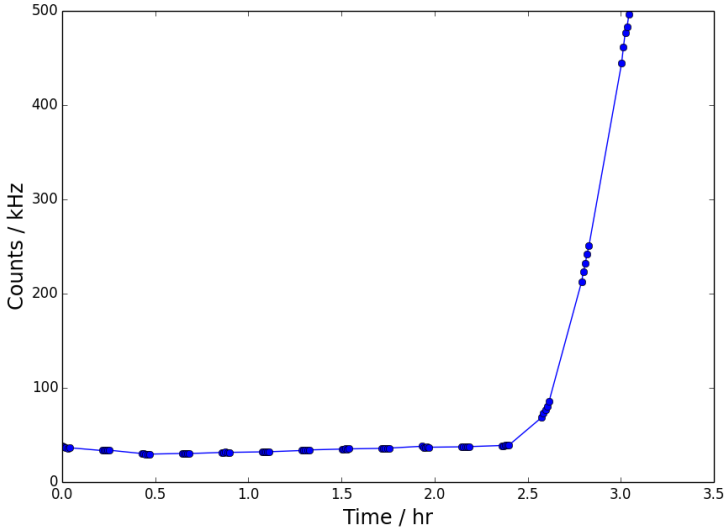

Figure 10.4. Scattering count rate during the early period of the photolysis 5 mM OOA as measured by illumination from a 532 nm laser.

Additionally, the timing of the initial uptick in counts is reproducible, occurring at roughly 2.5 hours across different experiments (Figure 10.5). This indicates that not only are the kinetics of the photolysis similar across runs but that the nature of aggregation is similar and dependent on the kinetics of the photochemistry. Differences in the slope of the increase in count rate are observed between the two wavelengths used to detect scattering, as the more powerful green laser is more sensitive to the increased scattering. The observed uptick in counts for all runs occurs within ~30 minutes of each other regardless of the laser used for detection.

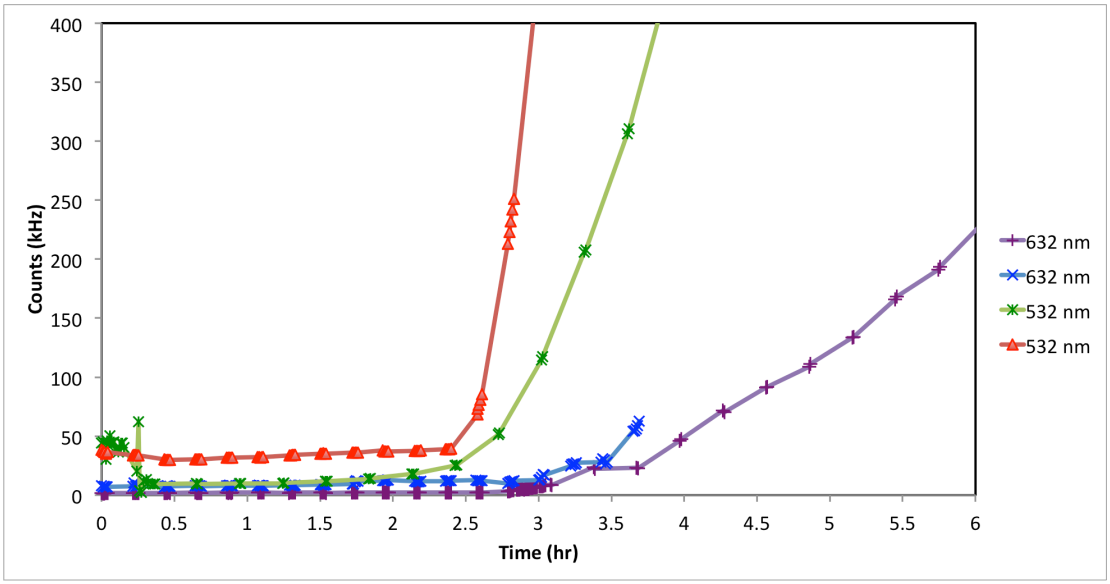

Figure 10.5. Reproducibility of the increase in count rate from scattering during the photolysis of 5 mM OOA as monitored by a 632 nm (purple, blue) and 532 nm laser.

As the counts increase, the auto-correlation functions also rapidly change from being dominated by noise to being measurements of real scattering (Figure 10.6A). The noise in the correlation function continues to decrease as the count rate increases (Figure 10.6B). These correlations are fit to a single exponential decay as described in the experimental section, and the good fit observed across the course of photolysis indicates that the aggregates formed are relatively monodisperse in size at any given time-point.

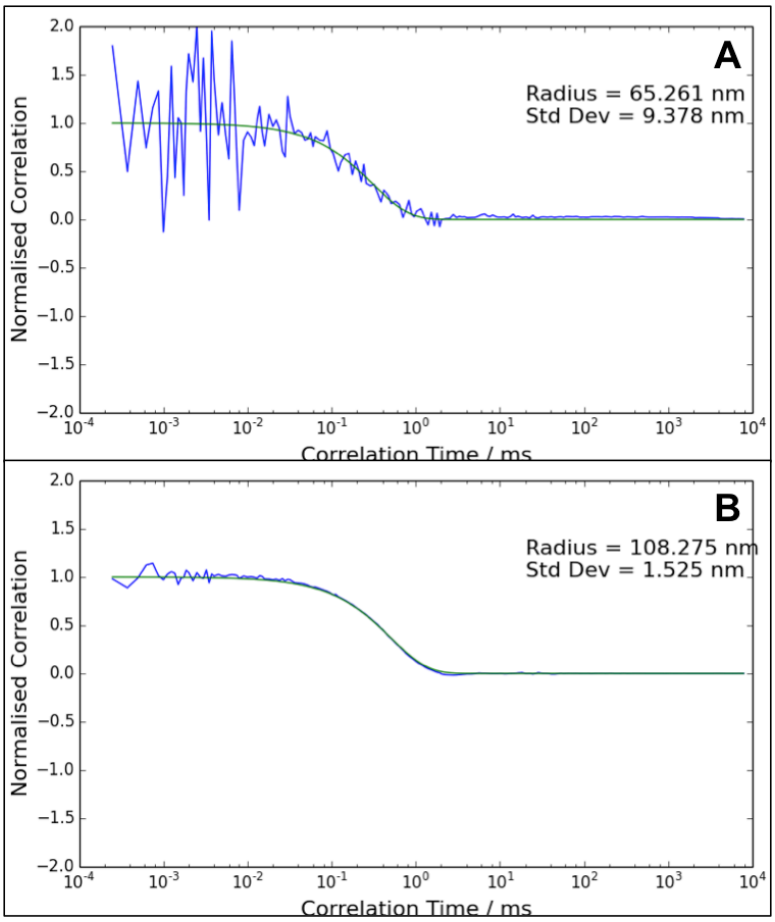

Figure 10.6. Representative normalized correlation data (blue) and fit (green) near the initial increase in count rate (A) and at a late time-point in the photolysis of OOA. Uncertainty given is the standard deviation of the fit using radius as the fit parameter.

While the counts due to scattering are observed to increase steadily over the course of photolysis once aggregates begin to form, the observed radii of the aggregates undergoes a much more abrupt transition, as seen in Figure 10.7. For clarity the unphysical radii extracted from the early time-points where the correlation data are noise-dominated have been set to 0 nm. As soon as counts begin to increase ~ 2.5 hours (Figure 10.5), aggregates with a radius of ~70 nm are observed (Figure 10.7). This abrupt, almost step-function-type transition is indicative that the system reaches some critical aggregation concentration of photoproducts and then forms aggregates, rather than a more gradual incremental aggregation process. Following this abrupt change, the average size of the aggregates slowly increases to ~120 nm in radius. Although importantly, the fit of the correlation

functions remains very good, suggesting that the aggregates continue to be relative monodisperse and additional populations of aggregates are not generated, meaning, for example, that the previously formed aggregates are not themselves coalescing.

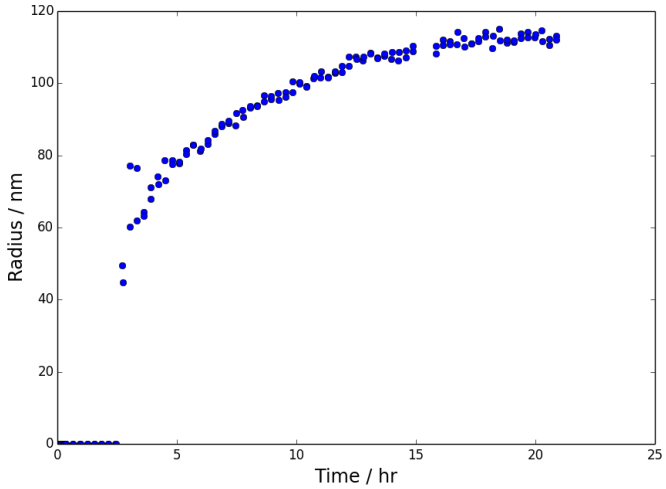

Figure 10.7. Radii of aggregates during the course of photolysis for 5 mM OOA extracted from the normalized correlation data.

The combination of apparent aggregate growth, as well as the continued photochemistry that generates more multi-tailed material, likely accounts for the steady increase in the count rate observed during photolysis. The aggregates are formed well before the solution becomes visibly cloudy. The apparent drift in particle size is particularly intriguing and deserves further attention. The initial aggregate radius size observed here matches very well with the previous measurements of aggregate size for this system using offline DLS measurements,[16] but the continued drift in radius size during photolysis means the aggregates at the end of photolysis are somewhat larger than have been seen previously.

All correlation functions were fit using the viscosity of pure water at ambient temperature, 1 cP. The apparent increase in size during the course of photolysis could be due to an increase in solution viscosity that begins to deviate from that of water. As multi-tailed species are synthesized and aggregates formed, it is not unreasonable to think that

this would be the case. This, combined with the need to dilute samples in order to use the DLS at CU Boulder, could explain the apparent larger size observed here. However, control experiments suggest that the explanation is not this simple. Dilution of samples with water by 1:10 and 1:100, give essentially the same correlation data, with no shift in correlation time that would relate to a change in apparent radius (Figure 10.8).

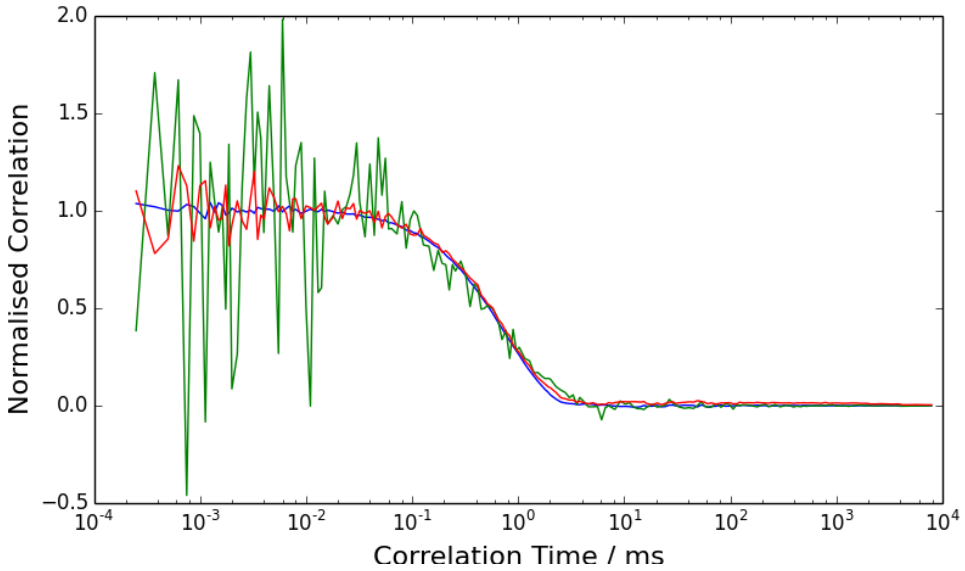

Figure 10.8. Normalized correlation data for post-photolysis solutions that have been diluted 1:10 (red) and 1:100 (green) compared to the undiluted sample (blue).

This suggests that it is unlikely that changes in viscosity are the major factor driving the observed increased in radius during photolysis. However, it is interesting to note that upon gentle heating of the sample from the ~21 °C of the lab to 26 °C the apparent size of the aggregates decreases linearly with temperature, even when the differences in temperature and water's viscosity are taken into account (Figure 10.9). This linear decrease does not appear to increase the polydispersity of the sample. It is not clear what is the cause of this apparent decrease in particle size with increasing temperature.

If changes in solution viscosity are not responsible for the observed drift in radius size, it is certainly possible that this change is due to an actual increase in particle size. Photolysis of OOA generates a mixture of multi-tailed oligomers.[1, 16] A major product,

dihexyltartaric acid, is double-tailed and formed from the recombination of two organic radicals generated from the photo-excitation of OOA. However, other oligomeric products are generated following multiple photochemical steps, including a triple-tailed dihydroxyoxoalkanoic acid product.[16] Because of the multiple photochemical steps required, it seems likely that the relative contribution of these species would be increased as photolysis proceeds. Species with a different number of alkyl chains or even different head groups would be expected to form aggregates, i.e. have a different packing parameter if the aggregates were vesicles.[20] Although, again, it is interesting that this increase in size appears to happen without an increase in polydispersity, suggesting the increase is due to an ordered process.

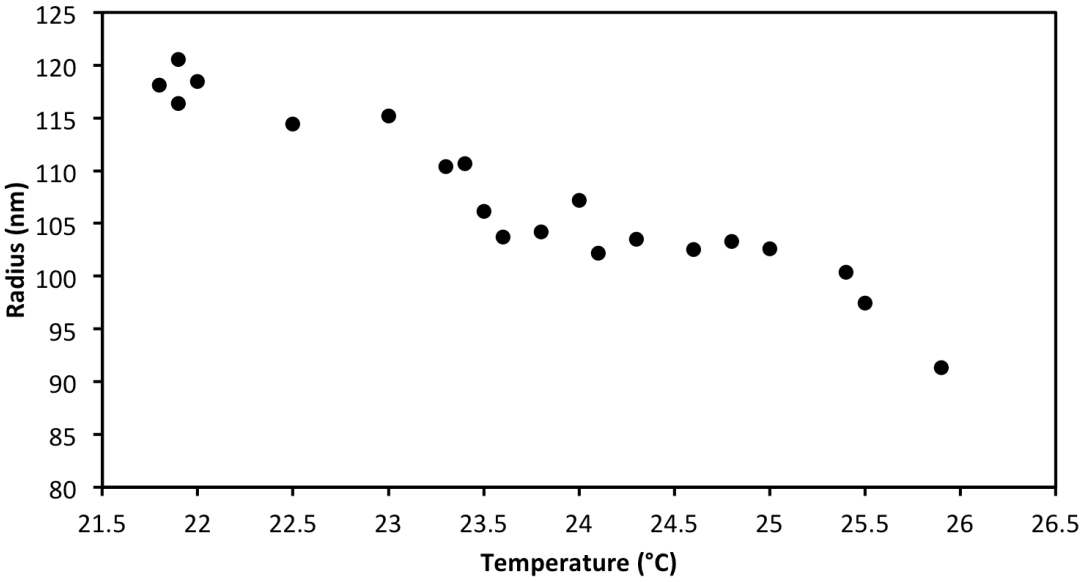

Figure 10.9. Observed temperature dependence of extracted radii of aggregates in a post-photolysis solution of 5 mM OOA (photolyzed using an Hg lamp). The decrease can be fit linearly with an R^2 value of 0.91.

The multi-tailed oligomers formed during photolysis are more surface-active than the single-tailed precursor.[1] This means that the local concentration of photoproducts will be higher at the air-water interface than in bulk solution, and it raises the interesting possibility that the aggregation observed for this system is mediated by the surface.

Visually, it is possible to see a gradation in the scattering of the post-photolysis solution in the cuvette (Figure 10.10). However, preliminary attempts to resolve the vertical dependence of the scattering and aggregate formation were inconclusive.

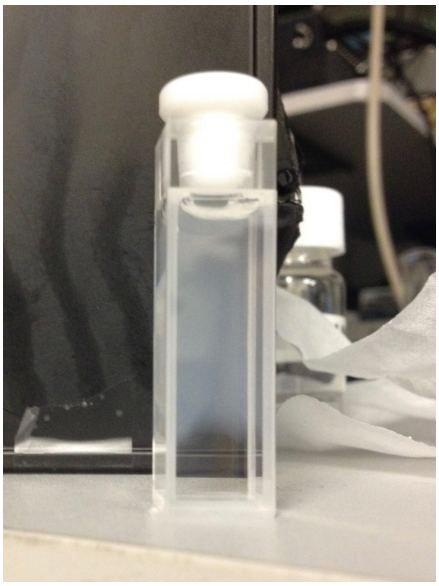

Figure 10.10. Visually observable gradient in scattering generated during photolysis of 5 mM OOA, where illumination of the cuvette was centered vertically.

While some questions remain, the time-resolved, *in situ* DLS measurements do provide information on the mechanism of formation of aggregates. It seems clear that as the photochemistry proceeds, a critical concentration of photoproducts is generated, resulting in aggregation. It is possible that small clusters of molecules of sizes and concentrations too small to be detected via DLS are present during the early stages of photolysis, but the incremental addition of molecules to these clusters does not appear to be the route of self-assembly. The observed slow drift in size following the abrupt formation of particles of ~70 nm in radius could be due to the partitioning of material to aggregates already present in solution, but this would need to occur relatively uniformly to maintain the observed monodispersity of aggregates in solution. The abrupt formation of aggregates combined with the apparent monodispersity is suggestive that an ordered process is at play. However, while DLS measurements can provide significant insight into the underlying self-assembly

processes, DLS is not capable of determining the nature of the aggregates themselves. For that, we turn to negative-staining and cryogenic transmission electron microscopy (TEM).

Negative-staining TEM shows the formation of significant quantities of aggregates from OOA after 5 hours of photolysis using the experimental set-up in Boulder (Figure 10.11). These aggregates are, indeed, spherical, as originally shown by phase contrast confocal microscopy,[1] and have an average diameter of ~120 nm with a standard deviation of ~30 nm. Cryo-TEM images show the presence of some larger aggregates as well (~600 nm) that are not observed in the negative-staining TEM, but collection of these images required concentration of the samples, which may have induced further aggregation or coalescence of material. The standard deviation of the aggregates may seem relatively large, but, even vesicles that have been extruded through a filter and separated on a size exclusion column to ensure monodispersity often have similar standard deviations in their size.[21] Therefore, we conclude that the aggregation process can be, indeed, characterized as monodisperse.

The negative-staining TEM radii closely match the radii observed via *in situ* DLS measurements during the initial stages of their formation. These particle sizes also match those observed when DLS measurements are taken of the post-photolysis solutions using the Titan DynaPro instrument at CU Boulder (~80 nm). However, there is little evidence of the larger particles that appear to be formed as photolysis continues in the DLS measurements. It is unclear what is the cause of this mismatch in sizes. It is possible that there is an explanation for the apparent increase in particle size that does not involve an actual increase in aggregate radii. While we have shown that it is unlikely this is due to changing viscosity, it is possible other changes in solution conditions could account for this difference. It is also possible that the difference in the rate of photochemical reactions between light sources may contribute to a change in the aggregation mechanism and favored particle size over the long time-scales required using the LDLS.

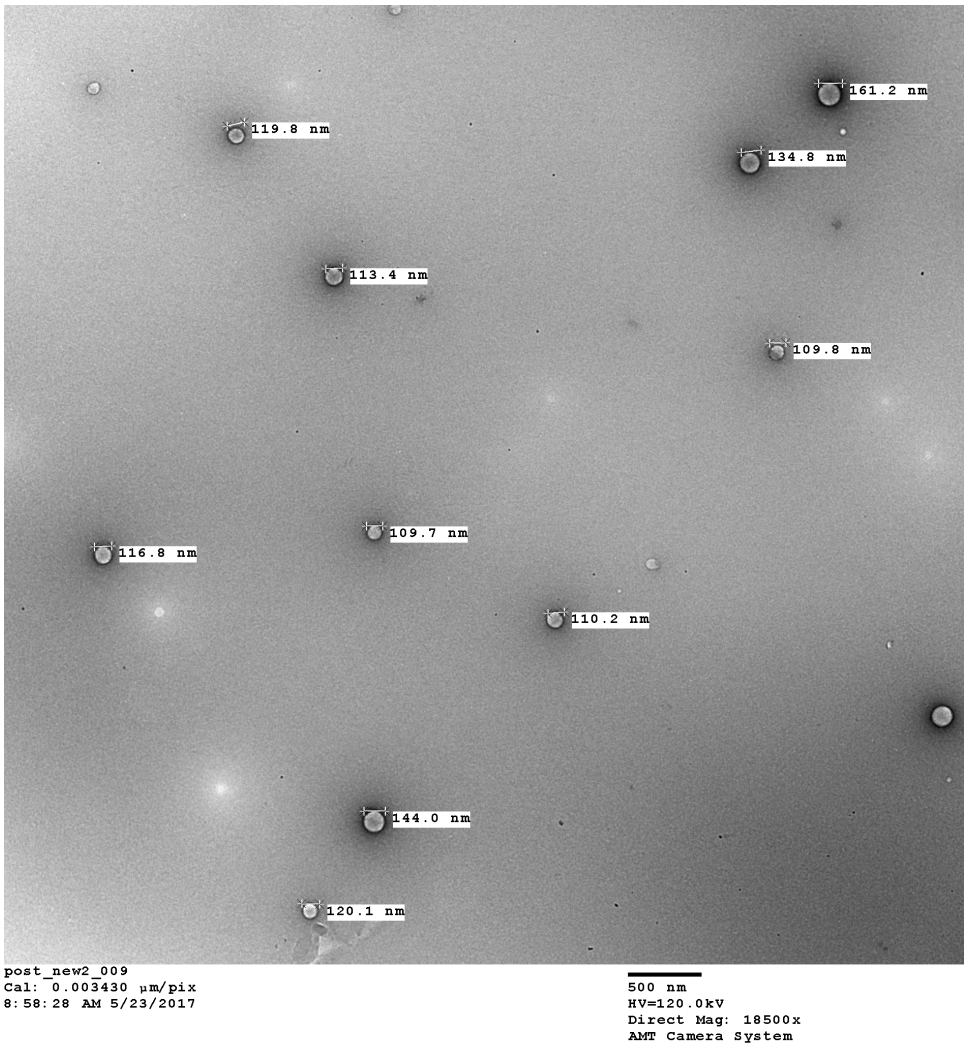

Figure 10.11. Negative-staining TEM images of aggregates formed by the photolysis of 6 mM OOA with their approximate diameters labeled. The scale bar is 500 nm.

There are also some indications that agitation may limit the size of the aggregates formed. Photolyses conducted during the time-resolved DLS measurements at LBL took place in a capped cuvette but were not purged with nitrogen. Conversely, the photolyses at CU Boulder are conducted in a sealed reactor that is continually purged with nitrogen that is bubbled through the aqueous solution.[16] This causes some mechanical agitation to the system that is not present in the solutions at LBL. Early experiments with this system revealed that active stirring of the solution appeared to slow photolysis, suggesting that such changes can affect the products. In cases where the photolysis reactor was not purged

with N_2, offline DLS measurements suggest an average radius of ~100 nm, which more closely matches those seen at LBL.[1] Additionally, negative-stain TEM images were taken of a post-photolysis solution that was photolyzed in July of 2013 in a reactor that was not purged with nitrogen. The images were taken to examine any changes in aggregation with time (Figure 10.12). While some coagulation has occurred, the individual spherical aggregates are still resolvable in many cases. These aggregates have an average radius of ~120 nm, which more closely matches the final radii observed in the *in situ* DLS measurements. However, because of the age of this solution, it is difficult determine whether the size of these aggregates has changed over four years of storage. Therefore, more experiments are needed to resolve the apparent difference in size between the photochemical experiments conducted in Boulder and those at LBL.

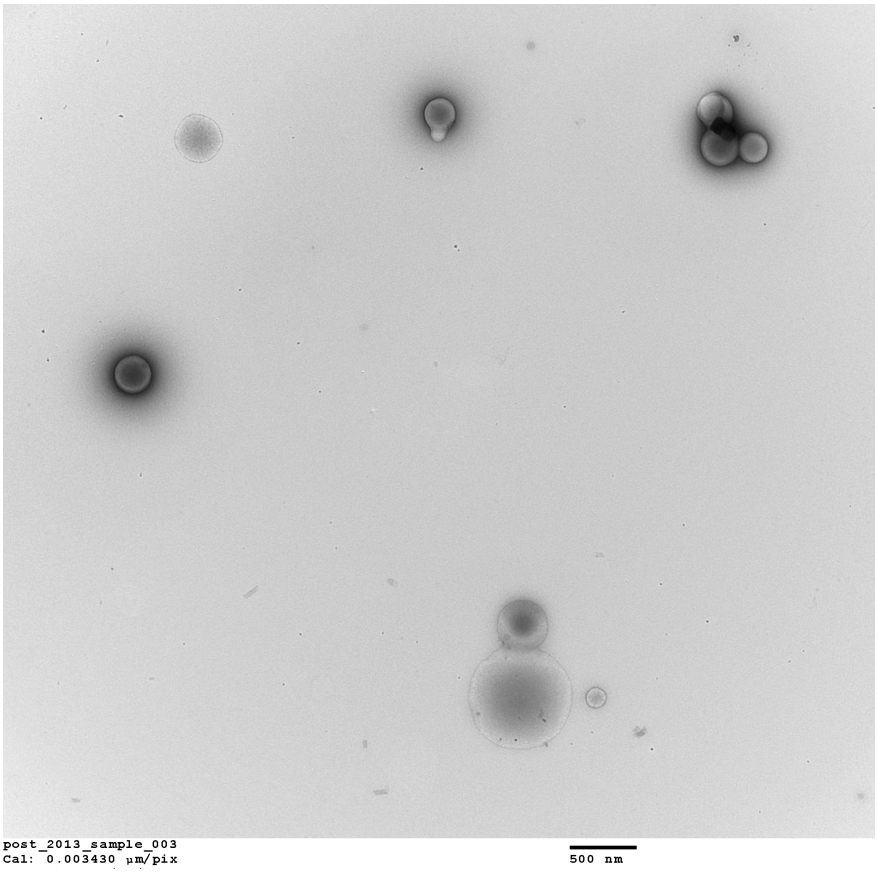

Figure 10.12. Negative-staining TEM images of aggregates formed by the photolysis of 6 mM OOA after 4 years of storage. The scale bar is 500 nm.

Additionally, the TEM images show that the aggregates formed are unlikely to be vesicles. Cryo-TEM images (Figure 10.13) of the aggregates do not have the telltale darker ring of material on the outside aggregate that would indicate the presence of a lamellar structure. Similarly, the post-photolysis solutions examined by negative-staining TEM (Figure 10.11) do not appear to have been disrupted or "popped" by the staining and drying process, as would be expected for vesicles. From this evidence, we conclude that the aggregates formed from photolysis of OOA are unlikely to be vesicles and are, instead, ordered colloidal particles.

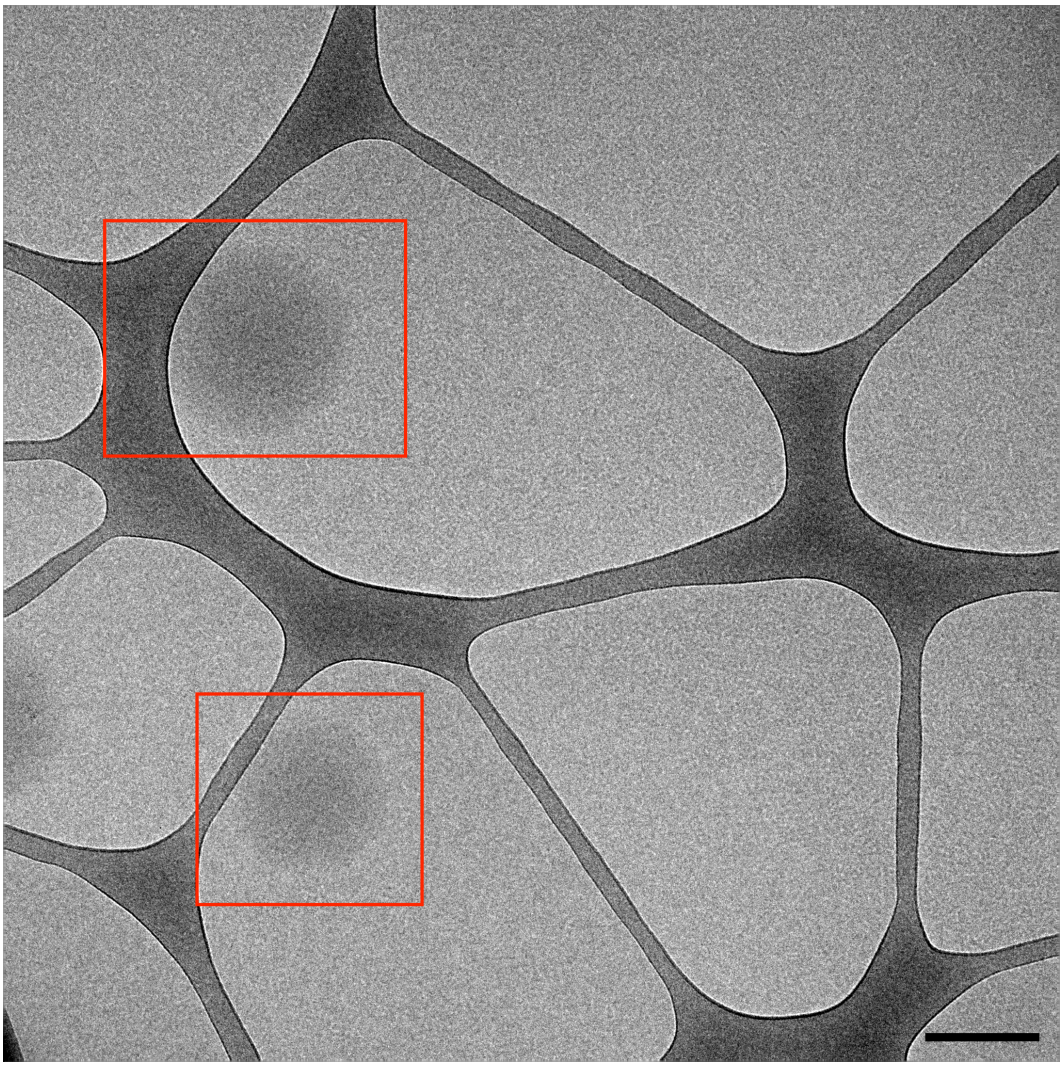

Figure 10.13. Cryo-TEM images of aggregates formed by the photolysis of 6 mM OOA (highlighted in red). The post-photolysis solution was evaporated to ~6X the nominal concentration to ensure particles were observable. The scale bar is 200 nm.

This does not exclude the possibility that vesicles could be formed from the oligomeric photoproducts under favorable solution conditions, such as those used for fatty acid vesicles,[12, 22] but it seems that the aggregates formed spontaneously during photolysis under acidic conditions are not lamellar in nature. The formation of ordered, monodisperse spherical aggregates that persist in solution on the order of years is interesting regardless of whether those aggregates are vesicles or not. This is a fundamentally interesting regime of self-assembly where material is incorporated into aggregates as the material is formed *in situ* and appears to accommodate more material throughout the course of photolysis. This leads to an increase in the size of the aggregates while the overall population of aggregates remains remarkably monodisperse. Additionally, the synthesis of long-lived colloidal aggregates is a key field of research in both materials and biomedical research, particularly with applications for drug delivery. Without any external perturbation to the system, the standard deviation in size of the observed particles is approximately that expected from a vesicle system that has been size-selected to ensure monodispersity.[21] It remains to determine the details of the physical principles underlying this behavior as well as the role of the surface in the self-assembly of aggregates.

10.4 Conclusions:

The photolysis of 2-oxoctanoic acid in aqueous solution generates oligomeric photoproducts that self-assemble into three-dimensional aggregates on the order of 100 nm in radius. These aggregates are formed suddenly once a critical aggregation concentration of photoproducts is reached. There is no evidence of incremental gradual growth of particles prior to when this concentration is reached, although the *in situ* DLS measurements appears to indicate that once aggregates are formed there is a drift in the size of particles with radius increasing slowly over the remainder of the photolysis. Importantly, it appears that the aggregates remain essentially monodisperse in size during the course of photolysis.

This monodispersity is also observed via electron microscopy, and the spherical shape of the particles is also confirmed. Despite the initial evidence pointing to the aggregates being vesicles in solution, we now suggest that they are non-lamellar colloidal aggregates.

10.5 Bibliography:

1. Griffith, E. C.; Rapf, R. J.; Shoemaker, R. K.; Carpenter, B. K.; Vaida, V. Photoinitiated synthesis of self-assembled vesicles. *J. Am. Chem. Soc.* **2014,** *136*, 3784-3787.

2. Morigaki, K.; Walde, P. Fatty acid vesicles. *Curr. Opin. Colloid Interface Sci.* **2007,** *12*, 75-80.

3. Menger, F. M. Remembrances of self-assemblies past. *Langmuir* **2011,** *27*, 5176-5183.

4. Keating, C. D. Aqueous phase separation as a possible route to compartmentalization of biological molecules. *Acc. Chem. Res.* **2012,** *45*, 2114-2124.

5. De Yoreo, J. J.; Gilbert, P. U. P. A.; Sommerdijk, N. A. J. M.; Penn, R. L.; Whitelam, S.; Joester, D.; Zhang, H.; Rimer, J. D.; Navrotsky, A.; Banfield, J. F., et al. Crystallization by particle attachment in synthetic, biogenic, and geologic environments. *Science* **2015,** *349*.

6. Wilber, A. W.; Doye, J. P. K.; Louis, A. A. Self-assembly of monodisperse clusters: Dependence on target geometry. *J. Chem. Phys.* **2009,** *131*, 175101.

7. Wilber, A. W.; Doye, J. P. K.; Louis, A. A.; Noya, E. G.; Miller, M. A.; Wong, P. Reversible self-assembly of patchy particles into monodisperse icosahedral clusters. *J. Chem. Phys.* **2007,** *127*, 085106.

8. Blando, J. D.; Turpin, B. J. Secondary organic aerosol formation in cloud and fog droplets: A literature evaluation of plausibility. *Atmos. Environ.* **2000,** *34*, 1623-1632.

9. Goltsov, A. N.; Barsukov, L. I. Synergetics of the membrane self-assembly: A micelle-to-vesicle transition. *J. Bio. Phys.* **2000,** *26*, 27-41.

10. Bergstrom, L. M.; Skoglund, S.; Danerlov, K.; Garamus, V. M.; Pedersen, J. S. The growth of micelles, and the transition to bilayers, in mixtures of a single-chain and a double-chain cationic surfactant investigated with small-angle neutron scattering. *Soft Matter* **2011,** *7*, 10935-10944.

11. Maurer, S. E.; Monnard, P.-A. Primitive membrane formation, characteristics and roles in the emergent properties of a protocell. *Entropy* **2011,** *13*, 466-484.

12. Maurer, S. E.; Nguyen, G. Prebiotic vesicle formation and the necessity of salts. *Origins Life Evol. Biosphere* **2016,** *46*, 215-222.

13. Cape, J. L.; Monnard, P.-A.; Boncella, J. M. Prebiotically relevant mixed fatty acid vesicles support anionic solute encapsulation and photochemically catalyzed trans-membrane charge transport. *Chem. Sci.* **2011,** *2*, 661-671.

14. Xu, H.; Du, N.; Song, Y.; Song, S.; Hou, W. Vesicles of 2-ketooctanoic acid in water. *Soft Matter* **2017,** *13*, 2246-2252

15. Xu, H.; Du, N.; Song, Y.; Song, S.; Hou, W. Microviscosity, encapsulation, and permeability of 2-ketooctanoic acid vesicle membranes. *Soft Matter* **2017,** *13*, 3514-3520.

16. Rapf, R. J.; Perkins, R. J.; Yang, H.; Miyake, G. M.; Carpenter, B. K.; Vaida, V. Photochemical synthesis of oligomeric amphiphiles from alkyl oxoacids in aqueous environments. *J. Am. Chem. Soc.* **2017,** *139*, 6946–6959.

17. Tanford, C., *The hydrophobic effect: Formation of micelles and biological membranes 2d ed*. J. Wiley.: 1980.

18. Reed Harris, A. E.; Ervens, B.; Shoemaker, R. K.; Kroll, J. A.; Rapf, R. J.; Griffith, E. C.; Monod, A.; Vaida, V. Photochemical kinetics of pyruvic acid in aqueous solution. *J. Phys. Chem. A* **2014,** *118*, 8505-8516.

19. Rapf, R. J.; Dooley, M. R.; Kappes, K.; Perkins, R. J.; Vaida, V. pH dependence of the aqueous photochemistry of α -keto acids *J. Phys. Chem. A* **2017**, DOI: 10.1021/acs.jpca.7b08192.

20. Antonietti, M.; Forster, S. Vesicles and liposomes: A self-assembly principle beyond lipids. *Adv. Mater.* **2003,** *15*, 1323-1333.

21. Perkins, R.; Vaida, V. Phenylalanine increases membrane permeability. *J. Am. Chem. Soc.* **2017,** *139*, 14388-14391.

22. Monnard, P. A.; Apel, C. L.; Kanavarioti, A.; Deamer, D. W. Influence of ionic inorganic solutes on self-assembly and polymerization processes related to early forms of life: Implications for a prebiotic aqueous medium. *Astrobio.* **2002,** *2*, 139-152.

11. Molecular Dynamics Simulations of the Diffusion of Hydrophobic Particles in Water

11.1 Introduction:

The characterization of aggregates in solution generally includes the determination of the size and polydispersity of the particles. In some cases, this can be done by direct visualization via techniques such as optical or electron microscopy. However, when this is not possible, indirect methods of size characterization, such as dynamic light scattering[1] or diffusion-ordered NMR spectroscopy (DOSY NMR),[2] are used instead. These techniques can be particularly useful for particles that are smaller than the diffraction limit of visible light. Unlike visualization, which measures aggregate diameter directly, these indirect techniques rely instead on the determination of diffusion constants. The experimentally determined diffusion constants, D, are then related to particle radius, R, using the Stokes-Einstein (SE) relation that states,

$$D \propto \frac{1}{R}.$$

In the following, we investigate whether this relationship holds for the diffusion of hydrophobic particles in water as a function of particle size, with particular interest in the behavior of particles near the dewetting transition.

Fluids are locally ordered. Insertion of a small particle into a fluid does relatively little to disrupt this local order, and very small particles tend to encounter a smooth boundary with the solvent. Larger particles, however, are more disruptive to solvent structure, as for instance, when water molecules can no longer maintain a full hydrogen-bonding network near a particle. Instead of a smooth boundary, the solute now forms an interface with the solvent (Figure 11.1). The change between these two regimes of solvation is a thermodynamic phenomenon, known as the dewetting or drying transition[3-5] and occurs for

particle radii of ~1 nm.[3, 4] In the following, we investigate the dynamical consequences of this thermodynamic process.

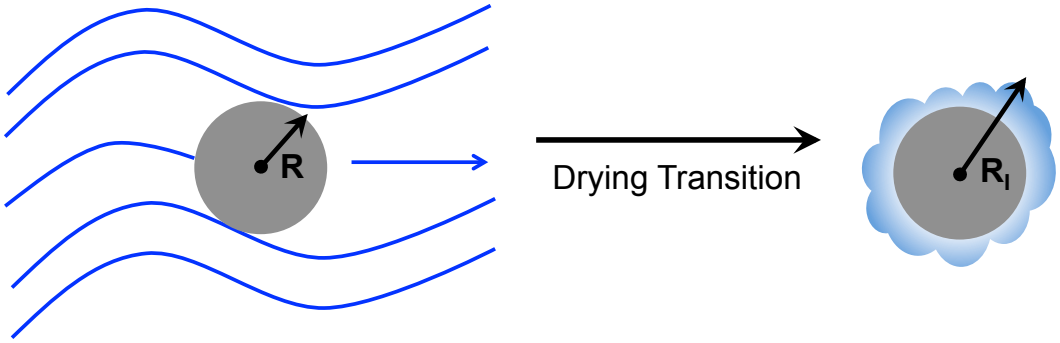

Figure 11.1. Cartoon of the nature of solvation of a hydrophobic particle during the drying transition, as the smooth boundary with solvent is replaced by an interface.

The inversely proportional relationship between the diffusion constant and particle radius can be derived from the Langevin equation of motion for a Brownian particle.[6, 7] The following derivation is shown for one-dimension, but can be easily related to three-dimensional movement, as each dimension is independent. The Langevin equation describes the forces acting on a Brownian particle in a fluid, including contributions from both friction with the solvent as well as the solvent's random density fluctuations,

$$F(t) = m\,a(t) = m\frac{dv}{dt} = -\zeta v(t) + \sqrt{2D}A(t)\ . \quad (1)$$

where m is the mass of the particle, ζ is the drag coefficient of the fluid, and A is the random force. This random force is defined to be statistically independent of the initial value of the velocity,

$$\langle A(t) \cdot v(0) \rangle = 0. \quad (2)$$

Dividing the Langevin equation by the drag coefficient gives

$$\frac{m}{\zeta}\frac{dv}{dt} = -v + \frac{\sqrt{2D}}{\zeta}A. \quad (3)$$

The term m/ζ has units of time, and is the characteristic decay time, τ, for the system. Solving the differential equation gives

$$v(t) = v(0)e^{-\frac{t}{\tau}} + \int_0^t ds\ \frac{\sqrt{2D}}{\zeta}e^{-\frac{t-s}{\tau}}A(s). \quad (4)$$

From this we can see for long timescales when t >> τ, the contributions from friction go to

zero and only random fluctuations contribute to the particle's velocity. That is, the motion of the particle is random and not correlated to its initial velocity in the long timescale limit. However, over shorter timescales there is a correlation between a particle's current and initial velocities, and the period of this correlation is determined by the decay time, τ.

It is these shorter timescales that are of interest, as they allow for the determination of the diffusion constant. The diffusion constant is determined from the velocity-velocity correlation function, which can be obtained by multiplying Equation 4 by the initial velocity, v(0) and taking the ensemble average,

$$\langle v(0) \cdot v(t) \rangle = \langle v(0)^2 \rangle e^{-t/\tau} + \int_0^t ds \, \frac{\sqrt{2D}}{\zeta} e^{-\frac{t-s}{\tau}} \langle v(0) \cdot A(s) \rangle \, . \quad (5)$$

However, because of our assumptions about the nature of the random force (Equation 2), the second term goes to zero. Additionally, due to the equipartition theorem, we know that value of $\langle v(0)^2 \rangle$ is simply $\frac{k_B T}{m}$. This then simplifies to,

$$C_{vv} = \langle v(0) \cdot v(t) \rangle = \frac{k_B T}{m} e^{-t/\tau}. \quad (6)$$

The integral of the velocity correlation function for all possible timesteps gives the diffusion constant of the particle,

$$D = \int_0^\infty dt \, \langle v(0) \cdot v(t) \rangle = \int_0^\infty dt \, \frac{k_B T}{m} e^{-t/\tau}, \quad (7)$$

or simply,

$$D = \frac{k_B T}{m} \tau. \quad (8)$$

Recalling that τ is simply m/ζ, we obtain,

$$D = \frac{k_B T}{\zeta}. \quad (9)$$

This equation says that the diffusion of a particle in solution is dependent on the solution's energy, as determined by temperature and the drag coefficient between the particle and solvent,

$$k_B T = D\zeta. \quad (10)$$

Interestingly, however, the diffusion is independent of the particle's mass, and, therefore, one would expect the same diffusion constant for all particles in the same fluid with the

same drag coefficient at the same temperature, regardless of their mass.

Equation 10 also provides a connection between the diffusion constant, a microscopic quantity that is dependent on the properties of the individual particle, with the drag coefficient, which is a macroscopic quantity. These two scales can be united because of the principles of fluctuation dissipation,[7] the Einstein relation.

Stokes' Law shows that the drag coefficient, ζ, is related to the radius, as

$$\zeta = c\eta R \ , \qquad (11)$$

where η is viscosity, and c is a constant that is either 6π or 4π depending on the choice of boundary conditions. Therefore, because $\zeta \propto R$, we can see from Equation 10 that D must be inversely proportional to R when the Stokes-Einstein relation holds, $D \propto \frac{1}{R}$.

The Stokes-Einstein relation (SE), however, often to does not hold for very small particles, that are smaller than the solute,[8-10], and there is evidence that it breaks down in water.[11] Furthermore, it is not clear that the Stokes-Einstein relation should hold for the diffusion of hydrophobic particles in water, especially for sizes near the drying transition. As particles undergo drying, the dimensionality of the interaction with the solvent changes, as the nature of the interface of solvent with the particle must be considered. This raises the question of whether the dependence of diffusion on particle radius might also change dimensionality in this region, scaling instead like $D \propto \frac{1}{R^{\nu}}$.

Understanding the behavior of particles in the size regime near the drying transition (~1 nm)[3, 4] is critical in part because this size is of relevance for small molecular clusters of simple lipids. As discussed in Chapters 10 and 12 and Appendix A, the self-assembly of many amphiphilic species is still not well understood. It is, for instance, not clear how simple single-chained amphiphiles behave in aqueous solution when at concentrations above the monomeric solubility limit but below reported bulk phase critical aggregation. It is likely small clusters are formed, and preliminary DOSY NMR results discussed in

Appendix A suggest that dimers held together by intermolecular forces are the primary components in solution rather than free monomers. This conclusion is based on the radii calculated from the experimentally-obtained diffusion constants, using the SE equation. Therefore, examination of the success of the SE relation in predicting diffusion behavior of both hydrophobic and amphiphilic particles in aqueous solution is necessary.

In this chapter, I report on an initial molecular dynamics study of the diffusion of repulsive Lennard-Jones particles in solution with bulk water as a function of particle size to determine whether the Stokes-Einstein relation holds for hydrophobic particles in aqueous solution on a molecular scale.

11.2 Methods:

Molecular dynamics simulations of bulk water were run with one hydrophobic particle embedded in the simulation box, using LAMMPS[12] and running simulations on the Janus and Summit Supercomputers at CU.[13-15] Bulk water was simulated using the rigid SPC/E potential.

11.2.1 Hydrophobe Parameterization and Simulation Details:

The hydrophobic particle was modeled with the same Van der Waals interactions as water but without hydrogen bonds, reducing the number of parameters in the model. Interactions between the hydrophobe and water were modeled using the WCA potential,[16]

$$U(R) = \begin{cases} 4\epsilon\left[\left(\frac{\sigma}{R}\right)^{12} - \left(\frac{\sigma}{R}\right)^{6}\right] + \epsilon, & R \leq 2^{\frac{1}{6}}\sigma \\ 0, & R > 2^{\frac{1}{6}}\sigma \end{cases},$$

where ε is the depth of the potential well and σ is the distance where the potential crosses zero. The particle was modeled using a Lennard-Jones potential for values of $R \leq 2^{1/6}\sigma$, and to simulate a purely repulsive particle, interactions were cut off at $2^{1/6}\sigma$, or the distance at which the minimum of the potential occurs in LAMMPS. This has the additional effect of

making the depth of the well, ε, arbitrary and a measure of the particle's "hardness." Here, ε was chosen to be 0.1553 kcal/mol. The nominal radius of the particles was also defined as $2^{1/6}\sigma$, where the force goes to zero, and the value of σ was adjusted accordingly to give particles of the desired size.

Simulations were conducted by inserting SPC/E water[17] molecules on a simple cubic lattice at a density of 1 g/cm^3. The hydrophobe of a given size was then inserted to this lattice and water molecules that fell within $2^{1/6}\sigma$ of the particle were removed. The system was then equilibrated in the NPT ensemble for 100 ps at 298 K and 1 bar. Temperature was scaled with a damping parameter of 200 fs, while the pressure damping parameter was 2 ps. Individual timesteps of 2 fs were used. The box size was averaged during the NPT equilibration. The simulation box was then re-sized to this average size over 10 ps in the NVT ensemble before changing ensembles to NVE, where, for 10 ps, the velocities were rescaled every 10 ps. Following these equilibration procedures, the actual simulations were run in the NVE ensemble for 1 ns without rescaling and data from these trials were used to obtain both radial distribution functions and diffusion constants.

Following benchmarking to optimize the processing efficiency, 24 processors were used per simulation, using the recommended command line switches for Intel Xenon processors to increase parallel efficiency. Simulation box sizes were chosen to ensure that the length of box, L, was large enough to recover the expected radial distribution function between the particle and the oxygen atoms of water, $g_{OP}(r)$, for a given particle radius, R. The particle radius, corresponding box lengths, and the maximum number of neighbors per particle used in these simulations are given in Table 11.1. The chosen hydrophobe radii are evenly spaced in R^{-1}.

Table 11.1. Simulation Box Parameters

R (Å)	L (Å)	Max. Neighbors
1.0	50	2000
1.2	50	2000
1.5	50	2000
2.0	50	2000
2.5	50	2000
3.33	50	2000
5.0	50	2000
6.67	50	2000
10	70	3000
20	110	12000

The hydrophobe radii, R, reported throughout are the nominal, mechanical radii based on the definition of $2^{1/6}\sigma$ discussed above. However, this is not the only way that the radius can be calculated. For each particle, it is also possible to calculate both the statistical radius, R_s, and the effective hard-sphere radius, R_{HS}, as shown in Figure 11.2. The statistical radius, R_s, is the distance where $g(R_s) = 0.5$ and is approximately 18% smaller than the mechanical radius. Similarly, the effective hard-sphere radius, R_{HS}, is about 17% smaller than the mechanical radius and is linear with σ when a WCA potential is used. R_{HS} is obtained by integrating the following,

$$R_{HS} = \int_0^\infty dr\left(1 - e^{-\beta U(r)}\right),$$

where $\beta = 1/k_BT$ and U(r) is the WCA potential.[18] The calculated hard-sphere radii in Figure 11.2 were obtained numerically, but it is possible to solve for these values analytically as well. Because both R_s and R_{HS} scale linearly with the mechanical radius, R, results obtained showing whether the SE relation is valid for the particles under study should be independent of which definition of radius is used. Therefore, we choose to report all results using the nominal, mechanical radius, R. However, the differences between these three types of radii may be important for other applications and should be considered before broadening the scope of these results.

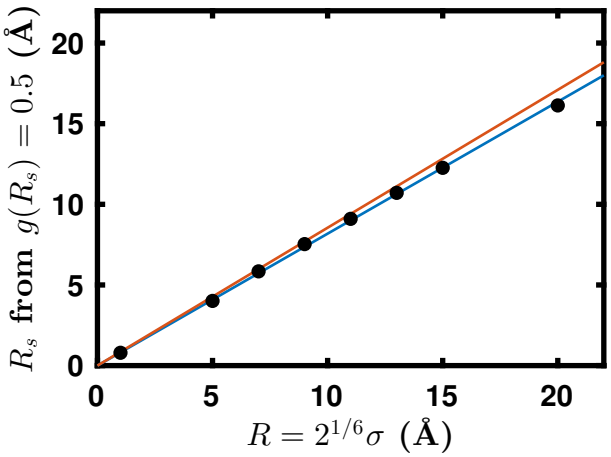

Figure 11.2. The statistical particle radius, R_s, computed from g(R_s) (black dots, fitted line in blue) and the hard-sphere radius, R_{HS} (red line), as a function of the nominal, mechanical radius, $R = 2^{1\backslash 6}\sigma$.

The SE equation does not explicitly consider a particle's mass, but in MD simulations each particle must be given an explicit mass. Here, we present results from three different cases for particle mass. In two cases, the mass was held constant regardless of particle size and fixed at either M = M_{H2O} or M = 100M_{H2O}. In the third case a constant density of 10 times the density of a water molecule was chosen, and the mass of the particle follows,

$$M = \left(\frac{\sigma}{\sigma_O}\right)^3 M_{H_2O},$$

where σ is the Lennard-Jones (LJ) parameter for the hydrophobe and σ_O is the LJ parameter for the water oxygen atom. Ten replicate simulations were performed for each hydrophobe size and mass.

In addition to the simulations of the hydrophobic particles in water, comparison was made to simulations of identical particles in an LJ fluid. The LJ fluid was modeled as "apolar" water and was composed of particles with the same mass and Van der Waals interactions as water but without the ability to form hydrogen bonds.

11.2.2 Calculation of Diffusion Constants:

Diffusion constants can be obtained by calculating the mean squared displacement

(MSD) for the particles using the Einstein relation for Brownian motion,

$$D = \frac{\langle(\vec{r_i}(t) - \vec{r_i}(0))^2\rangle}{6t}.$$

Diffusion constants were calculated by fitting the MSD for the first 0.25 ns of the 1 ns trial, omitting the initial 10 ps of the simulation to avoid the ballistic region. Average diffusion constants for each particle size were calculated in two ways. First, the MSD was computed for each trial separately, computing D for each trial, and then averaging the individual values of D. Second, the MSD was averaged across all trials, and then the average D was calculated. The results obtained from these two methods were essentially identical. Uncertainty in the diffusion constants was determined by bootstrapping over each trial of a given particle size to compute an average MSD and using the bootstrap distribution to estimate the confidence interval.

Calculated diffusion constants are known to be dependent on the system size of the simulation.[19] Using the same box size for all particle sizes is unnecessarily computationally expensive. Therefore, it is necessary to consider corrections to diffusion constants to account for differences in box size. We can apply the correction,

$$D_0 = D_{PBC} - \frac{k_B T \xi}{6\pi\eta L},$$

where D_{PBC} is the diffusion constant measured in a periodic simulation with side length, L, and the constant $\xi \approx 2.83729$.[19] However, as the constant $k_B T/6\pi\eta \approx 8*10^{-5}$ cm^{2}Å/s, and diffusion constants are typically on the order of D ~ 10^{-5} cm^2/s, the box size correction will be small. Indeed, testing reveals that this correction over the range of particle sizes tested here is negligible in all cases, and, therefore, has not been applied to these results.

11.3 Results and Discussion:

If the SE relation is valid, the diffusion constants simulated should scale as 1/R. By plotting the diffusion constant, D, against the particle's radius, R, on a log-log scale, we can more easily probe this relationship. The slope of these curves can be fit to a power law

function, $D \sim R^{-\alpha}$. If the fit value of $\alpha = 1$, then the SE relation holds for the particles in question.

As shown in Figure 11.3, it appears that, for the modeled hydrophobes with constant mass, the dependence of diffusion constant on particle radius does not follow a simple power law function. Rather, it appears that two behavior regimes are present, characterized by two different slopes distinguishing the behavior between small and large particles (Table 11.2). The cut-off between these two regimes was chosen by eye, and the slope of each was fit to give α_1 for small particles and α_2 for larger particles. Here, the value for α_2 is 1.0, meaning that the larger particles are in a regime that follows the expected SE behavior. However, for smaller particles, α_1 is larger than one, giving D a stronger dependence on R than would be expected from the SE relation. The breakdown in the SE equation for very small hydrophobic particles is, perhaps, not surprising. It is known that the SE relation often breaks down for small solutes whose size approaches that of the solvent molecule.[8, 9] This has been seen primarily when the solute molecule is 2-3 times larger than the solvent.[10]

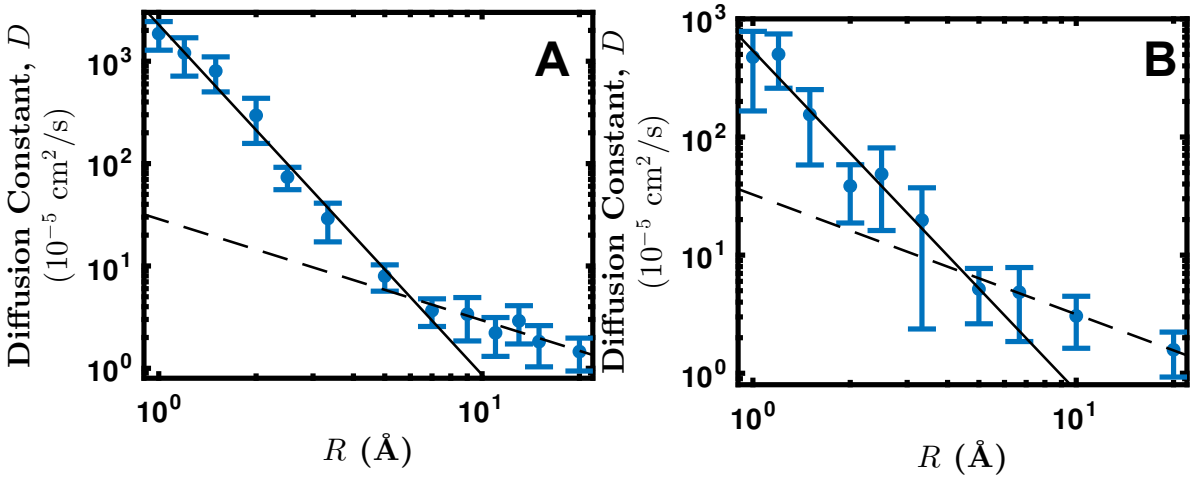

Figure 11.3. The diffusion constant, D, of a hydrophobe in water on a log-log scale as a function of radius for a particle of mass, $M = M_{H2O}$ (A) or $M = 100M_{H2O}$ (B). The data are fit to two power law functions $D \sim R^{-\alpha}$, and the parameters for the fits are given in Table 11.2.

Table 11.2. The power law fit parameters, $D \sim R^{-\alpha}$, for hydrophobic particles in water and a LJ fluid.

	α_1	α_2	Cutoff (Å)
Water			
Fixed Mass = M_{H2O}	3.4	1.0	7
Fixed Mass = $100M_{H2O}$	2.9	1.0	5
Fixed Density	4.3	1.5	3
LJ Fluid			
Fixed Mass = $100M_{H2O}$	2.6	1.0	4
Fixed Density	4.0	1.4	3

The radius size cutoff for the deviation from SE behavior observed in these simulations ranges from 7 Å for particles with the same mass as water and 5 Å for particles whose mass is ten times greater than a water molecule to 3 Å for particles of fixed density. Water molecules, themselves, are about 3 Å in size. This extends the size region of particles whose diffusion is not well modeled by SE from that of the expected size limit for this to occur, including solute particles whose radius is similar to that of the water molecules themselves. As the hydrophobe's size continues to increase, a cutoff in behavior is reached, and the diffusion behavior switches to that expected from SE for larger particles. This turnover in diffusion behavior is intriguingly suggestive of a switch between entropic and enthalpic solvation, as it appears to occur in roughly the same size regime as the dewetting transition.[4]

Some small differences between the particles with different mass, namely a larger value of α_1 and a larger cutoff size for the lighter hydrophobe, are observed. While the SE equation does not formally depend on mass, it is based on the assumption that the particles are in the Brownian limit, where the solute is much more massive than the solvent. This limit is achieved when the mass ratio of solute to solvent is about 100:1.[20] This ratio was used in the simulation of the heavier particles. Of course, the lighter particles whose mass is the same as water are never in this Brownian limit. It is, then, noteworthy that the SE

equation holds for any of the particle sizes for this lighter hydrophobe, showing the remarkable robustness of the SE relation outside of the initial parameters under which it was devised.

The diffusion of particles that have a constant density rather than a constant mass looks qualitatively very similar (Figure 11.4) to that of the hydrophobes with constant mass. The diffusion constant clearly depends on radius following two different power laws between the small and larger particle regimes. The size cut-off is slightly smaller, occurring at a radius of 3 Å. However, the power law that best fits the larger particles has an α_2 value of 1.5, not 1.0. This means that even the relatively large particles show some deviation from the expected SE behavior. This difference between the constant density and constant mass particles is interesting and not easily explained. Power law fits are not particularly accurate over the range of sizes considered here, and it is likely necessary to conduct further simulations to ensure this is a real difference between the types of particles.

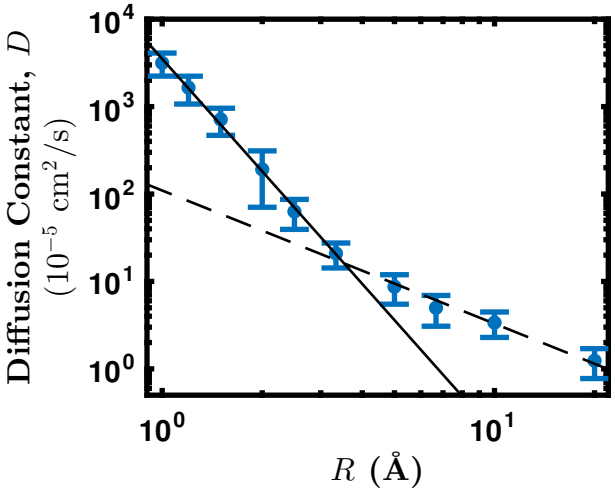

Figure 11.4. The diffusion constant, D, of a hydrophobe in water, on a log-log scale as a function of radius for a particle of constant density 10 times greater than that of a water molecule. The data are fit to two power law functions $D \sim R^{-\alpha}$, and the parameters for the fits are given in Table 11.2.

However, this observed deviation from the SE relation for the constant density particles is not limited to their diffusion in water. Comparison of the behavior of the same

hydrophobes diffusing in a Lennard-Jones (LJ) fluid (essentially apolar water) gives essentially identical results for the constant density particles (Figure 11.5A). The LJ fluid had the same properties as the SPC/E water, except that it is incapable of forming hydrogen bonds. A similar comparison of the diffusion of the heavier constant mass hydrophobes in a LJ fluid (Figure 11.5B) also shows similar behavior to that of the same particles in water; although, the size cutoff shrinks to 4 Å.

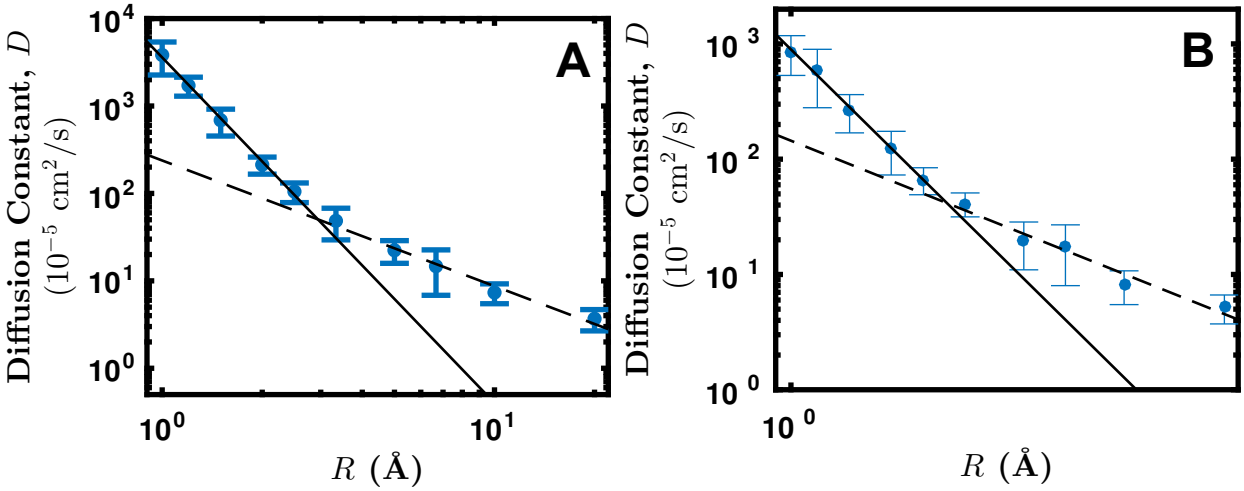

Figure 11.5. The diffusion constant, D, of a hydrophobe in a Lennard-Jones fluid, on a log-log scale as a function of radius for a particle of constant density 10 times greater than that of a water molecule (A) and of constant mass 100 times greater than that of water molecule (B). The data are fit to two power law functions $D \sim R^{-\alpha}$, and the parameters for the fits are given in Table 11.2. Note: radii are defined at $2^{1/6}\sigma$, the unit Å is used for ease of comparison with the particles in water but has no real meaning in an LJ fluid.

Examination of the radial distribution functions for the particles in water compared to those in the LJ fluid shows that some subtle differences exist between the two solvents (Figure 11.6). While an identical WCA particle with the same parameters is modeled in each solvent, the solute excludes more volume in water than in the LJ fluid. Additionally, as particle size is increased, the structured interface between the solvent and solute disappears in water. Conversely, in the LJ fluid, a structured interface is always present, except for the case of unphysically small particles. The cross-over between a structured and unstructured interface in water is likely due to the transition from entropic solvation to

enthalpic solvation,[3] as the particle becomes too large for the hydrogen-bonding network in water to accommodate the solute. Studying the comparable changes in solvation for the LJ fluid is more difficult, as the relevant range of interactions is longer, requiring a very large list of neighbors within the simulation.

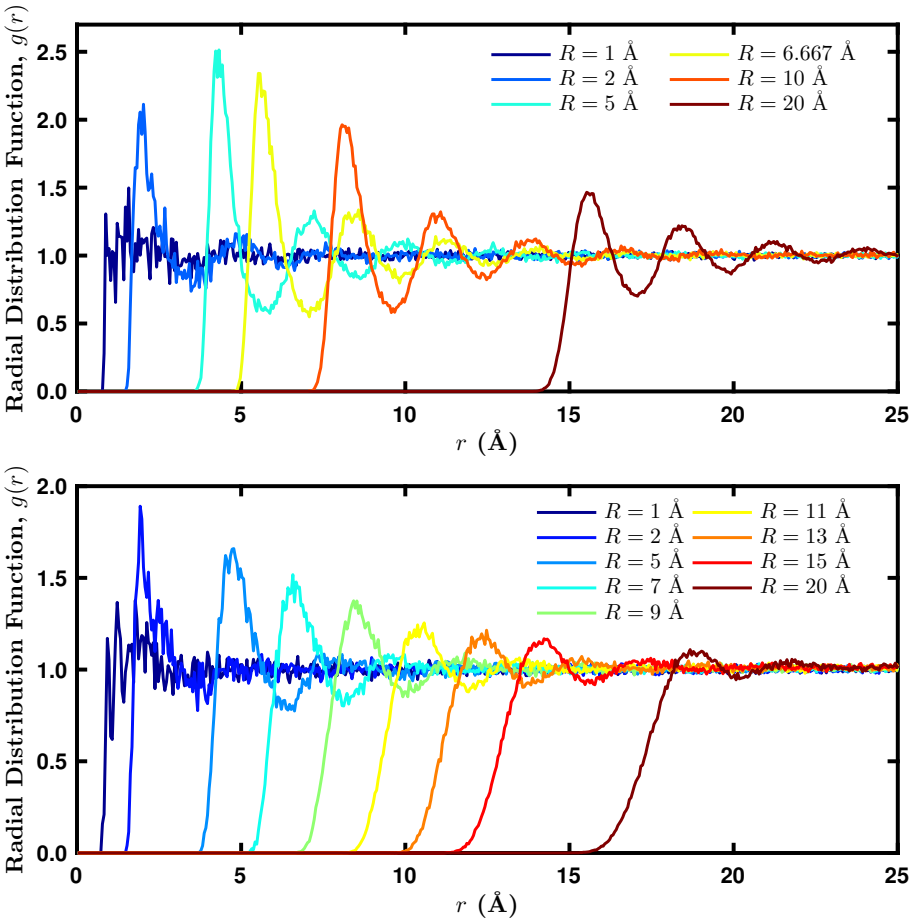

Figure 11.6. The radial distribution function between the solute particle and the solvent. The top panel is in LJ solvent and the bottom panel is in water.

The similar behavior of the diffusion constant for the hydrophobic particles regardless of solvent provides the opportunity to expand the observed results for water to a more generalized behavior for all fluids. The results suggesting that the constant density particles do not follow the expected SE behavior for all radii, relies upon a power law fit, and, therefore, should be confirmed through further trials. However, the turnover in diffusion behavior between small and large regimes appears to be a robust effect that is

generalizable across solvents. The nature of the processes governing this transition, including potential similarities to the dewetting transition should be investigated further.

Nevertheless, the results obtained from these simulations suggest that for the majority of particles with sizes that are relevant to experimentally-observed spherical colloidal aggregates, the SE relation holds. However, particles of constant mass in the "intermediate" size range (~5-7 Å), as well as particles with constant density do not appear to follow the SE relation. This is particularly interesting for those particles of constant density, which, in some respects, are the most directly relevant way to model the particles that form from increasingly larger clusters of a molecule of interest. This breakdown of the SE relation has implications for the analysis of the small clusters observed via DOSY NMR, as proposed in Appendix A. The extent of expansion of an alkyl chain in solution can be crudely estimated using a freely-jointed chain model that accounts for the short-range interactions of the chain.[21] Doing so gives an effective radius for molecules such as decanoic acid or 2-oxooctanoic acid, on the order of ~6 Å. This is in the regime of interest where the SE relation may not hold. Therefore, depending on how such molecules cluster in solution, this could effect the interpretation of results. For instance, if using the SE relation in a size regime where it does not hold, observed differences in experimental diffusion constants may be erroneously assigned to the expected difference between the diffusion of a monomer and the diffusion of a dimer held together by intermolecular forces. This is particularly important, if the diffusion constant in fact has a stronger dependence on the radius of the cluster than would be expected.

Of course, the diffusion of real molecules in solution as opposed to simple purely hydrophobic particles is more complex, and assignment of a hydrodynamic radius to an observed diffusion constant comes with its own complexities based on potential solvent-

solute interactions. Further refinements of these molecular dynamics simulations to better model experimental conditions may help resolve how the SE holds for such molecular systems and the corresponding small clusters. In particular, it would be interesting to understand if anything changes for amphiphilic particles rather than the purely hydrophobic particles under consideration here. The behavior of the simple hydrophobic particles studied here does, however, help clarify the regimes under which the SE relation can be reliably used, as well as highlighting potential regions where caution must be used in the interpretation of diffusion constant results.

11.4 Conclusions:

Molecular dynamics simulations were conducted to measure the diffusion of a single, purely repulsive hydrophobic particle in water as a function of particle radius. These simulations were run defining the mass of the particle in three different ways, and for very small particles, where the radius was less than ~5 Å, a breakdown in Stokes-Einstein relationship of $D \sim R^{-1}$ occurred. The expected Stokes-Einstein relationship was observed for larger particles of constant mass, either $M = M_{H2O}$ or $100M_{H2O}$, but in the case of the constant density particles ($10\rho_{H2O}$), the diffusion in the large particle limit was found to scale as $D \sim R^{-1.5}$. These results were found to hold in a Lennard-Jones fluid model of apolar water, although changes in the solvation behavior were observed between these two solvents, with a loss of the ordered interface between solute and solvent for large particles in water. While the above results are preliminary, they suggest that caution may be necessary before directly relating the diffusion constant to a particle's radius via Stokes-Einstein relation for some hydrophobic particles.

11.5 Bibliography:

1. Clark, N. A.; Lunacek, J. H.; Benedek, G. B. A study of Brownian motion using light scattering. *Am. J. Phys.* **1970,** *38*, 575-585.

2. Griffith, E. C.; Rapf, R. J.; Shoemaker, R. K.; Carpenter, B. K.; Vaida, V. Photoinitiated synthesis of self-assembled vesicles. *J. Am. Chem. Soc.* **2014,** *136*, 3784-3787.

3. Chandler, D. W. Interfaces and the driving force of hydrophobic assembly. *Nature* **2005,** *437*, 640-647.

4. Lum, K.; Chandler, D.; Weeks, J. D. Hydrophobicity at small and large length scales. *J. Phys. Chem. B* **1999,** *103*, 4570-4577.

5. Berne, B. J.; Weeks, J. D.; Zhou, R. Dewetting and hydrophobic interaction in physical and biological systems. *Annu. Rev. Phys. Chem.* **2009,** *60*, 85-103.

6. McQuarrie, D., *Statistical mechanics*. University Science Books: Sausalito, California, 2004.

7. Gillespie, D. T. Fluctuation and dissipation in Brownian motion. *Am. J. Phys.* **1993,** *61*, 1077-1083.

8. Sharma, M.; Yashonath, S. Breakdown of the Stokes−Einstein relationship: Role of interactions in the size dependence of self-diffusivity. *J. Phys. Chem. B* **2006,** *110*, 17207-17211.

9. Banerjee, P.; Yashonath, S.; Bagchi, B. Rotation driven translational diffusion of polyatomic ions in water: A novel mechanism for breakdown of Stokes-Einstein relation. *J. Chem. Phys.* **2017,** *146*, 164502.

10. Bhattacharyya, S.; Bagchi, B. Anomalous diffusion of small particles in dense liquids. *J. Chem. Phys.* **1997,** *106*, 1757-1763.

11. Walser, R.; Mark, A. E.; van Gunsteren, W. F. On the validity of Stokes' law at the molecular level. *Chem. Phys. Lett.* **1999,** *303*, 583-586.

12. Plimpton, S. Fast parallel algorithms for short-range molecular dynamics. *J. Comp. Phys.* **1995,** *117*, 1-19, lammps.sandia.gov.

13. Jonathon Anderson, P. J. B., Daniel Milroy, Peter Ruprecht, Thomas Hauser, and Howard Jay Siegel, Deploying RMACC Summit: An HPC resource for the rocky mountain region. In *Proceedings of PEARC17*, New Orleans, LA, USA, 2017; p 7.

14. This work utilized the RMACC Summit supercomputer, which is supported by the National Science Foundation (Awards ACI-1532235 and ACI-1532236), the University of Colorado Boulder, and Colorado State University. The Summit supercomputer is a joint effort of the University of Colorado Boulder and Colorado State University.

15. This work utilized the Janus supercomputer, which is supported by the National Science Foundation (Award number CNS-0821794) and the University of Colorado Boulder. The Janus supercomputer is a joint effort of the University of Colorado Boulder, the University of Colorado Denver and the National Center for Atmospheric Research.

16. Weeks, J. D.; Chandler, D.; Andersen, H. C. Role of repulsive forces in determining the equilibrium structure of simple liquids. *J. Chem. Phys.* **1971,** *54*, 5237-5247.

17. Berendsen, H.; Grigera, J.; Straatsma, T. The missing term in effective pair potentials. *J. Phys. Chem.* **1987,** *91*, 6269-6271.

18. Hansen, J.-P.; McDonald, I. R., *Theory of simple liquids*. Elsevier: 1990.

19. Yeh, I.-C.; Hummer, G. System-size dependence of diffusion coefficients and viscosities from molecular dynamics simulations with periodic boundary conditions. *J. Phys. Chem. B* **2004,** *108*, 15873-15879.

20. Schmidt, J.; Skinner, J. Hydrodynamic boundary conditions, the Stokes–Einstein law, and long-time tails in the Brownian limit. *J. Chem. Phys.* **2003,** *119*, 8062-8068.

21. Cowie, J. M. G.; Arrighi, V., *Polymers: Chemistry and physics of modern materials*. CRC Press: 2007.

12. Effects of Salinity on the Intermolecular Interactions of Fatty Acids at Aqueous Interfaces:

"The solubility of soaps at room temperature is usually greatly overestimated."
James W. McBain, 1948[1]

12.1 Introduction:

Fatty acids, carboxylic acids with an alkyl tail, are ubiquitous species in the natural environment. As metabolites and key degradation products of biology, especially from the hydrolysis of phospholipids, fatty acids persist at the sea surface microlayer[2, 3] and are significant components of the organic fraction of atmospheric aerosols.[2-6] This is in part because these simple lipids partition to the air-water interface, resulting in an increased local concentration of oriented molecules at the surface, modifying the properties of the bare interface. Beyond their importance in today's environment, understanding the surface activity and behavior of fatty acids is of considerable interest in the study of prebiotic chemistry and the origins of life. Fatty acids can be synthesized abiotically by Fischer-Tropsch-like processes,[7, 8] and have been identified in carbonaceous meteorites.[9, 10] For these reasons, they are generally considered to have been readily available on the early Earth and are often considered to be the most prebiotically-plausible lipids.[11] Accordingly, are used to replicate primitive enclosures and protocells.[12-19]

Vesicles composed of fatty acids have been widely used as models for primitive cellular constructs,[12, 20, 21] and their stability and permeability have been reported for a variety of environmental conditions.[12, 14, 15, 19, 20, 22-35] Unlike modern membrane components, such as double-tailed phosopholipids, the simpler, single-tailed fatty acids have a more complicated phase behavior leading to the formation of vesicles. In general, relatively high concentrations of fatty acids are required to form permeable but fragile vesicles, which are only stable over a narrow-range of environmental conditions of pH, salt, and temperature.

The current literature understanding of the mechanism of self-assembly for these species is summarized schematically in Figure 12.1.[33] It is assumed that below some critical aggregation concentration (CAC), or in this case, critical vesicle concentration (CVC), the fatty acids exists as monomers in solution. Once the concentration is raised above this CVC, three-dimensional structures are formed. These structures are generally considered to be equilibrium structures, rather than the kinetically-trapped structures formed by phospholipids, although this designation is somewhat controversial.[29, 33, 36-38] The nature of the three-dimensional structures formed is very dependent on the solution pH, and this is rationalized by invoking the extent of protonation of the carboxylic acid head group.

At high pH, the head groups are largely deprotonated, favoring the formation of micelles since their structure minimizes the repulsion between carboxylate ions by maximizing the distance between head groups while maintaining favorable Van der Waals interactions between the alkyl tails. On the other hand, oil droplets form at low pH when the head groups are protonated and do not experience repulsion. Fatty acid vesicles are thought to form when approximately half the head groups are deprotonated and half are protonated; this occurs when the pH of the solution is equivalent to the so-called pK_a of aggregation.[33] However, the pK_a of aggregation is approximately 7 for decanoic acid, and is significantly higher than the pK_a of the monomeric carboxylic acids of ~4.9.[39] This difference suggests that the ionization state of fatty acids in aggregates likely differs from that in the bulk. Indeed, it appears as though the ionization behavior in aggregates may more closely resemble that of fatty acids at the surface than in the bulk. At the air-water interface the pK_a of fatty acids is known to increase significantly,[40][Kanicky, 1999 #1477, 41, 42] with recent estimates of the surface pK_a of decanoic acid of ~6.4.[40] This difference between the bulk and aggregate ionization behavior suggests that the intermolecular interactions causing self-assembly are likely more complicated than the simple model outlined in Figure 12.1. The

stability of vesicles under changing pH conditions has been empirically studied,[31, 32, 34, 43] but the relationship between the head group interactions and membrane stability has not been quantified. Prior study of fatty acid behavior at varying pH has found that the fatty acid pK_a changes with chain length, and that, at the surface, changes to bulk pH can change the fatty acid's ionization state, and its ability to form films.[40]

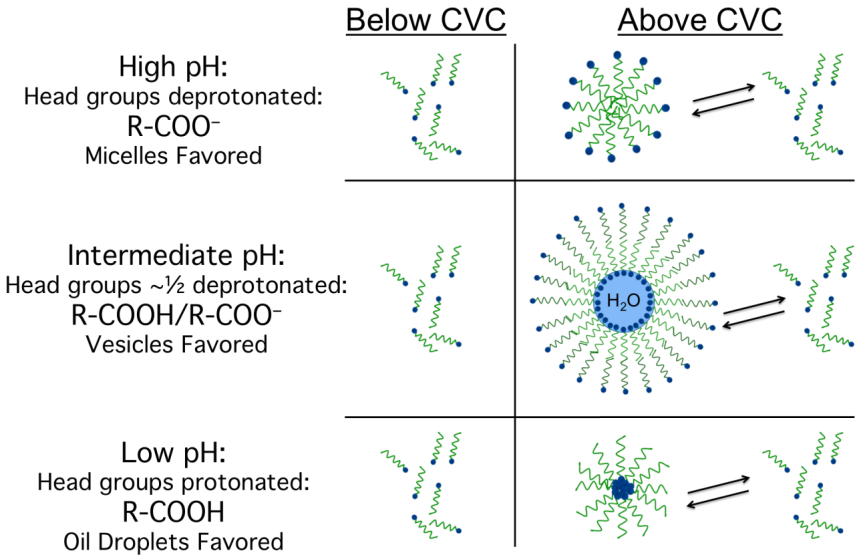

Figure 12.1.Schematic picture of the literature models for the phase behavior of fatty acids in aqueous solution where depending on the pH and concentration of fatty acid, oil droplets, vesicles, or micelles may be formed. These structures are all thought to be in equilibrium with monomers in solution. This diagram was inspired by a figure in Monnard and Deamer 2002.[33]

This schematic can be translated into a qualitative phase diagram (Figure 12.2) based on literature values describing the phase behavior of decanoic acid, one of the most commonly used fatty acid vesicle components used in the prebiotic literature.[31, 43, 44] Here, it is clear that the phase behavior is more complex than commonly appreciated. Perhaps the most interesting discrepancy is the large gap between the reported solubility of decanoic acid[45] and even the lowest reported critical aggregation concentrations. The behavior of decanoic acid in this regime has been largely ignored by the literature and is usually dismissed as undergoing some form of "pre-aggregation," but attempts to determine the

nature of this pre-aggregation" or, indeed to define the term have been lacking. We suggest in Appendix A based on preliminary DOSY NMR results that solutions of fatty acids in this concentration range may exist as small clusters composed of dimers of fatty acids held together by intermolecular forces. It is worth noting here that the monomeric solubility of decanoic acid of 0.37 mM at 30 °C reported by Eggenberger et al. in 1949[45] is not the value usually reported in handbooks, such as the CRC. The CRC reports a solubility value of 0.87 mM;[39] however, solutions of 0.8 mM decanoic acid at unadjusted pH form visible crystals in the solution flask when allowed to equilibrate at room temperature.[46]

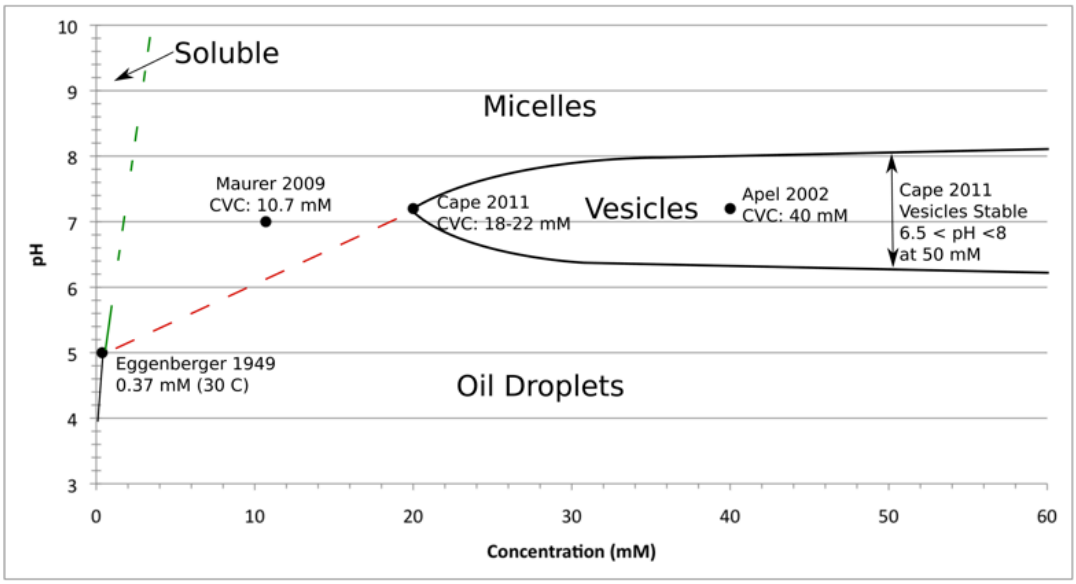

Figure 12.2. A schematic of the likely phase behavior of decanoic acid as a function of pH and concentration based off the CVC values reported by Cape et al.[31]. Two other literature CVC values are shown,[43, 44] as is the solubility of decanoic acid from Eggenberger et al.[45] The red and green dashed lines represent hypothetical phase transitions.

Closer examination of the literature also reveals considerable variance in the reported values for CVC, even under the same pH conditions, as shown in Figure 12.3.[15, 16, 31, 33, 34, 37, 43, 44, 47] This suggests that the phase behavior cannot be explained solely through the simple pH arguments that are often made. As shown in Table 12.1, the solutions of decanoic acid for which the CVC values were usually buffered and contained significant quantities of salt.[15, 31, 34, 37, 44, 47] Although the concentration of salt in solution is not always reported.

Indeed, Maurer and co-workers have shown that salt can have a large impact on the observed phase behavior of decanoic acid, and they suggest that the role of salt in these solutions has not been adequately addressed in the literature.[15]

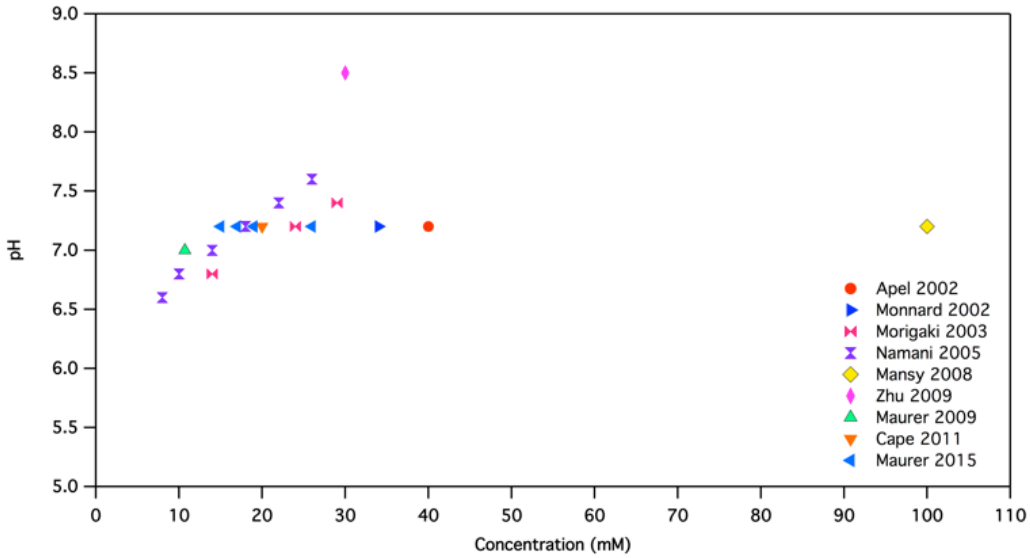

Figure 12.3. Reported literature values of the critical vesicle concentration for decanoic acid with varying pH.[15, 16, 31, 33, 34, 37, 43, 44, 47]

Table 12.1. Reported values for CVC and their corresponding solution conditions

Reported CVC (mM)	pH	Reported Buffer/Salt Conditions	Publication
40	7.2	Not Buffered	Apel et al. 2002[43]
43	7.2	Not Reported	Monnard and Deamer 2002[33]
14	6.8	100 mM Phosphate	Morigaki et al. 2003[37]
24	7.2		
29	7.4		
8	6.6	100 mM Phosphate	Namani and Walde 2005[34]
10	6.8		
14	7.0		
18	7.2		
22	7.4		
26	7.6		
≥100	(?)	Not Reported	Mansy et al. 2008[16]
10.7	7	100 mM Phosphate	Maurer et al. 2009[44]
30	8.5	200 mM Bicine	Zhu & Szostak 2009[47]
18-22	7.2	50 mM Phosphate	Cape 2011 et al.[31]
26	7.2	10 mM HEPES, 10 mM NaCl	Maurer and Nguyen 2016[15]
19		10 mM HEPES, 30 mM NaCl	
17		10 mM HEPES, 50 mM NaCl	
15		10 mM HEPES, 100 mM NaCl	

The role of salt in solutions of fatty acids is particularly interesting because of the sensitive balance required. Some salt is needed to form vesicles of fatty acids, but too much salt can cause them to rupture, flocculate, or otherwise fall apart.[31, 32, 37, 48] Fatty acid vesicles are known to be especially sensitive to divalent cations, such as Mg^{2+} and Ca^{2+},[32] an effect usually attributed to the tendency of salts of fatty acids to crystallize out of solution.[18, 32] Calcium ions in particular have been shown empirically to be more disruptive to vesicles than even other divalent cations, like Mg^{2+}.[32]

Studies of the effect of salts on fatty acid phase behavior can be somewhat limited, however, because the normal techniques of characterization require consideration of the bulk properties of a solution with many vesicles. Also, because of the stringent solvent conditions required to form vesicles from fatty acids, the aqueous solutions contain complex mixtures of these species, which makes it difficult to disentangle the effects of inorganic salts from the effects of either the buffer or the pH of the solution.

In such cases, it can be helpful to simplify the system under study and turn to examine the behavior of monolayer films using a Langmuir Trough. These monolayers can be more easily manipulated and observed than bulk solutions of bilayers. Furthermore, previous monolayer studies have been used to study the surface ionization of species[40, 49] and their aggregation behavior.[50] In this way, analysis of surfactants at the water surface can provide information about molecular interactions in aggregates, allowing them to inform our understanding of more complicated physical systems.

The phase behavior of long-tailed, insoluble fatty acids, such as stearic acid and palmitic acid, is very well-known in the literature, and some studies of the effects of salt on the compression isotherms of these species have been conducted.[51-56] Comparatively little is known about the behavior of shorter-chained fatty acids. Of these shorter fatty acids, the aggregation behavior of decanoic acid in bulk solution has been studied the most, making it

an attractive candidate for monolayer studies because direct comparison would be possible. However, it exists in a solubility regime that makes it experimentally infeasible to study using a Langmuir Trough. This soluble surfactant is too soluble to be studied like an insoluble surfactant, using compression isotherms, but it is also too insoluble to use normal techniques for the study of soluble surfactants, such as Gibbs adsorption isotherms.[46] Instead, the 14 carbon fatty acid, myristic acid, was chosen for these studies as a proxy for the shorter-chained fatty acids used to make vesicles. In the following, we report on the surface behavior of monolayer films of myristic acid deposited on aqueous solutions of varying salinity and the resultant effects on film stability.

12.2 Experimental Section:

For all experiments a custom-built 52 × 7 × 0.5 cm PTFE Langmuir trough with two computer-controlled mechanical PTFE barriers, using software from NIMA (KSV-NIMA, Finland). The barrier positions ranged from a surface area of 300 cm^2 to 30 cm^2, and were moved at a constant speed of 75 cm^2/min. The trough was coupled to a Wilhelmy balance that was used to measure surface pressure (π). Surface pressure is a measure of the decrease in surface tension from that of bare water ($\pi = \gamma_{H2O} - \gamma$). When an insoluble surfactant is deposited on top of the aqueous subphase, a monolayer film is formed. The two-dimensional phase of this film is controlled by moving the barriers, and a surface pressure-area (π-A) compression isotherm is obtained, giving surface thermodynamic information about the film. All isotherms were conducted at ambient temperature (~23 °C).

Myristic acid (≥99.0%) was dissolved in chloroform (≥99.8%) at 1 mg/mL. 25 μL of this solution was then deposited dropwise onto the aqueous subphase. The chloroform was allowed to evaporate, leaving a monolayer film of ~0.1 μmol of myristic acid. 18.2 MΩ (3 ppb TOC) water was used for the pure water subphase and was used to make all saline solutions. Aqueous solutions of sodium chloride (≥99.5%, BioXtra), potassium chloride

(≥99.0%, BioXtra), magnesium chloride (≥99.0%, BioXtra), and calcium chloride (≥99.0%, BioXtra) were made for a range of ionic strengths from 3 mM to 1 M. All chemicals were obtained from Sigma-Aldrich.

An example compression isotherm for myristic acid on water is shown in Figure 12.4. Myristic acid transitions from two-dimensional gas phase to a tilted-condensed (TC) phase before transitioning to the more ordered untilted-condensed (UTC) phase. The transition between the TC and UTC phase is characterized by a coexistence region where both phases exist. This region has a corresponding surface pressure associated with it, referred to as the coexistence pressure.

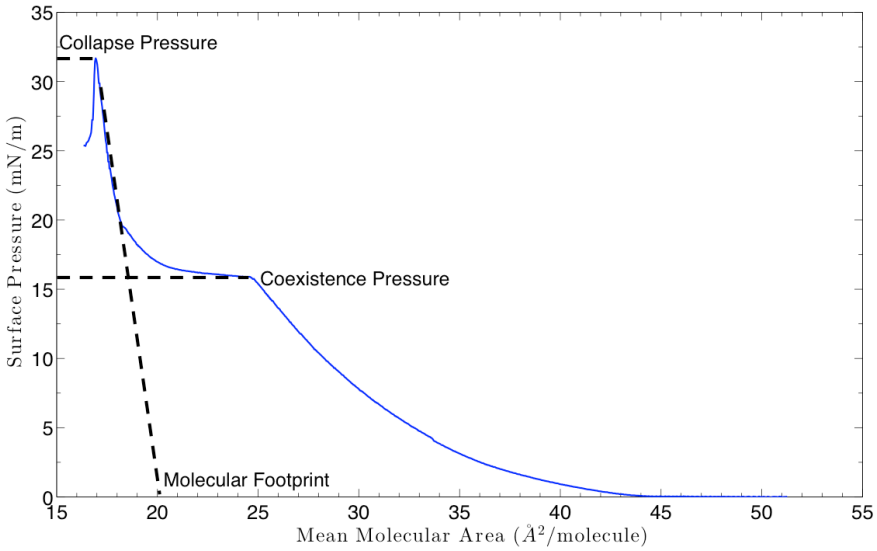

Figure 12.4. Sample myristic acid compression isotherm on clean water showing surface pressure as a function of mean molecular area. Three properties of interest are marked, showing the surface pressure of the coexistence region, collapse pressure, and the molecular footprint of the condensed film.

The surface pressure continues to increase as the UTC region is compressed further, until the film is no longer stable, at which point the film collapses into three-dimensional structures. The nature of this collapse depends on the film's properties, but can generally be characterized as either "constant area," where surface pressure rapidly decreases without

further compression (shown in Figure 12.4), or "constant pressure," where the surface pressure remains constant even as the film continues to be compressed. The surface pressure at which collapse occurs can be used as an indicator of a monolayer film's stability. Extrapolation from the slope of the surface pressure change in the UTC region gives myristic acid's footprint, or the average mean molecular area that a molecule of myristic acid takes up within the film. These three properties of the monolayer film were examined and used as proxies for understanding how the intermolecular interactions between molecules of myristic acid changes as a function of salinity, as described below.

12.3 Results and Discussion:

Compression isotherms of myristic acid films deposited on aqueous subphases of varying salinity were compared to that of bare water. We will first consider the effects of sodium chloride on myristic acid films before expanding our discussion to encompass the effects of potassium chloride, magnesium chloride, and calcium chloride as well. Sodium chloride is almost universally the salt of choice in making fatty acid vesicles, and, even when not added directly to solution, both sodium and chloride ions are often present due to the adjustment of solution pH by the addition of either sodium hydroxide or hydrochloric acid. In vesicular systems, therefore, it can be difficult to unravel the effects of the salt on the stability of the system from the pH effect. In fact, when fatty acid vesicles were first being studied, it was commonly thought that fatty acid vesicles could only be formed from lowering the pH of solutions of fatty acid micelles;[57] however, if the fatty acid is dissolved in a solution containing an equivalent amount of sodium chloride, it is not necessary to first raise and then lower the pH to obtain vesicles.[15] By studying monolayer films of myristic acid on saline solutions at unadjusted pH, we can begin to disentangle the role of salt from the effects of pH and buffer.

As shown in Figure 12.5, it is clear that the addition of salt has an immediate impact on

the monolayer films, even when present only at very dilute concentrations. As the concentration of sodium chloride is increased, the transition between the gas phase and the TC phase occurs at larger mean molecular area, and the molecular footprint likewise increased. The collapse pressure is also raised, and, interestingly, it appears under concentrated salt conditions, the collapse behavior transitions from the constant area regime to the constant pressure regime. The surface pressure of the coexistence region is relatively constant across salinity, but it appears to occur over a smaller relative range of mean molecular area as the salt concentration is increased.

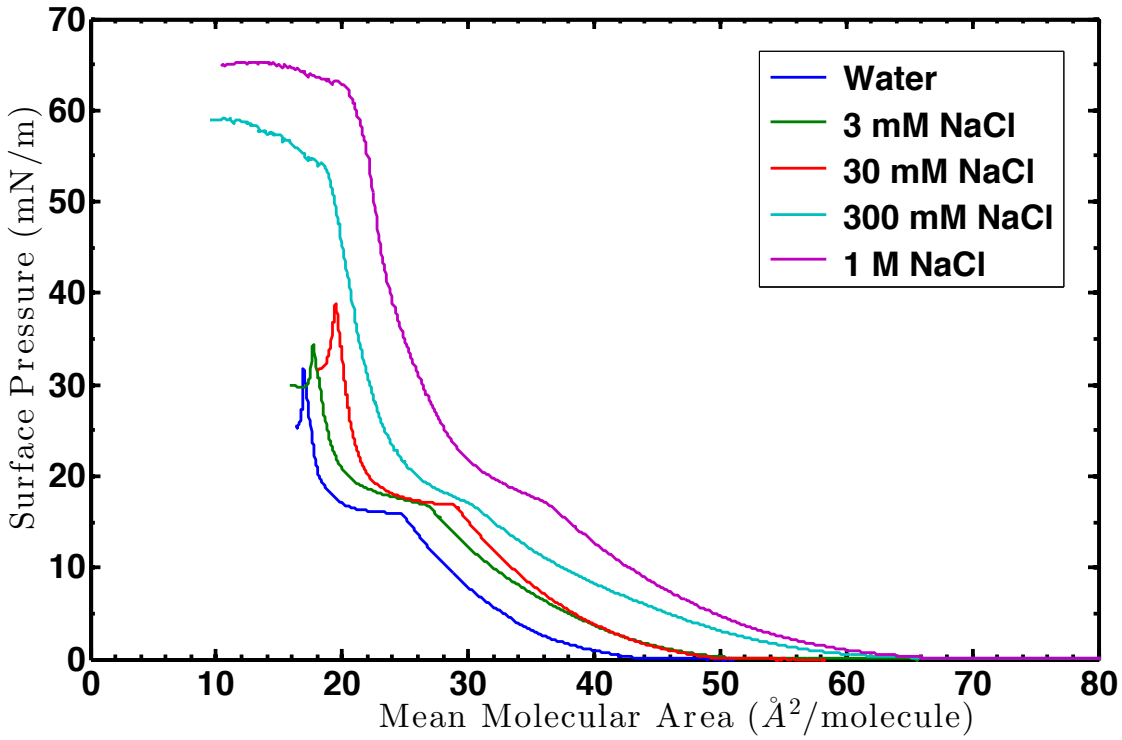

Figure 12.5. Representative compression isotherms for myristic acid deposited on pure water (blue) compared to films deposited on aqueous solutions of sodium chloride at concentrations of 3 mM (green), 30 mM (red), 300 mM (cyan), and 1 M (purple).

Taken together, these effects are all strongly indicative that the presence of sodium chloride stabilizes myristic acid films. This effect is consistent with previous observations in the literature of the stabilization of fatty acid monolayers by the addition of salt.[51, 53] This effect is usually explained as a result of ion pairing interactions between the cation, in this

case sodium, and the carboxylate head group of the fatty acid.[53] As salt ions screen the head group charge, the fatty acids experience less repulsion; this allows the film to condense more readily and leads to a monolayer that more readily lowers surface tension. This also explains the increased footprint of myristic acid at collapse, although this is perhaps counterintuitive. An earlier collapse does not necessarily indicate that a film is less stable, as collapse merely indicates the point at which the three-dimensional structures formed are more stable than maintaining the monolayer film. In the regimes where repulsions are minimized, this can happen for films with a larger footprint.

The stabilization of fatty acid films by the introduction of salt to the subphase has previously been observed primarily for films deposited onto a basic subphase (pH > 6.7).[53] It is certainly reasonable to assume that this effect would be greater for cases where more of the carboxylic acid head groups are deprotonated. Therefore, it is somewhat surprising that we see such relatively large changes in the surface behavior of myristic acid when deposited on an aqueous subphase, whose pH has not been adjusted (pH ~5). Additionally, fatty acids at the surface have a much higher pK_a than in the bulk. Myristic acid's surface pK_a is thought to be between 7.5 and 8,[41, 58] compared its bulk pK_a value of 4.9.[39] This means that less than 1% of the fatty acid molecules at the surface are likely to be deprotonated under our conditions. In this case very few molecules would be affected by ion pairing with sodium of the nature described in Adams et al. 2017.[53] It would also be expected that because so few carboxylate head groups are present in the film, the screening effects of sodium chloride would plateau rapidly, but this does not appear to occur. Therefore, it seems likely that the intermolecular interactions governing the stabilization of the myristic acid films may be more complex than this simple electrostatic model.

Expanding our study to other salts, as shown in Figures 12.6 and 12.7, we see the same broad trends in behavior that were observed for sodium chloride.

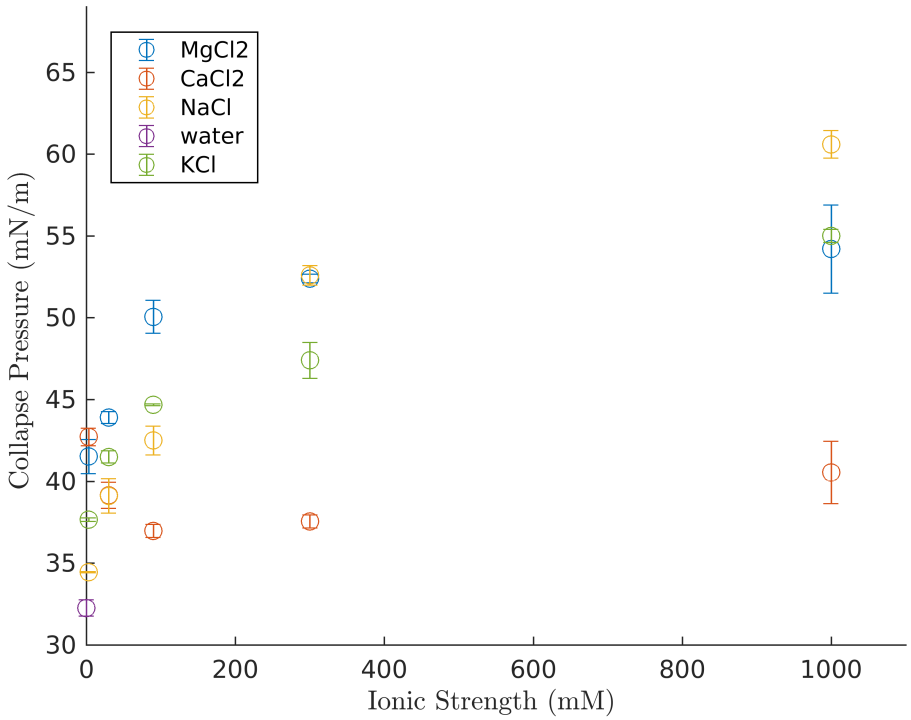

Figure 12.6. Observed collapse pressure of myristic acid films as a function of subphase ionic strength for aqueous solutions composed of sodium chloride (yellow), potassium chloride (green), magnesium chloride (blue), and calcium chloride (orange), compared to pure water (purple).

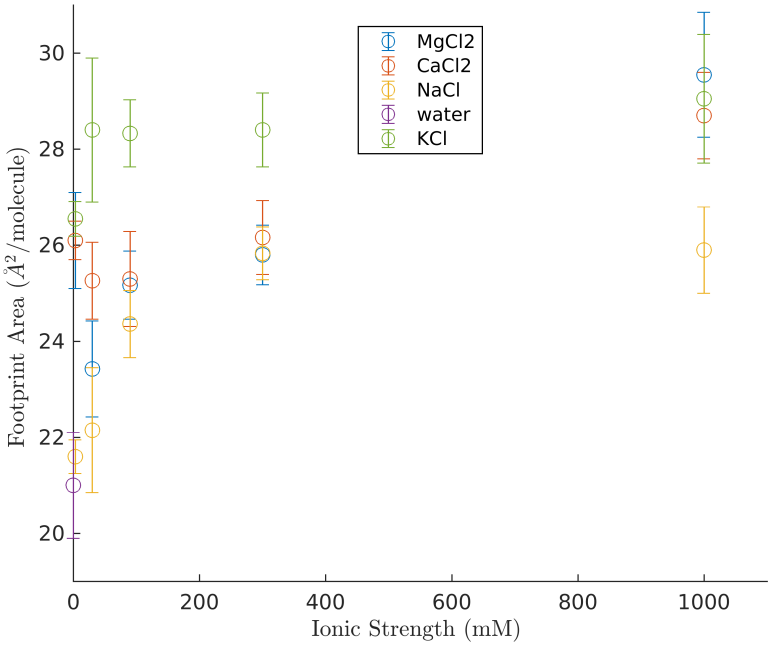

Figure 12.7. Observed molecular footprint of myristic acid films as a function of subphase ionic strength for aqueous solutions composed of sodium chloride (yellow), potassium chloride (green), magnesium chloride (blue), and calcium chloride (orange), compared to pure water (purple).

The collapse pressure is increased from that of myristic acid on pure water and generally continues to increase as the concentration of salt is raised. Similarly, the footprint of myristic acid is increased as salt is added and continues to increase slightly with increasing salinity, although this trend is less clear than for the collapse pressure. These changes suggest that the presence of salt, regardless of its chemical identity, generally stabilizes films of fatty acids, even under low pH conditions where few of the carboxylic acid head groups are deprotonated.

Beyond these overarching trends, closer inspection of these data reveals considerable differences in the effects of different salts on the phase behavior of pyruvic acid. For instance, the surface pressure of the coexistence region between the TC and UTC phases of myristic acid remains essentially the same as that found for bare water across all subphase ionic strengths for three of the salts, but this surface pressure is considerably lower for $CaCl_2$, even at an ionic strength of 3 mM (Figure 12.8). This is one example of a repeated theme: the effect of Ca^{2+} on films of myristic acid appears significantly different from that of other cations, including other divalent cations, such as Mg^{2+}.

Unlike the three other salts, calcium chloride stabilizes the myristic film most at low ionic strength, with films reaching their maximum collapse pressure for solutions where the ionic strength is 3 mM. Further addition of salt appears to have a minimal effect on the observed collapse pressure; although in every case, the collapse pressure is above that of bare water, suggesting some preferential stabilization. This behavior more closely resembles the salt effect that might be expected from the proposed model of electrostatic interactions leading to increased stability, where a plateau in the effect is rapidly reached because few of the head groups are deprotonated, in contrast to the effect of the other salts.

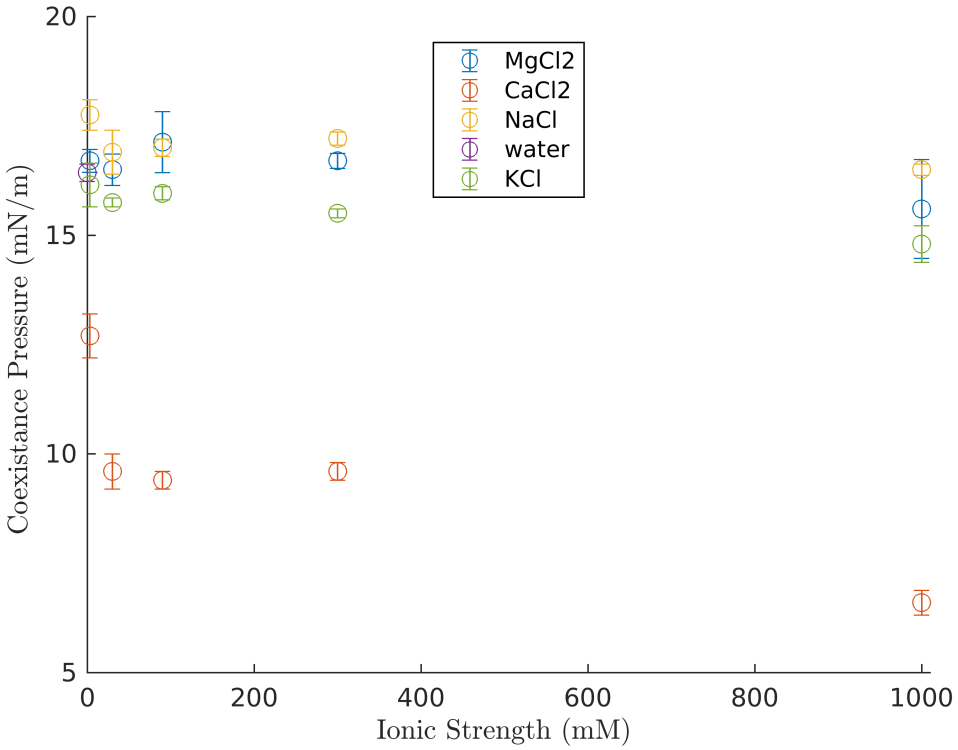

Figure 12.8. Observed surface pressure of the coexistence region of myristic acid films as a function of subphase ionic strength for aqueous solutions composed of sodium chloride (yellow), potassium chloride (green), magnesium chloride (blue), and calcium chloride (orange), compared to pure water (purple).

It is also interesting to note that the observed difference between the effects of Ca^{2+} and Mg^{2+} is not observed for monolayer films of palmitic acid, the 16 carbon fatty acids.[56] Films of palmitic acid deposited on aqueous calcium chloride with an ionic strength of 300 mM are considerably stabilized, with a collapse pressure of ~60 mN/m, and appear qualitatively similar to films deposited on a magnesium chloride subphase of the same ionic strength.[56] We have been able to replicate these results using palmitic acid in our laboratory, so it seems unlikely that the observed differences between myristic acid and palmitic acid are an artifact of experimental differences and are, instead, real. It is remarkable that the effect of Ca^{2+} phase behavior of two fatty acids that differ only by two CH_2 groups should be so different. While myristic acid is shorter than palmitic acid, it still acts as a well-behaved insoluble surfactant with no significant concentration in the bulk phase. It would also be

expected that salt would interact primarily with the carboxylic acid head groups, which are unchanged between molecules in this experiment. One possible explanation for this difference may be due to the Krafft temperatures (T_K) of the two species. T_K is the critical temperature where the solubility of an ionic surfactant in aqueous solution increases dramatically, and it is known to decrease with increasing salt concentration.[59] It is possible that the addition of Ca^{2+} to the aqueous subphase causes the Krafft temperature of myristic acid to be lowered sufficiently that it is reached at the ambient temperature used for our trough studies. If this is the case, it would be expected that the interactions of shorter-tailed fatty acids with Ca^{2+} would more closely resemble those of myrisitic acid than palmitic acid. It is, however, unclear why Ca^{2+} would be so much more efficient at lowering the Krafft temperature than other cations, including the divalent Mg^{2+}.

The effect of salts on fatty acids is often categorized by the valency of the cation. It is known that divalent cations generally are more disruptive to fatty acid vesicles than monovalent cations; although, it has been empirically observed that Ca^{2+} has a larger effect than Mg^{2+}.[32] Recent studies have also shown that Ca^{2+} coordinates more strongly to fatty acids than other cations.[55, 56] It seems unlikely that this difference can be explained solely by the size of Ca^{2+} as the larger K^+ appears to behave relatively similarly to Na^+. Similarly, simple explanations for the observed trends are not sufficient, even to explain the observed behavior of Na^+, K^+, and Mg^{2+}. The behavior of these three species does not follow the expected ordering based the Hofmeister series, for instance, which suggests that the ordering the cations follow should be $K^+ > Na^+ > Mg^{2+} > Ca^{2+}$.[60] However, it is observed that at high ionic strength the collapse pressure is highest for Na^+ and quite similar for K^+ and Mg^{2+}. Moreover, the relative trends for these species are not constant as a function of ionic strength. It appears that simple categorization of salts based on valency, size, or lyotropy is not sufficient to explain the observed behavior of fatty acid films with salinity. It is clear

that care must be taken before generalizing the results from a study of the effects of a single salt and fatty acid to other salts, or, indeed, to other fatty acids. Until there is a sufficient understanding of the intermolecular interactions underpinning these observed behaviors to be predictive, it is likely that detailed studies of each molecular system must be undertaken to establish the effects of a given salt on the phase behavior of the fatty acid in question.

12.4 Conclusions:

It is clear that the presence of salt has an important stabilizing effect on monolayer films of fatty acids, manifested by an increase in collapse pressure and footprint from those observed for bare water. However, the extent and nature of this stabilizing effect appears to be dependent on both the specific salt and the specific fatty acid being studied. Simple trends are not sufficient to explain the observed behavior. The effect of Ca^{2+} is particularly intriguing and warrants further investigation, especially given its known destabilizing effect on fatty acid vesicles.

The phase behavior of fatty acids is usually described by invoking the protonation state of the head group, but the effect of salt and ionic strength is rarely decoupled from the effect of changes in pH of solutions. Indeed, the stabilization of films by salts is surprisingly large even for systems that are primarily unionized. This suggests that purely electrostatic interactions may not account for the entirety of the observed effect. We suggest that there is a clear need for a better theoretical understanding of the intermolecular interactions between species that can be used to explain the empirically determined behaviors.

12.5 Bibliography:

1. McBain, J. W.; Sierichs, W. C. The solubility of sodium and potassium soaps and the phase diagrams of aqueous potassium soaps. *J. Am. Oil Chem. Soc.* **1948,** *25*, 221-225.

2. Cochran, R. E.; Laskina, O.; Jayarathne, T.; Laskin, A.; Laskin, J.; Lin, P.; Sultana, C.; Lee, C.; Moore, K. A.; Cappa, C. D. Analysis of organic anionic surfactants in fine and

coarse fractions of freshly emitted sea spray aerosol. *Environ. Sci. Technol.* **2016,** *50*, 2477-2486.

3. Cochran, R. E.; Laskina, O.; Trueblood, J. V.; Estillore, A. D.; Morris, H. S.; Jayarathne, T.; Sultana, C. M.; Lee, C.; Lin, P.; Laskin, J., et al. Molecular diversity of sea spray aerosol particles: Impact of ocean biology on particle composition and hygroscopicity. *Chem* **2017,** *2*, 655-667.

4. Tervahattu, H.; Juhanoja, J.; Vaida, V.; Tuck, A. F.; Niemi, J. V.; Kupiainen, K.; Kulmala, M.; Vehkamaki, H. Fatty acids on continental sulfate aerosol particles. *J. Geophys. Res.* **2005,** *110*, Article number D06207

5. Tervahattu, H.; Hartonen, K.; Kerminen, V. M.; Kupiainen, K.; Aarnio, P.; Koskentalo, T.; Tuck, A. F.; Vaida, V. New evidence of an organic layer on marine aerosols. *J. Geophys. Res.* **2002,** *107*, 4053-4060.

6. Gilman, J. B.; Eliason, T. L.; Fast, A.; Vaida, V. Selectivity and stability of organic films at the air-aqueous interface. *J. Colloid Interface Sci.* **2004,** *280*, 234-243.

7. McCollom, T. M.; Ritter, G.; Simoneit, B. R. Lipid synthesis under hydrothermal conditions by Fischer-Tropsch-Type reactions. *Origins Life Evol. Biosphere* **1999,** *29*, 153-166.

8. Rushdi, A. I.; Simoneit, B. R. T. Lipid formation by aqueous Fischer-Tropsch-Type synthesis over a temperature range of 100 to 400 °C. *Origins Life Evol. Biosphere* **2001,** *31*, 103-118.

9. Cooper, G.; Reed, C.; Nguyen, D.; Carter, M.; Wang, Y. Detection and formation scenario of citric acid, pyruvic acid, and other possible metabolism precursors in carbonaceous meteorites. *Proc. Natl. Acad. Sci.* **2011,** *108*, 14015-14020.

10. Pizzarello, S. Chemical evolution and meteorites: An update. *Origins Life Evol. Biosphere* **2004,** *34*, 25-34.

11. Luisi, P. L.; Walde, P.; Oberholzer, T. Lipid vesicles as possible intermediates in the origin of life. *Curr. Opin. Colloid Interface Sci.* **1999,** *4*, 33-39.

12. Hanczyc, M. M.; Fujikawa, S. M.; Szostak, J. W. Experimental models of primitive cellular compartments: Encapsulation, growth, and division. *Science* **2003,** *302*, 618-622.

13. Deamer, D.; Dworkin, J. P.; Sandford, S. A.; Bernstein, M. P.; Allamandola, L. J. The first cell membranes. *Astrobio.* **2002,** *2*, 371-381.

14. Maurer, S. E.; Monnard, P.-A. Primitive membrane formation, characteristics and roles in the emergent properties of a protocell. *Entropy* **2011,** *13*, 466-484.

15. Maurer, S. E.; Nguyen, G. Prebiotic vesicle formation and the necessity of salts. *Origins Life Evol. Biosphere* **2016,** *46*, 215-222.

16. Mansy, S. S.; Schrum, J. P.; Krishnamurthy, M.; Tobe, S.; Treco, D. A.; Szostak, J. W. Template-directed synthesis of a genetic polymer in a model protocell. *Nature* **2008,** *454*, 122-U10.

17. Budin, I.; Prywes, N.; Zhang, N.; Szostak, Jack W. Chain-length heterogeneity allows for the assembly of fatty acid vesicles in dilute solutions. *Biophys. J.* **2014,** *107*, 1582-1590.

18. Chen, I. A.; Salehi-Ashtiani, K.; Szostak, J. W. RNA catalysis in model protocell vesicles. *J. Am. Chem. Soc.* **2005,** *127*, 13213-13219.

19. Morigaki, K.; Walde, P. Fatty acid vesicles. *Curr. Opin. Colloid Interface Sci.* **2007,** *12*, 75-80.

20. Mansy, S. S. Membrane transport in primitive cells. *Cold Spring Harbor Persp. Biol.* **2010,** *2*, 14.

21. Budin, I.; Szostak, J. W. Physical effects underlying the transition from primitive to modern cell membranes. *Proc. Natl. Acad. Sci.* **2011,** *108*, 5249-5254.

22. Szostak, J. W.; Bartel, D. P.; Luisi, P. L. Synthesizing life. *Nature* **2001,** *409*, 387-390.

23. Mansy, S. S. Model protocells from single-chain lipids. *Int. J. Molec. Sci.* **2009,** *10*, 835-843.

24. Spencer, A. C.; Torre, P.; Mansy, S. S. The encapsulation of cell-free transcription and translation machinery in vesicles for the construction of cellular mimics. *J. Visual. Exp.* **2013**, e51304-e51304.

25. Pohorille, A.; Deamer, D. Self-assembly and function of primitive cell membranes. *Res. Microbiol.* **2009,** *160*, 449-456.

26. Stano, P.; D'Aguanno, E.; Bolz, J.; Fahr, A.; Luisi, P. L. A remarkable self-organization process as the origin of primitive functional cells. *Angew. Chem. Int. Ed.* **2013,** *52*, 13397-13400.

27. Chen, I. A.; Hanczyc, M. M.; Sazani, P. L.; Szostak, J. W., Protocells: Genetic polymers inside membrane vesicles. In *RNA world*, 3 ed.; Gesteland, R. F.; Cech, T. R.; Atkins, J. F., Eds. 2006; Vol. 43, pp 57-88.

28. Hazen, R. M.; Sverjensky, D. A. Mineral surfaces, geochemical complexities, and the origins of life. *Cold Spring Harbor Persp. Biol.* **2010,** *2*, a002162.

29. Monnard, P.-A.; Deamer, D. W., Membrane self-assembly processes: Steps toward the first cellular life. In *Minimal cell: The biophysics of cell compartment and origin of cell functionality*, Luisi, P. L.; Stano, P., Eds. 2011.

30. Monnard, P. A.; DeClue, M. S.; Ziock, H. J. Organic nano-compartments as biomimetic reactors and protocells. *Curr. Nanosci.* **2008,** *4*, 71-87.

31. Cape, J. L.; Monnard, P.-A.; Boncella, J. M. Prebiotically relevant mixed fatty acid vesicles support anionic solute encapsulation and photochemically catalyzed trans-membrane charge transport. *Chem. Sci.* **2011,** *2*, 661-671.

32. Monnard, P. A.; Apel, C. L.; Kanavarioti, A.; Deamer, D. W. Influence of ionic inorganic solutes on self-assembly and polymerization processes related to early forms of life: Implications for a prebiotic aqueous medium. *Astrobio.* **2002,** *2*, 139-152.

33. Monnard, P. A.; Deamer, D. W. Membrane self-assembly processes: Steps toward the first cellular life. *Anat. Rec.* **2002,** *268*, 196-207.

34. Namani, T.; Walde, P. From decanoate micelles to decanoic acid/dodecylbenzenesulfonate vesicles. *Langmuir* **2005,** *21*, 6210-6219.

35. Black, R. A.; Blosser, M. C.; Stottrup, B. L.; Tavakley, R.; Deamer, D. W.; Keller, S. L. Nucleobases bind to and stabilize aggregates of a prebiotic amphiphile, providing a viable mechanism for the emergence of protocells. *Proc. Natl. Acad. Sci.* **2013,** *110*, 13272-13276.

36. Guida, V. Thermodynamics and kinetics of vesicles formation processes. *Adv. Colloid Interface Sci.* **2010,** *161*, 77-88.

37. Morigaki, K.; Walde, P.; Misran, M.; Robinson, B. H. Thermodynamic and kinetic stability. Properties of micelles and vesicles formed by the decanoic acid/decanoate system. *Colloids Surf., A* **2003**, 37-44.

38. Laughlin, R. G. Equilibrium vesicles: Fact or fiction? *Colloids Surf., A* **1997,** *128*, 27-38.

39. Haynes, W. M., *CRC handbook of chemistry and physics*. CRC press: 2014.

40. Wellen, B. A.; Lach, E. A.; Allen, H. C. Surface pKa of octanoic, nonanoic, and decanoic fatty acids at the air-water interface: Applications to atmospheric aerosol chemistry. *Phys. Chem. Chem. Phys.* **2017**.

41. McLean, D. S.; Vercoe, D.; Stack, K. R.; Richardson, D. The colloidal pKa of lipophilic extractives commonly found in pinus radiata. *Appita Journal: Journal of the Technical Association of the Australian and New Zealand Pulp and Paper Industry* **2005,** *58*, 362.

42. Cistola, D. P.; Hamilton, J. A.; Jackson, D.; Small, D. M. Ionization and phase behavior of fatty acids in water: Application of the Gibbs phase rule. *Biochem.* **1988,** *27*, 1881-1888.

43. Apel, C. L.; Deamer, D. W.; Mautner, M. N. Self-assembled vesicles of monocarboxylic acids and alcohols: Conditions for stability and for the encapsulation of biopolymers. *Biochim. Biophys. Acta-Biomembranes* **2002,** *1559*, 1-9.

44. Maurer, S. E.; Deamer, D. W.; Boncella, J. M.; Monnard, P. A. Chemical evolution of amphiphiles: Glycerol monoacyl derivatives stabilize plausible prebiotic membranes. *Astrobio.* **2009,** *9*, 979-987.

45. Eggenberger, D.; Broome, F.; Ralston, A.; Harwood, H. The solubilities of the normal saturated fatty acids in water. *J. Org. Chem.* **1949,** *14*, 1108-1110.

46. Kessenich, B. Surface thermodynamics of decanoic acid. University of Colorado Boulder, 2015.

47. Zhu, T. F.; Szostak, J. W. Coupled growth and division of model protocell membranes. *J. Am. Chem. Soc.* **2009,** *131*, 5705-5713.

48. Douliez, J.-P.; Gaillard, C. Self-assembly of fatty acids: From foams to protocell vesicles. *New J. Chem.* **2014,** *38*, 5142-5148.

49. Griffith, E. C.; Vaida, V. Ionization state of l-phenylalanine at the air-water interface. *J. Am. Chem. Soc.* **2013,** *135*, 710-716.

50. Fedotenko, I. A.; Stefaniu, C.; Brezesinski, G.; Zumbuehl, A. Monolayer properties of 1,3-diamidophospholipids. *Langmuir* **2013,** *29*, 9428-9435.

51. Brzozowska, A. M.; Duits, M. H. G.; Mugele, F. Stability of stearic acid monolayers on artificial sea water. *Colloids Surf., A* **2012,** *407*, 38-48.

52. Kumar, N.; Wang, L.; Siretanu, I.; Duits, M.; Mugele, F. Salt dependent stability of stearic acid Langmuir–Blodgett films exposed to aqueous electrolytes. *Langmuir* **2013,** *29*, 5150-5159.

53. Adams, E. M.; Allen, H. C. Palmitic acid on salt subphases and in mixed monolayers of cerebrosides: Application to atmospheric aerosol chemistry. *Atmosphere* **2013,** *4*, 315-336.

54. Huang, Z.; Hua, W.; Verreault, D.; Allen, H. C. Influence of salt purity on Na+ and palmitic acid interactions. *J. Phys. Chem. A* **2013,** *117*, 13412-13418.

55. Tang, C. Y.; Allen, H. C. Ionic binding of Na+ versus K+ to the carboxylic acid headgroup of palmitic acid monolayers studied by vibrational sum frequency generation spectroscopy. *J. Phys. Chem. A* **2009,** *113*, 7383-7393.

56. Tang, C. Y.; Huang, Z.; Allen, H. C. Binding of Mg^{2+} and Ca^{2+} to palmitic acid and deprotonation of the COOH headgroup studied by vibrational sum frequency generation spectroscopy. *J. Phys. Chem. B* **2010,** *114*, 17068-17076.

57. Monnard, P.-A.; Deamer, D. W. Preparation of vesicles from nonphospholipid amphiphiles. *Methods Enzymol.* **2003,** *372*, 133-151.

58. Kanicky, J. R.; Poniatowski, A. F.; Mehta, N. R.; Shah, D. O. Cooperativity among molecules at interfaces in relation to various technological processes: Effect of chain length on the pKa of fatty acid salt solutions. *Langmuir* **1999,** *16*, 172-177.

59. Chu, Z.; Feng, Y. Empirical correlations between krafft temperature and tail length for amidosulfobetaine surfactants in the presence of inorganic salt. *Langmuir* **2012,** *28*, 1175-1181.

60. Cacace, M.; Landau, E.; Ramsden, J. The Hofmeister series: Salt and solvent effects on interfacial phenomena. *Quarterly reviews of biophysics* **1997,** *30*, 241-277.

13. Conclusion

"This dread and darkness of the mind cannot be dispelled by the sunbeams, ... but only by an understanding of the outward form and inner workings of nature."
Lucretius, ca. 99 – ca. 55 B.C.E.

Throughout this thesis, we have seen that the reactivity of even simple systems in aqueous environments can be deceptively complex. Using the example of α-keto acids, it becomes clear that even if a single, pure compound is the initial starting material, the complexity of the system rapidly increases as soon as the compound is dissolved in water. The mixture of molecular species formed is dependent on solution conditions, and these can, in turn, affect the photochemical reactivity of the system.

Photolysis of α-keto acids also increases the complexity of the solution in three distinct ways, particularly for longer-tailed alkyl α-keto acids. First, many of the products formed are covalently bonded dimers and trimers of the starting material. Photochemistry has, in this case, been used to build larger molecules by generating organic radicals that recombine, forming C-C bonds. This is an instance of the generation of molecular complexity.

Second, the observed photoproducts present in the post-photolysis solutions are often the result of secondary chemistry derived from reactive intermediate species. Once light is introduced to the system, a solution that initially contained only one photoactive species rapidly generates these reactive intermediates, some of which are themselves photoactive. For α-keto acids, these new photoactive species are usually also α-keto acids. These species, therefore, react in a similar manner and generate organic radicals. Organic radicals are indiscriminate, recombining with other radicals as they are encountered. This rapidly increases the number of photoproducts generated, and increases the chemical complexity of the system significantly. This effect is further amplified when additional compounds are

added to the solution, even when they are not photoactive because α-keto acids can also act as photo-initiators. Although, it is worth noting that these products can, in most cases, be predicted and identified using the detailed mechanistic framework that has been established. So, while the chemical complexity of the system is increased, the resultant mixture is not an impenetrable and intractable tar.

Finally, the photochemistry of the alkyl α-keto acids generates multi-tailed, surface-active lipids, and these lipids spontaneously self-assemble into ordered, spherical, monodisperse structures. The generation of aggregates and larger assemblages of molecules is an example of the generation of supramolecular complexity. Studies of the behavior of particles and the intermolecular interactions of lipid molecules in solution and at the air-water interface suggest that there are missing details to our fundamental understanding of the nature of aggregation, even for well-studied systems.

The level of complexity of these fundamental laboratory studies cannot approach that of the natural environment, and study of the environment in its full complexity requires the introduction of generalizations and coarse-graining. There is a natural tendency to try to explain systems as simply as possible using broad strokes, especially when considering aggregation and larger scale phenomena that are difficult to probe molecularly. We have seen throughout that this approach is not always successful, and that simple trends and explanations for behavior may not be capable of providing predictive understanding. However, there is a middle ground. As shown here, detailed studies of model systems can be used to fill in gaps in our fundamental understanding while providing a framework that allows for more successful and predictive generalizations as more complex systems are considered.

References

1. Abramov, O.; Kring, D. A.; Mojzsis, S. J. The impact environment of the Hadean Earth. *Chem. Erde Geochem.* **2013,** *73*, 227-248.

2. Abramov, O.; Mojzsis, S. J. Microbial habitability of the Hadean Earth during the late heavy bombardment. *Nature* **2009,** *459*, 419-422.

3. Adams, E. M.; Allen, H. C. Palmitic acid on salt subphases and in mixed monolayers of cerebrosides: Application to atmospheric aerosol chemistry. *Atmosphere* **2013,** *4*, 315-336.

4. Adamson, A. W.; Gast, A. P., *Physical chemistry of surfaces*. 6 ed.; John Wiley & Sons, Inc.: New York, 1997.

5. Al-Azmi, A.; Elassar, A. Z. A.; Booth, B. L. The chemistry of diaminomaleonitrile and its utility in heterocyclic synthesis. *Tetrahedron* **2003,** *59*, 2749-2763.

6. Albrecht, M.; Borba, A.; Barbu-Debus, K. L.; Dittrich, B.; Fausto, R.; Grimme, S.; Mahjoub, A.; Nedić, M.; Schmitt, U.; Schrader, L., et al. Chirality influence on the aggregation of methyl mandelate. *New J. Chem.* **2010,** *34*, 1266-1285.

7. Altieri, K.; Seitzinger, S.; Carlton, A.; Turpin, B.; Klein, G.; Marshall, A. Oligomers formed through in-cloud methylglyoxal reactions: Chemical composition, properties, and mechanisms investigated by ultra-high resolution FT-ICR mass spectrometry. *Atmos. Environ.* **2008,** *42*, 1476-1490.

8. Altieri, K. E.; Carlton, A. G.; Lim, H.-J.; Turpin, B. J.; Seitzinger, S. P. Evidence for oligomer formation in clouds: Reactions of isoprene oxidation products. *Environ. Sci. Technol.* **2006,** *40*, 4956-4960.

9. Alvarez-Idaboy, J. R.; Mora-Diez, N.; Boyd, R. J.; Vivier-Bunge, A. On the importance of prereactive complexes in molecule-radical reactions: Hydrogen abstraction from aldehydes by OH. *J. Am. Chem. Soc.* **2001,** *123*, 2018-2024.

10. Alves, C. A. Chemistry between the sea surface microlayer and marine aerosols. *Quim. Nova* **2014,** *37*, 1382-1400.

11. Alves, I. D.; Correia, I.; Jiao, C. Y.; Sachon, E.; Sagan, S.; Lavielle, S.; Tollin, G.; Chassaing, G. The interaction of cell-penetrating peptides with lipid model systems and subsequent lipid reorganization: Thermodynamic and structural characterization. *J. Pept. Sci.* **2009,** *15*, 200-209.

12. Anbar, A. D. Oceans elements and evolution. *Science* **2008,** *322* 1481-1483.

13. Andreae, M. O.; Talbot, R. W.; Li, S. M. Atmospheric measurements of pyruvic and formic acid. *J. Geophys. Res. Atmos.* **1987,** *92*, 6635-6641.

14. Antonietti, M.; Forster, S. Vesicles and liposomes: A self-assembly principle beyond lipids. *Adv. Mater.* **2003,** *15*, 1323-1333.

15. Apel, C. L.; Deamer, D. W.; Mautner, M. N. Self-assembled vesicles of monocarboxylic acids and alcohols: Conditions for stability and for the encapsulation of biopolymers. *Biochim. Biophys. Acta-Biomembranes* **2002,** *1559*, 1-9.

16. Arakaki, T.; Anastasio, C.; Kuroki, Y.; Nakajima, H.; Okada, K.; Kotani, Y.; Handa, D.; Azechi, S.; Kimura, T.; Tsuhako, A. A general scavenging rate constant for reaction of hydroxyl radical with organic carbon in atmospheric waters. *Environ. Sci. Technol.* **2013,** *47*, 8196-8203.

17. Asad, A.; Mmereki, B.; Donaldson, D. Enhanced uptake of water by oxidatively processed oleic acid. *Atmo. Chem. Phys.* **2004,** *4*, 2083-2089.

18. Axson, J. L.; Takahashi, K.; De Haan, D. O.; Vaida, V. Gas-phase water-mediated equilibrium between methylglyoxal and its geminal diol. *Proc. Natl. Acad. Sci.* **2010,** *107*, 6687-6692.

19. Bada, J. L. New insights into prebiotic chemistry from Stanley Miller's spark discharge experiments. *Chem. Soc. Rev.* **2013,** *42*, 2186.

20. Baek, S.; Field, R.; Goldstone, M.; Kirk, P.; Lester, J.; Perry, R. A review of atmospheric polycyclic aromatic hydrocarbons: Sources, fate and behavior. *Water, Air, Soil Pollut.* **1991,** *60*, 279-300.

21. Bahadur, K. Photosynthesis of amino-acids from paraformaldehyde and potassium nitrate. *Nature* **1954,** *173*, 1141.

22. Bahadur, K.; Ranganayaki, S.; Santamaria, L. Photosynthesis of amino-acids from paraformaldehyde involving the fixation of nitrogen in the presence of colloidal molybdenum oxide as catalyst. *Nature* **1958,** *182*, 1668.

23. Baly, E. C. C.; Heilbron, I. M.; Barker, W. F. Photocatalysis: Part I. The synthesis of formaldehyde and carbohydrates from carbon dioxide and water. *J. Chem. Soc. Trans.* **1921,** *119*, 1025-1035.

24. Banerjee, A.; Ganguly, G.; Tripathi, R.; Nair, N. N.; Paul, A. Unearthing the mechanism of prebiotic nitrile bond reduction in hydrogen cyanide through a curious association of two molecular radical anions. *Chem. Eur. J.* **2014,** *20*, 6348-6357.

25. Banerjee, P.; Yashonath, S.; Bagchi, B. Rotation driven translational diffusion of polyatomic ions in water: A novel mechanism for breakdown of Stokes-Einstein relation. *J. Chem. Phys.* **2017,** *146*, 164502.

26. Bao, L.; Matsumoto, M.; Kubota, T.; Sekiguchi, K.; Wang, Q.; Sakamoto, K. Gas/particle partitioning of low-molecular-weight dicarboxylic acids at a suburban site in Saitama, Japan. *Atmos. Environ.* **2012,** *47*, 546-553.

27. Bar-Nun, A.; Chang, S. Photochemical-reactions of water and carbon monoxide in Earth's primitive atmosphere. *J. Geophys. Res. Oceans* **1983,** *88*, 6662-6672.

28. Bar-Nun, A.; Hartman, H. Synthesis of organic-compounds from carbon monoxide and water by UV photolysis. *Origins Life Evol. Biosphere* **1978,** *9*, 93-101.

29. Barks, H. L.; Buckley, R.; Grieves, G. A.; Di Mauro, E.; Hud, N. V.; Orlando, T. M. Guanine, adenine, and hypoxanthine production in UV-irradiated formamide solutions: Relaxation of the requirements for prebiotic purine nucleobase formation. *ChemBioChem* **2010,** *11*, 1240-1243.

30. Barnes, G. The effects of monolayers on the evaporation of liquids. *Adv. Colloid Interface Sci.* **1986,** *25*, 89-200.

31. Becker, M. Über magnetische kernresonanzspektren wäßriger brenztraubensäurelösungen. *Ber. Bunsen-Ges. Phys. Chem* **1964,** *68*, 669-676.

32. Beer, J.; Mende, W.; Stellmacher, R. The role of the sun in climate forcing. *Quaternary Science Reviews* **2000,** *19*, 403-415.

33. Bell, R. P.; Rand, M. H.; Wynnejones, K. M. A. Kinetics of hydration of acetaldehyde. *Trans. Faraday Soc.* **1956,** *52*, 1093-1102.

34. Berendsen, H.; Grigera, J.; Straatsma, T. The missing term in effective pair potentials. *J. Phys. Chem.* **1987,** *91*, 6269-6271.

35. Berges, M. G.; Warneck, P. Product quantum yields for the 350 nm photodecomposition of pyruvic acid in air. *Ber. Bunsen-Ges. Phys. Chem* **1992,** *96*, 413-416.

36. Bergstrom, L. M.; Skoglund, S.; Danerlov, K.; Garamus, V. M.; Pedersen, J. S. The growth of micelles, and the transition to bilayers, in mixtures of a single-chain and a double-chain cationic surfactant investigated with small-angle neutron scattering. *Soft Matter* **2011,** *7*, 10935-10944.

37. Bernard, F.; Ciuraru, R.; Boréave, A.; George, C. Photosensitized formation of secondary organic aerosols above the air/water interface. *Environ. Sci. Technol.* **2016,** *50*, 8678-8686.

38. Berne, B. J.; Weeks, J. D.; Zhou, R. Dewetting and hydrophobic interaction in physical and biological systems. *Annu. Rev. Phys. Chem.* **2009,** *60*, 85-103.

39. Bernstein, M. P.; Dworkin, J. P.; Sandford, S. A.; Cooper, G. W.; Allamandola, L. J. Racemic amino acids from the ultraviolet photolysis of interstellar ice analogues. *Nature* **2002,** *416*, 401-403.

40. Bertram, A. K.; Ivanov, A. V.; Hunter, M.; Molina, L. T.; Molina, M. J. The reaction probability of OH on organic surfaces of tropospheric interest. *J. Phys. Chem. A* **2001,** *105*, 9415-9421.

41. Bhattacharyya, S.; Bagchi, B. Anomalous diffusion of small particles in dense liquids. *J. Chem. Phys.* **1997,** *106*, 1757-1763.

42. Bianco, C. D.; Torino, D.; Mansy, S. S. Vesicle stability and dynamics: An undergraduate biochemistry laboratory. *J. Chem. Educ.* **2014,** *91*, 1228-1231.

43. Bird, A. DNA methylation patterns and epigenetic memory. *Genes Dev.* **2002,** *16*, 6-21.

44. Black, R. A.; Blosser, M. C.; Stottrup, B. L.; Tavakley, R.; Deamer, D. W.; Keller, S. L. Nucleobases bind to and stabilize aggregates of a prebiotic amphiphile, providing a viable mechanism for the emergence of protocells. *Proc. Natl. Acad. Sci.* **2013,** *110*, 13272-13276.

45. Blake, R. E.; Chang, S. J.; Lepland, A. Phosphate oxygen isotopic evidence for a temperate and biologically active archaean ocean. *Nature* **2010,** *464*, 1029-1032.

46. Blando, J. D.; Turpin, B. J. Secondary organic aerosol formation in cloud and fog droplets: A literature evaluation of plausibility. *Atmos. Environ.* **2000,** *34*, 1623-1632.

47. Blodgett, K. B. Films built by depositing successive monomolecular layers on a solid surface. *J. Am. Chem. Soc.* **1935,** *57*, 1007-1022.

48. Blower, P. G.; Shamay, E.; Kringle, L.; Ota, S. T.; Richmond, G. L. Surface behavior of malonic acid adsorption at the air/water interface. *J. Phys. Chem. A* **2013,** *117*, 2529-2542.

49. Boris, A. J.; Desyaterik, Y.; Collett, J. L. How do components of real cloud water affect aqueous pyruvate oxidation? *Atmo. Res.* **2014,** *143*, 95-106.

50. Bosco, S.; Cirillo, A.; Timmons, R. B. Photolysis of formamides and acetamides studied by electron spin resonance. *J. Am. Chem. Soc.* **1969,** *91*, 3140-3143.

51. Boucher, O.; Randall, D.; Artaxo, P.; Bretherton, C.; Feingold, G.; Forster, P.; Kerminen, V. M.; Kondo, Y.; Liao, H.; Lohmann, U., et al., Clouds and aerosols. In *Climate change 2013: The physical science basis. Contribution of working group I to the fifth assessment report of the intergovernmental panel on climate change*, Stocker, T. F.; Qin, D.; Plattner, G. K.; Tignor, M.; Allen, S. K.; Boschung, J.; Nauels, A.; Xia, Y.; Bex, V.; Midgley, P. M., Eds. Cambridge Univ. Press, : Cambridge, U.K. and New York, NY, USA, 2013; pp 465-570.

52. Bougiatioti, A.; Nikolaou, P.; Stavroulas, I.; Kouvarakis, G.; Weber, R.; Nenes, A.; Kanakidou, M.; Mihalopoulos, N. Particle water and pH in the eastern Mediterranean: Source variability and implications for nutrient availability. *Atmos. Chem. Phys.* **2016,** *16*, 4579-4591.

53. Boulanger, E.; Anoop, A.; Nachtigallova, D.; Thiel, W.; Barbatti, M. Photochemical steps in the prebiotic synthesis of purine precursors from HCN. *Angew. Chem. Int. Ed.* **2013,** *52*, 8000-8003.

54. Brégonzio-Rozier, L.; Giorio, C.; Siekmann, F.; Pangui, E.; Morales, S.; Temime-Roussel, B.; Gratien, A.; Michoud, V.; Cazaunau, M.; DeWitt, H. Secondary organic aerosol formation from isoprene photooxidation during cloud condensation–evaporation cycles. *Atmo. Chem. Phys.* **2016,** *16*, 1747-1760.

55. Breslow, R. On the mechanism of the formose reaction. *Tetrahedron Lett.* **1959,** *1*, 22-26.

56. Brister, M. M.; Pollum, M.; Crespo-Hernandez, C. E. Photochemical etiology of promising ancestors of the RNA nucleobases. *Phys. Chem. Chem. Phys.* **2016**.

57. Brito, R. O.; Marques, E. F. Neat dodab vesicles: Effect of sonication time on the phase transition thermodynamic parameters and its relation with incomplete chain freezing. *Chem. Phys. Lipids* **2005,** *137*, 18-28.

58. Brocks, J. J.; Beckhaus, H.-D.; Beckwith, A. L.; Rüchardt, C. Estimation of bond dissociation energies and radical stabilization energies by ESR spectroscopy. *J. Org. Chem.* **1998,** *63*, 1935-1943.

59. Broekhuizen, K. E.; Thornberry, T.; Kumar, P. P.; Abbatt, J. P. Formation of cloud condensation nuclei by oxidative processing: Unsaturated fatty acids. *J. Geophys. Res. Atmos.* **2004,** *109*, D24206.

60. Brondsted Nielsen, M. Model systems for understanding absorption tuning by opsin proteins. *Chem. Soc. Rev.* **2009,** *38*, 913-924.

61. Brzozowska, A. M.; Duits, M. H. G.; Mugele, F. Stability of stearic acid monolayers on artificial sea water. *Colloids Surf., A* **2012,** *407*, 38-48.

62. Budin, I.; Prywes, N.; Zhang, N.; Szostak, Jack W. Chain-length heterogeneity allows for the assembly of fatty acid vesicles in dilute solutions. *Biophys. J.* **2014,** *107*, 1582-1590.

63. Budin, I.; Szostak, J. W. Physical effects underlying the transition from primitive to modern cell membranes. *Proc. Natl. Acad. Sci.* **2011,** *108*, 5249-5254.

64. Buick, R.; Dunlop, J. S. R.; Groves, D. I. Stromatolite recognition in ancient rocks - an appraisal of irregularly laminated structures in an early Archean chert-barite unit from North Pole, Western Australia. *Alcheringa* **1981,** *5*, 161-181.

65. Buick, R.; Groves, D. I.; Dunlop, J. S. R. Abiological origin of described stromatolites older than 3.2 Ga: Comment. *Geology* **1995,** *23*, 191.

66. Burton, A. S.; Stern, J. C.; Elsila, J. E.; Glavin, D. P.; Dworkin, J. P. Understanding prebiotic chemistry through the analysis of extraterrestrial amino acids and nucleobases in meteorites. *Chem. Soc. Rev.* **2012,** *41*, 5459-5472.

67. Buschmann, H. J.; Dutkiewicz, E.; Knoche, W. The reversible hydration of carbonyl compounds in aqueous solution. 2. The kinetics of the keto gem-diol transition. *Ber. Bunsen-Ges. Phys. Chem* **1982,** *86*, 129-134.

68. Buschmann, H. J.; Füldner, H. H.; Knoche, W. The reversible hydration of carbonyl compounds in aqueous solution. Part I, the keto/gem - diol equilibrium. *Ber. Bunsen-Ges. Phys. Chem* **1980,** *84*, 41-44.

69. Butkovskaya, N. I.; Kukui, A.; Pouvesle, N.; Le Bras, G. Rate constant and mechanism of the reaction of OH radicals with acetic acid in the temperature range of 229-300 K. *J. Phys. Chem. A* **2004,** *108*, 7021-7026.

70. Butlerov, A. Bildung einer zuckerartigen substanz durch synthese (Formation of a sugar-like substance by synthesis). *Justus Liebigs Ann Chem* **1861,** *120*, 295-298.

71. Cacace, M.; Landau, E.; Ramsden, J. The Hofmeister series: Salt and solvent effects on interfacial phenomena. *Quarterly reviews of biophysics* **1997,** *30*, 241-277.

72. Caffrey, M.; Fanger, G.; Magin, R. L.; Zhang, J. Kinetics of the premelting (l-beta-p-beta) and main transition (p-beta-l-alpha) in hydrated dipalmitoylphosphatidylcholine - a time resolved x-ray diffraction study using microwave-induced temperature jumps. *Biophys. J.* **1990,** *58*, 677-686.

73. Cairns-Smith, A. G.; Hartman, H., *Clay minerals and the origin of life*. Press Syndicate of the University of Cambridge: Cambridge, 1986.

74. Canuto, V. M.; Levine, J. S.; Augustsson, T. R.; Imhoff, C. L. UV radiation from the young sun and oxygen and ozone levels in the prebiological paleoatmosphere. *Nature* **1982,** *296*, 816-820.

75. Cape, J. L.; Monnard, P.-A.; Boncella, J. M. Prebiotically relevant mixed fatty acid vesicles support anionic solute encapsulation and photochemically catalyzed trans-membrane charge transport. *Chem. Sci.* **2011,** *2*, 661-671.

76. Carlton, A. G.; Turpin, B. J.; Lim, H.-J.; Altieri, K. E.; Seitzinger, S. Link between isoprene and secondary organic aerosol (SOA): Pyruvic acid oxidation yields low volatility organic acids in clouds. *Geophys. Res. Lett.* **2006,** *33*, L06822.

77. Carlton, A. G.; Wiedinmyer, C.; Kroll, J. H. A review of secondary organic aerosol (SOA) formation from isoprene. *Atmo. Chem. Phys.* **2009,** *9*, 4987-5005.

78. Cavosie, A. J.; Valley, J. W.; Wilde, S. A.; E.I.M.F. Magmatic $\delta^{18}O$ in 4400–3900 Ma detrital zircons: A record of the alteration and recycling of crust in the early Archean. *Earth. Planet. Sci. Lett.* **2005,** *235*, 663-681.

79. Cech, N. B.; Enke, C. G. Practical implications of some recent studies in electrospray ionization fundamentals. *Mass Spectrom. Rev.* **2001,** *20*, 362-387.

80. Cernicharo, J.; Agundez, M.; Kahane, C.; Guelin, M.; Goicoechea, J. R.; Marcelino, N.; De Beck, E.; Decin, L. Probing the dust formation region in IRC +10216 with the high vibrational states of hydrogen cyanide. *Astron. Astrophys.* **2011,** *529*, L3.

81. Chakraborty, P.; Zachariah, M. R. On the structure of organic-coated water droplets: From "net water attractors" to "oily" drops. *J. Geophys. Res.* **2011,** *116*, Art. Nr. D21205.

82. Chan, K. M.; Huang, D. D.; Li, Y. J.; Chan, M. N.; Seinfeld, J. H.; Chan, C. K. Oligomeric products and formation mechanisms from acid-catalyzed reactions of methyl vinyl ketone on acidic sulfate particles. *J. Atmos. Chem.* **2013,** *70*, 1-18.

83. Chandler, D. W. Interfaces and the driving force of hydrophobic assembly. *Nature* **2005,** *437*, 640-647.

84. Chang, X.-P.; Fang, Q.; Cui, G. Mechanistic photodecarboxylation of pyruvic acid: Excited-state proton transfer and three-state intersection. *J. Chem. Phys.* **2014,** *141*, 154311.

85. Chapman, C. R.; Cohen, B. A.; Grinspoon, D. H. What are the real constraints on the existence and magnitude of the late heavy bombardment? *Icarus* **2007,** *189*, 233-245.

86. Charlson, R. J.; Seinfeld, J. H.; Nenes, A.; Kulmala, M.; Laaksonen, A.; Facchini, M. C. Reshaping the theory of cloud formation. *Science* **2001,** *292*, 2025-2026.

87. Charnay, B.; Forget, F.; Wordsworth, R.; Leconte, J.; Millour, E.; Codron, F.; Spiga, A. Exploring the faint young sun problem and the possible climates of the Archean Earth with a 3D GCM. *J. Geophys. Res. Atmos.* **2013,** *118*, 10414-10431.

88. Chebbi, A.; Carlier, P. Carboxylic acids in the troposphere, occurrence, sources, and sinks: A review. *Atmos. Environ.* **1996,** *30*, 4233-4249.

89. Chen, H.; Nanayakkara, C. E.; Grassian, V. H. Titanium dioxide photocatalysis in atmospheric chemistry. *Chem. Rev.* **2012,** *112*, 5919-5948.

90. Chen, I. A.; Hanczyc, M. M.; Sazani, P. L.; Szostak, J. W., Protocells: Genetic polymers inside membrane vesicles. In *RNA world*, 3 ed.; Gesteland, R. F.; Cech, T. R.; Atkins, J. F., Eds. 2006; Vol. 43, pp 57-88.

91. Chen, I. A.; Roberts, R. W.; Szostak, J. W. The emergence of competition between model protocells. *Science* **2004,** *305*, 1474-1476.

92. Chen, I. A.; Salehi-Ashtiani, K.; Szostak, J. W. RNA catalysis in model protocell vesicles. *J. Am. Chem. Soc.* **2005,** *127*, 13213-13219.

93. Chen, I. A.; Walde, P. From self-assembled vesicles to protocells. *Cold Spring Harbor Persp. Biol.* **2010,** *2*.

94. Chen, L. H.; Geiger, C.; Perlstein, J.; Whitten, D. G. Self-assembly of styryl naphthalene amphiphiles in aqueous dispersions and interfacial films: Aggregate structure, assembly properties, photochemistry, and photophysics. *J. Phys. Chem. B* **1999,** *103*, 9161-9167.

95. Chen, L. H.; Lucia, L.; Whitten, D. G. Cooperative electron transfer fragmentation reactions. Amplification of a photoreaction through a tandem chain fragmentation of acceptor and donor pinacols. *J. Am. Chem. Soc.* **1998,** *120*, 439-440.

96. Chen, X.-B.; Fang, W.-H.; Fang, D.-C. An ab initio study toward understanding the mechanistic photochemistry of acetamide. *J. Am. Chem. Soc.* **2003,** *125*, 9689-9698.

97. Chiu, R.; Tinel, L.; Gonzalez, L.; Ciuraru, R.; Bernard, F.; George, C.; Volkamer, R. UV photochemistry of carboxylic acids at the air-sea boundary: A relevant source of glyoxal and other oxygenated VOC in the marine atmosphere. *Geophys. Res. Lett.* **2017,** *44*, 1079-1087.

98. Chu, Z.; Feng, Y. Empirical correlations between krafft temperature and tail length for amidosulfobetaine surfactants in the presence of inorganic salt. *Langmuir* **2012,** *28*, 1175-1181.

99. Cistola, D. P.; Hamilton, J. A.; Jackson, D.; Small, D. M. Ionization and phase behavior of fatty acids in water: Application of the gibbs phase rule. *Biochem.* **1988,** *27*, 1881-1888.

100. Ciuraru, R.; Fine, L.; Pinxteren, M. v.; D'Anna, B.; Herrmann, H.; George, C. Unravelling new processes at interfaces: Photochemical isoprene production at the sea surface. *Environ. Sci. Technol.* **2015**, 13199–13205.

101. Ciuraru, R.; Fine, L.; van Pinxteren, M.; D'Anna, B.; Herrmann, H.; George, C. Photosensitized production of functionalized and unsaturated organic compounds at the air-sea interface. *Sci. Rep.* **2015,** *5*, 12741

102. Claeys, M.; Graham, B.; Vas, G.; Wang, W.; Vermeylen, R.; Pashynska, V.; Cafmeyer, J.; Guyon, P.; Andreae, M. O.; Artaxo, P. Formation of secondary organic aerosols through photooxidation of isoprene. *Science* **2004,** *303*, 1173-1176.

103. Claire, M. W.; Sheets, J.; Cohen, M.; Ribas, I.; Meadows, V. S.; Catling, D. C. The evolution of solar flux from 0.1 nm to 160 mu m: Quantitative estimates for planetary studies. *Astrophys. J.* **2012,** *757*, 95.

104. Clark, N. A.; Lunacek, J. H.; Benedek, G. B. A study of Brownian motion using light scattering. *Am. J. Phys.* **1970,** *38*, 575-585.

105. Cleaves, H. J.; Chalmers, J. H.; Lazcano, A.; Miller, S. L.; Bada, J. L. A reassessment of prebiotic organic synthesis in neutral planetary atmospheres. *Origins Life Evol. Biosphere* **2008,** *38*, 105-115.

106. Cleaves, H. J.; Miller, S. L. Oceanic protection of prebiotic organic compounds from UV radiation. *Proc. Natl. Acad. Sci.* **1998,** *95*, 7260-7263.

107. Closs, G. L.; Miller, R. J. Photo-reduction and photodecarboxylation of pyruvic acid - applications of CIDNP to mechanistic photochemistry. *J. Am. Chem. Soc.* **1978,** *100*, 3483-3494.

108. Cochran, R. E.; Laskina, O.; Jayarathne, T.; Laskin, A.; Laskin, J.; Lin, P.; Sultana, C.; Lee, C.; Moore, K. A.; Cappa, C. D. Analysis of organic anionic surfactants in fine and coarse fractions of freshly emitted sea spray aerosol. *Environ. Sci. Technol.* **2016,** *50*, 2477-2486.

109. Cochran, R. E.; Laskina, O.; Trueblood, J. V.; Estillore, A. D.; Morris, H. S.; Jayarathne, T.; Sultana, C. M.; Lee, C.; Lin, P.; Laskin, J., et al. Molecular diversity of sea spray aerosol particles: Impact of ocean biology on particle composition and hygroscopicity. *Chem* **2017,** *2*, 655-667.

110. Cochran, R. E.; Ryder, O. S.; Grassian, V. H.; Prather, K. A. Sea spray aerosol: The chemical link between the oceans, atmosphere, and climate. *Acc. Chem. Res.* **2017,** *50*, 599-604.

111. Cockell, C. S. Biological effects of high ultraviolet radiation on early Earth: A theoretical evaluation. *J. Theor. Bio.* **1998,** *193*, 717-729.

112. Cockell, C. S. The ultraviolet history of the terrestrial planets: Implications for biological evolution. *Planet. Space Sci.* **2000,** *48*, 203-214.

113. Cody, G. D.; Boctor, N. Z.; Filley, T. R.; Hazen, R. M.; Scott, J. H.; Sharma, A.; Yoder, H. S. Primordial carbonylated iron-sulfur compounds and the synthesis of pyruvate. *Science* **2000,** *289*, 1337 -1340.

114. Colberg, M. R.; Watkins, R. J.; Krogh, O. D. Vibrationally excited carbon-dioxide produced by infrared multiphoton pyrolysis. *J. Phys. Chem.* **1984,** *88*, 2817-2821.

115. Condon, D. J.; Prave, A. R.; Benn, D. I. Neoproterozoic glacial-rainout intevals: Observations and implications. *Geology* **2002,** *30*, 35-38.

116. Cooper, A. J.; Redfield, A. G. Proton magnetic resonance studies of alpha-keto acids. *J. Biol. Chem.* **1975,** *250*, 527-32.

117. Cooper, G.; Reed, C.; Nguyen, D.; Carter, M.; Wang, Y. Detection and formation scenario of citric acid, pyruvic acid, and other possible metabolism precursors in carbonaceous meteorites. *Proc. Natl. Acad. Sci.* **2011,** *108*, 14015-14020.

118. Cottin, H.; Gazeau, M. C.; Raulin, F. Cometary organic chemistry: A review from observations, numerical and experimental simulations. *Planet. Space Sci.* **1999,** *47*, 1141-1162.

119. Cowie, J. M. G.; Arrighi, V., *Polymers: Chemistry and physics of modern materials*. CRC Press: 2007.

120. Crabtree, G. W.; Lewis, N. S. Solar energy conversion. *Physics Today* **2007,** *60*, 37-42.

121. Craig, R. L.; Nandy, L.; Axson, J. L.; Dutcher, C. S.; Ault, A. P. Spectroscopic determination of aerosol pH from acid–base equilibria in inorganic, organic, and mixed systems. *J. Phys. Chem. A* **2017,** *121*, 5690-5699.

122. Crespo-Hernandez, C. E.; Cohen, B.; Hare, P. M.; Kohler, B. Ultrafast excited-state dynamics in nucleic acids. *Chem. Rev.* **2004,** *104*, 1977-2019.

123. Crim, F. F. Selective excitation studies of unimolecular reaction dynamics. *Annu. Rev. Phys. Chem.* **1984,** *35*, 657-691.

124. Crutzen, P. J.; Zimmermann, P. H. The changing photochemistry of the troposphere. *Tellus B* **1991,** *43*, 136-151.

125. Cunliffe, M.; Engel, A.; Frka, S.; Gasparovic, B.; Guitart, C.; Murrell, J. C.; Salter, M.; Stolle, C.; Upstill-Goddard, R.; Wurl, O. Sea surface microlayers: A unified physiochemical and biological perspective of the air-ocean interface. *Prog. Oceanogr.* **2013,** *109*, 104-116.

126. Cwiertny, D. M.; Young, M. A.; Grassian, V. H. Chemistry and photochemistry of mineral dust aerosol. *Annu. Rev. Phys. Chem.* **2008,** *59*, 27-51.

127. da Silva, G. Decomposition of pyruvic acid on the ground-state potential energy surface. *J. Phys. Chem. A* **2015,** *120* 276–283.

128. Daniel, I.; Oger, P.; Winter, R. Origins of life and biochemistry under high-pressure conditions. *Chem. Soc. Rev.* **2006,** *35*, 858-875.

129. Davidson, R. S.; Goodwin, D. The role of electron transfer processes in the photoinduced decarboxylation reaction of α-oxo-carboxylic acids. *J. Chem. Soc., Perkin Trans. 2* **1982**, 1559-1564.

130. Davidson, R. S.; Goodwin, D.; de Violet, P. F. The mechanism of the norrish type II reaction of α-keto-acids and esters. *Tetrahedron Lett.* **1981,** *22*, 2485-2486.

131. Davidson, R. S.; Goodwin, D.; De Violet, P. F. The mechanism of the photo-induced decarboxylation of pyruvic acid in solution. *Chem. Phys. Lett.* **1981,** *78*, 471-474.

132. Davies, J. F.; Miles, R. E.; Haddrell, A. E.; Reid, J. P. Influence of organic films on the evaporation and condensation of water in aerosol. *Proc. Natl. Acad. Sci.* **2013,** *110*, 8807-8812.

133. De Man, J. The formation of diacetyl and acetoin from α - acetolactic acid. *Recl. Trav. Chim. Pays-Bas* **1959,** *78*, 480-486.

134. De Yoreo, J. J.; Gilbert, P. U. P. A.; Sommerdijk, N. A. J. M.; Penn, R. L.; Whitelam, S.; Joester, D.; Zhang, H.; Rimer, J. D.; Navrotsky, A.; Banfield, J. F., et al. Crystallization by particle attachment in synthetic, biogenic, and geologic environments. *Science* **2015,** *349*.

135. Deamer, D., Sources and syntheses of prebiotic amphiphiles. In *Self-production of supramolecular structures*, Springer: 1994; pp 217-229.

136. Deamer, D.; Dworkin, J. P.; Sandford, S. A.; Bernstein, M. P.; Allamandola, L. J. The first cell membranes. *Astrobio.* **2002,** *2*, 371-381.

137. Deamer, D.; Harang, E. Light-dependent pH gradients are generated in liposomes containing ferrocyanide. *BioSystems* **1990,** *24*, 1-4.

138. Deamer, D.; Weber, A. L. Bioenergetics and life's origins. *Cold Spring Harbor Persp. Biol.* **2010,** *2*, 1-16.

139. Deamer, D. W. Polycyclic aromatic hydrocarbons: Primitive pigment systems in the prebiotic environment. *Adv. Space Res.* **1992,** *12*, 183-189.

140. Deamer, D. W. The first living systems: A bioenergetic perspective. *Microbio. Mol. Bio. Rev.* **1997,** *61*, 239 - 261.

141. Decker, C.; Jenkins, A. D. Kinetic approach of oxygen inhibition in ultraviolet-and laser-induced polymerizations. *Macromolecules* **1985,** *18*, 1241-1244.

142. Demou, E.; Donaldson, D. J. Adsorption of atmospheric gases at the air-water interface. 4: The influence of salts. *J. Phys. Chem. A* **2002,** *106*, 982-987.

143. Demou, E.; Visram, H.; Donaldson, D.; Makar, P. A. Uptake of water by organic films: The dependence on the film oxidation state. *Atmos. Environ.* **2003,** *37*, 3529-3537.

144. Demtröder, W., *Molecular physics: Theoretical principles and experimental methods*. Blackwell Science: Oxford, 2005.

145. DeWitt, H. L.; Trainer, M. G.; Pavlov, A. A.; Hasenkopf, C. A.; Aiken, A. C.; Jimenez, J. L.; McKay, C. P.; Toon, O. B.; Tolbert, M. A. Reduction in haze formation rate on prebiotic Earth in the presence of hydrogen. *Astrobio.* **2009,** *9*, 447-453.

146. Dhanya, S.; Maity, D. K.; Upadhyaya, H. P.; Kumar, A.; Naik, P. D.; Saini, R. D. Dynamics of OH formation in photodissociation of pyruvic acid at 193 nm. *J. Chem. Phys.* **2003,** *118*, 10093-10100.

147. Dobson, C. M.; Ellison, G. B.; Tuck, A. F.; Vaida, V. Atmospheric aerosols as prebiotic chemical reactors. *Proc. Natl. Acad. Sci.* **2000,** *97*, 11864-11868.

148. Domcke, W.; Yarkony, D.; Köppel, H., *Conical intersections: Electronic structure, dynamics & spectroscopy*. World Scientific: 2004; Vol. 15.

149. Dommen, J.; Metzger, A.; Duplissy, J.; Kalberer, M.; Alfarra, M.; Gascho, A.; Weingartner, E.; Prevot, A.; Verheggen, B.; Baltensperger, U. Laboratory observation of oligomers in the aerosol from isoprene/NO_x photooxidation. *Geophys. Res. Lett.* **2006,** *33*.

150. Donaldson, D.; Valsaraj, K. T. Adsorption and reaction of trace gas-phase organic compounds on atmospheric water film surfaces: A critical review. *Environ. Sci. Technol.* **2010,** *44*, 865-873.

151. Donaldson, D. J.; George, C.; Vaida, V. Red sky at night: Long-wavelengths photochemistry in the atmosphere. *Environ. Sci. Technol.* **2010,** *44*, 5321-5326.

152. Donaldson, D. J.; Tervahattu, H.; Tuck, A. F.; Vaida, V. Organic aerosols and the origin of life: An hypothesis. *Origins Life Evol. Biosphere* **2004,** *34*, 57-67.

153. Donaldson, D. J.; Tuck, A. F.; Vaida, V. Atmospheric photochemistry via vibrational overtone absorption. *Chem. Rev.* **2003,** *103*, 4717-4729.

154. Donaldson, D. J.; Vaida, V. The influence of organic films at the air-aqueous boundary on atmospheric processes. *Chem. Rev.* **2006,** *106*, 1445-1461.

155. Dondi, D.; Merli, D.; Pretali, L., Prebiotic photochemistry. In *Photochemistry: Volume 38*, The Royal Society of Chemistry: 2010; Vol. 38, pp 330-343.

156. Dong, H.; Ignés-Mullol, J.; Claret, J.; Pérez, L.; Pinazo, A.; Sagués, F. Interfacial chiral selection by bulk species. *Chem. Eur. J.* **2014,** *20*, 7396-7401.

157. Douliez, J.-P.; Gaillard, C. Self-assembly of fatty acids: From foams to protocell vesicles. *New J. Chem.* **2014,** *38*, 5142-5148.

158. Driese, S. G.; Jirsa, M. A.; Ren, M.; Brantley, S. L.; Sheldon, N. D.; Parker, D.; Schmitz, M. Neoarchean paleoweathering of tonalite and metabasalt: Implications for reconstructions of 2.69 Ga early terrestrial ecosystems and paleoatmospheric chemistry. *Precambrian Res.* **2011,** *189*, 1-17.

159. Duvernay, F.; Trivella, A.; Borget, F.; Coussan, S.; Aycard, J. P.; Chiavassa, T. Matrix isolation fourier transform infrared study of photodecomposition of formimidic acid. *J. Phys. Chem. A* **2005,** *109*, 11155-11162.

160. Eggenberger, D.; Broome, F.; Ralston, A.; Harwood, H. The solubilities of the normal saturated fatty acids in water. *J. Org. Chem.* **1949,** *14*, 1108-1110.

161. Ehrenfreund, P.; Charnley, S. B. Organic molecules in the interstellar medium, comets, and meteorites: A voyage from dark clouds to the early Earth. *Ann. Rev. Astron. Astrophys.* **2000,** *38*, 427-483.

162. Ehrenfreund, P.; Rasmussen, S.; Cleaves, J.; Chen, L. H. Experimentally tracing the key steps in the origin of life: The aromatic world. *Astrobio.* **2006,** *6*, 490-520.

163. Eisch, J. J.; Munson, P. R.; Gitua, J. N. The potential of photochemical transitionmetal reactions in prebiotic organic synthesis. I. Observed conversion of methanol into ethylene glycol as possible prototype for sugar alcohol formation. *Origins Life Evol. Biosphere* **2004,** *34*, 441-454.

164. Eliason, T. L.; Gilman, J. B.; Vaida, V. Oxidation of organic films relevant to atmospheric aerosols. *Atmos. Environ.* **2004,** *38*, 1367-1378.

165. Ellison, G. B.; Tuck, A. F.; Vaida, V. Atmospheric processing of organic aerosols. *J. Geophys. Res. Atmos.* **1999,** *104*, 11633-11641.

166. Elsila, J. E.; Dworkin, J. P.; Bernstein, M. P.; Martin, M. P.; Sandford, S. A. Mechanisms of amino acid formation in interstellar ice analogs. *Astrophys. J.* **2007,** *660*, 911-918.

167. Engel, A.; Bange, H. W.; Cunliffe, M.; Burrows, S. M.; Friedrichs, G.; Galgani, L.; Herrmann, H.; Hertkorn, N.; Johnson, M.; Liss, P. S., et al. The ocean's vital skin: Toward an integrated understanding of the sea surface microlayer. *Front. Mar. Sci.* **2017,** *4*.

168. Engel, V.; Staemmler, V.; Vander Wal, R.; Crim, F.; Sension, R.; Hudson, B.; Andresen, P.; Hennig, S.; Weide, K.; Schinke, R. Photodissociation of water in the first absorption band: A prototype for dissociation on a repulsive potential energy surface. *J. Phys. Chem.* **1992,** *96*, 3201-3213.

169. Epstein, S. A.; Nizkorodov, S. A. A comparison of the chemical sinks of atmospheric organics in the gas and aqueous phase. *Atmo. Chem. Phys.* **2012,** *12*, 8205-8222.

170. Epstein, S. A.; Tapavicza, E.; Furche, F.; Nizkorodov, S. A. Direct photolysis of carbonyl compounds dissolved in cloud and fog droplets. *Atmo. Chem. Phys.* **2013,** *13*, 9461-9477.

171. Ervens, B. Modeling the processing of aerosol and trace gases in clouds and fogs. *Chem. Rev.* **2015,** *115*, 4157-4198.

172. Ervens, B.; Carlton, A. G.; Turpin, B. J.; Altieri, K. E.; Kreidenweis, S. M.; Feingold, G. Secondary organic aerosol yields from cloud-processing of isoprene oxidation products. *Geophys. Res. Lett.* **2008,** *35*, L02816.

173. Ervens, B.; Sorooshian, A.; Lim, Y. B.; Turpin, B. J. Key parameters controlling OH-initiated formation of secondary organic aerosol in the aqueous phase (aqSOA). *J. Geophys. Res. Atmos.* **2014,** *119*, 3997-4016.

174. Ervens, B.; Turpin, B. J.; Weber, R. J. Secondary aerosol formation in cloud droplets and aqueous particles (aqSOA): A review of laboratory, field and model studies. *Atmo. Chem. Phys.* **2011,** *11*, 11069-11102.

175. Ervens, B.; Volkamer, R. Glyoxal processing by aerosol multiphase chemistry: Towards a kinetic modeling framework of secondary organic aerosol formation in aqueous particles. *Atmo. Chem. Phys.* **2010,** *10*, 8219-8244.

176. Ervens, B.; Wang, Y.; Eagar, J.; Leaitch, W.; Macdonald, A.; Valsaraj, K.; Herckes, P. Dissolved organic carbon (DOC) and select aldehydes in cloud and fog water: The role of the aqueous phase in impacting trace gas budgets. *Atmo. Chem. Phys.* **2013,** *13*, 5117-5135.

177. Escabi-Perez, J. R.; Romero, A.; Lukac, S.; Fendler, J. H. Aspects of artificial photosynthesis. Photoionization and electron transfer in dihexadecyl phosphate vesicles. *J. Am. Chem. Soc.* **1979,** *101*, 2231-2233.

178. Eugene, A. J.; Guzman, M. I. Reactivity of ketyl and acetyl radicals from direct solar actinic photolysis of aqueous pyruvic acid. *J. Phys. Chem. A* **2017,** *121*, 2924–2935.

179. Eugene, A. J.; Xia, S.-S.; Guzman, M. I. Negative production of acetoin in the photochemistry of aqueous pyruvic acid. *Proc. Natl. Acad. Sci.* **2013,** *110*, E4274-E4275.

180. Evans, T. R.; Leermakers, P. A. Photochemistry of alpha-keto acids and alpha-keto esters VI. V. The Norrish Type II process in alpha-keto acids. Photolysis of alpha-ketodecanoic acid in benzene. *J. Am. Chem. Soc.* **1968,** *90*, 1840-1842.

181. Faccini, M. C.; Mircea, M.; Fuzzi, S.; Charlson, R. J. Cloud albedo enhancement by surface-active organic solutes in growing droplets. *Nature* **1999,** *401*, 257-259.

182. Fallah-Araghi, A.; Meguellati, K.; Baret, J.-C.; El Harrak, A.; Mangeat, T.; Karplus, M.; Ladame, S.; Marques, C. M.; Griffiths, A. D. Enhanced chemical synthesis at soft interfaces: A universal reaction-adsorption mechanism in microcompartments. *Phys. Rev. Lett.* **2014,** *112*.

183. Fedotenko, I. A.; Stefaniu, C.; Brezesinski, G.; Zumbuehl, A. Monolayer properties of 1,3-diamidophospholipids. *Langmuir* **2013,** *29*, 9428-9435.

184. Fernandez, D. I.; Sani, M.-A.; Gehman, J. D.; Hahm, K.-S.; Separovic, F. Interactions of a synthetic leu-lys-rich antimicrobial peptide with phospholipid bilayers. *Eur. Biophys. J. Biophy. 40*, 471-480.

185. Ferris, J. P. Montmorillonite-catalysed formation of RNA oligomers: The possible role of catalysis in the origins of life. *Philos. Trans. R. Soc. London, Ser. B* **2006,** *361*, 1777-1786.

186. Ferris, J. P.; Chen, C. T. Chemical evolution XXVI: Photochemistry of methane, nitrogen and water mixtures as a model for the atmosphere of primitive Earth. *J. Am. Chem. Soc.* **1975,** *97*, 2962-2967.

187. Finlayson-Pitts, B. J.; Pitts, J. N., *Chemistry of the upper and lower atmosphere.* Academic Press: San Diego, 1999.

188. Forsythe, J. G.; Yu, S.-S.; Mamajanov, I.; Grover, M. A.; Krishnamurthy, R.; Fernandez, F. M.; Hud, N. V. Ester-mediated amide bond formation driven by wet-dry cycles: A possible path to polypeptides on the prebiotic Earth. *Angew. Chem. Int. Ed.* **2015,** *54*, 9871-9875.

189. Frisch, M. J.; Trucks, G. W.; Schlegel, H. B.; Scuseria, G. E.; Robb, M. A.; Cheeseman, J. R.; Scalmani, G.; Barone, V.; Petersson, G. A.; Nakatsuji, H., et al. *Gaussian 09, revision d.01*, Gaussian, Inc.: Wallingford, CT, 2016.

190. Fu, H.; Ciuraru, R.; Dupart, Y.; Passananti, M.; Tinel, L.; Rossignol, S.; Perrier, S.; Donaldson, D. J.; Chen, J.; George, C. Photosensitized production of atmospherically reactive organic compounds at the air/aqueous interface. *J. Am. Chem. Soc.* **2015,** *137*, 8348-8351.

191. Galloway, M. M.; Powelson, M. H.; Sedehi, N.; Wood, S. E.; Millage, K. D.; Kononenko, J. A.; Rynaski, A. D.; De Haan, D. O. Secondary organic aerosol formation during evaporation of droplets containing atmospheric aldehydes, amines, and ammonium sulfate. *Environ. Sci. Technol.* **2014,** *48*, 14417-14425.

192. Gankanda, A.; Grassian, V. H. Nitrate photochemistry on laboratory proxies of mineral dust aerosol: Wavelength dependence and action spectra. *J. Phys. Chem. C* **2014,** *118*, 29117-29125.

193. Garcia, R. R.; López - Puertas, M.; Funke, B.; Marsh, D. R.; Kinnison, D. E.; Smith, A. K.; González - Galindo, F. On the distribution of CO_2 and CO in the mesosphere and lower thermosphere. *J. Geophys. Res. Atmos.* **2014,** *119*, 5700-5718.

194. George, C.; Ammann, M.; D'Anna, B.; Donaldson, D. J.; Nizkorodov, S. A. Heterogeneous photochemistry in the atmosphere. *Chem. Rev.* **2015,** *115*, 4218-4258.

195. George, C.; D'Anna, B.; Herrmann, H.; Weller, C.; Vaida, V.; Donaldson, D.; Bartels-Rausch, T.; Ammann, M., Emerging areas in atmospheric photochemistry. In *Atmospheric and aerosol chemistry*, Springer: 2014; pp 1-53.

196. Gerlach, T. M.; Nordlie, B. E. C-O-H-S gaseous system. 1. Composition limits and trends in basaltic cases. *Am. J. Sci.* **1975,** *275*, 353-376.

197. Gerlach, T. M.; Nordlie, B. E. C-O-H-S gaseous system. 2. Temperature, atomic composition, and molecular equilibria in volcanic gases. *Am. J. Sci.* **1975,** *275*, 377-394.

198. Gerlach, T. M.; Nordlie, B. E. C-O-H-S gaseous system. 3. Magmatic gases compatible with oxides and sulfides in basaltic magmas. *Am. J. Sci.* **1975,** *275*, 395-410.

199. Gibbs, J. W.; Bumstead, H. A., *Thermodynamics*. Longmans, Green and Company: 1906.

200. Gibian, M. J.; Corley, R. C. Organic radical-radical reactions. Disproportionation vs. Combination. *Chem. Rev.* **1973,** *73*, 441-464.

201. Gill, P.; Graedel, T.; Weschler, C. Organic films on atmospheric aerosol particles, fog droplets, cloud droplets, raindrops, and snowflakes. *Rev. Geophys.* **1983,** *21*, 903-920.

202. Gillespie, D. T. Fluctuation and dissipation in Brownian motion. *Am. J. Phys.* **1993,** *61*, 1077-1083.

203. Gilman, J. B.; Eliason, T. L.; Fast, A.; Vaida, V. Selectivity and stability of organic films at the air-aqueous interface. *J. Colloid Interface Sci.* **2004,** *280*, 234-243.

204. Gilman, J. B.; Tervahattu, H.; Vaida, V. Interfacial properties of mixed films of long-chain organics at the air-water interface. *Atmos. Environ.* **2006,** *40*, 6606-6614.

205. Gilman, J. B.; Vaida, V. Permeability of acetic acid through organic films at the air-aqueous interface. *J. Phys. Chem. A* **2006,** *110*, 7581-7587.

206. Gligorovski, S.; Strekowski, R.; Barbati, S.; Vione, D. Environmental implications of hydroxyl radicals (•OH). *Chem. Rev.* **2015,** *115*, 13051-13092.

207. Goldacre, R. J., Surface films, their collapse on compression, the shape and size of cells and the origin of life. In *Surface phenomena in chemistry and biology*, Danielli, J. F.; Parkhurst, K. G. A.; Riddiford, A. C., Eds. Pergamon Press: New York, 1958; pp 12 - 27.

208. Goltsov, A. N.; Barsukov, L. I. Synergetics of the membrane self-assembly: A micelle-to-vesicle transition. *J. Bio. Phys.* **2000,** *26*, 27-41.

209. Gradzielski, M. A. Vesicles and vesicle gels-structure and dynamics of formation. *J. Phys.: Condens. Matter* **2003,** *15*, R655.

210. Greene, J. E. Tracing the 4000 year history of organic thin films: From monolayers on liquids to multilayers on solids. *Appl. Phys. Rev.* **2015,** *2*, 011101.

211. Griffith, E. C. Chemical and physical changes unique in and on water: Implications for life and its origins. University of Colorado, Boulder, 2014.

212. Griffith, E. C.; Adams, E. M.; Allen, H. C.; Vaida, V. Hydrophobic collapse of a stearic acid film by adsorbed l-phenylalanine at the air-water interface. *J. Phys. Chem. B* **2012,** *116*, 7849-7857.

213. Griffith, E. C.; Carpenter, B. K.; Shoemaker, R. K.; Vaida, V. Photochemistry of aqueous pyruvic acid. *Proc. Natl. Acad. Sci.* **2013,** *110*, 11714-11719.

214. Griffith, E. C.; Rapf, R. J.; Shoemaker, R. K.; Carpenter, B. K.; Vaida, V. Photoinitiated synthesis of self-assembled vesicles. *J. Am. Chem. Soc.* **2014,** *136*, 3784-3787.

215. Griffith, E. C.; Shoemaker, R. K.; Vaida, V. Sunlight-initiated chemistry of aqueous pyruvic acid: Building complexity in the origin of life. *Origins Life Evol. Biosphere* **2013,** *43*, 341-352.

216. Griffith, E. C.; Tuck, A. F.; Vaida, V. Ocean-atmosphere interactions in the emergence of complexity in simple chemical systems. *Acc. Chem. Res.* **2012,** *45*, 2106-2113.

217. Griffith, E. C.; Vaida, V. In situ observation of peptide bond formation at the water-air interface. *Proc. Natl. Acad. Sci.* **2012,** *109*, 15697-15701.

218. Griffith, E. C.; Vaida, V. Ionization state of l-phenylalanine at the air-water interface. *J. Am. Chem. Soc.* **2013,** *135*, 710-716.

219. Gromov, E. V.; Burghardt, I.; Koeppel, H.; Cederbaum, L. S. Electronic structure of the PYP chromophore in its native protein environment. *J. Am. Chem. Soc.* **2007,** *129*, 6798-6806.

220. Gromov, E. V.; Burghardt, I.; Koeppel, H.; Cederbaum, L. S. Native hydrogen bonding network of the photoactive yellow protein (PYP) chromophore: Impact on the electronic structure and photoinduced isomerization. *J. Photochem. Photobiol., A* **2012,** *234*, 123-134.

221. Grosjean, D. Atmospheric reactions of pyruvic-acid. *Atmos. Environ.* **1983,** *17*, 2379-2382.

222. Groth, W. E.; Vonweyssenhoff, H. Photochemical formation of organic compounds from mixtures of simple gases. *Planet. Space Sci.* **1960,** *2*, 79-85.

223. Grotzinger, J.; Kasting, J. New constraints on Precambrian ocean composition. *J. Geol.* **1993,** *101*, 235-243.

224. Guenther, C. Estimates of global terrestrial isoprene emissions using MEGAN (model of emissions of gases and aerosols from nature). *Atmo. Chem. Phys.* **2006,** *6*.

225. Gueymard, C. A. Parameterized transmittance model for direct beam and circumsolar spectral irradiance. *Solar Energy* **2001,** *71*, 325-346.

226. Guggenheim, E.; Adam, N. The thermodynamics of adsorption at the surface of solutions. *Proc. R. Soc. London, Ser. A* **1933,** *139*, 218-236.

227. Guida, V. Thermodynamics and kinetics of vesicles formation processes. *Adv. Colloid Interface Sci.* **2010,** *161*, 77-88.

228. Guo, H.; Xu, L.; Bougiatioti, A.; Cerully, K. M.; Capps, S. L.; Hite Jr, J.; Carlton, A.; Lee, S.; Bergin, M.; Ng, N. Fine-particle water and pH in the southeastern United States. *Atmos. Chem. Phys* **2015,** *15*, 5211-5228.

229. Gürtler, P.; Saile, V.; Koch, E. Rydberg series in the absorption spectra of H_2O and D_2O in the vacuum ultraviolet. *Chem. Phys. Lett.* **1977,** *51*, 386-391.

230. Gustavsson, T.; Improta, R.; Markovitsi, D. DNA/RNA: Building blocks of life under UV irradiation. *J. Phys. Chem. Lett.* **2010,** *1*, 2025-2030.

231. Guzman, M. I.; Colussi, A. J.; Hoffmann, M. R. Photoinduced oligomerization of aqueous pyruvic acid. *J. Phys. Chem. A* **2006,** *110*, 3619-3626.

232. Guzman, M. I.; Hoffmann, M. R.; Colussi, A. J. Photolysis of pyruvic acid in ice: Possible relevance to CO and CO_2 ice core record anomalies. *J. Geophys. Res.* **2007,** *112*, D10123.

233. Guzman, M. I.; Martin, S. T. Prebiotic metabolism: Production by mineral photoelectrochemistry of alpha-ketocarboxylic acids in the reductive tricarboxylic acid cycle. *Astrobio.* **2009,** *9*, 833-842.

234. Haddad, I. E.; Liu, Y.; Nieto-Gligorovski, L.; Michaud, V.; Temime-Roussel, B.; Quivet, E.; Marchand, N.; Sellegri, K.; Monod, A. In-cloud processes of methacrolein under simulated conditions. Part 2: Formation of secondary organic aerosol. *Atmo. Chem. Phys.* **2009,** *9*, 5107-5117.

235. Hall, G. E.; Muckerman, J. T.; Preses, J. M.; Weston, R. E.; Flynn, G. W. Time-resolved FTIR studies of the photodissociation of pyruvic-acid at 193 nm. *Chem. Phys. Lett.* **1992,** *193*, 77-83.

236. Hallquist, M.; Wenger, J. C.; Baltensperger, U.; Rudich, Y.; Simpson, D.; Claeys, M.; Dommen, J.; Donahue, N. M.; George, C.; Goldstein, A. H., et al. The formation, properties and impact of secondary organic aerosol: Current and emerging issues. *Atmos. Chem. Phys.* **2009,** *9*, 5155-5236.

237. Hanczyc, M. M.; Fujikawa, S. M.; Szostak, J. W. Experimental models of primitive cellular compartments: Encapsulation, growth, and division. *Science* **2003,** *302*, 618-622.

238. Hanczyc, M. M.; Fujikawa, S. M.; Szostak, J. W. Experimental models of primitive cellular compartments: Encapsulation, growth, and division. *Science* **2003,** *302*, 618-622.

239. Hansen, J.; Sato, M.; Ruedy, R. Radiative forcing and climate response. *J. Geophys. Res. Atmos.* **1997,** *102*, 6831-6864.

240. Hansen, J.-P.; McDonald, I. R., *Theory of simple liquids*. Elsevier: 1990.

241. Hargreaves, W. R.; Mulvihill, S. J.; Deamer, D. W. Synthesis of phospholipids and membranes in prebiotic conditions. *Nature* **1977,** *266*, 78-80.

242. Harris, D. C., *Quantitative chemical analysis*. 7th ed.; W.H. Freeman and Company: New York, 2007.

243. Harrison, R. M.; Yin, J. Particulate matter in the atmosphere: Which particle properties are important for its effects on health? *Sci. Total Environ.* **2000,** *249*, 85-101.

244. Haynes, W. M., *CRC handbook of chemistry and physics*. CRC press: 2014.

245. Hazen, R. M. Mineral surfaces and the prebiotic selection and organization of biomolecules. *Am. Mineral.* **2006,** *91*, 1715-1729.

246. Hazen, R. M. Paleomineralogy of the Hadean eon: A preliminary species list. *Am. J. Sci.* **2013,** *313*, 807-843.

247. Hazen, R. M.; Deamer, D. W. Hydrothermal reactions of pyruvic acid: Synthesis, selection, and self-assembly of amphiphilic molecules. *Origins Life Evol. Biosphere* **2007,** *37*, 143-152.

248. Hazen, R. M.; Downs, R. T.; Kah, L.; Sverjensky, D., Carbon mineral evolution. In *Carbon in Earth*, Hazen, R. M.; Jones, A. P.; Baross, J. A., Eds. 2013; Vol. 75, pp 79-107.

249. Hazen, R. M.; Papineau, D.; Leeker, W. B.; Downs, R. T.; Ferry, J. M.; McCoy, T. J.; Sverjensky, D. A.; Yang, H. Mineral evolution. *Am. Mineral.* **2008,** *93*, 1693-1720.

250. Hazen, R. M.; Sverjensky, D. A. Mineral surfaces, geochemical complexities, and the origins of life. *Cold Spring Harbor Persp. Biol.* **2010,** *2*, a002162.

251. Heald, C. L.; Jacob, D. J.; Park, R. J.; Russell, L. M.; Huebert, B. J.; Seinfeld, J. H.; Liao, H.; Weber, R. J. A large organic aerosol source in the free troposphere missing from current models. *Geophys. Res. Lett.* **2005,** *32*, L18809.

252. Heller, E. J.; Davis, M. J. Molecular overtone bandwidths from classical trajectories. *J. Phys. Chem.* **1980,** *84*, 1999-2001.

253. Hennigan, C.; Izumi, J.; Sullivan, A.; Weber, R.; Nenes, A. A critical evaluation of proxy methods used to estimate the acidity of atmospheric particles. *Atmo. Chem. Phys.* **2015,** *15*, 2775.

254. Henry, B. R. Use of local modes in the description of highly vibrationally excited molecules. *Acc. Chem. Res.* **1977,** *10*, 207-213.

255. Henry, B. R.; Kjaergaard, H. G. Local modes. *Can. J. Chem.* **2002,** *80*, 1635-1642.

256. Herrmann, H. Kinetics of aqueous phase reactions relevant for atmospheric chemistry. *Chem. Rev.* **2003,** *103*, 4691-4716.

257. Herrmann, H.; Hoffmann, D.; Schaefer, T.; Bräuer, P.; Tilgner, A. Tropospheric aqueous-phase free-radical chemistry: Radical sources, spectra, reaction kinetics and prediction tools. *ChemPhysChem* **2010,** *11*, 3796-3822.

258. Herrmann, H.; Schaefer, T.; Tilgner, A.; Styler, S. A.; Weller, C.; Teich, M.; Otto, T. Tropospheric aqueous-phase chemistry: Kinetics, mechanisms, and its coupling to a changing gas phase. *Chem. Rev.* **2015,** *115*, 4259–4334.

259. Herrmann, J. M. Heterogeneous photocatalysis: Fundamentals and applications to the removal of various types of aqueous pollutants. *Catal. Today* **1999,** *53*, 115-129.

260. Hinds, W. C., *Aerosol technology : Properties, behavior, and measurement of airborne particles*. 2nd ed.; Wiley: New York, 1999.

261. Ho, K.; Lee, S.; Cao, J.; Kawamura, K.; Watanabe, T.; Cheng, Y.; Chow, J. C. Dicarboxylic acids, ketocarboxylic acids and dicarbonyls in the urban roadside area of Hong Kong. *Atmos. Environ.* **2006,** *40*, 3030-3040.

262. Hoffman, P. F.; Kaufman, A. J.; Halverson, G. P.; Schrag, D. P. A Neoproterozoic snowball Earth. *Science* **1998,** *281*, 1342-1346.

263. Hoffmann, M. R.; Martin, S. T.; Choi, W. Y.; Bahnemann, D. W. Environmental applications of semiconductor photocatalysis. *Chem. Rev.* **1995,** *95*, 69-96.

264. Hofmann, H. J.; Grey, K.; Hickman, A. H.; Thorpe, R. I. Origin of 3.45 Ga coniform stromatolites in Warrawoona group, Western Australia. *Geol. Soc. Am. Bull.* **1999,** *111*, 1256-1262.

265. Holland, H. D., *The chemical evolution of the atmosphere and oceans*. Princeton University Press: 1984; p 598.

266. Hoque, M. M. M.; Kawamura, K. Longitudinal distributions of dicarboxylic acids, ω-oxoacids, pyruvic acid, α-dicarbonyls, and fatty acids in the marine aerosols from the central Pacific including equatorial upwelling. *Global Biogeochem. Cycles* **2016,** *30*, 534-548.

267. Hoque, M. M. M.; Kawamura, K.; Uematsu, M. Spatio-temporal distributions of dicarboxylic acids, ω-oxocarboxylic acids, pyruvic acid, α-dicarbonyls and fatty acids in the marine aerosols from the north and south Pacific. *Atmo. Res.* **2017,** *185*, 158-168.

268. Horowitz, A.; Meller, R.; Moortgat, G. K. The UV–vis absorption cross sections of the α-dicarbonyl compounds: Pyruvic acid, biacetyl and glyoxal. *J. Photochem. Photobiol., A* **2001,** *146*, 19-27.

269. Hren, M.; Tice, M.; Chamberlain, C. Oxygen and hydrogen isotope evidence for a temperate climate 3.42 billion years ago. *Nature* **2009,** *462*, 205-208.

270. Huang, Z.; Hua, W.; Verreault, D.; Allen, H. C. Influence of salt purity on Na+ and palmitic acid interactions. *J. Phys. Chem. A* **2013,** *117*, 13412-13418.

271. Huber, C.; Wachtershauser, G. Peptides by activation of amino acids with CO on (Ni,Fe)S surfaces: Implications for the origin of life. *Science* **1998,** *281*, 670-672.

272. Huestis, D. L.; Berkowitz, J. Critical evaluation of the photoabsorption cross section of CO_2 from 0.125 to 201.6 nm at room temperature. *Adv. Geosci.* **2010,** *25*, 229-242.

273. Hugenholtz, J. Citrate metabolism in lactic acid bacteria. *FEMS Microbiol. Rev.* **1993,** *12*, 165-178.

274. Javaux, E. J.; Marshall, C. P.; Bekker, A. Organic-walled microfossils in 3.2-billion-year-old shallow-marine siliciclastic deposits. *Nature* **2010,** *463*, 934-938.

275. Jimenez, J. L.; Canagaratna, M. R.; Donahue, N. M.; Prevot, A. S. H.; Zhang, Q.; Kroll, J. H.; DeCarlo, P. F.; Allan, J. D.; Coe, H.; Ng, N. L., et al. Evolution of organic aerosols in the atmosphere. *Science* **2009,** *326*, 1525-1529.

276. Jonathon Anderson, P. J. B., Daniel Milroy, Peter Ruprecht, Thomas Hauser, and Howard Jay Siegel, Deploying RMACC Summit: An HPC resource for the Rocky Mountain Region. In *Proceedings of PEARC17*, New Orleans, LA, USA, 2017; p 7.

277. Joyce, G. F. The antiquity of RNA-based evolution. *Nature* **2002,** *418*, 214-221.

278. Kaganer, V. M.; Mohwald, H.; Dutta, P. Structure and phase transitions in Langmuir monolayers. *Rev. Mod. Phys.* **1999,** *71*, 779-819.

279. Kahan, T. F.; Kwamena, N. O. A.; Donaldson, D. J. Different photolysis kinetics at the surface of frozen freshwater vs. frozen salt solutions. *Atmo. Chem. Phys.* **2010,** *10*, 10917-10922.

280. Kaku, K.; Hegg, D.; Covert, D.; Santarpia, J.; Jonsson, H.; Buzorius, G.; Collins, D. Organics in the northeastern Pacific and their impacts on aerosol hygroscopicity in the subsaturated and supersaturated regimes. *Atmo. Chem. Phys.* **2006,** *6*, 4101-4115.

281. Kaltenegger, L.; Traub, W. A.; Jucks, K. W. Spectral evolution of an Earth-like planet. *Astrophys. J.* **2007,** *658*, 598.

282. Kameel, F. R.; Hoffmann, M. R.; Colussi, A. J. OH radical-initiated chemistry of isoprene in aqueous media. Atmospheric implications. *J. Phys. Chem. A* **2013,** *117*, 5117-5123.

283. Kameel, F. R.; Riboni, F.; Hoffmann, M.; Enami, S.; Colussi, A. Fenton oxidation of gaseous isoprene on aqueous surfaces. *Journal of Physical Chemistry C* **2014,** *118*, 29151-29158.

284. Kanakidou, M.; Seinfeld, J.; Pandis, S.; Barnes, I.; Dentener, F.; Facchini, M.; Dingenen, R. V.; Ervens, B.; Nenes, A.; Nielsen, C. Organic aerosol and global climate modelling: A review. *Atmo. Chem. Phys.* **2005,** *5*, 1053-1123.

285. Kanicky, J. R.; Poniatowski, A. F.; Mehta, N. R.; Shah, D. O. Cooperativity among molecules at interfaces in relation to various technological processes: Effect of chain length on the pKa of fatty acid salt solutions. *Langmuir* **1999,** *16*, 172-177.

286. Kasting, J. F. Earth's early atmosphere. *Science* **1993,** *259*, 920-926.

287. Kasting, J. F., Atmospheric composition of Hadean-early Archean Earth: The importance of CO. In *Earth's early atmosphere and surface environment*, Shaw, G. H., Ed. 2014; Vol. 504, pp 19-28.

288. Kasting, J. F.; Ono, S. Palaeoclimates: The first two billion years. *Philos. Trans. R. Soc. London, Ser. B* **2006,** *361*, 917-929.

289. Kawamura, K.; Kasukabe, H.; Barrie, L. A. Source and reaction pathways of dicarboxylic acids, ketoacids and dicarbonyls in Arctic aerosols: One year of observations. *Atmos. Environ.* **1996,** *30*, 1709-1722.

290. Kawamura, K.; Kasukabe, H.; Barrie, L. A. Secondary formation of water-soluble organic acids and alpha-dicarbonyls and their contributions to total carbon and water-soluble organic carbon: Photochemical aging of organic aerosols in the arctic spring. *J. Geophys. Res. Atmos.* **2010,** *115*, D21306.

291. Kawamura, K.; Umemoto, N.; Mochida, M.; Bertram, T.; Howell, S.; Huebert, B. J. Water-soluble dicarboxylic acids in the tropospheric aerosols collected over east Asia and western north Pacific by ACE-Asia C-130 aircraft. *J. Geophys. Res. Atmos.* **2003,** *108*, 8639.

292. Keating, C. D. Aqueous phase separation as a possible route to compartmentalization of biological molecules. *Acc. Chem. Res.* **2012,** *45*, 2114-2124.

293. Kempe, S.; Degens, E. T. An early soda ocean? *Chem. Geol.* **1985,** *53*, 95-108.

294. Kessenich, B. Surface thermodynamics of decanoic acid. University of Colorado Boulder, 2015.

295. Khare, B. N.; Sagan, C. Synthesis of cystine in simulated primitive conditions. *Nature* **1971,** *232*, 577-579.

296. Knauth, L. P. Salinity history of the Earth's early ocean [letter]. *Nature* **1998,** *395*, 554-555.

297. Knauth, L. P. Temperature and salinity history of the precambrian ocean: Implications for the course of microbial evolution. *Palaeogeogr. Palaeoclimatol. Palaeoecol.* **2005,** *219*, 53-69.

298. Knauth, L. P.; Lowe, D. R. High Archean climatic temperature inferred from oxygen isotope geochemistry of cherts in the 3.5 Ga Swaziland Supergroup, South Africa. *Geol. Soc. Am. Bull.* **2003,** *115*, 566-580.

299. Knobler, C. M.; Desai, R. C. Phase transitions in monolayers. *Annu. Rev. Phys. Chem.* **1992,** *43*, 207-236.

300. Kramer, Z. C.; Takahashi, H.; Vaida, V.; Skodje, R. T. Will water act as a photocatalyst for cluster phase chemical reactions? Vibrational overtone-induced dehydration reaction of methanediol. *J. Chem. Phys.* **2012,** *136*, 164302.

301. Kroll, J. H.; Ng, N. L.; Murphy, S. M.; Flagan, R. C.; Seinfeld, J. H. Secondary organic aerosol formation from isoprene photooxidation under high-NO_x conditions. *Geophys. Res. Lett.* **2005,** *32*, L18808.

302. Kroll, J. H.; Ng, N. L.; Murphy, S. M.; Flagan, R. C.; Seinfeld, J. H. Secondary organic aerosol formation from isoprene photooxidation. *Environ. Sci. Technol.* **2006,** *40*, 1869-1877.

303. Kumar, M.; Francisco, J. S. The role of catalysis in alkanediol decomposition: Implications for general detection of alkanediols and their formation in the atmosphere. *J. Phys. Chem. A* **2015,** *119*, 9821-9833.

304. Kumar, N.; Wang, L.; Siretanu, I.; Duits, M.; Mugele, F. Salt dependent stability of stearic acid Langmuir–Blodgett films exposed to aqueous electrolytes. *Langmuir* **2013,** *29*, 5150-5159.

305. Kunze, M.; Godolt, M.; Langematz, U.; Grenfell, J.; Hamann-Reinus, A.; Rauer, H. Investigating the early Earth faint young sun problem with a general circulation model. *Planet. Space Sci.* **2014,** *98*, 77-92.

306. Langmuir, I. The constitution and fundamental properties of solids and liquids. II. Liquids. *J. Am. Chem. Soc.* **1917,** *39*, 1848-1906.

307. Larsen, M. C.; Vaida, V. Near infrared photochemistry of pyruvic acid in aqueous solution. *J. Phys. Chem. A* **2012,** *116*, 5840-5846.

308. Laughlin, R. G. Equilibrium vesicles: Fact or fiction? *Colloids Surf., A* **1997,** *128*, 27-38.

309. Lee, O.-S.; Cho, V.; Schatz, G. C. Modeling the self-assembly of peptide amphiphiles into fibers using coarse-grained molecular dynamics. *Nano Lett.* **2012,** *12*, 4907-4913.

310. Lee, W.; Baasandorj, M.; Stevens, P. S.; Hites, R. A. Monitoring OH-initiated oxidation kinetics of isoprene and its products using online mass spectrometry. *Environ. Sci. Technol.* **2005,** *39*, 1030-1036.

311. Leermakers, P. A.; Vesley, G. F. Photochemistry of alpha-keto acids and alpha-keto esters. 1. Photolysis of pyruvic acid and benzoylformic acid. *J. Am. Chem. Soc.* **1963,** *85*, 3776-3779.

312. Leermakers, P. A.; Vesley, G. F. Photolysis of pyruvic acid in solution. *J. Org. Chem.* **1963,** *28*, 1160-1161.

313. Leermakers, P. A.; Vesley, G. F. Organic photochemistry and the excited state. *J. Chem. Educ* **1964,** *41*, 535.

314. Lelieveld, J.; Gromov, S.; Pozzer, A.; Taraborrelli, D. Global tropospheric hydroxyl distribution, budget and reactivity. *Atmos. Chem. Phys. Discuss.* **2016,** *2016*, 1-25.

315. Leopold, D. G.; Pendley, R. D.; Roebber, J. L.; Hemley, R. J.; Vaida, V. Direct absorption-spectroscopy of jet-cooled polyenes. 2. The 1 $^{1}B_{u}^{+}$ ← 1 $^{1}A_{g}^{-}$ transitions of butadienes and hexatrienes. *J. Chem. Phys.* **1984,** *81*, 4218-4229.

316. Leopold, D. G.; Vaida, V.; Granville, M. F. Direct absorption-spectroscopy of jet-cooled polyenes. 1. The 1 $^{1}B_{u}^{+}$ ← 1 $^{1}A_{g}^{-}$ transition of trans, trans-1,3,5,7-octatetraene. *J. Chem. Phys.* **1984,** *81*, 4210-4217.

317. Lerman, L., The primordial bubble: Water, symmetry-breaking, and the origin of life. In *Water and life: The unique properties of water*, Lynden-Bell, R. M.; Morris, S. C.; Barrow, J. D.; Finney, J. L.; Harper Jr., C. L., Eds. CRC Press: Boca Raton, FL, 2010; pp 259 - 290.

318. Lerman, L.; Teng, J., In the beginning. In *Origins: Genesis, evolution and diversity of life*, Seckbach, J., Ed. Kluwer Academic Publishers: Dordrecht, The Netherlands, 2004; pp 35 - 55.

319. Li, H. Y.; Savage, T.; Obermoeller, R. D.; Kazianis, S.; Walter, R. B. Parental 5-methylcytosine methylation patterns are stable upon interspecies hybridization of xiphophorus (Teleostei : Poeciliidae) fish. *Comp. Biochem. Phys. B* **2002,** *133*, 581-595.

320. Li, Y.; Ezell, M. J.; Finlayson-Pitts, B. J. The impact of organic coatings on light scattering by sodium chloride particles. *Atmos. Environ.* **2011,** *45*, 4123-4132.

321. Ligon, S. C.; Husar, B.; Wutzel, H.; Holman, R.; Liska, R. Strategies to reduce oxygen inhibition in photinduced polymerization. *Chem. Rev.* **2014,** *114*, 557-589.

322. Lim, Y. B.; Tan, Y.; Turpin, B. J. Chemical insights, explicit chemistry, and yields of secondary organic aerosol from OH radical oxidation of methylglyoxal and glyoxal in the aqueous phase. *Atmo. Chem. Phys.* **2013,** *13*, 8651-8667.

323. Liu, Y.; Siekmann, F.; Renard, P.; Zein, A. E.; Salque, G.; Haddad, I. E.; Temime-Roussel, B.; Voisin, D.; Thissen, R.; Monod, A. Oligomer and SOA formation through

aqueous phase photooxidation of methacrolein and methyl vinyl ketone. *Atmos. Environ.* **2012,** *49*, 123-129.

324. Lo, J.-H. A.; Lee, W.-M. G. Effect of surfactant film on solubility of hydrophobic organic compounds in fog droplets. *Chemosphere* **1996,** *33*, 1391-1408.

325. Loeffler, K. W.; Koehler, C. A.; Paul, N. M.; De Haan, D. O. Oligomer formation in evaporating aqueous glyoxal and methylglyoxal solutions. *Environ. Sci. Technol.* **2006,** *40*, 6318-6323.

326. Lohmann, U.; Feichter, J. Global indirect aerosol effects: A review. *Atmo. Chem. Phys.* **2005,** *5*, 715-737.

327. Long, C. A.; Ewing, G. E. Spectroscopic investigation of van der Waals molecules. 1. Infrared and visible spectra of O_2 *J. Chem. Phys.* **1973,** *58*, 4824-4834.

328. Long, M.; Keene, W.; Kieber, D.; Frossard, A.; Russell, L.; Maben, J.; Kinsey, J.; Quinn, P.; Bates, T. Light-enhanced primary marine aerosol production from biologically productive seawater. *Geophys. Res. Lett.* **2014,** *41*, 2661-2670.

329. Lopalco, A.; Dalwadi, G.; Niu, S.; Schowen, R. L.; Douglas, J.; Stella, V. J. Mechanism of decarboxylation of pyruvic acid in the presence of hydrogen peroxide. *J. Pharm. Sci.* **2016,** *105*, 705-713.

330. Lu, D. H.; Hase, W. L. Classical trajectory calculation of the benzene overtone spectra. *J. Phys. Chem.* **1988,** *92*, 3217-3225.

331. Luisi, P. L.; Walde, P.; Oberholzer, T. Lipid vesicles as possible intermediates in the origin of life. *Curr. Opin. Colloid Interface Sci.* **1999,** *4*, 33-39.

332. Lum, K.; Chandler, D.; Weeks, J. D. Hydrophobicity at small and large length scales. *J. Phys. Chem. B* **1999,** *103*, 4570-4577.

333. Magne, F. C.; Hughes, E. J.; Mod, R. R.; Skau, E. L. Binary freezing point diagrams for palmitic acid with substituted acetamides and other amides. *J. Am. Chem. Soc.* **1952,** *74*, 2793-2795.

334. Magne, F. C.; Mod, R. R.; Skau, E. L. Purification of long-chain saturated fatty acids by recrystallization of their molecular compounds with acetamide. *J. Am. Oil Chem. Soc.* **1957,** *34*, 127-129.

335. Magne, F. C.; Skau, E. L. Molecular compound formation between acetamide and long-chain saturated fatty acids. *J. Am. Chem. Soc.* **1952,** *74*, 2628-2630.

336. Maher, K. A.; Stevenson, D. J. Impact frustration of the origin of life. *Nature* **1988,** *331*, 612-614.

337. Maibaum, L.; Dinner, A. R.; Chandler, D. Micelle formation and the hydrophobic effect. *J. Phys. Chem. B* **2004,** *108*, 6778-6781.

338. Mamajanov, I.; MacDonald, P. J.; Ying, J.; Duncanson, D. M.; Dowdy, G. R.; Walker, C. A.; Engelhart, A. E.; Fernández, F. M.; Grover, M. A.; Hud, N. V. Ester formation and hydrolysis during wet–dry cycles: Generation of far-from-equilibrium polymers in a model prebiotic reaction. *Macromolecules* **2014,** *47*, 1334-1343.

339. Manov, G. G.; Bates, R. G.; Hamer, W. J.; Acree, S. Values of the constants in the Debye—Hückel equation for activity coefficients. *J. Am. Chem. Soc.* **1943,** *65*, 1765-1767.

340. Mansy, S. S. Model protocells from single-chain lipids. *Int. J. Molec. Sci.* **2009,** *10*, 835-843.

341. Mansy, S. S. Membrane transport in primitive cells. *Cold Spring Harbor Persp. Biol.* **2010,** *2*, 14.

342. Mansy, S. S.; Schrum, J. P.; Krishnamurthy, M.; Tobe, S.; Treco, D. A.; Szostak, J. W. Template-directed synthesis of a genetic polymer in a model protocell. *Nature* **2008,** *454*, 122-U10.

343. Mansy, S. S.; Szostak, J. W. Reconstructing the emergence of cellular life through the synthesis of model protocells. *Cold Spring Harb. Symp. Quant. Bio.* **2009,** *74*, 47 -54.

344. Marcum, J. C.; Kaufman, S. H.; Weber, J. M. UV-photodissociation of non-cyclic and cyclic mononucleotides. *Int. J. Mass Spectrom.* **2011,** *303*, 129-136.

345. Margulis, L.; Walker, J. C. G.; Rambler, M. Reassessment of roles of oxygen and ultraviolet light in precambrian evolution. *Nature* **1976,** *264*, 620-624.

346. Maroń, M. K.; Takahashi, K.; Shoemaker, R. K.; Vaida, V. Hydration of pyruvic acid to its geminal-diol, 2, 2-dihydroxypropanoic acid, in a water-restricted environment. *Chem. Phys. Lett.* **2011,** *513*, 184-190.

347. Martinez, I. S.; Peterson, M. D.; Ebben, C. J.; Hayes, P. L.; Artaxo, P.; Martin, S. T.; Geiger, F. M. On molecular chirality within naturally occurring secondary organic aerosol particles from the central amazon basin. *Phys. Chem. Chem. Phys.* **2011,** *13*, 12114-12122.

348. Martins-Costa, M. T. C.; Anglada, J. M.; Francisco, J. S.; Ruiz-Lopez, M. F. Reactivity of volatile organic compounds at the surface of a water droplet. *J. Am. Chem. Soc.* **2012,** *134*, 11821-11827.

349. Matthews, C. N.; Minard, R. D. Hydrogen cyanide polymers, comets and the origin of life. *Faraday Discuss.* **2006,** *133*, 393-401.

350. Maurer, S. E.; Deamer, D. W.; Boncella, J. M.; Monnard, P. A. Chemical evolution of amphiphiles: Glycerol monoacyl derivatives stabilize plausible prebiotic membranes. *Astrobio.* **2009,** *9*, 979-987.

351. Maurer, S. E.; Monnard, P.-A. Primitive membrane formation, characteristics and roles in the emergent properties of a protocell. *Entropy* **2011,** *13*, 466-484.

352. Maurer, S. E.; Nguyen, G. Prebiotic vesicle formation and the necessity of salts. *Origins Life Evol. Biosphere* **2016,** *46*, 215-222.

353. Mauzerall, D., Oceanic photochemistry and evolution of elements and cofactors in the early stages of the evolution of life. In *Evolution of primary producers in the sea*, Falkowski, P. G.; Knoll, A. H., Eds. Elsevier: Amsterdam, 2007; pp 7-19.

354. McBain, J. W.; Sierichs, W. C. The solubility of sodium and potassium soaps and the phase diagrams of aqueous potassium soaps. *J. Am. Oil Chem. Soc.* **1948,** *25*, 221-225.

355. McCollom, T. M. Miller-Urey and beyond: What have we learned about prebiotic organic synthesis reactions in the past 60 years? *Ann. Rev. Earth Planet. Sci.* **2013,** *41*, 207-229.

356. McCollom, T. M.; Ritter, G.; Simoneit, B. R. Lipid synthesis under hydrothermal conditions by Fischer-Tropsch-Type reactions. *Origins Life Evol. Biosphere* **1999,** *29*, 153-166.

357. McCollom, T. M.; Ritter, G.; Simoneit, B. R. T. Lipid synthesis under hydrothermal conditions by Fischer-Tropsch-Type reactions. *Origins Life Evol. Biosphere* **1999,** *29*, 153-166.

358. McLean, D. S.; Vercoe, D.; Stack, K. R.; Richardson, D. The colloidal pKa of lipophilic extractives commonly found in pinus radiata. *Appita Journal: Journal of the Technical Association of the Australian and New Zealand Pulp and Paper Industry* **2005,** *58*, 362.

359. McNeill, V. F.; Sareen, N.; Schwier, A. N., Surface-active organics in atmospheric aerosols. In *Atmospheric and aerosol chemistry*, McNeill, V. F.; Ariya, P. A., Eds. 2014; Vol. 339, pp 201-259.

360. McQuarrie, D., *Statistical mechanics*. University Science Books: Sausalito, California, 2004.

361. Mellouki, A.; Mu, Y. J. On the atmospheric degradation of pyruvic acid in the gas phase. *J. Photochem. Photobiol., A* **2003,** *157*, 295-300.

362. Menger, F. M. Remembrances of self-assemblies past. *Langmuir* **2011,** *27*, 5176-5183.

363. Menger, F. M.; Shi, L.; Rizvi, S. A. A. Self-assembling systems: Mining a rich vein. *J. Colloid Interface Sci.* **2010,** *344*, 241-246.

364. Menor-Salvan, C.; Marin-Yaseli, M. R. A new route for the prebiotic synthesis of nucleobases and hydantoins in water/ice solutions involving the photochemistry of acetylene. *Chem. Eur. J.* **2013,** *19*, 6488-6497.

365. Mercer-Smith, J. A.; Mauzerall, D. C. Photochemistry of porphyrins: A model for the origin of photosynthesis. *Photochem. Photobiol.* **1984,** *39*, 397-405.

366. Michaelian, K.; Iop, A non-linear irreversible thermodynamic perspective on organic pigment proliferation and biological evolution. In *4th national meeting in chaos, complex system and time series*, 2013; Vol. 475.

367. Michaelian, K.; Simeonov, A. Fundamental molecules of life are pigments which arose and co-evolved as a response to the thermodynamic imperative of dissipating the prevailing solar spectrum. *Biogeosciences* **2015,** *12*, 4913-4937.

368. Miller, S. L. A production of amino acids under possible primitive Earth conditions. *Science* **1953,** *117*, 528-529.

369. Miller, S. L.; Urey, H. C. Organic compound synthesis on the primitive early Earth. *Science* **1959,** *130*, 245-251.

370. Mitric, R.; Petersen, J.; Bonacic-Koutecky, V. Laser-field-induced surface-hopping method for the simulation and control of ultrafast photodynamics. *Phys. Rev. A* **2009,** *79*, 053416.

371. Miyazaki, Y.; Sawano, M.; Kawamura, K. Low-molecular-weight hydroxyacids in marine atmospheric aerosol: Evidence of a marine microbial origin. *Biogeosciences* **2014,** *11*, 4407-4414.

372. Mmereki, B. T.; Donaldson, D. Direct observation of the kinetics of an atmospherically important reaction at the air−aqueous interface. *J. Phys. Chem. A* **2003,** *107*, 11038-11042.

373. Mochida, M.; Kitamori, Y.; Kawamura, K.; Nojiri, Y.; Suzuki, K. Fatty acids in the marine atmosphere: Factors governing their concentrations and evaluation of organic films on sea-salt particles. *J. Geophys. Res. Atmos.* **2002,** *107*, 4325.

374. Mod, R. R.; Skau, E. L.; Planck, R. W. Binary freezing-point diagrams for alpha-and beta-eleostearic acids with each other and with acetamide. *J. Am. Oil Chem. Soc.* **1953,** *30*, 368-371.

375. Mojzsis, S. J.; Arrhenius, G.; McKeegan, K. D.; Harrison, T. M.; Nutman, A. P.; Friend, C. R. L. Evidence for life on Earth before 3,800 million years ago. *Nature* **1996,** *384*, 55-59.

376. Mojzsis, S. J.; Harrison, T. M.; Pidgeon, R. T. Oxygen-isotope evidence from ancient zircons for liquid water at the Earth's surface 4,300 Myr ago. *Nature* **2001,** *409*, 178-181.

377. Monks, P. S. Gas-phase radical chemistry in the troposphere. *Chem. Soc. Rev.* **2005,** *34*, 376-395.

378. Monnard, P.-A.; Deamer, D. W. Preparation of vesicles from nonphospholipid amphiphiles. *Methods Enzymol.* **2003,** *372*, 133-151.

379. Monnard, P.-A.; Deamer, D. W., Membrane self-assembly processes: Steps toward the first cellular life. In *Minimal cell: The biophysics of cell compartment and origin of cell functionality*, Luisi, P. L.; Stano, P., Eds. 2011.

380. Monnard, P.-A.; Walde, P. Current ideas about prebiological compartmentalization. *Life* **2015,** *5*, 1239-1263.

381. Monnard, P. A.; Apel, C. L.; Kanavarioti, A.; Deamer, D. W. Influence of ionic inorganic solutes on self-assembly and polymerization processes related to early forms of life: Implications for a prebiotic aqueous medium. *Astrobio.* **2002,** *2*, 139-152.

382. Monnard, P. A.; Deamer, D. W. Membrane self-assembly processes: Steps toward the first cellular life. *Anat. Rec.* **2002,** *268*, 196-207.

383. Monnard, P. A.; DeClue, M. S.; Ziock, H. J. Organic nano-compartments as biomimetic reactors and protocells. *Curr. Nanosci.* **2008,** *4*, 71-87.

384. Monod, A.; Carlier, P. Impact of clouds on the tropospheric ozone budget: Direct effect of multiphase photochemistry of soluble organic compounds. *Atmos. Environ.* **1999,** *33*, 4431-4446.

385. Montgomery, J. A.; Frisch, M. J.; Ochterski, J. W.; Petersson, G. A. A complete basis set model chemistry. VI. Use of density functional geometries and frequencies. *J. Chem. Phys.* **1999,** *110*, 2822-2827.

386. Morigaki, K.; Walde, P. Fatty acid vesicles. *Curr. Opin. Colloid Interface Sci.* **2007,** *12*, 75-80.

387. Morigaki, K.; Walde, P.; Misran, M.; Robinson, B. H. Thermodynamic and kinetic stability. Properties of micelles and vesicles formed by the decanoic acid/decanoate system. *Colloids Surf., A* **2003**, 37-44.

388. Morse, J. W.; Mackenzie, F. T. Hadean ocean carbonate geochemistry. *Aquat. Geochem.* **1998,** *4*, 301-319.

389. Mulkidjanian, A. Y.; Cherepanov, D. A.; Galperin, M. Y. Survival of the fittest before the beginning of life: Selection of the first oligonucleotide-like polymers by UV light. *BMC Evol. Bio.* **2003,** *3*, 12.

390. Munoz Caro, G. M.; Meierhenrich, U. J.; Schutte, W. A.; Barbier, B.; Arcones Segovia, A.; Rosenbauer, H.; Thiemann, W. H. P.; Brack, A.; Greenberg, J. M. Amino acids from ultraviolet irradiation of interstellar ice analogues. *Nature* **2002,** *416*, 403-6.

391. Murphy, D.; Thomson, D.; Mahoney, M. In situ measurements of organics, meteoritic material, mercury, and other elements in aerosols at 5 to 19 kilometers. *Science* **1998,** *282*, 1664-1669.

392. Murphy, J. G.; Gregoire, P.; Tevlin, A.; Wentworth, G.; Ellis, R.; Markovic, M.; VandenBoer, T. Observational constraints on particle acidity using measurements and modelling of particles and gases. *Faraday Discuss.* **2017**.

393. Nakata, K.; Fujishima, A. TiO_2 photocatalysis: Design and applications. *J. Photochem. Photobio. C* **2012,** *13*, 169-189.

394. Namani, T.; Walde, P. From decanoate micelles to decanoic acid-dodecylbenzenesulfonate vesicles. *Langmuir* **2005,** *21*, 6210-6219.

395. Nguyen, H. T.; Jeilani, Y. A.; Hung, H. M.; Nguyen, M. T. Radical pathways for the prebiotic formation of pyrimidine bases from formamide. *J. Phys. Chem. A* **2015,** *119*, 8871-8883.

396. Nguyen, T. B.; Bateman, A. P.; Bones, D. L.; Nizkorodov, S. A.; Laskin, J.; Laskin, A. High-resolution mass spectrometry analysis of secondary organic aerosol generated by ozonolysis of isoprene. *Atmos. Environ.* **2010,** *44*, 1032-1042.

397. Nilson, F. P. R. Possible impact of a primordial oil slick on atmospheric and chemical evolution. *Origins Life Evol. Biosphere* **2002,** *32*, 247-253.

398. Nilsson, M.; Connell, M. A.; Davis, A. L.; Morris, G. A. Biexponential fitting of diffusion-ordered NMR data: Practicalities and limitations. *Anal. Chem.* **2006,** *78*, 3040-3045.

399. Nilsson, M.; Morris, G. A. Improved DECRA processing of DOSY data: Correcting for non-uniform field gradients. *Magn. Reson. Chem.* **2007,** *45*, 656-660.

400. Noffke, N.; Christian, D.; Wacey, D.; Hazen, R. M. Microbially induced sedimentary structures recording an ancient ecosystem in the ca. 3.48 billion-year-old Dresser formation, Pilbara, Western Australia. *Astrobio.* **2013,** *13*, 1103-1124.

401. Noffke, N.; Eriksson, K. A.; Hazen, R. M.; Simpson, E. L. A new window into early Archean life: Microbial mats in Earth's oldest siliciclastic tidal deposits (3.2 Ga Moodies group, South Africa). *Geology* **2006,** *34*, 253-256.

402. Nuevo, M.; Auger, G.; Blanot, D.; d'Hendecourt, L. A detailed study of the amino acids produced from the vacuum UV irradiation of interstellar ice analogs. *Origins Life Evol. Biosphere* **2008,** *38*, 37-56.

403. Nurakhmetov, N.; Omarova, R.; Ospanov, K. K. Compounds of acetamide and its analogs with inorganic acids: Synthesis and properties. *Russ. J. Coord. Chem.* **2002,** *28*, 272-278.

404. O'Connor, R. T.; Mod, R. R.; Murray, M. D.; Skau, E. L. The x-ray diffraction and infrared spectra of molecular compounds of acetamide and long-chain saturated fatty acids. *J. Am. Chem. Soc.* **1955,** *77*, 892-895.

405. Odian, G., *Principles of polymerization*. John Wiley & Sons: Hoboken, New Jersey, 2004.

406. Ogata, Y.; Tomizawa, K.; Takagi, K. Photo-oxidation of formic, acetic, and propionic acids with aqueous hydrogen peroxide. *Can. J. Chem.* **1981,** *59*, 14-18.

407. Ogg, R. J.; Kingsley, R.; Taylor, J. S. WET, a T 1-and B 1-insensitive water-suppression method for in vivo localized ^{1}H NMR spectroscopy. *J. Magn. Reson., Ser B* **1994,** *104*, 1-10.

408. Ohtomo, Y.; Kakegawa, T.; Ishida, A.; Nagase, T.; Rosing, M. T. Evidence for biogenic graphite in early Archaean Isua metasedimentary rocks. *Nat. Geosci.* **2014,** *7*, 25-28.

409. Oneill, J. A.; Kreutz, T. G.; Flynn, G. W. IR diode-laser study of vibrational-energy distribution in CO_2 produced by UV excimer laser photofragmentation of pyruvic-acid. *J. Chem. Phys.* **1987,** *87*, 4598-4605.

410. Ortiz-Montalvo, D. L.; Lim, Y. B.; Perri, M. J.; Seitzinger, S. P.; Turpin, B. J. Volatility and yield of glycolaldehyde SOA formed through aqueous photochemistry and droplet evaporation. *Aerosol Sci. Technol.* **2012,** *46*, 1002-1014.

411. Pagni, R. M.; Sigman, M. E., The photochemistry of PAHs and PCBs in water and on solids. In *Environmental photochemistry*, Springer: 1999; pp 139-179.

412. Papanastasiou, G.; Ziogas, I. Simultaneous determination of equivalence volumes and acid dissociation constants from potentiometric titration data. *Talanta* **1995,** *42*, 827-836.

413. Park, S. C.; Burden, D. K.; Nathanson, G. M. Surfactant control of gas transport and reaction at the surface of sulfuric acid. *Acc. Chem. Res.* **2009,** *42*, 379-387.

414. Peck, W. H.; Valley, J. W.; Wilde, S. A.; Graham, C. M. Oxygen isotope ratios and rare earth elements in 3.3 to 4.4 Ga zircons: Ion microprobe evidence for high delta O-18 continental crust and oceans in the early Archean. *Geochim. Cosmochim. Acta* **2001,** *65*, 4215-4229.

415. Pedersen, K. J. The dissociation constants of pyruvic and oxaloacetic acid. *Acta Chem. Scand.* **1952,** *6*, 243-256.

416. Perkins, R.; Vaida, V. Phenylalanine increases membrane permeability. *J. Am. Chem. Soc.* **2017,** *139*, 14388-14391.

417. Perkins, R. J. Beyond hydrophobicity: Aqueous interfaces, interactions, and reactions. University of Colorado Boulder, 2017.

418. Perkins, R. J.; Shoemaker, R. K.; Carpenter, B. K.; Vaida, V. Chemical equilibria and kinetics in aqueous solutions of zymonic acid. *J. Phys. Chem. A* **2016,** *120*, 10096-10107.

419. Perkins, R. J.; Vaida, V. Zymonic acid as a prebiotic sugar analogue. *Origins Life Evol. Biosphere* **2017**, Submitted.

420. Perraud, V.; Bruns, E. A.; Ezell, M. J.; Johnson, S. N.; Yu, Y.; Alexander, M. L.; Zelenyuk, A.; Imre, D.; Chang, W. L.; Dabdub, D., et al. Nonequilibrium atmospheric secondary organic aerosol formation and growth. *Proc. Natl. Acad. Sci.* **2012,** *109*, 2836-2841.

421. Perri, M. J.; Seitzinger, S.; Turpin, B. J. Secondary organic aerosol production from aqueous photooxidation of glycolaldehyde: Laboratory experiments. *Atmos. Environ.* **2009,** *43*, 1487-1497.

422. Pestunova, O.; Simonov, A.; Snytnikov, V.; Stoyanovsky, V.; Parmon, V. Putative mechanism of the sugar formation on prebiotic Earth initiated by UV-radiation. *Adv. Space Res.* **2005,** *36*, 214-219.

423. Piccirilli, J. A.; Benner, S. A.; Krauch, T.; Moroney, S. E.; Benner, S. A. Enzymatic incorporation of a new base pair into DNA and RNA extends the genetic alphabet. *Nature* **1990,** *343*, 33-37.

424. Pierrehumbert, R. T. High levels of atmospheric carbon dioxide necessary for the termination of global glaciation. *Nature* **2004,** *429*, 646-649.

425. Pilpel, N.; Hunter, B. F. J. Oxidation and decomposition of monomolecular films of stearic acid under ultraviolet irradiation. *J. Colloid Interface Sci.* **1970,** *33*, 615-622.

426. Pinto, J. P.; Gladstone, G. R.; Yung, Y. L. Photochemical production of formaldehyde in earths primitive atmosphere. *Science* **1980,** *210*, 183-184.

427. Pizzarello, S. Chemical evolution and meteorites: An update. *Origins Life Evol. Biosphere* **2004,** *34*, 25-34.

428. Pizzarello, S. Prebiotic chemical evolution: A meteoritic perspective. *Rend. Lincei.* **2011,** *22*, 153-163.

429. Pizzarello, S.; Lahav, M. On the emergence of biochemical homochirality: An elusive beginning. *Origins Life Evol. Biosphere* **2010,** *40*, 1-2.

430. Pizzarello, S.; Weber, A. L. Stereoselective syntheses of pentose sugars under realistic prebiotic conditions. *Origins Life Evol. Biosphere* **2009,** *40*, 3-10.

431. Plankensteiner, K.; Reiner, H.; Rode, B. M. Amino acids on the rampant primordial Earth: Electric discharges and the hot salty ocean. *Molec. Divers.* **2006,** *10*, 3-7.

432. Plath, K. L.; Axson, J. L.; Nelson, G. C.; Takahashi, K.; Skodje, R. T.; Vaida, V. Gas-phase vibrational spectra of glyoxylic acid and its gem diol monohydrate. Implications for atmospheric chemistry. *React. Kinet. Catal. Lett.* **2009,** *96*, 209-224.

433. Plath, K. L.; Takahashi, K.; Skodje, R. T.; Vaida, V. Fundamental and overtone vibrational spectra of gas-phase pyruvic acid. *J. Phys. Chem. A* **2009,** *113*, 7294-7303.

434. Plimpton, S. Fast parallel algorithms for short-range molecular dynamics. *J. Comp. Phys.* **1995,** *117*, 1-19, lammps.sandia.gov.

435. Pockels, A. On the relative contamination of the water-surface by equal quantities of different substances. *Nature* **1892,** *46*, 418-419.

436. Pocker, Y.; Meany, J. E.; Nist, B. J.; Zadorojny, C. Reversible hydration of pyruvic acid. I. Equilibrium studies. *J. Phys. Chem.* **1969,** *73*, 2879-2882.

437. Pohorille, A.; Deamer, D. Self-assembly and function of primitive cell membranes. *Res. Microbiol.* **2009,** *160*, 449-456.

438. Pohorille, A.; Wilson, M. A. Molecular-dynamics studies of simple membrane water interfaces - structure and functions in the beginnings of cellular life. *Origins Life Evol. Biosphere* **1995,** *25*, 21-46.

439. Powner, M. W.; Gerland, B.; Sutherland, J. D. Synthesis of activated pyrimidine ribonucleotides in prebiotically plausible conditions. *Nature* **2009,** *459*, 239-242.

440. Powner, M. W.; Sutherland, J. D. Prebiotic chemistry: A new modus operandi. *Philos. Trans. R. Soc. London, Ser. B* **2011,** *366*, 2870-2877.

441. Prather, K. A.; Bertram, T. H.; Grassian, V. H.; Deane, G. B.; Stokes, M. D.; DeMott, P. J.; Aluwihare, L. I.; Palenik, B. P.; Azam, F.; Seinfeld, J. H., et al. Bringing the ocean into the laboratory to probe the chemical complexity of sea spray aerosol. *Proc. Natl. Acad. Sci.* **2013,** *110*, 7550-7555.

442. Prather, K. A.; Hatch, C. D.; Grassian, V. H. Analysis of atmospheric aerosols. *Annu. Rev. Anal. Chem.* **2008,** *1*, 485-514.

443. Prey, V.; Waldmann, E.; Berbalk, H. Zur kenntnis der brenztraubensäure. *Monatshefte für Chemie und verwandte Teile anderer Wissenschaften* **1955,** *86*, 408-413.

444. Price, R. L.; Jerome, W. G. J., *Basic confocal microscopy*. Springer Science & Business Media: 2011.

445. Quinn, P. K.; Collins, D. B.; Grassian, V. H.; Prather, K. A.; Bates, T. S. Chemistry and related properties of freshly emitted sea spray aerosol. *Chem. Rev.* **2015,** *115*, 4383-4399.

446. Ranjan, S.; Sasselov, D. D. Influence of the UV environment on the synthesis of prebiotic molecules. *Astrobio.* **2016,** *16*, 68-88.

447. Rao, M.; Eichberg, J.; Oro, J. Synthesis of phosphatidylcholine under possible primitive Earth conditions *J. Mol. Evo.* **1982,** *18*, 196-202.

448. Rapf, R. J.; Dooley, M. R.; Kappes, K.; Perkins, R. J.; Vaida, V. pH dependence of the aqueous photochemistry of α-keto acids *J. Phys. Chem. A* **2017**, DOI: 10.1021/acs.jpca.7b08192.

449. Rapf, R. J.; Perkins, R. J.; Carpenter, B. K.; Vaida, V. Mechanistic description of photochemical oligomer formation from aqueous pyruvic acid. *J. Phys. Chem. A* **2017,** *121*, 4272–4282.

450. Rapf, R. J.; Perkins, R. J.; Yang, H.; Miyake, G. M.; Carpenter, B. K.; Vaida, V. Photochemical synthesis of oligomeric amphiphiles from alkyl oxoacids in aqueous environments. *J. Am. Chem. Soc.* **2017,** *139*, 6946–6959.

451. Rapf, R. J.; Vaida, V. Sunlight as an energetic driver in the synthesis of molecules necessary for life. *Phys. Chem. Chem. Phys.* **2016,** *18*, 20067-20084.

452. Reed Harris, A. E. A kinetic and mechanistic study of the photochemistry of pyruvic acid: Implications for the atmosphere. University of Colorado Boulder, 2017.

453. Reed Harris, A. E.; Doussin, J.-F.; Carpenter, B. K.; Vaida, V. Gas-phase photolysis of pyruvic acid: The effect of pressure on reaction rates and products. *J. Phys. Chem. A* **2016,** *120*, 10123-10133.

454. Reed Harris, A. E.; Ervens, B.; Shoemaker, R. K.; Kroll, J. A.; Rapf, R. J.; Griffith, E. C.; Monod, A.; Vaida, V. Photochemical kinetics of pyruvic acid in aqueous solution. *J. Phys. Chem. A* **2014,** *118*, 8505-8516.

455. Reed Harris, A. E.; Pajunoja, A.; Cazaunau, M.; Gratien, A.; Pangui, E.; Monod, A.; Griffith, E. C.; Virtanen, A.; Doussin, J. F.; Vaida, V. Multiphase photochemistry of pyruvic acid under atmospheric conditions. *J. Phys. Chem. A* **2017,** *121*, 3327–3339.

456. Reeser, D.; Jammoul, A.; Clifford, D.; Brigante, M.; D'Anna, B.; George, C.; Donaldson, D. J. Photoenhanced reaction of ozone with chlorophyll at the seawater surface. *J. Phys. Chem. C* **2009,** *113*, 2071-2077.

457. Reeser, D. I.; George, C.; Donaldson, D. J. Photooxidation of halides by chlorophyll at the air-salt water interface. *J. Phys. Chem. A* **2009,** *113*, 8591-8595.

458. Reeves Jr, R. R.; Harteck, P.; Thompson, B. A.; Waldron, R. W. Photochemical equilibrium studies of carbon dioxide and their significance for the venus atmosphere. *J. Phys. Chem.* **1966,** *70*, 1637-1640.

459. Renard, P.; Reed Harris, A. E.; Rapf, R. J.; Rainer, S.; Demelas, C.; Coulomb, B.; Quivet, E.; Vaida, V.; Monod, A. Aqueous phase oligomerization of methyl vinyl ketone by atmospheric radical reactions. *J. Phys. Chem. C* **2014,** *118*, 29421-29430.

460. Renard, P.; Siekmann, F.; Gandolfo, A.; Socorro, J.; Salque, G.; Ravier, S.; Quivet, E.; Clement, J. L.; Traikia, M.; Delort, A. M., et al. Radical mechanisms of methyl vinyl ketone oligomerization through aqueous phase OH-oxidation: On the paradoxical role of dissolved molecular oxygen. *Atmo. Chem. Phys.* **2013,** *13*, 6473-6491.

461. Renard, P.; Siekmann, F.; Salque, G.; Demelas, C.; Coulomb, B.; Vassalo, L.; Ravier, S.; Temime-Roussel, B.; Voisin, D.; Monod, A. Aqueous-phase oligomerization of methyl vinyl ketone through photooxidation. Part 1: Aging processes of oligomers. *Atmo. Chem. Phys.* **2015,** *15*, 21-35.

462. Rideal, E. K.; Mitchell, J. S. Photochemical reactions in monolayers: I. Photochemical properties of the ketoimino linkage. *Proc. R. Soc. London, Ser. A* **1937,** *159*, 0206-0228.

463. Rinaldi, M.; Decesari, S.; Finessi, E.; Giulianelli, L.; Carbone, C.; Fuzzi, S.; Dowd, C. D.; Ceburnis, D.; Facchini, M. C. Primary and secondary organic marine aerosol and oceanic biological activity: Recent results and new perspectives for future studies. *Adv. Meteorol.* **2010,** *2010*, Article ID 310682.

464. Rincon, A. G.; Guzman, M. I.; Hoffmann, M. R.; Colussi, A. J. Optical absorptivity versus molecular composition of model organic aerosol matter. *J. Phys. Chem. A* **2009,** *113*, 10512-10520.

465. Rios, A. C.; Tor, Y. On the origin of the canonical nucleobases: An assessment of selection pressures across chemical and early biological evolution. *Isr. J. Chem.* **2013,** *53*, 469-483.

466. Ritson, D.; Sutherland, J. D. Prebiotic synthesis of simple sugars by photoredox systems chemistry. *Nature Chem.* **2012,** *4*, 895-899.

467. Robert, F.; Chaussidon, M. A palaeotemperature curve for the Precambrian oceans based on silicon isotopes in cherts. *Nature* **2006,** *443*, 969-972.

468. Robinson, G. W. Intensity enhancement of forbidden electronic transitions by weak intermolecular interactions. *J. Chem. Phys.* **1967,** *46*, 572-585.

469. Ronkainen, P.; Brummer, S.; Suomalainen, H. Diacetyl and formic acid as decomposition products of 2-acetolactic acid. *Acta Chem. Scand.* **1970,** *24*, 3404-3406.

470. Rosing, M. T. C-13-depleted carbon microparticles in > 3700-Ma sea-floor sedimentary rocks from west Greenland. *Science* **1999,** *283*, 674-676.

471. Rosing, M. T.; Bird, D. K.; Sleep, N. H.; Bjerrum, C. J. No climate paradox under the faint early sun. *Nature* **2010,** *464*, 744-747.

472. Rosing, M. T.; Frei, R. U-rich Archaean sea-floor sediments from Greenland - indications of >3700 Ma oxygenic photosynthesis. *Earth. Planet. Sci. Lett.* **2004,** *217*, 237-244.

473. Rossignol, S.; Tinel, L.; Bianco, A.; Passananti, M.; Brigante, M.; Donaldson, D. J.; George, C. Atmospheric photochemistry at a fatty acid–coated air-water interface. *Science* **2016,** *353*, 699-702.

474. Rudich, Y. Laboratory perspectives on the chemical transformations of organic matter in atmospheric particles. *Chem. Rev.* **2003,** *103*, 5097-5124.

475. Rudich, Y.; Donahue, N. M.; Mentel, T. F. Aging of organic aerosol: Bridging the gap between laboratory and field studies. *Annu. Rev. Phys. Chem.* **2007,** *58*, 321-352.

476. Rudich, Y.; Riziq, A.; Erlick, C.; Adler, G.; Trainic, M.; Lang, N. Optical properties of aerosols with organic components using cavity ring down spectrometry. *Geochim. Cosmochim* **2009**, A1130-A1130.

477. Rugheimer, S.; Segura, A.; Kaltenegger, L.; Sasselov, D. UV surface environment of earth-like planets orbiting FGKM stars through geological evolution. *Astrophys. J.* **2015,** *806*, 137.

478. Rushdi, A. I.; Simoneit, B. R. T. Lipid formation by aqueous Fischer-Tropsch-Type synthesis over a temperature range of 100 to 400 °C. *Origins Life Evol. Biosphere* **2001,** *31*, 103-118.

479. Russell, M. J.; Nitschke, W.; Branscomb, E. The inevitable journey to being. *Philos. Trans. R. Soc. London, Ser. B* **2013,** *368*, 20120254.

480. Ryden, B.; Peterson, B. M., *Foundations of astrophysics*. Addison-Wesley: San Francisco, 2010.

481. Sagan, C. Ultraviolet selection pressure on the earliest organisms. *J. Theor. Bio.* **1973,** *39*, 195-200.

482. Sagan, C.; Chyba, C. The early faint sun paradox: Organic shielding of ultraviolet-labile greenhouse gases. *Science* **1997,** *276*, 1217-1221.

483. Sagan, C.; Khare, B. N. Long-wavelength ultraviolet photoproduction of amino acids on primitive Earth. *Science* **1971,** *173*, 417-420.

484. Saito, K.; Sasaki, G.; Okada, K.; Tanaka, S. Unimolecular decomposition of pyruvic acid - an experimental and theoretical study. *J. Phys. Chem.* **1994,** *98*, 3756-3761.

485. Saladino, R.; Ciambecchini, U.; Crestini, C.; Costanzo, G.; Negri, R.; Di Mauro, E. One-pot TiO_2-catalyzed synthesis of nucleic bases and acyclonucleosides from formamide: Implications for the origin of life. *ChemBioChem* **2003,** *4*, 514-521.

486. Samoylova, E.; Lippert, H.; Ullrich, S.; Hertel, I. V.; Radloff, W.; Schultz, T. Dynamics of photoinduced processes in adenine and thymine base pairs. *J. Am. Chem. Soc.* **2005,** *127*, 1782-1786.

487. Sanchez, R. A.; Ferris, J. P.; Orgel, L. E. Studies in prebiotic synthesis. 2. Synthesis of purine precursors and amino acids from aqueous hydrogen cyanide. *J. Mol. Biol.* **1967,** *30*, 223-253.

488. Sanchez, R. A.; Ferris, J. P.; Orgel, L. E. Studies in prebiotic synthesis. 4. Conversion of 4-aminoimidazole-5-carbonitrile derivatives to purines. *J. Mol. Biol.* **1968,** *38*, 121-128.

489. Sanchez, R. A.; Orgel, L. E. Studies in prebiotic synthesis. 5. Synthesis and photo anomerization of pyrimidine nucleosides. *J. Mol. Biol.* **1970,** *47*, 531-543.

490. Santamaria, L.; Fleischmann, L. Photochemical synthesis of amino acids from paraformaldehyde catalysed by inorganic agents. *Experientia* **1966,** *22*, 430-431.

491. Sarker, P. K.; Takahashi, J.-i.; Obayashi, Y.; Kaneko, T.; Kobayashi, K. Photo-alteration of hydantoins against UV light and its relevance to prebiotic chemistry. *Adv. Space Res.* **2013,** *51*, 2235-2240.

492. Schidlowski, M. A 3,800-million-year isotopic record of life from carbon in sedimentary rocks. *Nature* **1988,** *333*, 313-318.

493. Schilke, P.; Menten, K. M. Detection of a second, strong submillimeter HCN laser line toward carbon stars. *Astrophys. J.* **2003,** *583*, 446-450.

494. Schmidt, J.; Skinner, J. Hydrodynamic boundary conditions, the Stokes–Einstein law, and long-time tails in the Brownian limit. *J. Chem. Phys.* **2003,** *119*, 8062-8068.

495. Schnitzler, E. G.; Seifert, N. A.; Ghosh, S.; Thomas, J.; Xu, Y.; Jäger, W. Hydration of the simplest α-keto acid: A rotational spectroscopic and ab initio study of the pyruvic acid–water complex. *Phys. Chem. Chem. Phys.* **2017,** *19* 4440-4446.

496. Schöne, L.; Herrmann, H. Kinetic measurements of the reactivity of hydrogen peroxide and ozone towards small atmospherically relevant aldehydes, ketones and organic acids in aqueous solutions. *Atmo. Chem. Phys.* **2014,** *14*, 4503.

497. Schöne, L.; Schindelka, J.; Szeremeta, E.; Schaefer, T.; Hoffmann, D.; Rudzinski, K. J.; Szmigielski, R.; Herrmann, H. Atmospheric aqueous phase radical chemistry of the isoprene oxidation products methacrolein, methyl vinyl ketone, methacrylic acid and acrylic acid–kinetics and product studies. *Phys. Chem. Chem. Phys.* **2014,** *16*, 6257-6272.

498. Schreiner, P. R.; Reisenauer, H. P.; Ley, D.; Gerbig, D.; Wu, C.-H.; Allen, W. D. Methylhydroxycarbene: Tunneling control of a chemical reaction. *Science* **2011,** *332*, 1300-1303.

499. Schwartz, A. W.; Chittenden, G. J. F. Synthesis of uracil and thymine under simulated prebiotic conditions. *Biosystems* **1977,** *9*, 87-92.

500. Schwartz, A. W.; De Graaf, R. The prebiotic synthesis of carbohydrates: A reassessment. *J. Mol. Evo.* **1993,** *36*, 101-106.

501. Seinfeld, J. H.; Pandis, S. N., *Atmospheric chemistry and physics: From air pollution to climate change*. John Wiley & Sons, Inc.: New York, 1998.

502. Sempere, R.; Kawamura, K. Comparative distributions of dicarboxylic acids and related polar compounds in snow, rain, and aerosols from urban atmosphere. *Atmos. Environ.* **1994,** *28*, 449-459.

503. Senanayake, S. D.; Idriss, H. Photocatalysis and the origin of life: Synthesis of nucleoside bases from formamide on TiO_2(001) single surfaces. *Proc. Natl. Acad. Sci.* **2006,** *103*, 1194-1198.

504. Serrano-Andres, L.; Merchan, M. Are the five natural DNA/RNA base monomers a good choice from natural selection? A photochemical perspective. *J. Photochem. Photobio. C* **2009,** *10*, 21-32.

505. Seta, P.; Bienvenue, E.; Moore, A. L.; Mathis, P.; Bensasson, R. V.; Liddell, P.; Pessiki, P. J.; Joy, A.; Moore, T. A.; Gust, D. Photodriven transmembrane charge separation and electron transfer by a carotenoporphyrin–quinone triad. *Nature* **1985,** *316*, 653-655.

506. Shah, D. O., The origin of membranes and related surface phenomena. In *Exobio.*, Ponnamperuma, C., Ed. North-Holland Publishing Co.: Amsterdam, 1972; pp 235 - 265.

507. Shapiro, R. Small molecule interactions were central to the origin of life. *Q. Rev. Bio.* **2006,** *81*, 105-125.

508. Sharma, M.; Yashonath, S. Breakdown of the Stokes−Einstein relationship: Role of interactions in the size dependence of self-diffusivity. *J. Phys. Chem. B* **2006,** *110*, 17207-17211.

509. Shaw, G. H. Earth's atmosphere–Hadean to early Proterozoic. *Chem. Erde Geochem.* **2008,** *68*, 235-264.

510. Sheldon, N. D. Precambrian paleosols and atmospheric CO_2 levels. *Precambrian Res.* **2006,** *147*, 148-155.

511. Shibuya, T.; Komiya, T.; Nakamura, K.; Takai, K.; Maruyama, S. Highly alkaline, high-temperature hydrothermal fluids in the early Archean ocean. *Precambrian Res.* **2010,** *182*, 230-238.

512. Sibert, E. L.; Hynes, J. T.; Reinhardt, W. P. Classical dynamics of highly excited CH and CD overtones in benzene and perdeuterobenzene. *J. Chem. Phys.* **1984,** *81*, 1135-1144.

513. Skoog, D. A.; Holler, F. J.; Mieman, T. A., *Principles of instrumental analysis*. 5th ed.; Brooks/Cole: United States, 1998.

514. Sleep, N. H. The Hadean-Archaean environment. *Cold Spring Harbor Persp. Biol.* **2010,** *2*, a002527.

515. Sleep, N. H.; Zahnle, K. J.; Kasting, J. F.; Morowitz, H. J. Annihilation of ecosystems by large asteroid impacts on the early Earth. *Nature* **1989,** *342*, 139-142.

516. Smith, R. D.; Berg, J. C. The collapse of surfactant monolayers at the air—water interface. *J. Colloid Interface Sci.* **1980,** *74*, 273-286.

517. Snyder, L. E.; Buhl, D. Observations of radio emission from interstellar hydrogen cyanide. *Astrophys. J.* **1971,** *163*, L47.

518. Sorjamaa, R.; Svenningsson, B.; Raatikainen, T.; Henning, S.; Bilde, M.; Laaksonen, A. The role of surfactants in Köhler theory reconsidered. *Atmo. Chem. Phys.* **2004,** *4*, 2107-2117.

519. Spencer, A. C.; Torre, P.; Mansy, S. S. The encapsulation of cell-free transcription and translation machinery in vesicles for the construction of cellular mimics. *J. Visual. Exp.* **2013**, e51304-e51304.

520. Spracklen, D.; Jimenez, J.; Carslaw, K.; Worsnop, D.; Evans, M.; Mann, G.; Zhang, Q.; Canagaratna, M.; Allan, J.; Coe, H. Aerosol mass spectrometer constraint on the global secondary organic aerosol budget. *Atmo. Chem. Phys.* **2011,** *11*, 12109-12136.

521. Stano, P.; D'Aguanno, E.; Bolz, J.; Fahr, A.; Luisi, P. L. A remarkable self-organization process as the origin of primitive functional cells. *Angew. Chem. Int. Ed.* **2013,** *52*, 13397-13400.

522. Stefan, M. I.; Bolton, J. R. Reinvestigation of the acetone degradation mechanism in dilute aqueous solution by the UV/H_2O_2 process. *Environ. Sci. Technol.* **1999,** *33*, 870-873.

523. Strehlow, H. Die kinetik der hydratation von α-ketocarbonsäuren. *Zeitschrift für Elektrochemie* **1962,** *66*, 392-396.

524. Sugisaki, R.; Horiuchi, Y.; Sugitani, K.; Adachi, M. Acid character of Archean ocean waters revealed by 3.3-Ga-old ferruginous chert compositions, Western Australia. *Proc. Jpn. Acad., Ser. B* **1995,** *71*, 170-174.

525. Sun, K.; Mauzerall, D. Charge transfer across a single lipid-water interface causes ion pumping across the bilayer. *Biophys. J.* **1996,** *71*, 309-316.

526. Sun, W.; Yang, L.; Yu, L.; Saeys, M. Ab initio reaction path analysis for the initial hydrogen abstraction from organic acids by hydroxyl radicals. *J. Phys. Chem. A* **2009,** *113*, 7852-7860.

527. Surratt, J. D.; Murphy, S. M.; Kroll, J. H.; Ng, N. L.; Hildebrandt, L.; Sorooshian, A.; Szmigielski, R.; Vermeylen, R.; Maenhaut, W.; Claeys, M. Chemical composition of secondary organic aerosol formed from the photooxidation of isoprene. *J. Phys. Chem. A* **2006,** *110*, 9665-9690.

528. Sutherland, J. D. The origin of life-out of the blue. *Angew. Chem. Int. Ed.* **2016,** *55*, 104-121.

529. Sutherland, J. D.; Whitfield, J. N. Prebiotic chemistry: A bioorganic perspective. *Tetrahedron* **1997,** *53*, 11493-11527.

530. Switzer, C.; Moroney, S. E.; Benner, S. A. Enzymatic incorporation of a new base pair into DNA and RNA. *J. Am. Chem. Soc.* **1989,** *111*, 8322-8323.

531. Szostak, J. W.; Bartel, D. P.; Luisi, P. L. Synthesizing life. *Nature* **2001,** *409*, 387-390.

532. Takahashi, K.; Plath, K. L.; Skodje, R. T.; Vaida, V. Dynamics of vibrational overtone excited pyruvic acid in the gas phase: Line broadening through hydrogen-atom chattering. *J. Phys. Chem. A* **2008,** *112*, 7321-7331.

533. Talbot, R.; Andreae, M.; Berresheim, H.; Jacob, D. J.; Beecher, K. Sources and sinks of formic, acetic, and pyruvic acids over central Amazonia: 2. Wet season. *J. Geophys. Res. Atmos.* **1990,** *95*, 16799-16811.

534. Tan, Y.; Carlton, A. G.; Seitzinger, S. P.; Turpin, B. J. SOA from methylglyoxal in clouds and wet aerosols: Measurement and prediction of key products. *Atmos. Environ.* **2010,** *44*, 5218-5226.

535. Tan, Y.; Perri, M. J.; Seitzinger, S. P.; Turpin, B. J. Effects of precursor concentration and acidic sulfate in aqueous glyoxal–OH radical oxidation and implications for secondary organic aerosol. *Environ. Sci. Technol.* **2009,** *43*, 8105-8112.

536. Tanford, C., *The hydrophobic effect: Formation of micelles and biological membranes 2d ed.* J. Wiley.: 1980.

537. Tang, C. Y.; Allen, H. C. Ionic binding of Na+ versus K+ to the carboxylic acid headgroup of palmitic acid monolayers studied by vibrational sum frequency generation spectroscopy. *J. Phys. Chem. A* **2009,** *113*, 7383-7393.

538. Tang, C. Y.; Huang, Z.; Allen, H. C. Binding of Mg^{2+} and Ca^{2+} to palmitic acid and deprotonation of the COOH headgroup studied by vibrational sum frequency generation spectroscopy. *J. Phys. Chem. B* **2010,** *114*, 17068-17076.

539. Taylor, R. The mechanism of thermal eliminations XXIII: [1] The thermal-decomposition of pyruvic-acid. *Int. J. Chem. Kinet.* **1987,** *19*, 709-713.

540. Tervahattu, H.; Hartonen, K.; Kerminen, V. M.; Kupiainen, K.; Aarnio, P.; Koskentalo, T.; Tuck, A. F.; Vaida, V. New evidence of an organic layer on marine aerosols. *J. Geophys. Res.* **2002,** *107*, 4053-4060.

541. Tervahattu, H.; Juhanoja, J.; Vaida, V.; Tuck, A. F.; Niemi, J. V.; Kupiainen, K.; Kulmala, M.; Vehkamaki, H. Fatty acids on continental sulfate aerosol particles. *J. Geophys. Res.* **2005,** *110*, Article number D06207

542. Thompson, B.; Harteck, P.; Reeves, R. Ultraviolet absorption coefficients of CO_2, CO, O_2, H_2O, N_2O, NH_3, NO, SO_2, and CH_4 between 1850 and 4000 A. *J. Geophys. Res.* **1963,** *68*, 6431-6436.

543. Thornton, D. C. O.; Brooks, S. D.; Chen, J. Protein and carbohydrate exopolymer particles in the sea surface microlayer (SML). *Front. Mar. Sci.* **2016,** *3*.

544. Tian, F.; Kasting, J. F.; Zahnle, K. Revisiting HCN formation in Earth's early atmosphere. *Earth. Planet. Sci. Lett.* **2011,** *308*, 417-423.

545. Tinel, L.; Rossignol, S.; Bianco, A.; Passananti, M.; Perrier, S.; Wang, X.; Brigante, M.; Donaldson, D. J.; George, C. Mechanistic insights on the photosensitized chemistry of a fatty acid at the air/water interface. *Environ. Sci. Technol.* **2016,** *50*, 11041-11048.

546. Tinel, L.; Rossignol, S.; Ciuraru, R.; Dumas, S.; George, C. Photosensitized reactions initiated by 6-carboxypterin: Singlet and triplet reactivity. *Phys. Chem. Chem. Phys.* **2016,** *18*, 17105-17115.

547. Toxvaerd, S. Origin of homochirality in biosystems. *Int. J. Molec. Sci.* **2009,** *10*, 1290-1299.

548. Trail, D.; Watson, E. B.; Tailby, N. D. The oxidation state of Hadean magmas and implications for early Earth's atmosphere. *Nature* **2011,** *480*, 79-82.

549. Trainer, M. G. Atmospheric prebiotic chemistry and organic hazes. *Curr. Org. Chem.* **2013,** *17*, 1710-1723.

550. Trainer, M. G.; Pavlov, A. A.; Curtis, D. B.; Mckay, C. P.; Worsnop, D. R.; Delia, A. E.; Toohey, D. W.; Toon, O. B.; Tolbert, M. A. Haze aerosols in the atmosphere of early Earth: Manna from heaven. *Astrobio.* **2004,** *4*, 409-419.

551. Trainer, M. G.; Pavlov, A. A.; DeWitt, H. L.; Jimenez, J. L.; McKay, C. P.; Toon, O. B.; Tolbert, M. A. Organic haze on Titan and the early Earth. *Proc. Natl. Acad. Sci.* **2006,** *103*, 18035-18042.

552. Tuck, A. The role of atmospheric aerosols in the origin of life. *Surv. Geophys.* **2002,** *23*, 379-409.

553. Tuck, A. F., *Atmospheric turbulence: A molecular dynamics perspective*. Oxford University Press: Oxford, U.K., 2008.

554. Turro, N. J.; Ramamurthy, V.; Scaiano, J. C., *Modern molecular photochemistry of organic molecules*. University Science Books: Sausalito, California, 2010.

555. Tverdislov, V. A.; Yakovenko, L. V. Physical aspects of the emergence of living cell precursors: The ion and chiral asymmetries as two fundamental asymmetry types. *Moscow Univ. Phys. Bull.* **2008,** *63*, 151-163.

556. Uzer, T.; Hynes, J. T.; Reinhardt, W. P. Classical dynamics of intramolecular energy-flow and overtone-induced dissociation in ho2h and ho2d. *J. Chem. Phys.* **1986,** *85*, 5791-5804.

557. Vaida, V. Spectroscopy of photoreactive systems: Implications for atmospheric chemistry. *J. Phys. Chem. A* **2009,** *113*, 5-18.

558. Vaida, V. Perspective: Water cluster mediated atmospheric chemistry. *J. Chem. Phys.* **2011,** *135*, Art. Nr. 020901.

559. Vaida, V. Ocean sea spray, clouds, and climate. *ACS Cent. Sci.* **2015,** *1*, 112-114.

560. Vaida, V. Atmospheric radical chemistry revisited. *Science* **2016,** *353*, 650-650.

561. Vaida, V.; Donaldson, D. J.; Sapers, S. P.; Naaman, R.; Child, M. S. Spectroscopic probe of intramolecular predissociation dynamics in clusters. *J. Phys. Chem.* **1989,** *93*, 513-520.

562. Vaida, V.; Feierabend, K. J.; Rontu, N.; Takahashi, K. Sunlight-initiated photochemistry: Excited vibrational states of atmospheric chromophores. *Int. J. Photoenergy* **2008**, Art. No. 138091.

563. Vaida, V.; McClelland, G. M. Electronic absorption-spectroscopy of cooled supersonic expansions - dynamics of the $^1B_{1u}$ state of trans-butadiene. *Chem. Phys. Lett.* **1980,** *71*, 436-439.

564. Veatch, S. L.; Polozov, I. V.; Gawrisch, K.; Keller, S. L. Liquid domains in vesicles investigated by NMR and fluorescence microscopy. *Biophys. J.* **2004,** *86*, 2910-2922.

565. Venot, O.; Fray, N.; Bénilan, Y.; Gazeau, M.-C.; Hébrard, E.; Larcher, G.; Schwell, M.; Dobrijevic, M.; Selsis, F. High-temperature measurements of vuv-absorption cross sections of CO_2 and their application to exoplanets. *Astron. Astrophys.* **2013,** *551*, A131.

566. Veres, P.; Roberts, J. M.; Burling, I. R.; Warneke, C.; de Gouw, J.; Yokelson, R. J. Measurements of gas-phase inorganic and organic acids from biomass fires by negative-ion proton-transfer chemical - ionization mass spectrometry. *J. Geophys. Res. Atmos.* **2010,** *115*, D23302.

567. Veres, P. R.; Roberts, J. M.; Cochran, A. K.; Gilman, J. B.; Kuster, W. C.; Holloway, J. S.; Graus, M.; Flynn, J.; Lefer, B.; Warneke, C., et al. Evidence of rapid production of organic acids in an urban air mass. *Geophys. Res. Lett.* **2011,** *38*, L17807.

568. Vesley, G. F.; Leermakers, P. A. Photochemistry of alpha-keto acids and alpha-keto esters. 3. Photolysis of pyruvic acid in vapor phase. *J. Phys. Chem.* **1964,** *68*, 2364-2366.

569. Viehe, H. G.; Janousek, Z.; Merenyi, R.; Stella, L. The captodative effect. *Acc. Chem. Res.* **1985,** *18*, 148-154.

570. Voet, D.; Voet, J. G., *Biochemistry*. 4 ed.; John Wiley and Sons, Inc: Hoboken, NJ, 2011.

571. Volkamer, R.; Jimenez, J. L.; San Martini, F.; Dzepina, K.; Zhang, Q.; Salcedo, D.; Molina, L. T.; Worsnop, D. R.; Molina, M. J. Secondary organic aerosol formation from anthropogenic air pollution: Rapid and higher than expected. *Geophys. Res. Lett.* **2006,** *33*.

572. Volman, D. H. The photochemistry of acetamide in water solution. *J. Am. Chem. Soc.* **1941,** *63*, 2000-2002.

573. Walser, R.; Mark, A. E.; van Gunsteren, W. F. On the validity of Stokes' law at the molecular level. *Chem. Phys. Lett.* **1999,** *303*, 583-586.

574. Wang, D.-N.; Stieglitz, H.; Marden, J.; Tamm, Lukas K. Benjamin Franklin, Philadelphia's favorite son, was a membrane biophysicist. *Biophys. J.* **2013,** *104*, 287-291.

575. Wang, X.; Sultana, C. M.; Trueblood, J.; Hill, T. C. J.; Malfatti, F.; Lee, C.; Laskina, O.; Moore, K. A.; Beall, C. M.; McCluskey, C. S., et al. Microbial control of sea spray aerosol composition: A tale of two blooms. *ACS Cent. Sci.* **2015,** *1*, 124-131.

576. Warneck, P. Multi-phase chemistry of C-2 and C-3 organic compounds in the marine atmosphere. *J. Atmos. Chem.* **2005,** *51*, 119-159.

577. Weast, R. C., *Handbook of chemistry and physics.* . 60th ed.; CRC Press Inc.: Boca Raton, Florida, 1979.

578. Weber, R. J.; Guo, H.; Russell, A. G.; Nenes, A. High aerosol acidity despite declining atmospheric sulfate concentrations over the past 15 years. *Nat. Geosci.* **2016,** *9*, 282-285.

579. Weeks, J. D.; Chandler, D.; Andersen, H. C. Role of repulsive forces in determining the equilibrium structure of simple liquids. *J. Chem. Phys.* **1971,** *54*, 5237-5247.

580. Wellen, B. A.; Lach, E. A.; Allen, H. C. Surface pKa of octanoic, nonanoic, and decanoic fatty acids at the air-water interface: Applications to atmospheric aerosol chemistry. *Phys. Chem. Chem. Phys.* **2017**.

581. Whitehill, A. R.; Jiang, B.; Guo, H.; Ono, S. SO_2 photolysis as a source for sulfur mass-independent isotope signatures in stratospheric aerosols. *Atmo. Chem. Phys.* **2015,** *15*, 1843-1864.

582. Whitehill, A. R.; Ono, S. Excitation band dependence of sulfur isotope mass-independent fractionation during photochemistry of sulfur dioxide using broadband light sources. *Geochim. Cosmochim. Acta* **2012,** *94*, 238-253.

583. Whitelam, S.; Rogers, C.; Pasqua, A.; Paavola, C.; Trent, J.; Geissler, P. L. The impact of conformational fluctuations on self-assembly: Cooperative aggregation of archaeal chaperonin proteins. *Nano Lett.* **2009,** *9*, 292-297.

584. Wilber, A. W.; Doye, J. P. K.; Louis, A. A. Self-assembly of monodisperse clusters: Dependence on target geometry. *J. Chem. Phys.* **2009,** *131*, 175101.

585. Wilber, A. W.; Doye, J. P. K.; Louis, A. A.; Noya, E. G.; Miller, M. A.; Wong, P. Reversible self-assembly of patchy particles into monodisperse icosahedral clusters. *J. Chem. Phys.* **2007,** *127*, 085106.

586. Wilde, S. A.; Valley, J. W.; Peck, W. H.; Graham, C. M. Evidence from detrital zircons for the existence of continental crust and oceans on the Earth 4.4 Gyr ago. *Nature* **2001,** *409*, 175-178.

587. Williams, R. J. P.; da Silva, J., *The natural selection of the chemical elements: The environment and life's chemistry*. Clarendon Press; Oxford University Press: 1996.

588. Wolf, E.; Toon, O. Hospitable Archean climates simulated by a general circulation model. *Astrobio.* **2013,** *13*, 656-673.

589. Wolf, E.; Toon, O. Controls on the Archean climate system investigated with a global climate model. *Astrobio.* **2014,** *14*, 241-253.

590. Wolf, E. T.; Toon, O. B. Fractal organic hazes provided an ultraviolet shield for early Earth. *Science* **2010,** *328*, 1266-1268.

591. Wolfe, S.; Kim, C.-K.; Yang, K.; Weinberg, N.; Shi, Z. Hydration of the carbonyl group: A theoretical study of the cooperative mechanism. *J. Am. Chem. Soc.* **1995,** *117*, 4240-4260.

592. Wolff, L. II. Ueber die parabrenztraubensäure. *Justus Liebigs Ann Chem* **1899,** *305*, 154-165.

593. Wolff, L. Ueber ein neues condensationsproduct der brenztraubensäure. *Justus Liebigs Ann. Chem.* **1901,** *317* 1–22.

594. Wood, C. F.; Oneill, J. A.; Flynn, G. W. Infrared diode-laser probes of photofragmentation products-bending excitation in CO_2 produced by excimer laser photolysis of pyruvic-acid. *Chem. Phys. Lett.* **1984,** *109*, 317-323.

595. Wyss, M. T.; Jolivet, R.; Buck, A.; Magistretti, P. J.; Weber, B. In vivo evidence for lactate as a neuronal energy source. *J. Neurosci.* **2011,** *31*, 7477-7485.

596. Xiao, Z. J.; Xu, P. Acetoin metabolism in bacteria. *Crit. Rev. Microbio.* **2007,** *33*, 127-140.

597. Xu, H.; Du, N.; Song, Y.; Song, S.; Hou, W. Vesicles of 2-ketooctanoic acid in water. *Soft Matter* **2017,** *13*, 2246-2252

598. Yamamoto, S.; Back, R. A. The photolysis and thermal decomposition of pyruvic acid in the gas phase. *Can. J. Chem.* **1985,** *63*, 549-554.

599. Yeh, I.-C.; Hummer, G. System-size dependence of diffusion coefficients and viscosities from molecular dynamics simulations with periodic boundary conditions. *J. Phys. Chem. B* **2004,** *108*, 15873-15879.

600. Young, A. H.; Keene, W. C.; Pszenny, A. A. P.; Sander, R.; Thornton, J. A.; Riedel, T. P.; Maben, J. R. Phase partitioning of soluble trace gases with size-resolved aerosols in near-surface continental air over northern Colorado, USA, during winter. *J. Geophys. Res. Atmos.* **2013,** *118*, 9414-9427.

601. Zahnle, K. J. Photochemistry of methane and the formation of hydrocyanic acid (HCN) in the earths early atmosphere. *J. Geophys. Res. Atmos.* **1986,** *91*, 2819-2834.

602. Zaia, D. A. M.; Zaia, C. T. B. V.; Santana, H. D. Which amino acids should be used in prebiotic chemistry studies? *Origins Life Evol. Biosphere* **2008,** *38*, 469-88.

603. Zhang, X.; Chen, Z.; Zhao, Y. Laboratory simulation for the aqueous OH-oxidation of methyl vinyl ketone and methacrolein: Significance to the in-cloud SOA production. *Atmo. Chem. Phys.* **2010,** *10*, 9551-9561.

604. Zhang, Z.; Cai, W.; Liu, L.; Liu, C.; Chen, F. Direct determination of thickness of sea surface microlayer using a pH microelectrode at original location. *Science in China Series B: Chemistry* **2003,** *46*, 339-351.

605. Zhang, Z. B.; Liu, L.; Liu, C.; Cai, W. Studies on the sea surface microlayer. II. The layer of sudden change of physical and chemical properties. *J. Colloid Interface Sci.* **2003,** *264*, 148-159.

606. Zhu, T. F.; Szostak, J. W. Coupled growth and division of model protocell membranes. *J. Am. Chem. Soc.* **2009,** *131*, 5705-5713.

607. Zilberter, Y.; Zilberter, T.; Bregestovski, P. Neuronal activity in vitro and the in vivo reality: The role of energy homeostasis. *Trends Pharmacol. Sci.* **2010,** *31*, 394-401.

Appendix A: Additional Applications of NMR Spectroscopy: A Proposed DOSY NMR Study of the Clustering Behavior of Fatty Acids in Aqueous Solution

Nuclear magnetic resonance (NMR) spectroscopy is one of the most powerful analytical tools available in the modern chemistry laboratory. However, for most of the studies described in this work, it has been used sparingly and high-resolution electrospray ionization mass spectrometry (ESI$^-$ MS) has been used as the primary means of identification of products. This is in part because NMR, particularly simple one-dimensional ^{1}H NMR, is of limited use in the analysis of complex mixtures of multiple species like those generated during the photolysis of α-keto acids. This difficulty is compounded for analysis of aqueous solutions, as the large peak due to water must be suppressed. Additionally, the identification of new products in the absence of analytical standards can be particularly challenging, especially because the chemical shifts of products are known to be dependent on solution conditions, including the presence of other organic species in solution.

Smaller organic molecules, such as pyruvic acid and its photoproducts, are generally easier to identify, but as the alkyl chain length is increased, the CH_2 groups on the alkyl chains experience very similar chemical environments regardless of the nature of the head group or other functionalized parts of the molecule. This can make it difficult to distinguish between the precursor and the photoproducts, or, indeed, between two different alkyl α-keto acids in solution. However, in some cases a slight splitting is observed (Figure A.1) that can be used to distinguish between two alkyl α-keto acids, in this case 2-oxooctanoic acid (OOA) and 2-oxodecanoic acid (ODA), that differ only by an additional two CH_2 groups present on the alkyl tail of ODA. The sum of ^{1}H NMR spectra of the two individual oxoacids recovers this splitting behavior and reproduces the experimental spectra of the mixture remarkably

well.

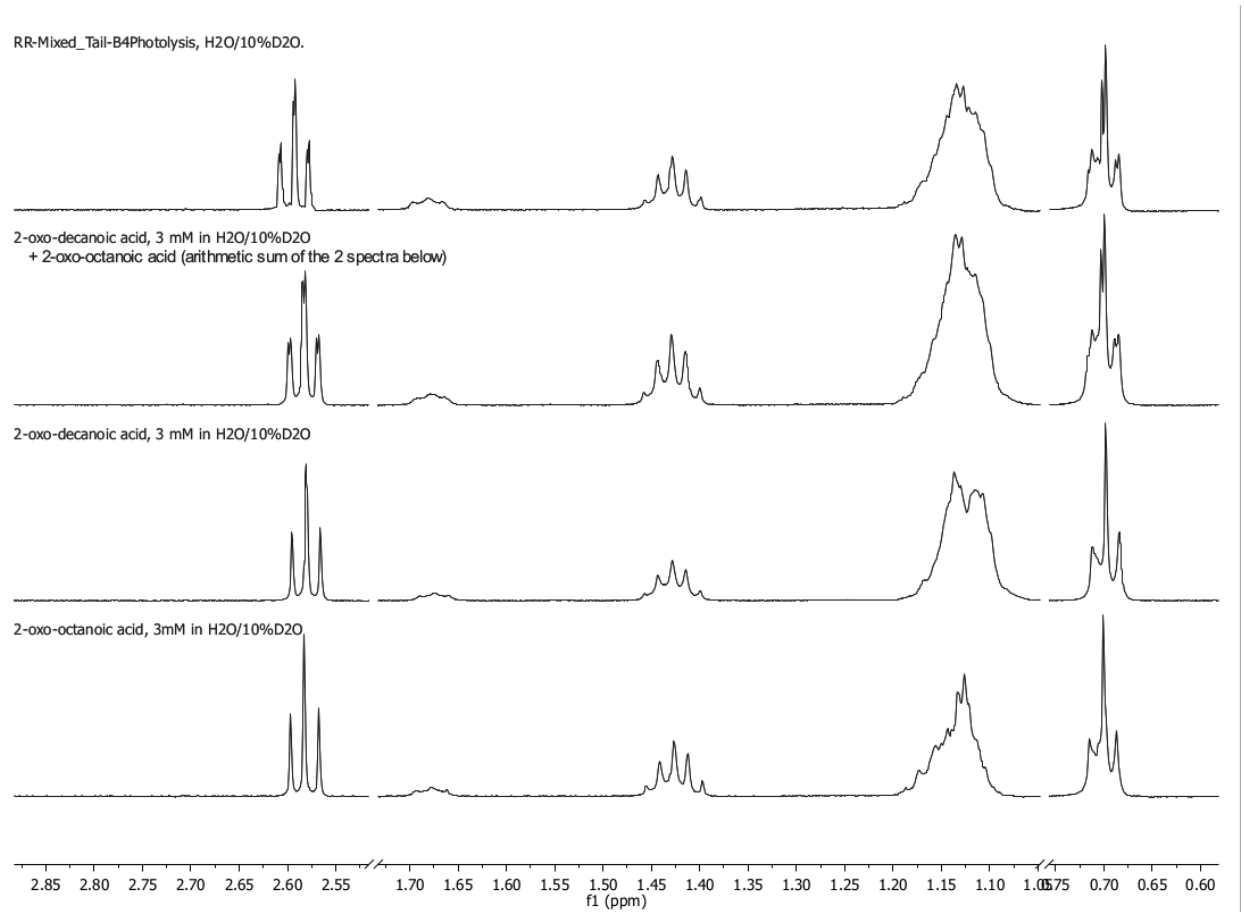

Figure A.1. Experimental ^{1}H NMR spectra of an aqueous solution containing a mixture of 3 mM OOA and 3 mM ODA (top) compared to an arithmetic sum of the two individual spectra (upper middle) of ODA (lower middle) and OOA (bottom).

A zoomed-in section of the spectra is given in Figure A.2 and shows we can assign the split peaks to the individual α-keto acids. It is possible that similar splittings could be used to resolve the assignment of species in more complicated mixtures as well, including, perhaps, differentiating among photoproducts and the precursor species. Such assignments are likely to be dependent on either the isolation and purification or the synthesis of photoproducts to be used as analytical standards before any such identification could occur.

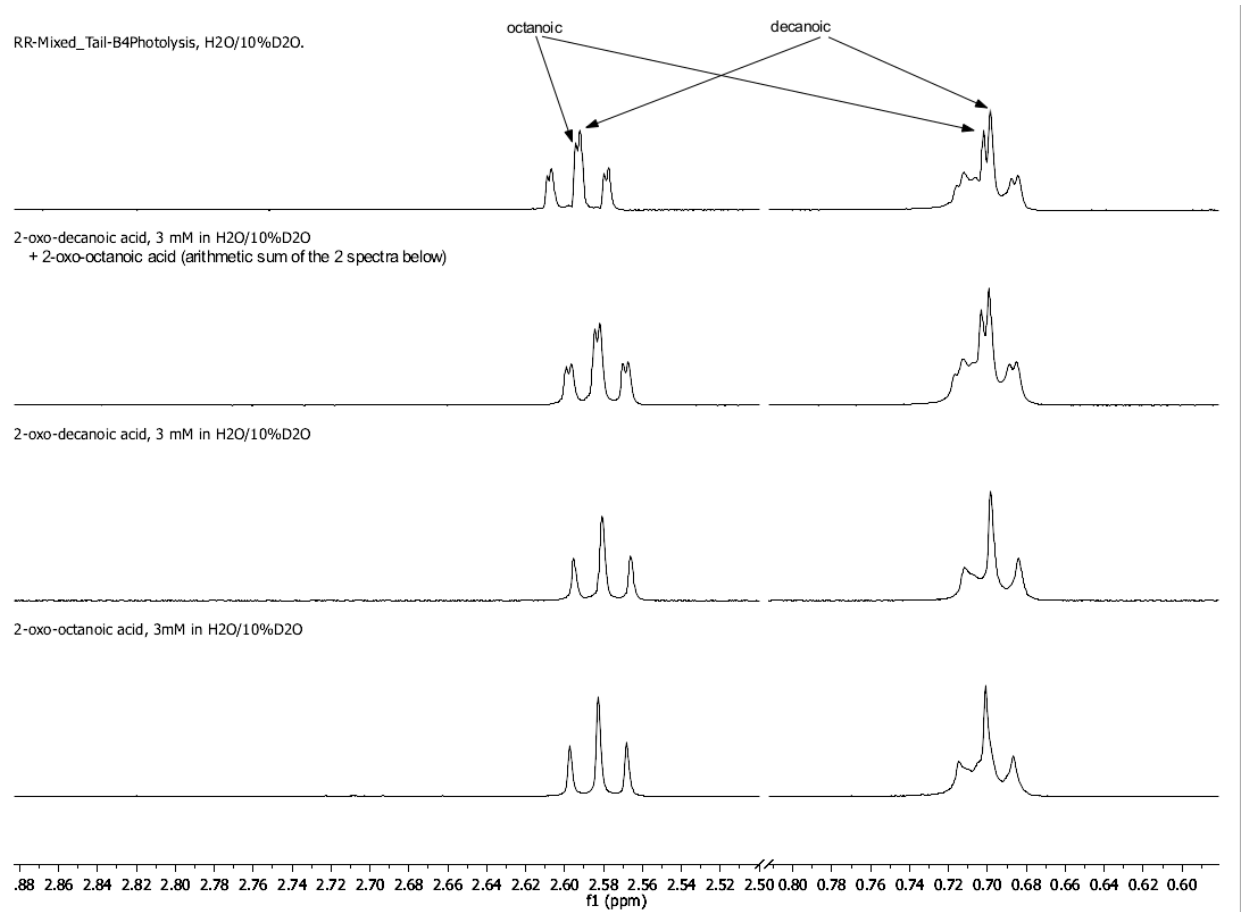

Figure A.2. Zoomed-in section of experimental ^{1}H NMR spectra of an aqueous solution containing a mixture of 3 mM OOA and 3 mM ODA (top) compared to an arithmetic sum of the two individual spectra (upper middle) of ODA (lower middle) and OOA (bottom). The splitting of the peaks has been assigned to individual α-keto acids.

In addition to simple one-dimensional ^{1}H NMR, two-dimensional NMR spectroscopies are incredibly powerful and, often, more useful at firmly identifying the components of mixtures. gCOSY NMR, for instance, has been used to great effect in the identification of key photoproducts of the photolysis of pyruvic acid.[1] Additionally, high-resolution diffusion-ordered spectroscopy NMR (DOSY NMR) has been used both for the identification of photoproducts[1] and to determine the size of aggregates generated from the photolysis of OOA.[2] 2-D DOSY NMR separates NMR signals of species that have different diffusion constants through a series of pulsed field gradients of different strengths. In this way, signal from larger molecules or aggregates is deconvoluted from signal of smaller species

that might have been overlapping in a one-dimensional NMR spectrum. While, it was possible to extract a diffusion constant for the large aggregates formed during the photolysis of OOA that was on the order of those obtained via DLS,[2] DOSY NMR is generally better at resolving smaller particles or clusters and has the potential to resolve differences in size that would result from the diffusion of small intermolecularly-bound clusters from the monomeric species diffusing in solution, if such clusters were sufficiently long-lived (~ms).

DOSY NMR spectra of 2-ocodecanoic acid following photolysis shows three major regions of signal (Figure A.3). There are the expected large aggregates that diffuse slowly in solution, there are smaller photoproducts that contain a methyl group, and there is signal from material with the expected alkyl tail of ODA or its oligomeric photoproducts that has not been incorporated into the larger aggregates. It is somewhat surprising that this free material appears to be well-described by one diffusion constant, ~$5.8*10^{-10}$ M^2/sec, as only about ~30% of the ODA is consumed during photolysis, and it seems highly likely that the free material would include both ODA as well as oligomeric photoproducts, most of which are covalently-bonded “dimers” of ODA.

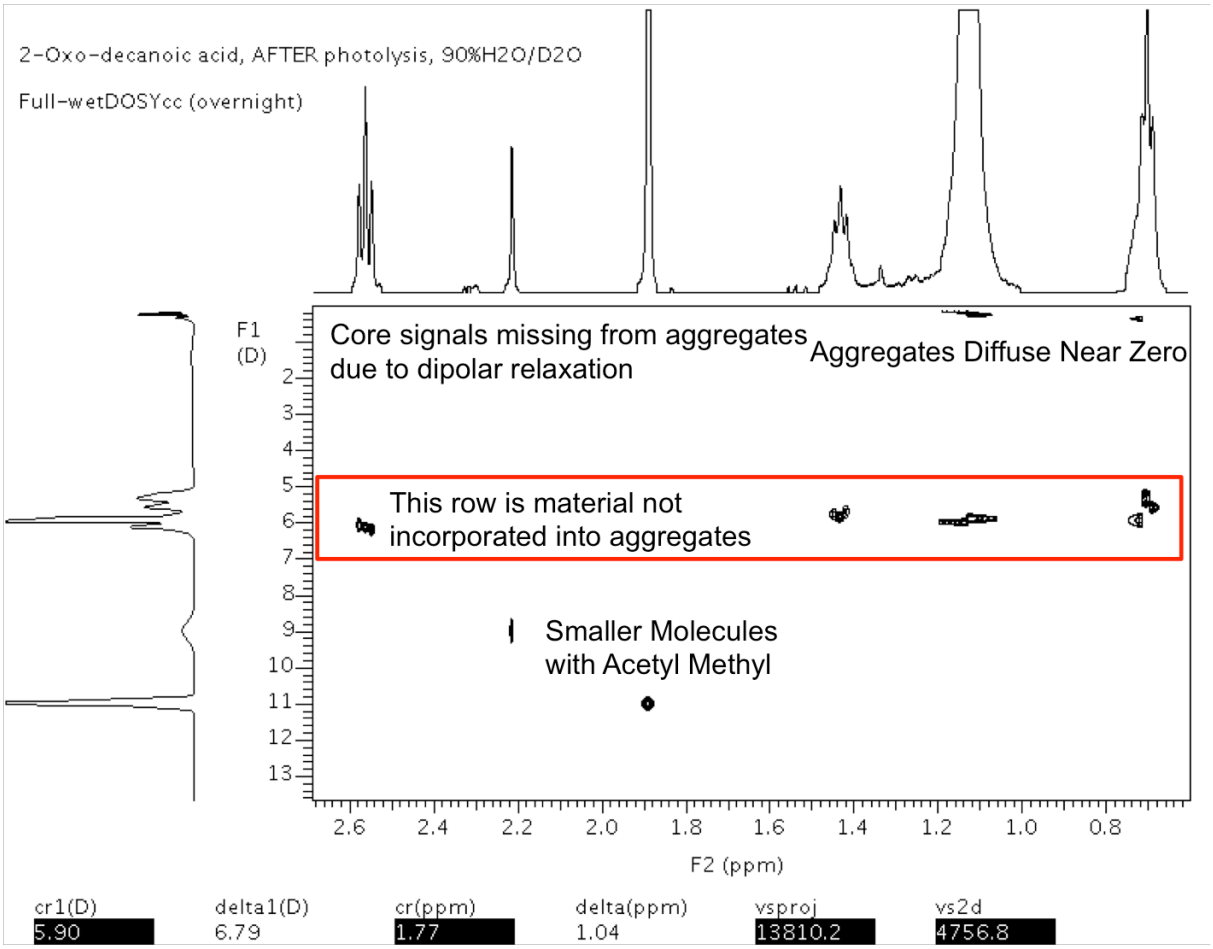

Figure A.3. DOSY NMR spectra of 3 mM ODA following 5 hours of photolysis.

Interestingly, the diffusion constant of the unphotolyzed ODA species in solution (Figure A.4), $5.80*10^{-10}$ M^2/sec, matches that obtained for the free material in the post-photolysis solutions. Solutions of ODA do not contain any covalently-bonded oligomeric species prior to photolysis. Additionally, the experimental diffusion constant obtained both before and after photolysis is closer to that which would be expected for a dimer of two intermolecularly-bound species than the monomer, using the Stokes-Einstein equation to obtain rough hydrodynamic radii. This suggests the possibility that pure ODA in solution is diffusing as dimers in solution rather than monomers. Here, we note that the term dimer is being used to refer to species held together by either Van der Waals forces or hydrogen bonding and does not refer to covalently-bound species, such as those that may be formed

photochemically.

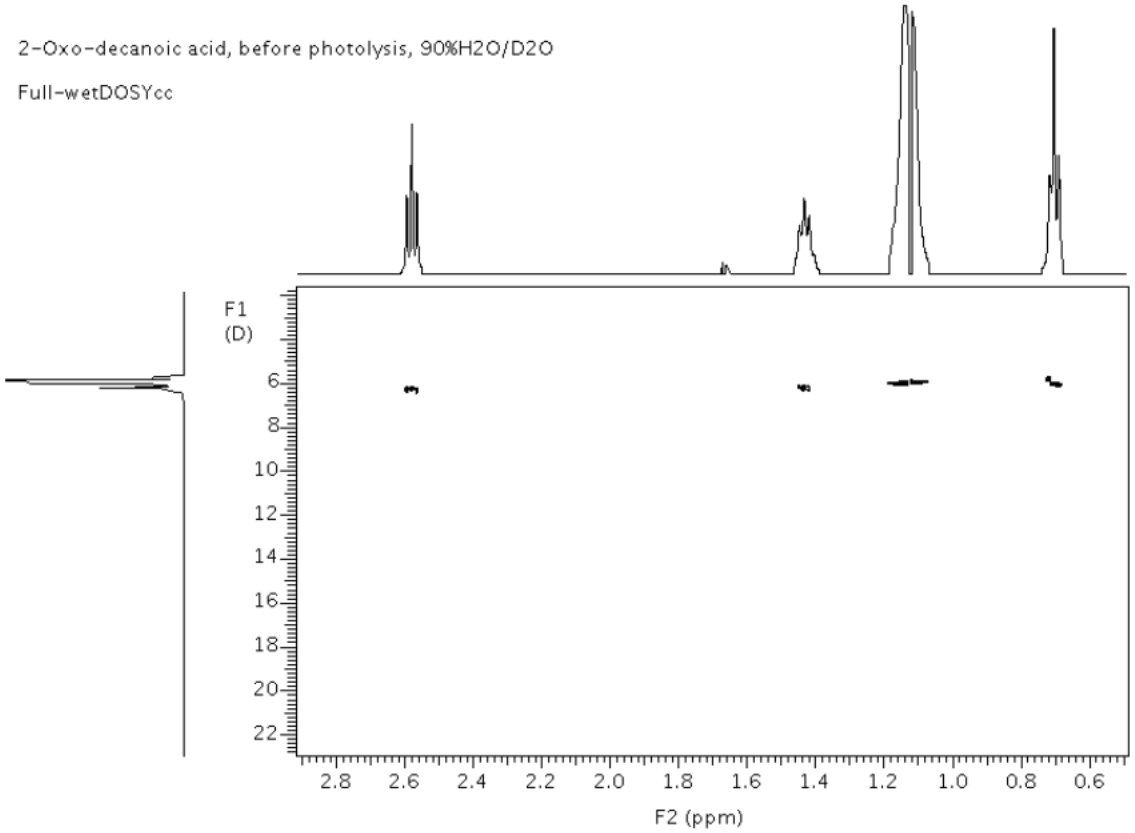

Figure A.4. DOSY NMR spectra of 3 mM ODA in aqueous solution.

This preliminary evidence suggesting that the simple, single-tailed lipid ODA is diffusing as a dimer in solution at 3 mM concentration is a highly intriguing in light of the questions about the phase behavior of fatty acids, similar simple, single-tailed lipids. The open questions surrounding the phase behavior of fatty acids are explored in more detail in Chapter 12, but, in general, there appears to be a gap between the reported monomeric solubility of a fatty acid and the reported critical aggregation concentrations.[3-5] It is possible that fatty acids form similar dimers or small clusters to those observed for ODA in solutions within this intermediate concentration regime. DOSY NMR is a unique tool to explore this possibility as it is equipped to examine the diffusion of low concentrations of small aggregates in a way that most bulk analysis techniques, such as light scattering or microscopy, cannot.

I suggest a future study to examine this possibility via a series of DOSY NMR experiments for fatty acids, such as decanoic acid and the smaller, more soluble hexanoic acid. By exploring the diffusion behavior of these fatty acids across a range of concentrations and solution pH, we aim to fill in critical information about the phase diagram governing the behavior of these species in water. It will be necessary to span a concentration regime that begins with very dilute solutions in order to attempt to observe a region where the diffusion of the monomer in solution is favored, allowing us to then understand where the cross-over to dimers and small clusters occurs. The behavior of this system under slightly higher concentrations will also be interesting, particularly to determine whether larger clusters are formed as concentration is increased in a smooth fashion, or, if there is an abrupt change to larger aggregates from the monomers or dimers in solution. By spanning a range of pH values, we can begin to understand the phase behavior of the fatty acids as the protonation state of the head group changes. The protonation state of the head group is known to play a key role in determining the favored structure of larger aggregates for fatty acids at higher concentrations, so it seems reasonable that it would also be an important factor governing smaller-scale interactions between molecules.

Experimentally, care will need to be taken to ensure that the viscosity and other solution parameters are held constant across experiments as the changes we hope to observed in the diffusion constants of these species are small and could easily be confounded by small changes in solution conditions. Similarly, it may be necessary to conduct all experiments in the presence of relatively high concentrations of salt to ensure that changes in ionic strength between conditions are minimized. Such changes could, again, mask the true diffusion behavior of fatty acids in solution. Analysis of the very low concentrations required to access any potential diffusion of monomeric species will also be

likely somewhat experimentally-challenging as long acquisition periods will be required to obtain strong enough signal above the noise threshold.

The DOSY NMR experiments proposed here will require strict attention to detail to ensure that confounding variables are minimized in order to ensure any observed changes are truly due to differences in the clustering behavior of fatty acids. Despite these challenges, these experiments have the potential to provide key information on the behavior of fatty acids in dilute solution; information that currently does not exist in the literature. The phase behavior observed for these species in the low concentration regime will help provide understanding about the fundamental molecular interactions that govern the larger aggregates observed in the higher concentration regime.

A.1 Bibliography:

1. Griffith, E. C.; Carpenter, B. K.; Shoemaker, R. K.; Vaida, V. Photochemistry of aqueous pyruvic acid. *Proc. Natl. Acad. Sci.* **2013,** *110*, 11714-11719.

2. Griffith, E. C.; Rapf, R. J.; Shoemaker, R. K.; Carpenter, B. K.; Vaida, V. Photoinitiated synthesis of self-assembled vesicles. *J. Am. Chem. Soc.* **2014,** *136*, 3784-3787.

3. Eggenberger, D.; Broome, F.; Ralston, A.; Harwood, H. The solubilities of the normal saturated fatty acids in water. *J. Org. Chem.* **1949,** *14*, 1108-1110.

4. Cape, J. L.; Monnard, P.-A.; Boncella, J. M. Prebiotically relevant mixed fatty acid vesicles support anionic solute encapsulation and photochemically catalyzed trans-membrane charge transport. *Chem. Sci.* **2011,** *2*, 661-671.

5. Maurer, S. E.; Nguyen, G. Prebiotic vesicle formation and the necessity of salts. *Origins Life Evol. Biosphere* **2016,** *46*, 215-222.

Appendix B: Additional Aggregate Characterization Methods

As described in Chapters 5, 9, and 10, a number of techniques were used for aggregate characterization, primarily dynamic light scattering (DLS) and DOSY NMR, as well as both optical and electron microscopy. Additional methods of characterization were also used, mainly with an eye towards the determination if the aggregates were lamellar in nature are described briefly below. The results from these techniques were inconclusive, likely because as revealed by the TEM images in Chapter 10, the aggregates formed are unlikely to, in fact, be vesicles.

Traditional methods of synthesizing vesicles[1] rely on dissolving the lipid of interest in a volatile solvent, forming a thin film of the lipid in a round bottom flask through rotary evaporation, and then re-suspending the lipid in the desired aqueous solution through sonication or vortexing. Fatty acid vesicles may also be formed directly by addition to the aqueous solution without the need for a thin lipid film. These vesicles are then often extruded through a membrane of a given pore size to ensure monodispersity.

For characterization, hydrophilic dye is often included in the aqueous solution used to make vesicles, and this dye is encapsulated within the vesicles. Following separation of the encapsulated dye from the free dye by using a size exclusion column, optical microscopy or fluorescence spectroscopy can be used to image the vesicles or obtain information about the permeability of the membrane.[1, 2] Encapsulation of dye is generally thought to be a sufficient requirement for the characterization of a system of aggregates as vesicles.

For obvious reasons, this method of encapsulation is not readily translated to the alkyl α-keto acid system, as it is not possible to introduce dye to the pre-photolysis solutions. Therefore, a number of attempts were made to disrupt the photochemically formed aggregates, introduce dye, and then allow the aggregates to reform. Working in

collaboration with Dr. Sheref Mansy and Laura Martini both in Trento, Italy, and in Boulder, I attempted to disrupt the aggregates both by sonication and by evaporation to form a thin film followed by resuspension. Following sonication, the solution was somewhat less turbid, but dye was never successfully encapsulated. Similarly, attempts to make a thin lipid film were unsuccessful, and it appeared as though visible "bumps" of aggregates were formed on the bottom of the round bottom flask rather than a thin film. This is in part because it was very difficult to then re-suspend the system once it had been dried. Several solvents were used, including in mixtures, but material still remained insoluble. The best success was had using water and heating to ~90 °C.

It is known that mixed systems of vesicles composed of more than one fatty acid are often more stable and less permeable than those composed of a single fatty acid,[3-5] therefore, we introduced decanoic acid to the system at 30 mM and attempted dye encapsulation. This was promising, and we were able to encapsulate dye, but it seems reasonable, in light of the discussion in Chapter 12, that this may have simply been due to the formation of decanoic acid vesicles without much contribution from the photochemically-synthesized lipids. It is possible that if photolysis of the α-keto acids was conducted in the presence of a fatty acid under the solution conditions required to make fatty acid vesicles, a mixed systems would be formed, including the covalently-bonded cross-product from reaction between the two species (Chapter 8).

Our system is notable for its temporal stability, with aggregates remaining in solution on the order of years. This led to the assumption that the aggregates formed must be soluble, rather than a simple colloidal suspension. Separation of the aggregates from the solution was attempted by centrifugation, and while UV-vis spectra showed slightly less scattering in the centrifuged sample suggesting some phase separation, the effect was small and somewhat inconclusive. It is possible that centrifugation at a higher speed may be more

effective.

In collaboration with Dr. Rob Walker and Christine Gobrogge at Montana State University, we also used differential scanning calorimetry (DSC) to attempt to understand the thermodynamics of the self-assembly of the aggregates. DSC can be used to monitor the stability of lipid bilayers.[6-8] By heating lipid vesicles in the DSC, it is possible to measure the phase transition enthalpy in bilayers, for example from a lamellar gel phase to a ripple intermediate phase and to a lamellar liquid crystalline phase.[7] DSC can be used to obtain detailed information about the nature and structure of a membrane.[9] For instance, vesicles composed of mixed surfactants show some differences in melting behavior,[6] as do vesicles that have been aged or sonicated to introduce polydispersity and membrane defects.[9] However, initial DSC measurements of the post-photolysis solutions of α-keto aicds did not show any phase transitions and were inconclusive. While it is possible more refinement of the experimental technique could yield more definitive results, it certainly seems possible that the aggregates formed photochemically are not "melting" in the DSC, as the colloidal structures formed are more stable than would be expected for a lamellar system.

B.1 Bibliography:

1. Bianco, C. D.; Torino, D.; Mansy, S. S. Vesicle stability and dynamics: An undergraduate biochemistry laboratory. *J. Chem. Educ.* **2014,** *91*, 1228-1231.

2. Cape, J. L.; Monnard, P.-A.; Boncella, J. M. Prebiotically relevant mixed fatty acid vesicles support anionic solute encapsulation and photochemically catalyzed trans-membrane charge transport. *Chem. Sci.* **2011,** *2*, 661-671.

3. Monnard, P. A.; Apel, C. L.; Kanavarioti, A.; Deamer, D. W. Influence of ionic inorganic solutes on self-assembly and polymerization processes related to early forms of life: Implications for a prebiotic aqueous medium. *Astrobio.* **2002,** *2*, 139-152.

4. Budin, I.; Prywes, N.; Zhang, N.; Szostak, Jack W. Chain-length heterogeneity allows for the assembly of fatty acid vesicles in dilute solutions. *Biophys. J.* **2014,** *107*, 1582-1590.

5. Morigaki, K.; Walde, P. Fatty acid vesicles. *Curr. Opin. Colloid Interface Sci.* **2007,** *12*, 75-80.

6. Alves, I. D.; Correia, I.; Jiao, C. Y.; Sachon, E.; Sagan, S.; Lavielle, S.; Tollin, G.; Chassaing, G. The interaction of cell-penetrating peptides with lipid model systems and subsequent lipid reorganization: Thermodynamic and structural characterization. *J. Pept. Sci.* **2009,** *15*, 200-209.

7. Caffrey, M.; Fanger, G.; Magin, R. L.; Zhang, J. Kinetics of the premelting (l-beta-p-beta) and main transition (p-beta-l-alpha) in hydrated dipalmitoylphosphatidylcholine - a time resolved x-ray diffraction study using microwave-induced temperature jumps. *Biophys. J.* **1990,** *58*, 677-686.

8. Fernandez, D. I.; Sani, M.-A.; Gehman, J. D.; Hahm, K.-S.; Separovic, F. Interactions of a synthetic leu-lys-rich antimicrobial peptide with phospholipid bilayers. *Eur. Biophys. J. Biophy. 40*, 471-480.

9. Brito, R. O.; Marques, E. F. Neat DODAB vesicles: Effect of sonication time on the phase transition thermodynamic parameters and its relation with incomplete chain freezing. *Chem. Phys. Lipids* **2005,** *137*, 18-28.

Appendix C: Toward the Identification of Possible Impurities in Fatty Acids and Alcohols

As mentioned in Chapter 8, there has been recent interest in the literature about the heretofore unknown photochemistry of fatty acids that invokes the presence of a surface-enhanced triplet state at ~270 nm to account for its apparent reactivity.[1, 2] We show in Chapter 8 that it is plausible that this absorbance is due, at least in part, to the presence of an impurity instead. This naturally raises the question of what is the identity of such an impurity. We suggest that it is possible that this impurity may be due to complexes of acetamide with the fatty acid or fatty alcohol.

Acetamide, CH_3CONH_2 (structure given in Figure C.1), forms molecular complexes with fatty acids.[3-6] These complexes have been used historically to help facilitate the purification of fatty acids through recrystallization.[7] It is unknown whether the modern day industrial processes use this same method of purification for fatty acids and fatty alcohols. Sigma-Aldrich declined to reveal whether acetamide was used in the preparation of the compounds purchased from them, as their large (confidential) industrial suppliers of these compounds consider their methods of production to be proprietary. Nevertheless, it seems possible that this molecule is used.

Free acetamide in solution has a UV absorption maximum at about ~200 nm[8, 9] however, this absorption is known to shift significantly to the red when it is complexed with inorganic acids in solution, in some cases to a $\lambda_{max} > 310$ nm.[9] It is conceivable, then, that a shift to an absorption maximum of ~270 nm could occur when a complex between acetamide and organic species is formed. Acetamide is known to react photochemically in aqueous solution[10-12] and generates free radicals by the scission of the C-C bond.[11]

Acetamide (≥99.0%, Sigma-Aldrich) was added to pure, distilled hexanoic acid, and the

mixture was heated to ~50 °C for ~1 hours to induce the formation of complexes. The UV-vis absorption spectra of 20 mM aqueous solutions of this mixture were then compared to 20 mM solutions of pure hexanoic acid (Figure C.1). There appears to be a small increase in the absorbance at 270 nm for solutions composed of hexanoic acid that was incubated with acetamide.

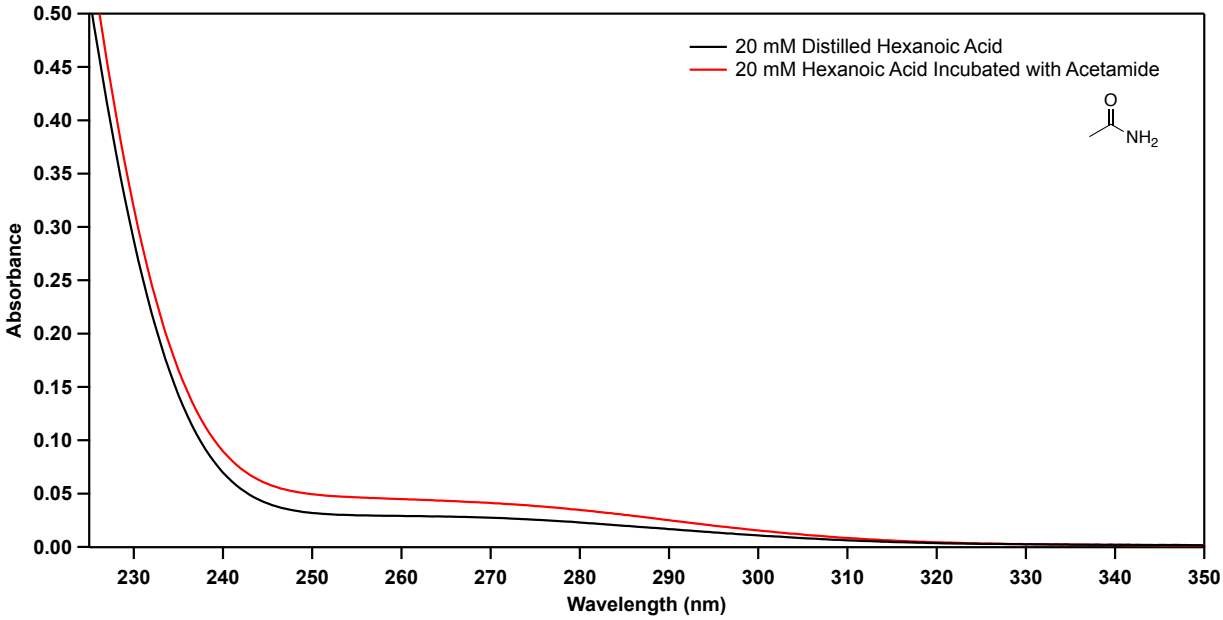

Figure C.1. UV-vis absorption spectra of 20 mM aqueous solutions of pure hexanoic acid (black) and hexanoic acid that has been incubated with acetamide.

While preliminary and largely circumstantial, the data presented here are suggestive that acetamide is a potential contaminant in solutions of fatty acids that is responsible for the absorption observed at ~270 nm and may serve as a photo-initiator. NMR studies of the fatty acids and alcohols that have been incubated with acetamide, in addition to elemental analysis, may be able to either confirm or reject this speculative assignment more definitively.

C.1 Bibliography:

1. Chiu, R.; Tinel, L.; Gonzalez, L.; Ciuraru, R.; Bernard, F.; George, C.; Volkamer, R. UV photochemistry of carboxylic acids at the air-sea boundary: A relevant source of glyoxal and other oxygenated VOC in the marine atmosphere. *Geophys. Res. Lett.* **2017,** *44*, 1079-1087.

2. Rossignol, S.; Tinel, L.; Bianco, A.; Passananti, M.; Brigante, M.; Donaldson, D. J.; George, C. Atmospheric photochemistry at a fatty acid–coated air-water interface. *Science* **2016,** *353*, 699-702.

3. Magne, F. C.; Skau, E. L. Molecular compound formation between acetamide and long-chain saturated fatty acids. *J. Am. Chem. Soc.* **1952,** *74*, 2628-2630.

4. Magne, F. C.; Hughes, E. J.; Mod, R. R.; Skau, E. L. Binary freezing point diagrams for palmitic acid with substituted acetamides and other amides. *J. Am. Chem. Soc.* **1952,** *74*, 2793-2795.

5. Mod, R. R.; Skau, E. L.; Planck, R. W. Binary freezing-point diagrams for alpha-and beta-eleostearic acids with each other and with acetamide. *J. Am. Oil Chem. Soc.* **1953,** *30*, 368-371.

6. O'Connor, R. T.; Mod, R. R.; Murray, M. D.; Skau, E. L. The x-ray diffraction and infrared spectra of molecular compounds of acetamide and long-chain saturated fatty acids. *J. Am. Chem. Soc.* **1955,** *77*, 892-895.

7. Magne, F. C.; Mod, R. R.; Skau, E. L. Purification of long-chain saturated fatty acids by recrystallization of their molecular compounds with acetamide. *J. Am. Oil Chem. Soc.* **1957,** *34*, 127-129.

8. Weast, R. C., *Handbook of chemistry and physics*. 60th ed.; CRC Press Inc.: Boca Raton, Florida, 1979.

9. Nurakhmetov, N.; Omarova, R.; Ospanov, K. K. Compounds of acetamide and its analogs with inorganic acids: Synthesis and properties. *Russ. J. Coord. Chem.* **2002,** *28*, 272-278.

10. Volman, D. H. The photochemistry of acetamide in water solution. *J. Am. Chem. Soc.* **1941,** *63*, 2000-2002.

11. Bosco, S.; Cirillo, A.; Timmons, R. B. Photolysis of formamides and acetamides studied by electron spin resonance. *J. Am. Chem. Soc.* **1969,** *91*, 3140-3143.

12. Chen, X.-B.; Fang, W.-H.; Fang, D.-C. An ab initio study toward understanding the mechanistic photochemistry of acetamide. *J. Am. Chem. Soc.* **2003,** *125*, 9689-9698.

Appendix D: Supporting Information for Chapter 4

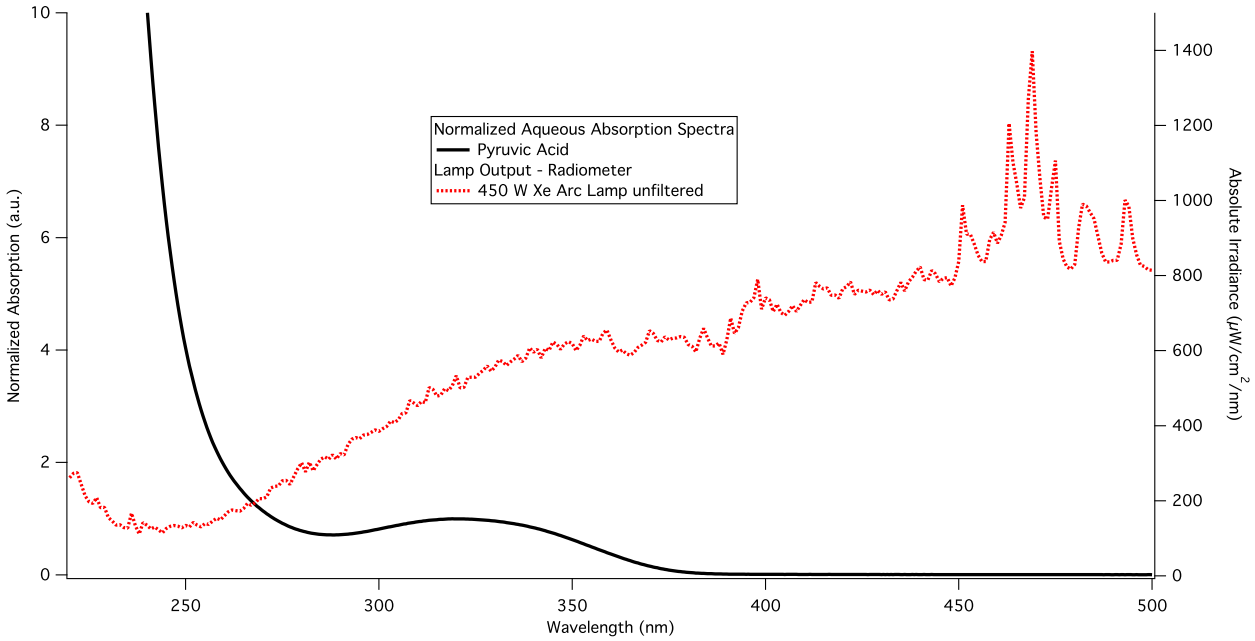

Figure D.1. Normalized aqueous absorption spectrum of pyruvic acid (black) overlaid with the spectral output of the unfiltered 450 W Xe arc lamp used for photolysis (dashed red).

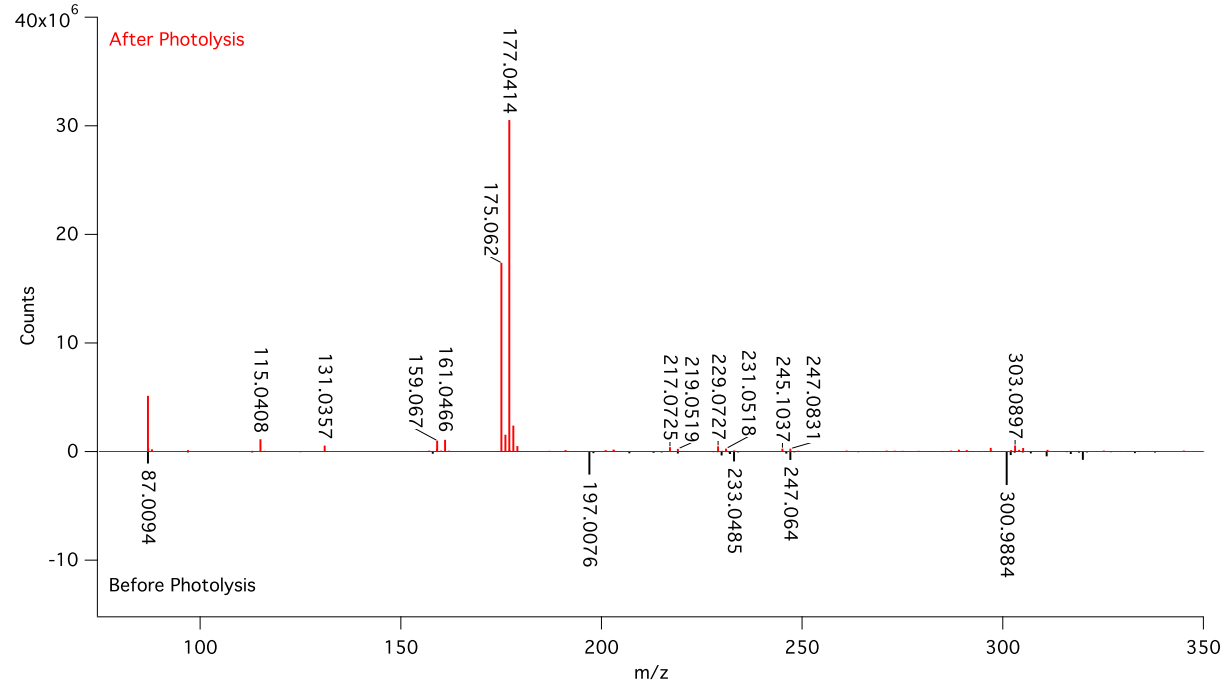

Figure D.2. Representative high resolution ESI- MS of 10 mM pyruvic acid before (black, counts multiplied by -1 for ease of presentation) and after (red) 5 hours of photolysis under N_2.

Table D1. Pyruvic Acid Photolysis Detailed ESI- MS Results

Assigned Formula [M-H]-	Assigned Structure	Avg Exp. m/z	Theor. m/z	Mass Diff. (ppm)	Exp. Nat. Abun	Avg. Nat. Abun	Pre-Photolysis	Post-Photolysis
$C_3H_3O_3$	Pyruvic Acid	87.0091 ± 0.0005	87.0082	10.8			Strong	Strong
		88.0124 ± 0.0004	88.0116	9.2	3.2%	3.8%		
$C_4H_7O_2$	Acetoin	87.0454 ± 0.0007	87.0446	8.7			Below Threshold	Medium
		88.0487 ± 0.0009	88.0480	7.8	4.3%	5.7%		
$C_3H_5O_3$	Lactic Acid	89.0239 ± 0.0003	89.0239	0.45			Below Threshold	Weak
$C_3H_5O_4$	2,2-DHPA	105.0190 ± 0.0007	105.0188	2.3			Weak	Below Threshold
$C_5H_7O_3$	Unassigned	115.0404 ± 0.0008	115.0395	8.1			Below Threshold	Medium
		116.0434 ± 0.0008	116.0429	4.6	5.4%	6.1%		
$C_5H_7O_4$	Acetolactic Acid	131.0354 ± 0.001	131.0345	6.6			Below Threshold	Medium
		132.0383 ± 0.0008	132.0378	3.7	5.4%	6.4%		
$C_6H_7O_5$	Unassigned	159.0300 ± 0.001	159.0294	3.5			Below Threshold	Medium
		160.0335 ± 0.0008	160.0327	5.1	6.5%	7.8%		
$C_7H_{11}O_4$	Unassigned	159.0666 ± 0.0007	159.0658	5.0			Below Threshold	Medium
		160.0695 ± 0.0007	160.0691	2.3	7.6%	8.9%		
$C_6H_9O_6$	Unassigned	161.0457 ± 0.001	161.0450	4.3			Below Threshold	Medium
		162.0487 ± 0.001	162.0484	2.1	6.5%	8.0%		
$C_6H_7O_6$	Parapyruvic Acid*	175.0243 ± 0.0004	175.0243	0.21			Weak	Below Threshold
$C_7H_{11}O_5$	DMOHA	175.0617 ± 0.0006	175.0607	5.5			Below Threshold	Strong
		176.0650 ± 0.0006	176.0640	5.5	7.6%	8.5%		
$C_6H_9O_6$	Dimethyl-tartaric Acid	177.0409 ± 0.0005	177.0400	5.0			Below Threshold	Strong
		178.0443 ± 0.001	178.0433	5.7	6.5%	7.6%		
$C_6H_6O_6Na$	Na Adduct of 2 PA-	197.0072 ± 0.0004	197.0062	5.2			Strong	Weak
		198.0102 ± 0.0005	198.0096	2.8	6.5%	7.3%		
Unidentified		217.0724 ± 0.0006					Below Threshold	Medium

		218.0757 ± 0.001				10.4%		
$C_8H_{11}O_7$	CDMOHA	219.0512 ± 0.0009	219.0505	3.2			Below Threshold	Medium
		220.0546 ± 0.0006	220.0539	3.3	8.7%	9.7%		
$C_{10}H_{13}O_6$	Unassigned	229.0717 ± 0.001	229.0713	1.7			Below Threshold	Medium
		230.0754 ± 0.001	230.0746	3.4	10.8%	11.7%		
$C_9H_{11}O_7$	Unassigned	231.0511 ± 0.001	231.0505	2.7			Below Threshold	Medium
		232.0544 ± 0.0008	232.0539	2.1	9.7%	11.5%		
$C_{10}H_{15}O_6$	Unassigned	231.0874 ± 0.0007	231.0869	2.3			Below Threshold	Medium
		232.0909 ± 0.002	232.0903	2.6	10.8%	11.5%		
Unidentified		233.0474 ± 0.0007					Medium for 10 mM PA, B.T. at low conc	Below Threshold
		234.0513 ± 0.0008				8.6%		
Unidentified		247.0635 ± 0.0005					Medium for 10 mM PA, B.T. at low conc	Below Threshold
		248.0684 ± 0.0009				11.1%		
$C_{10}H_{14}O_8Na$	Na Adduct of 2 Acetolactates	285.0597 ± 0.0007	285.0587	3.6			Below Threshold	Medium
		286.0622 ± 0.0009	286.0620	0.82	10.8%	11.8%		
$C_9H_{12}O_9Na$	Na Adduct of PA- and DMTA-	287.0391 ± 0.0006	287.0380	3.8			Below Threshold	Weak
$C_9H_9O_9Ca$	Ca Adduct of 3 PA-	300.9883 ± 0.0005	300.9873	3.3			Strong	Below Threshold
		301.9918 ± 0.0005	301.9907	3.7	9.7%	10.7%		
Unidentified		303.0899 ± 0.003					Below Threshold	Medium
		304.0821 ± 0.002				25.0%		
$C_9H_9O_9Na_2$	Na Adduct of 3 PA-	307.0052 ± 0.0006	307.0043	3.1			Medium	Below Threshold
		308.0086 ± 0.001	308.0076	3.2	9.7%	10.8%		

Notes: Chemical formulas are assigned as the ionized $[M\text{-}H]^-$ species, structures are assigned as the neutral species. The experimental m/z is the observed average across experiments, and the uncertainty given is the 95% confidence interval

2,2-DHPA = 2,2-Dihydroxypropanoic Acid, diol of pyruvic acid
DMOHA = 2,4-dihydroxy-2-methyl-5-oxohexanoic acid
CDMOHA = 4-carboxy-2,4-dihydroxy 2-methyl-5-oxohexanoic acid
*The peak assigned to parapyruvic acid likely also has contributions from the closed ring form of the zymonic acid diol as well.

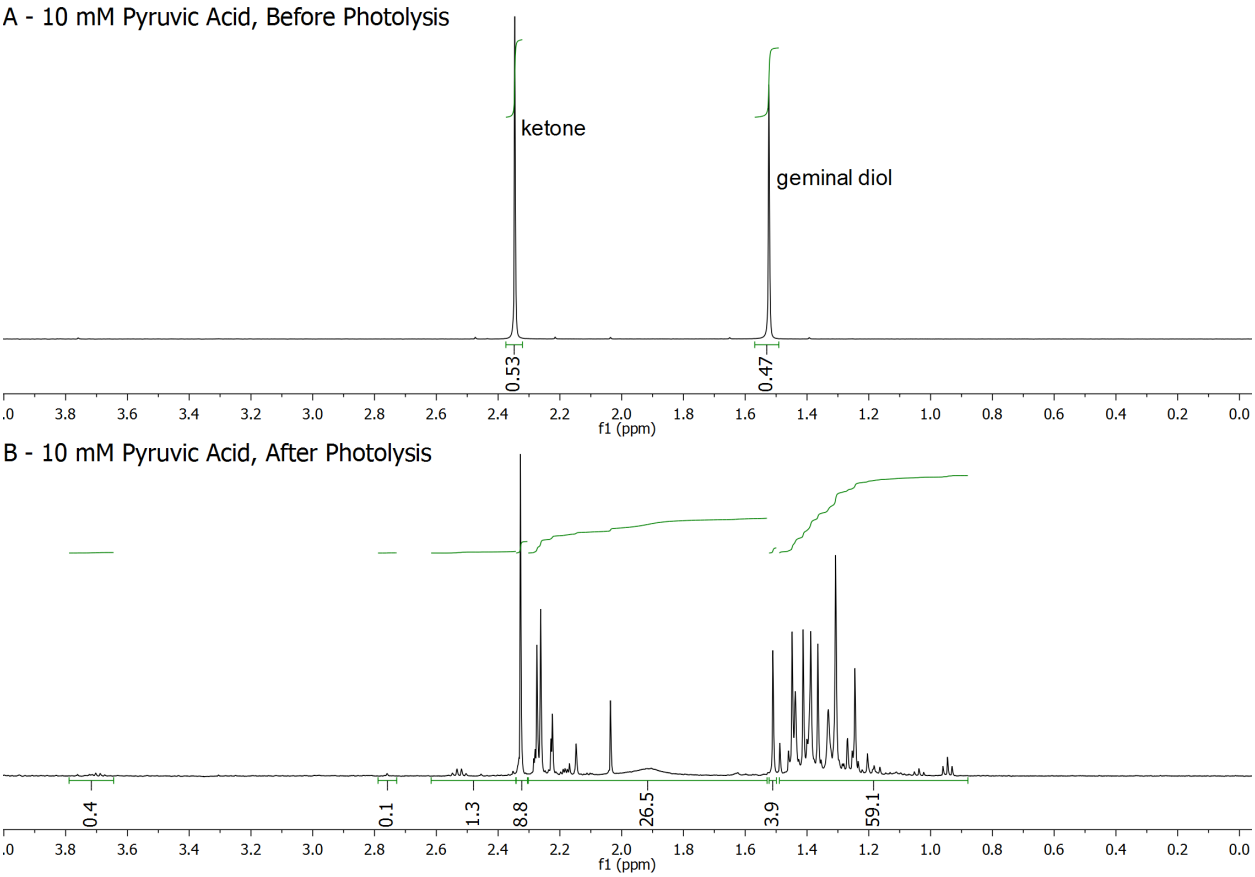

Figure D.3. [1]H NMR spectra of 10 mM pyruvic acid in aqueous solution before (A) and after (B) 5 hours of photolysis under N_2.

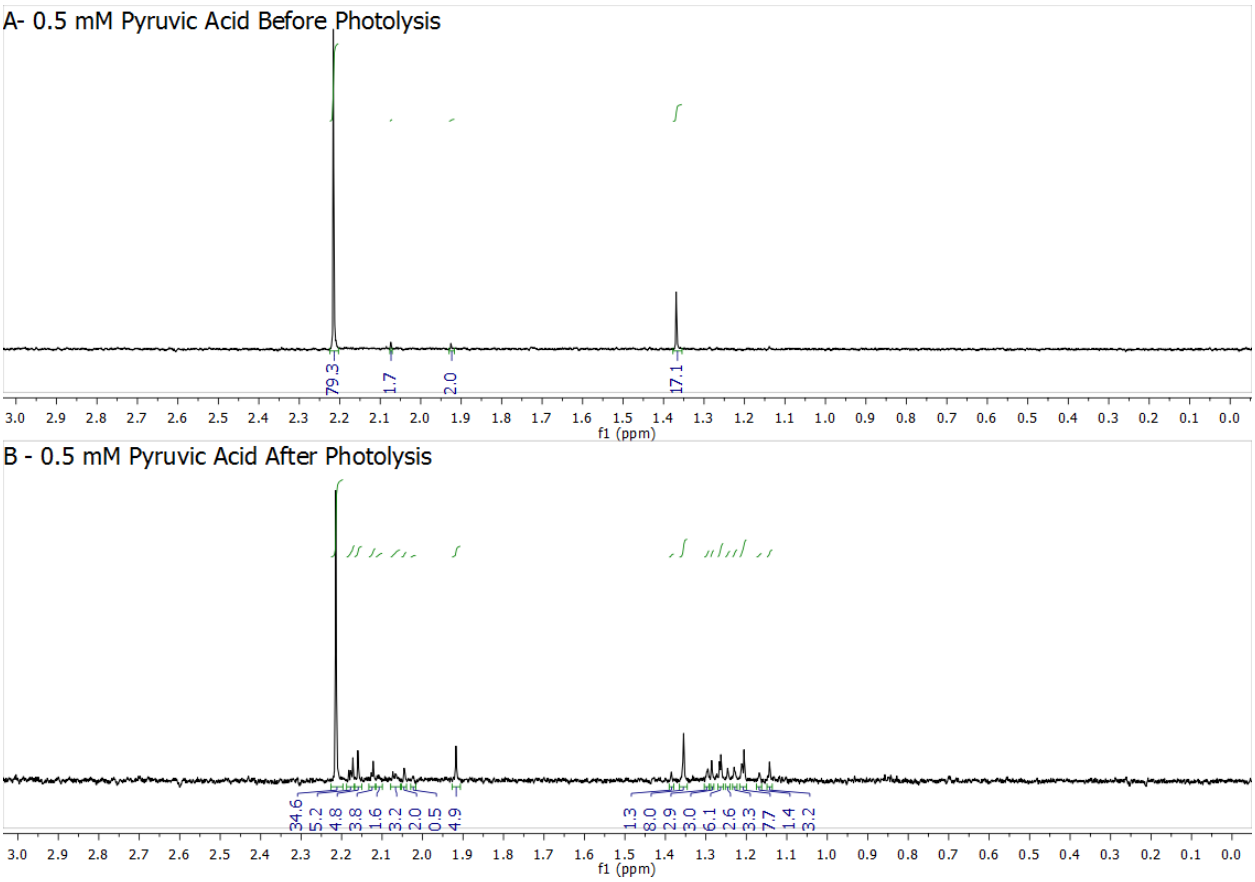

Figure D.4. [1]H NMR spectra of 0.5 mM pyruvic acid in aqueous solution before (A) and after (B) 5 hours of photolysis under N_2.

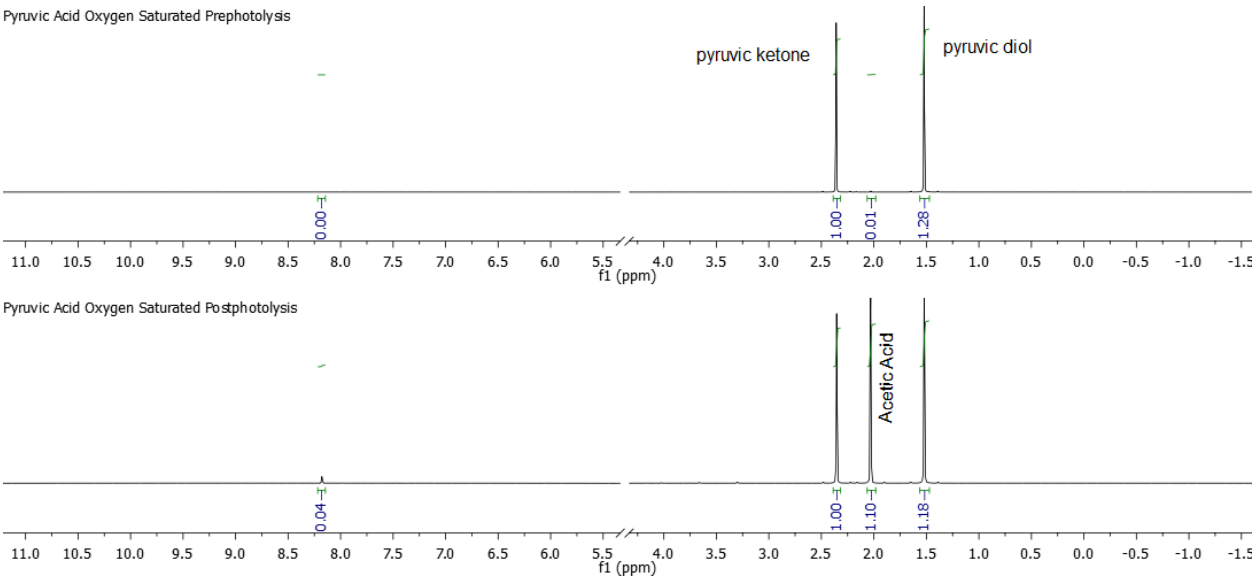

Figure D.5: [1]H NMR of 50 mM pyruvic acid bubbled O_2 through pre (A) and post (B) photolysis for 5 hours.

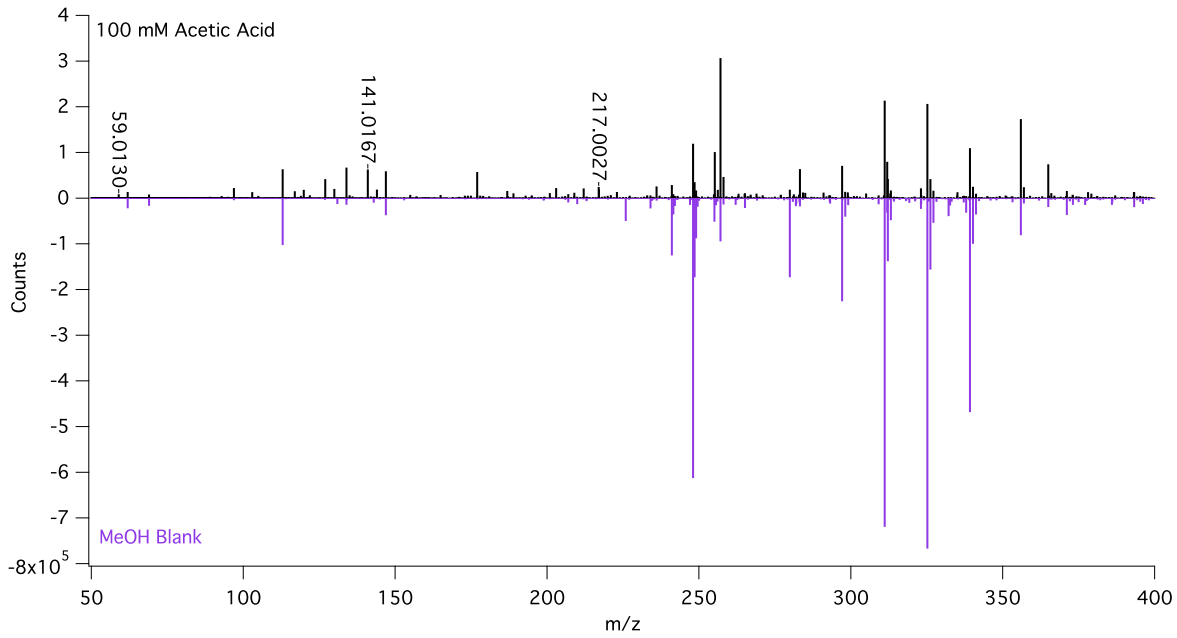

Figure D.6. ESI- MS spectrum of 100 mM acetic acid in aqueous solution (black) compared to a methanol blank spectrum (purple, counts multiplied by -1 for ease of presentation). Labeled peaks are contributions from acetic acid species: m/z of 59.0130 corresponds to acetic acid with [M-H]- of $C_2H_3O_2$, m/z of 141.0167 corresponds to an adduct of 2 AA- and Na with [M-H]- of $C_4H_6O_4Na$, and m/z of 217.0027 corresponds to an adduct of 3 AA- and Ca with [M-H]- of $C_6H_9O_6Ca$. The intensity of the [M-H]- of $C_2H_3O_2$ is 8500 counts, below the threshold for detection of 10^4 counts.

Appendix E: Supporting Information for Chapter 5

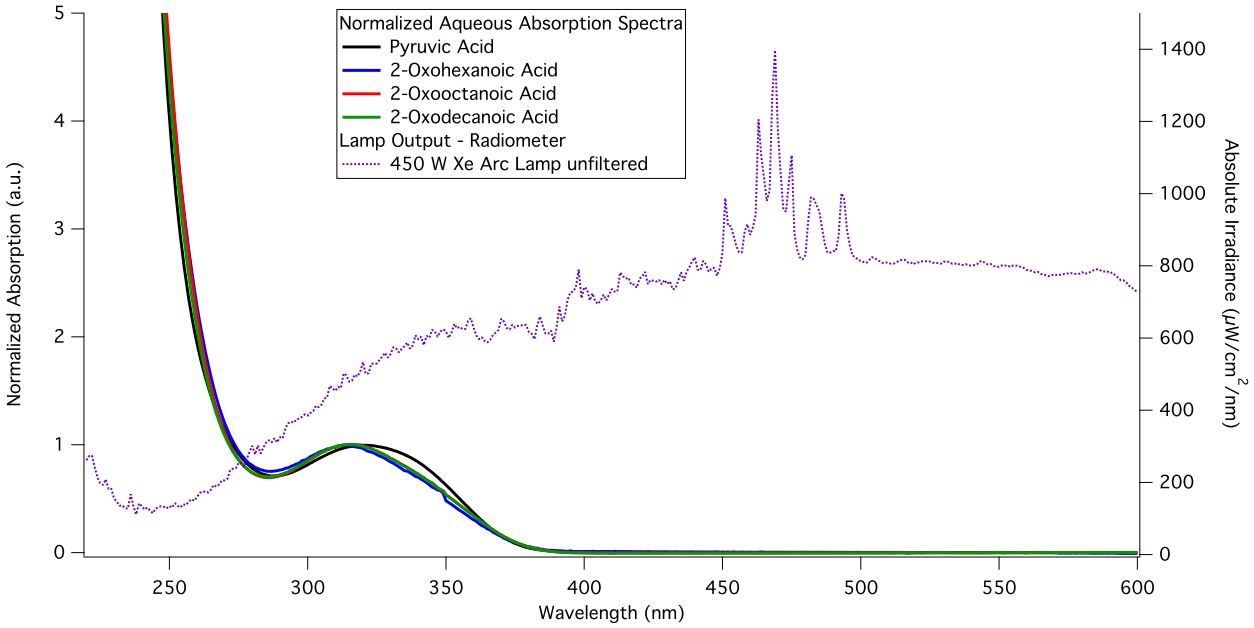

Figure E.1. Normalized UV aqueous absorption spectra for pyruvic acid (black, λ_{max} = 320 nm), 2-oxohexanoic acid (OHA, blue, λ_{max} = 313 nm), 2-oxooctanoic acid (OOA, red, λ_{max} = 315 nm), and 2-oxodecanoic acid (ODA, green, 315 nm).

The absorption maximum for the oxoacids shifts slightly to the blue as the tail length increases from the methyl group of pyruvic to the longer chained oxoacids, but there does not appear to be a further dependence of the cross-section on alkyl tail length as it continues to increase. The absorption maximum of the cross-section of 2-oxododecanoic acid (ODDA) also occurs at 315 nm, but it is not shown here because of the low solubility of ODDA in water. At concentrations needed to obtain UV-vis spectra, aggregates of ODDA form and cause scattering in the background of the spectra.

Synthesis of Alkyl Oxoacids:

Preparation of 2-Oxohexanoic Acid: A solution of the Grignard reagent, prepared from 1-bromobutane (3.01 g, 22 mmol) and the suspension of magnesium (1.07 g, 44 mmol) in THF (30 mL), was added dropwise under N_2 atmosphere to a cold (–78 °C) solution of diethyloxalate (2.92 g, 20 mmol) in THF (20 mL). After the addition was complete, the

reaction mixture was stirred at –78 °C for an additional 7 h. The reaction was quenched with 2 N HCl, the aqueous layer was extracted with ether (3 × 100 mL), and the combined organic layers were washed with saturated NaCl, dried over $MgSO_4$, and evaporated. The crude product was dissolved in acetic acid (120 mL) and HCl (37%, 30 mL). After 11 h, the reaction was concentrated directly, and the residue was purified by distillation under reduced pressure to give the pure product (1.63 g, 57%) as a colorless oil. ^{1}H NMR (300 MHz, $CDCl_3$, shown in SI Figure 2) δ 7.63 (s, 1H), 2.98 (t, *J* = 7.3 Hz, 2H), 1.87 – 1.53 (m, 2H), 1.53 – 1.27 (m, 2H), 0.96 (t, *J* = 7.3 Hz, 3H); ^{13}C NMR (75 MHz, $CDCl_3$) δ 195.6, 161.4, 99.2, 37.7, 24.8, 21.9, 13.5; HRMS (ESI): calcd. for $C_6H_9O_3^-$: 129.0552. Found 129.0549.

Preparation of 2-Oxodecanoic Acid: A solution of the Grignard reagent, prepared from the solution of 1-bromoctane (5.26 g, 27.2 mmol) in THF (8 mL) and the suspension of magnesium (1.32 g, 54.5 mmol) in THF (20 mL), was added dropwise under N_2 atmosphere to a cold (–78 °C) solution of diethyloxalate (3.72 g, 24.7 mmol) in THF (34 mL). After the addition was complete, the reaction mixture was stirred at –78 °C for an additional 1.3 h. The reaction was quenched with 2 N HCl, the aqueous layer was extracted with ether (3 × 150 mL), and the combined organic layers were washed with saturated NaCl, dried over $MgSO_4$, and evaporated. The crude product was dissolved in acetic acid (36 mL) and HCl (37%, 9.4 mL). After 16 h, most of the solvent of reaction was removed. The concentrated solution was diluted with water (80 mL) and diethyl ether (100 mL). The organic layer was washed with water (80 mL), saturated NaCl (80 mL), and dried over $MgSO_4$, and concentrated. The residue was recrystallized in hexanes to give the pure product (2.59 g, 51%) as white solid; ^{1}H NMR (300 MHz, $CDCl_3$, shown in SI Figure 3) δ 9.54 (s, 1H), 2.94 (t, *J* = 7.3 Hz, 2H), 1.67 (p, *J* = 7.3 Hz, 2H), 1.60 – 1.18 (m, 10H), 1.09 – 0.72 (m, 3H). ^{13}C NMR (75 MHz, $CDCl_3$) δ 195.7, 160.2, 37.5, 31.7, 29.2, 29.0, 28.9, 23.0, 22.6, 14.0; HRMS (ESI): calcd. for $C_{10}H_{17}O_3^-$: 185.1178. Found 185.1179.

Preparation of 2-Oxododecanoic Acid: A solution of the Grignard reagent, prepared from the solution of 1-bromodecane (6.02 g, 27.2 mmol) in THF (8 mL) and the suspension of magnesium (1.32 g, 54.5 mmol) in THF (40 mL), was added dropwise under N_2 atmosphere to a cold (–78 °C) solution of diethyloxalate (1.46 g, 10 mmol) in THF (34 mL). After the addition was complete, the reaction mixture was stirred at –78 °C for an additional 2.5 h. The reaction was diluted with hexanes (100 mL), and quenched with 2 N HCl. The aqueous layer was extracted with hexanes (2 × 100 mL), and the combined organic layers were washed with H_2O (100 mL), saturated NaCl (100 mL), dried over $MgSO_4$, and evaporated. The crude product was dissolved in HOAc (150 mL) and HCl (37%, 39 mL). After 16 h, most of the solvent of reaction was removed. The concentrated solution was diluted with water (80 mL) and diethyl ether (80 mL). The organic layer was extracted with diethyl ether (2 × 80 mL), and the combined organic layers were washed with water (80 mL), saturated NaCl (80 mL), and dried over $MgSO_4$, and concentrated. The residue was recrystallized in hexanes to give the pure product (0.673 g, 12%) as white solid. ^{1}H NMR (300 MHz, $CDCl_3$, shown in SI Figure 4) δ 8.47 (s, 1H), 2.96 (t, J = 7.3 Hz, 2H), 1.68 (p, J = 7.4 Hz, 2H), 1.30 (d, J = 12.4 Hz, 14H), 1.01 – 0.77 (m, 3H); ^{13}C NMR (75 MHz, $CDCl_3$) δ 195.9, 159.5, 37.3, 31.9, 29.5, 29.4, 29.3, 29.2, 28.9, 23.1, 22.7, 14.1; HRMS (ESI): calcd. for $C_{12}H_{21}O_3^-$: 213.1491. Found 213.1488.

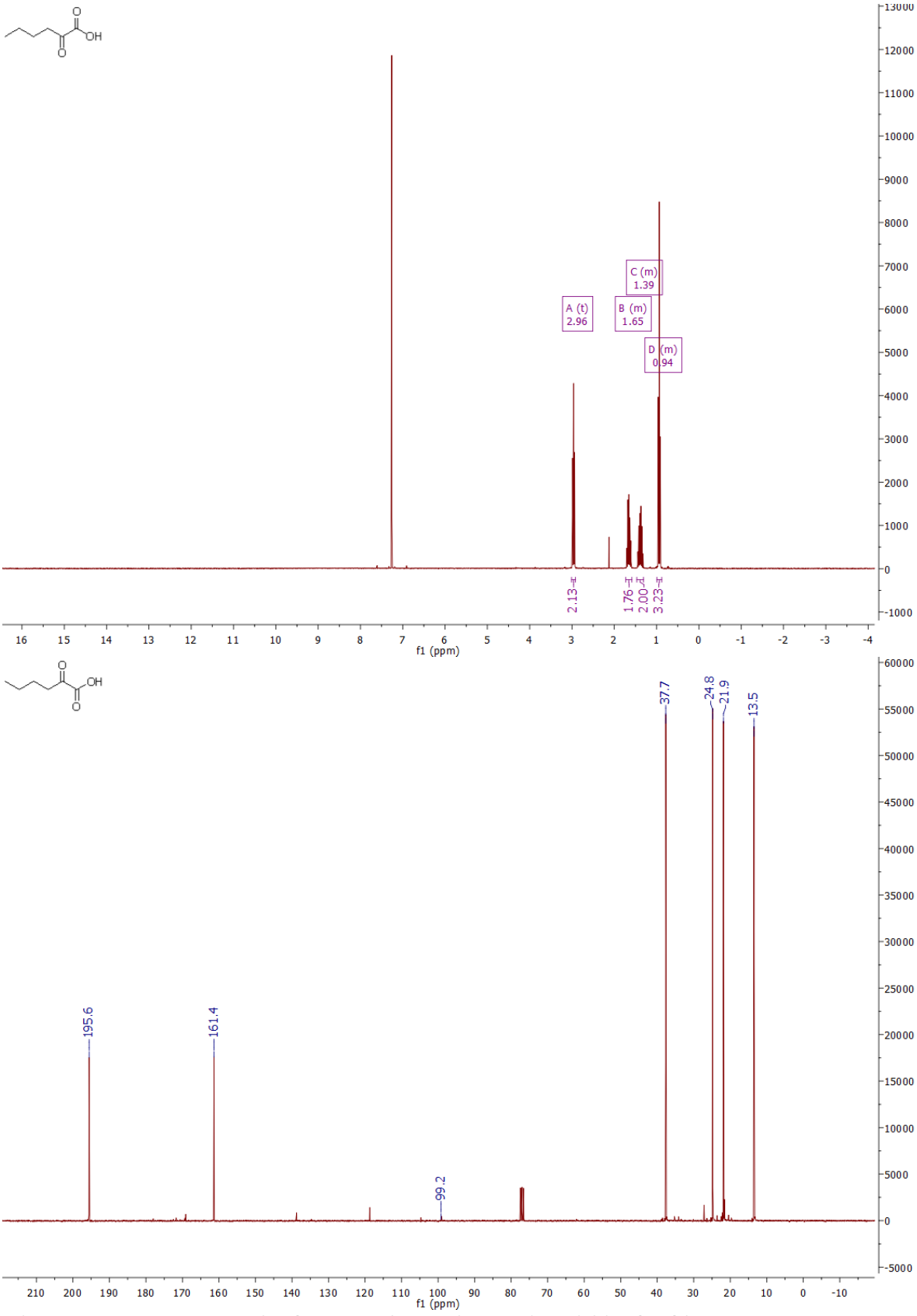

Figure E.2. [1]H NMR and [13]C NMR of 2-oxohexanoic acid in $CDCl_3$.

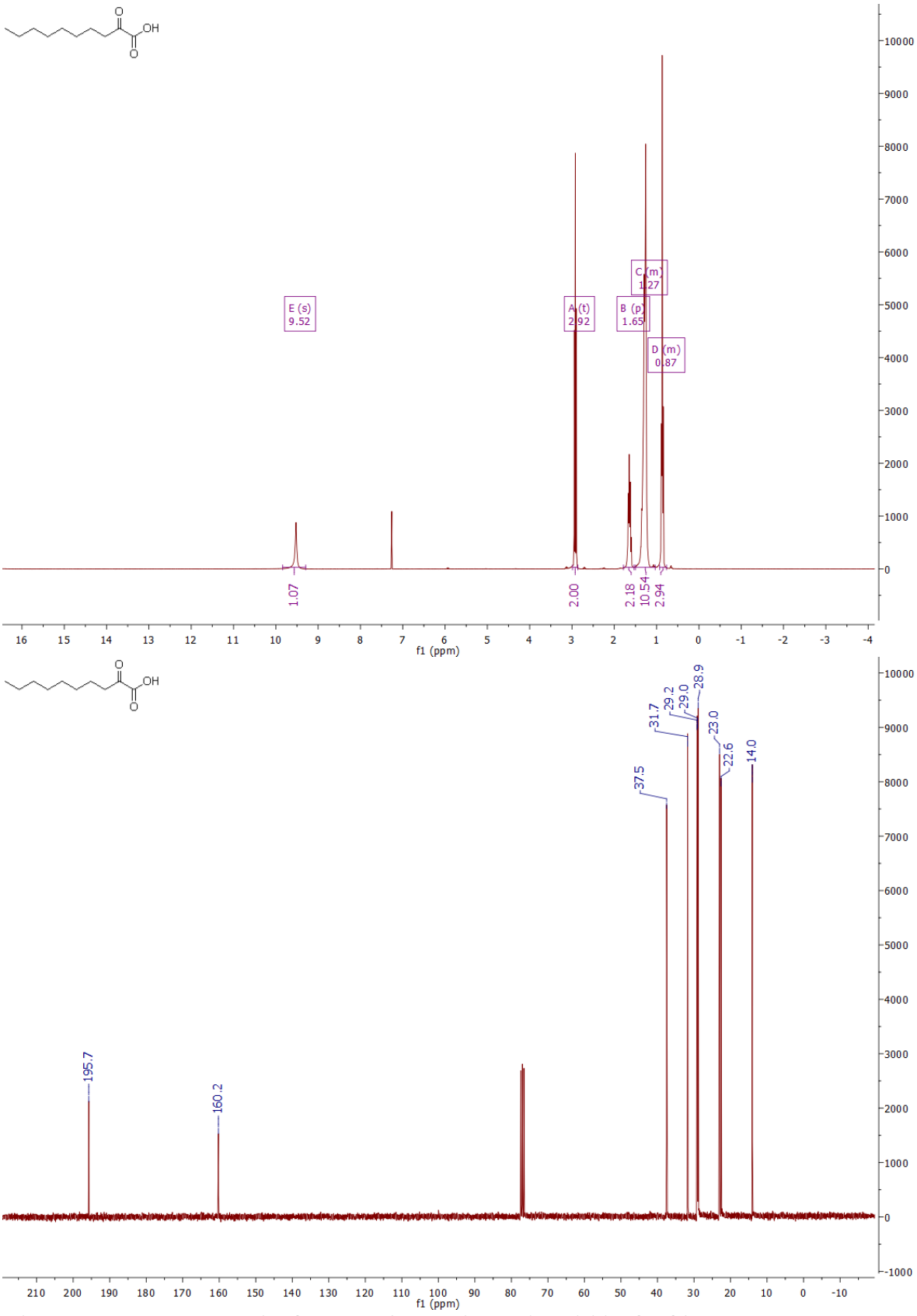

Figure E.3. [1]H NMR and [13]C NMR of 2-oxodecanoic acid in $CDCl_3$.

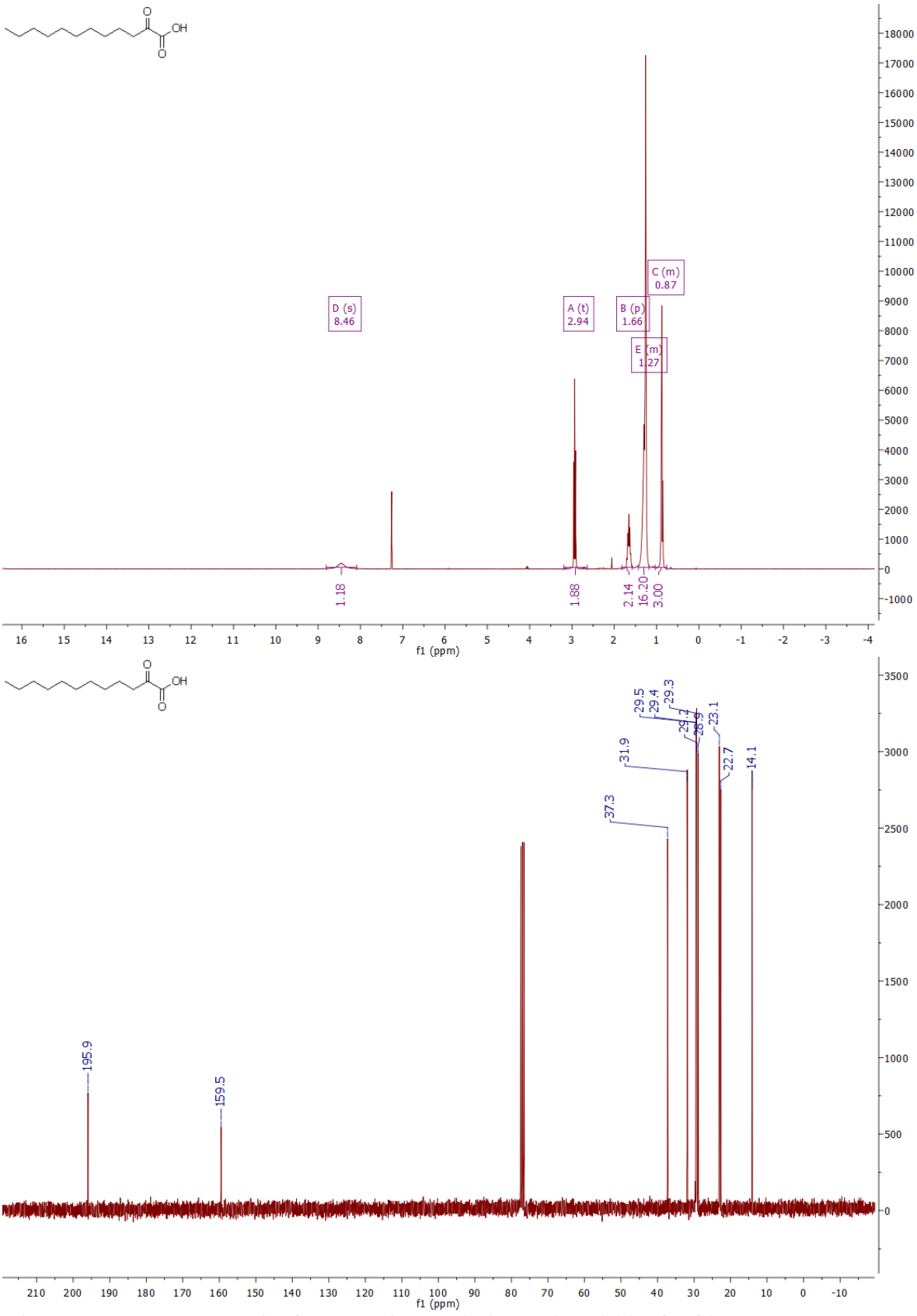

Figure E.4. ^{1}H NMR and ^{13}C NMR of 2-oxododecanoic acid in $CDCl_3$.

Table E.1. OOA Photolysis Detailed ESI-MS Results

Assigned Formula [M-H]-	Assigned Structure	Avg Exp. m/z	Theor. m/z	Mass Diff. (ppm)	Exp. Nat. Abun	Avg. Nat. Abun	Pre-Photolysis	Post-Photolysis
$C_3H_3O_3$	Pyruvic Acid	87.0092 ± 0.0006	87.0082	10.9			Below Threshold	Weak
$C_7H_{13}O_2$	Heptanoic Acid	129.0926 ± 0.0004	129.0916	8.2			Medium	Medium
		130.0961 ± 0.0004	130.0949	9.2	7.6%	8.1%		
$C_8H_{11}O_2$	Unassigned	139.0773 ± 0.0006	139.0759	9.6			Below Threshold	Medium
		140.0806 ± 0.0005	140.0793	9.6	8.7%	9.2%		
$C_8H_{13}O_3$	2-Oxooctanoic Acid	157.0880 ± 0.0005	157.0865	9.6			Strong	Strong
		158.0911 ± 0.0004	158.0899	8.1	8.7%	10.3%		
$C_9H_{17}O_2$	Nonanoic Acid	157.1248 ± 0.0005	157.1229	12.3			Weak	Weak
$C_8H_{13}O_4$	2,2-DHOA	173.0826 ± 0.0004	173.0814	7.0			Medium	Medium
		174.0861 ± 0.0004	174.0848	7.8	8.6%	9.3%		
$C_7H_{11}O_5$	DMOHA	175.0620 ± 0.001	175.0607	7.5			Below Threshold	Weak
$C_6H_9O_6$	Dimethyl-tartaric Acid	177.0411 ± 0.0005	177.0400	6.6			Below Threshold	Weak
$C_{14}H_{27}O_2$	8-hydroxy-tetradecan-7-one	227.2020 ± 0.0006	227.2011	3.9			Below Threshold	Weak
$C_{11}H_{17}O_6$	R-PPA	245.1034 ± 0.0007	245.1026	3.4			Below Threshold	Medium
		246.1067 ± 0.002	246.1059	3.1	11.9%	12.3%		
$C_{12}H_{21}O_5$	R-DHO Acid	245.1400 ± 0.0005	245.1389	4.4			Below Threshold	Medium
		246.1435 ± 0.0005	246.1423	4.9	13.0%	14.7%		
$C_{11}H_{19}O_6$	Methylhexyl-tartaric Acid	247.1193 ± 0.0005	247.1182	4.6			Below Threshold	Strong
		248.1231 ± 0.0005	248.1216	6.3	11.9%	12.9%		
$C_{15}H_{27}O_3$	Unassigned	255.1968 ± 0.0005	255.1960	2.8			Below Threshold	Medium
		256.2001 ± 0.0009	256.1994	2.9	16.2%	17.6%		
Unidentified		269.1763 ± 0.0004					Below Threshold	Medium
		270.1796 ± 0.0004				17.9%		

$C_{15}H_{27}O_4$	8-C-8-H-tetradecan-7-one	271.1919 ± 0.0006	271.1910	3.4			Below Threshold	Medium
		272.1950 ± 0.0007	272.1943	2.5	16.2%	16.7%		
$C_{15}H_{29}O_4$	Unassigned	273.2071 ± 0.0007	273.2066	2.0			Below Threshold	Weak
		274.2107 ± 0.0007	274.2100	2.5	16.2%	16.7%		
$C_{13}H_{28}O_5Na$*	Unassigned	287.1852 ± 0.002	287.1835	6.0			Below Threshold	Medium
		288.1905 ± 0.001	288.1868	12.7	14.1%	16.4%		
$C_{13}H_{21}O_7$	R-DHO Diacid	289.1301 ± 0.001	289.1288	4.7			Below Threshold	Medium
		290.1333 ± 0.001	290.1321	4.1	14.1%	14.9%		
$C_{16}H_{25}O_6$	R,R-DODA	313.1659 ± 0.0004	313.1652	2.4			Medium	Medium
		314.1692 ± 0.0005	314.1865	2.1	17.3%	18.2%		
$C_{16}H_{28}O_6$	R,R-PPA	315.1791 ± 0.001	315.1808	-5.3			Medium	Medium
		316.1831 ± 0.001	316.1842	-3.2	17.3%	17.7%		
$C_{17}H_{31}O_5$	R,R-DHO Acid	315.2181 ± 0.0006	315.2172	3.0			Below Threshold	Strong
		316.2213 ± 0.0003	316.2205	2.2	18.0%	19.6%		
$C_{16}H_{29}O_6$	Dihexyl-tartaric Acid	317.1973 ± 0.0005	317.1965	2.8			Below Threshold	Strong
		318.2009 ± 0.0004	318.1998	3.4	17.3%	19.1%		
$C_{16}H_{26}O_6Na$	Na Adduct of 2 OOA-	337.1634 ± 0.0004	337.1627	1.9			Strong	Medium
		338.1665 ± 0.0003	338.1661	1.2	17.3%	19.3%		
$C_{16}H_{26}O_7Na$	Na Adduct of OOA- and OOA Diol-	353.1571 ± 0.001	353.1577	-1.5			Medium	Medium
		354.1610 ± 0.0007	354.1610	-0.1	17.3%	18.1%		
$C_{18}H_{27}O_7$*	Unassigned	355.1736 ± 0.0006	355.1757	-6.0			Medium	Weak
		356.1770 ± 0.0006	356.1791	-5.8	19.5%	18.6%		
$C_{18}H_{31}O_7$	R,R-DHO Diacid	359.2071 ± 0.0007	359.2070	0.3			Below Threshold	Medium
		360.2108 ± 0.0005	360.2104	1.0	19.5%	20.2%		
$C_{22}H_{41}O_5$	R,R,R-DHO Acid	385.2958 ± 0.0003	385.2954	0.8			Below Threshold	Medium

		386.2994 ± 0.0004	386.2988	1.5	23.8%	24.8%		
$C_{23}H_{41}O_7$	R,R,R-DHO Diacid	429.2855 ± 0.0008	429.2860	-1.2			Below Threshold	Weak
$C_{26}H_{41}O_9$	Unassigned	497.2723 ± 0.0007	497.2751	-5.6			Below Threshold	Medium
		498.2762 ± 0.0007	498.2785	-4.5	28.1%	28.9%		
$C_{24}H_{39}O_9Ca$	Ca Adduct of 3 OOA-	511.2224 ± 0.0003	511.2221	0.8			Medium	Medium
		512.2255 ± 0.0004	512.2254	0.2	26.0%	27.8%		
$C_{24}H_{39}O_9Na_2$	Na Adduct of 3 OOA-	517.2388 ± 0.0005	517.2390	-0.4			Medium	Below Threshold
		518.2424 ± 0.0005	518.2424	0.2	26.0%	27.1%		

NOTES:
*Tentative chemical formula assignment.
2,2-DHOA = 2,2-Dihydroxyoctanoic Acid, Diol of OOA
DMOHA = 2,4-dihydroxy-2-methyl-5-oxohexanoic acid
8-C-8-H-tetradecan-7-one = 8-carboxy-8-hydroxy-tetradecan-7-one

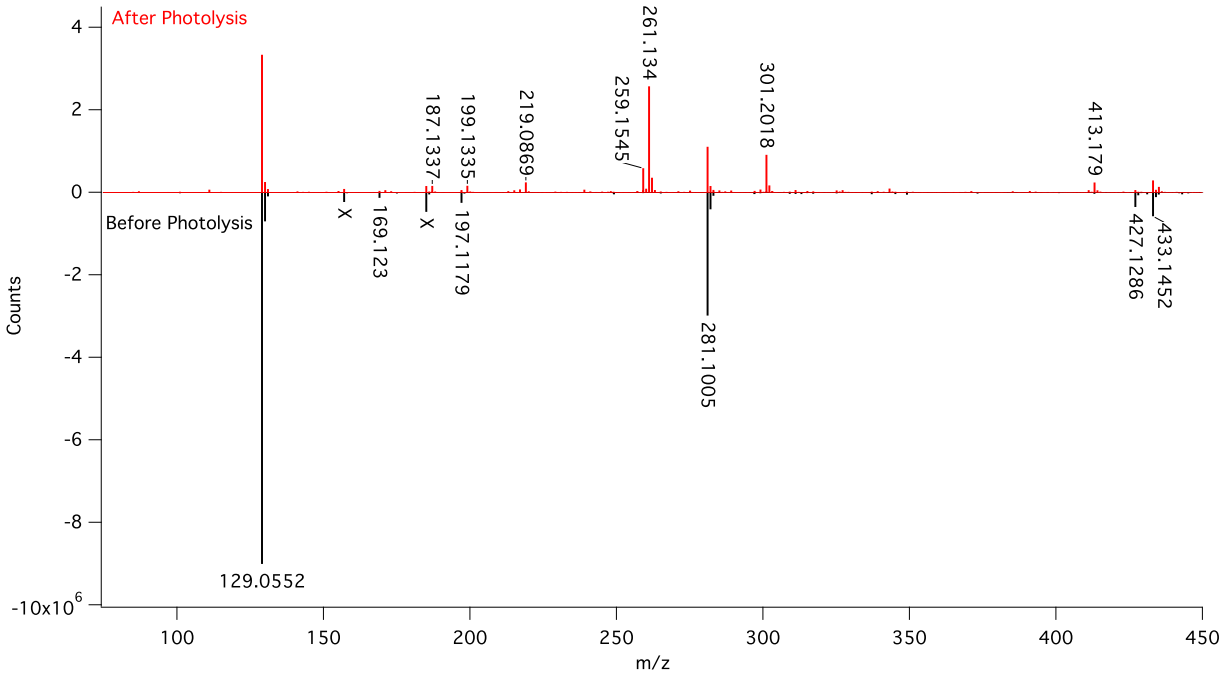

Figure E5. Representative high resolution ESI- MS of 1 mM OHA before (black, counts multiplied by -1 for ease of presentation) and after (red) 5 hours of photolysis under N_2. Peaks marked with an X are due to carry-over material from a previous sample and are not normally observed.

Table E.2. OHA Photolysis Detailed ESI-MS Results

Assigned Formula [M-H]-	Assigned Structure	Avg Exp. m/z	Theor. m/z	Mass Diff. (ppm)	Exp. Nat. Abun	Avg. Nat. Abun	Pre-Photolysis	Post-Photolysis
$C_3H_3O_3$	Pyruvic Acid	87.0080	87.0082	-3.3			Below Threshold	Weak
$C_5H_9O_2$	Pentanoic Acid	101.0601	101.0602	-1.9			Weak	Weak
$C_6H_9O_3$	2-Oxohexanoic Acid	129.0550	129.0552	-1.5			Strong	Strong
		130.0586	130.0586	0.4	6.5%	7.7%		
$C_9H_{17}O$	Unassigned	141.1278	141.1280	-1.1			Medium	Medium
		142.1311	142.1313	-1.5	9.7%	10.0%		
$C_6H_{11}O_4$	2,2-Dihydroxy hexanoic Acid (OHA Diol)	147.0655	147.0658	-2.1			Weak	Weak
$C_{10}H_{17}O_2$	Unassigned	169.1229	169.1229	-0.1			Medium	Weak
		170.1260	170.1262	-1.4	10.8%	11.4%		
$C_7H_{11}O_5$	DMOHA	175.0603	175.0607	-2.2			Below Threshold	Weak
$C_6H_9O_6$	Dimethyl-tartaric Acid	177.0398	177.0400	-0.8			Below Threshold	Weak
$C_{10}H_{19}O_3$	Unassigned	187.1336	187.1334	1.0			Below Threshold	Medium
		188.1370	188.1368	1.1	10.8%	11.1%		
$C_{11}H_{17}O_3$	Unassigned	197.1178	197.1178	0.2			Medium	Medium
		198.1215	198.1212	1.5	11.9%	12.9%		
$C_{11}H_{19}O_3$	Unassigned	199.1328	199.1334	-3.2			Below Threshold	Medium
		200.1366	200.1368	-1.0	11.9%	11.9%		
$C_{11}H_{19}O_4$	6-C-6-H-decan-5-one	215.1281	215.1284	-1.2			Below Threshold	Weak
$C_9H_{13}O_6$	R-PPA	217.0708	217.0713	-2.1			Below Threshold	Weak
$C_{10}H_{17}O_5$	R-DHO Acid	217.1077	217.1076	0.3			Below Threshold	Medium
		218.1108	218.1110	-0.9	10.8%	11.4%		
$C_9H_{15}O_6$	Methylbutyl-tartaric Acid	219.0868	219.0869	-0.5			Below Threshold	Medium
		220.0900	220.0903	-1.4	9.7%	10.4%		
$C_{12}H_{19}O_5$	Unassigned	243.1231	243.1233	-0.9			Medium	Medium

		244.1267	244.1266	0.2	13.0%	13.7%		
$C_{12}H_{17}O_6$	R,R-DODA	257.1025	257.1026	-0.1			Below Threshold	Weak
$C_{12}H_{19}O_6$	R,R-PPA	259.1175	259.1182	-2.9			Weak	Medium
		260.1200	260.1216	-6.0	13.0%	13.9%		
$C_{13}H_{23}O_5$	R,R-DHO Acid	259.1542	259.1546	-1.5			Below Threshold	Medium
		260.1581	260.1579	2.3	13.0%	15.1%		
$C_{12}H_{21}O_6$	Dibutyltartaric Acid	261.1339	261.1339	0.0			Below Threshold	Strong
		262.1370	262.1372	-0.8	13.0%	13.9%		
$C_{12}H_{18}O_6Na$	Na Adduct of 2 OHA-	281.1003	281.1001	0.4			Strong	Strong
		282.1037	282.1035	0.7	13.0%	14.1%		
$C_{16}H_{29}O_5$	R,R,R-DHO Acid	301.2017	301.2015	0.6			Below Threshold	Medium
		302.2048	302.2049	0.3	17.3%	18.7%		
$C_{14}H_{23}O_7$	R,R-DHO Diacid	303.1447	303.1444	0.8			Below Threshold	Medium
		304.1476	304.1478	0.6	15.1%	15.8%		
$C_{17}H_{30}O_7$	R,R,R-DHO Diacid	345.1909	345.1914	-1.4			Below Threshold	Medium
		346.1945	346.1947	-0.7	18.4%	18.8%		
$C_{18}H_{30}O_9Na$	Unassigned	413.1791	413.1788	0.7			Below Threshold	Medium
		414.1817	414.1822	-1.2	19.5%	20.3%		
$C_{18}H_{27}O_9Ca$	Ca Adduct of 3 OHA-	427.1281	427.1282	-0.1			Medium	Weak
		428.1311	428.1315	-0.9	19.5%	22.3%		
$C_{18}H_{27}O_9Na_2$	Na Adduct of 3 OHA-	433.1449	433.1451	-0.5			Medium	Weak
		434.1483	434.1485	-0.3	19.5%	20.8%		

NOTES:
DMOHA = 2,4-dihydroxy-2-methyl-5-oxohexanoic acid
6-C-6-H-decan-5-one = 6-carboxy-6-Hydroxy-decan-5-one

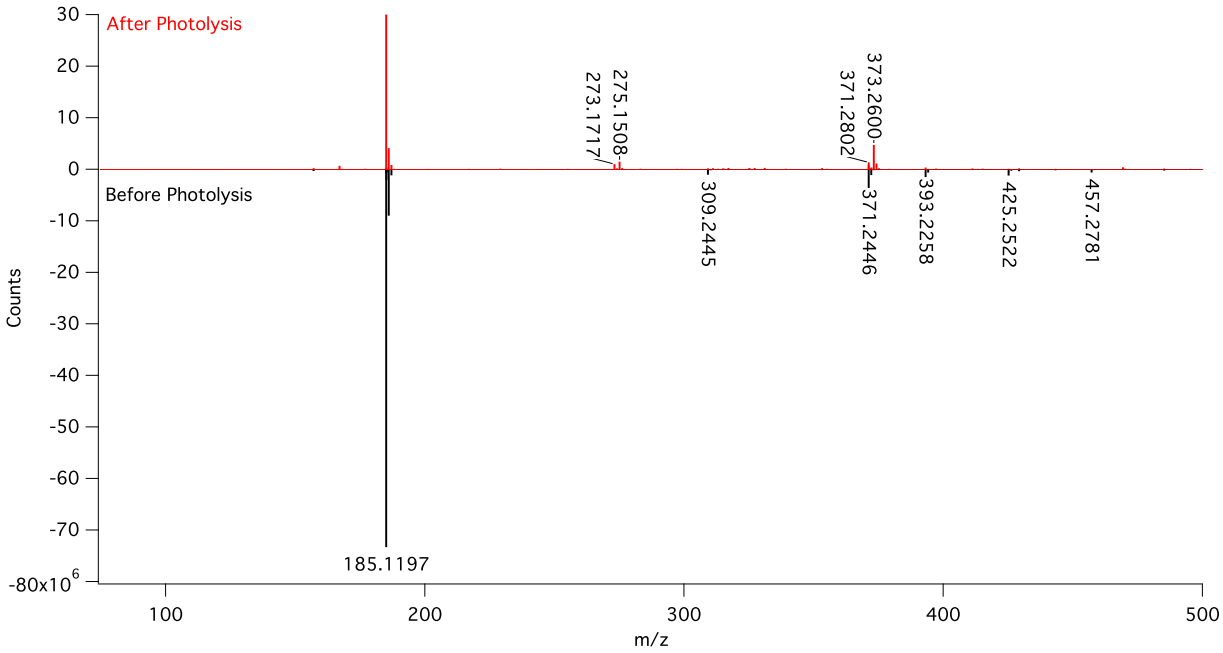

Figure E.6. Representative high resolution ESI- MS of 3 mM ODA before (black, counts multiplied by -1 for ease of presentation) and after (red) 5 hours of photolysis under N_2.

Table E.3. ODA Photolysis Detailed ESI-MS Results

Assigned Formula [M-H]-	Assigned Structure	Avg Exp. m/z	Theor. m/z	Mass Diff. (ppm)	Exp. Nat. Abun	Avg. Nat. Abun	Pre-Photolysis	Post-Photolysis
$C_3H_3O_3$	Pyruvic Acid	87.0086 ± 0.0009	87.0082	3.9			Below Threshold	Weak
$C_9H_{17}O_2$	Nonanoic Acid	157.1238 ± 0.0006	157.1229	5.6			Medium	Medium
		158.1270 ± 0.0006	158.1262	4.9	9.7%	9.6%		
$C_{10}H_{15}O_2$	Unassigned	167.1078 ± 0.0009	167.1072	3.2			Below Threshold	Medium
		168.1117 ± 0.001	168.1106	6.5	10.8%	10.9%		
$C_7H_{11}O_5$	DMOHA	175.0615 ± 0.001	175.0607	4.7			Below Threshold	Weak
$C_6H_9O_6$	Dimethyl-tartaric Acid	177.0408 ± 0.0009	177.0400	4.5			Below Threshold	Weak
$C_{10}H_{17}O_3$	2-Oxodecanoic Acid	185.1186 ± 0.0006	185.1178	4.5			Strong	Strong
		186.1218 ± 0.0006	186.1212	3.2	10.8%	12.6%		
$C_{10}H_{19}O_4$	2,2-DHDA (ODA Diol)	203.1293 ± 0.0003	203.1284	4.4			Medium	Medium
		204.1320 ± 0.0000	204.1317	1.4	10.8%	11.6%		
$C_{12}H_{21}O_4$	Unassigned	229.1445 ± 0.001	229.1440	2.1			Below Threshold	Medium

		230.1485 ± 0.001	230.1474	4.9	13.0%	13.4%		
$C_{13}H_{21}O_6$	R-PPA	273.1317 ± 0.001	273.1339	8.0			Below Threshold	Weak
$C_{14}H_{25}O_5$	R-DHO Acid	273.1708 ± 0.0009	273.1702	1.9			Below Threshold	Medium
		274.1740 ± 0.0008	274.1736	1.5	15.1%	15.8%		
$C_{13}H_{23}O_6$	MethylOctyl-Tartaric Acid	275.1500 ± 0.0008	275.1495	1.8			Below Threshold	Strong
		275.1500 ± 0.0008	276.1529	1.4	14.1%	14.8%		
$C_{19}H_{33}O_3$	Unassigned	309.2439 ± 0.0007	309.2430	2.8			Medium	Medium
		310.2470 ± 0.0006	310.2463	2.1	20.5%	21.4%		
$C_{15}H_{25}O7$	R-DHO Diacid	317.1580 ± 0.003	317.1601	-6.5			Below Threshold	Medium
		318.1620 ± 0.002	318.1634	-4.5	16.2%	18.2%		
$C_{19}H_{35}O_4$	10-C-10-H-octadecan-9-one	327.2538 ± 0.0009	327.2536	0.6			Below Threshold	Medium
		328.2570 ± 0.001	328.2569	0.3	20.5%	20.9%		
$C_{20}H_{33}O_6$	R,R-DODA	369.2270 ± 0.0008	369.2277	-2.0			Below Threshold	Weak
$C_{20}H_{37}O_7$	R,R-PPA	371.2435 ± 0.0005	371.2434	0.3			Strong	Medium
		372.2468 ± 0.0005	372.2468	0.0	21.6%	22.5%		
$C_{21}H_{39}O_5$	R,R-DHO Acid	371.2805 ± 0.001	371.27978	1.9			Below Threshold	Strong
		372.2838 ± 0.0009	372.2831	1.6	22.7%	24.2%		
$C_{20}H_{37}O_6$	Dioctyltartaric Acid	373.2595 ± 0.0006	373.2590	1.2			Below Threshold	Strong
		374.2625 ± 0.0006	374.2624	0.3	21.6%	22.7%		
$C_{20}H_{37}O_7$	ODA + ODA Diol + H	389.2540 ± 0.002	389.2540	0.1			Weak	Weak
		390.2573 ± 0.0007	390.2573	0.0	21.6%	23.6%		
$C_{20}H_{34}O_6Na$	Na Adduct of 2 ODA-	393.2256 ± 0.0004	393.2253	0.6			Strong	Medium
		394.2290 ± 0.0004	394.2287	0.8	21.6%	22.5%		
$C_{20}H_{36}O_7Na$	Na Adduct of ODA- and ODA Diol-	411.2360 ± 0.0000	411.2359	0.2			Medium	Below Threshold
		412.2397 ± 0.0007	412.2393	1.0	21.6%	23.7%		

$C_{22}H_{39}O_7$	R,R-DHO Diacid	415.2695 ± 0.0006	415.2696	-0.3			Below Threshold	Medium
		416.2733 ± 0.001	416.2730	0.8	23.8%	23.3%		
$C_{21}H_{38}O_7Na$	Unassigned	425.2518 ± 0.0004	425.2516	0.6			Medium	Below Threshold
		426.2550 ± 0.0000	426.2549	0.2	22.7%	24.0%		
$C_{22}H_{42}O_8Na$	Unassigned	457.2780 ± 0.0006	457.2778	0.5			Medium	Below Threshold
		458.2812 ± 0.0004	458.2811	0.1	23.8%	25.5%		
$C_{28}H_{53}O_5$	R,R,R-DHO Acid	469.3890 ± 0.0000	469.3893	-0.7			Below Threshold	Medium
		470.3927 ± 0.0007	470.3927	-0.05	30.3%	31.2%		
$C_{29}H_{53}O_7$	R,R,R-DHO Diacid	513.3790 ± 0.001	513.3792	-0.3			Below Threshold	Weak
$C_{30}H_{51}O_9Ca$	Ca Adduct of 3 ODA-	595.3154 ± 0.001	595.3160	-0.9			Medium	Below Threshold
		596.3187 ± 0.001	596.319	-1.1	32.4%	33.2%		
$C_{30}H_{51}O_9Na_2$	Na Adduct of 3 ODA-	601.3313 ± 0.00	601.3329	2.7			Weak	Below Threshold

NOTES:
2,2-DHDA = 2,2-Dihydroxydecanoic Acid, Diol of ODA
DMOHA = 2,4-dihydroxy-2-methyl-5-oxohexanoic acid
10-C-10-H-octadecan-9-one = 10-carboxy-10-hydroxy-octadecan-9-one

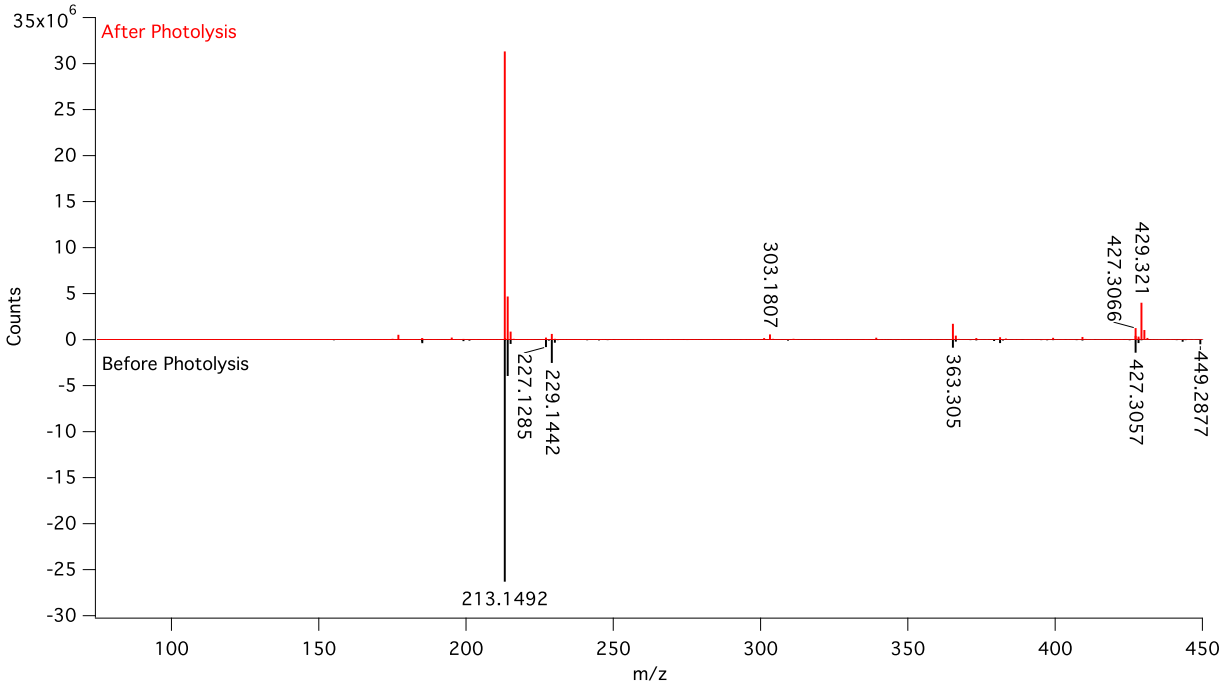

Figure E.7. Representative high resolution ESI- MS of 1 mM ODDA before (black, counts multiplied by -1 for ease of presentation) and after (red) 5 hours of photolysis under N_2.

Table E.4. ODDA Photolysis Detailed ESI-MS Results

Assigned Formula [M-H]-	Assigned Structure	Avg Exp. m/z	Theor. m/z	Mass Diff. (ppm)	Exp. Nat. Abun	Avg. Nat. Abun	Pre-Photolysis	Post-Photolysis
$C_3H_3O_3$	Pyruvic Acid	87.0089	87.0082	7.0			Below Threshold	Weak
$C_7H_{11}O_5$	DMOHA	175.0618	175.0607	6.4			Below Threshold	Weak
$C_6H_9O_6$	Dimethyl-tartaric Acid	177.0410	177.0400	5.9			Below Threshold	Medium
		178.0446	178.0433	7.0	6.5%	6.8%		
$C_{11}H_{21}O_2$	Undecanoic Acid	185.1559	185.1542	9.1			Medium	Medium
		186.1590	185.1575	7.7	11.9%	12.2%		
$C_{12}H_{19}O_2$	Unassigned	195.1399	195.1385	6.8			Below Threshold	Medium
		196.1430	196.1419	5.7	13.0%	13.2%		
$C_{11}H_{19}O_3$	Unassigned	199.1346	199.1334	5.6			Below Threshold	Medium
		200.1387	200.1368	9.2	11.9%	13.1%		
$C_{12}H_{21}O_3$	2-Oxodecanoic Acid	213.1503	213.1491	5.8			Strong	Strong
		214.1540	214.1525	7.1	13.0%	14.0%		
$C_{12}H_{19}O_4$	Unassigned	227.1295	227.1284	4.9			Medium	Medium
		228.1330	228.1317	5.7	13.0%	13.4%		
$C_{12}H_{19}O_4$	Unassigned	229.1454	229.1440	6.0			Medium	Medium
		230.1485	230.1474	4.9	13.0%	13.2%		
$C_{12}H_{23}O_4$	2,2-DHDDA (ODDA Diol)	231.1574	231.1597	-9.7			Weak	Weak
$C_{15}H_{25}O_6$	R-PPA	301.1655	301.1652	1.2			Below Threshold	Weak
$C_{16}H_{29}O_5$	R-DHO Acid	301.2025	301.2015	3.2			Below Threshold	Medium
		302.2055	302.2049	2.0	17.3%	16.5%		
$C_{15}H_{27}O_6$	Methyldecyl-tartaric Acid	303.1816	303.1808	2.6			Below Threshold	Medium
		304.1849	304.1842	2.3	16.2%	16.5%		
$C_{17}H_{29}O_7$	R-DHO Diacid	345.1915	345.1914	0.4			Below Threshold	Weak
$C_{23}H_{41}O_3$	Unassigned	365.3056	365.3056	-0.1			Strong	Strong

		366.3091	366.3090	0.4	24.9%	24.5%		
Unidentified		381.3011					Medium	Medium
		382.3046				25.15%		
$C_{23}H_{43}O_4$	12-C,12-H-docos-11-one	383.3155	382.3162	-1.7			Below Threshold	Weak
$C_{24}H_{41}O_6$	R,R-DODA	425.2908	425.2904	0.9			Weak	Weak
$C_{24}H_{43}O_6$	R,R-PPA	427.3065	427.3060	1.3			Medium	Medium
		428.3098	428.3094	0.9	26.0%	25.4%		
$C_{25}H_{47}O_5$	R,R-DHO Acid	427.3450	427.3424	6.1			Below Threshold	Medium
		428.3480	428.3457	5.3	27.0%	29.8%		
$C_{24}H_{45}O_6$	Didecyltartaric Acid	429.3213	429.3217	-0.8			Below Threshold	Strong
		430.3250	430.3250	0.0	26.0%	25.2%		
$C_{24}H_{42}O_6Na$	Na Adduct of 2 ODDA-	449.2881	449.2879	0.3			Medium	Weak
		450.2916	450.2913	0.7	26.0%	26.5%		
$C_{26}H_{47}O_7$	R,R-DHO Diacid	471.3320	471.3322	-0.5			Below Threshold	Weak
$C_{35}H_{65}O_7$	R,R,R-DHO Diacid	597.4730	597.4731	-0.1			Below Threshold	Weak

NOTES:
2,2-DHDDA = 2,2-Dihydroxydodecanoic Acid, Diol of ODDA
DMOHA = 2,4-dihydroxy-2-methyl-5-oxohexanoic acid
12-C,12-H-docos-11-one = 12-carboxy-12-hydroxy docos-11-one

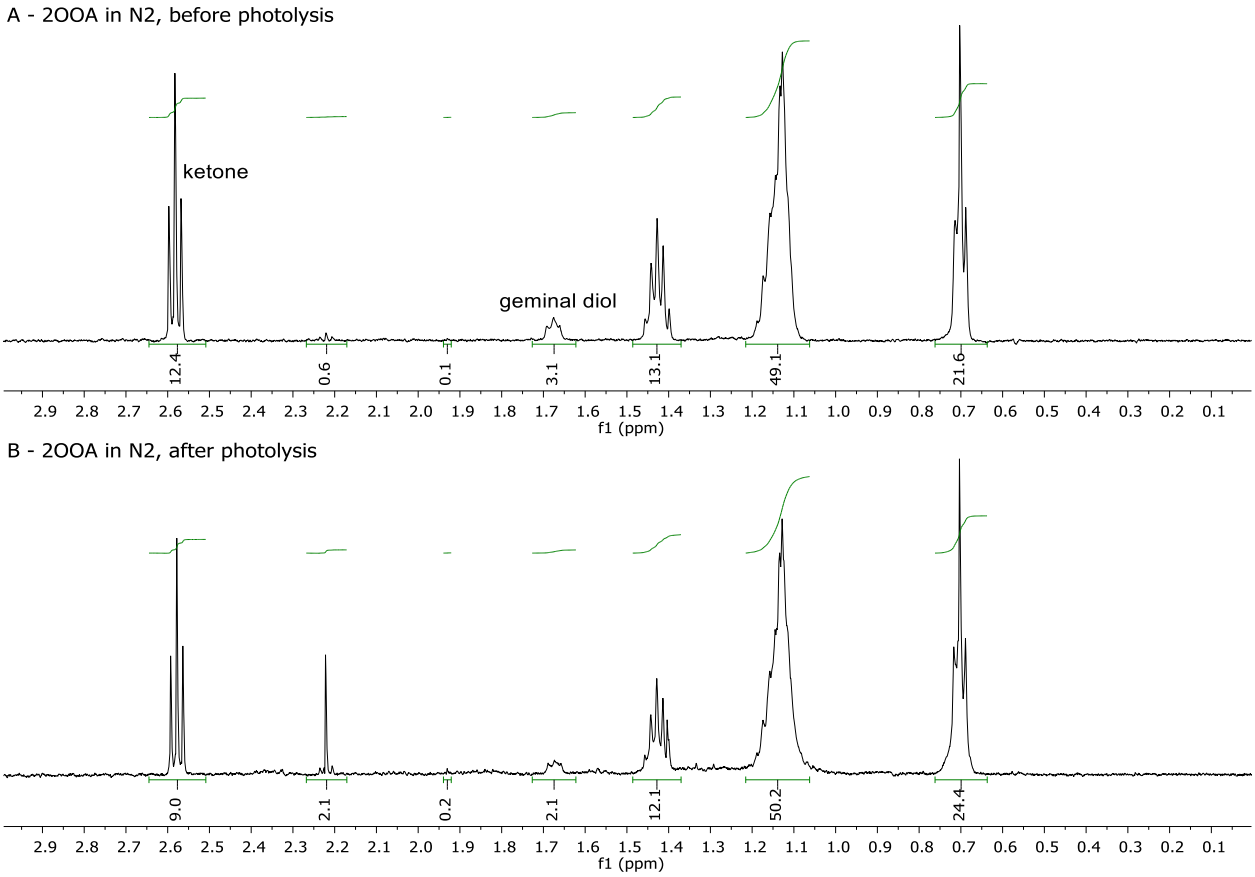

Figure E.8. NMR Spectra of 6 mM 2-oxooctanoic acid in aqueous solution before (A) and after (B) 5 hours of photolysis under N_2.

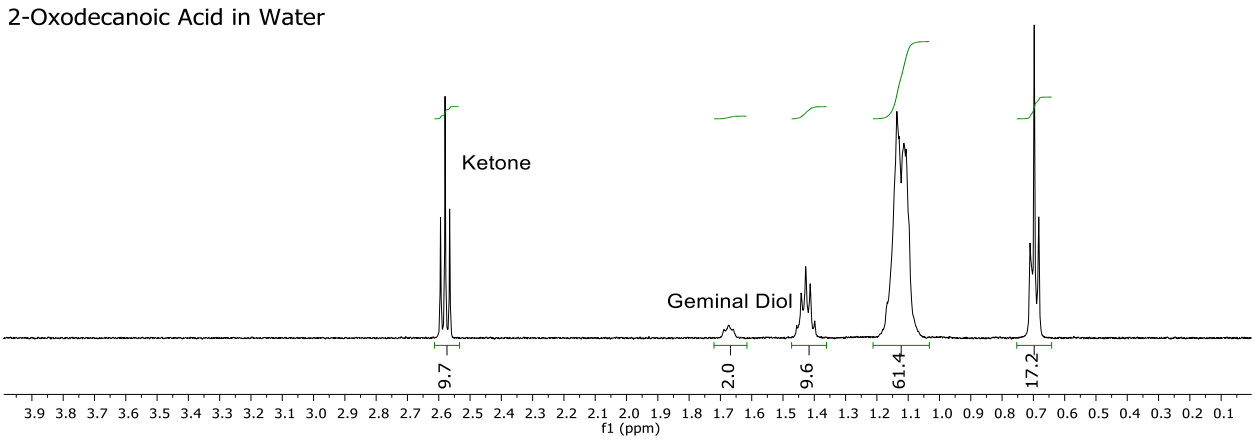

Figure E.9. NMR Spectra of 3 mM ODA in aqueous solution.

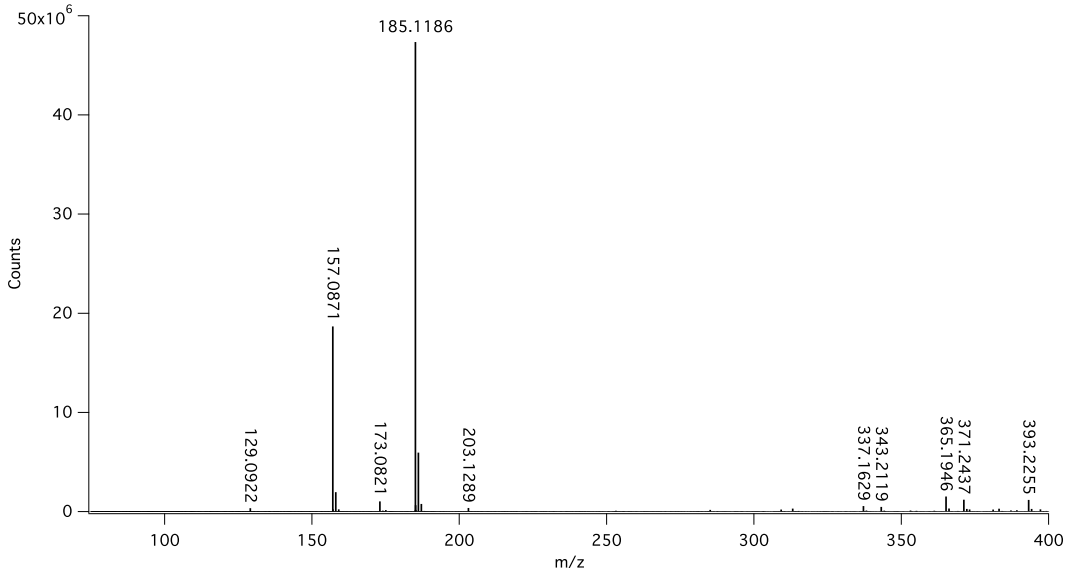

Figure E.10. Representative high resolution ESI-MS of a mixed solution of 3 mM OOA and 3 mM ODA before photolysis.

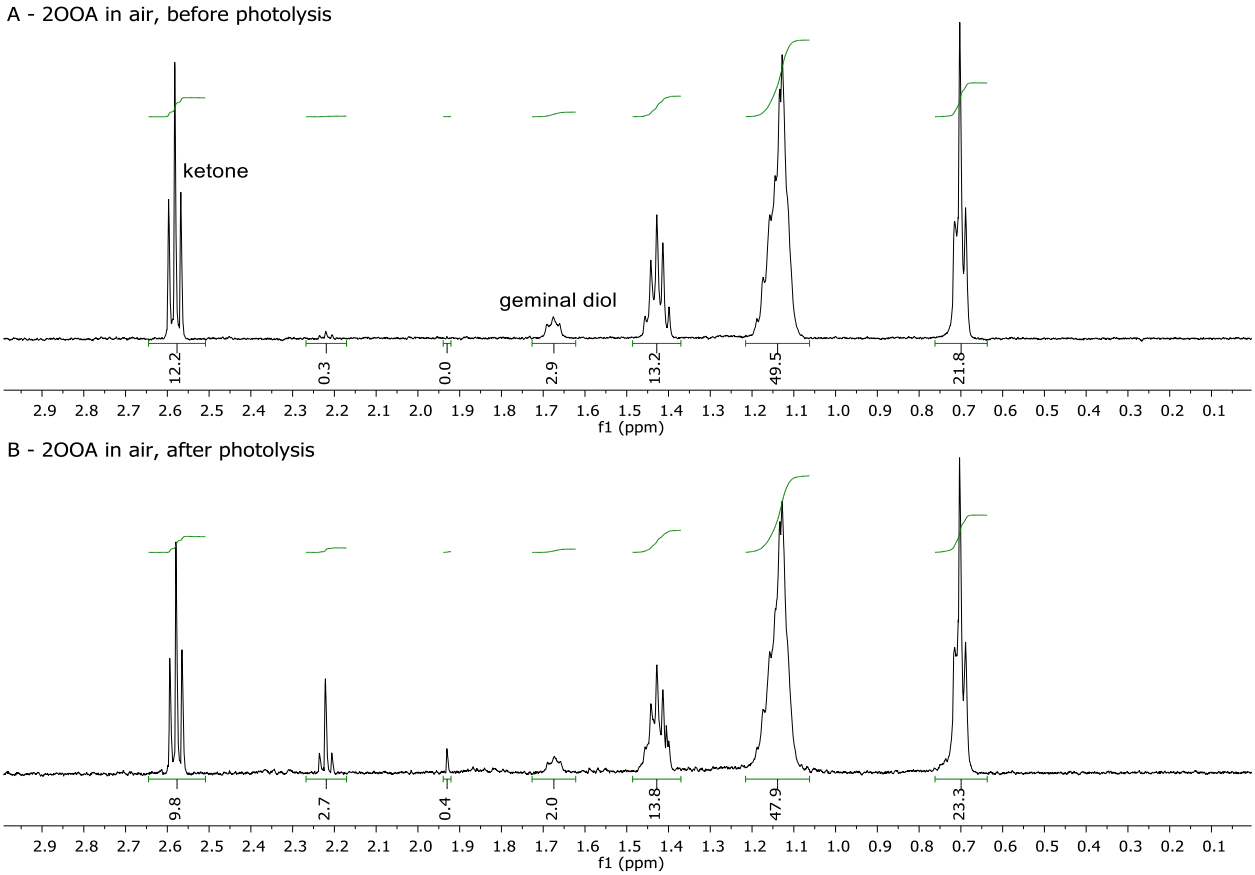

Figure E.11. NMR Spectra of 6 mM 2-oxoctanoic acid in aqueous solution before (A) and after (B) 5 hours of photolysis in air.

Appendix F: Supporting Information for Chapter 6

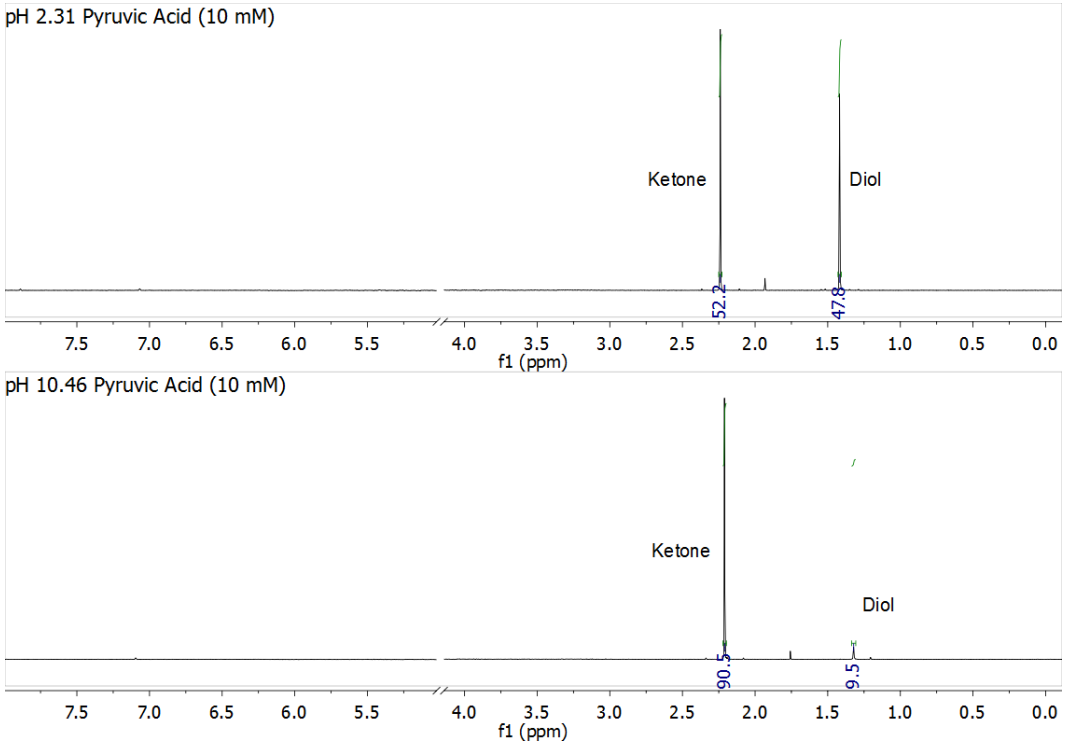

Figure F.1. Representative NMR spectra for 10 mM pyruvic acid at pH 2.31 (unadjusted, top) and pH 10.46 (bottom).

F.1 Fitting Procedure for Titration Curves

Acid dissociation constants were calculated from a plot of pH versus NaOH was used to calculate, following the fitting routine given in Harris's *Quantitative Chemical Analysis* textbook[2] with modifications to account for ionic strength taken from Papanastasiou and Ziogas 1995.[3] The pK_a was calculated using an iterative fitting routine described below.

Concentrations of $[H^+]$ and $[OH^-]$ were calculated from the experimental pH at each point of the titration. The fraction of dissociated acid, α_{A^-}, was then calculated for each data point using equation 1.

$$\textbf{\textit{Equation 1}}: \alpha_{A-} = \frac{K_a}{[H^+]+K_a}$$

The fraction of titration, ϕ, is determined using equation 2 and then can be used to find the volume of base added for each step of the titration, V_b, using equation 3.

$$\textbf{\textit{Equation 2}}: \phi = \frac{\alpha_{A-} - \frac{[H^+]-[OH^-]}{C_a}}{1+\frac{[H^+]+[OH^-]}{C_b}}$$

$$\textbf{\textit{Equation 3}}: V_b = \phi \times C_a \times \frac{V_a}{C_b}$$

In these equations, C_a is the concentration of acid, C_b is the concentration of base at each point, and V_a is the volume of acid.

For dilute solutions of acid, the addition of NaOH can significantly affect the overall ionic strength of the solution, which can, in turn, influence the experimental pK_a value. Therefore, the ionic strength was calculated using equation 4 for each point of the titration.

$$\textbf{\textit{Equation 4}}: I = [H^+] + C_b$$

This ionic strength value, I, is then used to calculate an effective activity coefficient, y_i, using the Debye-Hückel equation. The $\log(y_i)$ can be calculated using equation 5, where A and B are constants that depend on the physical properties of the solution. For our solutions, we used the values for water at room temperature, A = 0.5085, B = 0.3281.[4] The effective diameter of the ion, å, was taken to be 5 angstroms.[3]

$$\textbf{\textit{Equation 5}}: \log(y_i) = -\frac{A\sqrt{I}}{1+\text{å}B\sqrt{I}}$$

The proton concentrations at each point of the titration were corrected using these activity coefficients as in equation 6, where $[H^+]'$ is the corrected proton concentration. This correction is then iterative, due to the dependence of the effective activity coefficient on proton concentration.

$$\textbf{\textit{Equation 6}}: [H^+]' = \frac{[H^+]}{y_i}$$

Using this initial list of corrected proton concentrations and an initial guess for the value for the K_a, the residuals were calculated using equation 7 for each data point and then summed together. The offset in equation 7 accounts for the presence of deprotonated acid molecules prior to the addition of base.

$$\textbf{\textit{Equation 7}}: Residual = [(V_b + offset) - V_{predicted}]^2$$

The data were then fit by minimizing the sum of residuals using the Microsoft Excel solver function, allowing the base offset, acid concentration, and K_a to vary to obtain the best fit for K_a. Values for K_a were obtained for individual titration experiments and averaged to obtain the pK_a values reported here.

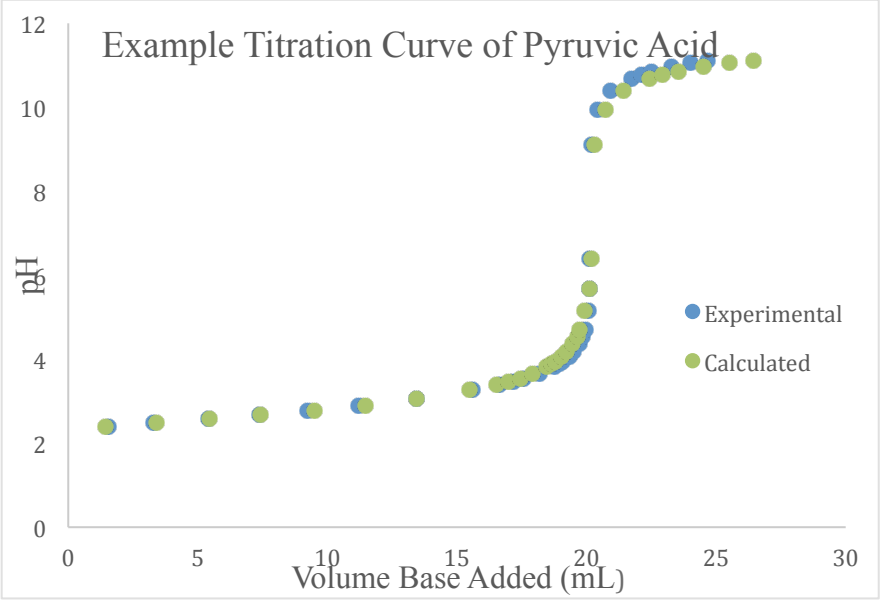

Figure F.2. Representative titration curve for 10 mM pyruvic acid with 15 mM sodium hydroxide, with experimental values given in blue and values from the calculated best fit given in green.

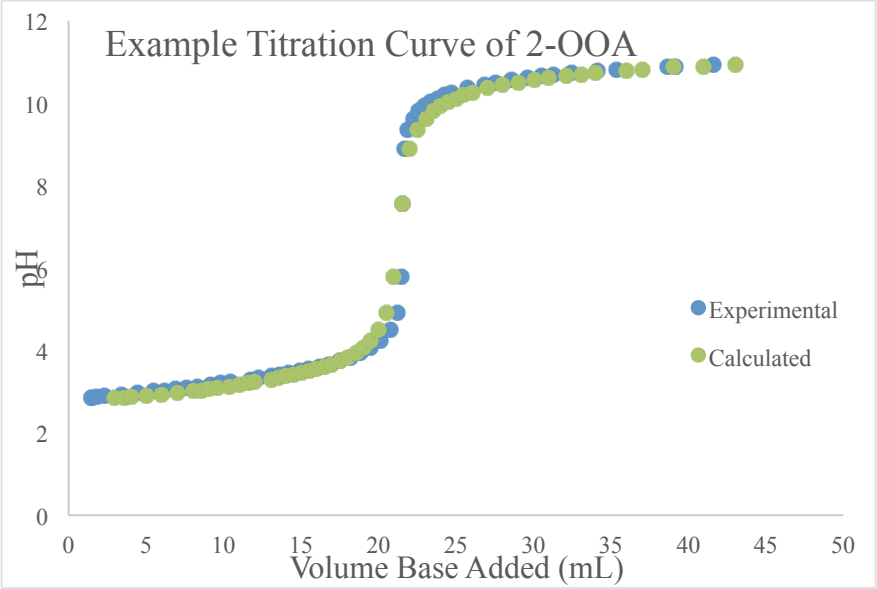

Figure F.3. Representative titration curve for 3 mM 2-oxooctanoic acid with 10 mM sodium hydroxide, with experimental values given in blue and values from the calculated best fit given in green.

F.2 Calculation of the composition of species in solution as a function of pH:

Pyruvic acid in solution exists as a four different species: protonated keto (HP), protonated diol (HD), deprotonated keto (P^-), and deprotonated diol (D^-) forms. The total concentration of the solution can be described as: $C_{pyruvic} = C_{keto} + C_{diol}$ and the concentrations of C_{Keto} and C_{Diol} can be calculated from the ratio of keto and diol forms found via NMR. The keto and diol forms have individual K_a values[5, 6] that are as follows,

Keto: $HP \rightleftharpoons H^+ + P^-$, $K_{aP} = [H^+][P^-]/[HP] = 6.607*10^{-3}$ and

Diol: $HD \rightleftharpoons H^+ + D^-$, $K_{aD} = [H^+][D^-]/[HD] = 2.512*10^{-4}$

And the self-ionization of water is also accounted for,

$H_2O \rightleftharpoons H^+ + OH^-$, $K_w = [H^+][OH^-] = 1*10^{-14}$

For those cases where the pH of the solution has been adjusted with NaOH, we assume all the NaOH is dissociated fully into Na^+ and OH^-.

The concentrations of species in solution are, then,

$C_{Keto} = [P^-] + [HP]$

$C_{Diol} = [D^-] + [HD]$

$C_{Na+} = [NaOH_{added}]$

The charge balance in solution can be represented as,

$[H^+] + [Na^+] = [P^-] + [D^-] + [OH^-]$.

Substituting into the above yields the following equation in terms of $[H^+]$:

$[H^+] + C_{Na+} = (C_{Keto}K_{aP}/([H^+] + K_{aP})) + (C_{Diol}K_{aD}/([H^+] + K_{aD})) + K_w/[H^+]$

This equation is solved numerically in Matlab for $[H^+]$, using literature values for K_{aP}, K_{aD}, and K_w and experimental values for C_{Keto}, C_{Diol}, and C_{Na+}.

The calculated $[H^+]$ is then substituted back in, obtaining values for $[P^-]$ and $[D^-]$. This calculated value for $[H^+]$ can also be used to extract an expected pH value for the solution that can be compared to the experimental pH. It's worth noting that the experimental pH values are very sensitive to the amount of NaOH added under these dilute conditions.

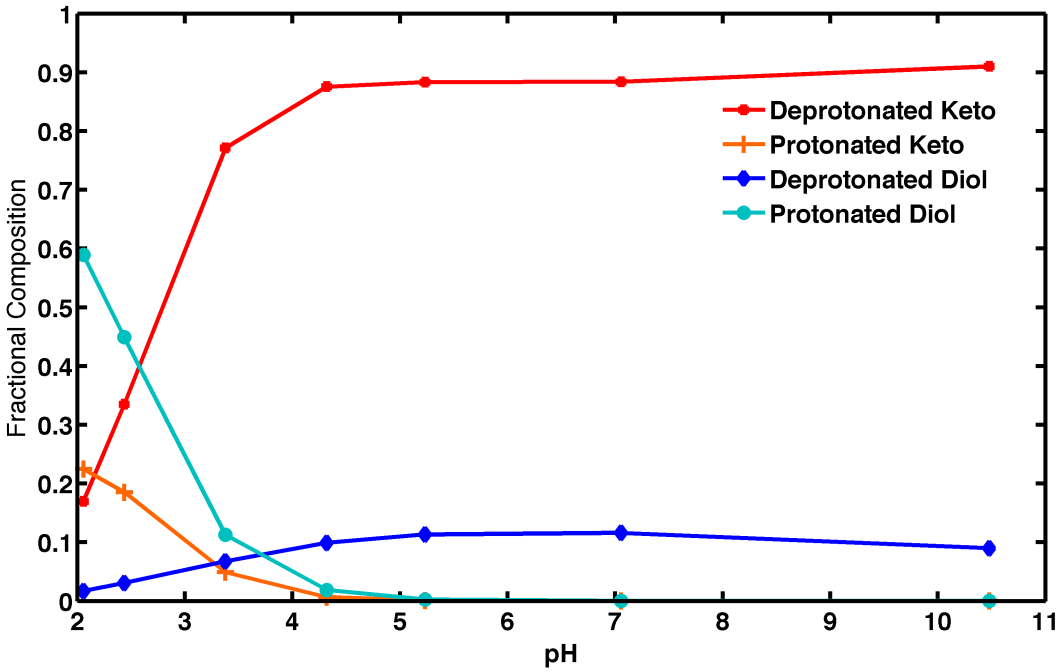

Figure F.4. Calculated fractional compositions of pyruvic acid species as a function of solution pH.

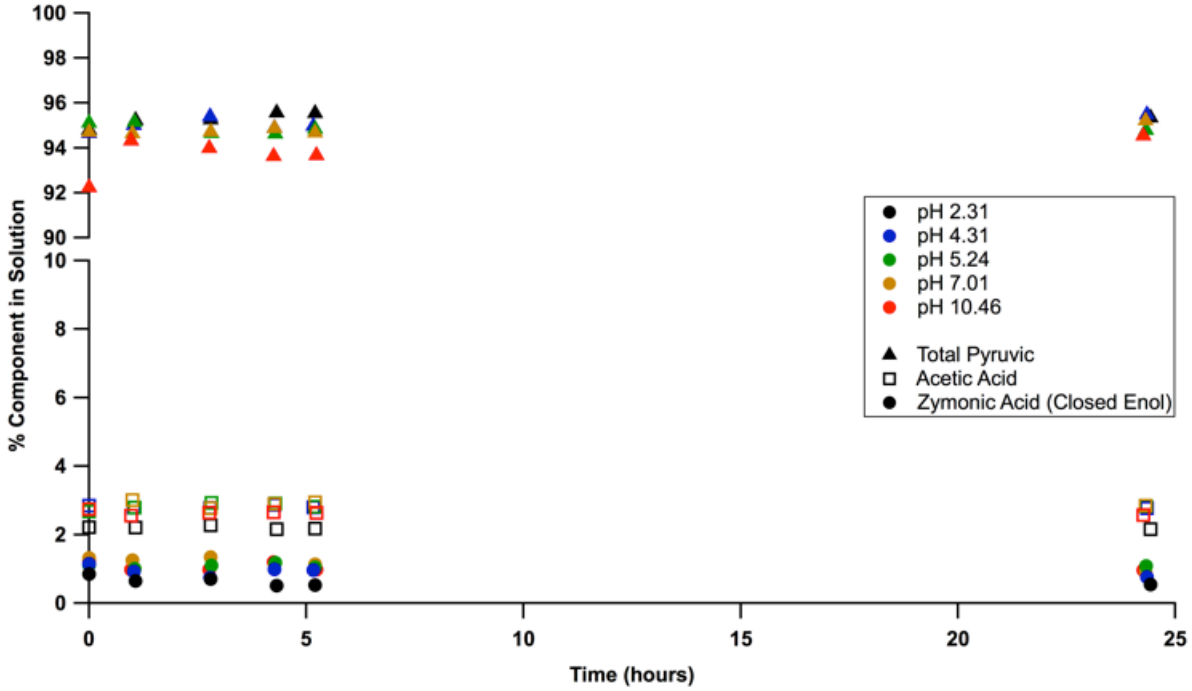

Figure F.5. Composition of 10 mM solutions of pyruvic acid for a range of pH conditions (from 2.31 to 10.46) monitored by NMR over time. Percentages of total pyruvic acid include contributions from both the keto and diol forms.

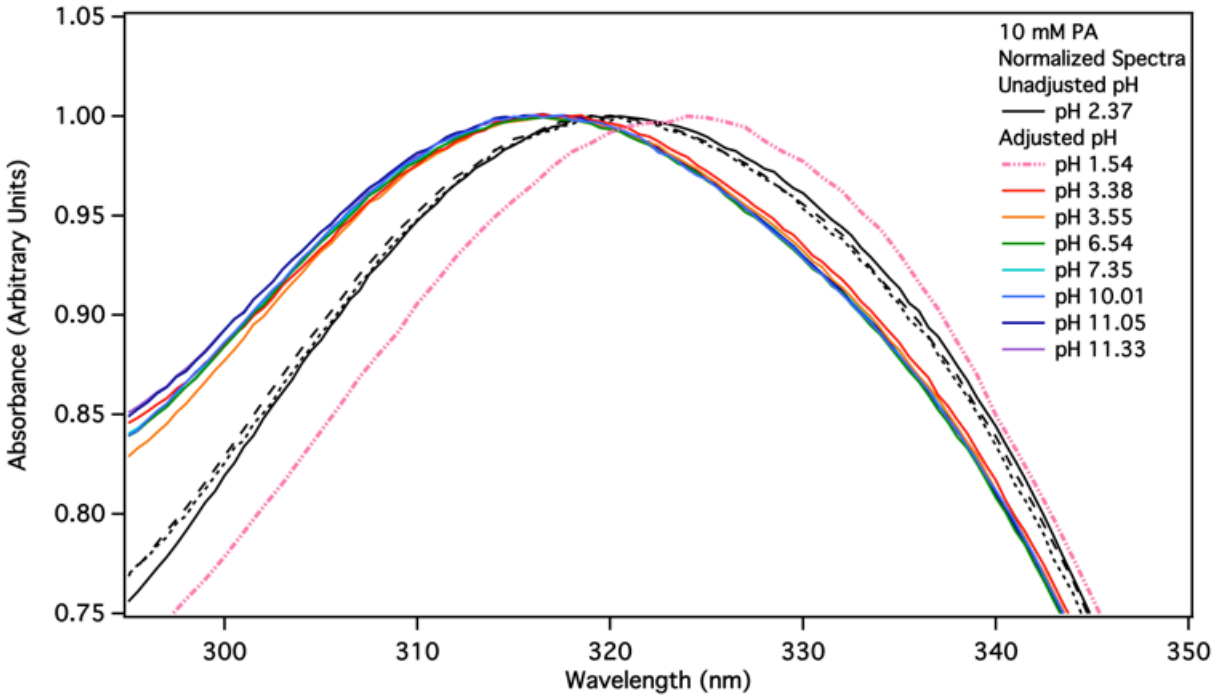

Figure F.6. Representative UV-vis absorption spectra of 10 mM pyruvic acid over a range of pH conditions from 1.54 to 11.33. All spectra were normalized at the λ_{max} of the transition, making the blue shift observed as pH is increased more apparent.

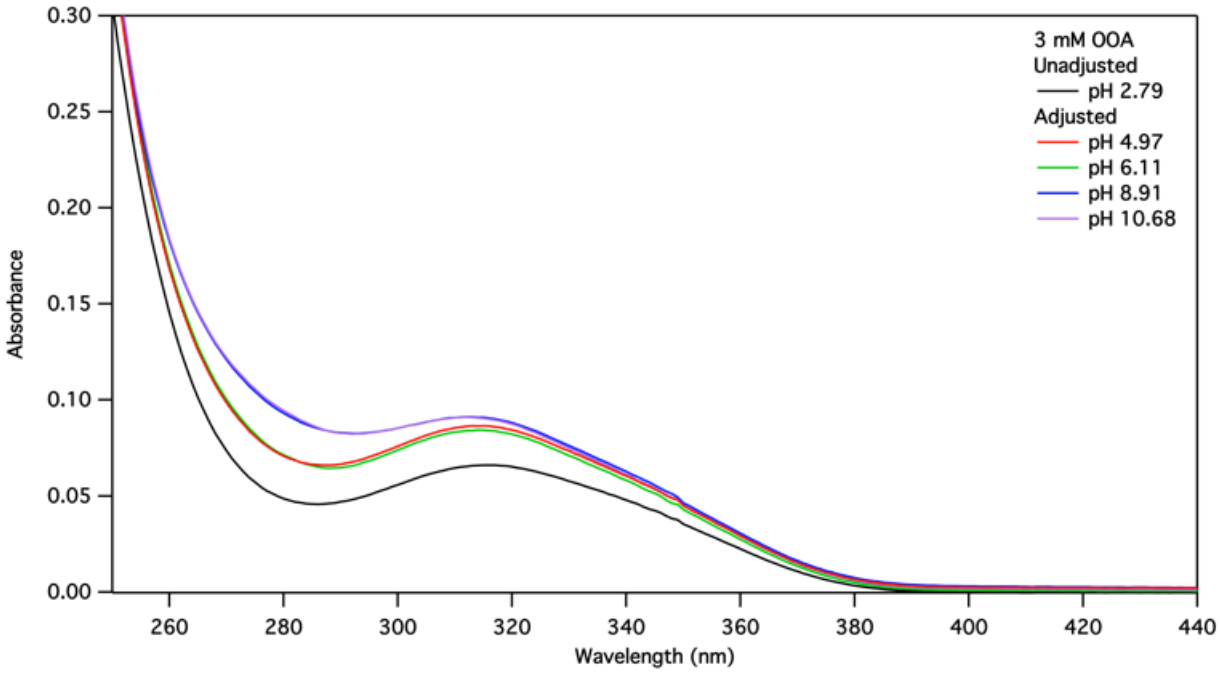

Figure F.7. Representative UV-vis absorption spectra of 3 mM 2-oxooctanoic acid solutions over a range of pH conditions from 2.79 to 10.68.

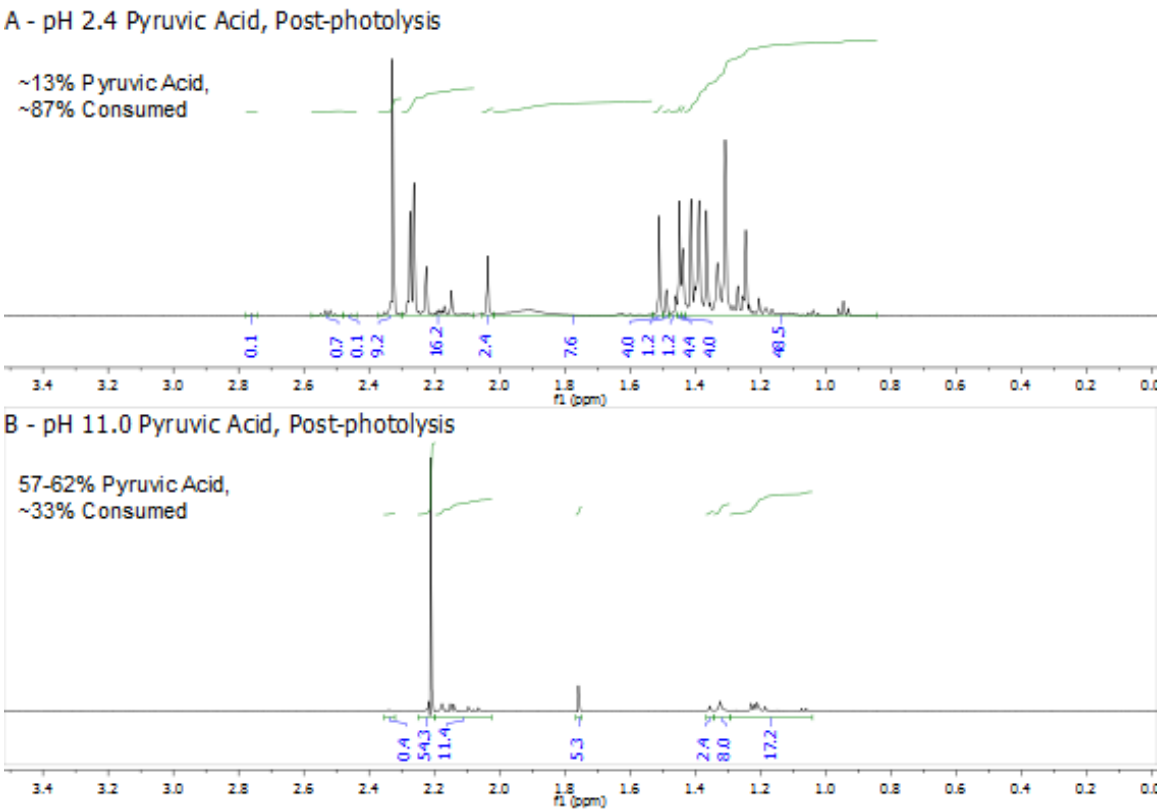

Figure F.8. Representative NMR spectra for 10 mM solutions of pyruvic acid with at unadjusted pH (initial pH = 2.4, top) and high pH (initial pH = 11.0 bottom) following 5 hours of photolysis.

Table F.1. Pyruvic Acid Photolysis Detailed ESI⁻ MS Results

							High pH		Unadjusted pH	
Assigned Formula [M-H]−	Assigned Structure	Avg Exp. m/z	Theor. m/z	Mass Diff. (ppm)	Theor. Nat. Abun	Avg. Nat. Abun	Pre	Post	Pre	Post
$C_3H_3O_3^-$	Pyruvic Acid	87.0085 ± 0.0003	87.0082	3.3			S	S	S	S
		88.0119 ± 0.0003	88.0116	3.1	3.2%	3.7%				
$C_4H_7O_2^-$	Acetoin	87.0447 ± 0.0004	87.0446	0.6			B.T.	W	B.T.	M
		88.0483 ± 0.0008	88.0480	3.9	4.3%	5.6%				
$C_3H_5O_3^-$	Lactic Acid	89.0234 ± 0.0006	89.0239	-5.3			B.T.	B.T.	B.T.	W
$C_3H_5O_4^-$	2,2-DHPA	105.0190 ± 0.0005	105.0188	1.6			B.T.	B.T.	W	B.T.
Unidentified		108.9905 ± 0.0003					M	M	B.T.	B.T.†
		109.9943 ± 0.0006				5.2%				

$C_5H_7O_3^-$	Unassigned	115.0398 ± 0.0005	115.0395	2.4			B.T.	W	B.T.	M
		116.0432 ± 0.0007	116.0429	2.9	5.4%	6.0%				
Unidentified		125.0219 ± 0.0006					M	M	B.T.	B.T.
		126.0251± 0.0004				5.8%				
$C_5H_7O_4^-$	Acetolactic Acid	131.0347 ± 0.0005	131.0345	1.8			B.T.	B.T.	B.T.	M
		132.0381 ± 0.0006	132.0378	2.0	5.4%	6.2%				
Unidentified		141.0168 ± 0.0005					W	W	B.T.	B.T.
Unidentified		154.9961 ± 0.0006					M	M	B.T.	B.T.
		155.9990 ± 0.0006				6.0%				
$C_7H_{11}O_4^-$	Unassigned	159.0660 ± 0.0005	159.0658	1.3			B.T.	M	B.T.	M
		160.0699 ± 0.0006	160.0691	4.8	7.6%	9.5%				
$C_6H_9O_6^-$	Unassigned	161.0453 ± 0.0007	161.0450	2.0			B.T.	B.T.	B.T.	M
		162.0488 ± 0.0008	162.0484	2.8	6.5%	7.7%				
$C_6H_7O_6^-$	Parapyruvic Acid*	175.0245 ± 0.0005	175.0243	1.2			W	B.T.	W	B.T.
$C_7H_{11}O_5^-$	DMOHA	175.0609 ± 0.0004	175.0607	0.9			B.T.	S	B.T.	S
		176.0644 ± 0.0005	176.0640	2.4	7.6%	8.6%				
$C_6H_9O_6^-$	Dimethyl-tartaric Acid	177.0403 ± 0.0005	177.0400	1.5			B.T.	M	B.T.	S
		178.0434 ± 0.0004	178.0433	0.4	6.5%	7.4%				
$C_6H_6O_6Na^-$	Na Adduct of 2 PA-	197.0066 ± 0.0003	197.0062	2.0			S	S	S	W
		198.0099 ± 0.0004	198.0096	1.4	6.5%	7.1%				
Unidentified		217.0719 ± 0.0006					B.T.	W	B.T.	M
		218.0754 ± 0.0008				10.6%				
$C_8H_{11}O_7^-$	CDMOHA	219.0509 ± 0.0007	219.0505	1.9			B.T.	B.T.	B.T.	M
		220.0546 ± 0.0006	220.0539	3.0	8.7%	9.6%				
Unidentified		233.0473 ± 0.0007					B.T.	B.T.	M	B.T.
		234.0510 ± 0.0006				8.5%				

Unidentified		240.9706 ± 0.0005					M	M	B.T.	B.T.
		241.9737 ± 0.0006				7.5%				
Unidentified		247.0632 ± 0.0004					B.T.	B.T.	S	B.T.
		248.0677 ± 0.001				10.6%				
$C_{10}H_{14}O_8Na^-$	Na Adduct of PA- and DMOHA-	285.0592 ± 0.0005	285.0587	1.7			B.T.	S	B.T.	M
		286.0621 ± 0.0005	286.0620	1.1	10.8%	11.8%				
$C_9H_{12}O_9Na^-$	Na Adduct of PA- and DMTA-	287.0383 ± 0.0006	287.0380	1.1			B.T.	B.T.	B.T.	W
$C_9H_9O_9Ca^-$	Ca Adduct of 3 PA-	300.9880 ± 0.0008	300.9873	5.6			M	W	M	B.T.
		301.9928 ± 0.001	301.9907	6.9	9.7%	10.5%				
$C_9H_9O_9Na_2^-$	Na Adduct of 3 PA-	307.0045 ± 0.0004	307.0043	0.5			S	M	M	B.T.
		308.0082 ± 0.0004	308.0076	1.8	9.7%	10.1%				

Notes: Chemical formulas are assigned as the ionized $[M-H]^-$ species, structures are assigned as the neutral species. The experimental m/z is the observed average across experiments, and the uncertainty given is the 95% confidence interval. S = Strong, M = Medium, W = Weak, and B.T. = Below Threshold (Threshold was set conservatively at 10^4 counts).
2,2-DHPA = 2,2-Dihydroxypropanoic Acid, diol of pyruvic acid; DMOHA = 2,4-dihydroxy-2-methyl-5-oxohexanoic acid; CDMOHA = 4-carboxy-2,4-dihydroxy 2-methyl-5-oxohexanoic acid
*The peak assigned to parapyruvic acid likely also has contributions from the closed ring form of the zymonic acid diol as well.
†When the post-photolysis solution of pyruvic acid at low pH is adjusted to high pH this analyte is observed.

Table F.2. 2-Oxooctanoic Acid Photolysis Detailed ESI^- MS Results

							High pH		Unadjusted pH	
Assigned Formula [M-H]-	Assigned Structure	Avg Exp. m/z	Theor. m/z	Mass Diff. (ppm)	Exp. Nat. Abun	Avg. Nat. Abun	Pre	Post	Pre	Post
$C_3H_3O_3^-$	Pyruvic Acid	87.0082 ± 0.0005	87.0082	-0.5			B.T.	W	B.T.	W
$C_7H_{13}O_2^-$	Heptanoic Acid	129.0918 ± 0.0003	129.0916	1.4			M	M	M	M
		130.0953 ± 0.0003	130.0949	3.0	7.6%	8.4%				
$C_8H_{11}O_2^-$	Unassigned	139.0762 ± 0.0004	139.0759	2.2			B.T.	M	B.T.	M
		140.0797 ± 0.0004	140.0793	2.6	8.7%	9.5%				
$C_7H_{13}O_3^-$*	Unassigned	145.0867 ± 0.0004	145.0865	1.8			M	M	W	W

		146.0899 ± 0.0001	146.0899	0.4	7.6%	9.3%				
$C_8H_{13}O_3^-$	2-Oxooctanoic Acid	157.0867 ± 0.0003	157.0865	1.7			S	S	S	S
		158.0902 ± 0.0004	158.0899	1.6	8.7%	10.2%				
$C_9H_{17}O_2^-$	Nonanoic Acid	157.1236 ± 0.0004	157.1229	4.7			W	W	W	W
$C_8H_{13}O_4^-$	2,2-DHOA	173.0816 ± 0.0003	173.0814	1.4			M	M	S	S
		174.0851 ± 0.0003	174.0848	1.6	8.6%	9.6%				
$C_6H_9O_6^-$	Dimethyl-tartaric Acid	177.0406 ± 0.0009	177.0400	3.2			B.T.	B.T.	B.T.	W
Unidentified		211.2065 ± 0.0003					B.T.	S	B.T.	B.T.[†]
		212.2096 ± 0.0002				16.1%				
Unidentified		225.0740 ± 0.0001					M	M	B.T.	B.T.[†]
		226.0772 ± 0.0001				11.2%				
$C_{14}H_{27}O_2^-$	8-hydroxy-tetradecan-7-one	227.2014 ± 0.0004	227.2011	1.1			B.T.	W	B.T.	W
$C_{11}H_{17}O_6^-$	R-PPA	245.1017 ± 0.001	245.1026	-3.5			B.T.	B.T.	B.T.	W
$C_{12}H_{21}O_5^-$	R-DHO Acid	245.1391 ± 0.0004	245.1389	0.9			B.T.	W	B.T.	M
		246.1428 ± 0.0005	246.1423	1.8	13.0%	14.2%				
$C_{11}H_{19}O_6^-$	Methylhexyl-tartaric Acid	247.1186 ± 0.0004	247.1182	1.6			B.T.	M	B.T.	S
		248.1220 ± 0.0004	248.1216	1.4	11.9%	12.9%				
Unidentified		253.1805 ± 0.0003					W	W	M	W
		254.1841 ± 0.0004				17.6%				
$C_{15}H_{27}O_3^-$	Unassigned	255.1961 ± 0.0004	255.1960	0.4			B.T.	S	B.T.	M
		256.1996 ± 0.0005	256.1994	0.7	16.2%	17.4%				
$C_{15}H_{27}O_4^-$	8-C-8-H-tetradecan-7-one	271.1912 ± 0.0004	271.1910	0.7			B.T.	M	B.T.	M
		272.1944 ± 0.0003	272.1943	0.5	16.2%	17.5%				
$C_{15}H_{29}O_4^-$	Unassigned	273.2066 ± 0.0005	273.2066	0.0			B.T.	M	B.T.	W
		274.2098 ± 0.0003	274.2100	-0.8	16.2%	17.2%				
$C_{13}H_{28}O_5Na^-$*	Unassigned	287.1857 ± 0.0006	287.1835	7.6			W	W	B.T.	W

		288.1892 ± 0.0005	288.1868	8.3	14.1%	19.1%				
$C_{13}H_{21}O_7^-$	R-DHO Diacid	289.1292 ± 0.0006	289.1288	1.2			B.T.	B.T.	B.T.	M
		290.1327 ± 0.0007	290.1321	2.1	14.1%	15.1%				
$C_{16}H_{25}O_6^-$	R,R-DODA	313.1653 ± 0.0003	313.1652	0.4			M	M	M	M
		314.1687 ± 0.0003	314.1865	0.6	17.3%	18.7%				
$C_{16}H_{28}O_6^-$	R,R-PPA	315.1783 ± 0.001	315.1808	-8.0			W	W	M	M
		316.1825 ± 0.001	316.1842	-5.5	17.3%	18.4%				
$C_{17}H_{31}O_5^-$	R,R-DHO Acid	315.2176 ± 0.0004	315.2172	1.4			B.T.	S	B.T.	S
		316.2206 ± 0.0003	316.2205	0.2	18.0%	19.5%				
$C_{16}H_{29}O_6^-$	Dihexyl-tartaric Acid	317.1959 ± 0.0006	317.1965	-2.0			B.T.	S	B.T.	S
		318.2000 ± 0.0003	318.1998	0.7	17.3%	18.8%				
$C_{16}H_{26}O_6Na^-$	Na Adduct of 2 OOA-	337.1326 ± 0.0002	337.1627	-0.3			S	S	S	M
		338.1658 ± 0.0002	338.1661	-1.0	17.3%	18.8%				
$C_{16}H_{26}O_7Na^-$	Na Adduct of OOA- and OOA Diol-	353.1564 ± 0.0007	353.1577	-3.6			M	M	M	M
		354.1598 ± 0.0007	354.1610	-3.5	17.3%	18.6%				
$C_{18}H_{31}O_7^-$	R,R-DHO Diacid	359.2069 ± 0.0005	359.2070	-0.3			B.T.	B.T.	B.T.	M
		360.2107 ± 0.0007	360.2104	0.7	19.5%	21.5%				
Unidentified		369.3000 ± 0.0003					B.T.	S	B.T.	B.T.
		370.3036 ± 0.0001				24.6%				
$C_{22}H_{41}O_5^-$	R,R,R-DHO Acid	385.2953 ± 0.0002	385.2954	-0.4			B.T.	S	B.T.	M
		386.2986 ± 0.0002	386.2988	-0.4	23.8%	25.5%				
$C_{23}H_{41}O_7^-$	R,R,R-DHO Diacid	429.2850 ± 0.001	429.2860	-2.3			B.T.	W	B.T.	W
$C_{26}H_{41}O_9^-$	Unassigned	497.2721 ± 0.0006	497.2751	-6.0			B.T.	M	B.T.	M
		498.2761 ± 0.0001	498.2785	-4.8	28.1%	27.4%				
$C_{24}H_{39}O_9Ca^-$	Ca Adduct of 3 OOA-	511.2233 ± 0.0006	511.2221	2.3			W	W	M	M

		512.2261 ± 0.0007	512.2254	1.3	26.0%	28.3%				
$C_{24}H_{39}O_9Na_2^-$	Na Adduct of 3 OOA-	517.2388 ± 0.0001	517.2390	-0.4			S	S	M	W
		518.2422 ± 0.0002	518.2424	-0.5	26.0%	27.1%				

Notes: Chemical formulas are assigned as the ionized $[M-H]^-$ species, structures are assigned as the neutral species. The experimental *m/z* is the observed average across experiments, and the uncertainty given is the 95% confidence interval. S = Strong, M = Medium, W = Weak, and B.T. = Below Threshold (Threshold was set conservatively at 10^4 counts).
2,2-DHOA = 2,2-Dihydroxyoctanoic Acid, Diol of OOA; DMOHA = 2,4-dihydroxy-2-methyl-5-oxohexanoic acid; 8-C-8-H-tetradecan-7-one = 8-carboxy-8-hydroxy-tetradecan-7-one
*Tentative chemical formula assignment.
†When the post-photolysis solution of OOA at low pH is adjusted to high pH this analyte is observed.

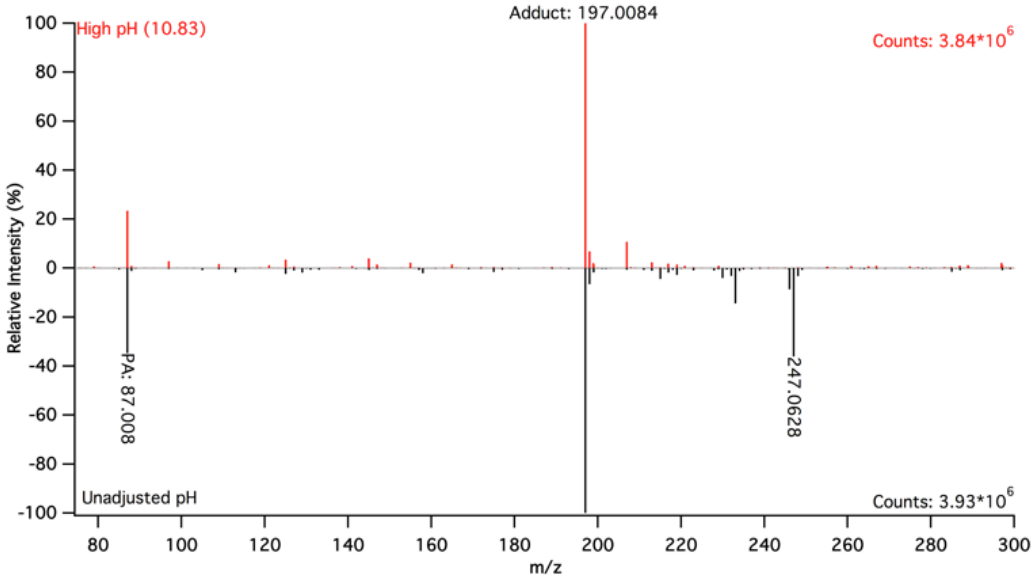

Figure F.9. Representative ESI- MS of 10 mM pyruvic acid solutions prior to photolysis at high (10.83, red) and low pH (unadjusted, black, multiplied by -1 for ease of presentation) conditions.

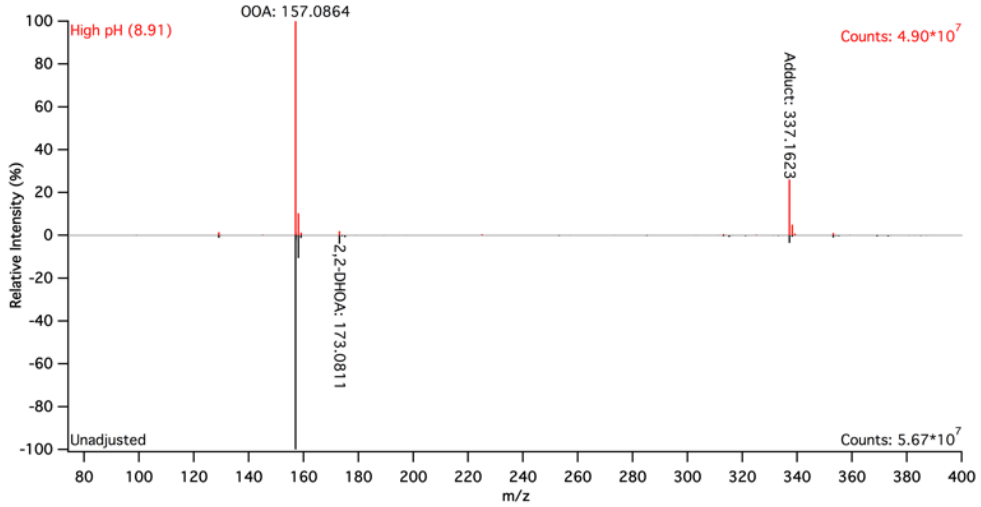

Figure F.10. Representative ESI- MS of 3 mM 2-oxooctanoic acid prior to photolysis at low (unadjusted, black, multiplied by -1 for ease of presentation) and high pH (pH = 8.91, red).

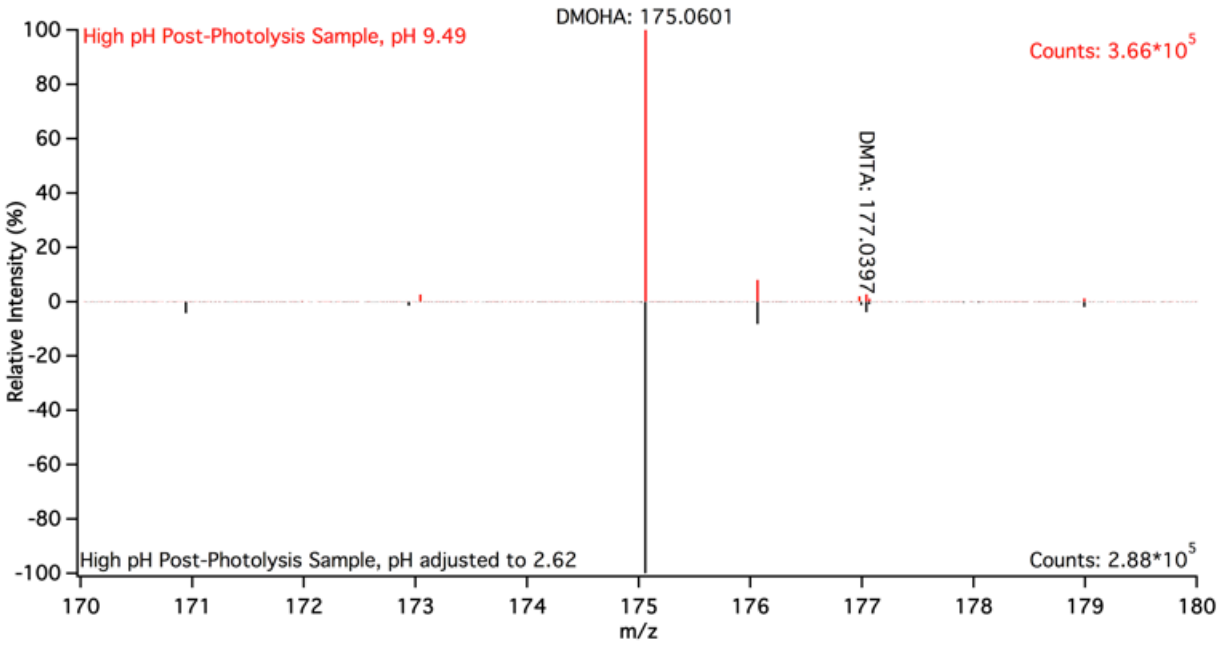

Figure F.11. Representative ESI- MS of 10 mM pyruvic acid after 5 hours of photolysis at pH ~10 (initial pH = 10.01), comparing spectra taken under both high pH (9.49, red) and low pH (2.62, adjusted with HCl, black, multiplied by -1 for ease of presentation) conditions.

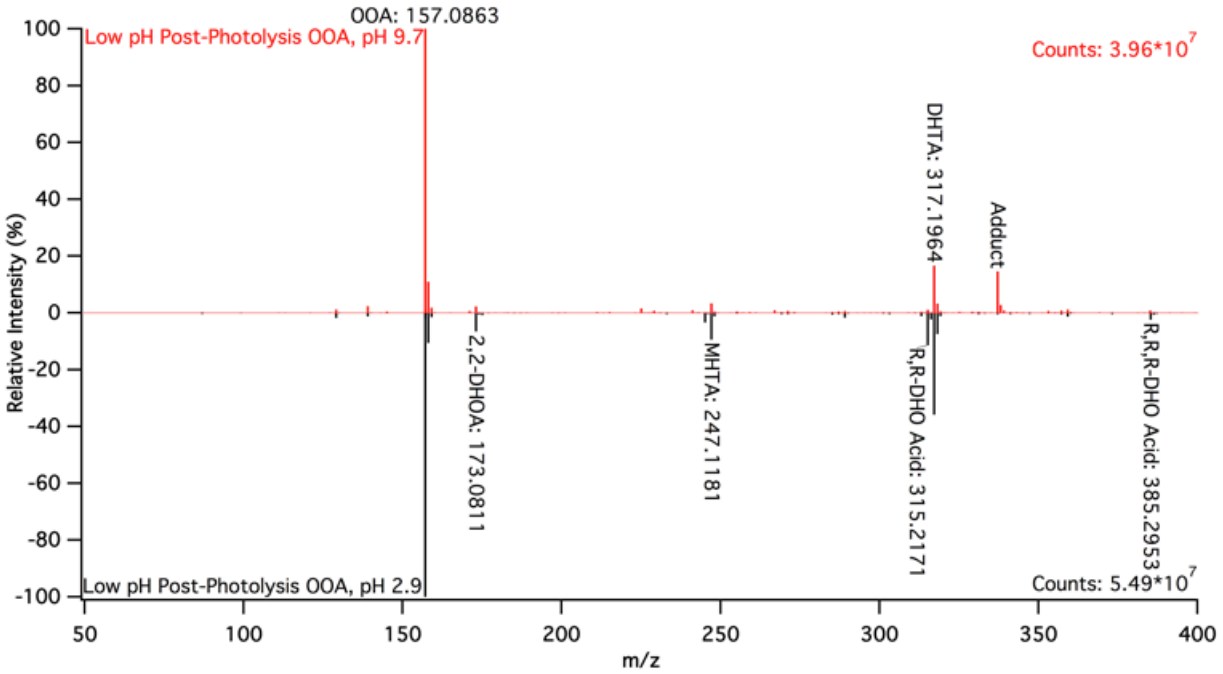

Figure F.12. Representative ESI- MS of 3 mM OOA after 5 hours of photolysis at unadjusted pH, comparing spectra taken under both high pH (9.72 adjusted with NaOH, red) and low pH (2.93, black, multiplied by -1 for ease of presentation) conditions.

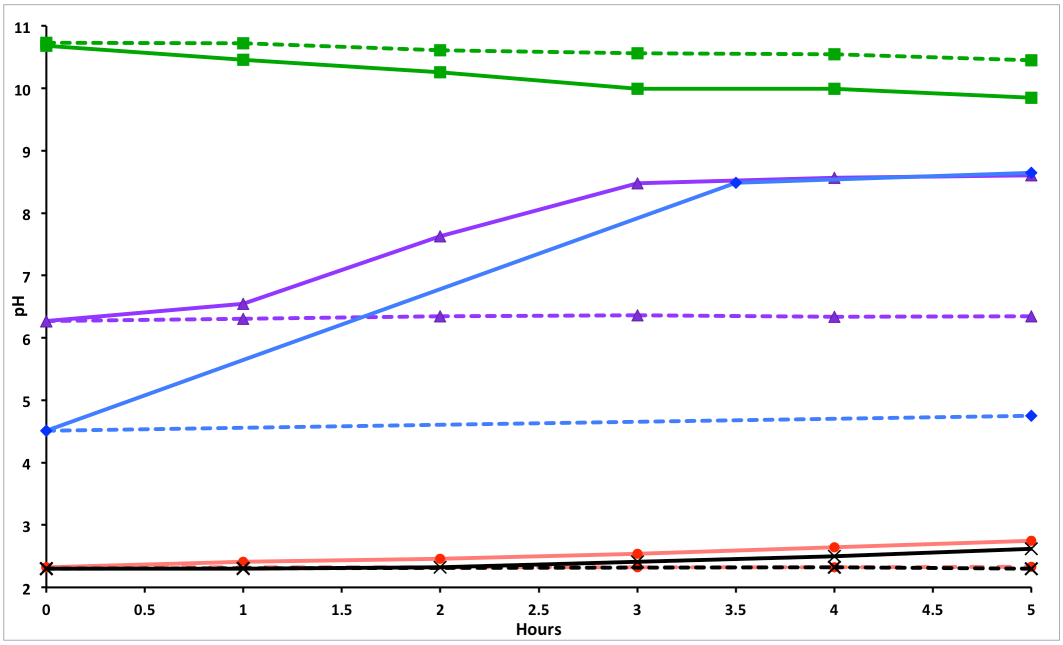

Figure F.13. Examples of the change in solution pH over the course of 5 hours of photolysis (solid) and comparison to dark controls (dashed) for 10 mM pyruvic acid at low pH (red circles and black crosses), intermediate pH (blue diamonds and purple triangles), and high pH (green squares).

F.3 Bibliography:

1. Ogg, R. J.; Kingsley, R.; Taylor, J. S. WET, a T 1-and B 1-insensitive water-suppressionmethod for in vivo localized ^{1}H NMR spectroscopy. *Journal of Magnetic Resonance, Series B* **1994,** *104*, 1-10.

2. Harris, D. C., *Quantitative Chemical Analysis*. 7th ed.; W.H. Freeman and Company: New York, 2007.

3. Papanastasiou, G.; Ziogas, I. Simultaneous determination of equivalence volumes and acid dissociation constants from potentiometric titration data. *Talanta* **1995,** *42*, 827-836.

4. Manov, G. G.; Bates, R. G.; Hamer, W. J.; Acree, S. Values of the constants in the Debye—Hückel equation for activity coefficients. *J. Am. Chem. Soc.* **1943,** *65*, 1765-1767.

5. Strehlow, H. Die Kinetik der Hydratation von α-Ketocarbonsäuren. *Zeitschrift für Elektrochemie* **1962,** *66*, 392-396.

6. Becker, M. Über magnetische Kernresonanzspektren wäßriger Brenztraubensäurelösungen. *Ber. Bunsen-Ges. Phys. Chem* **1964,** *68*, 669-676.

Appendix G: Supporting Information for Chapter 7

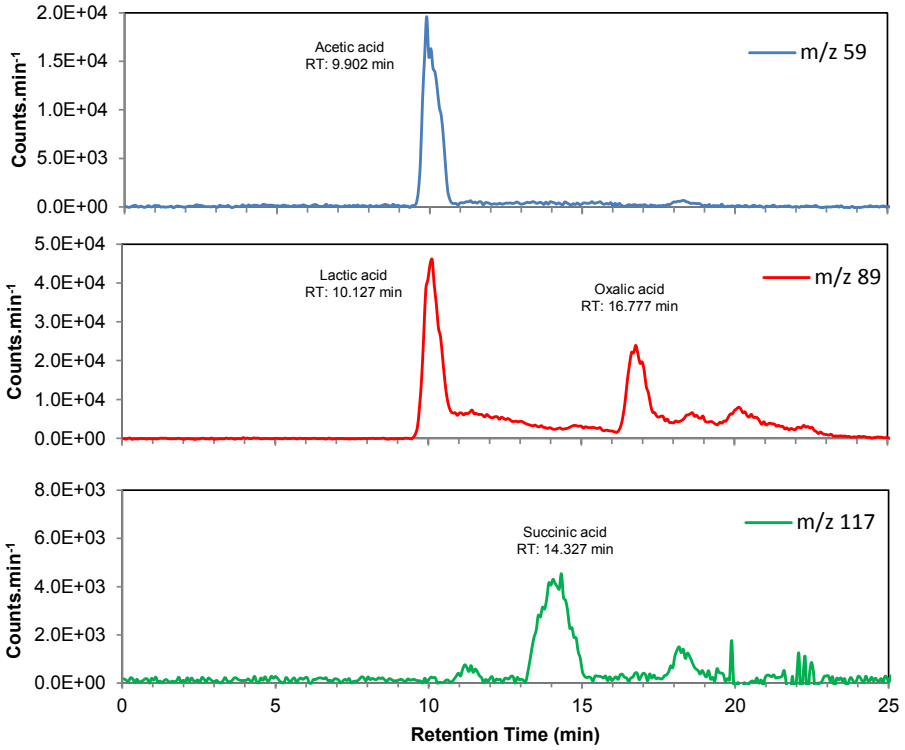

Figure G.1. Ionic chromatograms (SIM mode) from the photolysis of $[MVK]_0$ = 20mM and $[PA]_0$ = 100mM at t = 50 min. IC-MS analyses, i.e. chromatographic separations coupled to mass spectrometry, allow for identification of individual ions with different m/z or retention times.

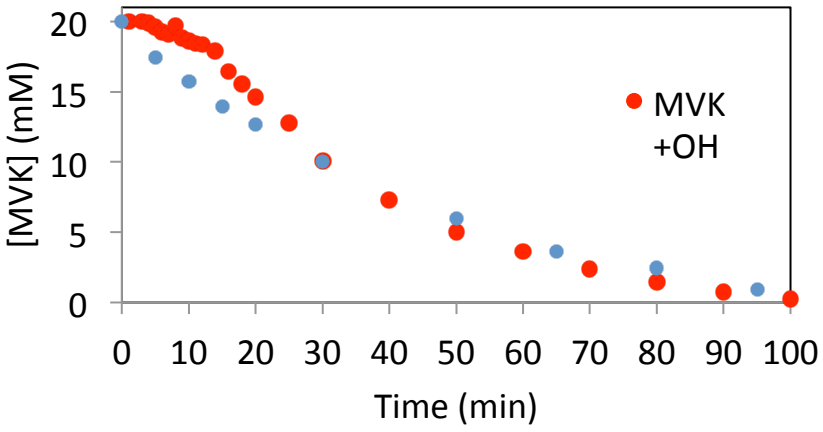

Figure G.2. Comparison of the decay of MVK between MVK •OH-oxidation and MVK PA-photolysis. During MVK •OH-oxidation ($[MVK]_0$ = 20 mM, $[H_2O_2]_0$ = 400 mM), oligomerization (propagation) is slowed by the presence of dissolved O_2, while, in the MVK PA-photolysis ($[MVK]_0$ = 20 mM, $[PA]_0$ = 100 mM), oligomerization is rapid at the start of the reaction due to the low dissolved O_2 concentrations.

Table G.1 Reaction Scheme for the Photolysis of H_2O_2 and formation of O_2

Reactions	Rate constant or pKa value at 25°C
$H_2O_2 + h\nu \xrightarrow{J} 2\ HO^{\cdot}$	J (s^{-1})
$H_2O_2 + HO^{\cdot} \xrightarrow{k_1} HO_2^{\cdot} + H_2O$	$k_1 = 2.7\times10^7\ M^{-1}\ s^{-1}$
$HO_2^{\cdot} + HO_2^{\cdot} \xrightarrow{k_2} H_2O_2 + O_2$	$k_2 = 8.3\times10^5\ M^{-1}\ s^{-1}$
$HO_2^{\cdot} + O_2^{\cdot-} + H^+ \xrightarrow{k_3} H_2O_2 + O_2$	$k_3 = 1\times10^8\ M^{-1}\ s^{-1}$
$O_2^{\cdot-} + O_2^{\cdot-} + 2H^+ \xrightarrow{k_4} H_2O_2 + O_2$	$k_4 = 0.3\ M^{-1}\ s^{-1}$
$HO_2^{\cdot} + HO^{\cdot} \xrightarrow{k_5} H_2O + O_2$	$k_5 = 7\times10^9\ M^{-1}\ s^{-1}$
$O_2^{\cdot-} + HO^{\cdot} \xrightarrow{k_6} OH^- + O_2$	$k_6 = 1\times10^{10}\ M^{-1}\ s^{-1}$
$HO_2^{\cdot} + H_2O \overset{K_a}{\Leftrightarrow} HO_3^+ + O_2^{\cdot-}$	$pK_a = 4.8$

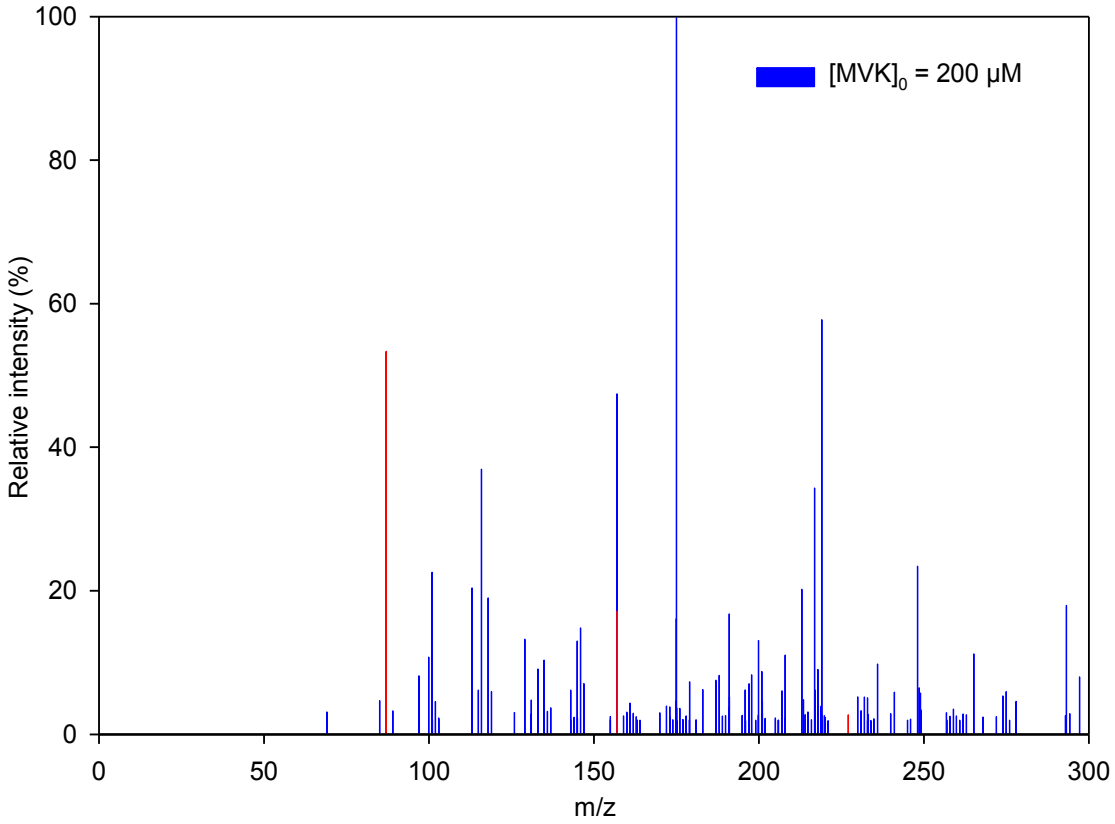

Figure G.3. Mass spectrum of the peak relative oligomer intensity of the MVK PA-photolysis at low initial precursor concentrations ($[MVK]_0$ = 200 µM, $[PA]_0$ = 4 mM, t = 5 min), obtained using LC-MS for the retention time range 0 to 4 min, in the negative mode. Series S160 PA-$(MVK)_n$ (see Table 7.1) is highlighted in red.

G.1 Comparison Of Initiation Rates Between MVK ·OH-Oxidation And MVK PA-Photolysis Reactions

Assuming PA-photolysis produces PA* (excited PA triplet state) and/or PA· and AA· radicals (both are called PA· in the following) that readily react on MVK, one can compare the initiation rates of MVK + ·OH and MVK + PA· reactions both for our experimental conditions and atmospherically relevant conditions. This calculation requires a number of assumptions, outlined below.

The rates of each reaction, i.e. $R_{MVK+\cdot OH}$ and $R_{MVK+PA\cdot}$ are given by:

$$R_{MVK+\cdot OH} = k_{MVK+\cdot OH}[\cdot OH][MVK]$$
$$R_{MVK+PA\cdot} = k_{MVK+\,PA\cdot}[PA\cdot][MVK],$$

where [·OH], [MVK], and [PA·] are the concentrations of the corresponding species in the solution, and $k_{MVK+\cdot OH}$ and $k_{MVK+\,PA\cdot}$ are the rate constants of MVK + ·OH and MVK + PA· reactions respectively.

The calculation of $R_{MVK+\cdot OH}$ and $R_{MVK+PA\cdot}$ therefore requires:

a) $k_{MVK+\cdot OH}$ and $k_{MVK+\,PA\cdot}$. The former is known ($k_{MVK+\cdot OH} = 7.3\times10^{9}$ M^{-1} s^{-1}),[37] while the latter is not. Generally, organic radicals are orders of magnitude less reactive toward organic compounds than ·OH radicals. In their review, Ligon et al., (2014)[1] list a series of rate constants for oligomer initiation of acrylate monomer by a series of different organic radicals. These rate constants range between 10^5 and 10^7 M^{-1} s^{-1}. Here, we consider this range of rate constants for the reaction of MVK + PA· (Tables G.2 and G.3).

b) The concentrations of ·OH and PA· radicals. The former can be estimated for either our experimental set up or atmospheric conditions; however, the latter is much more difficult. A pseudo-steady state approximation for [PA·] radical can be calculated using assumptions appropriate for either case. The following sections detail these assumptions.

G.1.1 Under Atmospheric Conditions:

b) The concentration of ·OH is estimated to be 10^{-13}-10^{-15} M in the atmosphere.[3] Using the following values for the calculation of [PA·]:

i) J_{PA} = 1 x 10^{-3} s^{-1} (atmospherically relevant photolysis rate constant for pyruvic acid)[13]
ii) [O_2] = 258 μM (at 25°C),
iii) [PA] = 0.1 M,
iv) [MVK] = 1 μM,

one obtains [PA·] ~ 10^{-10} M (Table G.2). The results for the estimation of $R_{MVK+\cdot OH}$ and $R_{MVK+PA\cdot}$ are indicated in Table G.2. The comparison indicates that, under conditions where aqueous concentrations of ·OH radicals are limited and where pyruvic acid is highly concentrated such as in wet aerosols, the rates of reactions MVK + PA· and MVK + ·OH can be of the same order of magnitude.

Table G.2. Estimated rates of MVK + ·OH and MVK + PA· under atmospheric conditions

Reaction	·OH concentrations assumed (M)	$R_{MVK+\cdot OH}$ (M s^{-1})
MVK + ·OH	10^{-15}	7 x 10^{-12}
	10^{-14}	7 x 10^{-11}
	10^{-13}	7 x 10^{-10}

Reaction	Assumed rate constant for MVK + PA· and PA + PA·	PA· concentrations estimated (M)	$R_{MVK+PA\cdot}$ (M s^{-1})
MVK + PA·	10^7 M^{-1} s^{-1}	7 x 10^{-11}	7 x 10^{-10}
	10^6 M^{-1} s^{-1}	10^{-10}	10^{-10}
	10^5 M^{-1} s^{-1}	2 x 10^{-10}	2 x 10^{-11}

G.1.2 Under Our Experimental Conditions:

b) The concentration of ·OH is estimated to be ~10^{-14} M in the reactor.[7] Using the following values for the calculation of [PA·]:

i) J_{PA}=3.5 x 10^{-5} s^{-1} (Photolysis rate constant for pyruvic acid calculated from PA-photolysis experiments (with no MVK) and using the same approach as the one by Reed-Harris et al., 2014),[2]

ii) [O_2] = 25 μM,
iii) [PA] = 0.1 M,
iv) [MVK] = 20 mM,

one obtains [PA˙] ~ 2-5 x 10^{-12} M, depending on the rate constant used for MVK + PA˙. (Table G.3 below). The resulting initiation rates, $R_{MVK+PA\cdot}$ and $R_{MVK+\cdot OH}$, are compared in Table G.3. It indicates that the reaction of MVK should be more efficient by ˙OH than by PA˙ radicals under our experimental conditions.

Table G.3. Comparison of the rates of reactions between MVK + PA˙ and MVK + ˙OH initiation steps under our experimental conditions, and for different values for the rate constants of MVK + PA˙ and PA + PA˙

Assumed rate constant for MVK + PA˙ and PA + PA˙ reactions	[PA˙] (steady state concentration) (M)	$R_{MVK+PA\cdot}$ (M s^{-1})	$R_{MVK+\cdot OH}$ (M s^{-1})
10^7 M^{-1} s^{-1}	2 x 10^{-12}	4 x 10^{-7}	10^{-6}
10^6 M^{-1} s^{-1}	4 x 10^{-12}	8 x 10^{-8}	10^{-6}
10^5 M^{-1} s^{-1}	5 x 10^{-12}	9 x 10^{-9}	10^{-6}

G.2 Bibliography:

1. Ligon, S. C.; Husar, B.; Wutzel, H.; Holman, R.; Liska, R. Strategies to reduce oxygen inhibition in photoinduced polymerization. *Chem. Rev.* **2014,** *114*, 557-589.

2. Reed Harris, A. E.; Ervens, B.; Shoemaker, R. K.; Kroll, J. A.; Rapf, R. J.; Griffith, E. C.; Monod, A.; Vaida, V. Photochemical kinetics of pyruvic acid in aqueous solution. *J. Phys. Chem. A* **2014,** *118*, 8505-8516.

Appendix H: Supporting Information for Chapter 8

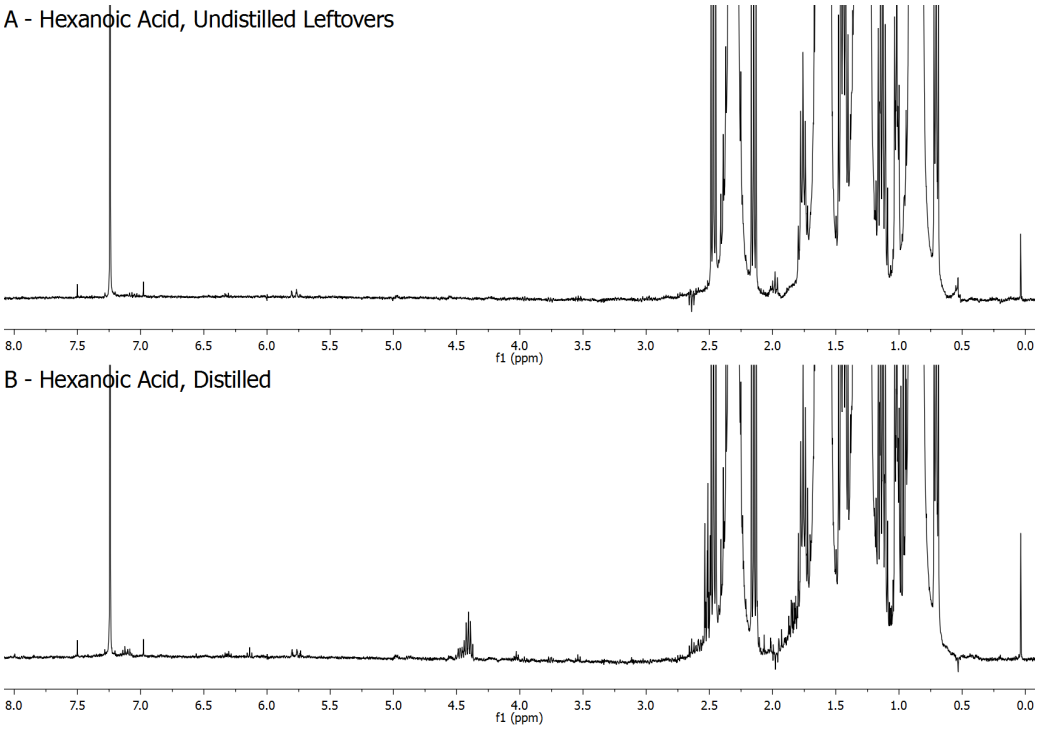

Figure H.1. Representative NMR spectra of hexanoic acid after (bottom) distillation compared to the remnant material that was left over following distillation (top).

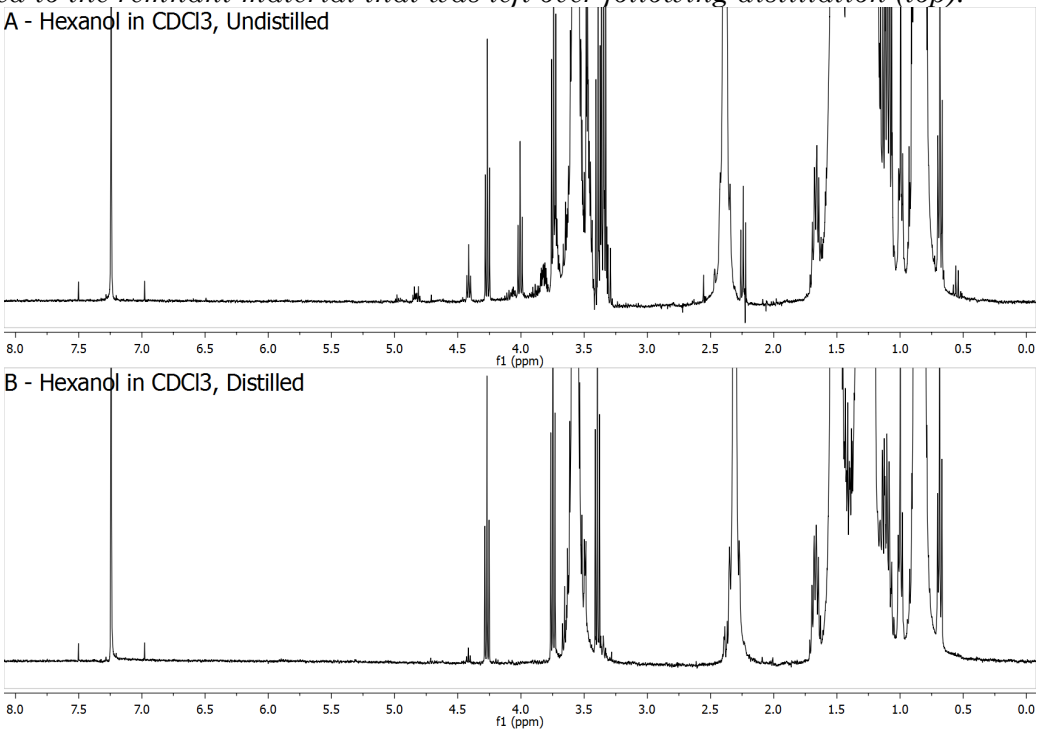

Figure H.2 Representative NMR spectra of 1-hexanol before (top) and after (bottom) distillation.

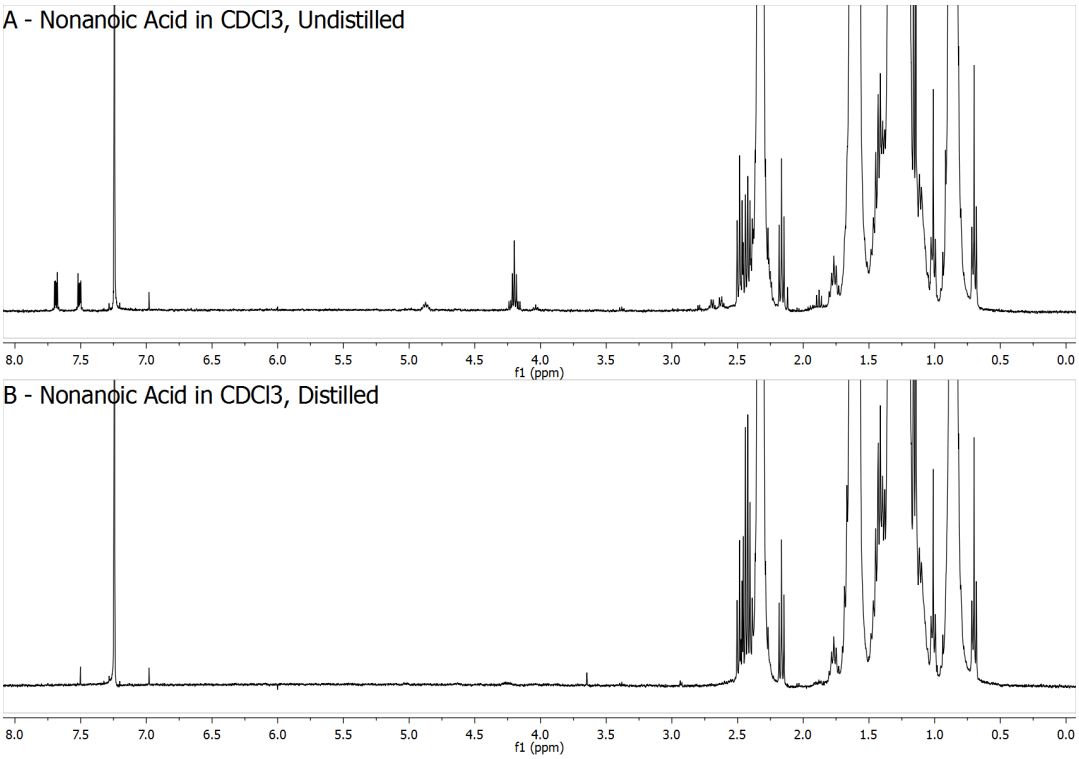

Figure H.3. Representative NMR spectra of nonanoic acid before (top) and after (bottom) distillation.

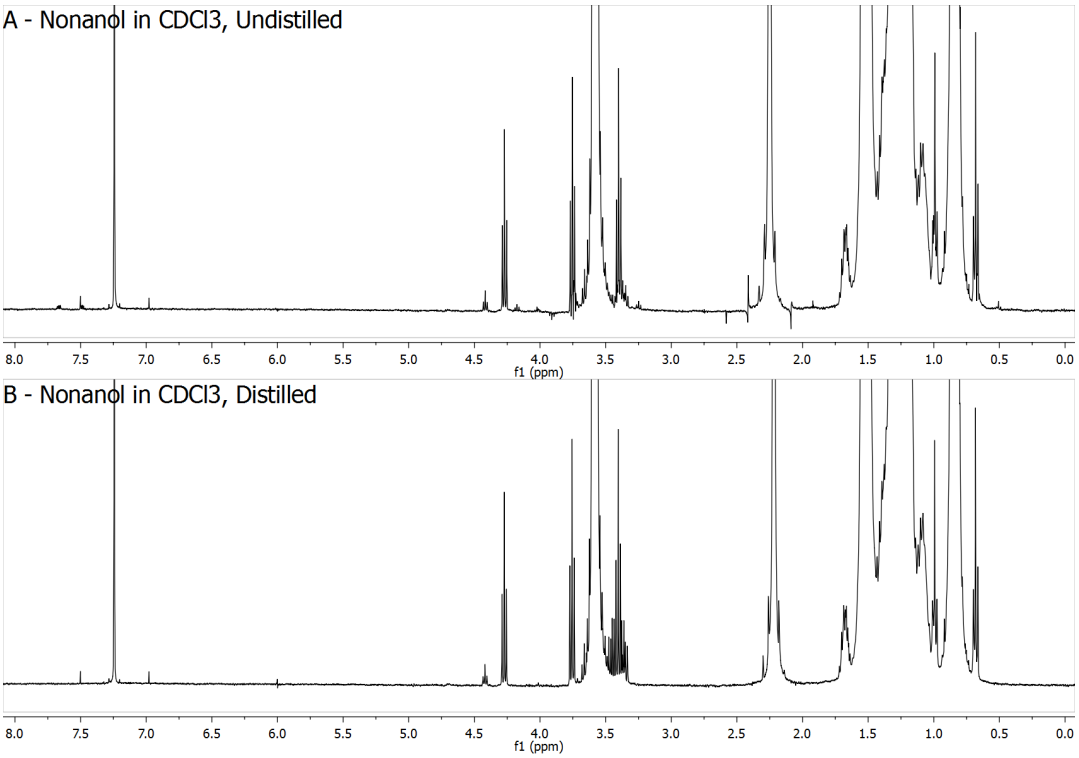

Figure H.4. Representative NMR spectra of nonanol before (top) and after (bottom) distillation.

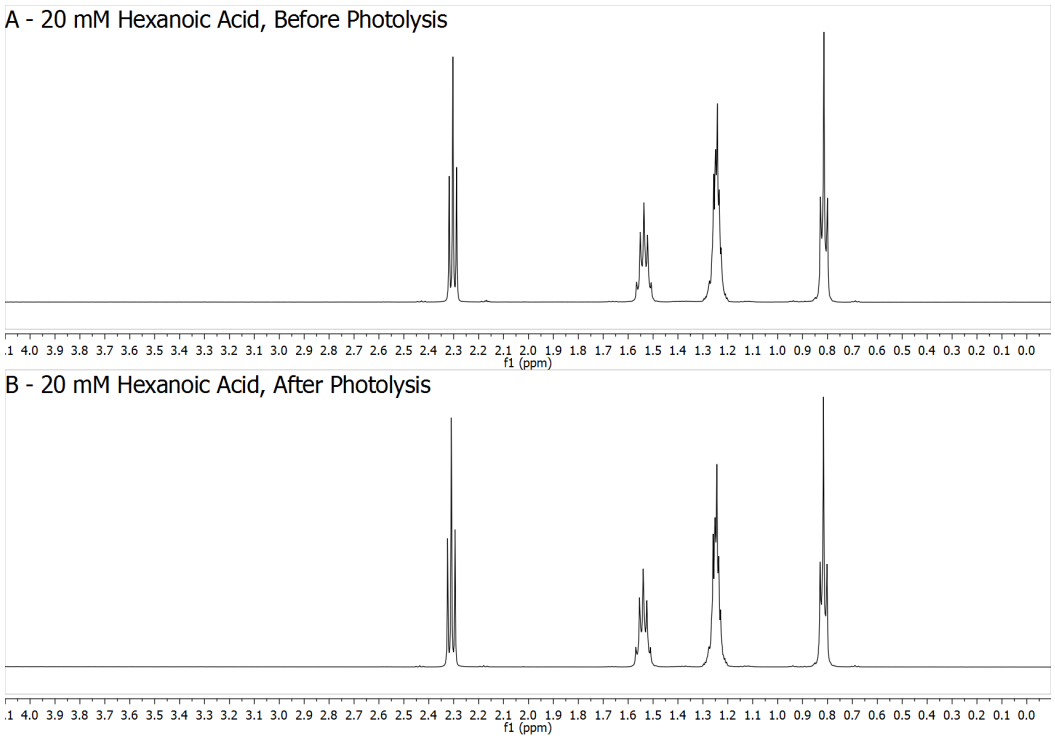

Figure H.5. Representative NMR spectra of 20 mM hexanoic acid before (top) and after (bottom) 5 hours of photolysis. No observable differences are present between the two solutions.

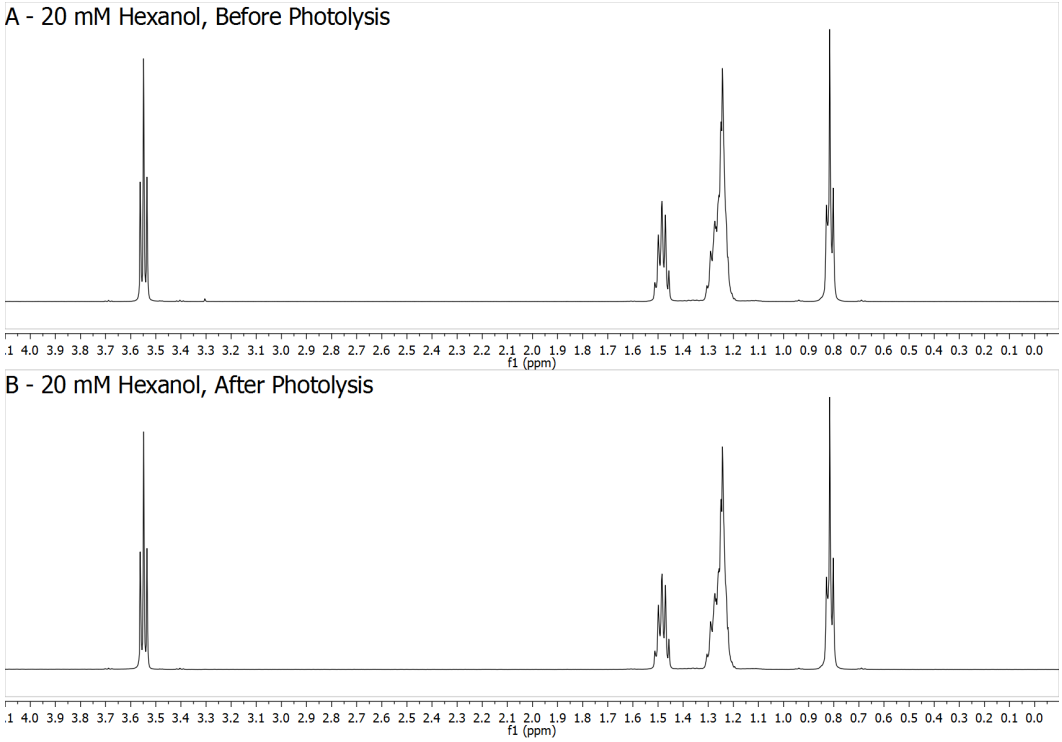

Figure H.6 NMR spectra of 20 mM hexanol before (top) and after (bottom) 5 hours of photolysis. No observable differences are present between the two solutions.

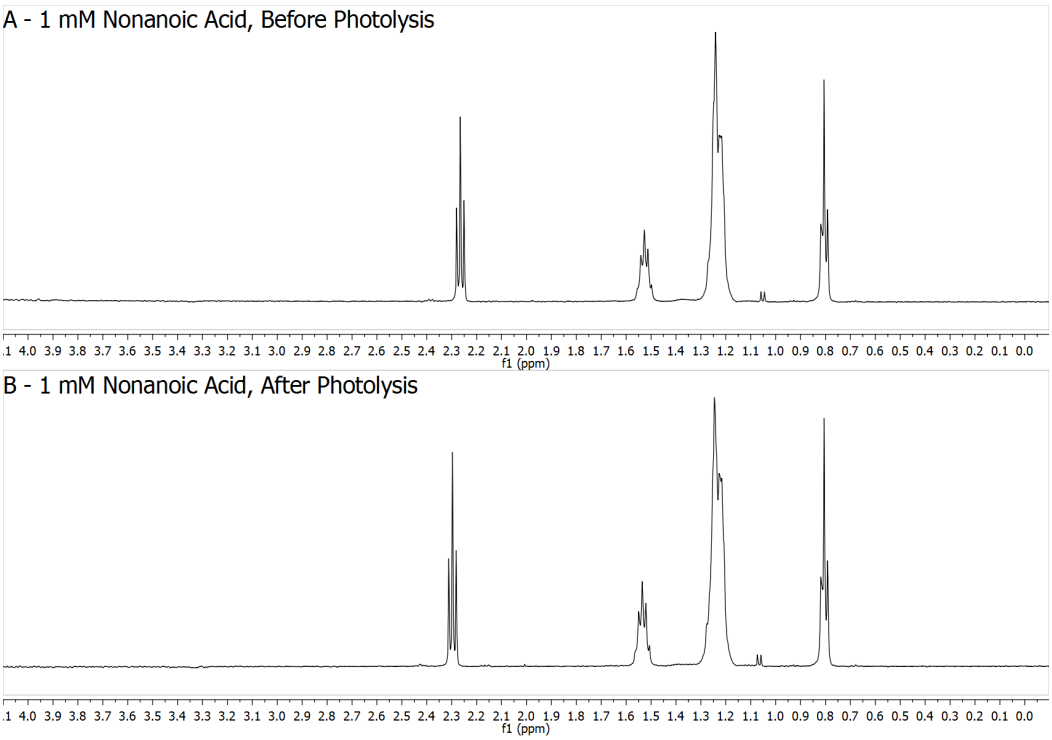

Figure H.7. Representative NMR spectra of 1 mM nonanoic acid before (top) and after (bottom) 5 hours of photolysis. No observable differences are present between the two solutions.

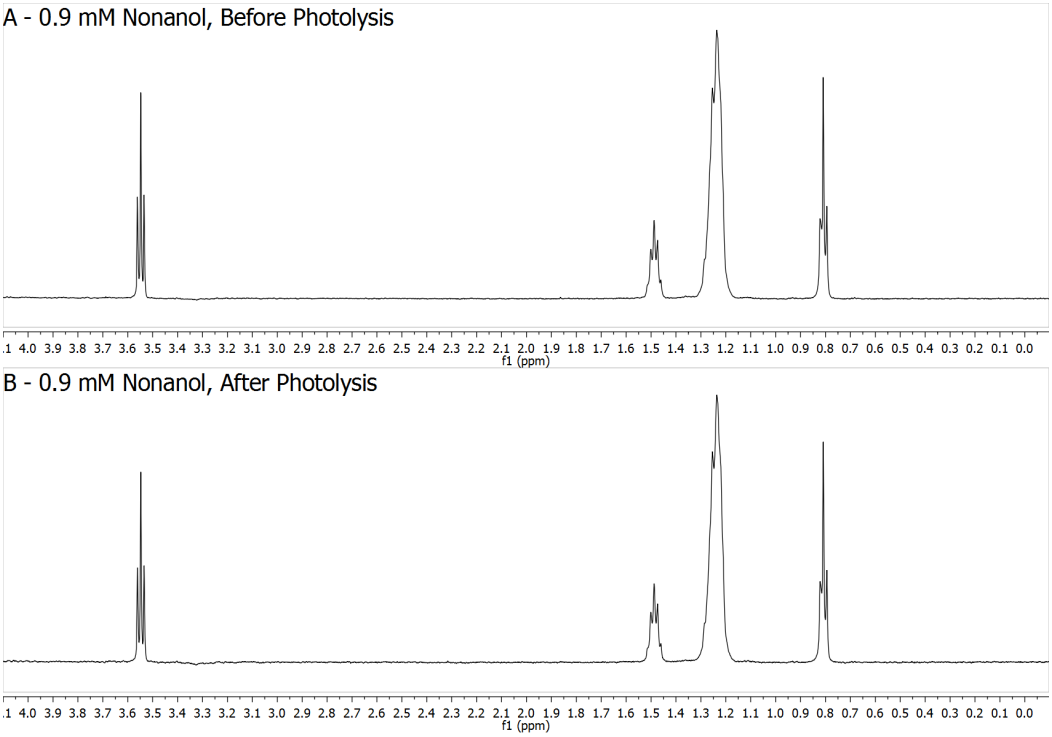

Figure H.8. Representative NMR spectra of 0.9 mM nonanol before (top) and after (bottom) 5 hours of photolysis. No observable differences are present between the two solutions.

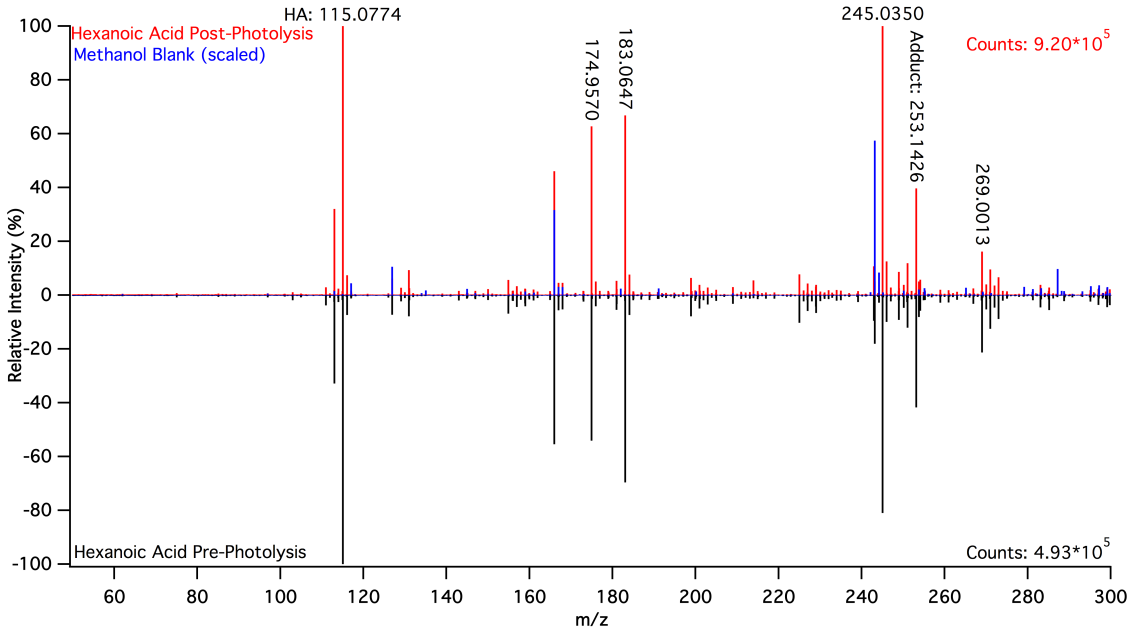

Figure H.9. Representative ESI⁻ MS of 20 mM hexanoic acid solutions before (black, multiplied by -1 for ease of presentation), after 5 hours of photolysis (red), and the corresponding methanol blank (blue). There is essentially no difference between the pre- and post-photolysis solutions.

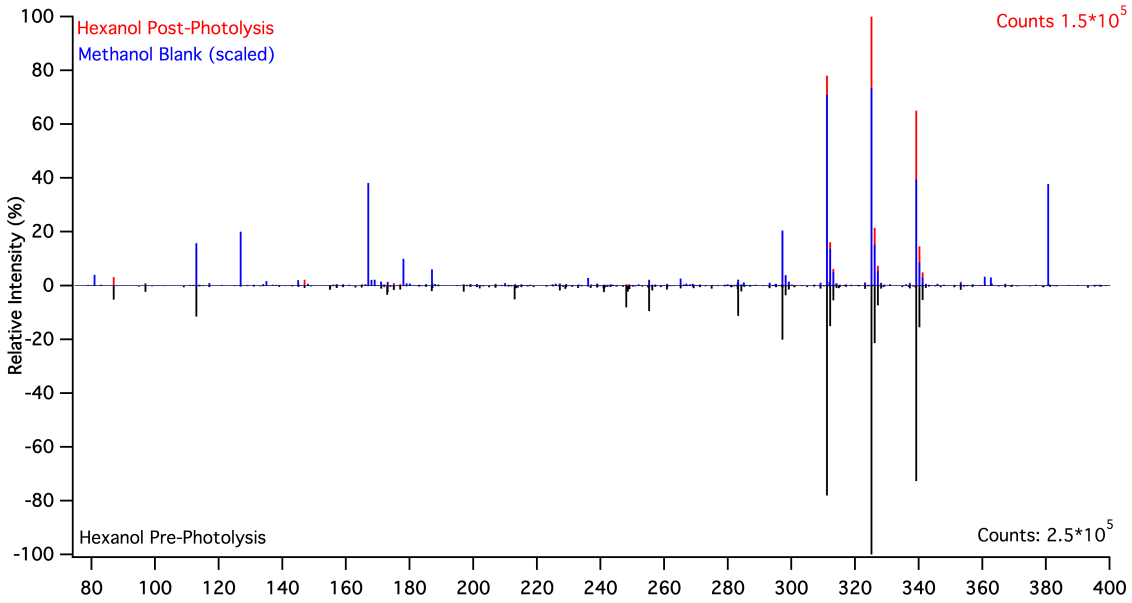

Figure H.10. Representative ESI⁻ MS of 20 mM hexanol solutions before (black, multiplied by -1 for ease of presentation), after 5 hours of photolysis (red), and the corresponding methanol blank (blue). Essentially all the observed signal is due to species also present in the methanol blank.

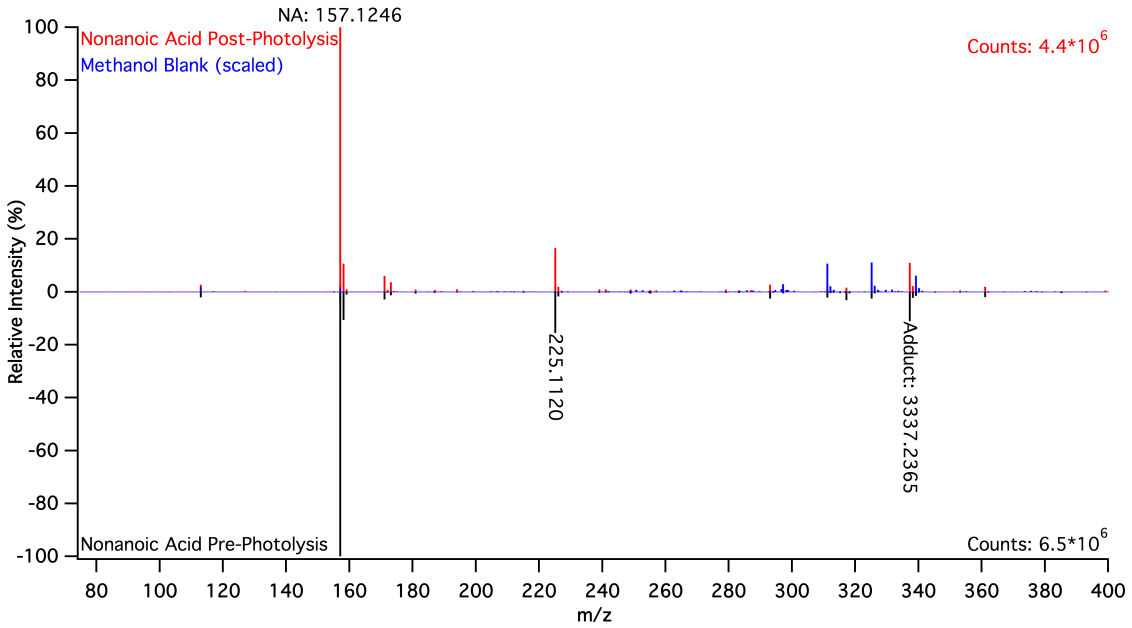

Figure H.11. Representative ESI⁻ MS of 1 mM nonanoic acid solutions before (black, multiplied by -1 for ease of presentation), after 5 hours of photolysis (red), and the corresponding methanol blank (blue). There is essentially no difference between the two samples.

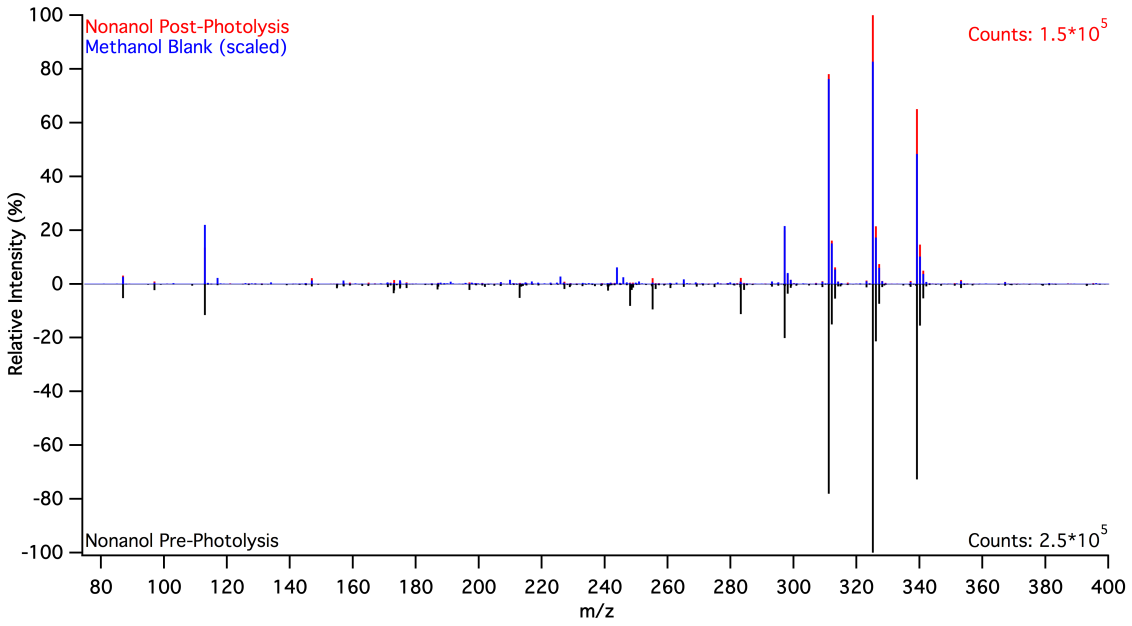

Figure H.12. Representative ESI⁻ MS of 0.9 mM nonanol solutions before (black, multiplied by -1 for ease of presentation), after 5 hours of photolysis (red), and the corresponding methanol blank (blue). Essentially all of the signal observed is due to species that are also present in the methanol blank.

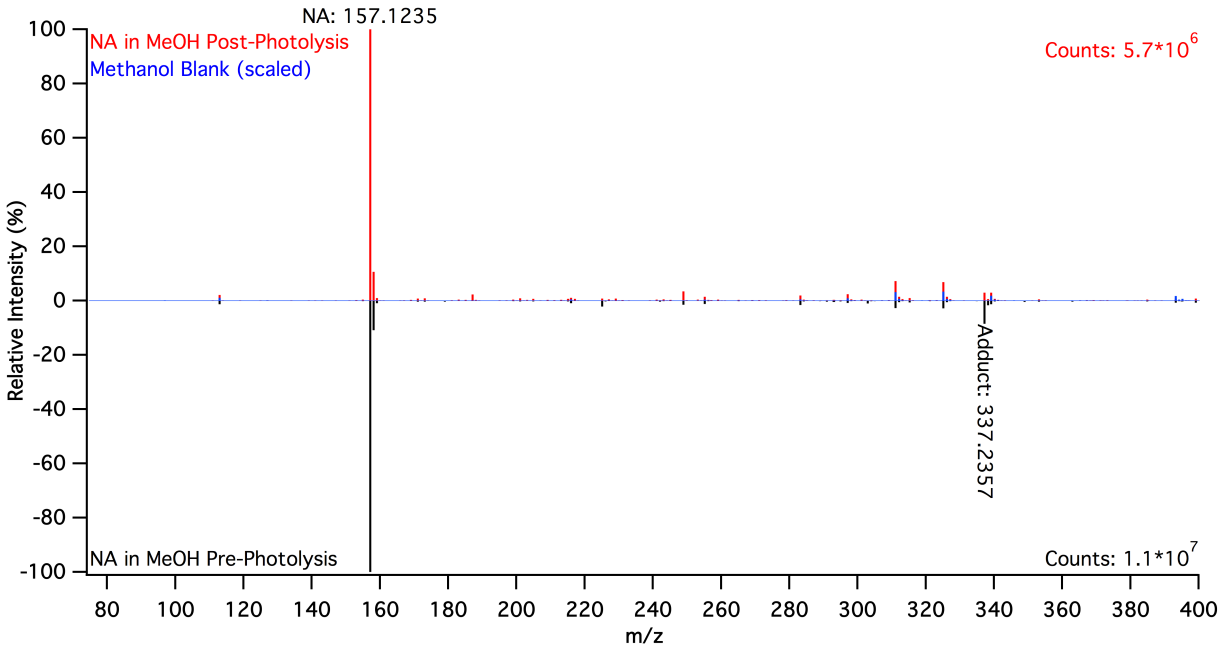

Figure H.13 Representative ESI- MS of 100 mM nonanoic acid dissolved in methanol before (black, multiplied by -1 for ease of presentation), after 5 hours of photolysis (red), and the corresponding methanol blank (blue). There is essentially no difference between the two samples.

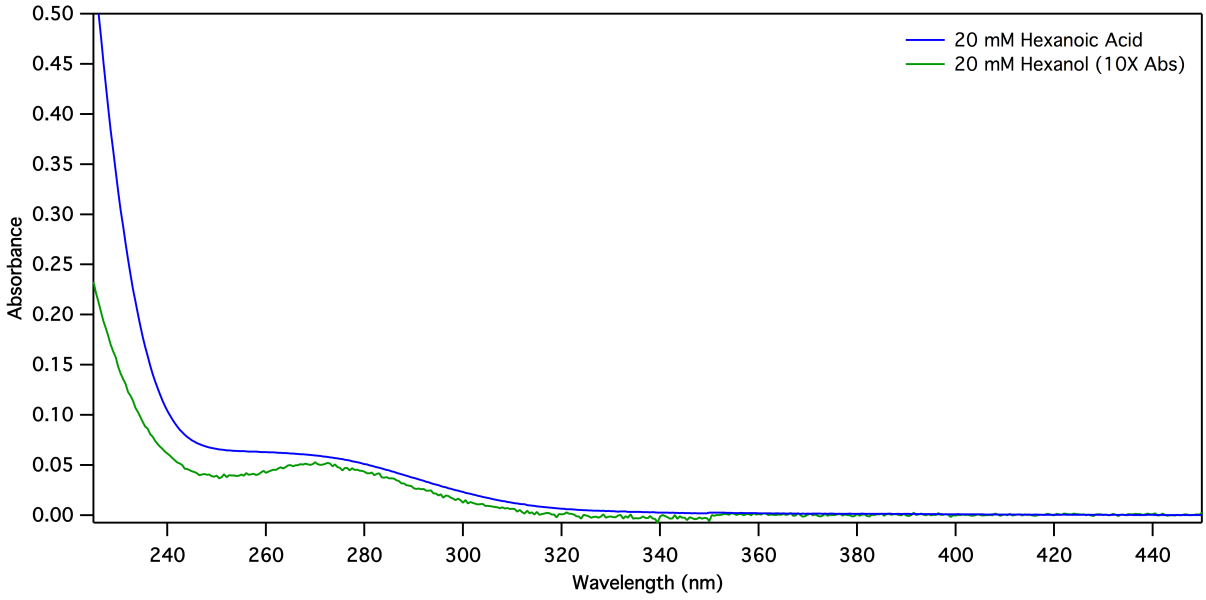

Figure H.14. Representative UV-vis absorption spectra of 20 mM hexanoic acid (blue) and 20 mM hexanol (green). The absorbance of hexanol has been multiplied by 10 for clarity.

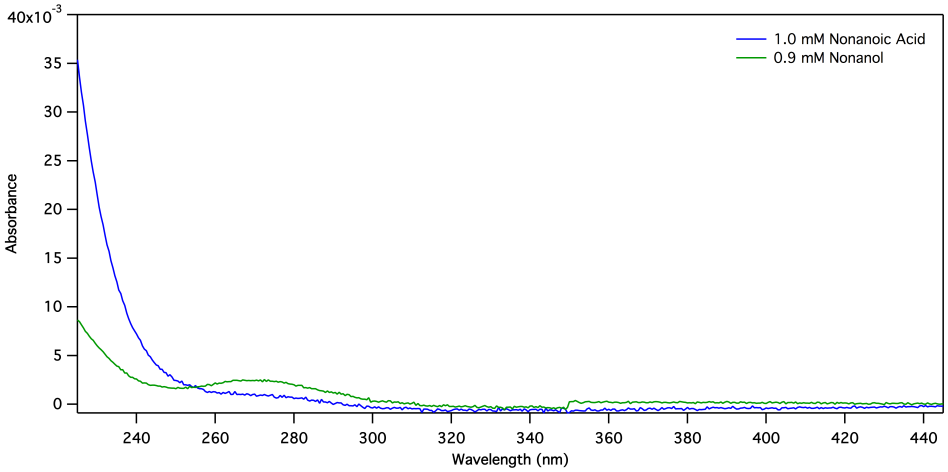

Figure H.15. Representative UV-vis absorption spectra of 1 mM nonanoic acid (blue) and 0.9 mM nonanol (green).

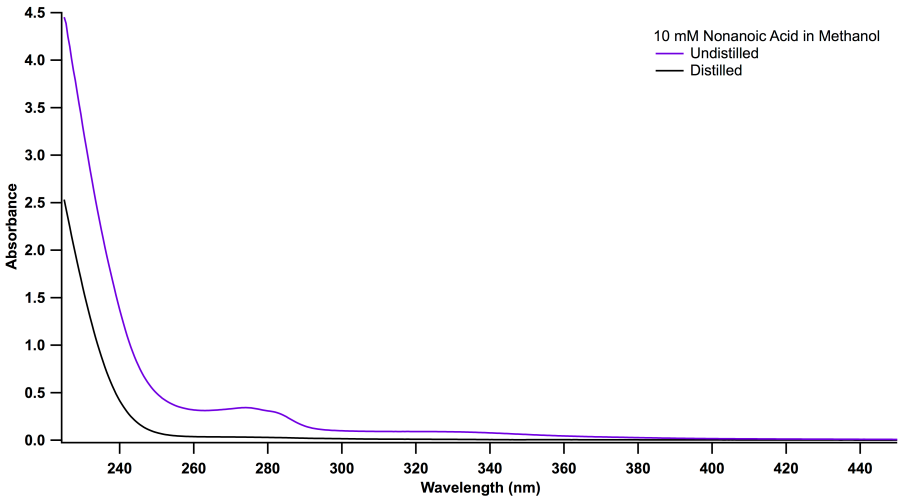

Figure H.16. Representative UV-vis absorption spectra of 10 mM nonanoic acid dissolved in methanol before (purple) and after (black) distillation.

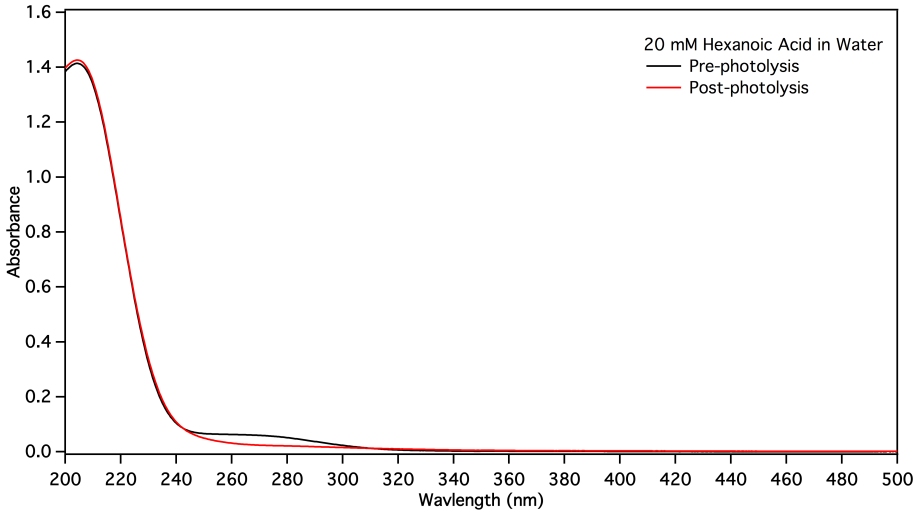

Figure H.17. UV-vis spectra of distilled 20 mM hexanoic acid before (black) and after (red) 5 hours photolysis.

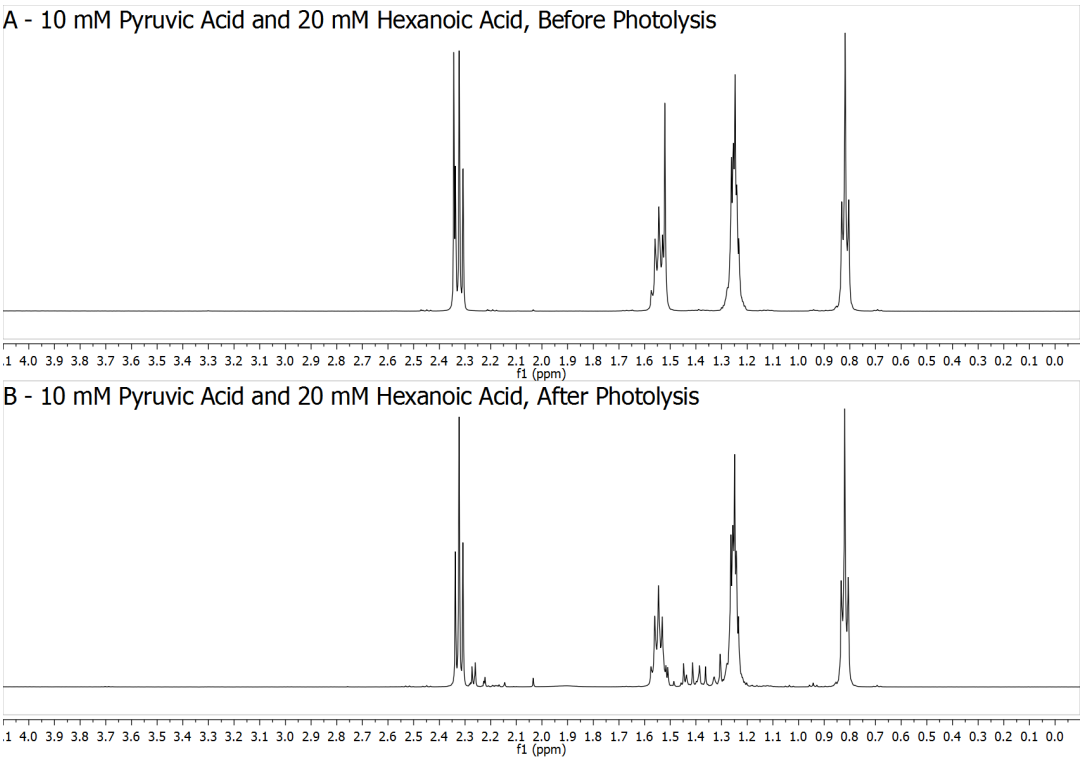

Figure H.18. Representative NMR spectra of 10 mM pyruvic acid and 20 mM hexanoic acid before (top) and after (bottom) 5 hours of photolysis.

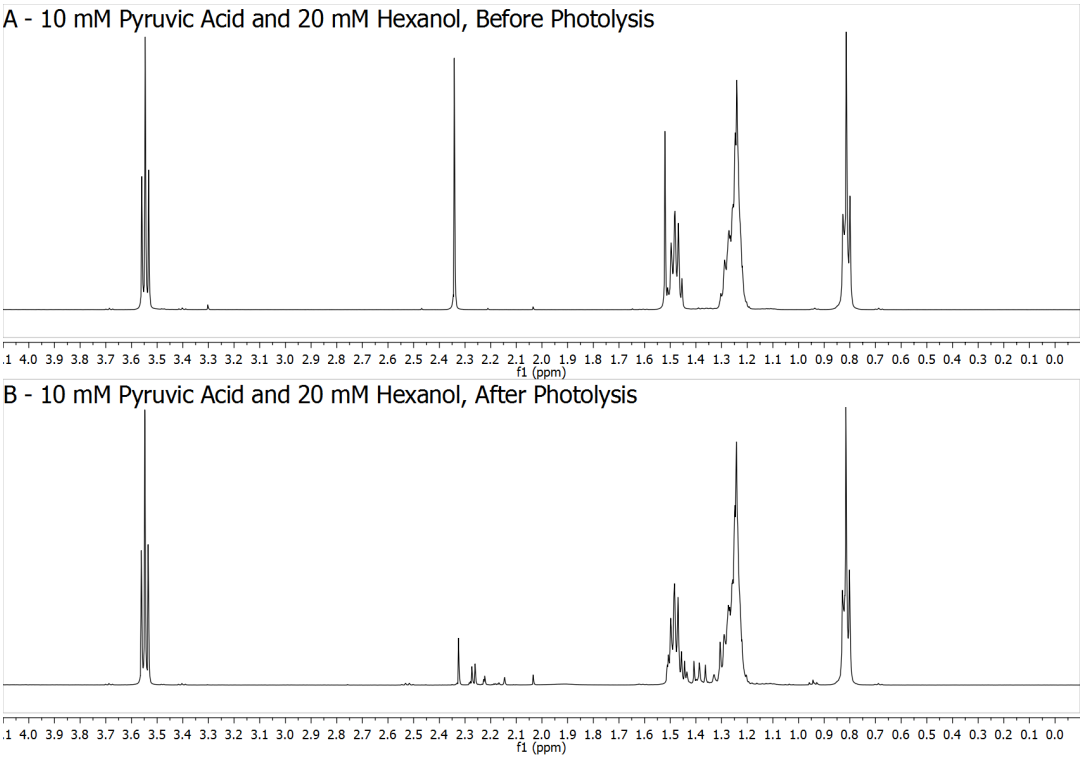

Figure H.19. Representative NMR spectra of 10 mM pyruvic acid and 20 mM hexanol before (top) and after (bottom) 5 hours of photolysis.

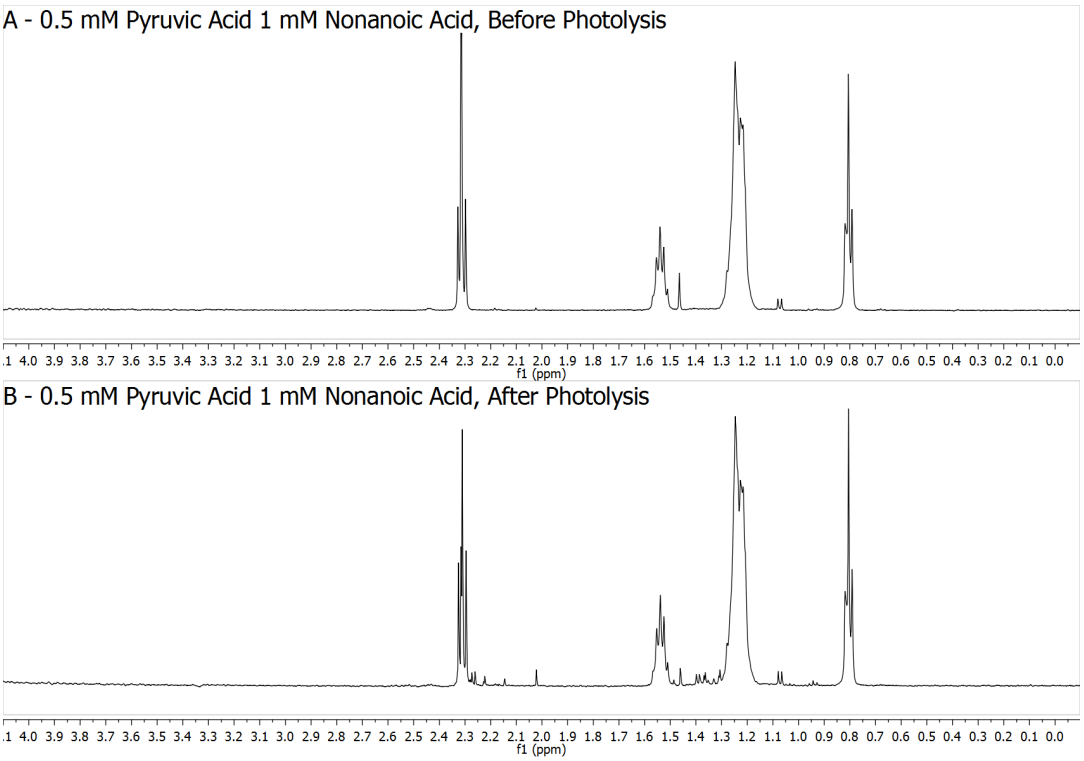

Figure H.20. Representative NMR spectra of 0.5 mM pyruvic acid and 1 mM nonanoic acid before (top) and after (bottom) 5 hours of photolysis.

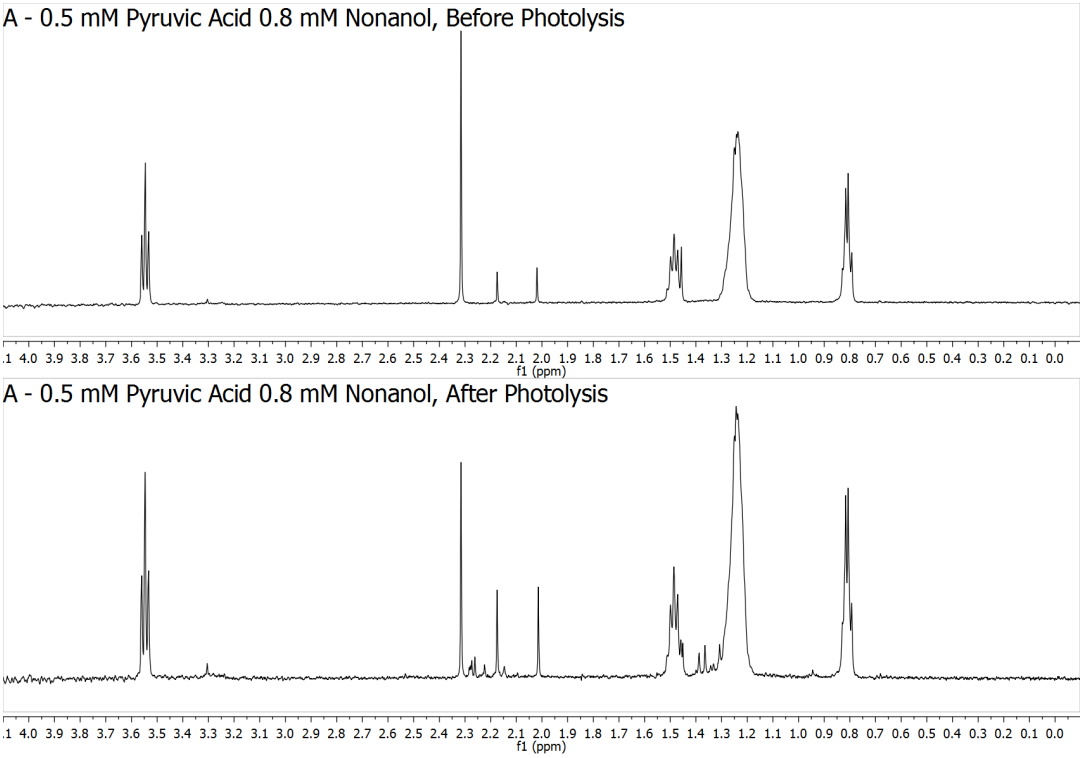

Figure H.21. Representative NMR spectra of 0.5 mM pyruvic acid and 0.8 mM nonanol before (top) and after (bottom) 5 hours of photolysis.

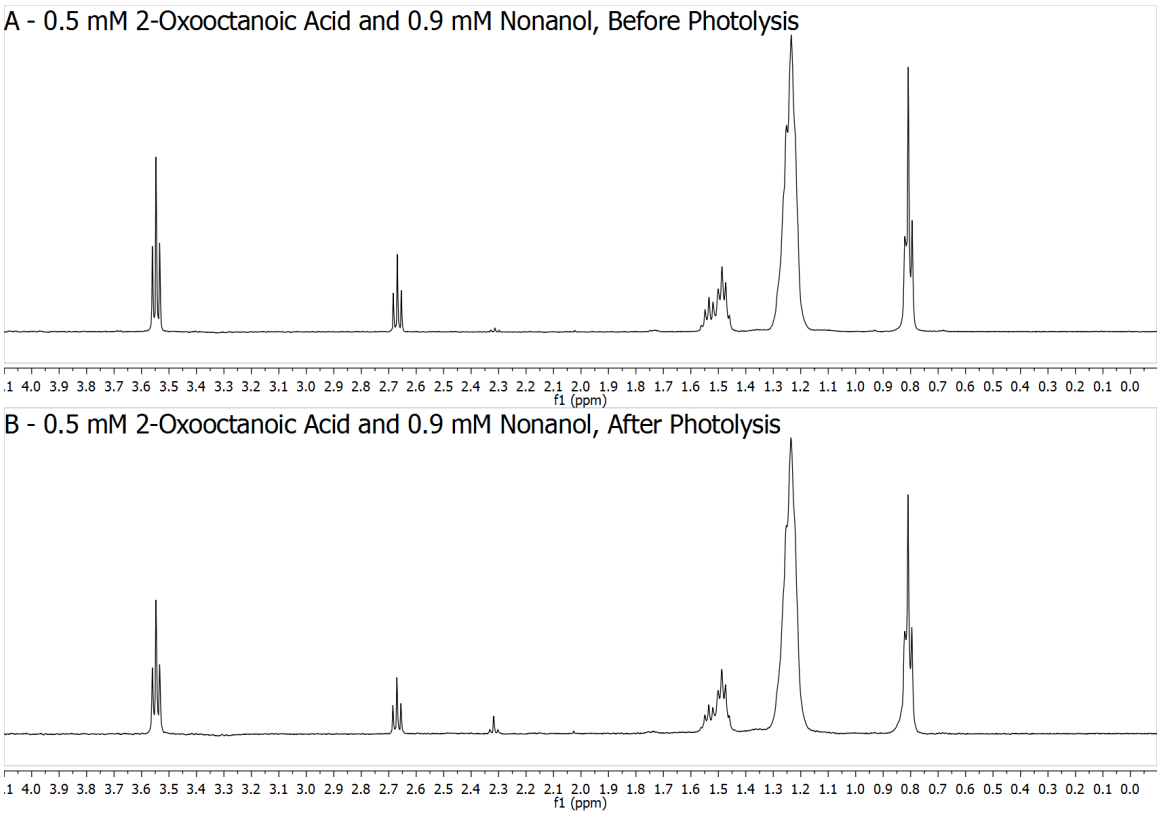

Figure H.22. Representative NMR spectra of 0.5 mM 2-oxooctanoic acid and 0.9 mM nonanol before (top) and after (bottom) 5 hours of photolysis.

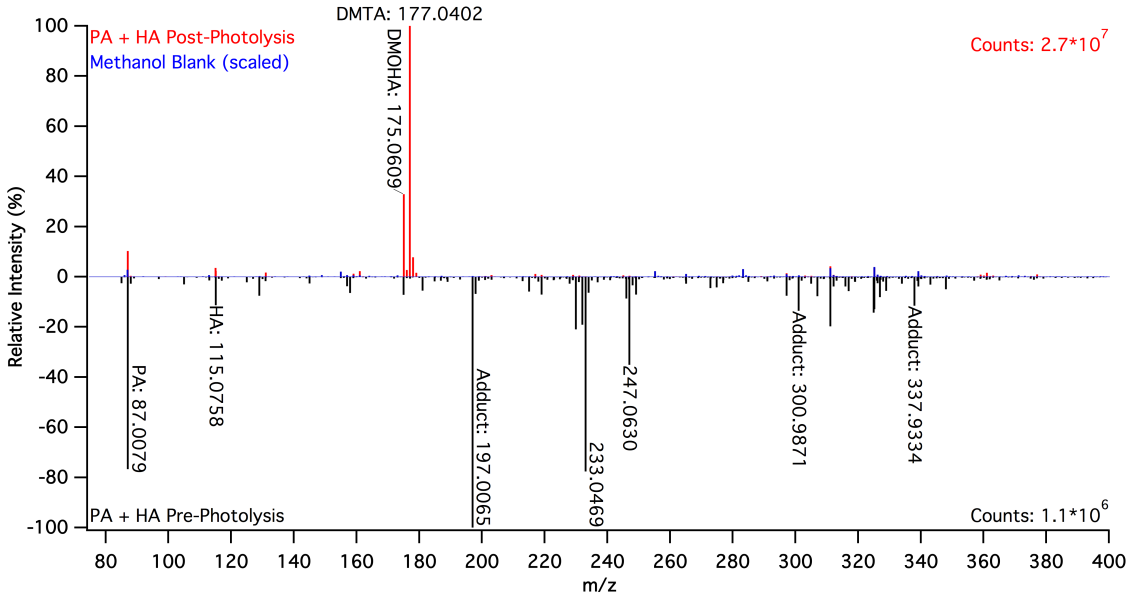

Figure H.23. Representative ESI- MS of a solution of 10 mM pyruvic acid and 20 mM hexanoic acid before (black, multiplied by -1 for ease of presentation), after 5 hours of photolysis (red), and the corresponding methanol blank (blue).

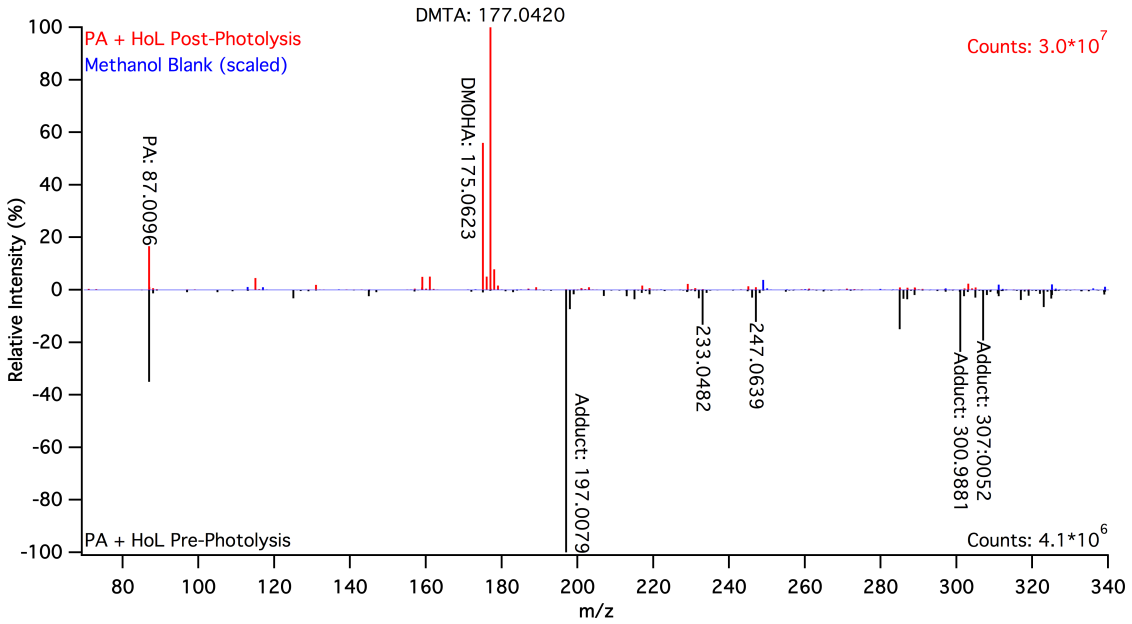

Figure H.24. Representative ESI- MS of a solution of 10 mM pyruvic acid and 20 mM hexanol before (black, multiplied by -1 for ease of presentation), after 5 hours of photolysis (red), and the corresponding methanol blank (blue).

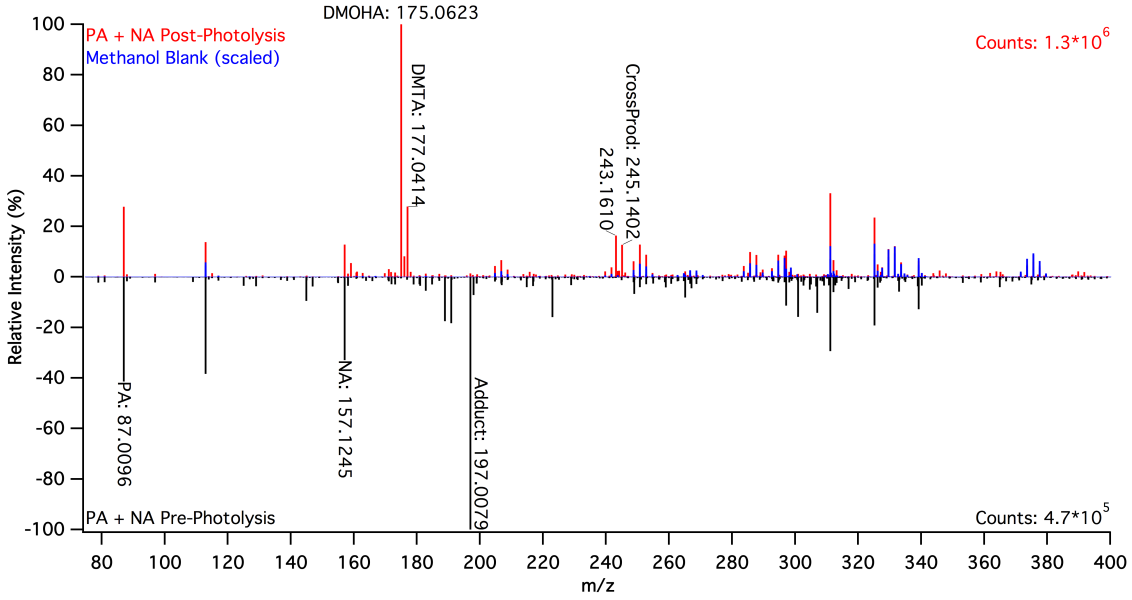

Figure H.25. Representative ESI- MS of a solution of 0.5 mM pyruvic acid and 1 mM nonanoic acid before (black, multiplied by -1 for ease of presentation), after 5 hours of photolysis (red), and the corresponding methanol blank (blue).

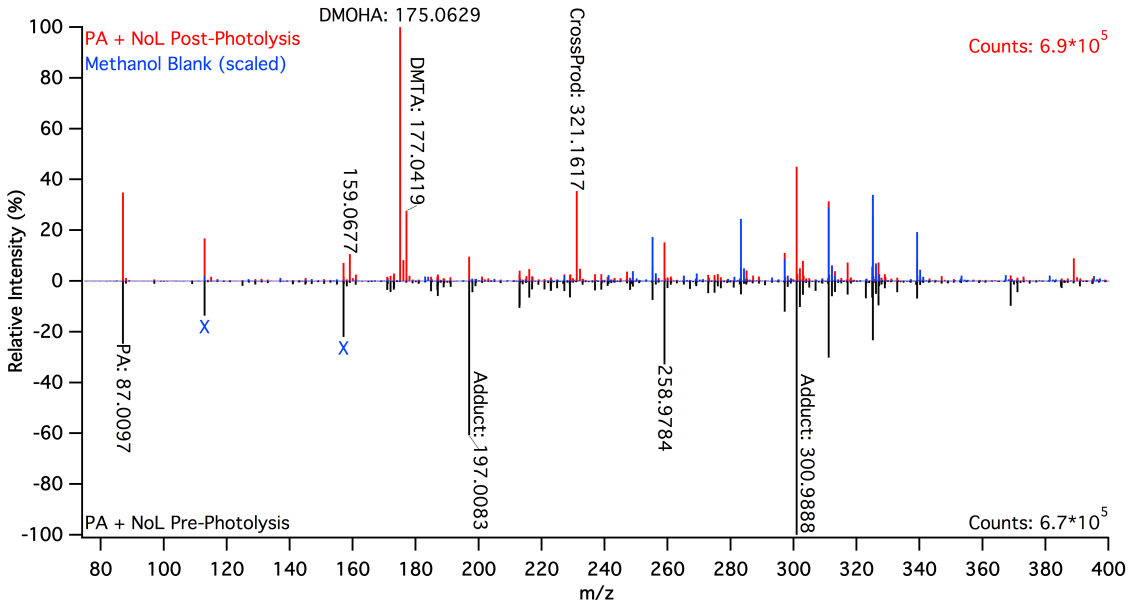

Figure H.26. Representative ESI- MS of a solution of 0.5 mM pyruvic acid and 0.8 mM nonanol before (black, multiplied by -1 for ease of presentation), after 5 hours of photolysis (red), and the corresponding methanol blank (blue). Blue X's indicate signal due to carry-over of material from previous experimental samples.

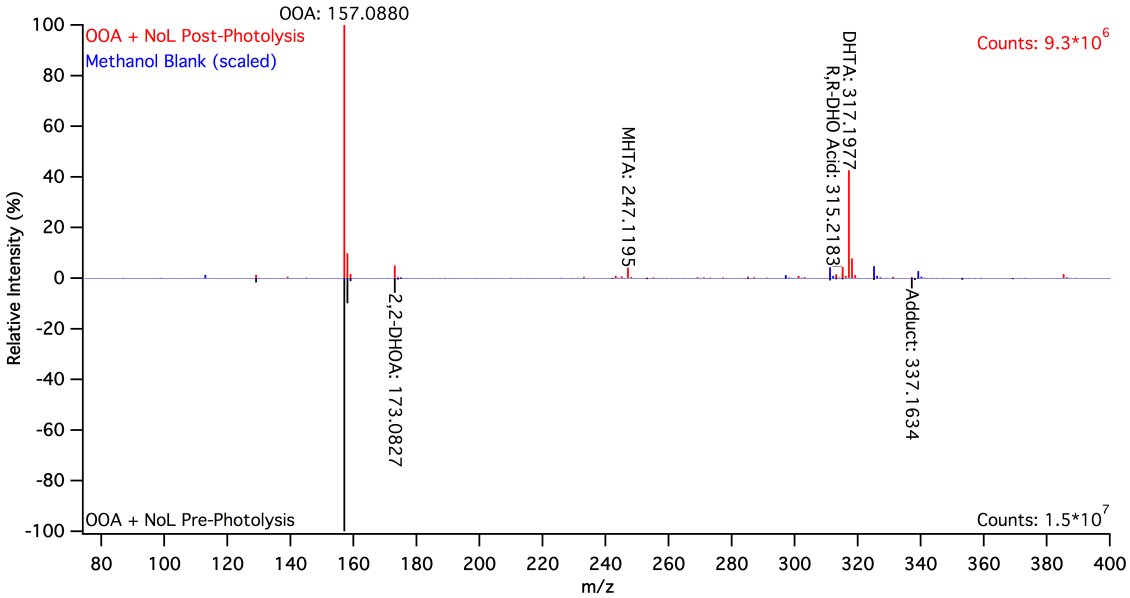

Figure H.27. Representative ESI- MS of a solution of 0.5 mM 2-oxooctanoic acid and 0.9 mM nonanol before (black, multiplied by -1 for ease of presentation) and after 5 hours of photolysis (red).

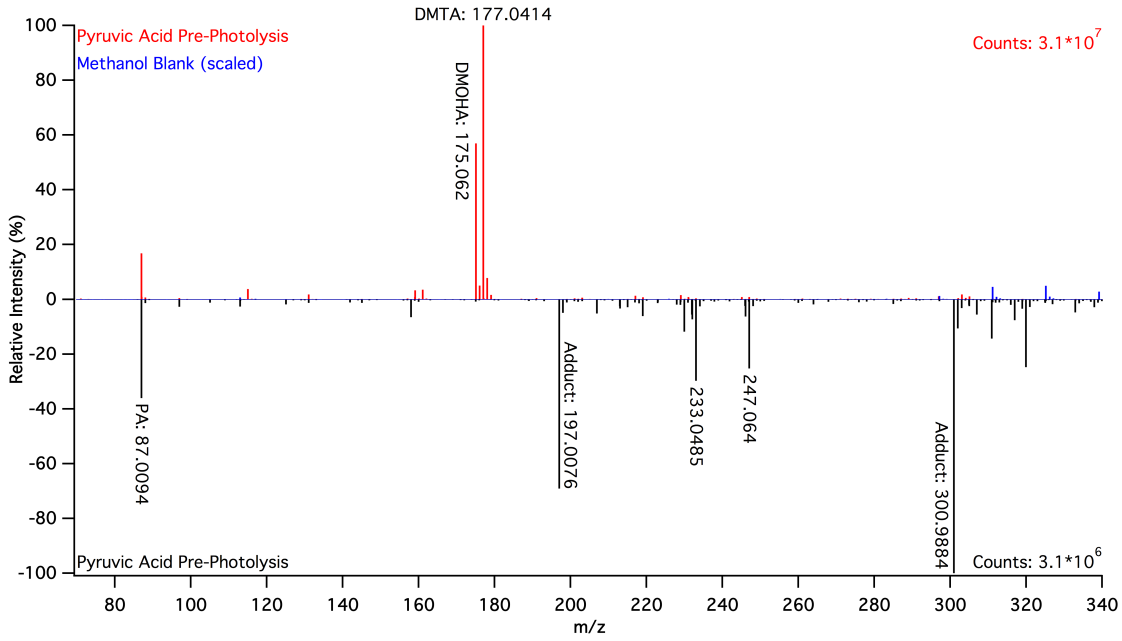

Figure H.28. Representative ESI- MS of a solution of 10 mM pyruvic acid before (black, multiplied by -1 for ease of presentation), after 5 hours of photolysis (red), and the corresponding methanol blank (blue).

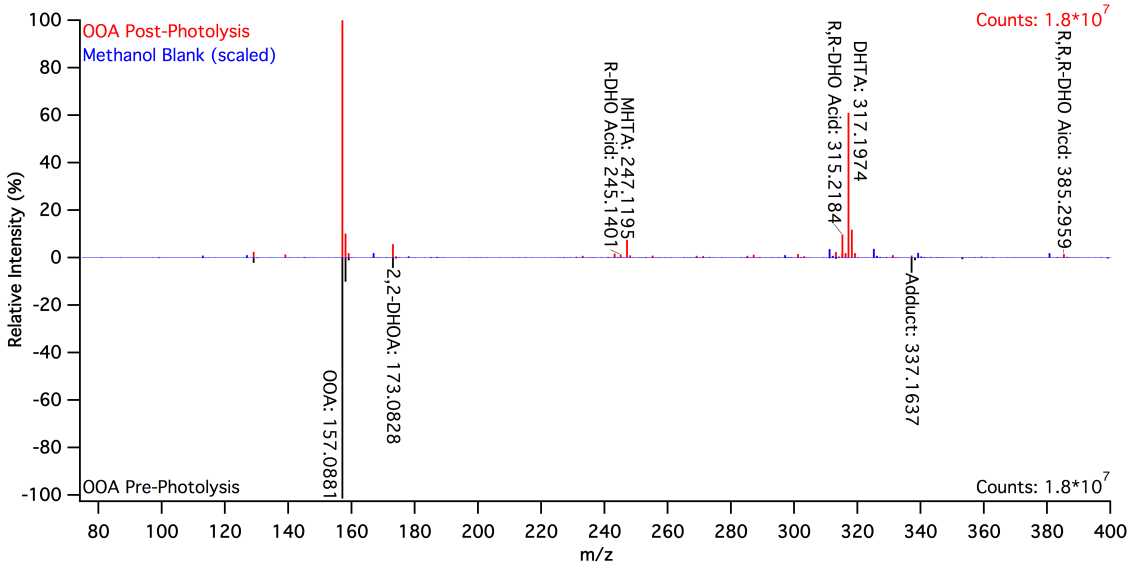

Figure H.29. Representative ESI- MS of a solution of 0.5 mM 2-oxocotanoic acid before (black, multiplied by -1 for ease of presentation), after 5 hours of photolysis (red), and the corresponding methanol blank (blue). Product species are labeled following the conventions of Chapter 5 and consist of two tartaric acid derivatives, dihexyltartaric acid (DHTA) and methylhexyltartaric acid (MHTA), as well as three dihydroxyoxoalkanoic acid species with between one and three alkyl tails (R-DHO acid, R,R-DHO acid, and R,R,R-DHO acid).

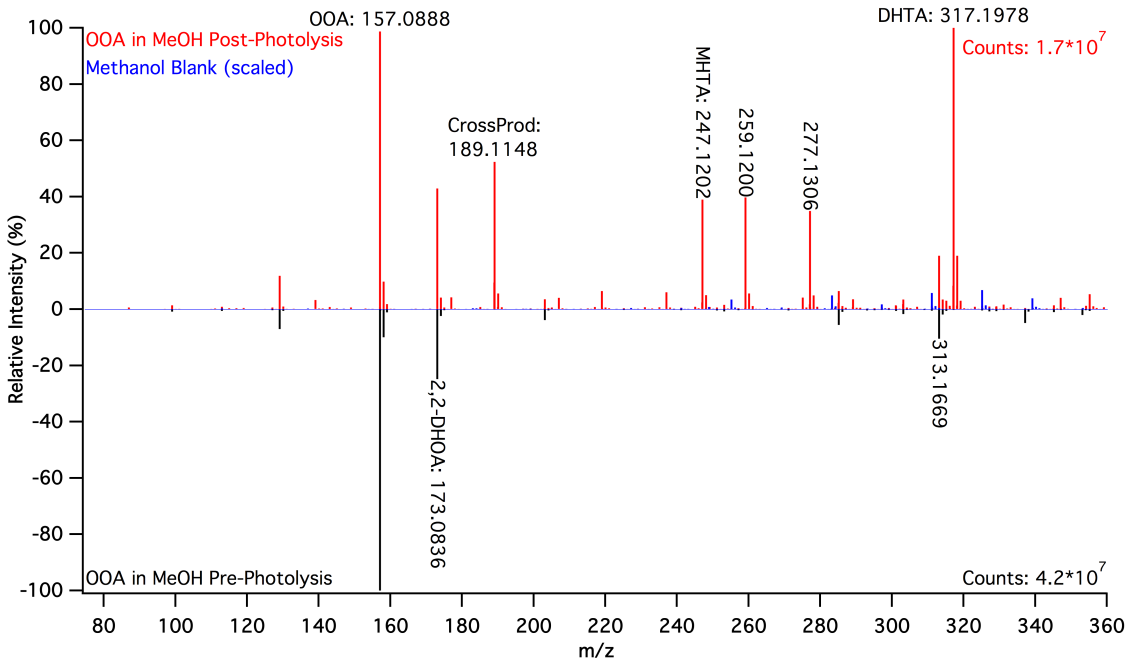

Figure H.30. Representative ESI⁻ MS of 6 mM 2-oxooctanoic acid dissolved in methanol before (black, multiplied by -1 for ease of presentation), after 5 hours of photolysis (red), and the corresponding methanol blank (blue).

Table H.1. Compiled ESI⁻ MS Data for Pyruvic Acid and Hexanoic Acid

			Pyruvic Acid		**Hexanoic Acid**		**Mixed PA + HA**	
Assigned Formula [M-H]-	Assigned Structure	Theor. m/z	Pre-hv	Post-hv	Pre-hv	Post-hv	Pre-hv	Post-hv
$C_3H_3O_3^-$	Pyruvic Acid	87.0082	S	S			S	S
$C_4H_7O_2^-$	Acetoin	87.0446		M				M
$C_3H_5O_3^-$	Lactic Acid	89.0239		W				W
$C_3H_5O_4^-$	2,2-DHPA	105.0188	W				W	
$C_5H_7O_3^-$	Unassigned	115.0395		M				M
$C_6H_{11}O_2^-$	Hexanoic Acid	115.07592			M	M	M	M
$C_5H_7O_4^-$	Acetolactic Acid	131.0345		M				M
$C_8H_{13}O_3^-$	Unassigned	157.0865						W
$C_7H_{11}O_4^-$	Unassigned	159.0658		M				M
$C_6H_9O_6^-$	Unassigned	161.0450		M				M
$C_9H_{11}O_4^-$†	Unassigned	Avg: 174.9569 ± 0.0001			M	M		

$C_6H_7O_6^-$	Parapyruvic Acid*	175.0243	W					
$C_7H_{11}O_5^-$	DMOHA	175.0607		S				S
$C_6H_9O_6^-$	Dimethyltartaric Acid	177.0400		S				S
Unidentified		Avg: 183.0647 ± 0.0001			M	M		W
Unidentified		Avg: 185.1189 ± 0.0005						W
$C_6H_6O_6Na^-$	Na Adduct of 2 PA-	197.0062	S	W			S	W
$C_9H_{15}O_5^-$	Cross-product of PA and HA	203.0920		W				M
Unidentified		Avg: 217.0719 ± 0.0006		M				M
$C_8H_{11}O_7^-$	CDMOHA	219.0505		M				M
$C_9H_{14}O_5Na^-$	Na Adduct of PA- and HA-	225.0739					W	W
$C_{10}H_{13}O_6^-$	Unassigned	229.0713		M				M
$C_9H_{11}O_7^-$	Unassigned	231.0505		M				M
$C_{10}H_{15}O_6^-$	Unassigned	231.0869		M				M
Unidentified		Avg: 233.0473 ± 0.0007	M				M	
Unidentified		Avg: 245.0350 ± 0.0000			M	M		W
Unidentified		Avg: 247.0632 ± 0.0004	S				M	
$C_{12}H_{22}O_4Na^-$	Na Adduct of HA-	253.1416			M	M	W	W
Unidentified		269.0014 ± 0.0001			M	M		
$C_{10}H_{14}O_8Na^-$	Na Adduct of PA- and DMOHA-	285.0587		M				W
$C_9H_{12}O_9Na^-$	Na Adduct of PA- and DMTA-	287.0380		W				W
$C_9H_9O_9Ca^-$	Ca Adduct of 3 PA-	300.9873	M				M	
$C_9H_9O_9Na_2^-$	Na Adduct of 3 PA-	307.0043	M				M	
Unidentified		Avg: 313.0218 ± 0.0001			M	M		
$C_{12}H_{20}O_8Na^-$	Na Adduct of DMTA- and HA-	315.1056					W	W
Unidentified		Avg: 315.1124 ± 0.0001			M	M		

Unidentified		Avg: 383.0997 ± 0.0001			M	M		
$C_{18}H_{33}O_6Ca^-$	Ca Adduct of 3 HA-	385.1903			M	M		
$C_{18}H_{33}O_6Na_2^-$	Na Adduct of 3 HA-	391.2073			W	W		

Notes: Chemical formulas are assigned as the ionized $[M-H]^-$ species, structures are assigned as the neutral species. The theoretical m/z for each species is given, where known. The experimental mass difference from this value were <15 ppm for each species assigned for each experiment, with typical values of <10 ppm. Where the peak has not been assigned, the average m/z value across experiments is given, with uncertainties given as a 95% confidence interval.
S = Strong, M = Medium, W = Weak
Blank entries indicate that the species was not observed with an intensity above the cut-off threshold, which was was set conservatively at 10^4 counts.
2,2-DHPA = 2,2-Dihydroxypropanoic Acid, diol of pyruvic acid
DMOHA = 2,4-dihydroxy-2-methyl-5-oxohexanoic acid
CDMOHA = 4-carboxy-2,4-dihydroxy 2-methyl-5-oxohexanoic acid
† Assignment is tentative
*The peak assigned to parapyruvic acid likely also has contributions from the closed ring form of the zymonic acid diol as well.

Table H.2. Compiled ESI^- MS Data for Pyruvic Acid and Hexanol

			Pyruvic Acid		**Hexanol**		**Mixed PA + HoL**	
Assigned Formula [M-H]-	Assigned Structure	Theor. m/z	Pre-hv	Post-hv	Pre-hv	Post-hv	Pre-hv	Post-hv
$C_3H_3O_3^-$	Pyruvic Acid	87.0082	S	S			S	S
$C_4H_7O_2^-$	Acetoin	87.0446		M				M
$C_3H_5O_3^-$	Lactic Acid	89.0239		W				
$C_3H_5O_4^-$	2,2-DHPA	105.0188	W				W	
$C_5H_7O_3^-$	Unassigned	115.0395		M				M
$C_5H_7O_4^-$	Acetolactic Acid	131.0345		M				M
$C_7H_{11}O_4^-$	Unassigned	159.0658		M				M
$C_6H_9O_6^-$	Unassigned	161.0450		M				M
$C_6H_7O_6^-$	Parapyruvic Acid*	175.0243	W	B.T.				B.T.
$C_7H_{11}O_5^-$	DMOHA	175.0607		S				S
$C_6H_9O_6^-$	Dimethyltartaric Acid	177.0400		S				S
$C_9H_{17}O_4^-$	Cross-product of PA and HoL	189.1127						M
$C_6H_6O_6Na^-$	Na Adduct of 2 PA-	197.0062	S	W			S	W
Unidentified		Avg: 217.0719 ± 0.0006		M				M

$C_8H_{11}O_7^-$	CDMOHA	219.0505		M				M
$C_{10}H_{13}O_6^-$	Unassigned	229.0713		M				M
$C_9H_{11}O_7^-$	Unassigned	231.0505		M				M
$C_{10}H_{15}O_6^-$	Unassigned	231.0869		M				M
Unidentified		Avg: 233.0473 ± 0.0007	M				M	
Unidentified		Avg: 247.0632 ± 0.0004	S				M	
$C_{10}H_{14}O_8Na^-$	Na Adduct of PA- and DMOHA-	285.0587		M				W
$C_9H_{12}O_9Na^-$	Na Adduct of PA- and DMTA-	287.0380		W				W
$C_9H_9O_9Ca^-$	Ca Adduct of 3 PA-	300.9873	M				M	W
$C_9H_9O_9Na_2^-$	Na Adduct of 3 PA-	307.0043	M				M	

Table H.3. Compiled ESI$^-$ MS Data for Pyruvic Acid and Nonanoic Acid

			Pyruvic Acid		**Nonanoic Acid**		**Mixed PA + NA**	
Assigned Formula [M-H]-	Assigned Structure	Theor. m/z	Pre-hv	Post-hv	Pre-hv	Post-hv	Pre-hv	Post-hv
$C_3H_3O_3^-$	Pyruvic Acid	87.0082	M	M			M	M
$C_4H_7O_2^-$	Acetoin	87.0446		W				W
$C_5H_7O_3^-$	Unassigned	115.0395		W				W
$C_5H_7O_4^-$	Acetolactic Acid	131.0345		W				
$C_9H_{17}O_2^-$	Nonanoic Acid	157.1229			S	S		
$C_7H_{11}O_4^-$	Unassigned	159.0658		W				W
$C_6H_9O_6^-$	Unassigned	161.0450						W
$C_6H_7O_6^-$	Parapyruvic Acid*	175.0243	W					
$C_7H_{11}O_5^-$	DMOHA	175.0607		S				S
$C_6H_9O_6^-$	Dimethyltartaric Acid	177.0400		M				M
$C_6H_6O_6Na^-$	Na Adduct of 2 PA-	197.0062	M	M			M	M
Unidentified		Avg: 217.0719 ± 0.0006		W				W

Unidentified		Avg: 225.1115 ± 0.0004			M	M		
$C_{10}H_{13}O_6^-$	Unassigned	229.0713						W
$C_{10}H_{15}O_6^-$	Unassigned	231.0869						W
Unidentified		Avg: 243.1607						M
$C_{12}H_{21}O_5^-$	Cross-Product of PA + NA	245.1389						M
$C_{10}H_{14}O_8Na^-$	Na Adduct of PA- and DMOHA-	285.0587		W				W
$C_9H_{12}O_9Na^-$	Na Adduct of PA- and DMTA-	287.0380		W				W
Unidentified		Avg: 293.0985 ± 0.0004			W	W		
$C_9H_9O_9Ca^-$	Ca Adduct of 3 PA-	300.9873	M	M			W	W
$C_9H_9O_9Na_2^-$	Na Adduct of 3 PA-	307.0043	W	W			W	
$C_{18}H_{34}O_4Na^-$	Na Adduct of 2 NA-	337.2355			M	M	W	
Unidentified		Avg: 403.2355 ± 0.0004			M	M		
Unidentified		Avg: 473.2107 ± 0.0004			M	M		
$C_{27}H_{51}O_6Ca^-$	Ca Adduct of 3 NA-	511.3312			W	W		
$C_{27}H_{51}O_6Na_2^-$	Na Adduct of 3 NA-	517.3481			M	M		

Table H.4. Compiled ESI$^-$ MS Data for Pyruvic Acid and Nonanol

			Pyruvic Acid		**Nonanol**		**Mixed PA + NoL**	
Assigned Formula [M-H]-	Assigned Structure	Theor. m/z	Pre-hv	Post-hv	Pre-hv	Post-hv	Pre-hv	Post-hv
$C_3H_3O_3^-$	Pyruvic Acid	87.0082	M	M			M	M
$C_4H_7O_2^-$	Acetoin	87.0446		W				
$C_5H_7O_3^-$	Unassigned	115.0395		W				W
$C_5H_7O_4^-$	Acetolactic Acid	131.0345		W				
$C_7H_{11}O_4^-$	Unassigned	159.0658		W				W
$C_6H_9O_6^-$	Unassigned	161.0450						W
$C_6H_7O_6^-$	Parapyruvic Acid*	175.0243	W					

$C_7H_{11}O_5^-$	DMOHA	175.0607		S				S
$C_6H_9O_6^-$	Dimethyltartaric Acid	177.0400		M				M
$C_6H_6O_6Na^-$	Na Adduct of 2 PA-	197.0062	M	M			M	W
Unidentified		Avg: 217.0719 ± 0.0006		W				W
$C_{12}H_{23}O_4^-$	Cross Product of PA and NoL	231.1597						M
Unidentified		Avg: 258.9780					W	W
$C_{10}H_{14}O_8Na^-$	Na Adduct of PA- and DMOHA-	285.0587		W				W
$C_9H_{12}O_9Na^-$	Na Adduct of PA- and DMTA-	287.0380		W				W
$C_9H_9O_9Ca^-$	Ca Adduct of 3 PA-	300.9873	M	M			M	W
$C_9H_9O_9Na_2^-$	Na Adduct of 3 PA-	307.0043	W	W			W	

Table H.5. Compiled ESI⁻ MS Data for OOA and Nonanol

			2-Oxooctanoic Acid		**Nonanol**		**Mix. OOA + NoL**	
Assigned Formula [M-H]-	Assigned Structure	Theor. m/z	Pre-hv	Post-hv	Pre-hv	Post-hv	Pre-hv	Post-hv
$C_3H_3O_3^-$	Pyruvic Acid	87.0082		W				W
$C_7H_{13}O_2^-$	Heptanoic Acid	129.0916	M	M			M	M
$C_8H_{11}O_2^-$	Unassigned	139.0759		M				W
$C_8H_{13}O_3^-$	2-Oxooctanoic Acid	157.0865	S	S			S	S
$C_9H_{17}O_2^-$	Nonanoic Acid	157.1229	W	W				
$C_8H_{13}O_4^-$	2,2-DHOA	173.0814	M	M			M	M
$C_6H_9O_6^-$	Dimethyltartaric Acid	177.0400		W				
$C_{14}H_{27}O_2^-$	8-hydroxy-tetradecan-7-one	227.2011		W				
$C_{11}H_{17}O_6^-$	R-PPA	245.1026		W				
$C_{12}H_{21}O_5^-$	R-DHO Acid	245.1389		M				W
$C_{11}H_{19}O_6^-$	Methylhexyl-tartaric Acid	247.1182		S				M
$C_{15}H_{27}O_3^-$	Unassigned	255.1960		M				W

Unidentified		Avg: 269.1763 ± 0.0004		M				W
$C_{15}H_{27}O_4^-$	8-C-8-H-tetradecan-7-one	271.1910		M				W
$C_{15}H_{29}O_4^-$	Unassigned	273.2066		W				W
$C_{13}H_{28}O_5Na^-$†	Unassigned	287.1835		W				W
$C_{13}H_{21}O_7^-$	R-DHO Diacid	289.1288		W				
$C_{17}H_{33}O_4^-$	Cross Product of OOA and NoL	301.2379						M
$C_{16}H_{25}O_6^-$	R,R-DODA	313.1652	M	M			W	M
$C_{16}H_{28}O_6^-$	R,R-PPA	315.1808	W	W			W	W
$C_{17}H_{31}O_5^-$	R,R-DHO Acid	315.2172		S				M
$C_{16}H_{29}O_6^-$	Dihexyltartaric Acid	317.1965		S				S
$C_{16}H_{26}O_6Na^-$	Na Adduct of 2 OOA-	337.1627	S	M			M	M
$C_{16}H_{26}O_7Na^-$	Na Adduct of OOA- and OOA Diol-	353.1577	M	W			W	
$C_{18}H_{31}O_7^-$	R,R-DHO Diacid	359.2070		W				W
$C_{22}H_{41}O_5^-$	R,R,R-DHO Acid	385.2954		M				W
$C_{23}H_{41}O_7^-$	R,R,R-DHO Diacid	429.2860		W				
$C_{26}H_{41}O_9^-$	Unassigned	497.2751		W				W
$C_{24}H_{39}O_9Ca^-$	Ca Adduct of 3 OOA-	511.2221	M	W			M	M
$C_{24}H_{39}O_9Na_2^-$	Na Adduct of 3 OOA-	517.2390	M				W	W

Notes: Chemical formulas are assigned as the ionized $[M-H]^-$ species, structures are assigned as the neutral species. The theoretical m/z for each species is given, where known. The experimental mass difference from this value were <15 ppm for each species assigned for each experiment, with typical values of <10 ppm. Where the peak has not been assigned, the average m/z value across experiments is given, with uncertainties given as a 95% confidence interval.

S = Strong, M = Medium, W = Weak

Blank entries indicate that the species was not observed with an intensity above the cut-off threshold, which was was set conservatively at 10^4 counts.

2,2-DHOA = 2,2-Dihydroxyoctanoic Acid, Diol of OOA

DMOHA = 2,4-dihydroxy-2-methyl-5-oxohexanoic acid

8-C-8-H-tetradecan-7-one = 8-carboxy-8-hydroxy-tetradecan-7-one

† Assignment is tentative

Table H.6. Compiled ESI⁻ MS Data for OOA Dissolved in Methanol

			OOA in MeOH	
Assigned Formula [M-H]-	Assigned Structure	Theor. m/z	Pre-hv	Post-hv
$C_3H_3O_3^-$	Pyruvic Acid	87.0082		M
$C_7H_{13}O_2^-$	Heptanoic Acid	129.0916	S	S
$C_8H_{11}O_2^-$	Unassigned	139.0759		M
$C_8H_{13}O_3^-$	2-Oxooctanoic Acid	157.0865	S	S
$C_9H_{17}O_2^-$	Nonanoic Acid	157.1229	W	W
$C_8H_{13}O_4^-$	2,2-DHOA	173.0814	S	S
$C_7H_{11}O_5^-$	DMOHA	175.0607		W
$C_6H_9O_6^-$	Dimethyltartaric Acid	177.0400		M
$C_9H_{17}O_4^-$	Cross Product of OOA and MeOH	189.1127	W	S
$C_{11}H_{19}O_4^-$	Unassigned	203.1284	M	M
Unidentified		207.0525		M
Unidentified		219.0527		M
$C_{14}H_{27}O_2^-$	8-hydroxy-tetradecan-7-one	227.2011		W
Unidentified		237.0631		M
$C_{11}H_{17}O_6^-$	R-PPA	245.1026		W
$C_{12}H_{21}O_5^-$	R-DHO Acid	245.1389		M
$C_{11}H_{19}O_6^-$	Methylhexyl-tartaric Acid	247.1182		S
$C_{15}H_{27}O_3^-$	Unassigned	255.1960		M
$C_{12}H_{19}O_6^-$	Unassigned	259.1182		S
Unidentified		Avg: 269.1763 ± 0.0004		M
$C_{15}H_{27}O_4^-$	8-C-8-H-tetradecan-7-one	271.1910		M
$C_{15}H_{29}O_4^-$	Unassigned	273.2066		W
Unidentified		275.1509		M
Unidentified		277.1306		S
Unidentified		285.1718	M	M
$C_{13}H_{28}O_5Na^-$*	Unassigned	287.1835		W

$C_{13}H_{21}O_7^-$	R-DHO Diacid	289.1288		W
$C_{16}H_{25}O_6^-$	R,R-DODA	313.1652	M	M
$C_{16}H_{28}O_6^-$	R,R-PPA	315.1808	W	W
$C_{17}H_{31}O_5^-$	R,R-DHO Acid	315.2172		S
$C_{16}H_{29}O_6^-$	Dihexyltartaric Acid	317.1965		S
$C_{16}H_{26}O_6Na^-$	Na Adduct of 2 OOA-	337.1627	S	M
$C_{16}H_{26}O_7Na^-$	Na Adduct of OOA- and OOA Diol-	353.1577	M	W
$C_{18}H_{31}O_7^-$	R,R-DHO Diacid	359.2070		W
$C_{22}H_{41}O_5^-$	R,R,R-DHO Acid	385.2954		M
$C_{23}H_{41}O_7^-$	R,R,R-DHO Diacid	429.2860		W
$C_{26}H_{41}O_9^-$	Unassigned	497.2751		W
$C_{24}H_{39}O_9Ca^-$	Ca Adduct of 3 OOA-	511.2221	M	W
$C_{24}H_{39}O_9Na_2^-$	Na Adduct of 3 OOA-	517.2390	M	

Appendix I. Contributions to This Work

The research contained in this thesis is, of course, not solely my work but the result of the efforts of many people. In the following, I outline the specific contributions that resulted in the preceding work. Unless otherwise specified, I conducted the majority of the experimental work and analysis and was main author of the text, and Veronica Vaida oversaw the design of the research and edited all text.

Chapter 4: Barry K. Carpenter (BKC) provided the new mechanism and electronic structure calculations. Russell J. Perkins (RJP) conducted NMR experiments and aided in the development of the new mechanism.

Chapter 5: Haishen Yang synthesized and purified 2-oxohexanoic acid, 2-oxodecanoic acid, and 2-oxododecanoic acid under the supervision of Garret M. Miyake. BKC provided mechanistic insight, and RJP conducted NMR analysis.

Chapter 6: Michael R. Dooley (MRD) conducted the majority of the experimental work as part of his undergraduate honors thesis under my direction. Keaten Kappes provided additional experimental data. RJP provided NMR analysis.

Chapter 7: Pascal Renard conducted all the photochemical experiments and wrote an initial draft of the manuscript under the direction of Anne Monod and assisted by Sylvain Ravier, Carine Demelas, Bruno Coulomb, and Etienne Quivet. I conducted the surface activity studies. Allison E. Reed Harris and I rewrote the manuscript.

Chapter 8: BKC provided electronic structure calculations and mechanistic insight. MRD and Jay A. Kroll distilled the pyruvic acid, fatty acids, and fatty alcohols and took UVvis spectra. RJP provided NMR analysis.

Chapter 9: Elizabeth C. Griffith conducted the majority of the experimental work and wrote the manuscript. Richard K. Shoemaker (RKS) did all NMR analysis. BKC provided

mechanistic insight. I conducted the experimental characterization of the aggregates, especially the DLS measurements, and edited the manuscript.

Chapter 10: James F. Davies under Kevin R. Wilson developed the experimental set-up for the time-resolved DLS measurements at LBL. I conducted the experiments at LBL with JFD and also did all photochemical experiments at Boulder. All electron microscopy was done at the University of Colorado, Boulder EM Services Core Facility in MCDB, with the technical assistance of facility staff.

Chapter 11: I developed the project in Joel D. Eaves (JDE) CHEM 5555 in the Fall of 2015 and performed initial MD simulations. Steven E. Strong refined the MD simulations and developed the analysis under the direction of JDE.

Chapter 12: I developed and directed the project with help from RJP. Brenda Kessenich did preliminary experiments on decanoic acid. Benjamin R. Williamson conducted all myrstic acid trough studies and did some initial analysis.

Appendix A: RKS conducted all NMR analyses. RJP contributed insights about the NMR data.

Appendix B: Sheref Mansy and Laura Martini taught me how to make vesicles in their lab in Trento, Italy. I conducted DSC experiments with Christine Gobrogge in Rob Walker's lab at Montana State University.

Appendix C: MRD made the acetamide and hexanoic acid solutions and took UV-vis spectra under my direction.